Improvement of the current therapy against *Helicobacter pylori*: biophysical studies of drug-membrane interactions and development of a drug delivery system

Daniela Lopes de Campos

D

2018

Daniela Priscila Rodrigues Lopes de Campos

Improvement of the current therapy against *Helicobacter pylori*: biophysical studies of drug-membrane interactions and development of a drug delivery system

Aos grandes amores da minha vida,

Deus, Samuel e Priscila Campos

"De entre todos, apenas vós
tendes direito a ver-me
fracassar. Onde caio
entre a vossa irónica
doçura implacável, convosco
partilho o pão e o espaço
e a rapidez dos olhos
sobre o que fica (sempre)
para dar ou dizer.
E de vós me levanto
e vos levo pesando
e ardendo até onde
me ajudais a ser
melhor ou talvez
menos só."

Vítor Matos e Sá, in 'Companhia Violenta'

Agradecimentos

A escrita desta tese é na verdade a concretização de um percurso longo, laborioso, árduo, mas gratificante. Todos os problemas e gigantes desafios que me cercaram foram enfrentados com alegria e otimismo graças ao apoio de imensos amigos.

À minha professora e orientadora Salette Reis, quero agradecer ter-me acompanhado no meu crescimento neste meio académico e científico. Desde o início de 2009 que sei que tenho em si um apoio constante em qualquer tipo de dificuldade. E esse apoio não se restringe à investigação. Todo o seu lado maternal me acolheu com grande amor neste seu grupo. Por isso serei eternamente grata.

À Cláudia, por tudo. Poderia enumerar todas as coisas que fizeste por mim, mas esta tese não chegaria para tal (e olha que é grande!). Obrigada por toda a tua orientação, cuidado, amizade, sensibilidade, carinho, brincadeiras, descompressão, e muito mais. Tornaste estes 4 anos um período muito mais leve.

Ao meu co-orientador Bruno Sarmento, agradeço toda disponibilidade que sempre demonstrou. Quando precisava, sabia que podia contar com a sua resposta "para ontem". Estou muito grata por todos os úteis comentários, sugestões e sabedoria.

Aos meus colaboradores e amigos que tanto contribuíram para este trabalho. À minha Ritinha, primeira aluna de mestrado, agradeço o quanto me fizeste crescer como orientadora. Foste uma aluna excecional e sou grata por ter podido acompanhar-te na tua tese. À Sofia Lima, agradeço todo o exemplo e experiência que me transmitiste nas culturas celulares e não só. Agradeço toda a amizade, preocupação e ajuda neste percurso. À Catarina Seabra, um enorme obrigada por tudo o que trouxeste para este trabalho. Obrigada pela amizade, pela companhia nas longas horas de trabalho, obrigada por todo o conhecimento pylorento que me transmitiste e por nunca me teres deixado "cair". À Catarina Pereira-Leite, agradeço do fundo do coração a colaboração que fizemos nos ensaios de biofísica. Tu consegues sempre ensinar-me alguma coisa e é ótimo ter-te por

perto. Acima de tudo, por toda a tua amizade e carinho. Tens um coração enorme. Agradeço também à Prof. Ana Coutinho e aos demais investigadores que colaboraram connosco nos ensaios de fluorescência (Joana C. Ricardo, Aleksander Fedorov e Prof. Manuel Prieto). Ao Tiago Santos, agradeço toda a disponibilidade e ajuda que me deste. A tua alegria e descontração acalmam sempre tudo. To Sven Jakobtorweihen, I am grateful for being so well-received in your research group at the Hamburg-Harburg University. Thank you for all the help with the computational simulations. You brought a whole new perspective to this work. To Philippe Fontaine, I thank all the help with the analysis of the GIXD results. Agradeço à Prof. Cristina Martins ter-me recebido no seu laboratório para a realização dos ensaios de eficácia. Fui muitíssimo bem-recebida e sou muito grata por toda a ajuda cientifica que me prestou. Foi muito bom colaborar consigo.

A todos do MB^2 que me acompanharam no laboratório. Agradeço verdadeiramente tudo o que fazem por mim. Muito obrigada por me facilitarem tanto as longas horas no laboratório. Muito obrigada por sempre procurarem o meu bem-estar, nem que seja trazendo um café enquanto estou numa correria. Muito obrigada por todos os sorrisos, abraços, lanches, etc. Agradeço à Joana, ao José, ao Alexandre, à Luise, à Virgínia, ao João, à Daniela Resende, à Ana Isabel, à Andreia Granja, à Catarina Alves, à Andreia Marinho, à Joyce, à Yong, à Marina, à Nini, ao Miguel, ao Iúri, à Rita Leal, à Mara, à Elizabete, ao Nuno, à Francisca, ao Abdu, ao Emílio, à Suellen, à Joana Queiroz, à Daniela Ribeiro, à Luisa, à Soraia, à Sara, ao João e tantos outros. Obrigada porque mesmo com contribuições "temporárias", vocês criaram o ambiente maravilhoso que o MB^2 possui. É um prazer trabalhar, conviver e "viver" convosco.

Agradeço também a todos os meus vizinhos de laboratório, especialmente à Inês, à Sara, à Luísa, à Patrícia, à Margarida, à Ana Marta, à Rosa Couto e ao Soares pela boa companhia nas longas horas de trabalho. Agradeço também às pessoas que me proporcionam sempre maravilhosas conversas, especialmente à Mafalda, ao Jorge, à Clara, à Marisa, à Daniela Ribeiro, à Sofia Rodrigues e à Marieta. A todos os professores do laboratório de Química Aplicada, agradeço a simpatia e a preocupação constante. Um obrigada especial ao Prof. José Costa Lima e ao Prof. Rui Lapa por me darem boas condições de trabalho. À Vânia, à D. Manuela e à Patrícia Moreira agradeço todo o apoio laboratorial, técnico, administrativo, mas sobretudo por todos os sorrisos e abraços que me animaram nos dias cinzentos.

Agradeço também a todas as meninas do laboratório da Cristina Martins e do Bruno Sarmento. Obrigada por toda a ajuda que me deram nesta "visita" à vossa casa. Obrigada por me receberem tão bem. Um obrigada especial à Cláudia Monteiro, Paula Parreira e Andreia Pereira. I would also to thank Nele, Denista and Prof. Irina Smirnova for receiving

me so well in your wonderful city (Hamburg). Estou grata à Sara Cravo pela ajuda no Laboratório de Química Orgânica.

Aos meu colegas Biotecanos, agradeço termos caminhado juntos. Não foi uma caminhada fácil, mas conseguimos tornar uma competição numa amizade e estou grata por todo o vosso cuidado. Ao Daniel Vasconcelos e à Catarina Leite Pereira agradeço todo o tempo que dispensaram para tratar dos nossos problemas "Biotecanos". Tornaram este percurso mais fácil. À Helena Martins agradeço a disponibilidade e a presença constante para resolver problemas administrativos e não só. Agradeço toda a sua ajuda.

A todos os meus amigos, agradeço o imenso cuidado e preocupação que tiveram por mim. Obrigada por me sustentarem quando tudo parecia tremer. Um agradecimento especial à Ana e ao Joel, à Rita Silva e à Rita Monteiro, às meninas do pequeno grupo (Florbela, Alda, Miriam, Eunice, Rachel, Jeff, Erin, Edna, Bruno) e à Cristel.

Agradeço a toda a minha família por sempre perguntarem como estou e orarem por mim. Agradeço especialmente aos meus pais. Sem vocês eu não estaria aqui hoje, não só pelas condições que me proporcionaram para poder estudar, mas sobretudo por todo o apoio e amor que demonstraram por mim toda a minha vida. Sabem que tenho péssima memória, mas sei (porque senti) que me amaram com tudo o que podiam e eu amo-vos de todo o coração. Espero um dia retribuir tudo o que fizeram por mim. À minha irmã, meu cunhado Ricardo, meus cunhados Sara e David e aos meus pequenos lindos sobrinhos Gabriel, Josué e Salomão agradeço a companhia, a amizade e todo o cuidado. Agradeço também à minha avó, à D. Leonilde e ao Sr. João por estarem sempre presentes.

Ao meu Samuel, não há palavras para agradecer. Devias ser doutor honoris causa somente por tudo o que contribuíste para este doutoramento. A tua paciência, o suportares fins-de-semana, noites e feriados de trabalho, o me apoiares sempre que as coisas complicavam, e sobretudo por todo o teu amor que sempre encheu o meu coração e a nossa casa. Sem ti, sem dúvida alguma, que isto não era possível. Agradeço à Priscila por toda a alegria que me trouxe. Um dia lerás isto filha e saberás que sempre foste a melhor parte do meu dia. Estar contigo é uma alegria e uma bênção incrível. Obrigada por seres a filha maravilhosa que és! Agradeço também a Deus. Sem Ele, não teria feito nada.

x

Publications

Ao abrigo do disposto do nº 2, alínea a) do artigo 31º do Decreto-Lei nº 115/2013 de 7 de Agosto, fazem parte integrante desta tese de doutoramento os seguintes trabalhos já publicados:

1) D. Lopes, C. Nunes, M. C. L. Martins, B. Sarmento, S. Reis. "Eradication of Helicobacter pylori: Past, present and future". Journal of Controlled Release 189 (2014) 169-186;

2) D. Lopes, C. Nunes, M. C. L. Martins, B. Sarmento, S. Reis. "Targeting strategies for the treatment of Helicobacter pylori infections". In Nano based drug delivery, pp.339-366. IAPC-OBP, 2015. ISBN 978-953-56942-2-9;

3) D. Lopes, C. Nunes, P. Fontaine, B. Sarmento, S. Reis. "Proof of pore formation and biophysical perturbations through a 2D Amoxicillin-lipid membrane interaction approach". Biochimica et Biophysica Acta – Biomembranes 1859 (2017) 803-812;

4) D. Lopes, S. Jakobtorweihen, C. Nunes, B. Sarmento, S. Reis. "Shedding light on the puzzle of drug-membrane interactions: experimental techniques and molecular dynamics simulations". Progress in Lipid Research 65 (2017) 24-44;

5) D. Lopes, R. Pinto, C. Nunes, B. Sarmento, S. Reis. "Oral administration of lipid-based delivery systems to combat infectious diseases". In Nanoparticles in Life Sciences and Biomedicine. Pan Stanford Publishing, 2018. ISBN 978-981- 4745-98- 7;

6) D. Lopes, C. Nunes, B. Sarmento, S. Jakobtorweihen, S. Reis. "Metronidazole within phosphatidylcholine lipid membranes: new insights to improve the design of imidazole derivatives". European Journal of Pharmaceutics and Biopharmaceutics 129 (2018) 204-214.

Abstract

Helicobacter pylori (*H. pylori*) is the main cause of chronic gastritis and peptic ulcers. The importance of the eradication of these bacteria at the first clinical symptoms is well-recognized. In fact, persistent infections can evolve into gastric cancer, which underlies their classification as human carcinogenic bacteria by the International Agency for Research on Cancer. Nevertheless, the treatment of *H. pylori* infections is hindered by several limitations, such as antimicrobial resistances, the protective location of the bacteria *in vivo*, the pharmacokinetic properties of antibiotics and their low residence time at the stomach, among others. This leads to eradication rates of 70-80%, which is distant from the desirable for infectious diseases. Hence, this thesis aimed to improve the current therapy against *H. pylori*.

The first-line triple therapy is composed of a proton-pump inhibitor, such as omeprazole, plus two antibiotics (e.g. amoxicillin and metronidazole). The first objective of this thesis was to study some pharmacokinetic limitations of these drugs by using mimetic model systems. Dipalmitoylphosphatidylcholine models were used to mimic lipid membranes of biological cells. Different biophysical techniques and mimetic models were combined for a more comprehensive puzzle of drug-membrane interactions. The main focus of omeprazole studies was the understanding of the effect of the absorption route on the topical action of the drug on biological membranes. The cytoprotective effect of omeprazole had already been reported *in vivo*; however, the mechanisms behind this effect were unknown. We discovered that when omeprazole is absorbed directly through the gastric mucosa at lower pH values (e.g. pH 5), it has an additional mechanism of action against peptic ulcers. This is due to its amphipathic properties that enable an intercalation among phospholipid molecules and, consequently, a higher packing and reinforcement of the protective barrier of the gastric mucosa. We also discovered that metronidazole is able to perturb the biophysical properties of lipid membranes at pH 7.4, which was visualized by the fluidizing effect and the decrease of the hydrophobicity of the membrane. Thus, we used molecular dynamics simulations to unveil which is the functional group that causes this toxic effect. The hydroxyl group of metronidazole side chain interacts with water molecules and with the phosphate group of phospholipids whereas the oxygen atoms of the other side chain are important for the partitioning of the drug. Hence, through these biophysical studies, we contributed to the structure-toxicity relationship of metronidazole, which can be

henceforward used to develop new imidazole derivatives. The study with amoxicillin showed that this drug perturbs the lipid membrane at acidic pH, leading to the formation of pores. At physiological pH, however, amoxicillin did not have a toxic effect on the lipid membrane.

The second objective of the thesis was to develop a drug delivery system. For that, lipid nanoparticles were optimized by a Box-Behnken design. The components were carefully chosen: Tween 80 and linolenic acid due to their antimicrobial properties and dioleoylphosphatidylethanolamine to bind to *H. pylori* receptors (active targeting). Permeability studies showed that the lipid nanoparticles were able to be retained at the site of infection once they did not permeate gastric cells. Furthermore, they interacted with mucins, which enhances their retention time at the stomach. The lipid nanoparticles killed *H. pylori* through the detachment of the bacterial membrane and the release of the cytoplasmic content. Moreover, due to the targeting agent, the lipid nanoparticles were bound to the bacteria within the first 15 min, which decreased the adhesion of the bacteria to gastric cells. These lipid nanoparticles were successfully used to load amoxicillin and protect it from the acidic pH. An *in vitro* infection model was developed during this thesis, considering the existence of a complex system that protects *H. pylori in vivo*, namely, the gastric epithelial barrier, mucins, and the acidic pH. Contrary to the observed with plain amoxicillin, amoxicillin-loaded lipid nanoparticles were effective in the *in vitro* infection model.

Overall, this thesis contributed to the improvement of the current therapy against *H. pylori* by: a) discovering an additional mechanism of action of omeprazole, which has direct implications on the choice of the treatment in the clinical practice; b) providing new insights regarding the structure-toxicity relationship of metronidazole, which can be used to design new imidazole derivatives; c) unveiling toxic mechanisms of amoxicillin at acidic pH; d) developing lipid nanoparticles that are able to be retained at the site of infection and that can target and kill the bacteria; e) developing an *in vitro* infection model that can be used by other researchers for the evaluation of antimicrobial compounds on a more realistic model than planktonic bacteria; and f) encapsulating amoxicillin in the delivery system to protect the drug from the acidic pH, which turns amoxicillin a more effective therapy.

Keywords: *Helicobacter pylori*, omeprazole, metronidazole, amoxicillin, membrane mimetic models, biophysical techniques, lipid nanoparticles, *in vitro* infection model.

Resumo

As infeções por *Helicobacter pylori* (*H. pylori*) são a principal causa de gastrite crónica e úlceras pépticas. É bem reconhecida a importância de erradicar estas bactérias quando aparecem os primeiros sintomas clínicos. De facto, as infeções persistentes podem evoluir para cancro gástrico, o que justifica a sua classificação como bactéria carcinogénica humana pela Agência Internacional de Pesquisa em Cancro. Contudo, o tratamento de infeções pela *H. pylori* é dificultado por diversas limitações, como a resistência aos antibióticos, a localização protegida da bactéria *in vivo*, as propriedades farmacocinéticas dos antibióticos e o seu reduzido tempo de residência no estômago, entre outras. Isto leva a taxas de erradicação de 70-80%, o que está distante do desejável para doenças infeciosas. Assim, esta tese teve como objetivo melhorar a terapia atual contra a infeção por *H. pylori*.

A terapia tripla de primeira linha é composta por um inibidor da bomba de protões, como o omeprazol, e dois antibióticos (ex. a amoxicilina e o metronidazole). O primeiro objetivo desta tese foi estudar algumas limitações farmacocinéticas destes fármacos usando modelos miméticos. Modelos compostos por dipalmitoilfosfatidilcolina foram usados para mimetizar as membranas lipídicas das células biológicas. A utilização de diferentes técnicas biofísicas e diferentes modelos miméticos permitiu construir um puzzle mais completo da interação fármaco-membrana. O principal foco dos estudos com o omeprazol foi entender o efeito da via de absorção na sua ação local ao nível das membranas biológicas. O efeito citoprotetor do omeprazol já tinha sido reportado *in vivo*. No entanto, os mecanismos que originam esse efeito eram desconhecidos. Nós descobrimos que quando o omeprazol é absorvido diretamente através da mucosa gástrica a valores de pH mais baixos (ex. pH 5), ele tem um mecanismo de ação adicional na cura de úlceras pépticas. A pH 5, o omeprazol possui propriedades anfipáticas, o que permite a sua intercalação entre os fosfolípidos, levando a um maior empacotamento e reforço da barreira protetora da mucosa gástrica. No caso do metronidazol, descobrimos que este fármaco perturba as propriedades biofísicas das membranas lipídicas a pH 7.4, o que foi comprovado pelo seu efeito de fluidificação e pela diminuição da hidrofobicidade da membrana. De forma a perceber qual o grupo funcional que causa o efeito, foram efetuadas simulações de dinâmica molecular. O grupo hidroxilo da cadeia lateral interage com moléculas de água e com o grupo fosfato dos fosfolípidos enquanto que os átomos de

oxigénio ligados ao azoto da outra cadeia lateral são importantes para a partição do fármaco. Assim, através destes estudos, pudemos contribuir para a relação estrutura-toxicidade do metronidazol, o que poderá ser futuramente usado para o desenvolvimento de novos derivados imidazólicos. O estudo com a amoxicilina mostrou que este fármaco perturba a membrana lipídica a pH ácido, induzindo a formação de poros. No entanto, a pH fisiológico, a amoxicilina não teve qualquer efeito tóxico na membrana lipídica.

O segundo objetivo da tese foi desenvolver um sistema de entrega de fármacos. Para isso, procedeu-se à otimização do desenvolvimento de nanopartículas lipídicas usando um desenho experimental do tipo Box-Behnken. Os componentes foram cuidadosamente escolhidos: o Tween 80 e o ácido linolénico foram usados pelas suas propriedades antimicrobianas e o dioleoilfosfatidiletanolamina para se ligar a recetores na *H. pylori* (vectorização ativa). Os estudos de permeabilidade mostraram que as nanopartículas lipídicas são capazes de ser retidas no local da infeção, uma vez que não permearam as células gástricas. Além disso, as nanopartículas interagiram com as mucinas, o que leva a um aumento do tempo de retenção no estômago. As nanopartículas mataram a *H. pylori* pela rutura da membrana bacteriana com consequente libertação do conteúdo citoplasmático. Além disso, devido ao agente de vectorização, as nanopartículas ligaram-se às bactérias nos primeiros 15 min de experiência, o que levou a uma diminuição da adesão das bactérias às células gástricas. Estas nanopartículas lipídicas foram utilizadas com sucesso na encapsulação da amoxicilina, protegendo-a do pH ácido. Um modelo de infeção *in vitro* foi desenvolvido durante a tese, o qual teve em conta a existência de um sistema complexo que protege a bactéria *in vivo*, nomeadamente, a barreira gástrica epitelial, as mucinas e o pH ácido. Ao contrário do observado com a amoxicilina livre, as nanopartículas contendo a amoxicilina foram eficazes no modelo de infeção.

Esta tese contribuiu para melhorar a terapia atual contra a *H. pylori* por: a) descobrir um mecanismo adicional de ação do omeprazol, o qual tem implicações diretas na escolha do tratamento na clínica; b) fornecer novos dados para a construção da relação estrutura-toxicidade do metronidazole, o que pode ser usado para o desenho de novos derivados imidazólicos; c) desvendar mecanismos de toxicidade da amoxicilina a pH ácido; d) desenvolver nanopartículas lipídicas que ficam retidas no local da infeção, se ligam e matam as bactérias; e) desenvolver um modelo de infeção *in vitro* que pode ser usado por outros investigadores para a avaliação de compostos antimicrobianos num ambiente mais realista que as bactérias planctónicas; e f) encapsular a amoxicilina num sistema de entrega de fármacos, protegendo-a assim do pH ácido e tornando a sua ação mais eficaz.

Keywords: *Helicobacter pylori*, omeprazol, metronidazol, amoxicilina, modelos miméticos membranares, técnicas de biofísica, nanopartículas lipídicas, modelo de infeção *in vitro.*

Contents

Lɪst of Figures

Chapter 2. Theoretical Background

1. *Helicobacter pylori*

2. Shedding light on the puzzle of drug-membrane interactions: Experimental techniques and molecular dynamics simulations

3. Eradication of *Helicobacter pylori*: Past, present and future

4. Oral Administration of Lipid-Based Delivery Systems to Combat Infectious Diseases

5. Targeting Strategies for The Treatment of *Helicobacter pylori* Infections

Chapter 4. Methods to evaluate drug-lipid membrane interactions

Chapter 5. Methods to develop and characterize the drug delivery systems

Chapter 6. Progress beyond the state of the art

1. Topical interaction with lipid membranes as a new additional mechanism of immediate-release omeprazole

2. Molecular mechanisms behind the new additional mechanism of action of immediate-release omeprazole

3. Metronidazole within phosphatidylcholine lipid membranes: new insights to improve the design of imidazole derivatives

4. Proof of pore formation and biophysical perturbations through a 2D amoxicillin-lipid membrane interaction approach

5. Delivering amoxicillin at the infection site – a rational design through lipid nanoparticles

6. Targeting and killing the ever-challenging ulcer bug: an antibiotic-free strategy

7. Efficacy of amoxicillin-loaded lipid nanoparticles on an *in vitro* infection model of *Helicobacter pylori*

Chapter 7. Concluding remarks and future perspectives

LList of Tables

Chapter 4. Methods to evaluate drug-lipid membrane interactions

Chapter 6. Progress beyond the state of the art

1. Topical interaction with lipid membranes as a new additional mechanism of immediate-release omeprazole

2. Molecular mechanisms behind the new additional mechanism of action of immediate-release omeprazole

3. Metronidazole within phosphatidylcholine lipid membranes: new insights to improve the design of imidazole derivatives

4. Proof of pore formation and biophysical perturbations through a 2D amoxicillin-lipid membrane interaction approach

5. Delivering amoxicillin at the infection site – a rational design through lipid nanoparticles

List of abbreviations

AE	Association efficiency
AMX	Amoxicillin
ATP	Adenosine triphosphate
BabA	Blood group antigen-binding adhesins
BAM	Brewster angle microscopy
BB	Brucella broth
CagA	Cytotoxin-associated gene A product
CFU	Colony forming unit
DOPE	Dioleoylphosphatidylethanolamine
DPH	1,6-Diphenyl-1,3,5-hexatriene
DPPC	1,2-Dipalmitoyl-*sn*-glycero-3-phosphocholine
FBS	Fetal bovine serum
FDA	Food and Drug Administration
fwhm	Full width at half maximum
GIXD	Grazing incidence X-ray diffraction
H. pylori	*Helicobacter pylori*
IR-OME	immediate-release omeprazole
LC	Loading capacity
LNPs	Lipid nanoparticles
LUVs	Large unilamellar vesicles
MD	Molecular dynamics
MLVs	Multilamellar vesicles
MND	Metronidazole
OipA	Outer inflammatory protein
OME	Omeprazole

PDI	Polydispersion index
PM-IRRAS	Polarization modulation-infrared reflection-absorption spectroscopy
PPI	Proton-pump inhibitor
RDF	Radial distribution function
SabA	Sialic acid-binding adhesins
SAXS	Small-angle X-ray scattering
SEM	Scanning electron microscopy
TEM	Transmission electron microscopy
TMA-DPH	1-(4-Trimethylammoniumphenyl)-6-phenyl-1,3,5-hexatriene p-toluenesulfonate
US	Umbrella sampling
UV-Vis	Ultraviolet visible
VacA	Vacuolating cytotoxin
WAXS	Wide-angle X-ray scattering
WHAM	Weighted histogram analysis method

List of Symbols

[L]	Lipid molar concentration
[Q]	Total quencher concentration
[Q]$_m$	Membrane concentration of quencher
A_F	Absorbance values at the wavelength of excitation of the fluorophore in the absence of the drug
A_L	Area per lipid
A_Q	Absorbance values at the wavelength of excitation of the fluorophore in the presence of the drug
B	Cooperativity
C_T	Total molar concentration of drug
d	Long and short-range distances
D_T	Derivative value obtained from the absorption data of the total amount of drug
D_w	Derivative value obtained from the absorption data of the amount of drug in the aqueous phase
E_m	Drug molar absorptivity in the lipid phase
E_w	Drug molar absorptivity in the aqueous phase
I	Fluorescence intensity
I_0	Fluorescence intensity of the probe in the absence of quencher
I_{cor}	Corrected fluorescence intensity
K_a	Acid dissociation constant in aqueous medium
K_D	Dynamic quenching constant
K_P	Partition coefficient
K_S	Static quenching constant
K_{SV}	Stern-Volmer constant
L_o	Liquid-ordered phase of lipid bilayers
log D $_{DS}$	Distribution coefficient obtained by derivative spectrophotometry

log D_{MD}	Distribution coefficient obtained by molecular dynamics simulation
log $D_{O/w}$	Octanol:water distribution coefficient
L_α	Liquid-crystalline phase of lipid bilayers
p_1	Slope of linear fits to the data before the phase transition region
p_2	Slope of linear fits to the data after the phase transition region
pK_a	Logarithmic acid dissociation constant in aqueous medium
$P_{\beta'}$	Ripple gel phase of lipid bilayers
Q	Peak distances
Q_{xy}	In-plane component of the scattering vector
Q_z	Out-of-plane component of the scattering vector
$r(0)$	Initial anisotropies of the decays
$r(t)$	Anisotropy decay
r_∞	Limiting anisotropy
r_0	Fundamental anisotropy
r_s	Steady-state fluorescence anisotropy
r_{s1}	Y-intercepts of linear fits to the data before the phase transition region
r_{s2}	Y-intercepts of linear fits to the data after the phase transition region
S_{CD}	Deuterium order parameter
τ	Fluorescence lifetime
τ_0	Fluorescence lifetime in the absence of drug
τ_i	Lifetime of the ith fluorescence decay component
T_m	Main phase transition temperature
V_φ	Lipid molar volume
α_i	Amplitude of the ith fluorescence decay component
β_i	Amplitude correlation time of the ith anisotropy decay component
ΔG	Gibbs free energy
λ	Wavelength

ξ Correlation length

ϕ_i Rotational correlation time of the ith anisotropy decay component of the anisotropy

Chapter 1

Thesis structure

"First comes thought; then organization of that thought, into ideas and plans; then transformation of those plans into reality."

Napoleon Hill

This thesis is organized in 7 chapters, based on the manuscripts that this work has originated.

Chapter 1: Thesis structure

This chapter guides the reader through the thesis by providing a summary of the contents of each chapter.

Chapter 2: Theoretical Background

This chapter provides the knowledge base that underlies the motivation, the objectives, and the strategies that were followed within this thesis. Firstly, it presents a brief description of the morphology and the pathogenicity of *Helicobacter pylori* (*H. pylori*), the current eradication therapy, and new strategies that have been developed. In the follow-up, four publications were included, namely, two review papers and two book chapters:

1- **Shedding light on the puzzle of drug-membrane interactions: experimental techniques and molecular dynamics simulations** (Prog. Lipid Res. 65 (2017) 24-44).

The first review paper provides new insights about the usefulness of combining experimental techniques with molecular dynamics simulations to study drug-membrane interactions.

2- **Eradication of *Helicobacter pylori*: Past, present and future** (J. Control. Release 189 (2014) 169-86).

This review paper describes the limitations of the current therapy against *H. pylori* infections, and it provides an overview of the strategies that have been developed, highlighting micro- and nanotechnology.

3- **Oral Administration of lipid-based delivery systems to combat Infectious diseases** (*in* Nanoparticles in Life Sciences and Biomedicine, 2018; ISBN 978-981-4745-98-7)

This book chapter describes the features of lipid nanoparticles that make them an interesting oral delivery system against infectious diseases.

4- **Targeting strategies for the treatment of *Helicobacter pylori* infections** (*in* Nano Based Drug Delivery, 2015; ISBN 978-953-56942-2-9).

This book chapter provides new strategies for targeting the gastric mucosa and/or the bacteria and to evaluate the efficacy of that targeting.

Chapter 3: Motivation and objectives

In this section, the motivation that drove the development of this thesis is explained. The motivation led to the outline of general and specific objectives that are clearly pointed out.

Chapter 4: Methods to evaluate drug-lipid membrane interactions

A combination of membrane models and techniques is required to study drug-lipid membrane interactions. This chapter contains the scientific basis behind the membrane models and the biophysical techniques that were used throughout this thesis.

Chapter 5: Methods to design and characterize the drug delivery systems

This chapter presents the theoretical background of the techniques that were used to design and characterize the drug delivery system.

Chapter 6: Progress beyond the state of the art

The experimental work of this thesis originated 7 papers:

1- **Topical interaction with lipid membranes as a new additional mechanism of action of immediate-release omeprazole** (to be submitted)

2- **Molecular mechanisms behind the new additional mechanism of action of immediate-release omeprazole** (to be submitted)

3- **Metronidazole within phosphatidylcholine lipid membranes: new insights to improve the design of imidazole derivatives** (submitted)

4- **Proof of pore formation and biophysical perturbations through a 2D amoxicillin-lipid membrane interaction approach** (Biochim. Biophys. Acta 1859 (2017) 803-812)

5- **Delivering amoxicillin at the infection site – a rational design through lipid nanoparticles** (to be submitted)

6- **Targeting and killing the ever-challenging ulcer bug: an antibiotic-free strategy** (to be submitted)

7- **Efficacy of amoxicillin-loaded lipid nanoparticles on an *in vitro* infection model of *Helicobacter pylori*** (to be submitted)

Chapter 7: Concluding remarks and future perspectives

A critical global analysis of this thesis is provided. The main findings and conclusions are drawn. Furthermore, the limitations of the experimental work and future perspectives are also discussed.

Appendix

The authorization for reproduction of the book chapter entitled "Oral Administration of lipid-based delivery systems to combat Infectious diseases" is provided in this section.

Chapter 2   5

Theoretical Background

"Eradication of the ubiquitous "ulcer bug" is the first step in freeing patients with chronic dyspepsia and/or ulcer disease from an expensive lifetime of chronic medication use."

Prof. Barry Marshall

1. *Helicobacter pylori*

Helicobacter pylori (*H. pylori*), the so-called "ulcer bug", has been the focus of several research groups since Barry Marshall proved the association between these bacteria and peptic ulcers [1]. It was difficult for the scientific community to handle with the idea that a bacterium could survive through the harsh conditions of the gastrointestinal tract [1]. There are indeed several factors that hinder the colonization of a human stomach, such as the acidity of the lumen, its peristaltic movements, the nutrient availability, the host immune system, and other competing microbes [2]. Over time, the unique characteristics of *H. pylori* were known, and the ability of these bacteria to colonize the antrum of the stomach is now well-recognized [1].

1.1 Morphology and pathogenicity

H. pylori is a gram-negative and microaerophilic bacterium that usually adopts a spiral shape with 0.5 x 5 μm in length (Figure 1, A) [1, 3]. Under hostile conditions, it changes to resistant structures (coccus) (Figure 1, B) [3]. *H. pylori* is the only human bacterium that is able to persistently colonize the gastric mucus [4]. This is due to several virulent factors that enable the bacterium not only to resist to the acidic pH of the stomach lumen, but also to be pathogenic. A spiral shape combined with 5 to 7 polar flagella enable the motility through the mucus layer [1, 4]. Furthermore, one of the *H. pylori* genes is acid-regulated, and it is able to induce the secretion of urease by which the bacterium neutralizes the acidic pH [4]. *H. pylori* also secretes some cytotoxins that are involved in their pathogenicity, such as the cytotoxin-associated gene A product (CagA), the vacuolating cytotoxin (VacA), and the

outer inflammatory protein (OipA) [5]. The CagA is the most studied virulence factor, and it is classified as a bacteria-derived carcinogen [5]. It was already shown that who were infected by CagA positive *H. pylori* strains had a higher risk of development of peptic ulcers and gastric cancer [5]. The VacA cytotoxin can damage epithelial cells by forming pores within the host cell membrane [6]. It can also bind to several epithelial cell receptors and induce peptic ulcers [4, 6]. OipA is an outer membrane protein that acts as an adhesin and induces inflammation [5]. *H. pylori* has also other adhesins, such as the sialic acid-binding adhesins (SabA) and the blood group antigen-binding adhesins (BabA), that bind to Lewis b antigens on epithelial cells [4]. Strains that possess the BabA adhesins are associated with higher epithelial proliferation and higher risk of development of ulcers [4]. Although *H. pylori* does cause inflammation processes and does activate immune cells, the bacterium developed mechanisms to evade the immune system [4]. *H. pylori* has surface components, like lipopolysaccharides, that hinder the recognition by immune cells [4]. It can also combat the bactericidal oxidative stress, inhibit the production of nitric oxide by immune cells, and downregulate chemokine receptors on neutrophils [4].
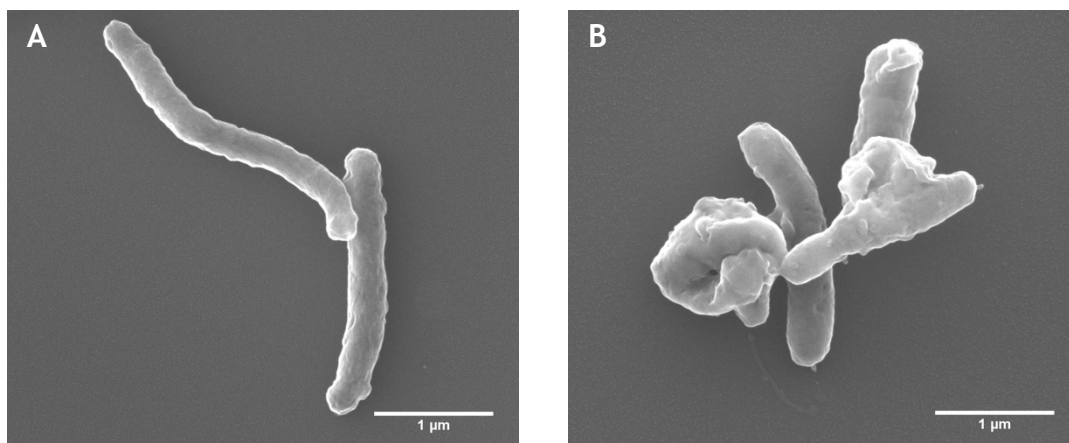
Figure 1. *H. pylori* morphology by scanning electron microscopy: spiral shape (A) and coccoid shape (B) (Lopes-de-Campos, 2017).

Some of the experts in *H. pylori* consider that these bacteria may have symbiotic or pathogenic properties, depending on the context [7]. In fact, in some cases, the colonization by *H. pylori* can even be beneficial [7]. For instance, *H. pylori* infections have been associated with a decrease in the prevalence of allergic and autoimmune diseases [7]. Nevertheless, the bacteria can also be pathogenic, depending on the virulence of the strain, on the extent of the immune response by the host, and on modulating factors, such as smoking and diet [4]. The infection by *H. pylori* is highly common worldwide and not every

one that is infected has clinical and pathogenic signs. A recent (2017) global systematic review showed that approximately 4.4 billion individuals were infected worldwide in 2015 [8], which corresponds to approximately 60% of the population. The prevalence varies significantly among regions, with higher prevalence in developing countries [8]. In Portugal, the prevalence of infection is one of the highest (almost 87%) [8]. In general, 20% of the individuals that are infected manifest some histological changes that can lead to serious gastric conditions [9]. In fact, persistent infections can lead to chronic inflammatory processes and epithelial damages that result in the development of ulcers and gastric adenocarcinomas [4]. *H. pylori* can also induce the development of gastric cancer, being involved in the initiation, the promotion, and the progression of cancer cells [6]. For instance, 89% of non-cardia gastric cancer are associated with persistent infections by *H. pylori* [10]. Consequently, *H. pylori* is considered a human carcinogenic by the World Health Organization [11]. Moreover, *H. pylori* has been associated with extragastric and extradigestive conditions, including haematological, cardiovascular, and neurological diseases [12].

1.2 Eradication therapy

The relationship between *H. pylori* and its host is ambiguous [13]. The balance between the benefits and the risks of having *H. pylori* should be carefully analysed before any treatment. Nevertheless, in some cases, the severity of the diseases promoted by these bacteria requires the follow-up of specific treatment guidelines. The eradication of *H. pylori* is strongly recommended in cases of peptic ulcers, mucosa-associated lymphoid tissue lymphoma, atrophic gastritis, post-gastric cancer resection, and in the cases where the patient has relatives with gastric cancer [14]. In these cases, the treatment is supported by several consensuses worldwide (e.g., [15-19]).

It is difficult to determine a standard and global treatment to manage *H. pylori* infections once they vary among regions and countries [20]. It is necessary to consider the prevalence of *H. pylori* infections, the prevalence of gastric cancer, the resistance rate to antibiotic treatments, the availability of resources, such as of bismuth or diagnostic tests, the ethnicity, previous treatments, the local efficacy of the common first-line treatments, among other factors [20]. Nevertheless, two first-line regimens are commonly used. The first-line triple therapy is composed of a proton-pump inhibitor (PPI) plus two antibiotics, such as amoxicillin, clarithromycin, or metronidazole [20]. The other regiment is a quadruple therapy, which adds bismuth to the triple therapy [20]. In the cases where the resistance against clarithromycin is common, the sequential and the concomitant therapy are

considered first-line treatments [21]. In the sequential therapy, a PPI is associated with amoxicillin for 5 days, followed by a triple therapy with a PPI, clarithromycin, and tinidazole for another 5 days [21]. In the concomitant regiment, a PPI is administered with three antibiotics (clarithromycin, amoxicillin, and metronidazole) [21]. In regions with high dual clarithromycin and metronidazole resistance, other drugs (e.g. levofloxacin and rifabutin) can be used [16].

Despite the guidelines for managing *H. pylori* infections, a successful treatment is still a challenge. There are several factors that hinder the eradication of these bacteria. For one hand, there are some difficulties that arise from the characteristics of *H. pylori*. More specifically, antimicrobial resistances, the number of multiple strains at the site of infection, the protective mechanism of the mucus layer, and the intracellular location of some bacteria [12]. Other limitations are associated with the patient, namely, their compliance to the treatment and some physiological features (e.g. age and enzymatic polymorphisms) [12]. Furthermore, there are also limitations associated with the pharmacokinetic properties of antibiotics, such as the degradation by the acidic pH, the low residence time in the stomach, and the difficulty to cross the mucus layer to reach the bacteria [22, 23].

1.3 New treatment strategies

The study of the limitations of the current therapy is a crucial step to develop effective new treatment strategies. The efficacy of antibiotics depends on their pharmacokinetic properties [24]. The interaction of antibiotics with membranes are essential for their absorption, diffusion, distribution, and accumulation. Thus, the study of drug-membrane interactions can be helpful to understand some pharmacokinetic limitations (**Chapter 2.2**) and, ultimately, to develop new drugs with higher efficacy and reduced toxicity [25].

Alternative strategies have been developed, specially to overcome the resistance that has been growing over the last years. Nanotechnology has been the focus of several studies due to their potential to directly or indirectly eradicate *H. pylori* (**Chapter 2.3**). Among the commonly studied nanoparticles, lipid-based nanoparticles are highlighted for their ability to be an effective and safe strategy to combat infectious diseases by oral administration (**Chapter 2.4**). Furthermore, the possibility of using functionalized or "smart" nanoparticles to target either *H. pylori* or the gastric mucosa (**Chapter 2.5**) makes nanotechnology an interesting and worthy of in-depth study strategy.

References

[1] *Helicobacter pylori*: physiology and genetics, ASM Press, Washington DC, 2001.

[2] T.L. Cover, M.J. Blaser, *Helicobacter pylori* in health and disease, Gastroenterology 136(6) (2009) 1863-73.

[3] L. Boyanova, I. Mitov, B. Vladimirov, *Helicobacter pylori*, Caister Academic Press, Norfolk, 2011.

[4] J.C. Atherton, The pathogenesis of *Helicobacter pylori*-induced gastro-duodenal diseases, Annu. Rev. Pathol. Mech. 1 (2006) 63-96.

[5] Y. Yamaoka, Mechanisms of disease: *Helicobacter pylori* virulence factors, Nat. Rev. Gastroenterol. Hepatol. 7(11) (2010) 629-41.

[6] M. Hatakeyama, T. Brzozowski, Pathogenesis of *Helicobacter pylori* infection, Helicobacter 11 (2006) 14-20.

[7] S. Mishra, Is *Helicobacter pylori* good or bad?, Eur. J. Clin. Microbiol. Infect. Dis. 32 (2013) 301-304.

[8] J.K.Y. Hooi, W.Y. Lai, W.K. Ng, M.M.Y. Suen, F.E. Underwood, D. Tanyingoh, P. Malfertheiner, D.Y. Graham, V.W.S. Wong, J.C.Y. Wu, F.K.L. Chan, J.J.Y. Sung, G.G. Kaplan, S.C. Ng, Global Prevalence of *Helicobacter pylori* Infection: Systematic Review and Meta-Analysis, Gastroenterology 153(2) (2017) 420-429.

[9] S.S. Kim, V.E. Ruiz, J.D. Carroll, S.F. Moss, *Helicobacter pylori* in the pathogenesis of gastric cancer and gastric lymphoma, Cancer Lett. 305(2) (2011) 228-238.

[10] IARC working group report. Volume 8: *Helicobacter pylori* eradication as a strategy for preventing gastric cancer, International Agency for Research on Cancer, 2014.

[11] A review of human carcinogens. Part B: Biological agents, IARC Working Group on the Evaluation of the Carcinogenic Risks to Human, Lyon, France, 2009.

[12] S.D. Georgopoulos, V. Papastergiou, S. Karatapanis, Current options for the treatment of *Helicobacter pylori*, Expert Opin. Pharmacother. 14(2) (2013) 211-223.

[13] K.M. Bocian, E.K. Jagusztyn-krynicka, The controversy over Anti-*Helicobacter pylori* therapy, Pol. J. Microbiol. 61(4) (2012) 239-246.

[14] P. Malfertheiner, F. Mégraud, C. O'Morain, Guidelines for the management of *Helicobacter pylori* infections, Business Briefing: Eur. Gastroenterol. Rev. (2005) 59-62.

[15] R.M. Zagari, M. Romano, V. Ojetti, R. Stockbrugger, S. Gullini, B. Annibale, F. Farinati, E. Ierardi, G. Maconi, M. Rugge, C. Calabrese, F. Di Mario, F. Luzza, S. Pretolani, A. Savio, G. Gasbarrini, M. Caselli, Guidelines for the management of *Helicobacter pylori* infection in Italy: The III Working Group Consensus Report 2015, Dig. Liver Dis. 47(11) (2015) 903-12.

[16] P. Malfertheiner, F. Megraud, C.A. O'Morain, J.P. Gisbert, E.J. Kuipers, A.T. Axon, F. Bazzoli, A. Gasbarrini, J. Atherton, D.Y. Graham, R. Hunt, P. Moayyedi, T. Rokkas, M. Rugge, M. Selgrad, S. Suerbaum, K. Sugano, E.M. El-Omar, Management of *Helicobacter pylori* infection-the Maastricht V/Florence Consensus Report, Gut 66(1) (2017) 6-30.

[17] W.D. Chey, G.I. Leontiadis, C.W. Howden, S.F. Moss, ACG Clinical Guideline: treatment of *Helicobacter pylori* infection, Am. J. Gastroenterol. 112(2) (2017) 212-239.

[18] C.A. Fallone, N. Chiba, S.V. van Zanten, L. Fischbach, J.P. Gisbert, R.H. Hunt, N.L. Jones, C. Render, G.I. Leontiadis, P. Moayyedi, J.K. Marshall, The Toronto Consensus for the Treatment of *Helicobacter pylori* Infection in Adults, Gastroenterology 151(1) (2016) 51-69 e14.

[19] J.P. Gisbert, J. Molina-Infante, J. Amador, F. Bermejo, L. Bujanda, X. Calvet, M. Castro-Fernández, A. Cuadrado-Lavín, J.I. Elizalde, E. Gene, F. Gomollón, Á. Lanas, C. Martín de Argila, F. Mearin, M. Montoro, Á. Pérez-Aisa, E. Pérez-Trallero, A.G. McNicholl, IV Spanish Consensus Conference on *Helicobacter pylori* infection treatment, Gastroenterología y Hepatología (English Edition) 39(10) (2016) 697-721.

[20] *Helicobacter pylori* in developing countries, World Gastroenterology Organisation Global Guidelines, 2010, pp. 1-15.

[21] S.Y. Kim, D.J. Choi, J.-W. Chung, Antibiotic treatment for *Helicobacter pylori*: is the end coming?, World J Gastrointest. Pharmacol. Ther. 6(4) (2015) 183-198.

[22] R.B. Umamaheshwari, N.K. Jain, Receptor-mediated targeting of lipobeads bearing acetohydroxamic acid for eradication of *Helicobacter pylori*, J. Control. Release 99(1) (2004) 27-40.

[23] P.-L. Bardonnet, V. Faivre, P. Boullanger, J.-C. Piffaretti, F. Falson, Pre-formulation of liposomes against *Helicobacter pylori:* characterization and interaction with the bacteria, Eur. J. Pharm. Biopharm. 69 (2008) 908-22.

[24] J.C. Yang, C.W. Lu, C.J. Lin, Treatment of *Helicobacter pylori* infection: current status and future concepts, World J. Gastroenterol. 20(18) (2014) 5283-93.

[25] M. Lúcio, J.L.F.C. Lima, S. Reis, Drug-membrane interactions: significance for Medicinal Chemistry, Curr. Med. Chem. 17 (2010) 1795-1809.

Chapter 2.2

Shedding light on the puzzle of drug-membrane interactions: Experimental techniques and molecular dynamics simulations

The first objective of this thesis was to understand some pharmacokinetic limitations of the current therapy using biomimetic models. My background encompassed experimental biophysical studies; however, one of the challenges was to use computational simulations as a piece of this puzzle. This review paper was then written to answer one of the questions that arose from the first objective: "How can we combine experimental techniques with molecular dynamics simulations?".
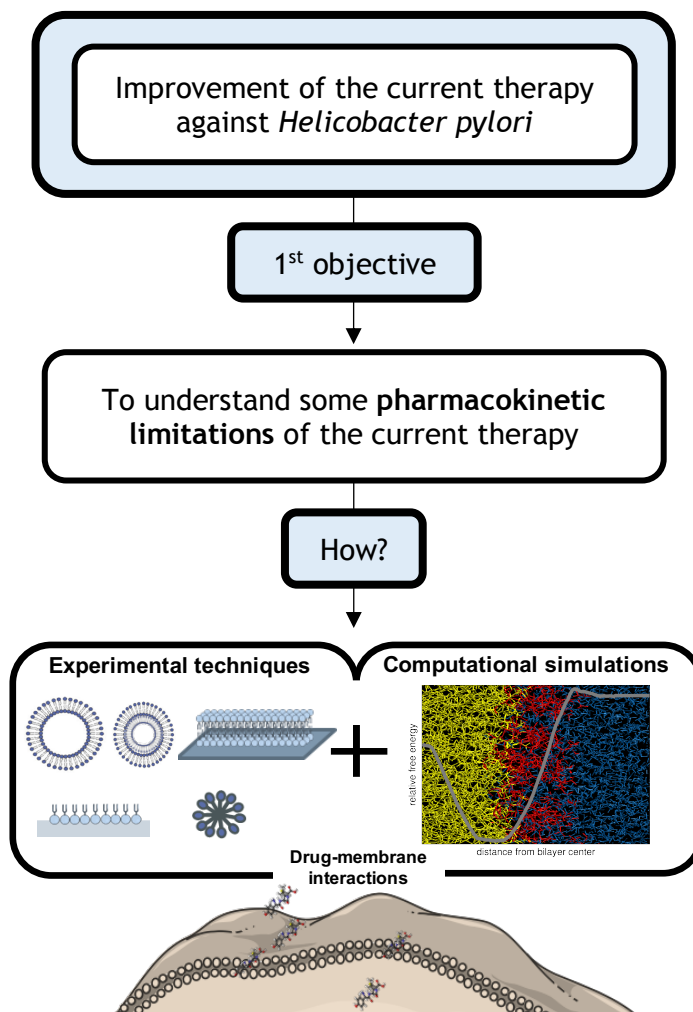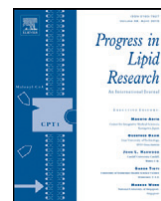
Review

Shedding light on the puzzle of drug-membrane interactions: Experimental techniques and molecular dynamics simulations

Daniela Lopes [a], Sven Jakobtorweihen [b,*], Cláudia Nunes [a], Bruno Sarmento [c,d], Salette Reis [a]

[a] UCIBIO, REQUIMTE, Departamento de Ciências Químicas, Faculdade de Farmácia, Universidade do Porto, Portugal
[b] Institute of Thermal Separation Processes, Hamburg University of Technology, Germany
[c] INEB-Instituto de Engenharia Biomédica, Universidade do Porto, Portugal
[d] IINFACTS - Instituto de Investigação e Formação Avançada em Ciências e Tecnologias da Saúde, Instituto Superior de Ciências da Saúde-Norte, Gandra, PRD, Portugal

ARTICLE INFO

ABSTRACT

Lipid membranes work as barriers, which leads to inevitable drug-membrane interactions in vivo. These interactions affect the pharmacokinetic properties of drugs, such as their diffusion, transport, distribution, and accumulation inside the membrane. Furthermore, these interactions also affect their pharmacodynamic properties with respect to both therapeutic and toxic effects. Experimental membrane models have been used to perform in vitro assessment of the effects of drugs on the biophysical properties of membranes by employing different experimental techniques. In in silico studies, molecular dynamics simulations have been used to provide new insights at an atomistic level, which enables the study of properties that are difficult or even impossible to measure experimentally. Each model and technique has its advantages and disadvantages. Hence, combining different models and techniques is necessary for a more reliable study. In this review, the theoretical backgrounds of these (in vitro and in silico) approaches are presented, followed by a discussion of the pharmacokinetic and pharmacodynamic properties of drugs that are related to their interactions with membranes. All approaches are discussed in parallel to present for a better connection between experimental and simulation studies. Finally, an overview of the molecular dynamics simulation studies used for drug-membrane interactions is provided.

© 2016 Elsevier B.V. All rights reserved.

Contents

1. Introduction

Membranes are essential to life. They are responsible for preserving the homeostatic environment inside a cell and maintaining crucial cellular functions [1]. They are generally composed of phospholipids, proteins, and glycoproteins in varying proportions, according to the membrane type and their distinct and specific functions [1]. The membranes themselves are also involved in cell signalling, and they are significantly altered in the presence of environmental stimuli [2]. They work as a barrier, and both cell culture and in vivo studies have already shown that they strongly affect the pharmacokinetic properties of drugs, namely their diffusion, transport, distribution, and accumulation [3]. For instance, several resistance mechanisms of cancer cells are related to the alteration of the membrane biophysics through a change in their phospholipid composition, and consequently, their fluidity, order, lipid packing, and membrane potential [4]. A review of the properties of cancer cells, with respect to membrane biophysics and its impact on anticancer drug-membrane interactions, was recently published [5]. The well-known P-glycoprotein multidrug efflux pump is also a recognized resistance mechanism due to its key role as a hydrophobic vacuum cleaner [6]. Its function is highly related to drug-membrane interactions, as reported by several studies, which confirmed that this transporter selects drugs from the membrane rather than from the aqueous medium [6]. Therefore, lipophilic drugs, which easily penetrate cancer cell membranes, are also easily expelled by the P-glycoprotein [6]. Bacteria have also been reported to develop membrane-related strategies, such as changing their outer membrane composition and charge to modify their affinity to antibiotics [7,8]. Drug-membrane interactions are unavoidable since absorption and even therapeutic action depend on them. In fact, approximately half of the current commercial drugs target a membrane protein [1]. Additionally, drugs can also have intracellular targets or act directly on the membrane curvature or phase behaviour [9]. However, because a membrane is a consequence of a balanced environment, the topical action of a drug may result in the disturbance of its biophysical properties, including its integrity [2]. This can result in either therapeutic or toxic effects, depending on the target membrane.

To gain new insight into drug-membrane interactions, several biophysical techniques have been developed through the use of membrane models. Additionally, molecular dynamics (MD) simulations have been used to provide complementary information at the atomistic scale. Since no data of drug-membrane interactions are used in the method development, the simulations for these systems are predictive. Therefore, the main advantages of MD simulations are the capabilities to predict relevant properties and to obtain detailed atomistic information, where the latter is often not accessible by experimental methods. The disadvantage of simulations is their computational cost, which prohibits the possibility of performing screening studies with MD simulations. This might change in the future, as a recent example using MD methods in fragment-based drug design has demonstrated that MD might be possible for screening studies [10]. This review will provide a brief overview of the most common experimental techniques applied in the study of drug-membrane interactions. Furthermore, we will provide a theoretical background of MD simulations and their application in this field, particularly their usefulness in the determination of key pharmacokinetic properties, such as the partition and the location of a drug within a bilayer. Moreover, the use of MD simulations to study the effects of drugs on the biophysical properties of a membrane and on both therapeutic and toxic mechanisms will be discussed. Hence, by discussing MD methods and experimental techniques in parallel, the goal of this review is to better connect the two different approaches. In fact, the combination of experimental techniques and MD simulations has recently been used to investigate drug-membrane interactions (e.g., [11–13]). After introducing the theoretical background of the methods, we will provide details on the most important pharmacokinetic and pharmacodynamic properties. For these properties, we will discuss the corresponding experimental methods and the application of MD simulations to predict these properties. Additionally, we will provide an overview of MD studies that have investigated drug-membrane interactions, which are restricted to Food and Drug Administration (FDA) approved drugs.

2. Theoretical background

2.1. Membrane models and experimental techniques

Although the study of drug-cell membranes interactions is important, the complexity, heterogeneity and fragility of cells make it hard to successfully perform biophysical studies [3]. For instance, the influence of some variables, viz., pH, temperature and ionic strength, on cells is difficult to study since cell viability depends on a homeostatic environment. Furthermore, the study of specific bacterial membranes that belong to pathogenic strains requires access to particular facilities and is restricted by a number of security regulations. To overcome these difficulties, membrane model systems with a lipid organization that is similar to those observed in natural cell membranes have been developed [3,9]. These models can be used to perform an in vitro assessment of the membrane's biophysical properties [3,9]. The most commonly used models are micelles, lipid monolayers, supported lipid bilayers and liposomes [3,9]. Liposomes can vary in size (small, large or giant), and they can be divided into unilamellar or multilamellar liposomes depending on the number of bilayers [14]. The selection of the model and size depends on the specific aim of the study and the properties to be investigated. For instance, the amount of a sample present in multilamellar systems can be an advantage compared to that in unilamellar systems for the application of some experimental techniques, such as solid-state nuclear magnetic resonance, differential scanning calorimetry and X-ray scattering analysis [14]. On the other hand, unilamellar vesicles are reported to have a curvature that is more similar to biological cells and, consequently, they have been extensively used to study drug-membrane interactions [9]. Similarly, micelles can be used to study the effect of drugs on the structural organization of lipids due to their hydrophilic surface and hydrophobic core [14]. However, properties, such as the lateral pressure, packing and topology of the surfaces, are difficult to measure in three-dimensional spherical models, such as micelles and liposomes [14]. Thus, lipid monolayers at the air-water interface are useful for studying these properties [14]. Additionally, it is easier to evaluate the effect of drugs on the

interface in monolayer models [15]. There are also some techniques where a flat surface is required, for example, atomic force microscopy [16]. In these cases, supported lipid bilayers, with planar bilayers adsorbed on a solid surface, should be used [16]. It is important to know that each model has its advantages and disadvantages, and a more reliable analysis can be performed if different models and techniques are used [14].

In addition to selecting the membrane model, it is crucial to have an appropriate lipid composition based on the target membrane. For instance, chlorhexidine is an antibiotic, whose mechanism of action relies on the disruption of the bacterial membrane [17]. However, MD simulations showed that the amount of this drug that could be incorporated into a DMPC membrane was higher than the minimum inhibitory concentration [17]. Therefore, the authors questioned the validity of DMPC as a membrane model for studying the effect of chlorhexidine [17]. Nevertheless, for partition coefficient studies, it was already shown that liposomes composed of a single lipid type are good models for bacterial chromatophores and for partitions in worms [18,19]. Furthermore, there are different types of lipids in cells, such as glycerolipids, sphingolipids or saccharolipids, among others [20]. Cells from different tissues have different types of lipids in varying proportions, which affects the membrane fluidity, curvature and function [15]. Moreover, Khakbaz and Klauda used MD simulations of the cytoplasmic *E. coli* membrane to demonstrate the importance of lipid diversity in determining the properties of biological membranes [20]. Furthermore, MD studies revealed local lipid compositions in lipid bilayers [21–24], which can also affect solute partitioning [25–29]. The complexity of the models can be increased by using of mixtures of lipids and inserting proteins to improve the similarity with biological membranes and the reliability of the results. The field of lipidomics has emerged and evolved in recent years as an important way to improve on this similarity. Lipidomics encompasses the study of the lipidome of biological tissues by evaluating their entire lipid composition [30]. In general, this field goes beyond the quantitative analysis of lipids by also covering their location, function, distribution and interaction in space and time [30,31]. Lipidomics has been used for the diagnosis and therapy of several diseases, as it involves the study of the dynamic adaptation of lipids to harsh conditions and the metabolic pathways of lipids [30,32]. The qualitative and quantitative analysis of the lipidome of a cell enables the use of a more accurate composition of model systems in both experimental and simulation studies. Therefore, lipidomics is essential for a better connection between mimetic model systems and biological cells. The analytical techniques used in this field have been extensively described elsewhere [30,31,33–36], and they will not be described in this review. MD methods have not been directly used in lipidomics; however, Wassenaar et al. introduced a method that could be used as a starting point for computational lipidomics [37].
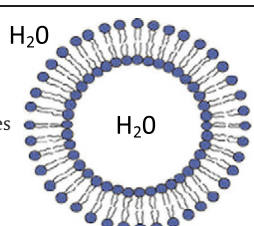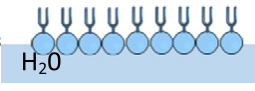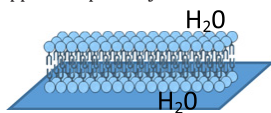
It has been proven that the physical characteristics of mimetic models, such as the thickness, refractive index and capacitance, and their specific properties, can be extrapolated to biological cells [15]. For instance, Sousa et al. compared the effect of nonsteroidal anti-inflammatory drugs on liposomes to their effect on biological cells, viz., mouse and human cell lines [38]. In the following year, the same research group compared the effect of phenols on liposomes to their effect on mouse cell lines [39]. In both studies, they used fluorescence measurements to evaluate the drug location and membrane fluidity, and a good parallelism was obtained by comparing the membrane models to the cell lines [38,39].

Biophysical techniques can be used to evaluate drug partitioning and its effect on the membrane equilibrium, such as the perturbation of the lipid order [14]. Table 1 summarizes the main biophysical techniques used for each model. Some techniques will be covered in this review (see Sections 3 and 4). For a full description of the preparation methods of the models and the protocols for the experimental techniques, please see the following reviews [9,14,40].

2.2. Molecular dynamics simulations

Molecular simulations are used to investigate systems at an atomistic scale. Two main techniques exist: Monte Carlo simulations and molecular dynamics simulations. In this review, only the latter will be discussed in detail. The first MD simulation was performed by Alder and Wainwright in the 1950s [41]. MD simulations for biomolecular systems began when McCammon et al. simulated the dynamics of

Table 1
Biophysical tools to study drug-membrane interactions using membrane models (based on [14]).

Membrane model	Biophysical experimental techniques	Properties studied
Liposomes	- Derivative spectroscopy - Fluorescence quenching studies - Membrane permeabilization studies - Förster resonance energy transfer - Binding studies using intrinsic fluorescence - Fluorescent anisotropy studies - Dynamic and electrophoretic light scattering - Electron microscopy - Infrared spectroscopy - Isothermal titration calorimetry - Differential scanning calorimetry - Nuclear magnetic resonance	- Partition coefficient - Drug location - Effect on the membrane permeabilization - Drug location - Binding constants - Lipid phase transition and order - Size and zeta-potential - Morphology and size - Molecular interaction with specific groups - Thermodynamic parameters - Phase transition temperature and thermodynamic parameters - Drug location and the effect on the lipid phase
Micelles	- Derivative spectroscopy - Dynamic and electrophoretic light scattering	- Partition coefficient - Size and zeta-potential
Lipid monolayers	- Brewster angle microscopy - Langmuir isotherms - Infrared spectroscopy - Grazing incidence X-ray scattering	- Morphology and size of domains - Adsorption or penetration by lipid packing changes - Molecular interaction with specific groups - Lipid conformation and structural arrangements
Supported lipid bilayers	- Atomic force microscopy	- Morphology and size of membrane domains
Multilayers in capillaries	- Small and wide angle X-ray scattering	- Lipid order and structure

15

folded proteins [42]. The main advantage of MD simulations is their atomistic scale, which is often not accessible by experimental techniques. Furthermore, MD simulations can be used for systems where experiments are impossible, dangerous or highly expensive [43].

MD simulations are based on Newton's classical mechanics. From the forces that act on all particles, their successive positions and velocities can be calculated. As an atom has three coordinates and three velocity components, a microscopic system is described by a $6N$-dimensional phase space, where N is the number of atoms. Thus, a phase space trajectory can be determined by using MD simulations. Numerical integrators must be used to solve the equation of motion. These integrators have to fulfil several criteria (e.g., conservation of the total energy); more details about integrators can be found elsewhere [44,45].

The connection between the macroscopic properties and the behaviour of molecules (the microscopic system) is obtained by statistical thermodynamics. A fundamental finding of statistical thermodynamics is that a macroscopic property cannot be calculated from one microscopic configuration. Instead, it is an average obtained over a large set of microscopic configurations. Therefore, in principle, the observation time should be infinite. Since it is impossible to extend the measurement to an infinite time, it is important to measure for a sufficiently long (but finite) time [45]. If the observation time is long enough, an equilibrated thermodynamic system will pass through all possible microstates. In other words, we can assume the ergodic hypothesis, where a time average is equal to the average over all possible microstates. This resulted in the introduction of the ensemble concept in statistical thermodynamics. An ensemble is the collection of all possible microstates under predefined macroscopic conditions. There are several ensembles, where each one depends on different fixed macroscopic properties. In a microcanonical ensemble (NVE), the number of particles (N), the volume (V) and the total energy (E) are fixed. The isobaric/isothermal ensemble (NPT), with a constant number of particles and constant pressure (P) and temperature (T), is commonly used, since it resembles common experimental set-ups in which these variables are kept constant.

In addition to the fixed macroscopic properties, there are other important parameters that should be considered before starting an MD simulation. An overview of the input parameters, requirements, basic principles and limitations of MD simulations is shown in Fig. 1. These parameters will be discussed in the following sections with a focus on biomembrane simulations. Note that we can only give a broad overview of the algorithms of MD simulations for membranes. In general, more information about MD studies can be found in textbooks [44,45], and more specific details for membrane and drug simulations in provided in other review articles [46–49].

2.2.1. Simulation parameters

The ensemble must be appropriate for the system and properties under study. As the NVE ensemble is the "natural" ensemble for MD simulations, other ensembles need special algorithms. For instance, a thermostat algorithm is required to simulate a system at a constant temperature. The choice among several thermostat algorithms is crucial. If dynamic properties will be studied, the thermostat must be carefully chosen to avoid alterations in the system dynamics. For simulations at a constant pressure, a barostat is needed. These barostat algorithms change the volume to reach and maintain the target pressure. The coupling of the three dimensions of the simulation box can be performed, such that all directions are changed simultaneously (isotropic coupling) or each direction is changed independently (anisotropic coupling). For membrane simulations, a semi-isotropic coupling should be used. By considering the symmetry of the system, the direction parallel to the membrane normal is coupled independently from the other two directions. Different thermostats and barostats are discussed in textbooks [45] and in the manuals of MD software packages.

Moreover, the time step size must be carefully chosen, where its maximum is governed by the fastest motion in the system. A rule of thumb is to use one tenth of the shortest period of motion [44]. In MD simulations, the fastest vibrations are due to bond stretches involving hydrogen atoms. These bonds would require a shorter time step size, which leads to longer simulation times. Hence, they are often treated as rigid bonds. Constraints are used to fix intramolecular distances. There are different algorithms for applying constraints in MD simulations, such as the LINCS algorithm [50]. By constraining all bonds to hydrogen atoms, a time step of 2 fs is often used, depending on the force field.

As the number of atoms in MD simulations is much smaller than that in real systems, the boundaries of the system (e.g., the container walls)
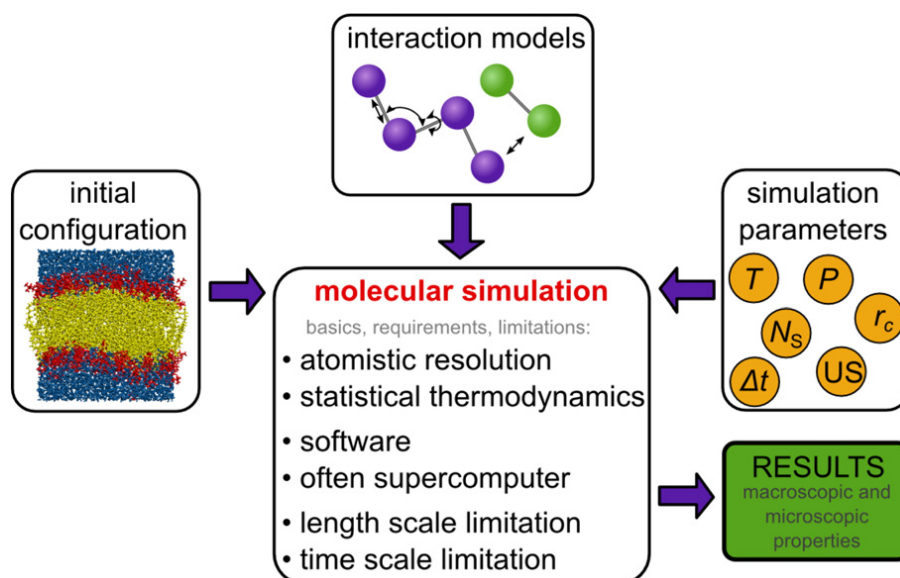
Fig. 1. Ingredients of a molecular simulation. An initial configuration (see Section 2.2.2) and the interaction models (force field) of the system are required (see Section 2.2.3). Furthermore, various simulation parameters are needed (see Section 2.2.1), which depend on the type of simulation. Here, only a small selection of parameters, which are usually required for an MD simulation, is shown, such as the time step size (Δt), the number of time steps (N_S) and the cutoff radii (r_c). If the simulation is performed in the NPT ensemble, the temperature (T) and the pressure (P) should be specified. If special algorithms are used, such as umbrella sampling (US), the required input has to be provided. Molecular simulations are based on the laws of statistical thermodynamics and they are subject to some requirements and limitations (see Section 2.2.4).

will have a huge impact on the measured properties [43]. Therefore, periodic boundary conditions are used to avoid this effect. The system is enclosed in a box with previously defined dimensions and copies of itself surrounding it. Consequently, particles always have neighbouring particles, independent of their location at the centre or at the edge of a box. When a particle crosses the boundaries of the box, it enters the box again at the opposite side. Hence, periodic boundary conditions keep the number of particles constant and remove boundary effects.

2.2.2. Initial configurations

A simulation starts from an initial structure, which is defined by the initial positions and velocities of the atoms (points in the phase space). For membranes, it is possible to start from a random distribution of lipids and water and then to let them self-assemble [51]. However, long simulations are required to obtain an equilibrated membrane from self-assembly simulations. Therefore, for drug-membrane interaction studies, it is more efficient to start from a pre-assembled membrane. Different tools are available to arrange lipids into a bilayer configuration. A review of the different approaches that may be used to build lipid bilayers was recently published (2016) [52]. The membrane builder from the CHARMM-GUI project can be used to construct membranes with lipids available in the CHARMM force field [53]. Other tools to build membranes using lipids with different force fields are available [37,54–57]. PACKMOL is an easy to use and flexible tool for building initial configurations of various systems [58]. In addition, all these tools are capable of setting up heterogeneous lipid membranes. MD simulations of micro-domain formations are computationally demanding due to the slow lateral lipid diffusion. However, several new studies have recently been published, which provide an atomistic detail on domain formation (see Section 3.6).

For drug-membrane interaction studies, it is important that the membrane has been previously equilibrated to achieve equilibrium among water molecules, ions and the membrane. The system must lose any memory of the initial conditions, thus allowing a result that is independent of the initial configuration. The first step is often an energy minimization, where an algorithm (e.g., the steepest descent algorithm) is used to lower the potential energy. Afterwards, one or more MD simulations are performed to equilibrate the membrane system. Anézo et al. showed that at least 10 or 20 ns of equilibration are needed to generate an equilibrated thermodynamic system when phospholipid bilayers are simulated [59]. However, the equilibration time will depend on the molecular system, the thermodynamic state point and the properties that should be analysed. For example, longer equilibration times are required for bilayers composed of a mixture of different lipids than for membranes of a single lipid type. To study the interactions with drug molecules, these molecules are inserted into the membrane system. There are different methods for this insertion, depending on the system [60,61]. Further equilibration steps are usually necessary to reach a microscopic state of the ensemble. The equilibration steps depend on the system, the insertion method and the study that will be performed afterwards.

2.2.3. Force fields

The behaviour of a molecular system is determined by atom-atom interactions (potential energy). Hence, models for these interactions are needed. A set of interaction models is called a force field, which contains all functions and values of their parameters. The choice of the force field is a crucial step, and it should be carefully chosen since it strongly affects the results of an MD simulation. The parameterization is not a trivial task [62]. The transferability of the force field parameters is an important property of force fields. Transferability is the ability to use the same parameters successfully for systems other than the ones used for the parameterization. The force field parameters are fitted to experimental and quantum mechanical data to match the spectroscopic, thermodynamic and crystallographic data of the molecule [63,64]. In force fields, the potential energy is usually divided into two parts, the
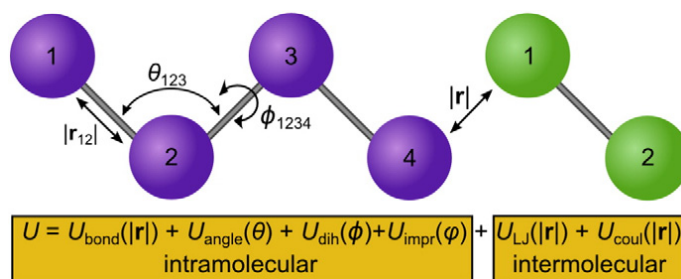
Fig. 2. Schematic representation of force fields, which contain all functions and their parameters to model the interactions within a molecule (intramolecular/bonded) and between different molecules (intermolecular/non-bonded). The usual intramolecular interaction terms are shown in the left molecule (purple). Bond stretching (U_{bond}) is defined by the positions of two bonded atoms. The bond bending term (U_{angle}) is defined by the bond angle θ, which is defined by the positions of three atoms. The dihedral angle term (U_{dih}) defines the rotation φ around a bond, where the dihedral angle is defined by the positions of four atoms. Not shown in this figure is the improper dihedral angle ϕ, which is used to model planar groups. Larger molecules contain also non-bonded intramolecular interactions, that is, atoms in the same molecule can interact via the intermolecular terms. The intermolecular terms are usually modelled with a Lennard-Jones term (U_{LJ}) and a Coulomb term (U_{coul}), where both depend on the distance of the interacting atoms.

intramolecular potential energy (the bonded part) and the intermolecular potential energy (the non-bonded part) (see Fig. 2). Bonded atoms are affected by the stretching (U_{bond}), the bending (U_{angle}) and the torsion (U_{dih}) of the bonds. For some molecules, a so-called improper dihedral (U_{impr}) term is used to model their planar groups. The non-bonded potential energy is modelled as Lennard-Jones interactions (U_{LJ}) and electrostatic interactions (U_{coul}). These models are also applied between atoms of the same molecule, which are more than three bonds apart. Atoms that are 3 bonds apart (1–4 pairs) are treated differently in each force field; sometimes they are not used, sometimes they are used at full strength, and sometimes they are used at a reduced strength (scaled).

Many force fields are available, and most of them are introduced for a special purpose (e.g., biological systems at physiological conditions, phase equilibria for a large pressure range, etc.). Biomolecular force fields contain parameters for lipids, carbohydrates, proteins and nucleic acids. In addition, they usually provide a library with parameters for other molecules, such as drug molecules. Each force field has a different parameterization procedure. Thus, the combination of parameters from different force fields in one simulation is inadequate. The common biological force fields are "AMBER", "CHARMM", "GROMOS", and "OPLS". The CHARMM force field contains parameters for different lipid types [65,66], and the CHARMM general force field has parameters for drug-like molecules [67]. The AMBER force field also has parameters for lipids [68] and a branch (the general AMBER force field) for drug-like molecules [69]. The OPLS force field contains lipids [70], whereas there are different GROMOS-based models for lipids [71,72]. All of these force fields have their pros and cons, and they have been compared in different publications [73–75]. It has to be ensured that the same algorithms (e.g., cutoff schemes) used during the parameterization are used for the MD simulation [76].

Recently, Paloncýová et al. tested the interaction of 11 organic compounds with a DMPC membrane that was modelled using different force fields (Berger, Slipids, CHARMM36, GROMOS 43A1-S3 and GAFFlipids) [77]. By comparing the free energy profiles and the partition coefficients calculated for each force field, Slipids appeared to be the most precise method, and it is recommended for complex molecular systems [77]. CHARMM36 is the best option for studying hydrophilic molecules [77].

The most time-consuming step of a simulation is the determination of the non-bonded interactions since, in principle, they are calculated

for each pair of atoms. As the interactions are almost negligible for long distances, a non-bonded cutoff is usually applied to minimize the computational time required. In other words, intermolecular interactions are only determined when the distance between two atoms is smaller than the predetermined cutoff radius. The Lennard-Jones interactions at a distance greater than the cutoff are often completely neglected. Electrostatic interactions are however long ranged and must be considered even beyond the cutoff radius. Therefore, several strategies can be used, including reaction field methods and Ewald summations, such as the particle-particle/particle-mesh (P^3M) method [78] and the particle-mesh-Ewald (PME) method [79,80]. To enable accurate calculation of electrostatic forces, it is necessary to have an electrostatically neutral system. Thus, counterions are usually added to neutralize charged molecules. Additionally, ions can be added to mimic a particular ionic strength. The selection of the correct ions is important for a correct assessment of the topical effects of the drug on the membrane. For instance, Song et al. simulated salicylate within a DPPC membrane with NaCl [81]. The effect of salicylate on the membrane resulted in a decrease of the area per lipid and in an increase of the lipid order [81]. The trend of these results was the opposite of what was found by experimental techniques (Raman microscopy and monolayers experiments) [82]. Therefore, Khandelia et al. evaluated the influence of ions (Na^+, K^+ and TMA^+) in MD simulations [82]. Specifically, the effect of salicylate on a DMPC membrane depended on the ion type, and the authors suggested that the presence of Na^+ masked the disordering effect of the drug in the previous simulation [82]. Recently, Venable et al. revised the Lennard-Jones radii of ions in the CHARMM force field to calibrate the results to the experimental NMR deuterium order parameters, which minimized possible artefacts caused by the binding of ions to the lipid headgroups [83].

One possible approach to accelerate time-consuming simulations is the use of coarse-grained models [84]. In these models, groups of atoms are lumped together into single interaction sites. Different coarse-grained models have been successfully applied for the simulation of phospholipids, for example, models by Shelley et al. [85], Marrink et al. [86], Orsi and Essex [87], and Lu and Voth [88]. These models are simplistic and, consequently, they have some limitations, and it is necessary to evaluate whether the selected model fits the purpose of the simulation [86]. However, these models have been used to evaluate drug-membrane interactions, such as volatile anaesthetics [89], antiparasitic drugs [90] and antimicrobial peptides [91–98]. Bereau and Kremer showed that MD simulations with coarse-grained models can lead to free energy profiles that are similar to those obtained by all-atom simulations [99]. There are also a number of studies that use a dual-resolution model, where the lipid membrane and the water are simulated using a coarse-grain model, and the drugs, such as β-blocker drugs and antibiotics, are simulated using an atomistic model [100,101]. However, in this review, the focus will be on all-atom MD simulations.

2.2.4. Limitations

In addition to all their advantages, MD simulations have certain limitations. The phenomena and systems that can be studied with MD simulations are especially limited by their length- and time-scales. Furthermore, for drug-like molecules, the force field limitation is a problem. Due to the enormously large size of the chemical space, it is not possible to develop special parameters for every molecule. Therefore, as mentioned previously, the transferability of parameters is an important issue in force field design. Nevertheless, due to the number of functional groups and their combinations in drug molecules, parameters for drug molecules are often unavailable. Moreover, checking whether all the parameters are available (scanning force field databanks for all needed chemical groups and their linkages) can be a tedious task. As a first step, automatic tools were developed to obtain missing parameters from force field databanks by structural analogy [102–105]; whereby, no new parameters are calculated. In fact, the introduction of tools that automatically parameterize small molecules, in accordance with a specific force field, represents a big step forward, not only for the simulation of drug molecules [106–110].

Setting up and analysing a molecular simulation require a fair amount of expertise, as various parameters for different methods in different software packages must be considered [62]. Once a force field and a method are chosen, software that supports both has to be found. Many MD simulation packages are available for biomolecular simulations, such as GROMACS [111], NAMD [112], CHARMM [113], AMBER [114], GROMOS [115], and Desmond [116]. As biological systems are made up of a large number of atoms, super-computers are usually required to carry out MD simulations for these systems.

Van Gunsteren et al. [43] described the limitations of biomolecular simulations by considering four general problems. The so-called force field problem was already identified above as a primary limitation for drug-like molecules. The rough energy surface of biomolecular systems and therefore, the difficulty of finding the global minimum was referred to as the search problem [43]. The huge number of configurations required was called the ensemble problem [43]. The fourth problem was termed the experimental problem, and it illustrates that enough experimental data are often not available, results are often hard to interpret and results are sometimes not precise enough [43]. We hope that this review will help to alleviate the last problem identified by van Gunsteren et al. by reducing the gap between experiments and simulations.

While van Gunsteren et al. discussed general limitations of the MD method, Wong-Ekkabut and Karttunen recently discussed practical issues that can occur when applying MD [117]. In particular, the different influences of parameters on different systems are discussed using case studies. Furthermore, some algorithms (e.g., thermostats) are discussed in detail to explain which algorithm should be used for which system and what should be checked to ensure that the simulation results are unbiased [117]. Ultimately, the person who sets up the simulation is identified as the most significant source of errors [117].

2.2.5. Drug-membrane interactions studies

Table 2 summarizes, to the best of our knowledge, all studies of FDA approved drug-membrane interactions applying MD simulations, with the exception of anti-inflammatory and anaesthetic drugs that will be presented in the following sections. The usual simulation parameters selected for each study (the number of molecules, type of membrane, temperature, type and time of simulation) are also presented. A number of studies are not mentioned in Table 2 since they combined different classes of drugs in the same report. For more information about these studies, please see references [26,100,118–128]. Some examples will be discussed in detail in the following sections. There are also dozens of MD studies of the presence of antimicrobial peptides within a membrane (see reviews [129–131]). However, they will not be discussed in this review since the majority of these compounds are still under evaluation by the FDA [132].

2.3. COSMOmic

COSMOmic is a relatively new molecular method that is capable of predicting the partition behaviour in biological membranes. It is an extension of the "conductor-like screening model for realistic solvation" (COSMO-RS) to anisotropic systems, such as biomembranes and micelles [179]. In COSMOmic, the system is considered to be a layered liquid, which can be cylindrical or spherical in the case of micelles or flat layers for membranes, as represented in Fig. 3 [179].

The distribution of the atoms over the layers should be given as an input, which can be obtained, for example, from MD simulations [180]. Additionally, a "density functional theory (DFT)/COSMO file", with information regarding the polarization charge density of each molecule, is required [179]. By considering different solute orientations, the relative (with respect to the water phase) free energy in each layer can be calculated. Thus, COSMOmic is capable of calculating free energy

Table 2

Drug-membrane interactions studied by MD simulations. Both unbiased (UB) and biased (B) simulation methods were applied. In the latter case, a set of different simulations often has to be carried out. The number of simulations (n_B) is mentioned in this case. The simulation time corresponds to the production run. Note that studies combining different classes of drugs [26,100,118–128] are not mentioned in this table.

Drug (no. of drugs)	Lipids (no. of lipids)	T (K)	Simulation	Ref. (year)
Antiviral drugs				
Amantadine (1)/rimantadine (1)/memantine (1)	POPC (52)	310	B – 13 ns × 190 n_B	[133] (2008)
Amantadine (1)	DMPC (68)	310	UB – 10 ns	[134] (2008)
Enfuvirtide (1)	POPC:Chol (126:0 or 120:120)	300	UB – 100 ns	[135] (2011)
Darunavir (1 or 5)	DMPC (128)	310	UB – 60 ns	[136] (2012)
Antiparasitic drugs				
Miltefosine (1)	7 different lipid compositions	300/323	B – 200/420/600 ns	[90] (2015)
Antibacterial drugs				
Gramicidin A (1)	DMPC (16)	340	UB – 100/300/600 ps	[137] (1996)
Gramicidin S (1)	DMPC (38)	305	UB – 3 ns	[138] (2000)
Fusidic acid (18)	DPPC (110)	323	UB - 80 ns	[139] (2006)
Gramicidin A (1)	DMPC (125)	310	UB – 20 ns	[140] (2007)
Vancomycin (2 or 4)	Lipid II:POPC (1:127; 3:125 or 6:122)	310	UB – 50/60/200 ns; B – 9 ns × 21/29 n_B	[141] (2011)
Gramicidin A (1)	DLPC/DMPC/DOPC/POPC (180)	303	UB – 100 ns	[142] (2012)
Ciprofloxacin (10 or 1)	DLPC (128)	310	UB – 300 ns; B – 7.5 ns × 35 n_B	[143] (2012)
Gramicidin A (1)	DMPC/DSPC (128)	307/338	UB – 25 ns	[144] (2012)
Gramicidin A (1)	DLPC/DMPC/POPC/DAPC (128)	300	UB – 130 ns	[145] (2014)
Thioridazine (0, 16, 32 or 64)	POPC (128)/POPC:POPS (104:26)	310	UB - different times	[146] (2014)
Chlorhexidine (1, 4 or 12)	DMPC (128)	309/323	UB – 100 ns	[17] (2014)
Polymyxin B1 (2, 6, 7, 8, 9 or 12)	Different compositions	313/323	UB - different times	[147] (2015)
Antifungal drugs				
Amphotericin B (8)	DMPC (34):Chol (8)	300	UB – 60 ps	[148] (1997)
Amphotericin B (8)	DMPC (34):Chol/ergosterol (8)	300	UB – 250 ps	[149] (2002)
Amphotericin B (1)	DMPC (200)	300	UB – 1.1 or 1.0 ns	[150] (2004)
Amphotericin B (12 or 8)	DMPC (128):Chol/ergosterol (42)	300	UB – 30 ns	[151] (2006)
Amphotericin B (4 or 1)	DMPC (94)	300	UB – 30 ns; B – 2 ns × 324 n_B	[152] (2009)
Amphotericin B (4)	DMPC (124):Chol/ergosterol (38)	300	UB – 100 ns	[153] (2009)
Amphotericin B (1)	DMPC (63):Chol/ergosterol (28)	300	B – 200 ns × 16 n_B	[154] (2010)
Amphotericin B (2)	DMPC (98):Chol/ergosterol (44)	300	B – 500 ns × 21 n_B	[155] (2013)
Amphotericin B (1)	DMPC (97)/DMPC (97):Chol/ergosterol (44)	310	B – 400 ns × 37 n_B	[156] (2016)
β-Blocker drugs				
Alprenolol (1)/atenolol (1)/pindolol (1)	DPPC (72)	323	B – 3/4 ns × 6 n_B	[157] (2005)
Propranolol	POPC (128)	310	UB – 50 ns; B – 5 ns × 26 n_B	[158] (2014)
Atenolol (1)/nadolol (1)/pindolol (1)/propranolol (1)/metoprolol (1)/alprenolol (1)	POPC (128)	310	B – 2 ns × 19 n_B	[159] (2016)
Propranolol (1, 2 or 4)/oxprenolol (1, 2 or 4)	DPPC (128)	323	UB – 100 ns; B – 10 ns × 18 n_B	[160] (2016)
Anticancer drugs				
Doxorubicin (1)	DPPC:Chol (128:0; 110:20 or 94:40)	323	B – 4 ns × 38 n_B	[161] (2011)
5-Fluorouracil (4)	DMPC:Chol (128:0; 96:32 or 64:64)	323	UB – 20 ns; B – 4 ns × 13 n_B	[29] (2014)
Cytarabine (1)	DOPC:Chol (128:0; 102:26 or 76:52)	323	UB – 20 ns	[162] (2014)
Paclitaxel (1 or 60)	POPC (59, 420 or 483)	310	UB – 100/346/352 ns; B – 40 ns[a]	[163] (2014)
Tamoxifen (20)	POPC:POPG (162:18)	298	UB – 100 ns	[164] (2015)
Doxorubicin (1)/ellipticine (1)	POPC (n.s.)/POPC:Chol (n.s.)	310	B – 300/400 ns × 41 n_B	[13] (2016)
Photodynamic therapy				
5-Aminolevulinic acid (2 or 4)	DPPC (64)	323	UB - 20 ns; B – 1 ns × 46 n_B	[165,166] (2008)
Anticoagulant drug				
Warfarin (1 or 2)	DOPC (72)	310	UB – 10 ns; B – 500 ps × 31 n_B	[167] (2013)
Central nervous system drugs				
Valproic acid (1)	DPPC (64)	323	B - 0.4–0.8 ns per position	[168] (2003)
Chlorpromazine (1)	DPPC/DPPG (2 monolayers of 36 each)	323	UB – 5 ns	[169,170] (2006/07)
Sumatriptan (2, 15 or 50)	POPC (150)	310	UB – 100 ns	[171] (2013)
Sumatriptan (2 or 50)/naratriptan (2 or 50)	POPC (150)	310	UB – 100 ns	[172] (2014)
Antihypertensive drugs				
Nifedipine (1)	DMPC (49)	310	UB - 150 ps	[173] (1997)
Nifedipine (1)	DMPC (49)	310	UB – 100 ps	[174] (1998)
Nifedipine (1)	DMPC (42)	325	UB – 600 ps	[175] (1998)
Losartan (8)	DPPC (484)	323	UB – 480 ns	[176] (2014)
Amlodipine (4)/atenolol (4)/lisinopril (4)	DMPC (128)	310	UB – 100 ns; B – 15 ns × 15 n_B	[177] (2015)
Aliskiren (1, 5 or 11)	DMPC (128)/DPPC (128)	325	UB – 250 ns	[178] (2015)

n.s. not specified.

[a] This reference did not mention the number of simulations, instead the spacing was given to be 0.25 nm.

profiles, which are not accessible by experimental methods. MD simulations can also be used to obtain these profiles (see below). COSMOmic was recently optimized for charged solutes, with regards to the membrane dipole potential [181]. COSMOmic has proved its usefulness for the determination of membrane/water partition coefficients for different solutes [77,126,179–187] and for micelle/water partition coefficients [183,188–191]. It was also shown that the results of COSMOmic and MD simulations are comparable [126,182]. COSMOmic does not consider the structural changes of the membrane induced by a drug. Hence, some properties, such as a change in the tail order parameters of the membrane and pore formation, can only be analysed by MD studies.
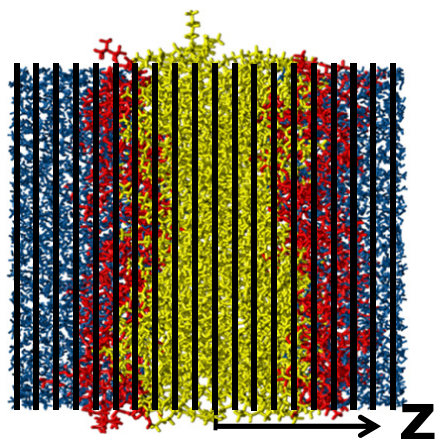
Fig. 3. Representation of a membrane as a layered liquid for COSMOmic calculations.
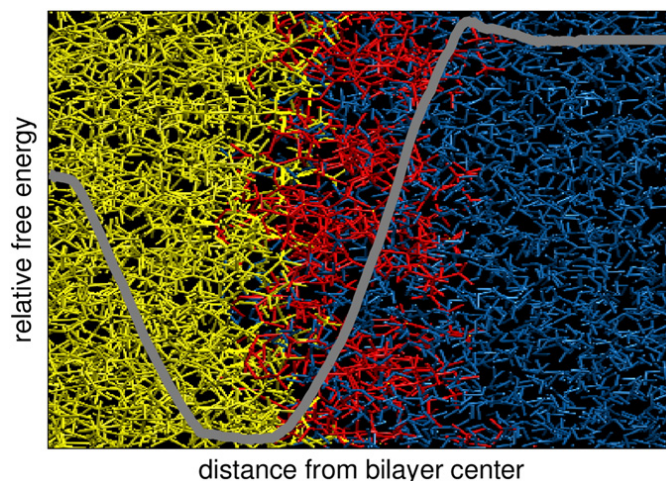
Fig. 4. Simultaneous representation of a free energy profile (grey line) and a bilayer with hydrophobic tails and hydrophilic heads of the lipids in yellow and red, respectively, and water in blue. ΔG is set to zero in the water phase and, consequently, the ΔG in the membrane is the difference to the water phase value. Through the Gibbs energy, it is possible to infer where the drug has higher probabilities to be located.

3. Pharmacokinetic properties

3.1. Free energy

Thermodynamic potentials describe the behaviour of a system in equilibrium. The free energy is especially important since it includes both enthalpy and entropy, and it indicates the most stable state. Moreover, other properties are directly related to the free energy, for example the pK_a, partition coefficients, permeability and location (see the subsequent sections).

Experimentally, it is possible to obtain thermodynamic parameters, namely, the enthalpy (ΔH), entropy (ΔS) and Gibbs free energy, by determining the drug partition coefficients as a function of temperature [192]. The Van't Hoff equation associates the partition coefficient values (K_p) at different temperatures in Kelvin (T) to the thermodynamic parameters [192]:

$$\ln(K_p) = -\frac{\Delta H}{RT} + \frac{\Delta S}{R} \tag{1}$$

where R represents the gas constant. Another strategy is to use isothermal titration calorimetry (ITC) to obtain enthalpy values. Here, two approaches are possible, namely, the titration of a liposome suspension with a drug solution and vice versa [193,194]. In each case, the heat flow is recorded, and K_p and the binding constants can be calculated using mathematical expressions [193,194]. ITC is performed at a constant temperature. In contrast, differential scanning calorimetry (DSC) is performed at increasing temperatures [195,196]. Thus, DSC enables the determination of the heat exchange associated with lipid phase transitions and gives information regarding the enthalpy, entropy and cooperativity of the process [15]. Since it is a non-perturbing technique, it provides a quick and reliable way to obtain thermodynamic parameters of the phase transition of the membrane in the presence and absence of a drug [195,196].

Experimental techniques allow the free energies of the partitioning between two phases to be determined. No details about the underlying processes within the phases can be obtained, but these are interesting processes in the particular case of anisotropic systems, such as membranes. With MD simulations, it is possible to calculate the local free energies, such as the free energy as a function of the distance to the bilayer centre (the direction of the bilayer normal). COSMOmic is another method by which this information can be obtained (see Section 2.3). These so-called free energy profiles are useful in explaining all the thermodynamic processes involved in the interaction of a drug with a membrane. For instance, the most favourable region of a drug within a membrane can be determined through the free energy profiles (see Fig. 4). In fact, relative free energies are calculated, that is, all states

are relative to a reference state, which is often the water phase. The free energy of the reference state is set to zero.

To distinguish between different thermodynamic states, the first step is always to define the coordinate along which the free energy should be calculated [197], which is called the reaction coordinate (ξ). For drug partitioning into membranes, this is usually the direction of the bilayer normal. The variation of the free energy along a coordinate is closely related to the potential of mean force [198,199]. The free energy profile can be calculated from the probability of visiting different regions along the reaction coordinate, which is averaged over all possible configurations that can occur at each position. In other words, all possible microstates must occur during the simulation to achieve a complete and accurate free energy profile. However, regions of high free energies are rarely visited in an equilibrium (unbiased) simulation. In these
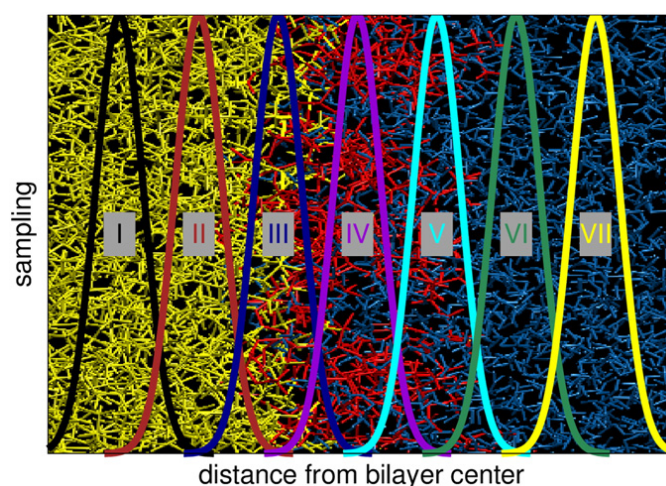
Fig. 5. Output example of seven independent umbrella sampling (US) simulations (I to VII). In each simulation, the drug molecule is harmonically restrained at a different position along the reaction coordinate (here the distance to the bilayer centre). Hence, the different regions (hydrophobic membrane core in yellow, hydrophilic heads in red, and water in blue) are independently sampled. The lines show the number of visits (sampling) of the positions along the reaction coordinate. Neighbouring distributions must overlap to connect the individual US output to one unbiased free energy profile using the weighted histogram analysis method (WHAM). Note that this is a schematic representation. In real applications, the distributions can have different shapes and more than 30 individual US simulations are usually carried out for one free energy profile in lipid bilayers.

20

cases, biased or non-Boltzmann methods can be applied. There are different biased MD methods, and they have been compared and reviewed in a number of publications [60,200–202]. One example is umbrella sampling (US) [203,204]. In this method, the system is divided into small layers (windows) along the reaction coordinate (Fig. 5). Then, a biasing potential is added to restrain a solute in a specific window. The bias potential ensures that the solute in a particular window i is kept close to the reference point (ξ_i^{ref}) of the window (see Fig. 5). Therefore, the entire reaction coordinate is sampled using independent simulations. Different functional forms can be used for the US potential [197, 205], although a harmonic potential is commonly used.

$$u_i^{\text{US}}(\xi) = \frac{k^{\text{US}}}{2}\left(\xi - \xi_i^{\text{ref}}\right)^2 \qquad (2)$$

where k^{US} is the strength of the bias.

The drug is not constrained, but instead, it is restrained, which allows fluctuations around the reference point. Usually, the drug is restrained in one coordinate but free to move in the other coordinates. To remove the introduced bias and to obtain an unbiased (the "real") free energy profile from a set of US simulations, different approaches can be used [197], such as the weighted histogram analysis method (WHAM) [206,207] and the umbrella integration method [208]. For WHAM, it is important that the drug distributions of adjacent windows sufficiently overlap (Fig. 5).

The calculation of the free energy profiles for drug molecules in lipid bilayers is computationally demanding, as a significant amount of sampling has to be performed, and the convergence can be slow. In a recent review, Neale and Pomes discussed sources of errors in this type of simulation [209]. It is noteworthy that brute-force methods may not be suitable for some drugs. Oosten et al. recently reported that holding the doubly charged chlorhexidine within the membrane, in regions deeper than its minimum free energy location, may perturb the bilayer [17]. This can promote the opening of a hole in the membrane and the movement of water into the membrane [17].

Although thermodynamic parameters of drug-membrane interactions can be determined using experimental techniques, the free energy profile along the membrane is a property that is impossible to measure experimentally. Given the insights provided by free energy profiles, namely the partition coefficients and locations, it can be a very useful tool to complement experimental data even though the calculation is computationally demanding.

3.2. pK$_a$ in the membrane

The ionization state of a drug within the membrane is related to its acidity constant (pK$_a$) in that environment. In fact, the pK$_a$ can change drastically from the aqueous phase to the centre of a membrane [210]. This strongly affects the drug permeability, bioavailability and ability to interact with target proteins. Hence, the prediction of this parameter within the membrane can be used to optimize drug design [211].

Using a thermodynamic cycle (Fig. 6), the acidity constant in the membrane (K_m) can be calculated from the acidity constant in the water phase (K_a) and the partition coefficients of each protonation state (K_p^{AH} and $K_p^{\text{A}-}$); the calculation of the latter will be discussed in Section 3.3 [212]. There are several methods to experimentally determine the pK$_a$ in an aqueous phase, namely potentiometry, conductometry, calorimetry, nuclear magnetic resonance, electrophoresis, UV/Vis spectrometry, and fluorometry, among others. For a description of these techniques, see [213]. The advantage of MD simulations is that the pK$_a$ can be calculated as a function of the drug position inside the membrane [210]. The protonation/deprotonation reaction cannot be directly simulated [210], but the free energy of the partitioning of a drug in both (protonated and deprotonated) states can be determined. Fig. 6 compares the calculation of the acidity constant in the membrane using experimental methods and MD simulations. The protonation/
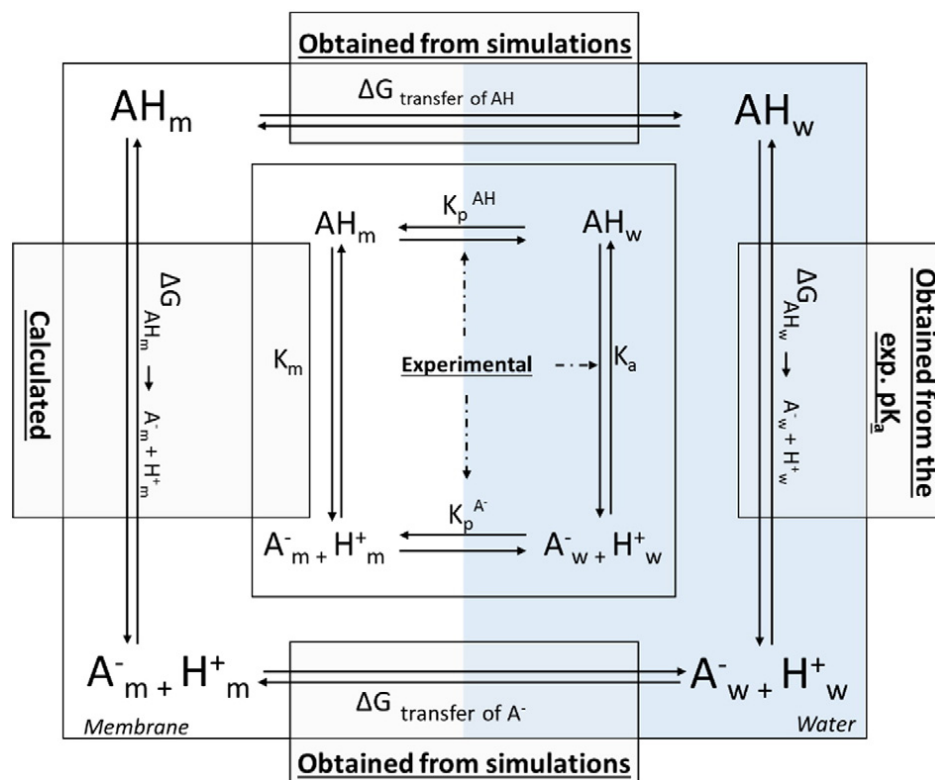
Fig. 6. Thermodynamic cycle, which enables the calculation of the pK$_a$ in the membrane. The internal and the external cycles represent its determination using experimental techniques and MD simulations, respectively. K_a is the drug acidity constant in water and $K_p^{\text{A}-}$ and K_p^{AH} are the partition coefficients of the negatively charged (A−) and the neutral (AH) drug, respectively. K_m is the acidity constant in the membrane and can be calculated using the thermodynamic cycle. In MD simulations, the free energy of the dissociation of the substance within the membrane (AH$_m$) can be calculated from the thermodynamic cycle (left side). This value can then be used to calculate the pK$_a$ (see Eq. (3)). A notable difference to experimental studies is that the simulated free energies are obtained in spatial resolution, hence, the pK$_a$ at every membrane position can be calculated.

deprotonation reaction in bulk water is not simulated; rather, its free energy is obtained from the known pK_a, given that $\Delta G = -2.303RT$ (pK_a-pH) [168,210]. Knowing this parameter and the free energy of drug partitioning for both protonation states, the protonation/deprotonation as a function of the membrane depth can be calculated. Hence, the preferred protonation state at each membrane position can be obtained [210].

Using MD simulations, the drug pK_a can be calculated from the free energy difference of the two protonation states at a given depth [210]:

$$pK_a = \Delta G_{AH_m \to A_m^- + H_m^+} / (2.303RT) + pH \tag{3}$$

where R is the gas constant and T is the temperature. Here, the assumption is made that the H^+ concentration of the bulk water phase corresponds to its concentration at all positions [212]. This method was used by Chew et al. to study the interaction of POPC membranes with adamantane derivatives [133]. These drugs are usually used to treat influenza A and Parkinson's diseases due to their interaction with specific membrane proteins [133]. For all three drugs (amantadine, rimantadine and memantine), they reported a significant reduction of the pK_a value in the centre of the bilayer, which favours the formation of the deprotonated state [133]. This state was considered to be the membrane-permeant state, with no barriers at the centre of the bilayer [133]. The authors also concluded that the drugs´ protonation states and their locations within the membrane may be important to explain their interactions with their therapeutic targets [133].

3.3. Partition coefficient

A partition coefficient is used to quantify the ability of a drug to penetrate a membrane. It is defined as the ratio of the two solute concentrations found in the two phases at equilibrium, such as a membrane and a water phase. The knowledge of drug partition coefficients can be used to optimize commercialized drugs and to design new drugs. For instance, Karlsson et al. studied the partition of warfarin in different structural arrangements (neutral isomers, the open side chain form and the cyclic form) [167]. Based on their results, they proposed that the partition may result in an isomerization process with the adaptation of the drug under different membrane environments [167]. This information along with the interaction type can give new insight into the development of a controlled release formulation [167]. Furthermore, the partition process can be strongly related with the mechanism of action, as in the case of a local anaesthetic [127].

The most common experimental model is the partition in an octanol/water system or other isotropic systems [214]. However, these systems have been replaced by membrane model systems, which can provide an anisotropic environment that is similar to those observed in cell membranes [215]. Therefore, a better representation of the different interactions that occur in vivo are achieved, including the electrostatic interactions and hydrogen bonds that are not reproduced by octanol/water systems [187,214,215]. Liposomes have been used extensively as model systems, where the determination of the partition coefficient can be carried out by potentiometry, isothermal titration calorimetry, differential scanning calorimetry, equilibrium dialysis and different chromatographic techniques, namely, electrokinetic chromatography and immobilized liposome chromatography [193,214–216]. Different spectroscopic techniques, namely, UV–Vis absorption spectrophotometry and fluorescence studies, have also been used [217]. The main advantage of optical techniques is that a physical separation is not required and, therefore, the equilibrium perturbation is negligible [217].

Moreover, it is possible to predict the partition coefficients with MD simulations by using the previously detailed free energy profiles (see Section 3.1). Different equations can be used to calculate the partition coefficient from the free energy profile [182]. The system is commonly divided into two parts, one representing the membrane phase and

another representing the bulk water phase, as described by the following:

$$K^{(N,N)} = \frac{\sum_{i=1}^{n_{lip}} V(z_i) \exp(-\beta \Delta G(z_i))}{\sum_{j=n_{lip}+1}^{n} V(z_j) \exp(-\beta \Delta G(z_j))} \tag{4}$$

Each part is divided into n layers along the bilayer normal: the membrane phase is represented by layers 1 to n_{lip}, and the water phase is represented by layers $n_{lip} + 1$ to n. Depending on the quantity used to define the amount or concentration of the solute, the partition coefficients can have different units. In Eq. (4), the superscript (N,N) denotes that the coefficient is based on the amounts of substance in each phase. Experimentally, partition coefficients in units of L_{water}/kg_{lipid} are often obtained. To compare the partition coefficients obtained from different sources, it is necessary to consider their units. The MD coefficients can easily be transferred to the L_{water}/kg_{lipid} units by using the volume of the water phase (V^w) and the mass of the lipid phase (m^L), $K^{(b,c)} = K^{(N,N)}V^w / m^L$ [182]. Note that this unit is equivalent to other units for liposome/water systems [185]. By converting a free energy profile into a partition coefficient, considerable information is lost. The simulations give more information than just the value of the partition coefficients. The free energy profiles provide detailed information about the partitioning process, which can assist a rational drug design. Furthermore, MD simulations can provide atomistic information on different types of drug movement across membranes, namely, passive membrane permeation or facilitated transport by membrane proteins [218]. Detailed information about the application of in silico models to study these processes has been recently reviewed [218]. Partition coefficients from MD simulations have been compared to experimental values, often with good agreement [182]. As MD simulations of solute partitioning are computationally demanding, they are usually not used for partition coefficient screening studies. COSMOmic [179] is capable of predicting membrane/water partition coefficients more efficiently [126,182]. However, compared to COSMOmic, MD simulations also provide information about the structural changes of the membrane.

There are several experimental methods for determining the drug partitioning using membrane models, and some of them have already been optimized for high throughput screening. For instance, Magalhaes et al. reported a new method using microplates to determine the partition coefficient by derivative spectrophotometry [219]. The group of K.-U. Goss collected measured membrane/water partition coefficients for neutral compounds [185] and ionized compounds [181] from the literature.

3.4. Permeability

Drug permeability is the ability of a drug to cross a lipid bilayer. Drug permeability is important, as the ADMET properties (absorption, distribution, metabolism, elimination and toxicity) depend on it [124,214]. The permeability is quantified by the permeability coefficient P (in $m\ s^{-1}$), and it is defined as $P = J/(c_2 - c_1)$, where J represents the flux in $mol\ m^{-2}\ s^{-1}$, and c is the drug concentration in the compartments separated by the membrane. By assuming that the membrane is a homogenous system and by using Fick's law and the definition of the partition coefficient, the permeability can be calculated from the diffusion coefficient (D) and the partition coefficient according to the following equation:

$$P = \frac{DK^{(c,c)}}{d} \tag{5}$$

where d is the thickness of the membrane. This model is called the homogeneous (or bulk) solubility-diffusion model. Assuming the membrane as a homogenous phase dates back to the Meyer-Overton rule. This is a relatively drastic assumption since the system is anisotropic in the direction of the membrane normal (z-direction). Therefore,

Diamond and Katz introduced the inhomogeneous solubility-diffusion model [220]:

$$1/P = \int_0^d \frac{dz}{D(z)K(z)} \qquad (6)$$

This equation takes the anisotropy into account by letting the diffusion coefficient and partition coefficient depend on the position inside the membrane. Experimentally, it is not possible to measure spatially resolved coefficients, whereas MD simulations can provide such data.

Experimentally, Caco-2 cell permeability assays are still the most commonly used assay to determine the permeability in vitro [221]. Despite its high reliability when extrapolated to in vivo absorption, this assay still has several limitations, such as the time-consuming step of cell growth and the associated costs [221]. Therefore, other methods, such as the parallel artificial membrane permeability assay and immobilized artificial membrane (IAM) chromatography, have been used due to their simplicity and speed [128]. In the first assay, instead of Caco-2 cells, porous filters coated with lipids in an inert organic solvent are used to separate two compartments, one with the drug and the other with the aqueous solvent [15,221]. The amount of drug that permeates the barrier is then quantified. In the second assay, the affinity of a drug to the lipids immobilized onto a silica surface is measured, which was already correlated with the drug permeability through the Caco-2 cells and with the human skin permeability of different compounds [222]. These in vitro model methods consider the passive diffusion, and their results depend on the buffer and the lipid composition, which makes phospholipid mixtures a better choice for comparison with Caco-2 cells [221].

In MD studies, the inhomogeneous solubility-diffusion model (see Eq. (6)) is usually used to calculate the permeability coefficient. Marrink and Berendsen were the first to adopt it for MD simulations [223]. For this model, local diffusivities and local partition coefficients are needed. The latter is directly related to the free energy profile via $K(z) = \exp(-dG(z) / RT)$ (the calculation of these profiles is detailed in Section 3.1). The most commonly used method of calculating the self-diffusion coefficients is via the Einstein equation using the mean squared displacements. However, in general, it is difficult to use this equation for local diffusivities. Moreover, it is not applicable for systems with large changes in the free energy, which is the case for membrane systems [48,223]. Therefore, the force-autocorrelation function is often used instead [48,224]. This method can only be applied when the drug is constrained (fixed at its position), for example, in combination with the z-constraint method [223], which is another method used for free energy profile calculations. In general, it is preferable to calculate the free energies and self-diffusion coefficients from the same MD simulation. Therefore, Hummer introduced a method to calculate the local diffusion coefficients for cases where the drug is restrained (allowed to fluctuate around a reference position) [225]. Hence, with this approach, the local diffusivities can be calculated in US simulations. The different methods for calculating local diffusion coefficients were compared in several publications (e.g., [226]). When using MD simulations to calculate the parameters of the inhomogeneous solubility-diffusion model, the major limitation is the low accuracy in dynamic properties (e.g., diffusion) [227]. In spite of all these difficulties, MD simulations have been used to calculate permeability coefficients [48]. A good summary of the prediction of the non-facilitated membrane permeation of several solutes is provided elsewhere [228]. The agreement with experimental methods was qualitatively good, but quantitative agreement can be poor, as deviations by an order of magnitude [48], or even larger [229], were observed. However, the experimental data also show deviations by orders of magnitude [100,227,230,231].

Despite its computational costs and its uncertainties in quantitative predictions, a detailed atomic description of the permeability process can be achieved through molecular dynamics. For instance, Carpenter et al. used MD simulations to predict the blood-brain barrier permeability [128]. They used a 1,2-dioleoyl-*sn*-glycero-3-phosphocholine (DOPC) membrane and tested 12 compounds [128]. By considering the computed effective permeability ($logP_{eff}$), the permeability through the blood-brain barrier (logBB) was predicted, which was in good agreement with the experimental results and differed by less than 0.2 log units [128].

Computational methods to predict drug permeability are important. In vitro and in vivo methods cannot always be applied in early stage molecules due to the time-consuming nature of and/or costs associated with screening studies [123]. Consequently, computational methods are useful due to the high throughput screening in the early stages of drug design [123]. However, MD simulations are not among the computational methods that can be used for screening studies, and only simpler models are used for these studies. The advantage of MD is the detailed atomistic data. Quantitative structure–activity relationship (QSAR) models, in which a mathematical model is applied to relate compound properties and structures with their biological activity, have been applied to calculate the membrane permeability of new drugs [128,232]. Nevertheless, they have some limitations, namely, the dataset can be insufficient to predict the biological activity with a high enough accuracy. These methods are based on a set of descriptors, which have a strong dependency on the training data set used for the model development. Furthermore, they do not provide information on the underlying atomistic mechanism [232]. Swift and Amaro compared results from QSAR methods with predictions from MD simulations [232]. They conclude that MD studies have the potential to replace QSAR methods in the near future. In particular, new QSAR methods have been combined with MD simulations [118,122,123,233]. In these methods, drug-membrane interaction descriptors obtained by MD simulations are used in combination with the conventional drug-solvent interaction descriptors and general intramolecular descriptors [118]. The descriptors obtained by MD simulations are mainly energy parameters [118,122]. Other methods for permeability calculations are based on empiric correlations. For example, the permeability was correlated with the permeate size [234], reference solvents [234,235], and free energy barriers [100, 101]. Furthermore, cellular automata models have been developed for estimating the membrane permeability of drugs [236,237].

In summary, predictions of permeability coefficients are difficult. MD simulations provide a detailed atomistic picture but are computational demanding, and quantitative predictions are not always possible. Experimental techniques provide reliable permeability values; however, atomistic detail is lacking, which is important to enable a better understanding and to help drug development in general. On the other hand, high throughput screening methods in the drug development process demand screening tools, and both MD and experimental methods remain too expensive for this purpose. Therefore, permeability calculations often rely on QSAR methods. These methods require a significant amount of training data to obtain the descriptors. The results are then dependent on the training set and are often only suitable for similar molecules [232]. There is hope that MD simulations can substitute QSAR models in the near future [232], aided by new MD approaches [227,238].

3.5. Location

In addition to the partition coefficients, the location of a drug within a membrane is extremely important to determine specific effects of drugs on the membranes. Because a high percentage of drugs have membrane proteins as a target, the location can provide new insight on pharmacodynamics.

Experimentally, it is possible to use probes (fluorophores) with a well-known location to evaluate the proximity of a quencher by fluorescence quenching studies [239]. DPH, 1,6-diphenyl-1,3,5-hexatriene, is one of the most commonly used probes; it presents no fluorescence emission in the aqueous phase and a high emission in a membrane environment [239]. It is mainly located parallel to the acyl chains of lipids

[239]. However, it is possible to add a trimethylammonium group to form the TMA-DPH probe, which has a more superficial location [239]. These are only two examples among a high variety of probes [240]. The use of amphipathic probes enables the study of the interaction at the biointerface [241]. Moreover, it can also provide information regarding the local effect of a drug on the biophysical properties of the membrane, e.g., the order parameter (if the probe is oriented parallel to the apolar chains of phospholipids) [241]. The location can also be determined using Förster resonance energy transfer (FRET), in which a fluorescent donor excites an acceptor fluorophore [242]. Since the transference is distance dependent, it is possible to predict the locations of drugs within the membrane [242].

Using MD studies, drug locations can be directly observed from the trajectory or from the density or free energy profiles. The lower the free energy is in a specific region within the bilayer (see Fig. 4), the higher the probability that the drug is located at that position. Hansen et al. reported that propofol, an anaesthetic, is preferably located near the polar heads of phospholipids by analysing its electron density profile [243]. The simulation was corroborated by the analysis of DSC results, which showed that the phase transition enthalpy was constant; this indicates that the hydrocarbon chains of the phospholipids are relatively unperturbed [243]. The combination of experimental results with MD simulations can also be used to obtain molecular information [158]. Forst et al. used the time-dependent fluorescence shift of fluorescent probes with precise locations within a POPC membrane to study the location of β-blockers [158]. By complementing their experiments with MD studies, the authors concluded that propranolol interacts with both polar and hydrophobic groups of the lipids through the establishment of hydrophobic interactions between the naphthalene ring of propranolol and the lipid chains [158]. Therefore, the spectral changes observed in the experiments were explained by the clarification of the location and specific interactions between propranolol and the membrane obtained by MD simulations [158]. Hence, the combination of experimental and MD methods here has resulted in a comprehensive understanding of these interactions.

The main advantage of adding MD information to these experimental data is that fluorescence quenching provides only relative and imprecise information, whereas MD simulations can give a more detailed location. Furthermore, the combination of drug locations with specific drug conformations within the membrane, which can be provided by MD simulations, can give new insight regarding their mode of action and side effects [158].

3.6. Influence of environmental stimuli and compounds

Drug-membrane interactions are strongly affected by environmental stimuli and by biological and external compounds. Membranes change their packing and structure in response to stimuli, such as temperature, ionic strength, pH, pressure, hydration, and the presence of ions [244]. Some examples will be presented on how MD simulations and experimental techniques can be combined to gain a deeper understanding of these influences.

Chau et al. used MD simulations to evaluate the interactions of anaesthetics with DMPC membranes at different pressures [245]. A main purpose was to understand why the pressure reversal mechanism affects the activity of anaesthetics [245]. The authors suggested that halothane aggregates under pressure and is thus unable to interact with the putative binding site [245]. They continued the work by testing a lower concentration and changing the composition of the membrane to POPC to avoid the effect of the concentration and specific halothane-DMPC interactions [246]. Aggregation was also found at 2×10^7 Pa, but it was not detected at 4×10^7 Pa, which is in accordance with experimental results [246]. They suggested several experimental techniques, such as wide-angle X-ray scattering, to complement their results and to further clarify the effect of the aggregation on the phospholipid arrangement [246].

The ionic strength was reported as a key factor for partition behaviour, especially for ionized drugs [247]. Austin et al. measured the partition of salmeterol and proxicromil from water to unilamellar vesicles of dioleoylphosphatidylcholine (DOPC) and from water to octanol [247]. The ionic strength affected both partitions by changing the surface charge in the first system and by extracting ion pairs in the second one [247]. Cascales and Costa used MD simulations to study the influence of both interfacial tension and ionic strength on the penetration of benzocaine, a local anaesthetic, into DPPC/DPPS membranes [248]. They reported that an increase in the amount of charged phospholipids (DPPS) and in the ionic strength causes a decrease in the thermodynamic barrier [248]. This is strongly related to the interfacial tension between the phospholipid bilayer and the aqueous solution, which was calculated by integrating the lateral pressure profile across the lipid bilayer [248].

The influence of cholesterol has also been extensively studied since it is one of the key components of eukaryotic cells, and it modulates their physicochemical properties, such as fluidity and packing [3,249]. Thus, it has a direct influence on the translocation, partition, and location of a drug within a membrane. Experimentally, it was already proven that the presence of cholesterol reduces the solute partition coefficients due to its intercalation between the hydrophobic chains of phospholipids, which increases their packing [250]. Using MD simulations, Zocher et al. showed that cholesterol can influence the local partition coefficients at the lipid headgroups and at the lipid tails in different manners [27]. This can be attributed to by the contrary effect that cholesterol has on lipid packing in both regions, namely, it decreases the packing at the lipid headgroups and increases the packing at the hydrophobic tails [27]. Additionally, Wennberg et al. studied the influence of cholesterol on the partitioning of different solutes (no drug molecules) in different membranes [25]. They found some deviations between the MD simulations and experiments and attributed these deviations to the formation of micro-domains in the experiments that were not modelled in their simulations. Khajeh and Modarress applied US simulations to determine the potential of mean force of the partition of a hydrophilic anticancer drug (5-fluorouracil) in a DMPC membrane with different concentrations of cholesterol [29]. The free energy barrier increased as the cholesterol concentration increased [29]. This was attributed to the effect that cholesterol has on the thickness, ordering, rigidity and packing of phospholipids [29]. They also reported the influence of cholesterol on ibuprofen-membrane interactions [28]. They showed that ibuprofen slightly enhanced the order of DMPC lipids, whereas in the presence of 50 mol% cholesterol, the opposite effect was observed [28]. The presence of cholesterol also affects the activity of efflux pumps, such as P-glycoprotein [26]. For instance, Subramanian et al. evaluated the free energy profiles of several drugs within POPC lipid bilayers [26]. In the case of doxorubicin and nifedipine, cholesterol reduced their free energy in the centre of the bilayer [26]. Thus, it increased their local concentration in the membrane and, consequently, enhanced P-glycoprotein's ability to expel these drugs [26]. The effect of cholesterol has also been studied by MD simulations, especially with regards to its effect on the formation of lipid domains (e.g., [21,22,24,251,252]). In fact, the interest in lipid domains has risen due to their key role in several functions of cells in vivo, such as the communication with other cells or extracellular matrices [244]. Lipid domains are associated with heterogeneities that are formed due to different lipid affinities, which govern the association and location of lipids [253–255]. Therefore, they affect membrane properties and, consequently, should be considered when studying drug-membrane interactions. Experimentally, giant unilamellar vesicles (GUVs) and supported lipid bilayers are the most commonly used models because microscopy can be used to assess lipid domains [256]. MD simulations can provide atomistic information on domain formation. Certainly, the interaction parameters for the different lipid types must be known (see Section 2.2.3). The main limitation is the slow lateral diffusion of lipids within a membrane (the time scale limitation). Furthermore, the number of

simulated molecules must be increased compared to that of single component membrane systems (the length scale limitation). Nevertheless, the number of MD studies investigating domain formation has increased in recent years. Basically, two procedures are used to overcome the above limitations. Preferably, all-atom simulations with modern hardware and software are used, for example, the simulations in [21, 252]. Another possibility is to use coarse-grained models (see Section 2.2.3) to study mixed bilayers, for example, the simulations in [23,37, 88,257,258].

A more complex membrane system can even be used, for example, by adding transmembrane proteins to evaluate their influence on the diffusion of drugs. There are several experimentally used membrane models that allow proteins to be inserted, such as monolayers, supported lipid bilayers and liposomes [259]. However, the protein activity may be hard to preserve after inserting them into the models [259]. Nevertheless, their influence on drug partitioning may be independent on their activity. For example, Amjad-Iranagh et al. studied the interaction of the anaesthetic articaine with a DMPC membrane [260]. In addition to studying the protonation state influence, they also incorporated a drug transporter, viz., an EmrD protein [260]. They reported an unexpected decrease of the diffusion coefficients of articaine, possibly due to the bonds formed between the drug and the protein and between the protein and water molecules, which increased the potential barrier for drug penetration [260]. A few years earlier, Gaspar et al. used monolayers with the phospholipase A_2 enzyme to study the inhibitory ability of nonsteroidal anti-inflammatory drugs (ibuprofen and piroxicam) [261]. The authors reported that the biophysical properties of the lipid layer affect the inhibitory effects of the drugs on the enzymatic capability of the phospholipase A_2 [261].

Since several stimuli can have a significant impact on drug-membrane interactions, it is important to consider these effects for an accurate evaluation of the pharmacokinetic properties.

4. Pharmacodynamic properties

Some biophysical properties of membranes can be altered by the penetration of a drug. This may result in therapeutic or in toxic effects, depending on the target membrane.

The area per lipid is one of the most important properties of lipid bilayers. It is defined as the average area occupied by the lipids (in one leaflet of the membrane). Experimentally, the area per lipid can be obtained by combining neutron and X-ray scattering techniques or by using deuterium nuclear magnetic resonance (NMR) [262,263]. It can be altered by the penetration of a drug since a drug can occupy spaces between lipid molecules [264]. Monolayers can be used as membrane models to measure the Langmuir isotherms, which provides useful information regarding changes in the area per lipid in the presence of a drug [265]. Through MD simulations, the area per lipid can be calculated using the area of the simulation box that is perpendicular to the membrane normal (most times defined by the *x*- and *y*-size of the box) divided by the number of lipids per leaflet. In mixtures of lipids, more complex equations can be used to determine the area per lipid of each type of lipid [266]. Because it is easy to calculate and since a correct area per lipid reflects a modelled membrane with reasonable properties [59], the area per lipid is often used as a first check in MD studies. Anézo et al. showed that the area per lipid in MD simulations strongly depends on the simulation conditions, especially concerning the treatment of long-range electrostatics [59].

The topical effects of drugs on membranes can result in the alteration of the main temperature of the lipid phase transition and the cooperativity of that process. Experimentally, these effects can be assessed using steady-state anisotropy measurements or DSC [195, 196,265]. Another important parameter related to the lipid phase is the tail order, which is a measure of the orientation of the hydrogens of the hydrophobic tails with respect to the normal of the membrane [267]. There are several experimental techniques that can be used to elucidate the effects of drugs on bilayer structure, order and packing, such as small and wide-angle X-ray diffraction (SAXS and WAXS, respectively), nuclear magnetic resonance (NMR) and electron paramagnetic resonance (EPR) [40]. Indirectly, the effects can also be determined using anisotropy studies, where changes in the rotational movement of a membrane probe reflect the influence of a drug on the membrane fluidity [239,268].

The order parameter *S* is commonly defined as follows:

$$S = \left\langle \frac{3}{2}(cos^2\theta) - \frac{1}{2} \right\rangle \tag{7}$$

where θ is the angle formed between the C—H bond and the normal of the lipid bilayer, and the angular brackets represent the average over time and over all lipids. Higher *S* values reflect a higher order (more chains are aligned). A recent review (2016) compared the order parameters, spin relaxation rates and scattering form factors of MD simulations with experimental results [269]. The authors concluded that these properties of hydrophobic chains of phospholipids are usually accurately modelled [269]. Nevertheless, their polar heads are sometimes incorrectly described and should be carefully analysed in processes where their chemical structure may play a key role in biological interactions [269].

Alterations of lipid domains, chain conformations and specific lipid groups (viz., phosphate and carbonyl regions) can be assessed using infrared spectroscopy (PM-IRRAS), Brewster angle microscopy (BAM) and grazing incident X-ray diffraction (GIXD) in monolayers [14]. MD simulations can be used to study the formation of hydrogen bonds, which are determined by defining cutoffs for the acceptor-donor-hydrogen angle (e.g., angles O—H—O and O—H—N higher than 90°) and for the hydrogen-acceptor distances (e.g., less than 2.5 Å) [270,271].

The formation of pores in membranes can also be studied experimentally. One example is the release of a self-quenched carboxyfluorescein or calcein probe that is incorporated in lipid vesicles and released due to leakage of the vesicle [40,272]. Using fluorescence spectroscopy, the release can be monitored over time [40,273]. Other strategies rely on microscopy using inverted optical microscopy for giant unilamellar vesicles (GUVs) or atomic force microscopy (AFM) for supported lipid bilayers [265,274]. Computer simulations have been extensively used to study pore formation by antimicrobial peptides [130,275]; however, as previously mentioned, they will not be discussed in this review since the majority of antimicrobial peptides are not FDA approved. One of the exceptions is gramicidin. Its effect on channel formation in different membranes was studied by Kim et al. [142]. The effect of external electric fields on a mixed gramicidin/phospholipid system was studied by Siu and Bockmann [140].

All these biophysical parameters are related to the stability and the function of biological membranes. Depending on the target membrane, the topical action of a drug may result in therapeutic or toxic effects. For the rest this chapter, some examples of both therapeutic and toxic actions will be discussed.

4.1. Therapeutic properties

Experimentally, the interaction of membranes with drugs from different classes, such as anti-inflammatory drugs, antibiotics, anticancer drugs and anaesthetics, among others, have been extensively studied using biophysical techniques and membrane models [242]. From the determination of the above-mentioned properties, a deeper understanding of the therapeutic properties of drugs in vivo can be obtained [242]. For instance, the higher affinity of antipsychotic agents for lipids similar to the ones present in nervous cells can be related to in vivo efficacy [242]. On the other hand, the therapeutic mechanisms concerning drug interactions with membrane proteins have also been related to the drug location and its effect on the membrane order [242,276]. A good correlation between the biophysical perturbations of membranes and

Table 3

Anaesthetic-membrane interactions studied by MD simulations. Both unbiased (UB) and biased simulation (B) methods were applied. In the latter case, a set of different simulations often has to be carried out. The number of simulations (n_B) is mentioned in this case. The simulation time corresponds to the production runs.

Drug (no. of drugs)	Lipids (no. of lipids)	T (K)	Simulation	Ref. (year)
Benzyl alcohol (3)	DMPC (72)	325	UB – 900 ps	[267] (1998)
Halothane (4)	DPPC (64)	323	UB - 1.6 ns	[282] (1998)
Halothane (32)	DPPC (64)	323	UB - 1.5 ns	[283] (2000)
Halothane (10)	DMPC (182)	305	UB – 2.2 ns	[284] (2002)
Halothane (0, 64, 128, 256, 384 or 512)	DMPC (512)	303	UB - 5 ns	[89] (2005)
Halothane (10 or 1)	DOPC (147 or 72)	305	UB – 16 ns; B – 16 n_B	[285] (2006)
Halothane (32)	DMPC (100)	310	UB - 800 ps	[245,286] (2007/09)
Lidocaine (12)	DMPC (128)	310	UB - 50 ns	[287] (2007)
Prilocaine (40)	POPC (120)	310	UB - 20 ns	[288] (2008)
Lidocaine (12 or 36)	DMPC (128)	313	UB - 50 ns	[278] (2008)
Halothane (1)	DMPC (100)	310	B - 500 ps × 4 n_B	[289] (2008)
			B - 12 or 16 ns × 4 n_B	[290] (2012)
Prilocaine (40)/etidocaine (40)	POPC (120)	310	UB - 20 ns	[291] (2009)
Benzocaine (2)	DPPC:DPPS (54:12)	350	B – 40 ns × 36 n_B	[292] (2009)
Ketamine (0–16)	POPC (200)	310	UB - 50 ns	[280] (2010)
Articaine (12 or 36)	DMPC (128)	310	UB - 100 ns	[293] (2010)
Articaine (1)	POPC (128)	300	UB - 100 ns	[277] (2011)
Benzocaine (1)	DPPC:DPPS (72:0, 60:12, 48:24, 24:48, 0:72)	350	B - 50 ns × 36 n_B	[248,294] (2011/13)
Halothane (16)	POPC (128)	310	UB - 10 ns	[246] (2012)
Halothane (36 or 72)/enflurane (96)	DPPC (256)	300	UB – 15 ns	[295] (2012)
Benzocaine (1)	DPPC (64)	320	UB - 50 ns	[296] (2012)
Bupivacaine (40)	POPC (120)	310	UB - 50 ns	[297] (2012)
Xenon (0, 1, 1.5, 2, 2.5 or 3 per lipid)	DOPC (288 or 576)	310	UB - 20 ns or 40 ns	[281] (2013)
Articaine (1)	DMPC (128)	310	UB - 10 ns; B - 15 ns × 50 n_B	[260] (2013)
Propofol (32)	DPPC (128)	330	UB - 70 ns	[243] (2013)
Lidocaine (1)	DMPC (64)	303	B – 65 ns × 80 n_B	[298] (2013)
Tetracaine (5)	DPPC (200)	310	UB - 30 ns	[299] (2013)
Desflurane (1 or A/L[a] = 1/5)/isoflurane (1 or A/L[a] = 1/5)/sevoflurane (1 or A/L[a] = 1/5)/propofol (1 or A/L[a] = 1/5)	POPC (216)	298	UB – 100 ns B - 9.5 ns × 38 n_B	[300] (2014)
Halothane (36 or 72)/enflurane (96)	DPPC (256)	310	UB – 20 ns	[301] (2015)
Capsaicin (4)	POPC (256)	323	UB – 500 ns, B – 5 ns × 76 n_B	[302] (2015)
Isoflurane (19)	POPC (512)	310	UB – 100 ns	[303] (2015)

[a] A/L denotes anaesthetics/lipid ratio.

both cell uptake and the therapeutic properties have been proven in several studies [3]. More atomistic detail can however be provided by combining experiments with MD simulations.

MD simulations have been extensively used to study the interaction of anaesthetic drugs with membranes (Table 3). Therapeutic properties can be related to the ability of the drugs to overcome the initial hydrophobic barrier and to penetrate into the membrane. By applying computer simulations, Skjevik et al. found that one of the reasons for articaine's higher ability to traverse bone and tissue in comparison with other local anaesthetics may be the formation of intramolecular hydrogen bonds [277]. These bonds may increase the lipophilicity of articaine, improving its efficacy [277]. This finding can be important for the design of new local anaesthetics [277]. Furthermore, MD simulations have been used to elucidate the mechanisms of action of anaesthetics. For instance, Cascales et al. simulated benzyl alcohol molecules at surgical concentrations within a DMPC membrane to clarify the two different mechanisms that had been suggested [267]. More specifically, both the structural alterations of the membrane and the interaction with membrane proteins were proposed as possible action mechanisms of anaesthetics [267]. By analysing the thickness of the hydrocarbon region, the surface area per lipid and the atom distribution across the membrane, the authors concluded that no significant alterations were verified [267]. The most significant alteration was in the order of the lipid tails; however, this could hardly explain the anaesthetic action [267]. Therefore, further studies were performed to evaluate other biophysical properties. One biologically relevant property of lipid bilayers is their electrostatic potential, which is important, for example, for the functionality of ion channels [278]. The electrostatic potential is established due to the dipoles of the phospholipid headgroups and of

the water molecules and due to their orientations [278]. In 2001, Koubi et al. reported that the presence of halothane in a DPPC membrane caused an increased hydration of the choline group of the polar heads and an alteration of the phosphate-nitrogen dipole orientation [279]. Thus, an alteration of the electrostatic potential was verified [279]. In 2008, Högberg and Lyubartsev studied the interaction of lidocaine with a DMPC membrane and calculated the electrostatic potential as a function of the dielectric constants and the charge density along the bilayer normal [278]. The changes in the electrostatic potential may affect the voltage-gated ion channels [278]. On the other hand, Jerabek et al. combined small-angle X-ray diffraction (SAXD) and MD simulations to verify that ketamine did not change the area per lipid and the thickness of a POPC membrane [280]. However, its presence changed the lateral pressure and shifted the pressure towards the centre of the POPC membrane, which affected the probability that an ion channel would be open [280]. The area per lipid can also be altered in some cases, for example, in the presence of xenon, a volatile anaesthetic [281]. In their study, Booker and Sum used DSC analysis to show that xenon increased the area per lipid of a DOPC membrane, which indicates an increase in the membrane fluidity [281]. Other biophysical alterations were also observed in MD studies, such as the increase of both the space between head groups and the bilayer thickness [281]. A further observation was a modulation of the lateral pressure, which affects the ion transportation through the channels [281].

Biophysical alterations can also support therapeutic actions of drugs. For instance, Falck et al. studied the interaction of fusidic acid with a DPPC membrane by combining experimental techniques and MD simulations [139]. All experimental techniques, viz., capillary electrochromatography, DSC and fluorescence spectroscopy

measurements, showed drug incorporation into the bilayer and their effect on the membrane biophysical properties, whereas MD studies provided information regarding the drug locations [139]. Putting all the pieces together, the authors concluded that fusidic acid induced a lateral microheterogeneity and increased its own availability to interact with its target protein [139].

MD simulations can also be helpful in explaining the lack of drug efficiency. For example, Canto et al. studied the interaction between membranes and enfuvirtide, which is a peptide that reduces the progression of HIV by inhibiting its fusion [135]. They used MD simulations to study its interaction with POPC and POPC/cholesterol membranes [135]. They reported that the lower efficiency compared to other peptides may be related to its lower ability to interact with membranes [135]. Consequently, there is a lower concentration of the peptide within the membrane, which is a weak reservoir for this anti-fusion peptide [135]. The interaction with lipids can also be favourable for other anti-HIV drugs. For instance, Leonis et al. reported that the conformation of darunavir as an HIV-protease inhibitor was sustained in the membrane by the hydrogens bonds formed with lipids and with water molecules [136].

In general, MD simulations can add new perspectives on the origin of some effects observed experimentally, especially regarding drug conformations and locations within a membrane.

4.2. Toxic effects

It is widely recognized that nonsteroidal anti-inflammatory drugs (NSAID) have gastric toxicity due to the inhibition of a protective cyclo-oxygenase, namely COX-1 [9]. Furthermore, it has been extensively determined that the hydrophobicity and the acid-resistant properties of the mucosal barrier may be affected due to the disruption of the biophysical properties of the membrane as a result of the NSAIDs topical action [9]. Several experimental studies proved this phenomenon, namely, DSC, fluorescence anisotropy studies, X-ray diffraction studies at small and wide angles and atomic force microscopy, among others [9]. MD simulations have been used to provide additional insight into anti-inflammatory drug-membrane interactions (Table 4). Since the toxic action of NSAIDs depends on their partition and because the absorption occurs in the gastric mucosa (which has a well-known pH-gradient), it is important to study the drug partition at different protonation states. For instance, Boggara and Krishnamoorti studied the neutral and the anionic state of both aspirin and ibuprofen in DPPC bilayers [304]. Their results showed, in line with experiments, that different structures and charges result in different partition coefficients, although the quantitative agreement between the simulation and experiment was poor [304]. Liu et al. studied ibuprofen in POPC bilayers and showed that the ionization state of this drug may change

when it penetrates the membrane [211]. Importantly, it should be noted that for some studies, a single drug molecule is used; hence, it is unlikely that meaningful perturbations in the membrane can be observed [304]. One strategy is to use different concentrations of the drug or to even study the simultaneous effect of different drugs, as performed by Yousefpour et al. [270]. They showed a dosage-dependent effect, and they concluded that drug mixtures have a larger effect even at a lower dosage compared to the dosage needed for a single drug [270].

As mentioned before, the electrostatic potential of lipid bilayers is essential for the functionality of ion channels [264]. Hence, the presence of a drug may disturb its functionality. The effect of paracetamol on the electrostatic potential of two different membranes, namely DPPC and DMPC, was analysed by MD simulations [264]. A decrease of 10 mV for DPPC headgroups and 50 mV for DMPC headgroups was found in the presence of the drug [264]. On the other hand, in the hydrophobic region, the paracetamol molecules increased the electrostatic potential, which is possibly due to deformation of lipid tails [264]. This effect depends on the number of drug molecules, which highlights the importance of studying the appropriate concentration. Paracetamol also decreased the order of both bilayers [264].

Markiewicz et al. selected POPC and cholesterol due to their predominance in the human gastric mucus to test different NSAIDs, namely, ketoprofen, aspirin, and piroxicam [305]. In addition to the area per lipids and tail orders, they determined NSAID-water, NSAID-POPC and NSAID-cholesterol hydrogen bonds because they can have a direct effect on the stability of the membrane [305]. For instance, NSAID-ion interactions, as exemplified by the binding of aspirin to sodium ions, may affect the bilayer surface and its mechanical properties [305]. Additionally, the ability of ketoprofen to penetrate deeper into the bilayer and to bind to water molecules to a higher extent may result in the accumulation of water molecules in the bilayer core [305]. Ultimately, it may result in the alteration of the hydrophobicity of the bilayer and in the formation of pores [305]. Another study showed that the presence of ibuprofen also affected the thickness and the hydration of a DOPC membrane [306]. Furthermore, the hydrophobic tail orders also changed in presence of NSAIDs. Experimentally, Basak et al. showed by isotherms of lipid monolayers that piroxicam induced fluidization [12]. Using MD simulations, they were able to visualize the effect on each carbon atom, which indicated that the disorder effect varied depending on the region [12].

More recently, Alsop et al. used POPC membranes to evaluate the effect of cortisone [11]. By using MD simulations, they reported that cortisone decreases the thickness of the membrane and the POPC tail orders, thereby increasing the area per lipid [11]. The location of cortisone within the membrane was found to depend on the concentration, with a higher preference for the interface at lower concentrations, which was demonstrated by both MD studies and X-ray diffraction

Table 4

Anti-inflammatory drug-membrane interactions studied by using MD simulations. Both unbiased (UB) and biased simulation (B) methods were used. In the latter case, a set of different simulations often has to be carried out. The number of simulations (n_B) is mentioned in this case. The simulation time corresponds to the production run.

Drug (no. of drugs)	Lipids (no. of lipids)	T (K)	Simulation	Ref. (year)
Salicylate (4 or 20)	DPPC (256)	323	UB – 25 ns	[81] (2005)
Aspirin (1)/ibuprofen (1)	DPPC (128)	323	B – 4 ns × 16 n_B	[304] (2010)
Ibuprofen (64)	DPPC (128)	323	UB – 60 ns	[307] (2010)
Salicylate (10 or 20)	DMPC (128 or 512)	310	UB - 120 or 60 ns	[82] (2010)
Ketoprofen (16)/aspirin (16)/piroxicam (16)	POPC:Chol (126:34)	310	UB – 30 ns	[305] (2011)
Ibuprofen (32 or 64)	DOPC (128)	323	UB – 20 ns	[306] (2012)
Aspirin (n.s.)/ibuprofen (n.s.)/naproxen (n.s.)	DPPC (128)	323	UB – 60 ns	[308] (2012)
Paracetamol (4 or 8)	DPPC (128)	323	UB - 50 ns; B – 10 ns × 16 n_B	[264] (2013)
	DMPC (128)	310		
Naproxen (12 or 18)/relafen (12 or 18)/naproxen:relafen (6:6 or 9:9)	DMPC (128)	310	UB – 40 ns	[270] (2013)
Ibuprofen (4 or 1)	DMPC:Chol (128:0; 96:32 or 64:64)	323	UB – 100 ns; B – 8 ns × 14 n_B	[28] (2014)
Ibuprofen (1)	POPC (128)	310	B – 2 ns × 19 n_B	[211] (2014)
Piroxicam (drug/lipid = 0.025 or 0.100)	DMPC (240)	298	UB – 20 ns	[12] (2015)
Cortisone (1 − 100)	POPC (100–128)	300	UB – 160 ns; B – 70 ns[a]	[11] (2016)

n.s. not specified.

[a] This reference did not mention the number of simulations, instead the spacing was given to be 0.1 nm.

studies [11]. However, at higher concentrations, cortisone is able to crystallize [11]. This effect was only observed by X-ray diffraction studies but not in the MD simulations [11]. Two hypotheses for this discrepancy were mentioned: i) the time of the simulations was not long enough for the occurrence of crystallization or ii) the force field used may not be appropriate [11]. Nevertheless, by combining all the information acquired by MD simulations and X-ray diffraction experiments, they concluded that cortisone affects the biophysical properties of membranes, and its crystallization may occur within a lipid environment [11].

There are some drugs that have enantiomers with different toxic effects, such as bupivacaine, which has a more toxic R-(+) enantiomer compared to S-(−) [297]. To determine the root of this difference, Martini and Pickholz compared simulations of the different enantiomers in a POPC membrane [297]. They reported that their locations within the membrane were different, resulting in different effects on the area per lipid, the distance between two phosphate groups and the tail order [297]. In particular, the enhancement of the fluidity caused by the R-(+) enantiomer can be related to its cardiotoxicity since fluidity changes may affect the blockade of cardiac sodium currents, the permeability and ultimately, the activity of cardiac receptors embedded in the membranes [297].

Yacoub et al. observed a toxic effect of anticancer drugs [161]. They studied the effects of doxorubicin on a DPPC/cholesterol membrane [161]. Doxorubicin was able to promote an increase of the curvature and an increase in the water penetration due to the attraction of the drug to the polar heads of the lipids [161].

Toxic effects as a consequence of drug-membrane interactions have been inferred from experimental results for different drugs, such as NSAIDS, anticancer and antimicrobial drugs, among others [9,242]. Toxic effects can be related to the alteration of the biophysical properties of membranes, such as their packing and electrostatic potential, which affect their homeostasis and function [2,15]. MD simulations are useful for providing detailed atomic information [305]. In addition to experiments, further information concerning drug-lipid, drug-water and drug-ion interactions can be determined from the results of these simulations, which can provide new insights regarding drug effects.

5. Conclusions

The bioavailability and efficacy of drugs are strongly determined by drug-membrane interactions. Therefore, studies of these interactions have been extensively performed to determine pharmacokinetic properties and to elucidate unknown action and toxic mechanisms. These properties are related to the ability of a drug to significantly impact the biophysical properties of biological membranes [309]. Variables such as protonation states and drug concentrations influence the nature and the magnitude of this impact [309]. Thus, gaining insight into these properties and their relation to drug properties can enable an improvement in drug design.

One of the key aspects required for an accurate extrapolation of in vivo drug-membrane interactions is selecting a suitable membrane for the purpose in mind. Additionally, it is crucial to understand that there is no perfect membrane model, and each assay should be a single piece of the puzzle, which should comprehensively include different experimental techniques and different membrane models. MD simulations represent another key to solve this puzzle. Most experimental techniques give macroscopic results. By supplementing them with MD studies, a new insight on the atomistic scale can be obtained. In particular, MD simulations provide information on both the space (atomic) and time (sub-picosecond) resolution that is difficult or even impossible to access with experimental methods. Furthermore, insight regarding the locations and orientations of drugs within a membrane and the local effects of drugs on the neighbouring atoms can be obtained. However, it is important to realize that due to time scale limitations, some processes cannot be studied with MD methods. Moreover, the

applicability of MD simulations depends strongly on the accuracy of the force field used. However, new tools for automatically generated force field parameters, fast computers (including the use of GPUs) and new algorithms will expand the applicability of MD simulations for drug design.

With recent and future advances in molecular dynamics methods and with the variety of experimental techniques, the combination of MD simulations with experimental approaches will help to shed more light on the puzzle of drug-membrane interactions and will therefore lead to an optimized drug design.

References

[1] Xu Y, Tillman TS, Tang P. Chapter 3: membranes and drug action. In: Hacker M, Bachmann K, Messer W, editors. Pharmacology: principles and practises. London: Elsevier; 2009.
[2] Seddon AM, Casey D, Law RV, Gee A, Templer RH, Ces O. Drug interactions with lipid membranes. Chem Soc Rev 2009;38(9):2509–19.
[3] Peetla C, Stine A, Labhasetwar V. Biophysical interactions with model lipid membranes: applications in drug discovery and drug delivery. Mol Pharm 2009;6(5):1264–76.
[4] Peetla C, Vijayaraghavalu S, Labhasetwar V. Biophysics of cell membrane lipids in cancer drug resistance: implications for drug transport and drug delivery with nanoparticles. Adv Drug Deliv Rev 2013;65(13–14):1686–98.
[5] Alves AC, Ribeiro D, Nunes C, Reis S. Biophysics in cancer: the relevance of drug-membrane interaction studies. BBA - Biomembranes 2016;1858(9):2231–44.
[6] Sharom FJ. Complex interplay between the P-glycoprotein multidrug efflux pump and the membrane: its role in modulating protein function, front. Oncologia 2014;4:41.
[7] Delcour AH. Outer membrane permeability and antibiotic resistance. Biochim Biophys Acta 2009;1794(5):808–16.
[8] Dunnick JK, O'Leary WM. Correlation of bacterial lipid composition with antibiotic resistance. J Bacteriol 1970;101(3):892–900.
[9] Pereira-Leite C, Nunes C, Reis S. Interaction of nonsteroidal anti-inflammatory drugs with membranes: in vitro assessment and relevance for their biological actions. Prog Lipid Res 2013;52(571–584).
[10] Steinbrecher TB, Dahlgren M, Cappel D, Lin T, Wang L, Krilov G, et al. Accurate binding free energy predictions in fragment optimization. J Chem Inf Model 2015;55(11):2411–20.
[11] Alsop RJ, Khondker A, Hub JS, Rheinstadter MC. The lipid bilayer provides a site for cortisone crystallization at high cortisone concentrations. Sci Rep 2016;6:22425.
[12] Basak UK, Datta A, Bhattacharyya D. Stability and softening of a lipid monolayer in the presence of a pain-killer drug. Colloids Surf B Biointerfaces 2015;132:34–44.
[13] Zhang L, Bennett WF, Zheng T, Ouyang PK, Ouyang X, Qiu X, et al. Effect of cholesterol on cellular uptake of cancer drugs pirarubicin and ellipticine. J Phys Chem B 2016;120(12):3148–56.
[14] Lúcio M, Nunes C, Lima JLFC, Reis S. A biophysical approach to the study of the therapeutic and toxic effects of non-steroidal anti-inflammatory drugs. In: Jurado A, editor. A toxicological/pharmacological approach to chemico-biological interactions at a membrane level. Transworld Research Network; 2012.
[15] Drug-membrane interactions: analysis, drug distribution, modeling. Wiley-VCH; 2002.
[16] Rascol E, Devoisselle JM, Chopineau J. The relevance of membrane models to understand nanoparticles-cell membrane interactions. Nanoscale 2016;00(1–3):1–21.
[17] Van Oosten B, Marquardt D, Komljenovic I, Bradshaw JP, Sternin E, Harroun TA. Small molecule interaction with lipid bilayers: a molecular dynamics study of chlorhexidine. J Mol Graph Model 2014;48:96–104.
[18] Escher BI, Schwarzenbach RP. Partitioning of substituted phenols in liposome–water, biomembrane–water, and octanol–water systems. Environ Sci Technol 1996;30(1):260–70.

[19] Jonker MTO, Heijden SAVd. Bioconcentration factor hydrophobicity cutoff: an artificial phenomenon reconstructed. Environ Sci Technol 2007;41(21):7363–9.

[20] Khakbaz P, Klauda JB. Probing the importance of lipid diversity in cell membranes via molecular simulation. Chem Phys Lipids 2015;192:12–22.

[21] Sodt AJ, Sandar ML, Gawrisch K, Pastor RW, Lyman E. The molecular structure of the liquid-ordered phase of lipid bilayers. J Am Chem Soc 2014;136(2):725–32.

[22] Bennett WF, Tieleman DP. Computer simulations of lipid membrane domains. Biochim Biophys Acta 2013;1828(8):1765–76.

[23] Ingolfsson HI, Melo MN, van Eerden FJ, Arnarez C, Lopez CA, Wassenaar TA, et al. Lipid organization of the plasma membrane. J Am Chem Soc 2014;136(41): 14554–9.

[24] Diaz-Tejada C, Ariz-Extreme I, Awasthi N, Hub JS. Quantifying lateral inhomogeneity of cholesterol-containing membranes. J Phys Chem Lett 2015;6(23):4799–803.

[25] Wennberg CL, van der Spoel D, Hub JS. Large influence of cholesterol on solute partitioning into lipid membranes. J Am Chem Soc 2012;134(11):5351–61.

[26] Subramanian N, Schumann-Gillett A, Mark AE, O'Mara ML. Understanding the accumulation of P-glycoprotein substrates within cells: the effect of cholesterol on membrane partitioning. BBA-Biomembranes 2015.

[27] Zocher F, van der Spoel D, Pohl P, Hub JS. Local partition coefficients govern solute permeability of cholesterol-containing membranes. Biophys J 2013;105(12): 2760–70.

[28] Khajeh A, Modarress H. The influence of cholesterol on interactions and dynamic of ibuprofen in a lipid bilayer. Biochim Biophys Acta 2014;1838:2431–8.

[29] Khajeh A, Modarress H. Effect of cholesterol on behavior of 5-fluorouracil (5-FU) in a DMPC lipid bilayer, a molecular dynamics study. Biophys Chem 2014;187–188: 43–50.

[30] Wang M, Wang C, Han RH, Han X. Novel advances in shotgun lipidomics for biology and medicine. Prog Lipid Res 2016;61(83–108).

[31] Jung HR, Sylvänne T, Koistinen KM, Tarasov K, Kauhanen D, Ekroosv K. High throughput quantitative molecular lipidomics. Biochim Biophys Acta 2011;1811: 925–34.

[32] Zhao Y-Y, Miao H, Cheng X-L, Wei F. Lipidomics: novel insight into the biochemical mechanism of lipid metabolism and dysregulation-associated disease. Chem Biol Interact 2015;240:220–38.

[33] Kasugaa K, Sugab T, Mano N. Bioanalytical insights into mediator lipidomics. J Pharm Biomed Anal 2015;113:151–62.

[34] Sandra K, Sandra P. Lipidomics from an analytical perspective. Curr Opin Chem Biol 2013;17:847–53.

[35] Rolima AEH, Henrique-Araújo R, Ferraz EG, Dultra FKdAA, Fernandez LG. Lipidomics in the study of lipid metabolism: current perspectives in the omic sciences. Gene 2015;554:131–4.

[36] Navas-Iglesias N, Carrasco-Pancorbo A, Cuadros-Rodríguez L. From lipids analysis towards lipidomics, a new challenge for the analytical chemistry of the 21st century. Part II: analytical lipidomics. Trends Anal Chem 2009;29(4):393–403.

[37] Wassenaar TA, Ingolfsson HI, Bockmann RA, Tieleman DP, Marrink SJ. Computational lipidomics with insane: a versatile tool for generating custom membranes for molecular simulations. J Chem Theory Comput 2015;11(5):2144–55.

[38] Sousa C, Nunes C, Lucio M, Ferreira H, Lima JL, Tavares J, et al. Effect of nonsteroidal anti-inflammatory drugs on the cellular membrane fluidity. J Pharm Sci 2008; 97(8):3195–206.

[39] Nunes C, Sousa C, Ferreira H, Lúcio M, Lima JLC, Tavares J, et al. Substituted phenols as pollutants that affect membrane fluidity. J Environ Biol 2008;29(5): 733–8.

[40] Deleu M, Crowet JM, Nasir MN, Lins L. Complementary biophysical tools to investigate lipid specificity in the interaction between bioactive molecules and the plasma membrane: a review. Biochim Biophys Acta 2014;1838(12):3171–90.

[41] Alder BJ, Wainwright TE. Phase transition for a hard sphere system. J Chem Phys 1957;27(5):1208.

[42] McCammon JA, Gelin BR, Karplus M. Dynamics of folded proteins. Nature 1977; 267(16):585–90.

[43] van Gunsteren WF, Bakowies D, Baron R, Chandrasekhar I, Christen M, Daura X, et al. Biomolecular modeling: goals, problems, perspectives. Angew Chem Int Ed 2006;45(25):4064–92.

[44] Leach AR. Molecular modelling: principles and applications. 2nd ed. Harlow: Pearson Education; 2001.

[45] Frenkel D, Smit B. Understanding molecular simulation: from algorithms to applications. San Diego, California: Academic Press; 1996.

[46] Ebro H, Kim YM, Kim JH. Molecular dynamics simulations in membrane-based water treatment processes: a systematic overview. J Membr Sci 2013;438:112–25.

[47] Durrant JD, McCammon JA. Molecular dynamics simulation and drug discovery. BMC Biol 2011;9(71):1–9.

[48] Xiang TX, Anderson BD. Liposomal drug transport: a molecular perspective from molecular dynamics simulations in lipid bilayers. Adv Drug Deliv Rev 2006; 58(12–13):1357–78.

[49] Martinez-Seara H, Rog T. Molecular dynamics simulations of lipid bilayers: simple recipe of how to do it. Methods Mol Biol 2013;924:407–29.

[50] Hess B. P-LINCS: a parallel linear constraint solver for molecular simulation. J Chem Theory Comput 2008;4(1):116–22.

[51] Marrink SJ, Lindahl E, Edholm O, Mark AE. Simulation of the spontaneous aggregation of phospholipids into bilayers. J Am Chem Soc 2001;123(35):8638–9.

[52] Javanainen M, Martinez-Seara H. Efficient preparation and analysis of membrane and membrane protein systems. BBA-Biomembranes 2016;1858(10): 2468–82.

[53] Wu EL, Cheng X, Jo S, Rui H, Song KC, Davila-Contreras EM, et al. CHARMM-GUI membrane builder toward realistic biological membrane simulations. J Comput Chem 2014;35(27):1997–2004.

[54] Bovigny C, Tamo G, Lemmin T, Maino N, Dal Peraro M. LipidBuilder: a framework to build realistic models for biological membranes. J Chem Inf Model 2015;55(12): 2491–9.

[55] Sommer B, Dingersen T, Gamroth C, Schneider SE, Rubert S, Kruger J, et al. CELLmicrocosmos 2.2 MembraneEditor: a modular interactive shape-based software approach to solve heterogeneous membrane packing problems. J Chem Inf Model 2011;51(5):1165–82.

[56] Knight CJ, Hub JS. MemGen: a general web server for the setup of lipid membrane simulation systems. Bioinformatics 2015;31(17):2897–9.

[57] Ghahremanpour MM, Arab SS, Aghazadeh SB, Zhang J, Spoel Dvd. MemBuilder: a web-based graphical interface to build heterogeneously mixed membrane bilayers for the GROMACS biomolecular simulation program. Bioinformatics 2014;30(3): 439–41.

[58] Martinez L, Andrade R, Birgin EG, Martinez JM. PACKMOL: a package for building initial configurations for molecular dynamics simulations. J Comput Chem 2009; 30(13):2157–64.

[59] Anézo C, Vries AHd, Höltje H-D, Tieleman DP, Marrink S-J. Methodological issues in lipid bilayer simulations. J Phys Chem B 2003;107(35):9424–33.

[60] Paloncýová M, Berka K, Otyepka M. Convergence of free energy profile of coumarin in lipid bilayer. J Chem Theory Comput 2012;8(4):1200–11.

[61] Neale C, Bennett WF, Tieleman DP, Pomes R. Statistical convergence of equilibrium properties in simulations of molecular solutes embedded in lipid bilayers. J Chem Theory Comput 2011;7(12):4175–88.

[62] Maginn EJ. From discovery to data: what must happen for molecular simulation to become a mainstream chemical engineering tool. AICHE J 2009;55(6): 1304–10.

[63] Werner T, Morris MB, Dastmalchi S, Church WB. Structural modelling and dynamics of proteins for insights into drug interactions. Adv Drug Deliv Rev 2012;64(4): 323–43.

[64] Klauda JB, Venable RM, MacKerell Jr AD, Pastor RW. Considerations for lipid force field development. In: Sundararajan V, Feller SE, Simon SA, Benos DJ, editors. Computational modeling of membrane bilayers. New York: Academic Press; 2008. p. 1–48.

[65] Klauda JB, Venable RM, Freites JA, O'Connor JW, Tobias DJ, Mondragon-Ramirez C, et al. Update of the CHARMM all-atom additive force field for lipids: validation on six lipid types. J Phys Chem B 2010;114(23):7830–43.

[66] Pastor RW, Mackerell Jr AD. Development of the CHARMM force field for lipids. J Phys Chem Lett 2011;2(13):1526–32.

[67] Vanommeslaeghe K, Hatcher E, Acharya C, Kundu S, Zhong S, Shim J, et al. CHARMM general force field: a force field for drug-like molecules compatible with the CHARMM all-atom additive biological force fields. J Comput Chem 2010;31(4):671–90.

[68] Dickson CJ, Madej BD, Skjevik AA, Betz RM, Teigen K, Gould IR, et al. Lipid14: the amber lipid force field. J Chem Theory Comput 2014;10(2):865–79.

[69] Wang J, Wolf RM, Caldwell JW, Kollman PA, Case DA. Development and testing of a general amber force field. J Comput Chem 2004;25(9):1157–74.

[70] Maciejewski A, Pasenkiewicz-Gierula M, Cramariuc O, Vattulainen I, Rog T. Refined OPLS all-atom force field for saturated phosphatidylcholine bilayers at full hydration. J Phys Chem B 2014;118(17):4571–81.

[71] Kukol A. Lipid models for united-atom molecular dynamics simulations of proteins. J Chem Theory Comput 2009;5(3):615–26.

[72] Poger D, Van Gunsteren WF, Mark AE. A new force field for simulating phosphatidylcholine bilayers. J Comput Chem 2010;31(6):1117–25.

[73] Piggot TJ, Pineiro A, Khalid S. Molecular dynamics simulations of phosphatidylcholine membranes: a comparative force field study. J Chem Theory Comput 2012; 8(11):4593–609.

[74] Botan A, Favela-Rosales F, Fuchs PF, Javanainen M, Kanduc M, Kulig W, et al. Toward atomistic resolution structure of phosphatidylcholine headgroup and glycerol backbone at different ambient conditions. J Phys Chem B 2015;119(49): 15075–88.

[75] Lyubartsev AP, Rabinovich AL. Force field development for lipid membrane simulations. Biochim Biophys Acta 2016.

[76] Lee J, Cheng X, Swails JM, Yeom MS, Eastman PK, Lemkul JA, et al. CHARMM-GUI input generator for NAMD, GROMACS, AMBER, OpenMM, and CHARMM/OpenMM simulations using the CHARMM36 additive force field. J Chem Theory Comput 2016;12(1):405–13.

[77] Paloncýová M, Fabre G, DeVane RH, Trouillas P, Berka K, Otyepka M. Benchmarking of force fields for molecule–membrane interactions. J Chem Theory Comput 2014; 10(9):4143–51.

[78] Hockney RW, Eastwood JW. Computer simulation using particles. 2nd ed. Bristol: Institute of Physics Publishing; 1988.

[79] Darden T, York D, Pedersen L. Particle mesh Ewald: an N·log(N) method for Ewald sums in large systems. J Chem Phys 1993;98(12):10089.

[80] Petersen HG. Accuracy and efficiency of the particle mesh Ewald method. J Chem Phys 1995;103(9):3668.

[81] Song Y, Guallar V, Baker NA. Molecular dynamics simulation of salicylate effects on the micro- and mesoscopic properties of a dipalmitoylphosphatidylcholine bilayer. Biochem J 2005;44(41):13425–38.

[82] Khandelia H, Witzke S, Mouritsen OG. Interaction of salicylate and a terpenoid plant extract with model membranes: reconciling experiments and simulations. Biophys J 2010;99(12):3887–94.

[83] Venable RM, Luo Y, Gawrisch K, Roux B, Pastor RW. Simulations of anionic lipid membranes: development of interaction-specific ion parameters and validation using NMR data. J Phys Chem B 2013;117(35):10183–92.

[84] Coarse-graining of condensed phase and biomolecular systems. Boca Raton: CRC Press; 2009.

[85] Shelley JC, Shelley MY, Reeder RC, Bandyopadhyay S, Klein ML. A coarse grain model for phospholipid simulations. J Phys Chem B 2001;105(19):4464–70.

[86] Marrink SJ, Vries AHd, Mark AE. Coarse grained model for semiquantitative lipid simulations. J Phys Chem B 2004;108(2):750–60.

[87] Orsi M, Essex JW. The ELBA force field for coarse-grain modeling of lipid membranes. PLoS One 2011;6(12):1–22.

[88] Lu L, Voth GA. Systematic coarse-graining of a multicomponent lipid bilayer. J Phys Chem B 2009;113(5):1505–10.

[89] Pickholz M, Saiz L, Klein ML. Concentration effects of volatile anesthetics on the properties of model membranes: a coarse-grain approach. Biophys J 2005;88(3):1524–34.

[90] de Sa MM, Sresht V, Rangel-Yagui CO, Blankschtein D. Understanding miltefosine-membrane interactions using molecular dynamics simulations. Langmuir 2015;31(15):4503–12.

[91] Lin D, Grossfield A. Thermodynamics of antimicrobial lipopeptide binding to membranes: origins of affinity and selectivity. Biophys J 2014;107(8):1862–72.

[92] Horn JN, Sengillo JD, Lin D, Romo TD, Grossfield A. Characterization of a potent antimicrobial lipopeptide via coarse-grained molecular dynamics. Biochim Biophys Acta 2012;1818(2):212–8.

[93] Farrotti A, Bocchinfuso G, Palleschi A, Rosato N, Salnikov ES, Voievoda N, et al. Molecular dynamics methods to predict peptide locations in membranes: LAH4 as a stringent test case. Biochim Biophys Acta 2015;1848(2):581–92.

[94] Horn JN, Cravens A, Grossfield A. Interactions between fengycin and model bilayers quantified by coarse-grained molecular dynamics. Biophys J 2013;105(7):1612–23.

[95] von Deuster CI, Knecht V. Antimicrobial selectivity based on zwitterionic lipids and underlying balance of interactions. Biochim Biophys Acta 2012;1818(9):2192–201.

[96] von Deuster CI, Knecht V. Competing interactions for antimicrobial selectivity based on charge complementarity. Biochim Biophys Acta 2011;1808(12):2867–76.

[97] Sikorska E, Dawgul M, Greber K, Ilowska E, Pogorzelska A, Kamysz W. Self-assembly and interactions of short antimicrobial cationic lipopeptides with membrane lipids: ITC, FTIR and molecular dynamics studies. Biochim Biophys Acta 2014;1838(10):2625–34.

[98] Cruz VL, Ramos J, Melo MN, Martinez-Salazar J. Bacteriocin AS-48 binding to model membranes and pore formation as revealed by coarse-grained simulations. Biochim Biophys Acta 2013;1828(11):2524–31.

[99] Bereau T, Kremer K. Automated parametrization of the coarse-grained martini force field for small organic molecules. J Chem Theory Comput 2015;11(6):2783–91.

[100] Orsi M, Essex JW. Permeability of drugs and hormones through a lipid bilayer: insights from dual-resolution molecular dynamics. Soft Matter 2010;6(16).

[101] Orsi M, Noro MG, Essex JW. Dual-resolution molecular dynamics simulation of antimicrobials in biomembranes. J R Soc Interface 2011;8(59):826–41.

[102] Yesselman JD, Price DJ, Knight JL, Brooks 3rd CL. MATCH: an atom-typing toolset for molecular mechanics force fields. J Comput Chem 2012;33(2):189–202.

[103] Vanommeslaeghe K, MacKerell Jr AD. Automation of the CHARMM general force field (CGenFF) I: bond perception and atom typing. J Chem Inf Model 2012;52(12):3144–54.

[104] Vanommeslaeghe K, Raman EP, MacKerell Jr AD. Automation of the CHARMM general force field (CGenFF) II: assignment of bonded parameters and partial atomic charges. J Chem Inf Model 2012;52(12):3155–68.

[105] Wang J, Wang W, Kollman PA, Case DA. Automatic atom type and bond type perception in molecular mechanical calculations. J Mol Graph Model 2006;25(2):247–60.

[106] Huang L, Roux B. Automated force field parameterization for nonpolarizable and polarizable atomic models based on ab initio target data. J Chem Theory Comput 2013;9(8):3543–56.

[107] Malde AK, Zuo L, Breeze M, Stroet M, Poger D, Nair PC, et al. An automated force field topology builder (ATB) and repository: version 1.0. J Chem Theory Comput 2011;7(12):4026–37.

[108] Koziara KB, Stroet M, Malde AK, Mark AE. Testing and validation of the automated topology builder (ATB) version 2.0: prediction of hydration free enthalpies. J Comput Aided Mol Des 2014;28(3):221–33.

[109] Mayne CG, Saam J, Schulten K, Tajkhorshid E, Gumbart JC. Rapid parameterization of small molecules using the force field toolkit. J Comput Chem 2013;34(32):2757–70.

[110] Betz RM, Walker RC. Paramfit: automated optimization of force field parameters for molecular dynamics simulations. J Comput Chem 2015;36(2):79–87.

[111] Abraham MJ, Murtola T, Schulz R, Páll S, Smith JC, Hess B, et al. GROMACS: high performance molecular simulations through multi-level parallelism from laptops to supercomputers. SoftwareX 2015;1–2:19–25.

[112] Phillips JC, Braun R, Wang W, Gumbart J, Tajkhorshid E, Villa E, et al. Scalable molecular dynamics with NAMD. J Comput Chem 2005;26(16):1781–802.

[113] Brooks BR, Brooks 3rd CL, Mackerell Jr AD, Nilsson L, Petrella RJ, Roux B, et al. CHARMM: the biomolecular simulation program. J Comput Chem 2009;30(10):1545–614.

[114] Case DA, Cheatham 3rd TE, Darden T, Gohlke H, Luo R, Merz Jr KM, et al. The amber biomolecular simulation programs. J Comput Chem 2005;26(16):1668–88.

[115] Kunz AP, Allison JR, Geerke DP, Horta BA, Hunenberger PH, Riniker S, et al. New functionalities in the GROMOS biomolecular simulation software. J Comput Chem 2012;33(3):340–53.

[116] Bowers KJ, Chow E, Xu H, Dror RO, Eastwood MP, Gregersen BA, et al. Scalable algorithms for molecular dynamics simulations on commodity clustersProceedings of the ACM/IEEE conference on supercomputing (SC06), Tampa, Florida, November 11–17; 2006.

[117] Wong-Ekkabut J, Karttunen M. The good, the bad and the user in soft matter simulations. Biochim Biophys Acta 2016;1858(10):2529–38.

[118] Iyer M, Mishra R, Han Y, Hopfinger AJ. Predicting blood-brain barrier partitioning of organic molecules using membrane-interaction QSAR analysis. Pharm Res 2002;19(11):1611–21.

[119] Chen LL, Yao J, Yang JB, Yang J. Predicting MDCK cell permeation coefficients of organic molecules using membrane-interaction QSAR analysis. Acta Pharmacol Sin 2005;26(11):1322–33.

[120] Omote H, Al-Shawi MK. Interaction of transported drugs with the lipid bilayer and P-glycoprotein through a solvation exchange mechanism. Biophys J 2006;90(11):4046–59.

[121] Liu J, Yang L. Effect of cholesterol on DMPC phospholipid membranes and QSAR model construction in membrane-interaction QSAR study through molecular dynamics simulation. Bioorg Med Chem 2006;14(7):2225–34.

[122] Chen C, Yang J. MI-QSAR models for prediction of corneal permeability of organic compounds. Acta Pharmacol Sin 2006;27(2):193–204.

[123] Shinde RN, Srikanth K, Sobhia ME. Insights into the permeability of drugs and drug-like molecules from MI-QSAR and HQSAR studies. J Mol Model 2012;18(3):947–62.

[124] Meng F, Xu W. Drug permeability prediction using PMF method. J Mol Model 2013;19(3):991–7.

[125] Paloncýová M, Berka K, Otyepka M. Molecular insight into affinities of drugs and their metabolites to lipid bilayers. J Phys Chem B 2013;117(8):2403–10.

[126] Paloncýová M, DeVane R, Murch B, Berka K, Otyepka M. Amphiphilic drug-like molecules accumulate in a membrane below the head group region. J Phys Chem B 2014;118(4):1030–9.

[127] Martin LJ, Chao R, Corry B. Molecular dynamics simulation of the partitioning of benzocaine and phenytoin into a lipid bilayer. Biophys Chem 2014;185:98–107.

[128] Carpenter TS, Kirshner DA, Lau EY, Wong SE, Nilmeier JP, Lightstone FC. A method to predict blood-brain barrier permeability of drug-like compounds using molecular dynamics simulations. Biophys J 2014;107(3):630–41.

[129] Almeida PF. Membrane-active peptides: binding, translocation, and flux in lipid vesicles. Biochim Biophys Acta 2014;1838(9):2216–27.

[130] Galdiero S, Falanga A, Cantisani M, Vitiello M, Morelli G, Galdiero M. Peptide-lipid interactions: experiments and applications. Int J Mol Sci 2013;14(9):18758–89.

[131] Di Luca M, Maccari G, Nifosi R. Treatment of microbial biofilms in the post-antibiotic era: prophylactic and therapeutic use of antimicrobial peptides and their design by bioinformatics tools. Pathog Dis 2014;70(3):257–70.

[132] Steckbeck JD, Deslouches B, Montelaro RC. Antimicrobial peptides: new drugs for bad bugs? Expert Opin Biol Ther 2013;14(2):1–4.

[133] Chew CF, Guy A, Biggin PC. Distribution and dynamics of adamantases in a lipid bilayer. Biophys J 2008;95(12):5627–36.

[134] Li C, Yi M, Hu J, Zhou HX, Cross TA, Solid-state NMR. MD simulations of the antiviral drug amantadine solubilized in DMPC bilayers. Biophys J 2008;94(4):1295–302.

[135] do Canto AM, Carvalho AJ, Ramalho JP, Loura LM. Molecular dynamics simulations of T-20 HIV fusion inhibitor interacting with model membranes. Biophys Chem 2011;159(2–3):275–86.

[136] Leonis G, Czyznikowska Z, Megariotis G, Reis H, Papadopoulos MG. Computational studies of darunavir into HIV-1 protease and DMPC bilayer: necessary conditions for effective binding and the role of the flaps. J Chem Inf Model 2012;52(6):1542–58.

[137] Woolf TB, Roux B. Structure, energetics, and dynamics of lipid-protein interactions: a molecular dynamics study of the gramicidin A channel in a DMPC bilayer. Proteins Struct Funct Genet 1996;24:92–114.

[138] Mihailescu D, Smith JC. Atomic detail peptide-membrane interactions: molecular dynamics simulation of gramicidin S in a DMPC bilayer. Biophys J 2000;79(4):1718–30.

[139] Falck E, Hautala JT, Karttunen M, Kinnunen PK, Patra M, Saaren-Seppala H, et al. Interaction of fusidic acid with lipid membranes: implications to the mechanism of antibiotic activity. Biophys J 2006;91(5):1787–99.

[140] Siu SW, Bockmann RA. Electric field effects on membranes: gramicidin A as a test ground. J Struct Biol 2007;157(3):545–56.

[141] Jia Z, O'Mara ML, Zuegg J, Cooper MA, Mark AE. The effect of environment on the recognition and binding of vancomycin to native and resistant forms of lipid II. Biophys J 2011;101(11):2684–92.

[142] Kim T, Lee KI, Morris P, Pastor RW, Andersen OS, Im W. Influence of hydrophobic mismatch on structures and dynamics of gramicidin A and lipid bilayers. Biophys J 2012;102(7):1551–60.

[143] Cramariuc O, Rog T, Javanainen M, Monticelli L, Polishchuk AV, Vattulainen I. Mechanism for translocation of fluoroquinolones across lipid membranes. Biochim Biophys Acta 2012;1818(11):2563–71.

[144] Saito H, Iwayama M, Takagi H, Nishimura M, Miyakawa T, Kawaguchi K, et al. Molecular dynamics study of gramicidin a in lipid bilayer: structure and lateral pressure profile. Int J Quantum Chem 2012;112(24):3834–9.

[145] Basu I, Chattopadhyay A, Mukhopadhyay C. Ion channel stability of gramicidin A in lipid bilayers: effect of hydrophobic mismatch. Biochim Biophys Acta 2014;1838(1 Pt B):328–38.

[146] Kopec W, Khandelia H. Reinforcing the membrane-mediated mechanism of action of the anti-tuberculosis candidate drug thioridazine with molecular simulations. J Comput Aided Mol Des 2014;28(2):123–34.

[147] Berglund NA, Piggot TJ, Jefferies D, Sessions RB, Bond PJ, Khalid S. Interaction of the antimicrobial peptide polymyxin B1 with both membranes of E. coli: a molecular dynamics study. PLoS Comput Biol 2015;11(4):e1004180.

[148] Baginski M, Resat H, McCammon JA. Molecular properties of amphotericin B membrane channel: a molecular dynamics simulation. Mol Pharmacol 1997;52:560–70.

[149] Baginski M, Resat H, Borowski E. Comparative molecular dynamics simulations of amphotericin B - cholesterol/ergosterol membrane channel. Biochim Biophys Acta 2002;1567:63–78.

[150] Sternal K, Czub J, Baginski M. Molecular aspects of the interaction between amphotericin B and a phospholipid bilayer: molecular dynamics studies. J Mol Model 2004;10(3):223–32.

[151] Czub J, Baginski M. Modulation of amphotericin B membrane interaction by cholesterol and ergosterol - a molecular dynamics study. J Phys Chem B 2006;110(33): 16743–53.

[152] Czub J, Neumann A, Borowski E, Baginski M. Influence of a lipid bilayer on the conformational behavior of amphotericin B derivatives - a molecular dynamics study. Biophys Chem 2009;141(1):105–16.

[153] Neumann A, Czub J, Baginski M. On the possibility of the amphotericin B-sterol complex formation in cholesterol- and ergosterol-containing lipid bilayers: a molecular dynamics study. J Phys Chem B 2009;113(48):15875–85.

[154] Neumann A, Baginski M, Czub J. How do sterols determine the antifungal activity of amphotericin B? Free energy of binding between the drug and its membrane targets. J Am Chem Soc 2010;132(51):18266–72.

[155] Neumann A, Baginski M, Winczewski S, Czub J. The effect of sterols on amphotericin B self-aggregation in a lipid bilayer as revealed by free energy simulations. Biophys J 2013;104(7):1485–94.

[156] Neumann A, Wieczor M, Zielinska J, Baginski M, Czub J. Membrane sterols modulate the binding mode of amphotericin B without affecting its affinity for a lipid bilayer. Langmuir 2016;32(14):3452–61.

[157] Bemporad D, Luttmann C, Essex JW. Behaviour of small solutes and large drugs in a lipid bilayer from computer simulations. Biochim Biophys Acta 2005;1718(1–2): 1–21.

[158] Forst G, Cwiklik L, Jurkiewicz P, Schubert R, Hof M. Interactions of beta-blockers with model lipid membranes: molecular view of the interaction of acebutolol, oxprenolol, and propranolol with phosphatidylcholine vesicles by time-dependent fluorescence shift and molecular dynamics simulation. Eur J Pharm Biopharm 2014;87:559–69.

[159] Wang H, Ren X, Meng F. Molecular dynamics simulation of six β-blocker drugs passing across POPC bilayer. Mol Simul 2016;42(1):56–63.

[160] Azizi H, Koli MG. Molecular dynamics simulations of oxprenolol and propranolol in a DPPC lipid bilayer. J Mol Graph Model 2016;64:153–64.

[161] Yacoub TJ, Reddy AS, Szleifer I. Structural effects and translocation of doxorubicin in a DPPC/Chol bilayer: the role of cholesterol. Biophys J 2011;101(2):378–85.

[162] Karami L, Jalili S. Effects of cholesterol concentration on the interaction of cytarabine with lipid membranes: a molecular dynamics simulation study. J Biomol Struct Dyn 2015;33(6):1254–68.

[163] Kang M, Loverde SM. Molecular simulation of the concentration-dependent interaction of hydrophobic drugs with model cellular membranes. J Phys Chem B 2014;118(41):11965–72.

[164] Khadka NK, Cheng X, Ho CS, Katsaras J, Pan J. Interactions of the anticancer drug tamoxifen with lipid membranes. Biophys J 2015;108(10):2492–501.

[165] Erdtman E, dos Santos DJVA, Löfgren L, Eriksson LA. Modelling the behavior of 5-aminolevulinic acid and its alkyl esters in a lipid bilayer. Chem Phys Lett 2008; 463(1–3):178–82.

[166] Erdtman E, dosSantos DJVA, Löfgren L, Eriksson LA. Erratum to 'Modelling the behavior of 5-aminolevulinic acid and its alkyl esters in a lipid bilayer' [Chem. Phys. Lett. 463 (2008) 178]. Chem Phys Lett 2009;470(4–6):369.

[167] Karlsson BC, Olsson GD, Friedman R, Rosengren AM, Henschel H, Nicholls IA. How warfarin's structural diversity influences its phospholipid bilayer membrane permeation. J Phys Chem B 2013;117(8):2384–95.

[168] Ulander J, Haymet ADJ. Permeation across hydrated DPPC lipid bilayers: simulation of the titrable amphiphilic drug valproic acid. Biophys J 2003;85(6): 3475–84.

[169] Pickholz M, Oliveira ON, Skaf MS. Molecular dynamic simulations of neutral chlorpromazine in zwitterionic phospholipid monolayers. J Phys Chem B 2006;110(17): 8804–14.

[170] Pickholz M, Oliveira Jr ON, Skaf MS. Interactions of chlorpromazine with phospholipid monolayers: effects of the ionization state of the drug. Biophys Chem 2007; 125(2–3):425–34.

[171] Wood I, Pickholz M. Concentration effects of sumatriptan on the properties of model membranes by molecular dynamics simulations. Eur Biophys J 2013; 42(11–12):833–41.

[172] Wood I, Pickholz M. Triptan partition in model membranes. J Mol Model 2014; 20(10).

[173] Gupta D, Kothekar V. Conformation of nifedipine in hydrated 1,2-di-myristoyl-sn-glycero-3-phosphorylcholine bilayer molecular dynamics simulation. J Biosci 1997;22(2):177–92.

[174] Gupta D, Kothekar V. Molecular dynamics simulation of the interaction of nifedipine and its *meta* and *para* NO$_2$ analogs with a hydrated dimyristoyl-sn-glycero-3-phosphorylcholine (DMPC) bilayer. J Mol Struct 1998;431:17–31.

[175] Aiello M, Moran O, Pisciotta M, Gambale F. Interaction between dihydropyridines and phospholipid bilayers: a molecular dynamics simulation. Eur Biophys J 1998; 27:211–8.

[176] Zervou M, Cournia Z, Potamitis C, Patargias G, Durdagi S, Grdadolnik SG, et al. Insights into the molecular basis of action of the AT1 antagonist losartan using a combined NMR spectroscopy and computational approach. Biochim Biophys Acta 2014;1838(3):1031–46.

[177] Yousefpour A, Modarress H, Goharpey F, Amjad-Iranagh S. Interaction of PEGylated anti-hypertensive drugs, amlodipine, atenolol and lisinopril with lipid bilayer membrane: a molecular dynamics simulation study. Biochim Biophys Acta 2015; 1848(8):1687–98.

[178] Sadeghpour A, Rappolt M, Ntountaniotis D, Chatzigeorgiou P, Viras K, Megariotis G, et al. Comparative study of interactions of aliskiren and AT1 receptor antagonists with lipid bilayers. Biochim Biophys Acta 2015;1848:984–94.

[179] Klamt A, Huniar U, Spycher S, Keldenich J. COSMOmic: a mechanistic approach to the calculation of membrane water partition coefficients and internal distributions within membranes and micelles. J Phys Chem B 2008;112:12148–57.

[180] Jakobtorweihen S, Ingram T, Smirnova I. Combination of COSMOmic and molecular dynamics simulations for the calculation of membrane-water partition coefficients. J Comput Chem 2013;34(1332–1340).

[181] Bittermann K, Spycher S, Endo S, Pohler L, Huniar U, Goss KU, et al. Prediction of phospholipid-water partition coefficients of ionic organic chemicals using the mechanistic model COSMOmic. J Phys Chem B 2014;118:14833–42.

[182] Jakobtorweihen S, Zuniga AC, Ingram T, Gerlach T, Keil FJ, Smirnova I. Predicting solute partitioning in lipid bilayers: free energies and partition coefficients from molecular dynamics simulations and COSMOmic. J Chem Phys 2014; 141(4):045102.

[183] Ingram T, Storm S, Kloss L, Mehling T, Jakobtorweihen S, Smirnova I. Prediction of micelle/water and liposome/water partition coefficients based on molecular dynamics simulations, COSMO-RS, and COSMOmic. Langmuir 2013;29(11): 3527–37.

[184] Paloncýová M, DeVane RH, Murch BP, Berka K, Otyepka M. Rationalization of reduced penetration of drugs through ceramide gel phase membrane. Langmuir 2014;30(46):13942–8.

[185] Endo S, Escher BI, Goss KU. Capacities of membrane lipids to accumulate neutral organic chemicals. Environ Sci Technol 2011;45(14):5912–21.

[186] Spycher S, Smejtek P, Netzeva TI, Escher BI. Toward a class-independent quantitative structure-activity relationship model for uncouplers of oxidative phosphorylation. Chem Res Toxicol 2008;21(4):911–27.

[187] Bittermann K, Spycher S, Goss KU. Comparison of different models predicting the phospholipid-membrane water partition coefficients of charged compounds. Chemosphere 2016;144:382–91.

[188] Storm S, Jakobtorweihen S, Smirnova I. Solubilization in mixed micelles studied by molecular dynamics simulations and COSMOmic. J Phys Chem B 2014;118(13): 3593–604.

[189] Storm S, Jakobtorweihen S, Smirnova I, Panagiotopoulos AZ. Molecular dynamics simulation of SDS and CTAB micellization and prediction of partition equilibria with COSMOmic. Langmuir 2013;29(37):11582–92.

[190] Yordanova D, Smirnova I, Jakobtorweihen S. Molecular modeling of triton X micelles: force field parameters, self-assembly, and partition equilibria. J Chem Theory Comput 2015;11(5):2329–40.

[191] Ritter E, Yordanova D, Gerlach T, Smirnova I, Jakobtorweihen S. Molecular dynamics simulations of various micelles to predict micelle water partition equilibria with COSMOmic: influence of micelle size and structure. Fluid Phase Equilib 2016;422: 43–55.

[192] Nunes C, Lopes D, Pinheiro M, Pereira-Leite C, Reis S. *In vitro* assessment of NSAIDs-membrane interactions: significance for pharmacological actions. Pharm Res 2013; 30(8):2097–107.

[193] Osanai H, Ikehara T, Miyauchi S, Shimono K, Tamogami J, Nara T, et al. A study of the interaction of drugs with liposomes with isothermal titration calorimetry. J Biophys Chem 2013;04(01):11–21.

[194] Matos C, Lima JLC, Reis S, Lopes A, Bastos M. Interaction of antiinflammatory drugs with EPC liposomes: calorimetric study in a broad concentration range. Biophys J 2004;86(2):946–54.

[195] Jelesarov I, Bosshard HR. Isothermal titration calorimetry and differential scanning calorimetry as complementary tools to investigate the energetics of biomolecular recognition. J Mol Recognit 1999;12:3–18.

[196] Lúcio M, Nunes C, Gaspar D, Gołębska K, Wisniewski M, Lima JLFC, et al. Effect of anti-inflammatory drugs in phosphatidylcholine membranes: a fluorescence and calorimetric study. Chem Phys Lett 2009;471(4–6):300–9.

[197] Kästner J. Umbrella sampling. WIREs Comput Mol Sci 2011;1(6):932–42.

[198] Kirkwood JG. Statistical mechanics of fluid mixtures. J Chem Phys 1935;3(5).

[199] Roux B. The calculation of the potential of mean force using computer simulations. Comput Phys Commun 1995;91:275–82.

[200] Trzesniak D, Kunz AP, van Gunsteren WF. A comparison of methods to compute the potential of mean force. Chemphyschem 2007;8(1):162–9.

[201] Chipot, Pohorille C, Andrew, editors. Free energy calculations: theory and applications in chemistry and biology. Germany: Springer; 2007.

[202] Hansen N, van Gunsteren WF. Practical aspects of free-energy calculations: a review. J Chem Theory Comput 2014;10(7):2632–47.

[203] Torrie GM, Valleau JP. Monte Carlo free energy estimates using non-Boltzmann sampling: applications to the sub-critical Lennard-Jones fluid. Chem Phys Lett 1974;28(4):578–81.

[204] Torrie GM, Valleau JP. Nonphysical sampling distributions in Monte Carlo free-energy estimation: umbrella sampling. J Comput Phys 1977;23:187–99.

[205] Mills M, Andricioaei I. An experimentally guided umbrella sampling protocol for biomolecules. J Chem Phys 2008;129(114101):1–13.

[206] Kumar S, Bouzida D, Swendsen RH, Kollman PA, Rosenberg JM. The weighted histogram analysis method for free-energy calculations on biomolecules. I. The method. J Comput Chem 1992;13(8):1011–21.

[207] Souaille M, Roux B. Extension to the weighted histogram analysis method: combining umbrella sampling with free energy calculations. Comput Phys Commun 2001; 135:40–57.

[208] Kastner J, Thiel W. Bridging the gap between thermodynamic integration and umbrella sampling provides a novel analysis method: "umbrella integration". J Chem Phys 2005;123(14):144104.

[209] Neale C, Pomes R. Sampling errors in free energy simulations of small molecules in lipid bilayers. Biochim Biophys Acta 2016;1858(10):2539–48.

[210] MacCallum JL, Bennett WF, Tieleman DP. Distribution of amino acids in a lipid bilayer from computer simulations. Biophys J 2008;94(9):3393–404.

[211] Liu W, Zhang S, Meng F, Tang L. Molecular simulation of ibuprofen passing across POPC membrane. J Chem Theory Comput 2014;13(4):1–14.

[212] Castro Bd, Gameiro P, Lima JLFC, Matos C, Reis S. A fast and reliable spectroscopic method for the determination of membrane-water partition coefficients of organic compounds. Lipids 2001;36(1):89–96.

[213] Reijenga J, van Hoof A, van Loon A, Teunissen B. Development of methods for the determination of pKa values. Anal Chem Insights 2013;8:53–71.

[214] Franzen U, Ostergaard J. Physico-chemical characterization of liposomes and drug substance-liposome interactions in pharmaceutics using capillary electrophoresis and electrokinetic chromatography. J Chromatogr A 2012;1267:32–44.

[215] van Balen GP, Martinet C, Caron G, Bouchard G, Reist M, Carrupt PA, et al. Liposome/water lipophilicity: methods, information content, and pharmaceutical applications. Med Res Rev 2004;24(3):299–324.

[216] El Maghraby GM, Williams AC, Barry BW. Drug interaction and location in liposomes: correlation with polar surface areas. Int J Pharm 2005;292(1–2):179–85.

[217] Santos N, Prietob M, Castanho MARB. Quantifying molecular partition into model systems of biomembranes: an emphasis on optical spectroscopic methods. Biochim Biophys Acta 2003;1612(2):123–35.

[218] Di Meo F, Fabre G, Berka K, Ossman T, Chantemargue B, Paloncýová M, et al. *In silico* pharmacology: Drug membrane partitioning and crossing. Pharmacol Res 2016; 111:471–86.

[219] Magalhaes LM, Nunes C, Lucio M, Segundo MA, Reis S, Lima JL. High-throughput microplate assay for the determination of drug partition coefficients. Nat Protoc 2010;5(11):1823–30.

[220] Diamond JM, Katz Y. Interpretation of nonelectrolyte partition coefficients between dimyristoyl lecithin and water. J Membr Biol 1974;17:121–54.

[221] Reis JM, Sinko B, Serra CHR. Parallel artificial membrane permeability assay (PAMPA) - is it better than Caco-2 for human passive permeability prediction? Mini Rev Med Chem 2010;10(11):1071–6.

[222] Yang CY, Cai SJ, Liu H, Pidgeon C. Immobilized artificial membranes - screens for drug membrane interactions. Adv Drug Deliv Rev 1996;23:229–56.

[223] Marrink S-J, Berendsen HJC. Simulation of water transport through a lipid membrane. J Phys Chem 1994;98(15):4155–68.

[224] Roux B, Karplus M. Ion transport in a gramicidin-like channel: dynamics and mobility. J Phys Chem 1991;95(12):4856–68.

[225] Hummer G. Position-dependent diffusion coefficients and free energies from Bayesian analysis of equilibrium and replica molecular dynamics simulations. New J Phys 2005;7:34.

[226] Gaalswyk K, Awoonor-Williams E, Rowley CN. Generalized Langevin methods for calculating transmembrane diffusivity. J Chem Theory Comput 2016.

[227] Comer J, Schulten K, Chipot C. Calculation of lipid-bilayer permeabilities using an average force. J Chem Theory Comput 2014;10(2):554–64.

[228] Awoonor-Williams E, Rowley CN. Molecular simulation of nonfacilitated membrane permeation. Biochim Biophys Acta 2016;1858(7 Pt B):1672–87.

[229] Swift RV, Amaro RE. Modeling the pharmacodynamics of passive membrane permeability. J Comput Aided Mol Des 2011;25(11):1007–17.

[230] Orsi M, Seanderson WE, Essex JW. Permeability of small molecules through a lipid bilayer: a multiscale simulation study. J Phys Chem B 2009;113(35):12019–29.

[231] Shinoda W, Mikami M, Baba T, Hato M. Molecular dynamics study on the effects of chain branching on the physical properties of lipid bilayers: 2. Permeability. J Phys Chem B 2004;108(26):9346–56.

[232] Swift RV, Amaro RE. Back to the future: can physical models of passive membrane permeability help reduce drug candidate attrition and move us beyond QSPR? Chem Biol Drug Des 2013;81(1):61–71.

[233] Hong X, Hopfinger AJ. Molecular modeling and simulation of mycobacterium tuberculosis cell wall permeability. Biomacromolecules 2004;5(3):1066–77.

[234] Xiang TX, Anderson BD. The relationship between permeant size and permeability in lipid bilayer membranes. J Membr Biol 1994;140:111–22.

[235] Mayer PT, Anderson BD. Transport across 1,9-decadiene precisely mimics the chemical selectivity of the barrier domain in egg lecithin bilayers. J Pharm Sci 2002;91(3):640–6.

[236] Kier LB, Cheng C-K, Cellular Automata A. Model of membrane permeability. J Theor Biol 1997;186:75–80.

[237] Kubica K, Kuczera J. An application of cellular automata to model a lipid membrane. Appl Math Comput 1990;39:49–59.

[238] Sun R, Dama JF, Tan JS, Rose JP, Voth GA, Transition-Tempered Metadynamics I. A promising tool for studying the permeation of drug-like molecules through membranes. J Chem Theory Comput 2016;12(10):5157–69.

[239] Lakowicz JR. Principles of fluorescence spectroscopy. 3rd ed. Springer; 2006.

[240] Kaiser RD, London E. Location of diphenylhexatriene (DPH) and its derivatives within membranes: comparison of different fluorescence quenching analyses of membrane depth. Biochem J 1998;37:8180–90.

[241] Vázquez JL, Montero MT, Merino S, Domènech Ò, Berlanga M, Viñas M, et al. Location and nature of the surface membrane binding site of ciprofloxacin: a fluorescence study. Langmuir 2001;17:1009–14.

[242] Lúcio M, Lima JLFC, Reis S. Drug-membrane interactions: significance for medicinal chemistry. Curr Med Chem 2010;17:1795–809.

[243] Hansen AH, Sorensen KT, Mathieu R, Serer A, Duelund L, Khandelia H, et al. Propofol modulates the lipid phase transition and localizes near the headgroup of membranes. Chem Phys Lipids 2013;175–6.

[244] Denich TJ, Beaudette LA, Lee H, Trevors JT. Effect of selected environmental and physico-chemical factors on bacterial cytoplasmic membranes. J Microbiol Methods 2003;52:149–82.

[245] Chau PL, Jedlovszky P, Hoang PNM, Picaud S. Pressure reversal of general anaesthetics: a possible mechanism from molecular dynamics simulations. J Mol Liq 2009;147(1–2):128–34.

[246] Tu KM, Matubayasi N, Liang KK, Todorov IT, Chan SL, Chau PL. A possible molecular mechanism for the pressure reversal of general anaesthetics: aggregation of halothane in POPC bilayers at high pressure. Chem Phys Lett 2012;543:148–54.

[247] Austin RP, Barton P, Davis AM, Manners CN, Stansfield MC. The effect of ionic strength on liposome–buffer and 1-octanol–buffer distribution coefficients. J Pharm Sci 1998;87(5):599–607.

[248] Lopez Cascales JJ, Oliveira Costa SD. Effect of the interfacial tension and ionic strength on the thermodynamic barrier associated to the benzocaine insertion into a cell membrane. Biophys Chem 2013;172:1–7.

[249] Krause MR, Regen SL. The structural role of cholesterol in cell membranes: from condensed bilayers to lipid rafts. Acc Chem Res 2014;47(12):3512–21.

[250] Krämer SD. Liposome/water partitioning: theory, techniques, and applications. In: Testa B, Waterbeemd Hvd, Folkers G, Guy R, editors. Pharmacokinetic optimization in drug research: biological, physicochemical, and computational strategies. Germany: Wiley-VCH; 2001.

[251] de Joannis J, Coppock PS, Yin F, Mori M, Zamorano A, Kindt JT. Atomistic simulation of cholesterol effects on miscibility of saturated and unsaturated phospholipids: implications for liquid-ordered/liquid-disordered phase coexistence. J Am Chem Soc 2011;133(10):3625–34.

[252] Sodt AJ, Pastor RW, Lyman E. Hexagonal substructure and hydrogen bonding in liquid-ordered phases containing palmitoyl sphingomyelin. Biophys J 2015;109(5): 948–55.

[253] Andersson Trojer M, Brezesinski G. Self-assembly of lipid domains in the extracellular leaflet of the plasma membrane and models thereof. Curr Opin Colloid Interface Sci 2016;22:65–72.

[254] Garcia-Saez AJ, Schwille P. Stability of lipid domains. FEBS Lett 2010;584(9): 1653–8.

[255] Fan J, Sammalkorpi M, Haataja M. Formation and regulation of lipid microdomains in cell membranes: theory, modeling, and speculation. FEBS Lett 2010;584(9): 1678–84.

[256] Mouritsen OG, Bagatolli LA. Lipid domains in model membranes: a brief historical perspective. Essays Biochem 2015;57:1–19.

[257] Srivastava A, Voth GA, Hybrid Approach A. For highly coarse-grained lipid bilayer models. J Chem Theory Comput 2013;9(1):750–65.

[258] Hills Jr RD, McGlinchey N. Model parameters for simulation of physiological lipids. J Comput Chem 2016;37(12):1112–8.

[259] Shen HH, Lithgow T, Martin L. Reconstitution of membrane proteins into model membranes: seeking better ways to retain protein activities. Int J Mol Sci 2013; 14(1):1589–607.

[260] Amjad-Iranagh S, Yousefpour A, Haghighi P, Modarress H. Effects of protein binding on a lipid bilayer containing local anesthetic articaine, and the potential of mean force calculation: a molecular dynamics simulation approach. J Mol Model 2013; 19(9):3831–42.

[261] Gaspar D, Lucio M, Wagner K, Brezesinski G, Rocha S, Costa Lima JL, et al. A biophysical approach to phospholipase A2 activity and inhibition by anti-inflammatory drugs. Biophys Chem 2010;152(1–3):109–17.

[262] Dynamics of soft matter: neutron applications. Springer; 2012.

[263] Petrache HI, Dodd SW, Brown MF. Area per lipid and acyl length distributions in fluid phosphatidylcholines determined by ^{2}H NMR spectroscopy. Biophys J 2000; 79(6):3172–92.

[264] Nademi Y, Iranagh SA, Yousefpour A, Mousavi SZ, Modarress H. Molecular dynamics simulations and free energy profile of paracetamol in DPPC and DMPC lipid bilayers. J Chem Sci 2014;126(3):637–47.

[265] Nunes C, Brezesinski G, Pereira-Leite C, Lima JL, Reis S, Lucio M. NSAIDs interactions with membranes: a biophysical approach. Langmuir 2011;27(17):10847–58.

[266] Hofsäβ C, Lindahl E, Edholm O. Molecular dynamics simulations of phospholipid bilayers with cholesterol. Biophys J 2003;84(4):2192–206.

[267] Cascales JJL, Cifre JGH, Torre JGdl. Anaesthetic mechanism on a model biological membrane: a molecular dynamics simulation study. J Phys Chem B 1998;102(3): 625–31.

[268] Nunes C, Brezesinski G, Lopes D, Lima JL, Reis S, Lucio M. Lipid-drug interaction: biophysical effects of tolmetin on membrane mimetic systems of different dimensionality. J Phys Chem B 2011;115(43):12615–23.

[269] Ollila OH, Pabst G. Atomistic resolution structure and dynamics of lipid bilayers in simulations and experiments. BBA-Biomembranes 2016;1858(10):2512–28.

[270] Yousefpour A, Iranagh SA, Nademi Y, Modarress H. Molecular dynamics simulation of nonsteroidal antiinflammatory drugs, naproxen and relafen, in a lipid bilayer membrane. Int J Quantum Chem 2013;113:1919–30.

[271] Xu Q, Ni Z, Yao P, Li Y. Molecular dynamics simulation of anionic clays containing glutamic acid. J Mol Struct 2010;977(1–3):165–9.

[272] Weinstein JN, Yoshikami S, Henkart P, Blumenthal R, Hagins WA. Liposome-cell interaction: transfer and intracellular release of a trapped fluorescent marker. Science 1977;195:489–92.

[273] Gabel D, Awad D, Schaffran T, Radovan D, Daraban D, Damian L, et al. The anionic boron cluster (B12H11SH)2- as a means to trigger release of liposome contents. ChemMedChem 2007;2(1):51–3.

[274] Manzini MC, Perez KR, Riske KA, Bozelli Jr JC, Santos TL, da Silva MA, et al. Peptide:lipid ratio and membrane surface charge determine the mechanism of action of the antimicrobial peptide BP100. Conformational and functional studies. Biochim Biophys Acta 2014;1838(7):1985–99.

[275] Hu Y, Sinha SK, Patel S. Investigating hydrophilic pores in model lipid bilayers using molecular simulations: correlating bilayer properties with pore-formation thermodynamics. Langmuir 2015;31(24):6615–31.

[276] Tsuchiya H, Mizogami M. Interaction of local anesthetics with biomembranes consisting of phospholipids and cholesterol: mechanistic and clinical implications for anesthetic and cardiotoxic effects. Anesthesiol Res Pract 2013;2013:297141.

[277] Skjevik AA, Haug BE, Lygre H, Teigen K. Intramolecular hydrogen bonding in articaine can be related to superior bone tissue penetration: a molecular dynamics study. Biophys Chem 2011;154(1):18–25.

[278] Högberg CJ, Lyubartsev AP. Effect of local anesthetic lidocaine on electrostatic properties of a lipid bilayer. Biophys J 2008;94(2):525–31.

[279] Koubi L, Tarek M, Bandyopadhyay S, Klein ML, Scharf D. Membrane structural perturbations caused by anesthetics and nonimmobilizers: a molecular dynamics investigation. Biophys J 2001;81(6):3339–45.

[280] Jerabek H, Pabst G, Rappolt M, Stockner T. Membrane-mediated effect on ion channels induced by the anesthetic drug ketamine. J Am Chem Soc 2010;132:7990–7.

[281] Booker RD, Sum AK. Biophysical changes induced by xenon on phospholipid bilayers. Biochim Biophys Acta 2013;1828(5):1347–56.

[282] Tu K, Tarek M, Klein ML, Scharf D. Effects of anesthetics on the structure of a phospholipid bilayer: molecular dynamics investigation of halothane in the hydrated liquid crystal phase of dipalmitoylphosphatidylcholine. Biophys J 1998;75: 2123–34.

[283] Koubi L, Tarek M, Klein ML, Scharf D. Distribution of halothane in a dipalmitoylphosphatidylcholine bilayer from molecular dynamics calculations. Biophys J 2000;78:800–11.

[284] Tang P, Xu Y. Large-scale molecular dynamics simulations of general anesthetic effects on the ion channel in the fully hydrated membrane: the implication of molecular mechanisms of general anesthesia. Proc Natl Acad Sci U S A 2002;99(25): 16035–40.

[285] Vemparala S, Saiz L, Eckenhoff RG, Klein ML. Partitioning of anesthetics into a lipid bilayer and their interaction with membrane-bound peptide bundles. Biophys J 2006;91(8):2815–25.

[286] Chau PL, Hoang PNM, Picaud S, Jedlovszky P. A possible mechanism for pressure reversal of general anaesthetics from molecular simulations. Chem Phys Lett 2007; 438(4–6):294–7.

[287] Högberg CJ, Maliniak A, Lyubartsev AP. Dynamical and structural properties of charged and uncharged lidocaine in a lipid bilayer. Biophys Chem 2007;125(2–3):416–24.

[288] Pickholz M, Fernandes Fraceto L, de Paula E. Distribution of neutral prilocaine in a phospholipid bilayer: insights from molecular dynamics simulations. Int J Quantum Chem 2008;108(13):2386–91.

[289] Chau PL, Tu KM, Liang KK, Chan SL, Matubayasi N. Free-energy change of inserting halothane into different depths of a hydrated DMPC bilayer. Chem Phys Lett 2008; 462(1–3):112–5.

[290] Chau PL, Tu KM, Liang KK, Todorov IT, Roser SJ, Barker R, et al. The effect of pressure on halothane binding to hydrated DMPC bilayers. Mol Phys 2012;110(13):1461–7.

[291] Pickholz M, Fraceto LF, de Paula E. Preferential location of prilocaine and etidocaine in phospholipid bilayers: a molecular dynamics study. Synth Met 2009;159(21–22):2157–8.

[292] Porasso RD, Bennett WF, Oliveira-Costa SD, Cascales JJL. Study of the benzocaine transfer from aqueous solution to the interior of a biological membrane. J Phys Chem B 2009;113(29):9988–94.

[293] Mojumdar EH, Lyubartsev AP. Molecular dynamics simulations of local anesthetic articaine in a lipid bilayer. Biophys Chem 2010;153(1):27–35.

[294] Cascales JJ, Costa SD, Porasso RD. Thermodynamic study of benzocaine insertion into different lipid bilayers. J Chem Phys 2011;135(13).

[295] Darvas M, Hoang PN, Picaud S, Sega M, Jedlovszky P. Anesthetic molecules embedded in a lipid membrane: a computer simulation study. Phys Chem Chem Phys 2012;14(37):12956–69.

[296] Bernardi RC, Pascutti PG, Hybrid QM. MM molecular dynamics study of benzocaine in a membrane environment: how does a quantum mechanical treatment of both anesthetic and lipids affect their interaction. J Chem Theory Comput 2012;8(7): 2197–203.

[297] Martini MF, Pickholz M. Molecular dynamics study of uncharged bupivacaine enantiomers in phospholipid bilayers. Int J Quantum Chem 2012;112(20):3341–5.

[298] Jambeck JP, Lyubartsev AP. Implicit inclusion of atomic polarization in modeling of partitioning between water and lipid bilayers. Phys Chem Chem Phys 2013;15(13): 4677–86.

[299] Sierra-Valdez FJ, Forero-Quintero LS, Zapata-Morin PA, Costas M, Chavez-Reyes A, Ruiz-Suárez JC. The influence of nonpolar and polar molecules in mouse motile cells membrane and pure lipid bilayers. PLoS One 2013;8(4):1–6.

[300] Arcario MJ, Mayne CG, Tajkhorshid E. Atomistic models of general anesthetics for use in in silico biological studies. J Phys Chem B 2014;118(42):12075–86.

[301] Fabian B, Darvas M, Picaud S, Sega M, Jedlovszky P. The effect of anaesthetics on the properties of a lipid membrane in the biologically relevant phase: a computer simulation study. Phys Chem Chem Phys 2015;17(22):14750–60.

[302] Hanson SM, Newstead S, Swartz KJ, Sansom MS. Capsaicin interaction with TRPV1 channels in a lipid bilayer: molecular dynamics simulation. Biophys J 2015;108(6): 1425–34.

[303] Wieteskaa JR, Welchea PRL, Tub K-M, ElGamacyc M, Csanyid G, Paynea MC, et al. Isoflurane does not aggregate inside POPC bilayers at high pressure: implications for pressure reversal of general anaesthesia. Chem Phys Lett 2015;638:116–21.

[304] Boggara MB, Krishnamoorti R. Partitioning of nonsteroidal antiinflammatory drugs in lipid membranes: a molecular dynamics simulation study. Biophys J 2010;98(4): 586–95.

[305] Markiewicz M, Pasenkiewicz-Gierula M. Comparative model studies of gastric toxicity of nonsteroidal anti-inflammatory drugs. Langmuir 2011;27(11):6950–61.

[306] Boggara MB, Mihailescu M, Krishnamoorti R. Structural association of nonsteroidal anti-inflammatory drugs with lipid membranes. J Am Chem Soc 2012;134(48): 19669–76.

[307] Boggara MB, Faraone A, Krishnamoorti R. Effect of pH and ibuprofen on the phospholipid bilayer bending modulus. J Phys Chem B 2010;114:8061–6.

[308] Lichtenberger LM, Zhou Y, Jayaraman V, Doyen JR, O'Neil RG, Dial EJ, et al. Insight into NSAID-induced membrane alterations, pathogenesis and therapeutics: characterization of interaction of NSAIDs with phosphatidylcholine. Biochim Biophys Acta 2012;1821:994–1002.

[309] Kopec W, Telenius J, Khandelia H. Molecular dynamics simulations of the interactions of medicinal plant extracts and drugs with lipid bilayer membranes. FEBS J 2013;280(12):2785–805.

Chapter 2.3

Eradication of *Helicobacter pylori*: Past, present and future

The need to write this review paper came from the second objective, which was to develop a drug delivery system. For that, it was necessary to be aware of the history of *H. pylori* eradication attempts, particularly in terms of the new strategies that have been tried. Hence, this review was written to summarize and highlight the usefulness of nanotechnology in the treatment of *H. pylori* infections.
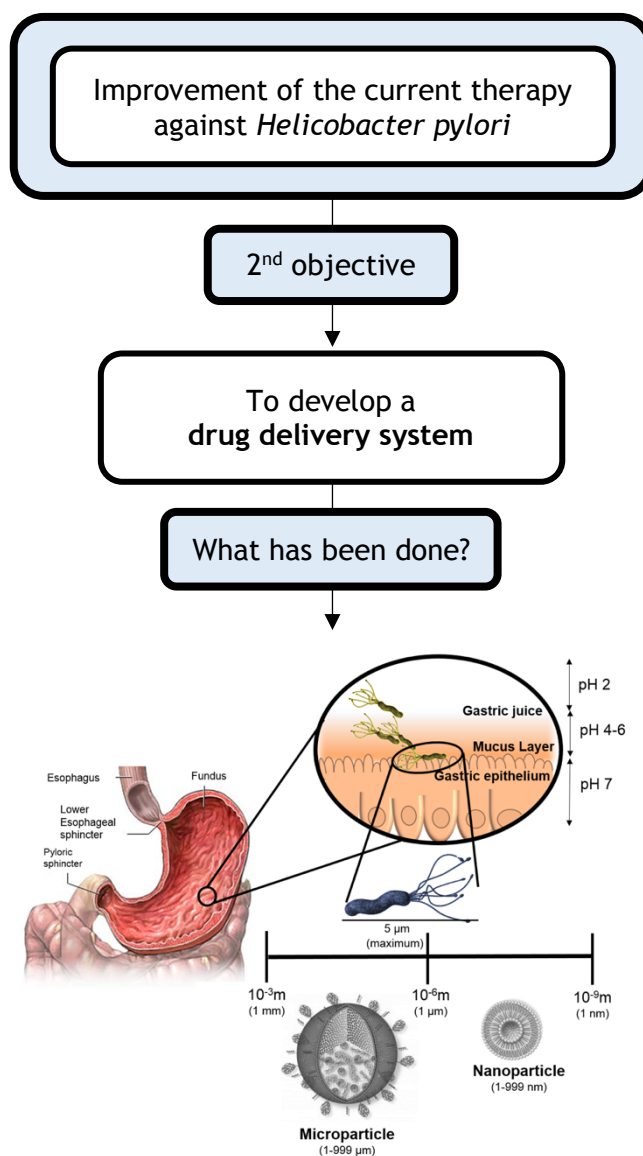
Review

Eradication of *Helicobacter pylori*: Past, present and future

Daniela Lopes [a], Cláudia Nunes [a], M. Cristina L. Martins [b,c], Bruno Sarmento [b,d], Salette Reis [a,*]

[a] REQUIMTE, Departamento de Ciências Químicas, Faculdade de Farmácia, Universidade do Porto, Porto, Portugal
[b] INEB – Instituto de Engenharia Biomédica, Universidade do Porto, Porto, Portugal
[c] ICBAS — Instituto de Ciências Biomédicas Abel Salazar, Universidade do Porto, Porto, Portugal
[d] IINFACTS — Instituto de Investigação e Formação Avançada em Ciências e Tecnologias da Saúde, Instituto Superior de Ciências da Saúde-Norte, Gandra-PRD, Portugal

ARTICLE INFO

ABSTRACT

Helicobacter pylori is the major cause of chronic gastritis and peptic ulcers. Since the classification as a group 1 carcinogenic by International Agency for Research on Cancer, the importance of the complete *H. pylori* eradication has obtained a novel meaning. Hence, several studies have been made in order to deepen the knowledge in therapy strategies. However, the current therapy presents unsatisfactory eradication rates due to the lack of therapeutic compliance, antibiotic resistance, the degradation of antibiotics at gastric pH and their insufficient residence time in the stomach. Novel approaches have been made in order to overcome these limitations. The purpose of this review is to provide an overview about the current therapy and its limitations, while highlighting the possibility of using micro- and nanotechnology to develop gastric drug delivery systems, overcoming these difficulties in the future.

© 2014 Elsevier B.V. All rights reserved.

Contents

1. Introduction

Helicobacter pylori (*H. pylori*) is a gram-negative bacterium, usually in a spiral-shaped form, that can be converted in coccoid cells under a hostile environment [1,2]. These bacteria present several structural and morphological characteristics that favor their penetration within the mucosa and consequently the colonization of the gastric antrum and the human duodenal mucosa [2,3]. Their major virulence factors lie on four to six flagella enhancers of their mobility, urease production, phospholipase secretion, cytotoxin production and their ability to adhere to the target cells [1–3]. These virulence factors enable their mobility through the gastric mucus and the colonization of the surface between the mucus gel layer and the epithelial cells [3,4]. Adhesins are responsible for the adherence to carbohydrates of the mucosa and to epithelial cells, namely through the adhesion to polysaccharides, laminins and Lewis b antigen among others, playing an important role in the pathogenesis of the bacteria [3–6].

Currently, the worldwide population infected is around 50%, being even higher in developing countries [7]. Prevalence rates of *H. pylori* infection varies according to race/ethnicity, socioeconomic conditions and age, being highest with aging [7]. Commonly, their colonization is asymptomatic, resulting only in histological signs of chronic gastritis [8,9]. However, approximately 20% of the infected population evolves into a clinical condition, commonly chronic gastritis and peptic ulcer [8,9]. This incomprehensive and complex *H. pylori*–human relationship, where only a portion of the infected people manifests a disease, have led to a controversy about the seriousness of *H. pylori* infection [8]. Nevertheless, the risk resulting from an unsuccessful eradication is higher in the cases of clinical manifestation, since persistent infections may lead to gastric cancer, such as gastric mucosa-associated lymphoma tissue and adenocarcinomas [7,8,10]. In fact, bacteria eradication in patients with low-grade lymphomas often results in the remission of the cancer [7]. According to these facts, the International Agency for Research on Cancer (IARC), subordinated to the World Health Organization (WHO), declared *H. pylori* as a human carcinogenic (group 1) [7].

Although without a clear explanation, other extradigestive conditions, namely idiopathic thrombocytopenic purpura, iron deficiency anemia, ischemic heart disease, stroke, Parkinson's disease and Alzheimer's disease have been recently related to the presence of *H. pylori* [11].

The importance of the therapy in clinical manifestation of *H. pylori* is unquestionable. However, despite all the endeavors, the current therapy presents many limitations which have led to the failure of *H. pylori* eradication. This review provides an overview about the traversed pathway until the current therapy and its limitation. Furthermore, a summary of all the reports with micro- and nanoparticles applied to gastric delivery through active or passive targeting to the bacteria or through mucoadhesiveness to the gastric mucosa will also be discussed.

2. Treatment of *H. pylori* infection

2.1. Overview of the discovery of H. pylori

The discovery of *H. pylori* resulted from a slow and gradual progression (Fig. 1). The first report about gastric ulceration was written in 1586 by an Italian physician named Marcello Donati [1,12,13]. During several years, the pathogenesis of this disease was exclusively associated to stress and dietary factors, being treated by resorting to bed rest and special diet [1]. In the second half of 18th century, the use of bismuth compounds, namely bismuth subnitrate, to treat gastric ulcers became very popular as a result of the work of Gorham and Kussmaul [13,14]. Actually, bismuth compounds have antibacterial properties that were unknown at that time [13,14].

In 1875, Bottcher and Letulle noticed the existence of bacteria in ulcer margins and suggested their relation to gastric disease [14]. However, the presence of spiral organisms in human gastric washings was reported by W. Jaworski, a Poland professor, only in 1889 [15]. He also theorized that the bacteria may be related to the development of gastric ulcers [1]. Nevertheless, his research work was poorly publicized since it was written in Polish [15]. The first recognized report appeared only in the latter half of the 19th century, when Bizzozero observed the
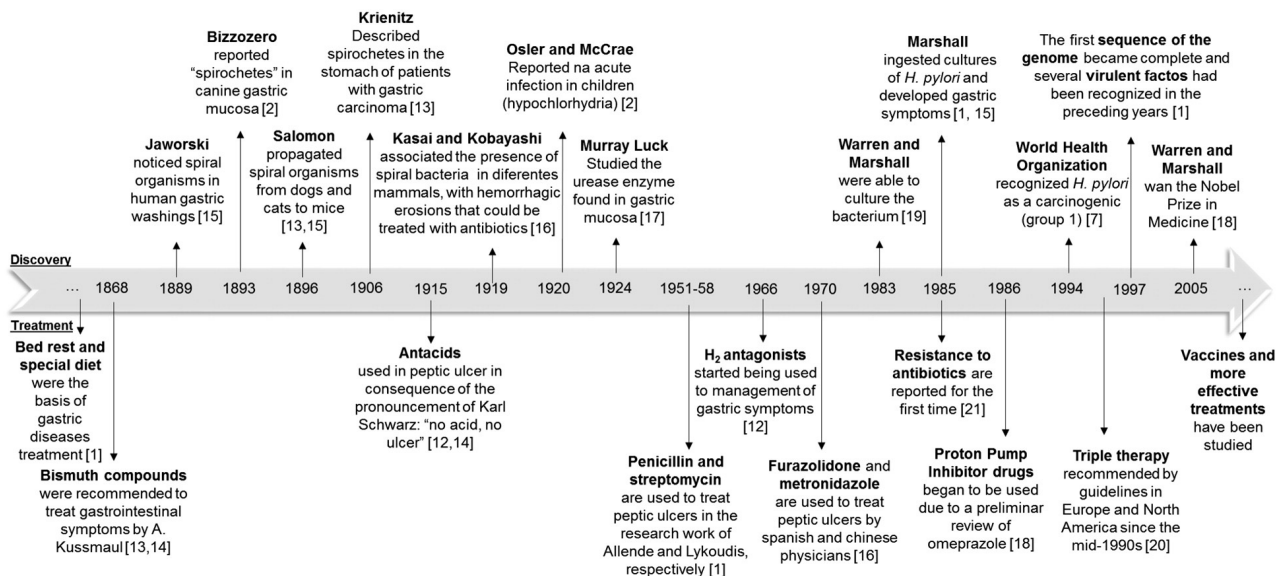
Fig. 1. Timeline of the *H. pylori* discovery and the progress of the therapy against the bacterium.

presence of "spirochetes" in canine gastric mucosa [2]. Bizzozero hypothesized that the bacterium could turn off acid secretion or tolerate the acidic environment [16]. Bizzozero's work was followed by Salomon, through the discovery of the propagation of spiral bacteria from dogs and cats to mice in 1896 [13,15]. These findings are the groundwork of the current studies of vaccines using *H. felis*-infected mouse [2]. Afterwards, spirochetes were found in the stomach of patients with gastric carcinoma by W. Krienitz, in 1906 [13].

In 1910, the Croatian Karl Schwarz pronounced the famous phrase "no acid, no ulcer" that lead to the use of antacids (*e.g.* magnesium and aluminium hydroxide) for symptomatic relief of ulcers in 1915 [12,14]. In 1919, Kasai and Kobayashi reported the presence of the spiral bacteria in several mammals, recognizing that it could cause hemorrhagic erosions which could be healed by resorting to several antimicrobials [16]. One year later, Osler and McCrae described an epidemic acute infection in children, characterized by a vomiting with neutral pH of the gastric juice, denominated hypochlorhydria [2]. In 1924, Murray Luck studied the urease enzyme found in gastric mucosa, mistakenly believing that it was naturally produced by gastric mucosa cells [17]. In the 1950s, the study of urease continues with the research work of Fitzgerald and Murphy, who found gastric urease in patients with peptic ulcers and believed that urease was produced to protect gastric mucosa [17].

Although participants in a society that considered the stomach as a sterile environment due to the acidic environment, Allende and Lykoudis reported the treatment of peptic ulcers with penicillin (1951) and streptomycin (1958), respectively [1]. However, this hypothesis was rejected by the medical community [1]. During the year of 1957, Charles Lieber and LeFevre discovered that the treatment with antibiotic promoted the decrease of the conversion from urea to ammonium [16]. They concluded that the gastric urease must be related to the presence of the bacteria [16]. Around 1966, H_2-antagonists came to be used to improve the management of gastric symptoms as a consequence of the discovery of gastric histamine receptors [12]. During the 70s, several Spanish and Chinese physicians reported efficacy of furazolidone and metronidazole to treat patients with ulcers [16].

The interest in these spirochetes began to spread worldwide, involving researchers from several countries, who reported the presence of the bacteria in the human gastric mucosa and noticed the curing of gastric diseases using antibiotic therapy [16,18]. However, in the 1960s and 1970s, physicians and microbiologists believed that the stomach was sterile since they obtained negative bacterial cultures and therefore all the evidences of the presence of spirochetes in the stomach were undervalued [17].

Against the skepticism of almost all the scientific community, Robin Warren and Barry Marshall believed that there was a direct association between the bacteria and gastric ulceration [13]. Evidences that served as clues included the presence of spiral bacteria in the stomach and its possible relation to gastric urease, epidemic hypochlorhydria and the efficacy of antibiotics to treat peptic ulcers [16]. Warren and Marshall noticed the immune response in hosts of *H. pylori* and described microbiological properties of these bacteria, including the similarity with the *Campylobacter* species [14]. During Easter break, a plate was incubated during 5 days, more than the usual attempt of 3 days, and when Marshall returned to the laboratory he found numerous colonies of *Campylobacter*-like organism [15,17]. Firstly named *Campylobacter pyloridis* and afterwards corrected to *Campylobacter pylori*, the bacterium is currently named *Helicobacter pylori* as it is a completely different genus [1,15]. In 1983, they reported in *Lancet* the first culture of the bacteria and, in 1985, Marshall ingested cultures of *H. pylori* in an attempt to fulfill the Koch postulate, promoting gastric symptoms healed afterwards by resorting to antibiotics and bismuth salts [1,15,19]. The magnitude of this discovery is a direct consequence of the persistence against the acid-induced ulceration dogma and skepticism, being recognized in 2005, by the award of the Nobel Prize in Physiology or Medicine [13,18].

In 1986, an initiatory review of omeprazole was published, opening the use of the proton pump inhibitor drugs [18]. The treatment of

H. pylori infection was improving from a double ineffective therapy, combining a PPI plus clarithromycin or amoxicillin to the current triple therapy recommended by guidelines in Europe and North America since the mid-1990s [1,20]. However, the first report of the resistance to metronidazole had already been published in 1985, followed by reports mentioning the resistance to other antibiotics, namely β-lactams, tetracyclines, fluoroquinolones, rifamycins and nitrofurans [2,21].

In 1994, the US National Institute of Health recognized *H. pylori* as the main cause of peptic ulcers and, in the same year, it was categorized by the World Health Organization as a carcinogenic (group 1) [1,7]. With the recognition of the foremost role of *H. pylori* in the origin of gastric diseases, thousands of research works have been published about the microbiology of the bacterium, including the sequence of the genome (1997), novel virulent factors and mechanisms of resistance to antibiotics [1]. Improvements in diagnostic tests and prophylactic methods (vaccines) are also being studied [1]. Nowadays, one of the foremost research subjects is the improvement of the current therapy.

2.2. Current therapy and its limitations

The treatment plan currently adopted as a first-line option includes a combination of a proton pump inhibitor, clarithromycin and amoxicillin or metronidazole/tinidazole, according to International Guidelines [10, 22]. This therapy persists during 7 to 14 days, twice a day [10]. Eradication rates of *H. pylori* treated with a 14-day triple therapy reached only 70% in non-ulcer dyspepsia patients and 80% in patients with peptic ulcer [10]. In Europe, Asia and North America rates of 20 to 45% have been reported [23]. This eradication rate is distant from the desirable rate to infectious diseases and from that proposed by the WHO [22, 24]. The main limitation of the current therapy results from the lack of therapeutic compliance, due to the incidence of side effects and the discomfort resulting from the multiple doses [25,26]. This factor may lead to the development of antibiotic resistance [26]. Moreover, antimicrobial agents such as amoxicillin and clarithromycin are degraded by gastric acid [24]. Therefore it is necessary to use higher doses, which is reflected in the increase of gastrointestinal side effects, namely diarrhea, nausea, vomiting, bloating and abdominal pain, and consequently the discontinuation of the therapy [26]. Another important reason is the antibiotic resistance that *H. pylori* has been developing, for instance the resistance to metronidazole has reached around 40% in developed countries and exceeds 90% in developing countries [27]. The resistance to clarithromycin has also been increasing, reaching more than 20% in southern Europe [23]. The bacteria are sensitive to other antimicrobial drugs, nevertheless they cannot be used in acidic medium [24]. Notwithstanding, the antibiotic residence time in the stomach is insufficient to achieve significant concentrations capable of crossing the gastric mucosa and reaching the surface between the mucus gel layer and the epithelial cells, where the *H. pylori* resides [3,4]. Although drug solutions reach the gastric luminal region, their absorption into deeper layers of the gastric mucosa is hampered by the mucous layer barrier [28].

In order to increase the efficacy of *H. pylori* eradication, different proposals have been made, namely a bismuth-containing quadruple (BCQ) therapy, sequential and concomitant treatment and the use of novel antibiotics, such as rifabutin [11,29]. However, these options may have to take into account that the complexity of the treatment plan, including the switch halfway in the sequential treatment and the large number of pills in concomitant and BCQ therapy, may decrease therapeutic compliance [11,29]. To overcome these limitations, novel effective therapies have been proposed: probiotics [30,31], phytomedicine [31], gastroretentive systems, namely floating drug delivery systems [32,33] and in a preventive approach, the attempt to develop an effective vaccine [23]. One of the foremost promising therapies that have recently emerged is based on the use of micro- or nanoparticles for direct contact with the *H. pylori*, through drug delivery techniques or mucoadhesive properties. This review will summarize all of the assays reported using micro/

nanoparticles applied to gastric delivery in order to increase *H. pylori* eradication rates.

3. Micro- and nanotechnology applied to eradication of *H. pylori*

Small particles (SPs), more specifically microparticles (MPs) and nanoparticles (NPs), have unique physical and chemical properties resulting from their small size, such as the high surface-to-volume ratio and their reactivity [34]. According to the concept used by the majority of the authors cited, the terms "microparticle" and "nanoparticle" will be used to refer to particles with a diameter of 1–999 μm and 1–999 nm, respectively. Each of these particles can be manipulated in order to achieve size, shape, chemical characteristics and specific ligands enhancers of molecular interactions [34]. For instance, positively charged particles may be attracted to gastric mucosa, since it is negatively charged due to several surface groups, *viz.* sialic acid, carboxyl or sulfate groups [28,35]. Additionally, *H. pylori* also is negatively charged, which may play an important role in the interaction with SPs [24]. Faced with the serious emerging problem of bacterial resistance to antibiotics, several antibiotic-loaded SPs have proven their usefulness and efficacy both *in vitro* and in animal models [36]. SPs also allow a sustained therapy since they can achieve higher retention time in the human body compared with small molecules of antibiotics [37]. Approaching the ideal "magic bullet", it is possible to use this technology to target almost exclusively the bacteria, allowing the use of higher doses without increasing side effects [38]. Some authors defend that size plays a central role in the SPs' diffusion into the gastric mucosa to reach *H. pylori*, since NPs with more than 200 nm have a decreased diffusion [24,39,40]. In fact, Hasani et al. (2009) referred to a size-dependent particle deposition in the inflamed tissue of gastric ulcers, observing that NPs of 50 nm present higher adhesion than NPs of 750 nm [39]. Additionally, some authors believe that submicrometer size is the key to the bacteriostatic effect of nanoparticles since their ability to penetrate the damaged bacterial membrane depends on their size [41]. On the other hand, NPs have an evident tendency to premature drug leakage [39]. Additionally, it is argued that microparticles, such as magnetic particles, are also able to pass between epithelial cells

and present lower toxicity and interaction with the immune system [42]. Polymeric microparticles have also been used as drug carriers due to the possibility to use mucoadhesiveness to target mucus and increase the retention time in the stomach [43]. It is also defended that SPs cannot be excessively small to avoid internalization by gastric cells and to enhance the *H. pylori*:particle ratio [44]. The relation between MP and NP size and the length of a *H. pylori* bacterium are demonstrated in Fig. 2.

Other advantages of encapsulated antibiotics include the controllable release and identical distribution in the infected tissue, the increase of pharmacokinetic properties of antibiotics, namely lipophilicity, and the reduction of collateral effects leading to the increase of therapeutic compliance [37]. Another pharmacokinetic limitation that may be overcome with drug delivery is the degradation of antimicrobial drugs by acidic pH. In fact, the pH of the stomach lumen is about 1 to 2 [45]. However, adding the secretion of HCO_3^- molecules to the capability of the mucus layer to resist to protons diffusion, a pH gradient is established from acid in the lumen to near neutral at the interface between the mucosa and epithelial cells (Fig. 2) [45,46]. Hence, the pH of the gastric mucus layer varies between 4 and 6.5, with the exception of occasional acid decreases to pH < 2 when the mucus layer is injured [47]. Additionally, the production of urease by the bacterium results in the production of ammonia, maintaining periplasmic and cytoplasmic pH of the bacterium near to neutral even in the presence of acid shocks [1,47]. Therefore, the release of the antimicrobial drug near the site of infection of *H. pylori* may protect the drug from acid degradation. Furthermore, it is improbable that bacteria might develop resistance to SPs because numerous and complex gene mutations would be necessary to overcome either the multiple mechanisms of action of antimicrobial SPs as well as the possibility to combine different antimicrobial drugs in the same carrier [38]. Their micro- and nanosize can also be used to develop vaccines since they are recognized by the immune system through their similarity to the bacteria and virus size [37]. Hence different particles (MPs and NPs) have been studied in order to increase the eradication rate of *H. pylori* infection. These novel systems will be the focus of this review, particularly liposomes and polymeric, magnetic and metallic systems.
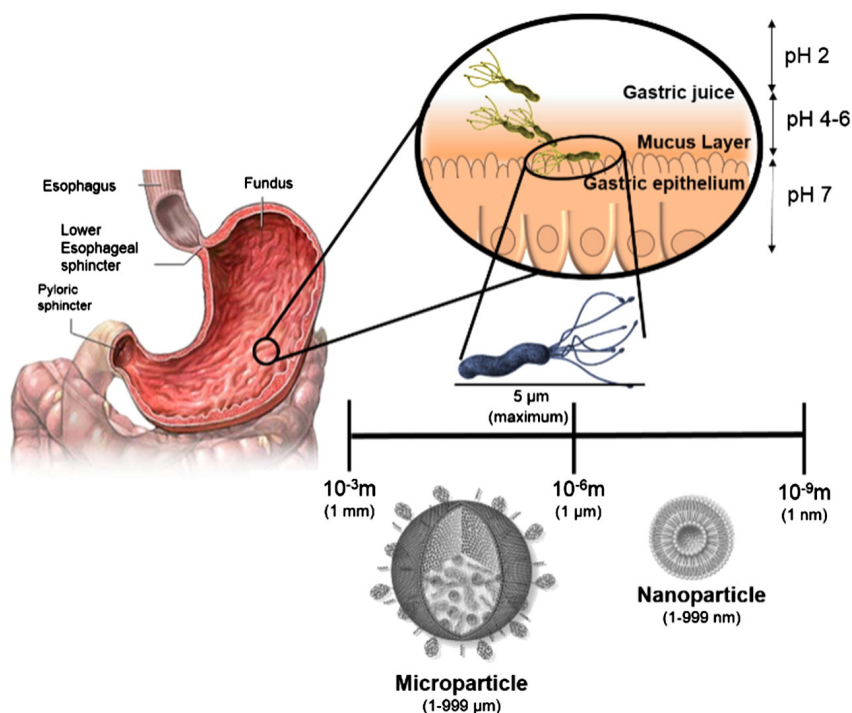
Fig. 2. Use of micro- and nanotechnology to active and passive targeting of *H. pylori*, highlighting the relation between the size of MPs and NPs and the length of the *H. pylori* bacterium.

40

3.1. Liposomes

Liposomes are spherical vesicles composed of amphiphilic lipids in a bi- or multilayer with an aqueous core. Liposomes have been used to encapsulate several compounds, such as enzymes, proteins and drugs with different targets [37]. Liposomes are also the most studied NP worldwide to deliver antimicrobial drugs [37]. The foremost important advantage is the use of biocompatible and biodegradable constituents, which allows the use of liposomes without significant toxicity [47,48]. They are also versatile drug carriers since their physicochemical properties can be easily transformed by changing the phospholipids, their proportion and size, their charge and even their sensitivity to external stimuli, such as pH and temperature [47,48]. Their versatility applies even to the drugs capable of being encapsulated, allowing the encapsulation of both hydrophilic and hydrophobic drugs and the coencapsulation of two or more drugs [28,48]. Additionally, their similarity to the cell membrane allows fusion with microbes by endocytosis [34,37]. In fact, it has been shown that the probability of inducing drug resistance is lower when the basis of the antibacterial mechanism is a fusion between the liposome and the bacteria [27].

In the specific case of H. pylori infection, phospholipids can also create a hydrophobic layer able to avoid bacterial attachment to the mucosa and provide fatty acids to repair the gastric mucosa [28]. Additionally, it is possible to benefit from the vacuolated protein synthesized by most of H. pylori strains to destabilize the bilayer [24]. Further, it is possible to use phosphatidylethanolamine (PE) for selective binding to the receptors present on the bacterium, allowing active targeting and blocking the adhesion of the bacteria to the gastric mucosa [3,24].

Given all the abovementioned advantages, several studies have been performed in order to develop a novel system for H. pylori eradication through the use of liposomes (Table 1).

3.1.1. Simple liposomes

Simple liposomes have been studied in order to encapsulate antibiotics. For instance, Bardonnet et al. (2008) designed two different liposomes loading metronidazole and ampicillin, consisting of 1,2-dipalmitoyl-sn-glycero-3-phosphocholine (DPPC) or epikuron 170 (E170) and both having cholesterol (Ch) [24]. In both formulations a synthetic glycolipid containing fucose was incorporated since some strains of H. pylori are able to link to fucosylated Lewis b antigens

Table 1
Physicochemical properties of reported liposomes and their mechanism of action associated with H. pylori eradication.

		Particle composition	Physicochemical properties of the optimized particle		Mechanism of action	Ref. (year)
Simple liposomes	Antibiotics	1. Cholesterol + DPPC 2. Cholesterol + E170 (with at least 10% of phosphatidilethanolamine (PE)) At both formulation a synthetic glycolipid was added	Size (nm) ζ-potential (mV) PDI %EE	147 –> 163 -20.0 (E170-Ch-glycolipid) –> -2.9 (DPPC-Ch-glycolipid) 0.10 –> 0.11 4.8 (DPPC-Ch-glycolipid with Ampicillin) –> 13.9 ± 1.0 (E170-Ch with Ampicillin)	Encapsulation of antimicrobial drugs (Metronidazole and Ampicillin). Glycolipid containing fucose and PE in formulations with E170 are used as a specific ligand to H. pylori	[24] (2008)
		a) Hydrogenated L-α-phosphatidylcholine b) Cholesterol c) Linolenic acid	Size (nm) PDI ζ-potential (mV)	88 ± 3 0.17 ± 0.01 -78 ± 4	The liposome fuses with the bacterial membrane, loading linolenic acid, which presents antibacterial activity	[27] (2012)
	Vaccines	a) Phosphatidylcholine b) Cholesterol	Size (nm) %EE	100 – 500 71.4 before and 68.6 after 1 month of storage at 4 ºC	Delivery of a recombinant peptide composed of CTB and urease B subunit epitope to induce prophylactic and therapeutic protection	[51] (2007)
		a) Dioleyphosphatidylethanolamine b) Dimethylaminoethanecarbamolch olesterol c) Polyethylene glycol 2000-PE	No data available		Delivery of a multi-epitope DNA-prime/peptide-boost vaccine to induce immune protection	[52] (2011)
	Antisense oligonucleotides	Cationic liposome using a commercial transfection reagent (N-[1-(2,3-dioleoyloxy)propyl]-N,N,N-trimethylammonium methyl-sulfate)	No data available		Encapsulation of an antisense oligonucleotide for p-50 (NF-kB dimer) in order to decrease the gastric injuries induced by the activation of iNOS	[53] (2001)
Double liposomes	Antibiotics	Common to inner and outer liposomes: a) Phosphatidylcholine b) Cholesterol Specific of inner liposome: a) Stearylamine (SA) Specific of outer liposome: a) Phosphatidilethanolamine	Optimized formulation: PC:Ch:SA (7:3:0.1) and PC:Ch:PE (7:3:0.1)		Delivery of an antimicrobial drug (AMOX in outer liposome) and a drug with both antimicrobial and antacid properties (RBC in inner liposome). PE is used as a specific ligand to the bacteria	[47] (2011)
			Size (μm) % EE (RBC/ inner liposome)	1.2 –> 2.4 (inner liposomes) 6.7 –> 8.2 (outer liposomes) 33		
			Optimized formulation: PC:Ch:SA (7:3:0.5) and PC:Ch:PE (7:3:0.2)			[54] (2012)
			Size (nm) PDI ζ-potential (mV) %EE	791.6 ± 0.4 0.087 11 ± 0.8 Amoxicillin: 67.9 ± 1.1 RBC: 72.6 ± 1.2		

PDI = polydispersity index.
EE = encapsulation efficiency = ratio between the actual and theoretical amount of amoxicillin drug loaded.

through a membrane protein (BabA2) [24]. Characteristics of the NP are described in Table 1. The encapsulation efficiency (EE) varies among the formulations, depending on the phospholipid and on the drug, reaching the maximum of 13.9% in the formulation with E170 and Ch [24]. Despite the low EE, liposomes with DPPC–glycolipid–Ch contained sufficient antimicrobial drug to achieve an antimicrobial effect [24]. Nevertheless, the authors assumed that the method can be improved [24]. Epifluorescent microscopy studies showed that Ch may play an important role in the interaction between the bacteria and liposomes, due to the already studied affinity of *H. pylori* to this steroid [24]. The synthesized glycolipid demonstrated to be important in the interaction with coccoid forms of specific *H. pylori* strains, namely those which expressed BabA2 [24]. In spite of the promising results from the evaluation of the bacterium–liposome interaction, effectiveness studies of this interaction in killing the bacteria are lacking [24]. The same research group performed new assays to evaluate the stability of liposomes in acidic conditions [49]. The results showed that these liposomes decrease the internal pH to pH 4 when drastic conditions are imposed, namely pH 1.2 to 2 [49]. This fact makes this system suitable to be used to encapsulate drugs such as amoxicillin and clarithromycin whose half-life time is significantly higher at pH 4 compared to pH 2 [49]. Actually, the half-life time of these drugs are 19.0 h and 176.9 h (amoxicillin) and 1.3 h and 96.7 h (clarithromycin), at pH 2 and pH 4, respectively [49]. Additionally, agglutination assays confirmed the chemical stability of the synthetic glycolipid [49]. In 2012, Obonyo et al. developed a novel antibacterial nanoparticle, using linolenic acid as an antibacterial drug [27]. Amphiphilic properties of linolenic acid (LLA) allowed the incorporation into the phospholipid bilayer of a liposome composed of hydrogenated L-α-phosphatidylcholine, cholesterol and LLA [27]. Contrary to that observed in conventional therapy, namely amoxicillin, the novel NP killed both spiral and coccoid forms of the bacterium [27]. The NP was also effective in killing all strains of *H. pylori*, even a strain resistant to metronidazole [27]. The bacterium did not acquire drug resistance when sub-bactericidal concentrations of the NP were evaluated, opposed to those observed with metronidazole and free LLA [27].

Simple liposomes have also been studied as an alternative to overcome the limitations of the development of successful vaccines. Although a prophylactic approach may seem a powerful and economic way to control the infection by *H. pylori*, especially in developing countries, the development of a vaccine able to cause full sterilizing immunity in animal models have faced several problems [50–52]. In fact, pharmaceutical companies have decreased their investment in this field for the past 10 years [50]. However, novel vaccination strategies have emerged using selected antigens correlated with the pathogenesis of this infection [51]. Liposomes are an attractive delivery system because they are able to protect the payload from the hostile gastric environment making oral delivery possible, promote a sustained release and cause immunological responses [51]. In 2007, Zhao et al. used *Escherichia coli* to express a fusion peptide (CtUBE) composed of a cholera toxin B subunit (CTB) and a urease B linear epitope [51]. CTB was used due to its properties as a carrier, adjuvant and immunogen compound [51]. Despite a small portion of vaccinated mice (14.3%) that developed minor or moderate gastritis, urease and histological tests and quantification of *H. pylori* colonies in mouse stomach showed that vaccinated mice were significantly protected from *H. pylori* infection [51]. The nanoparticle also showed therapeutic properties, promoting a significant reduction in the load of *H. pylori* in the stomach [51]. The increase of specific serum IgG and mucosa IgA corroborated abovementioned results [51]. Although protection response was correlated with Th1 lymphocyte response, further studies are necessary to understand the mechanism behind its prophylactic and therapeutic actions [51]. Later, Moss et al. resorted to informatic tools to design an intranasal multi-epitope DNA-prime/peptide-boost vaccine encapsulated in liposomes [52]. Contrary to that observed in the administration of *H. pylori* lysate or an empty plasmid intranasally or even the novel vaccine administered intramuscularly, the intranasal vaccine showed therapeutic effects [52]. As a consequence of the induced immune response, *H. pylori*

infection significantly decreased [52]. Further studies are necessary to understand the enhanced effectiveness of the intranasal route [52].

In an indirect approach, liposomes have also been used to encapsulate antisense oligonucleotides since they can improve their stability and intracellular delivery [53]. Previous studies showed that inducible nitrite synthase is increased in gastric mucosa of *H. pylori* infected patients, being the production of NO responsible for gastric injuries [53]. In fact, Lim et al. (2001) reported the relation between *H. pylori* and the activation of an oxidant-sensitive transcription factor (nuclear factor κB or NF-κB), which led to the induction of iNOS expression and nitrite NO production [53]. Ultimately, it was shown that the bacteria induce apoptosis in gastric epithelial AGS cells (human gastric adenocarcinoma cell line) [53]. Similar to what had been observed with antioxidants, catalase and an inhibitor of NF-κB, a liposome loading antisense oligonucleotides for p50 (NF-κB dimer) was able to inhibit the increase of p50 and decrease iNOS expression and nitrite production [53]. Thus, apoptosis of gastric cells decrease [53].

3.1.2. Double liposomes

Given the lack of conventional liposomes, such as low entrapment efficiency, instability and unsustained release due to the possibility of a breach in the phospholipid bilayer, double liposomes have been studied [47]. They are composed of smaller liposomes inside a lipid bilayer, which protect inner liposomes against external risk [47]. Double liposomes have a higher drug loading capacity, higher stability and can prevent chemical change in free drugs, being seen as an effective delivery system [47,54]. However, the instability resulting from storage at high temperatures may be more pronounced in double liposomes due to their large size [54].

Singh et al. (2011) developed a double liposome loading ranitidine bismuth citrate (RBC) in the inner liposome and amoxicillin trihydrate in the outer liposome [47]. *In vitro* drug release showed that after 12 h, only 32.6 ± 1.5% of amoxicillin and 20.3 ± 2.8% of RBC were released [47]. Although higher than what had been observed with plain amoxicillin + RBC, the % of growth inhibition was 86.75% [47]. Agglutination assays revealed clumps of *H. pylori* when treated with double liposomes, reflecting the vectorization towards the bacterium when the nanoparticle is functionalized with PE [47]. In the following year, Jain et al. performed novel assays with a new optimization of the double liposome designed by Singh et al. [54]. *In vitro* drug release studies showed a sustained release of both drugs [54]. Stability studies showed an increased size of vesicles and a decrease in the number of vesicles/mm³ when stored at 28 °C [54]. Additionally, a significant loss of drug was observed after 30 days of storing both at 4 °C and 28 °C [54]. Despite the instability under room temperature, the results of *ex vivo* and *in vivo* studies are promising. *H. pylori* growth inhibition was higher in the presence of DL, compared with free amoxicillin + RBC [54]. *In vivo* studies using albino rats supported the enhanced antisecretory and ulcer-protective action of double liposomes when compared to amoxicillin + RBC [54].

3.2. Polymeric particles

Polymeric particles are extensively studied due to their mechanical stability and loading capacity [3]. Additionally, it is possible to modify their biodistribution characteristics, resorting to the change of physicochemical properties such as size [55]. Indeed, the surface of polymeric particles can be personalized in order to augment interactions with the target cell and with the immune system [56]. Several polymers also have mucoadhesive properties, which are suited to enhance the residence time in the stomach and to overcome lower absorption of several drugs [25,55]. Polymeric particles can also protect drugs from proteolytic enzymes, increasing oral bioavailability [56]. Furthermore, polymers usually present several mechanisms to combat microbes, hence it is unlikely that *H. pylori* would develop resistance against

them [38]. Therefore, polymers have been the subject of study for application in *H. pylori* eradication.

3.2.1. Polyacrylic acid

Polyacrylic acid or carbopol is a mucoadhesive polymer, being used to encase other compounds in order to increase their mucoadhesiveness [57]. In fact, mucoadhesion to the stomach and small intestine of rats was proven both *in vitro* and *in vivo* [57].

In 2001, Cuña et al. developed an amoxicillin-loaded ion-exchange resin encased in a polymeric microsphere [58]. The size of the microsphere was 133 ± 39 μm and the mass percentage of the drug relative to the coated drug-resin complex was 7.87 ± 0.35% (w/w) [58]. The authors concluded that carbopol 934 microparticles as well as an attempt with polycarbophil failed in significantly prolonging retention time in the stomach [58]. Additionally, distribution of amoxicillin-resin on the mucosa was better when no-polymer was coated [58]. In 2012, Harsha developed an oral suspension with pure amoxicillin and amoxicillin loaded in nanospheres of 200 to 404 nm [59]. Encapsulation efficiency was 85.5 ± 0.7% [59]. Studies of drug release demonstrated an initial burst effect, followed by a controlled release during 12 h [59]. The formulation was stored as dry suspension and further reconstituted with xantham gum before use [59]. At low temperatures (3–5 °C) or at room temperature and during 12 months, amoxicillin did not change either in external morphology or drug content [59].

3.2.2. Proteins

There are several advantages in using proteins as drug carriers (summarized in Table 2), highlighting their biodegradability, non-antigenic properties, nutritional value and the existence of rich and renewable sources [60].

Gliadin consists in a group of proteins extracted from gluten [61]. Gliadin nanoparticles have been studied as a possible drug carrier for *H. pylori* eradication due to theirs mucoadhesive properties and their tropism for upper gastrointestinal areas [61]. Additionally, their small size allows penetration into the gastric mucosa and their hydrophobicity permits the development of nanoparticles able to protect the antibiotic and control its release [62,63]. Umamaheshwari and Jain (2003) used acetohydroxamic acid-loaded gliadin nanoparticles (GNP) combined with fucose-specific (Ulex Europaeus agglutinin I lectin — UEA I) or with mannose-specific (conconavalin A lectin — Con A) lectins to eradicate *H. pylori* [62]. In fact, lectins are known to bind to bacterial surface carbohydrates, allowing active targeting [62]. Additionally, peptides and proteins coated with lectin ensure higher protection against digestion and enhance uptake [60]. Studies confirmed the enhancement of affinity to pig gastric mucins and the ability to agglutinate *H. pylori*, contrary to that observed with GNP alone [62]. *In vitro* growth inhibition studies demonstrated the efficacy of GNP functionalized with lectins, reaching about 95% when Con A GNP is used [62]. *In situ* adherence studies demonstrated the capacity of lectins to plug the carbohydrate receptors and, subsequently, the inhibition of the attachment of the bacteria to the mucosa [62]. In the following year, the same research group used gliadin nanoparticles to delivery amoxicillin [63]. Amoxicillin release was controlled by gliadin nanoparticles, however in the presence of pepsin (stomach enzyme) the release rate was higher due to the digestion of gliadin [63]. Evaluating mucoadhesion in albino rats, the authors found that 82% of the nanoparticles remained after 2.5 h which corroborates the mucoadhesiveness of gliadin nanoparticles [63]. Although plain amoxicillin showed faster and complete growth inhibition *in vitro*, *in vivo* clearance demonstrated that complete eradication was not achieved even when using the highest dose, contrary to that

Table 2
Physicochemical characteristics and mechanism of action of micro- and nanoparticles composed of proteins, more specifically gliadin and gelatin, and applied to *H. pylori* eradication.

	Particle composition	Physicochemical properties of the optimized particle			Mechanism of action	Ref. (year)
Proteins to deliver antibiotics	a) Gliadin b) Pluronic F68 c) Con A or UEA I	Size (nm)	422 ± 12 (UEA–GNP)		Carrying of acetohydroxamic acid to eradicate *H. pylori* using active targeting	[62] (2003)
			419 ± 20 (ConA – GNP)			
		ζ–potential (mV)	26.6 ± 0.8 (without functionalization)			
		% EE (w/w)	58.2 ± 3.2			
	a) Gliadin b) Pluronic F68	Size (nm)	312 ± 12		Delivery of amoxicillin using mucoadhesiveness of gliadin nanoparticles	[63] (2004)
		ζ–potential (mV)	26.6 ± 0.8			
		% Payload	61.52 ± 2.2			
		% EE	66.54 ± 3.8			
	a) Gliadin b) PluronicF68	Size (nm)	250 → 500	Varying drug: gliadin ratio	Delivery of clarithromycin using mucoadhesiveness of gliadin nanoparticles	[64] (2006)
		ζ–potential (mV)	22.8			
		% EE	43.7 ± 2.3 → 73.1 ± 1.3			
	a) Gliadin b) Pluronic F68	Size (nm)	450–600	Varying drug: gliadin ratio	Encapsulation of clarithromycin (antibacterial properties) and omeprazole (antacid properties) using gliadin as a mucoadhesive component	[61] (2008)
		ζ–potential (mV)	22.8			
		% EE (maximum)	CLA: 53 ± 2.3 → 86.1 ± 1.3			
			OME: 49.6 ± 2.8 → 73.7 ± 3.9			
	a) Gliadin b) Pluronic F68 c) Con A	Size (nm)	620 ± 83		Encapsulation of a triple therapy (amoxicillin, clarithromycin and omeprazole) using gliadin as a mucoadhesive component and lectin as a specific binding	[65] (2008)
		ζ–potential (mV)	27.46			
		% EE	AMOX: 84.6 ± 1.34			
			CLA: 90.28 ± 1.83			
			OME: 66.2 ± 2.27			
	a) Aminated gelatin b) Glutaraldehyde	Size (μm)	46 –> 55 (depending on the % of glutaraldehyde)		Delivery of amoxicillin using mucoadhesiveness of aminated gelatin	[66] (2000)
	a) Gelatin	Size (nm)	50–1000 (average diameter was 571 nm)		Immediate and sustained release of amoxicillin	[67] (2013)
		% drug content	89.2 ±0.5			

EE = encapsulation efficiency = ratio between the actual and theoretical amount of amoxicillin drug loaded.
Payload = encapsulated drug/gliadin nanoparticle yield.
Drug content = weight of drug in nanoparticle/total weight of the nanoparticle.

43

observed with nanoparticles [63]. In 2006, they tried to use gliadin nanoparticles to encapsulate clarithromycin [64]. These nanoparticles proved their mucoadhesiveness through *in vitro* and *in vivo* studies, being suitable for localized delivery, especially to the upper region of the stomach [64].

In 2008, Ramteke and Jain tested clarithromycin- and omeprazole-containing gliadin nanoparticles [61]. A sustained release and mucoadhesiveness were proved through *in vitro* and *in vivo* methods and a synergic effect in *H. pylori* growth inhibition was observed when clarithromycin-NP and omeprazole-NP were used simultaneously [61]. This synergic effect may be due to the improvement of antibacterial activity of clarithromycin at higher pH [61]. Although higher than that of the plain drugs, % of growth inhibition of both NPs combined was only 83.7% [61]. The same research group (2008) developed lectin-conjugated gliadin nanoparticles in order to deliver a triple and synergic therapy (amoxicillin, clarithromycin and omeprazole) [65]. When compared with gliadin nanoparticles, lectin-conjugated gliadin nanoparticles revealed an enhancement in *in vitro* antibacterial studies and *in vivo* clearance, reaching 94.83% and 83.3% of eradication and clearance rate, respectively [65]. Similarly, *in vitro* and *in vivo* studies of mucoadhesive properties showed a slight increase of adhesion to the mucosa when the nanoparticles were coated with lectin [65].

Gelatin has also been studied due to its long history of security and safety, being used in pharmaceuticals, cosmetics and food, based on its Food and Drug Administration (FDA) classification as GRAS (generally regarded as safe) [60]. Wang et al. (2000) tested aminated gelatin microspheres due to the possibility of a positive charge increase in electrostatic attraction to the mucosa [66]. Several parameters, such as the % of

glutaraldehyde, the time of cross-linking reaction and the higher pH, contributed to a sustained release [66]. Modified gelatin microspheres demonstrated a slower release comparatively with microspheres of regular gelatin with the same % of glutaraldehyde [66]. *In vivo* studies proved that aminated gelatin microspheres have a higher gastric retention time, however further studies are necessary to understand the mechanism behind mucoadhesiveness of these microspheres [66].

Harnessing the mucoadhesiveness of gelatin, Harsha (2013) designed a suspension for immediate and sustained release of amoxicillin using gelatin nanoparticles [67]. Amoxicillin-loaded gelatin microspheres were added to a suspension containing xantham gum, D-sorbitol powder and citric acid as major components [67]. Nanoparticles were able to induce a sustained and controlled release of amoxicillin during 12 h and were stable for 24 months even under hostile conditions (25 °C and 60% humidity) [67]. Supplementary studies are necessary to confirm their effectiveness in *H. pylori* eradication [67].

3.2.3. Polysaccharides

Polymeric carbohydrate molecules, named polysaccharides, such as chitosan and alginate, have also been used against *H. pylori* (Table 3).

Chitosan is a linear and cationic polymer, composed of D-glucosamine and obtained from chitin deacetylation [68]. It has been suggested as a promising drug carrier owing to its mucoadhesiveness and biocompatibility [25]. Since it is positively charged, it can interact with sialic acid residues of mucin in the stomach which present a negative charge [69]. It also may be useful for drug release in response to pH decrease, due to swelling of chitosan microspheres in acidic medium [69]. Furthermore, several reports proved a broad-spectrum antimicrobial effect of chitosan

Table 3
Physicochemical properties and mechanism of action of particles composed of polysaccharides, namely chitosan and alginate, applied to eradication of *H. pylori*.

		Particle composition	Physicochemical properties		Mechanism of action	Ref. (year)
Polysaccharides	Chitosan to deliver antibiotics	a) Chitosan (87% degree of deacetylation (DA))	Size (μm)	Amoxicillin 50	Metronidazole 50	Local amoxicillin and metronidazole delivery	[73] (1999)
			%EE	81.2 ± 4.5	99.4 ± 6.9		
		a) Chitosan (>80% DA)	Size (μm)	Amoxicillin ~10	Metronidazole ~10	Delivery of amoxicillin or metronidazole using mucoadhesiveness of chitosan	[74] (2002)
			%EE	Close to 100	29 → 60 (varying with reacetylation time)		
		a) Chitosan (85% DA) b) Glutaraldehyde	Size (μm)	50.4 → 98.2	At different polymer:drug ratio	Delivery of amoxicillin through encapsulation in a mucoadhesive microsphere	[25] (2007)
			%EE	38 → 70	and stirring speed		
		a) Chitosan (84%DA)	Size (μm)	2.5		Encapsulation of amoxicillin in a mucoadhesive microsphere	[77] (2012)
			%EE	76			
		a) Chitosan (87% DA)	Size (μm)	2.0-3.0		Delivery of tetracycline through encapsulation in a mucoadhesive microspheres	[69] (2002)
			ζ-potential (mV)	26.68			
			%EE	8.04 ± 0.00 when added before cross-linking			
				69.37 ± 5.84 when added to preformed microspheres			
	Chitosan and its antibacterial effect	a) Chitosan (88.5% DA) Or a) Chitosan (95% DA)		88.5% DA	95% DA	Use antibacterial properties of chitosan to eradicate *H. pylori*	[41] (2009)
			Size (nm)	96.12 (70 → 130)	96.16 (71 → 129)		
			PDI	0.16 ± 0.03	0.18 ± 0.05		
			ζ-potential (mV)	23 (pH 2) → -10 (pH 7)	25 (pH 2) → -8 (pH 7)		
		a) Chitosan (15% DA) b) Genipin c) Sodium triphosphate pentabasic	Size (μm)	170 ± 15		Use antibacterial and mucoadhesive properties of chitosan to remove bacteria from the stomach of infected people	[44,68] (2013)
			ζ-potential (mV)	-6 -> 30 (Depending on pH, crosslinking and on time periods of crosslinking)			
	Alginate and vaccines	a) Hidrophobically modified alginate	Size (μm)	9		Encapsulation of *H. pylori* urease in order to promote *in vivo* immunization	[82] (2004)
			%EE	65-70			

EE = encapsulation efficiency = ratio between the actual and theoretical amount of amoxicillin drug loaded.
PDI = polydispersity index.

[41,70]. A serious disadvantage is its higher solubility at acidic pH [68]. Nevertheless, this problem has been overcome by resorting to a crosslinking agent, such as glutaraldehyde or genipin [68]. Genipin, which is a naturally occurring cross-linking agent, presents lower cell toxicity compared to glutaraldehyde and can inhibit *H. pylori* colonization [71,72].

Several studies have been performed based upon the abovementioned in order to encapsulate antibiotics. For instance, Shah et al. (1999) developed chitosan microspheres in order to deliver amoxicillin and metronidazole to the site of infection [73]. However, a sustained release into simulated gastric fluid (pH 1.2) was not achieved, since chitosan microspheres were highly porous, which led to the release of amoxicillin and metronidazole in 2 h [73]. In 2002, Portero et al. used reacetylated chitosan microspheres to encapsulate amoxicillin and metronidazole since previous work had proven the interaction between these microspheres and the mucosa and the sustained delivery of amoxicillin [74,75]. Reacetylation was used to reduce chitosan solubility and its influence on *in vitro* release and antimicrobial properties of drugs was evaluated [74]. Reacetylation affected the encapsulation of metronidazole, reducing the encapsulation efficiency [74]. Antimicrobial activity depends on the reacetylation time, however if short reacetylation time is used, a sustained release is achieved without loss of antimicrobial properties [74]. Chitosan microspheres were also used by Patel et al. (2007) to encapsulate amoxicillin and the influence of different variables was tested [25]. Mucoadhesion decreased with the increase of stirring speed and with the decrease of polymer:drug ratio [25]. Stirring speed also had a negative effect on drug entrapment efficiency [25]. *In vitro* mucoadhesive tests also showed that some microspheres adhered even after 12 h [25]. Release studies demonstrated that amoxicillin was released more promptly in acidic pH than in basic pH [25]. *In vivo* studies revealed higher *H. pylori* clearance when microspheres were used compared to that observed with plain amoxicillin [25]. In 2010, Raval et al. characterized spray dried microspheres of amoxicillin [76]. Physicochemical and morphological studies revealed that by increasing glutaraldehyde concentration and the duration of crosslinking, the ability to swell decreases [76]. Additionally, the percentage of swelling is correlated with *in vitro* drug release, hence it may be possible to control permeability to solutes adjusting abovementioned parameters [76]. In 2012, Patel and Patil tested the synthesis of amoxicillin mucoadhesive microparticles using supercritical CO_2 as an alternative to conventional processing methods [77]. Application of this supercritical fluid technology to the development of novel microparticles was successful [77]. High mucoadhesion and a sustained release at both pH 1.2 and 7.8 was achieved [77]. *In vivo* studies with administration twice a day for three consecutive days revealed a higher antimicrobial effect of amoxicillin-loaded microparticles when compared to powder amoxicillin [77].

Tetracycline had also been encapsulated in chitosan microspheres despite being more stable than amoxicillin in acidic medium [69]. The first report was published by Hejazi et al. in 2002 [69]. Tetracycline-microspheres were dissolved at pH 1.2 and 2.0, leading to an abrupt and rapid release of the drug [69]. Although more gradual, the release at pH 3.0 and 5.0 was similar, releasing almost 70% after only 3 h [69]. Hejazi and Amiji continued this research and published in 2003 a novel report where they studied the gastric residence time of tetracycline-loading chitosan microspheres in gerbils using radioiodinated [^{125}I] chitosan microspheres and tritiated-[^{3}H]-tetracycline [78]. The results were disappointing, showing a similar retention profile between the tetracycline loaded and the plain tetracycline in aqueous solution [78]. The main conclusion of this study is that chitosan microspheres prepared by ionic cross-linking are not suitable if the aim is a longer residence time [78]. In this context, Hejazi et al. (2004) studied the influence of crosslinking on the gastric residence, obtaining higher residence times with microspheres produced by chemical crosslinking as opposed to those produced by ionic precipitation [79]. A review of their complete work was also published [80]. *In vivo* studies showed that although more efficacious than plain tetracycline, tetracycline-loaded chitosan microspheres revealed

lower reduction of the levels of the bacteria as well as the serum gastrin levels in comparison to a triple therapy (lansoprazole, amoxicillin and clarithromycin) [80].

Chitosan has also been used for a different purpose. Its bactericide effect and mucoadhesiveness may enable the use of particles of chitosan to adhere, kill and remove *H. pylori* from the stomach. With this purpose in mind, Luo et al. (2009) studied the antibacterial effect of nanoparticles of chitosan [41]. This research group performed *in vitro* and *in vivo* studies to confirm that chitosan nanoparticles present higher anti-*H. pylori* efficacy than chitosan powder [41]. In 2013, Nogueira et al. studied the influence of the gastric medium in the effectiveness of chitosan microspheres mimicked through an ultrathin chitosan film [70]. Chitosan was considered suitable for gastrointestinal use at pH 2.6, 4 and 6 and independent of the presence of urea [70]. However, adhesion of *H. pylori* to chitosan films was lower at higher pH and was remarkably reduced in the presence of pepsin [70]. Similarly, pepsin reduced the death of chitosan-adherent *H. pylori* [70]. Nevertheless, the antibacterial effect of chitosan was proven, reaching death of 93% at pH 2 and more than 75% of the bacteria at pH 6, when urea and pepsin were absent [70]. In the same context, Fernandes et al. studied the characteristics of genipin-stabilized chitosan microspheres under acidic pH [44]. In order to achieve stability in acidic medium without diminishing the microspheres' ability to link to mucins of the mucosa, crosslinking was performed using 10 mM of genipin and during 1 h [44]. Despite swelling to twice their size, these microspheres were stable during 7 days in SGF and revealed the ability to remain in the stomach during 2 h [44]. Further studies were performed, revealing the ability to bind different strains of *H. pylori* independently of pH and of the presence of pepsin, contrary to that observed in previous studies where Nogueira et al. used an ultrathin chitosan film [68]. These novel studies demonstrated microsphere efficiency in reducing the attachment between the bacteria and gastric cells in 50–76% and in 47–56% when added after and before *H. pylori*-gastric cell pre-incubation, respectively [68]. Although reducing 20% of cell metabolic activity, these microspheres were not considered cytotoxic according to ISO international standard 10993-5 [68]. Nonetheless, additional studies are necessary to verify if repeated treatments are sufficient to complete eradication of *H. pylori* [68].

Alginate is also a promising option for drug delivery due to its biocompatibility, low toxicity and inexpensiveness [81]. A hydrophobically modified alginate-based microparticle was developed by Leonard et al. (2004) with the purpose of creating a vaccine against *H. pylori* [82]. Hydrophobic interactions allowed good retention of proteins which are released upon addition of a surfactant or by hydrolysis by lipases [82]. Despite mucoadhesiveness of these microparticles, subcutaneous vaccination of mice obtained more promising results when compared with oral and nasal routes [82]. However, no statistically relevant conclusions can be deduced from these preliminary studies [82].

3.2.4. Copolymers

A few studies have been performed in order to study physicochemical properties of micro- and nanoparticles composed of a mixture of polymers with no loaded drug. For instance, in 2003, Miyazaki et al. developed microspheres composed of cellulose acetate butyrate and dextran derivatives and evaluated their mucoadhesiveness and retention time in the stomach [83]. Dextrans, which are polysaccharides used worldwide in the medical field, were able to increase mucoadhesive properties both *in vitro* and *in vivo* [83]. In 2009, Lin et al. resorted to a combination of the benefits of chitosan referred to in Section 3.2.3 with the advantages of heparin, namely its ability to heal gastric ulcers, to develop a particle with about 130 nm [84]. These nanoparticles were pH-sensitive through the ionization of chitosan and heparin at pH 1.2–6.5, resulting in a polyelectrolyte complex [84]. At pH 7.0, chitosan becomes deprotonated leading to the disintegration of the nanoparticles [84]. Fluorescence studies using AGS cells and mouse gastric epithelium showed the adhesion and uptake of nanoparticles by gastric cells and, as

Table 4

Physicochemical characteristics and mechanism of action of micro- and nanoparticles composed of polymer mixture to be applied to *H. pylori* eradication.

Particle composition	Physicochemical properties of the		optimized particle	Mechanism of action	Ref. (year)
a) Carboxyvinyl polymer b) Curdlan	Size (µm)	250-335		Delivery of amoxicillin using mucoadhesiveness	[85] (1998)
a) Polyethylcyanoacrylate b) Pluronic F68 c) PEG(Different formulations were tested varying the molecular weight of PEG		PEG 600 Size (nm) 280 ± 8 PDI 0.60 ζ-potential (mV) -10.9 ± 1.5 %drug (w/w) 3.5 ± 0.11	PEG 2000 230 ± 15 0.40 -7.8 ± 1.3 7.5 ± 0.21	PEG 4000 220 ± 10 0.28 -5.1 ± 1.1 8.1 ± 0.23 Encapsulation of amoxicillin to drug delivery, resorting to mucoadhesive properties of polymers	[55] (2001)
a) Cholestyramine b) Cellulose acetate butyrate	Size (µm)	20 ± 2		Encapsulation of AHA an urease inhibitor, to local delivery	[86] (2003)
a) Poly(acrylic acid) b) Poly(vinyl pyrrolidone)	Size (µm) % EE	Amoxicillin 62.7 ± 4.7 57.5 ± 3.5	Clarithromycin 65.4 ± 4.6 93.5 ± 5.7	Delivery of amoxicillin or clarithromycin using mucoadhesive microspheres	[87] (2005)
a) Carbopol-934P b) Ethyl cellulose	Size (µm)	400-1000		Delivery of amoxicillin	[88] (2005)
	Size (µm) %EE	86.89 ± 12.45 → 129.72 ±13.87 48.35 ± 2.41 → 78.25 ± 2.65	} Varying composition	Delivery of clarithromycin	[89] (2008)
	Size (µm) %EE	109 56		Delivery of amoxicillin	[90] (2009)
a) Ethylcellulose b) Concanavalin-A c) Chitosan d) Polyvinyl alcohol	Size (µm) ζ-potential (mV) %EE	144.35 ± 22 7.56 ± 0.7 72.13 ± 1.4		Use functionalized microspheres for a controlled and local delivery of clarithromycin	[91] (2008)
a) Eudragit S100® b) Polyvinyl alcohol (PVA) c) Concanavalin-A	Size (µm) ζ-potential (mV) %EE	188.18 ± 2.46 18.7 ± 0.38 70.22 ± 0.14		Use Con-A microspheres to deliver amoxicillin	[92] (2014)
a) Sodium alginate b) Carbopol 934P c) Polycarbophil	Size (µm) %EE	208.5 → 408.5 35.249 ± 4.623 → 95 ± 2.835	} Varying composition	Encapsulation of clarithromycin into mucoadhesive microspheres	[93] (2009)
a) Chitosan b) Glutamic Acid c) α-l-fucose	Size (nm) % EE	874.97 ± 25.49 88.5 ± 2.8 (Amoxicillin) 91.1 ± 2.3 (Clarithromycin) 58.4 ± 3.7 (Metronidazole)		Use affinity of *H. pylori* receptors to fucose and use of mucoadhesiveness of polymers to create a triple drug delivery system	[94] (2009)
a) Chitosan (85% DA) b) Y-PGA	Size (nm) ζ-potential (mV) %EE	149.6 ± 6.3 18.9 ± 3.1 23.5 ± 2.7		Delivery of amoxicillin, using mucoadhesive nanoparticles	[95] (2010)
a) NIPASM b) AA c) HEM d) BPO e) TEGDMA	Size (nm) %EE	65 → 158 70.2 → 91.4	} Varying composition	Encapsulation of amoxicillin to drug delivery, resorting to mucoadhesive properties of polymers	[97] (2010)
a) Eudragit RL 100 b) Carbopol-974P	Size (µm) %EE	155-306 82 ± 1.13 → 90 ± 1.67	} Varying composition	Use polymer mucoadhesiveness to deliver loaded clarithromycin to localized action	[98] (2010)
a) Sodium alginate b) HPMC K4M Or b) Carbopol-974 P	Size (µm) %EE	602 ± 1.03 → 784 ± 5.11 66 ± 1.88 → 93 ± 2.02	} Varying composition		[43] (2011)
a) Eudragit RL 100 b) Carbopol 934P c) HPMC K4M	Size (µm) %EE	224 → 358 80 ± 1.25 → 92 ± 2.20	} Varying composition	Use polymer mucoadhesiveness to deliver loaded furazolidone to localized action	[100] (2010)
a) Eudragit RS 100 b) Carbopol-974P c) KPMC K4M	Size (µm) %EE	123 ± 8.35 → 524 ± 11.54 56.71 ± 1.66 → 89 ± 3.11	} Varying composition	Use polymer mucoadhesiveness to deliver loaded amoxicillin	[101, 102] (2010 /2011)
	Size (µm) %EE	118.5 ± 6.51 -> 493.3 ± 11.23 52.62 ± 0.72 → 87.97 ± 0.83	} Varying composition	Use polymer mucoadhesiveness to deliver loaded clarithromycin	[103] (2012)

Copolymers to deliver antibiotics

PDI = polydispersity index.

%drug (w/w) = percentage of the drug amount contained in 100 mg of dried material.

EE = encapsulation efficiency = ratio between the actual and theoretical amount of amoxicillin drug loaded.

% loading = weight of drug in SPs / total weight of the SPs.

a result, degradation of nanoparticles by lysosomes [84]. These nanoparticles were also able to interact locally with sites of *H. pylori* infection [84].

A mixture of polymers has also been applied to encapsulate antibiotics (Table 4). Nagahara et al. (1998) developed an amoxicillin-loaded mucoadhesive microsphere using carboxyvinyl polymers and

46

Table 4 (continued)

Particle composition	Physicochemical properties of the		optimized particle	Mechanism of action	Ref. (year)
a) Ethylcellulose b) Eudragit ® EPO c) Poly(vinyl alcohol) d) Glycerol monooleate	Size (μm) %loading	500-1000 6.82		Use mucoadhesiveness of GMO to deliver psoralen, a linear furanocoumarin compound	[104] (2011)
a) Polycationic chitosan b) Polyanionic alginate c) Pluronic F-127	Size (nm) ζ-potential (mV) % EE	651 59.76 91.23		Delivery of an antimicrobial agent, namely amoxicillin resorting to mucoadhesiveness and mucopenetrating properties	[35] (2011)
a) Sodium alginate b) Carbopol-934P c) Calcium chloride di-hydrate	Size (μm) %EE	890 ± 2.8 → 980 ± 3.2 68.2 ± 2.5 → 78.0 ± 2.1	Varying composition	Use mucoadhesiveness of polymers to vectorize clarithromycin to stomach	[105] (2011)
a) Chitosan (85% DA) b)Heparin (aqueous phase of a water-in-oil emulsification)	Size (nm) ζ-potential (mV) %EE % loading	296.5 ± 6.3 29.8 ± 3.1 54.3 ± 2.8 19.2 ± 1.2		Delivery of amoxicillin using advantages of chitosan and heparin	[106] (2012)
a) Sodium alginate b) Sodium carboxymethy cellulose c) Magnesium aluminium silicate d) Chitosan	Size (μm) %EE % loading	745 → 889 52 ± 0.78 → 92 ± 1.2 5.2 ± 0.78 → 11.0 ± 0.8	Varying composition	Use coat of chitosan to vectorize amoxicillin to the stomach	[107] (2012)
a) Sodium alginate b) Pectin c) Calcium chloride d) Ethylcellulose	Size (μm) %EE	17 ± 1 83 ± 1.3		Use a blend polymeric matrix to controlled release of clarithromycin	[108] (2013)
a) Chitosan (85% DA) b) Heparin c) Genipin d) Fucose e) Sodium cyanoborohydride	Size (nm) ζ-potential (mV) % EE	249.6 ± 4.2 27.2 ± 1.6 48.7 ± 2.8		Active and passive targeting of amoxicillin using fucose and pH-sensibility, respectively	[71] (2013)
a) Eudragit ® RS	Size (μm) PDI ζ-potential (mV) %EE %Loading	1.1283 ± 0.0551 → 9.9936 ± 0.0921 0.141 ± 0.029 → 0.294 ± 0.040 44.25 ± 1.08 → 65.39 ± 2.39 (SGF) 15.77 ± 3.44 → 31.72 ± 3.55 (water) 99.47 ± 2.06 → 100.10 ± 3.21 8.07 ± 1.14 → 25.79 ± 2.06	Varying composition	Sustained release of metronidazole	[109] (2014)

curdlan [85]. Stomach residence time and *in vivo* clearance were enhanced three and ten times, respectively, compared to plain amoxicillin suspension [85]. In 2001, Fontana et al. took into account polyethylenoglycol (PEG) properties, specifically their ability to avoid macrophage opsonization and, consequently, escape from the immune system, in order to develop a novel nanoparticle for amoxicillin delivery [55]. Experimental studies showed PEG influence on particle size, potential zeta and drug entrapment and proved that PEG coating certainly reduced the opsonization by macrophages [55]. PEG was also responsible for the reduction of drug release in human plasma, conversely to that observed in drug release assays at pH 7.4 [55]. The release of amoxicillin followed a biphasic profile, being rapidly released at the first stage [55]. Experimental studies also evidenced the effect of urease in increasing amoxicillin release owing to NP degradation [55].

A mixture of cholestyramine and cellulose acetate butyrate was also used to create a drug delivery system by Umamaheshwari et al. (2003) [86]. Cholestyramine is a mucoadhesive polymer which may locally interact with gastric mucosa through electrostatic forces [86]. Additionally, it can be used to encapsulate any drug of anionic species [86]. Acetohydroxamic acid release was higher at pH 1.2 than at pH 7.4 [86]. Additionally, the developed microparticles revealed both mucoadhesiveness and floating properties, being suitable for enhancing the retention time in the stomach [86]. Further studies are necessary to prove their efficiency in killing *H. pylori* [86].

In order to reduce water solubility of poly(acrylic acid), a well-known mucoadhesive and biocompatible polymer, Chun et al. (2005) developed a complex microsphere adding poly(vinyl pyrrolidone) [87]. In fact, the dissolution of the complex was significantly diminished when compared to PVP alone and was expressively slower at pH 2.0 than at pH 6.8, being useful for gastric delivery [87]. While the release of amoxicillin was almost independent of the pH, resulting from diffusion mechanisms, clarithromycin release varied with pH and resulted from the dissolution of PAA/PVP matrix [87].

In 2005, Liu et al. used a nanoparticle composed of ethylcellulose coated with carbopol-934P to encapsulate amoxicillin [88]. Adding mucoadhesiveness and biodegradable properties of carbopol to a matrix polymer composed of ethyl cellulose, a nanoparticle with affinity to mucosa was obtained, which was proved through *in vitro* and *in vivo* mucoadhesiveness evaluation [88]. Preliminary studies of *in vivo* H. pylori clearance were very promising, showing complete clearance at multidosage administration (twice a day, during three consecutive days) [88]. Three years later, the same idea was applied to design a clarithromycin-loaded ethyl cellulose-carbopol 934P microparticle by Rajinikanth et al. [89]. Microparticles manifested bioadhesiveness and *in vitro* floating during 20 h [89]. As a result, higher *H. pylori* clearance rates were obtained in Mongolian gerbils infected compared to those of a suspension of clarithromycin [89]. In 2009, Patel and Chavda took the previous idea of amoxicillin-loaded ethyl cellulose-carbopol 924P and synthesized it with different proportions and solvents [90]. Once again, increased retention time in stomach was obtained due to mucoadhesiveness [90]. *In vivo H. pylori* clearance tests revealed no

bacteria colony nor urease test positive in rats after administration of microspheres twice a day, during three consecutive days [90].

Jain and Jangdey (2008) took advantage of the affinity of Con A to different cells, via carbohydrate portions, and created a functionalized chitosan-ethylcellulose microsphere [91]. Mucoadhesive studies in vivo were performed and revealed the gastroretentive behavior of the developed formulation [91]. Additionally, the release of clarithromycin was sustained and controlled in simulated gastric fluids [91]. The same research group used Con A conjugated with microspheres of Eudragit S100® and PVA to encapsulate amoxicillin [92]. The proposed formulation showed mucoadhesive properties and a sustained release during 24 h at pH 1.2 [92]. Future perspectives include in vivo studies to evaluate H. pylori eradication [92].

In 2009, Thorat et al. reported the design of mucoadhesive microspheres in order to load clarithromycin, accompanied by a 3^2-full factorial [93]. In vitro studies revealed good mucoadhesiveness and a sustained release of the drug [93]. In the same year, Ramteke et al. developed a chitosan–glutamic acid nanoparticle for triple delivery (amoxicillin, clarithromycin and omeprazole) [94]. Once again, affinity of the bacteria to fucose was used as active targeting [94]. The developed nanoparticle achieved a remarkable 97% eradication rate, superior to that of nonconjugated nanoparticles and plain triple therapy [94]. A complete eradication was obtained in vivo, using Swiss albino mice, and histopathological studies revealed absence of infection [94]. With the same basis, Chang et al. (2010) designed amoxicillin-loaded chitosan/poly- -glutamic acid (-PGA) nanoparticles, carrying a pH-sensitive hydrogel to overcome instability in the acidic medium [95]. -PGA is a biocompatible polymer which can form a gel by electrostatic interactions with chitosan [96]. Subsequent to adhesion to the gastric mucosa, calcium-alginate-gelatin hydrogels will swell and collapse, leading to the release of nanoparticles and infiltration into the mucus [95]. It was evident that at pH 7.0 chitosan/ -PGA nanoparticles swelled and disintegrated, allowing rapid release of amoxicillin [95]. Confocal laser scanning microscopy revealed the location of the novel nanoparticle at the sites of H. pylori infection (intercellular spaces and cell cytoplasm) [95].

Another copolymer was synthesized by Moogooee and his research team through the crosslinking of N-isopropylacrylamide (NIPASM), acrylic acid (AA) and hydroxyethyl methacrylate (HEM) using benzoyl peroxide (BPO) as an initiator and triethyleneglycol dimethacrylate (TEGDMA) as a crosslinking agent [97]. The release of amoxicillin was higher at pH 1.0 than at pH 7.4 [97]. A sustained and controlled release was achieved with smaller nanoparticles but they present lower loading capacity [97]. In vivo studies performed on gastric tissues of rats showed an enhancement of gastric concentration of amoxicillin compared with plain amoxicillin [97].

Still in 2010, Venkateswaramurthy et al. developed clarithromycin-loaded microparticles with Eudragit RL100 as matrix and adding Carbopol 974P, acrylic and methacrylic-based polymers, respectively, to ensure mucoadhesive properties [98]. In vitro studies revealed bioadhesive properties, which might be reflected in an enhancement of the retention time in the stomach [98]. In the next year, another clarithromycin-loaded mucoadhesive microsphere was tested and bioadhesive properties were also proved through in vitro studies [43]. At gastric pH, carbopol 934P forms a slightly viscous gel, which influences drug release [99]. Hence, in order to improve mucoadhesive properties and the sustained release of the drug, this research group tried a mixture of carbopol 924P and hydroxy propyl methyl cellulose (HPMC) K4M, using Eudragit RL 100 or Eudragit RS 100 to disperse the polymers [99]. This novel composition was applied to encapsulate furazolidone (2010) [100], amoxicillin (2010–2011) [101,102] and clarithromycin (2012) [103]. In 2013, Venkateswaramurthy et al. administered twice daily for three consecutive days a mixture of amoxicillin-loaded MPs and clarithromycin-loaded MPs to male Wistar rats [99]. A complete eradication was achieved contrary to that observed with a solution of plain drugs (amoxicillin + clarithromycin) [99].

Liu et al. (2011) joined a mixture of polymers as matrix with a coat of a bioadhesive polymer, namely glycerol monooleate, in order to create a floating and mucoadhesive system [104]. Glycerol monooleate was used owing to its ability to form an in situ liquid crystal phase, characterized by high viscosity and bioadhesiveness in vivo [104]. Additionally, it is an FDA-approved additive due to its non-toxicity [104]. Drug release studies revealed a pH-dependency, being higher at acidic pH [104]. Mucoadhesiveness and buoyancy were proven both in vitro and in vivo and pharmacokinetics analysis of the drug revealed and enhancement of the plasmatic half-life time [104]. In an endeavor to improve mucoadhesive particles, Arora et al. (2011) developed a nanoparticle also able to penetrate into the gastric mucosa [35]. To achieve this aim, it was necessary to modify the charge of the chitosan surface in order to decrease mucoadhesiveness and decrease particle size to less than the mesh size of mucin fibers [35]. In vivo mucopenetration studies revealed the permanency of NPs during 6 h in the deeper layers of the mucosa, near epithelial cells [35]. Still in 2011, Pal et al. developed a polymeric mucoadhesive microsphere in order to encapsulate clarithromycin [105]. Mucoadhesiveness was proven by in vivo studies, with 72% remaining after 5 h and 37% after 7 h [105]. In vitro antibacterial effect was lower than 25% of growth inhibition after 8 h [105]. Studies of stability were also performed, revealing higher stability at lower temperatures with no degradation after 30 days at 4–8 °C [105].

In 2012, Lin et al. tried to improve the challenging encapsulation of low molecular weight hydrophilic drugs in nanoparticles composed of chitosan and heparin using water-in-oil emulsification [106]. The developed system presented a sustained release of amoxicillin at pH 1.2, collapsing at pH 7.0 [106]. This evidence is important since the surrounding pH of the bacteria is neutralized by urease secretion [106]. The results also showed a specific interaction between the nanoparticle and AGS cell monolayers infected with the bacteria [106]. Although incomplete, the NPs revealed a more complete H. pylori eradication than plain amoxicillin [106]. Still with the purpose to increase the entrapment efficiency of water soluble drugs and to modulate their release, Angadi et al. (2012) developed microbeads of well-known polymers coated with chitosan to enhance mucoadhesiveness [107]. In fact, the composition of the polymer matrix was decisive to obtain higher %EE, more precisely higher amounts of sodium carboxymethy cellulose and magnesium aluminium silicate resulted in higher %EE [107]. These microspheres were also efficient in obtaining controlled release of amoxicillin [107].

Taking into account the advantages of a blend of polysaccharide matrix, namely their worldwide use, their flexibility in management of drug-release profile and cost effectiveness, Tripathi (2013) used sodium alginate and pectin to create a pH sensitive microparticle [108]. This formulation showed favorable results both in vitro and in vivo, with a maximum percentage of growth inhibition of 85% and a more effective clearance than plain clarithromycin [108].

Appending mechanical stability conferred by genipin and active targeting provided by fucose, a genipin-cross-linked fucose-chitosan/heparin nanoparticle was developed [71]. According to what had been expected, at pH 1.2 amoxicillin was controllably released while at pH 7.0 the NP collapsed leading to a rapid release [71]. Although with a higher degree of contact with H. pylori due to its positively charged surface, the developed nanoparticle merely achieved 53.5 ± 6.3 of growth inhibition [71]. In vivo H. pylori growth inhibition studies and histological examinations revealed an enhancement of the clearance and a decrease of the inflammation [71]. Similar to what had been observed in the previous study, these NPs were able to locally interact with the sites of H. pylori infection, namely cell–cell junctions and cell cytoplasm, reducing the disruption of cell–cell junction protein [71]. The effect of the NP on bacteria morphology was also evaluated, showing changes from a helical to a coccoid form [71].

The most recent study dated from 2014, in which a porous Eudragit® RS microparticle fabricated via electrospray method was analyzed [109]. In vitro release studies revealed a sustained release, which may be beneficial when added to the ability to be retained in the

Table 5
Physicochemical characteristics and mechanism of action of particles composed of a mixture of polymers in order to treat *H. pylori* infections (probiotic, phytomedicine, antacids) or through immunization (vaccines).

	Particle composition	Physicochemical properties of the optimized particle				Mechanism of action	Ref. (year)
Probiotics	a) Chitosan (90% DA) b) Y-PGA	**ζ-potential (mV)**	-3.7 → + 23.25	depending on the		Encapsulation of *Lactobacillus casei* ATCC 393 (probiotic)	[96] (2011)
		%EE	76.2 → 82.4	% of chitosan			
Phytomedicine	a) Chitosan (85% DA) b) Heparin	**Size (nm)**	256.5 ± 2.3			Delivery of berberine, a plant alkaloid with antimicrobial properties. Using of chitosan as bioadhesive polymer and heparin due to healing properties	[110] (2011)
		PDI	0.26 ± 0.02				
		ζ-potential (mV)	-46.1 ± 0.4				
		% EE	54.4 ± 3.4				
	a) Chitosan (92.5% DA) b) Eudragit L100 (multi-cores) c) Sodium tripolyphosphate	**Size (μm)**	327.6 → 391.3	depending on		Use a multi-core chitosan microsphere to obtain a controlled release of berberine	[111] (2012)
		%EE	66.1 ± 1.6 → 71.5 ± 1.1	drug:eudragit ratio			
	a) Ethylcellulose b) Methylcellulose		**Water**	**pH 2.0**	**pH 7.4**	Use mucoadhesiveness of nanoparticles to encapsulate *Garcinia mangostana* extract	[112] (2013)
		Size (nm)	625±20	672±13	672±10		
		PDI	0.305±0.041	0.310±0.037	0.277±0.044		
		ζ-potential (mV)		1.88±0.32	0.93±0.01		
		%EE	98.9 ± 6.3				
	a) Ethylcellulose b) Carbopol 934P	**Size (μm)**	139.881 ± 2.56			Encapsulation of curcumin in mucoadhesive microspheres	[113] (2014)
		%EE	50.256 ± 1.38				
Antacids	a) Hydroxypropyl methyl cellulose (HPMC K4M) b) Eudragit®S100	**Size (μm)**	30.8			Encapsulation of pantoprazole in order to protect it from degradation before absorption	[114] (2006)
		% EE	98.2				
Vaccines	a) Poly(D-L-lactide-co-glycolide) (PLGA)	**Size (μm)**	0.16 – 0.85 (mean = 0,32)			Encapsulation of *Helicobacter pylori* lysates in order to achieve oral immunization	[115] (1999)
		%EE	67				
	a) Poly (D, L – lactide)-polyethylene glycol	**Size (μm)**	3.20 – 4.05				[116] (2002)
		%EE	74.9 - 82.2				
	a) Chitosan b) Sodium deoxycholate (DS) or a) Chitosan b) Alginate (Alg) c) Sodium tripolyphosphate (TPP)		**Chitosan/DS**	**Chitosan/Alg/TPP**		Development of a multiantigenic *H. pylori* vaccine through encapsulation into a chitosan-based nanoparticle	[117] (2012)
		Size (nm) pDNA Protein	242 ± 8 894 ± 6	195 ± 1 328 ± 7			
		%EE pDNA Protein	100 70 ± 10	100 70 ± 8			

EE = encapsulation efficiency = ratio between the actual and theoretical amount of amoxicillin drug loaded.
PDI = polydispersity index.

stomach for 8 h [109]. *In vivo* clearance studies support the effectiveness of this novel formulation, with a more complete clearance of *H. pylori* and lower gastric inflammation in *H. pylori*-infected mice models than with a pure drug solution [109].

A mixture of polymers has also been applied to the encapsulation of probiotics (Table 5). For example, Ko et al. (2011) developed a microsphere to encapsulate *Lactobacillus casei* ATCC 393 [96]. These organisms are used as probiotics, being able to produce some compound inhibitors of toxic activity of some pathogen organisms, namely *H. pylori* [96]. Additionally, it can manage side-effects of the current therapy which may result from qualitative and quantitative changes of gastric microflora [26]. At pH 1.5 a significant amount of the probiotic was released after 60 min due to the instability of the microsphere at acidic pH [96]. *H. pylori* growth inhibition and anti-adhesive effect of *Lactobacillus* were sustained during 60 min even under pH 1.5, whereas a non-encapsulated probiotic presented a higher initial efficacy without maintaining the effect during the 60 min [96].

The use of phytomedicine to eradicate *H. pylori* and the possibility to use micro- and nanotechnology to overcome its limitations have also been studied (Table 5). Berberine, a plant alkaloid compound with the ability to inhibit *H. pylori* growth and protect gastric mucosa, has also been the target of study [110]. The strategy of combining chitosan and

heparin was applied by Chang et al. (2011) to carry berberine [110]. *In vitro* studies proved the dose-dependence of *H. pylori* growth inhibition, reaching around 53% with 12 mg L^{-1} of berberine [110]. The novel NP showed a significant efficacy in increasing AGS cell viability after pre-incubation with *H. pylori* [110]. Further studies are required for *in vivo* application of this NP combined with other antibiotics [110]. Since chitosan microspheres are insufficient to obtain a controlled release of hydrophilic drugs, a novel strategy was chosen by Zhu et al. (2012) [111]. The usual strategies pursued resulted in the reduction of flexibility and the amount of amino groups, hence a loss of the mucoadhesiveness properties of chitosan [111]. Chitosan microspheres with multiple Eudragit®L100 cores were chosen by Zhu et al. (2012) to encapsulate berberine [111]. *In vitro* release studies revealed a controlled release of berberine, maintaining the mucoadhesiveness properties of chitosan [111]. In the following year, Pan-in et al. used a mixture of ethylcellulose and methylcellulose to encapsulate *Garcinia mangostana* extract (GME) [112]. GME with 56% by weight of α-mangostin was used due to several pharmacological effects, highlighting antioxidant, anti-inflammatory and antibacterial activity [112]. The selection of the polymers is based on their ability to adhere to the mucosa and, simultaneously, retain their forms without fast degradation or swelling at acidic pH [112]. The designed nanoparticle revealed antiadhesion and *in vitro* anti-

49

H. pylori efficacy, with a MIC similar to that of metronidazole, nevertheless it was significantly higher than clarithromycin or amoxicillin [112]. Compared to that observed with the unencapsulated GME and to free clarithromycin, administration of GME-loaded nanoparticles during 3 consecutive days revealed higher, although uncompleted, *in vivo* eradication [112]. Recently (2014), Ali et al. used mucoadhesive microspheres to encapsulate curcumin, which is able to reduce the enhancement of metalloproteinases levels caused by *H. pylori* and responsible for gastric injuries [113]. Mathematical models were used to optimize the formulation and experimental results revealed that entrapment efficiency and *in vitro* bioadhesiveness increased with the increase of polymer concentration [113]. Release studies showed a sustained release during 8 h [113].

Antacids are frequently used to complement antimicrobial therapy and SPs may be used to encapsulate them (Table 5). Pantoprazole is a common antacid used to complement the therapy against *H. pylori* [114]. However, when it reacts with acid before absorption, its effectiveness significantly decreases [114]. Thus, Raffin et al. (2006) used microparticles composed of Eudragit®S100 and HPMC to encapsulate sodium pantoprazole [114]. The aim of this research work was the evaluation of the success of a novel preparation method, namely spray drying on pilot scale [114]. Validation studies of microparticle preparation by pilot scale showed reproducible physicochemical properties as well as gastro-resistance profile [114].

A mixture of polymers has also been tested in order to produce vaccines through the encapsulation of antigens in order to induce immunization against *H. pylori* (Table 5). For instance, in 1999, a copolymer composed of lactic acid and glycolic acid was used in order to achieve oral immunization [115]. In fact, poly(D-L-lactide-co-glycolide) (PLGA), a FDA approved biodegradable copolymer, was used to encapsulate *H. pylori* lysates since it can be uptaken by M cells and carried to the mesenteric lymph nodes and spleen [115]. Thus, it is possible to use these microparticles not only to protect the antigen but also to target induction sites [115]. Results revealed that *H. pylori* lysate-loaded microparticles were able to induce immune system, namely Th2-type responses in Balb/c mice [115]. However this response was weaker than that observed with cholera toxin-*H. pylori* immunized mice [115]. Further studies are necessary to optimize immunization schedules, doses and intervals [115]. *H. pylori* lysates were also incorporated in a microsphere composed of poly(D,L-lactide)-polyethylene glycol copolymer [116]. Due to their small size, microspheres could induce mucosal and systemic immune responses and, in fact, encapsulated antigens achieved higher enhancement of specific antibodies than soluble antigen [116]. In 2012, Figueiredo et al. applied two based chitosan nanoparticles, namely chitosan/sodium deoxycholate and chitosan/sodium alginate/sodium tripolyphosphate, to induce immunization against *H. pylori* [117]. Two different approaches were tested to construct a multiantigenic vaccine, specifically DNA-vaccine and protein-vaccine, administered in two different routes (oral and intramuscular (i.m.)) [117]. Mucosal immunity was facilitated when chitosan-based nanoparticles were used through oral immunization, however i.m. immunization achieved a more equilibrated cellular/humoral immune response [117].

3.3. Hybrid systems with liposomes and polymeric particles

Liposomes have been used as drug delivery systems due to the several advantages mentioned above. However, they can be unstable during storage and even in biological fluids [28]. One of the major reasons of their instability is the propensity to fuse with other liposomes, leading to a payload loss [118]. Their instability is enhanced when in the presence of acidic medium, divalent cations and blood cells [3,118]. The coating with PEG is an alternative to overcome this limitation. Nonetheless, it is unsuitable to be used in the design of nanoparticles for the treatment of *H. pylori* because it makes fusion with the bacterial membrane difficult by which drug release would occur [118].

Furthermore, the loading capacity of liposomes is limited [119]. On the other hand, polymeric nanoparticles have mechanical stability without having the valuable surface properties of liposomes [3]. New hybrid systems combining the advantages of liposomes and polymeric nanoparticles have been studied.

3.3.1. Polymeric core coated with a phospholipid bilayer

Hybrids composed of a polymeric core encased in a phospholipid bilayer presents as main advantage the manipulation of the phospholipid bilayer, being possible to use techniques for active and passive targeting similar to those observed in liposomes [3]. These techniques may include a stimulus-sensitive drug release and a receptor- or antibody-mediated drug targeting [3].

Umamaheshwari et al. (2004) applied the idea of the lipobeads described by Jin et al. (1996) to the treatment of *H. pylori* infection [3]. With this purpose in mind, they developed a system composed of a hydrogel polymer core (polyvinyl alcohol) coated with a lipid bilayer of PE to encapsulate acetohydroxamic acid (AHA) [3]. Palmitoyl chloride was used to prepare acylated PVA beads and the shell was composed of a mixture of PE, oleic acid and cholesterol [3]. The result was microspheres of 75 $\pm$ 10 μm with an encapsulation efficiency of 65.3% [3]. The release of AHA was controlled by the PE bilayer [3]. Agglutination assays revealed the ability of lipobeads to agglutinate *H. pylori*, perchance due to the presence of PE in the phospholipid bilayer [3]. In fact, lipobeads showed a capacity to plug and seal the PE receptor in adherence assays, decreasing the adhesion of the bacteria to KATO-III cells (radiolabeling assay) and *in situ* adherence assay using human stomach cells [3]. Furthermore, lipobeads revealed rates of 100% *in vitro* growth inhibition after 6 h [3]. However, *in vivo* growth inhibition studies, using animal models, are necessary to prove the effectiveness of this NP [3]. In 2013, Jain and Jain designed a similar NP to encapsulate amoxicillin and RBC [119]. The core was composed of PVA and after acylation with palmitoyl choride; the shell was formed using PE and cholesterol [119]. Nanoparticles of 774.3 $\pm$ 4.3 nm and with a polydispersity index of 0.153 were synthesized [119]. ζ-potential was $+5.6 \pm 0.3$ mV and encapsulation efficiency was 86.1 ± 2.1 and 65.3 ± 3.2 for RBC and amoxicillin, respectively [119]. *In vitro* release of amoxicillin and RBC was sustained and controlled and the NP showed a higher percentage of growth inhibition compared to that of the plain drugs [119]. It also revealed a selective binding to bacteria receptors and mucoadhesive properties through agglutination and *in situ* adherence studies, respectively [119]. *In vivo* studies demonstrated effectiveness in the clearance rate of *H. pylori* and the ability to protect the gastric mucosa [119].

3.3.2. Liposome coated with biocompatible polymers

Jain et al. (2009) noticed that the strategy to enhance the stability of liposomes can also be accomplished through the coating of liposomes with alternate layers of polycations and polyanions (polyelectrolytes) [28]. Taking advantage of the positive charge of the outer layer of the NP, it is possible to increase the attachment to the mucosal surface which is negatively charged [28]. Hence, positively charged liposomes composed of egg phosphatidylcholine, cholesterol and stearylamine were coated with poly(acrylic acid) and poly(allylamine hydrochloride) [28]. Multilayered liposomes had 352 $\pm$ 21 nm, with 0.145 $\pm$ 0.018 of polydispersity index and a ζ-potential of $+31.64 \pm 0.37$ mV [28]. They used these nanoparticles to encapsulate amoxicillin and metronidazole, with a percentage of encapsulation efficiency of 47.71 ± 3.65 and 52.14 ± 3.58, respectively [28]. *In vitro* drug release studies showed a controlled and sustained release in simulated gastric fluid (pH 1.2) [28]. This steady release induced growth inhibition rates of 99%, lower than that obtained with the drugs without any formulation due to the direct contact between the bacteria and the plain drugs together [28]. The components of the NP also caused around 94% of growth inhibition, revealing antibacterial properties [28]. The ability to bind to the bacteria and the mucoadhesive properties of the NP were revealed in agglutination and adherence studies [28]. Contrary to that observed *in vitro*,

in vivo bacterial clearance studies revealed that NP had higher efficacy than free antibiotics [28]. This clearance is possibly a consequence of the decreased *H. pylori* attachment to the mucosa [28]. In spite of the promising results, cationic polymers may be toxic and supplementary studies are necessary [28]. Another strategy to increase the stability of liposomes was developed by Thamphiwatana et al. (2013), using charged nanoparticles to induce steric repulsion and reduce surface tension [118]. The authors used small gold nanoparticles modified with chitosan which are protonated at acidic pH and deprotonated at neutral pH [118]. Therefore, at gastric pH the liposome, composed of egg phosphatidylcholine and 1,2-dioleoyl-sn-glycerol-3-phosphate (sodium salt), would be stabilized by the linkage to chitosan-modified gold nanoparticles (AuChi) [118]. Synthesized nanoparticles had a diameter of 95.2 ± 1.3 nm, a polydispersity index of 0.11 ± 0.01 and a ζ-potential of $+57.4 \pm 0.7$ mV [118]. At neutral pH, AuChi would detach from liposomes, allowing the destabilization of the phospholipid bilayer and hence the release of the drug [118]. This property of AuChi was proved through fluorescence studies with rhodamine quenching at pH 1.2 [118]. Equally, an increased fusion between liposomes and bacterial membranes of *H. pylori* and higher rates of doxycycline release were noticed at pH 7.4 [118]. *In vitro* studies revealed the effectiveness of NP in killing completely the bacteria [118].

3.4. Metallic nanoparticles

Metallic nanoparticles may be composed of different elements, such as silver, zinc and bismuth-containing nanoparticles [38]. These nanoparticles are able to protect drugs from external threats, such as acidic pH, and can vectorize the drug to the target avoiding immune system activation and cytotoxicity [34]. In the ability to kill and/or inhibit growth of bacteria, there are several different mechanisms and they have strong antimicrobial effect even in lower doses [38,120]. Hence, the resistance development by the bacteria is improbable [38]. In point of fact, previous studies reported that bacteria do not develop resistance to metal NPs in a naturally occurring manner [37]. Recent studies (2014) also revealed the possibility to use complexes of Fe(III) and Co(II) with omeprazole to enhance antimicrobial activity against *H. pylori* [121]. Therefore, different metallic nanoparticles have been studied with the purpose to eradicate *H. pylori*.

3.4.1. Zinc nanoparticles

ZnO NPs are nontoxic and biocompatible, being recognized by FDA as generally recognized as safe [120]. Therefore, they have been widely used in drug carrier, cosmetic and medical materials [37]. Antimicrobial action of these NPs has also been proved, evolving different and complex mechanisms [38]. The most important disadvantage of ZnO NPs is the aggregation in water, which can be minimized by resorting to polymers [120]. Thus, Chakraborti et al. (2013) developed a zinc oxide nanoparticle functionalized with polyethyleneimine with 20 nm diameter [120]. In addition to the improvement of ZnO NP dispersion in biological fluids, polyethyleneimine acts as a permeabilizing agent for Gram-negative bacterial membranes and a specific target for lipopolysaccharides present in the outer membrane [120]. Results revealed a relative stability under a significant range of pH (2–7) and toxicity to metronidazole resistant bacteria [120]. Action mechanisms include generation of intracellular reactive oxygen species which results in membrane and RNA damage [120]. Using concentrations of ZnO–PEI NPs considered toxicologically safe and adding ampicillin under minimum inhibitory concentration, a synergic effect was observed reaching more than 80% of growth inhibition [120].

3.4.2. Silver nanoparticles

Since ancient times, antimicrobial properties of silver have been known [37]. With the discovery of penicillin, silver became rarely used until the emergence of strains resistant to some antibiotics which revived the study of antimicrobial properties of silver [37]. Silver NPs kill bacteria through multiple mechanisms of action, which may be the explanation for the effectiveness against a wide array of microbes [38]. They have also been reported as anti-ulcer agents [122]. However, some studies reported silver NP toxicity as concentration-dependent and further studies are necessary to elucidate its toxicity *in vivo* [37].

Amin et al. (2012) tested the application of silver NPs synthesized through reduction with *Solanum xanthocarpum* L. berry extract [122]. Nanoparticles with 10 nm diameter revealed in *in vitro* studies a higher antibacterial efficacy than that of ionic silver (silver nitrate) [122]. This evidence corroborates the importance of the high surface area to volume ratio of NPs to enhance the contact with the bacteria [122]. The inhibition of *H. pylori* growth was noteworthy with these nanoparticles, being higher than that of metronidazole, equal to tetracycline and lower than amoxicillin and clarithromycin [122]. Silver NPs were also effective even in antibiotic-resistant strains and presented urease inhibitory activities [122].

3.4.3. Bismuth compounds

Bismuth compounds have been used as a component of the triple therapy due to their antibacterial properties [122]. Bismuth nanoparticles have been studied as a promising drug carrier, however it was reported that bismuth nanoparticles show more toxicity than most reported bismuth compounds [123].

In 2006, Chen et al. reported the antibacterial effects of bismuth subcarbonate $((BiO)_2CO_3)$ nanotubes with a diameter of 4.0 ± 0.5 nm and a length from a hundred nm to several μm [124]. These nanotubes had a more potent inhibitory effect than the clinically used antiulcer drug (colloidal bismuth subcitrate) whereas bismuth oxide nanoparticles slightly inhibit bacteria growth [124]. The authors concluded that it may be a promising drug delivery system [124]. In 2010, they tried bismuth subcarbonate $((BiO)_2CO_3)$ nanoparticles of 9.2 ± 1.0 nm instead of nanotubes [125]. The results showed a similar anti-*H. pylori* effect to that observed with colloidal bismuth subcitrate [125].

In 2013, Nazari et al. evaluated the antibacterial activity of bismuth nanoparticles, which were synthesized using bismuth subnitrate and *Serratia marcescens* [126]. In fact, the antimicrobial effect of bismuth nanoparticles with less than 5 nm was higher than that of bismuth ions [126]. The analysis of the released metabolites from the bacterium indicated that these NPs were able to interfere with biochemical pathways in *H. pylori*, namely Krebs cycle, nucleotide and amino acid metabolism [126].

3.4.4. Iron microparticles

Magnetic vectorization has also been studied as an alternative to enhance the residence time in the stomach [42]. Through the incorporation of antibiotics in polymerized magnetic particles and resorting to an external magnet, the time of drug absorption will increase [42]. In 2009, Silva et al. developed a magnetic system composed of a magnetite core (superparamagnetic particle) coating with pH-sensitive polymers (Eudragit®S100) [42]. These polymers were able to protect magnetite particles from gastric dissolution and to load amoxicillin [42]. The size of these microparticles presented an irregular distribution around the medium value of 17.2 μm [42]. This research work was an early study of the fabrication of magnetic particles for drug delivery in the stomach, highlighting the influence of the spray-drying process and the magnetite content in the initial susceptibility and saturation magnetization of the microsystem developed [42]. Further studies are necessary [42].

4. Conclusion

The treatment against *H. pylori* has evolved according to the discovery of morphology and pathogenicity of the bacteria. However, the current therapy still presents various serious limitations. In this context, numerous efforts have been made in order to improve the current treatment.

One of the strategies adopted is the use of micro- and nanotechnology to overcome these limitations.

Even though presenting *in vitro* and *in vivo* studies as promising, fewer approaches present complete eradication of the bacteria and novel nanoparticles might be studied. In fact, studies reported the efficacy of dendrimers to overcome bacterial resistance mechanisms [38]. Ultimately, they can even destroy microbial cell membrane [38]. Lipid nanoparticles might also be an alternative, since they can protect drugs against external environment and are flexible in controlling the release of the antimicrobial loaded [127]. Nanoparticles of clarithromycin and L-ascorbic acid 2-glucoside were developed by Inoue et al. (2007) and may be a promising approach to treat *H. pylori* [128]. This nanoparticle might be applied to cure ulcers, since it has the combined antimicrobial properties of clarithromycin and antioxidant properties of ascorbic acid which were correlated with antiulcer properties [129].

In the majority of the studies it was common to evaluate the release at an acidic pH, mimicking the pH of the gastric medium. Nevertheless, generally other important compounds present in the gastric tract are not taken into account , namely pepsin. The proteolytic activity and even peristaltic movement of gastric mucosa may influence the ability to adhere to mucosa [35]. Another limitation of the majority of the studies is the devaluation of the degradation rate of antimicrobial drugs at acidic pH in release studies.

Despite the benefit of mucoadhesive micro or nanoparticles, the ideal is a particle that may also penetrate into the mucosa since the thick viscoelastic mucosa gel may decrease the diffusion of solely mucoadhesive particles [35]. Indeed, the great mucoadhesiveness may even prejudice the penetration within the mucosa due to the decrease of mobility [35]. Mucoadhesiveness may also be affected by the high turnover of the gastric mucosa [39].

Further studies are also necessary to evaluate micro- and nanotoxicity. In fact, their useful small size and large surface area may be associated with toxicity *in vivo* [130]. Previous studies reported the insufficiency of *in vitro* studies when related to nanotoxicology, once other mechanisms may be evolved *in vivo*, such as translocation, toxicokinetics and coordinated response of tissues [130]. SPs can interact with cells, tissues and organs *in vivo* and, consequently, it is difficult to predict the ideal dose, administration route and the adverse effects resulting from that interaction [37].

In conclusion, the helpfulness of SPs in the combat against *H. pylori* infection is unquestionable. However, supplementary studies are necessary to evaluate *in vivo* effectiveness and toxicity.

Acknowledgments

References

[1] L. Boyanova, I. Mitov, B. Vladimirov, *Helicobacter pylori*, Caister Academic Press, Norfolk, 2011.

[2] *Helicobacter pylori*: Physiology and genetics, ASM Press, Washington DC, 2001.

[3] R.B. Umamaheshwari, N.K. Jain, Receptor-mediated targeting of lipobeads bearing acetohydroxamic acid for eradication of *Helicobacter pylori*, J. Control. Release 99 (2004) 27–40.

[4] L. Yang, J. Eshraghi, R. Fassihi, A new intragastric delivery system for the treatment of *Helicobacter pylori* associated gastric ulcer: *in vitro* evaluation, J. Control. Release 57 (1999) 215–222.

[5] D. Ilver, A. Arnqvist, J. Ogren, I.-M. Frick, D. Kersulyte, E.T. Incecik, D.E. Berg, A. Covacci, L. Engstrand, T. Bore, *Helicobacter pylori* adhesin binding fucosylated histo-blood group antigens revealed by retagging, Science 279 (1998) 373–377.

[6] P. Falk, K.A. Roth, T. Borén, T.U. Westblom, J.I. Gordon, S. Normark, An *in vitro* adherence assay reveals that *Helicobacter pylori* exhibits cell lineage-specific tropism in the human gastric epithelium, Proc. Natl. Acad. Sci. 90 (1993) 2035–2039.

[7] A review of human carcinogens. Part B: biological agents, IARC Working Group on the Evaluation of the Carcinogenic Risks to Humans, Lyon, France, 2009.

[8] S. Mishra, Is *Helicobacter pylori* good or bad? Eur. J. Clin. Microbiol. Infect. Dis. 32 (2013) 301–304.

[9] S.S. Kim, V.E. Ruiz, J.D. Carroll, S.F. Moss, *Helicobacter pylori* in the pathogenesis of gastric cancer and gastric lymphoma, Cancer Lett. 305 (2011) 228–238.

[10] A. Zullo, C. Hassan, L. Ridola, V. de Francesco, D. Vaira, Standard triple and sequential therapies for *Helicobacter pylori* eradication: an update, Eur. J. Intern. Med. 24 (2012) 16–19.

[11] S.D. Georgopoulos, V. Papastergiou, S. Karatapanis, Current options for the treatment of *Helicobacter pylori*, Expert. Opin. Pharmacother. 14 (2013) 211–223.

[12] M.J.M. Buckley, C.A. O'Morain, *Helicobacter* biology — discovery, Br. Med. Bull. 54 (1998) 7–16.

[13] M. Kidd, I.M. Modlin, A century of *Helicobacter pylori*, Digestion 59 (1998) 1–15.

[14] J. Gustafson, D. Welling, "No acid, no ulcer"—100 years later: a review of the history of peptic ulcer disease, Am. Coll. Surg. 210 (2010) 110–116.

[15] J.W. Konturek, Discovery by Jaworski of *Helicobacter pylori* and its pathogenetic role in peptic ulcer, gastritis and gastric cancer, J. Physiol. Pharmacol. 54 (Suppl. 3) (2003) 23–41.

[16] B. Marshall, Gastric spirochaetes: 100 years of discovery before and after Kobayashi, Keio J. Med. 51 (Suppl. 2) (2002) 33–37.

[17] B.J. Marshall, The *Campylobacter pylori* story, Scand. J. Gastroenterol. 23 (Suppl. 146) (1988) 58–66.

[18] C. Ciacci, G. Mazzacca, The history of *Helicobacter pylori*: a reflection on the relationship between the medical community and industry, Dig. Liver Dis. 38 (2006) 778–780.

[19] B.J. Marshall, J.R. Warren, Unidentified curved bacilli in the stomach of patients with gastritis and peptic ulceration, Lancet (1984) 1311–1315.

[20] K.M. Bocian, E.K. Jagusztyn-krynicka, The controversy over anti-*Helicobacter pylori* therapy, Pol. J. Microbiol. 61 (2012) 239–246.

[21] C.A. McNulty, J. Dent, R. Wise, Susceptibility of clinical isolates of *Campylobacter pyloridis* to 11 antimicrobial agents, Antimicrob. Agents Chemother. 28 (1985) 837–838.

[22] P. Malfertheiner, F. Megraud, C.A. O'Morain, J. Atherton, A.T. Axon, F. Bazzoli, G.F. Gensini, J.P. Gisbert, D.Y. Graham, T. Rokkas, E.M. El-Omar, E.J. Kuipers, Management of *Helicobacter pylori* infection—the Maastricht IV/Florence Consensus Report, Gut 61 (2012) 646–664.

[23] M. Selgrad, P. Malfertheiner, New strategies for *Helicobacter pylori* eradication, Curr. Opin. Pharmacol. 8 (2008) 593–597.

[24] P.-L. Bardonnet, V. Faivre, P. Boullanger, J.-C. Piffaretti, F. Falson, Pre-formulation of liposomes against *Helicobacter pylori*: characterization and interaction with the bacteria, Eur. J. Pharm. Biopharm. 69 (2008) 908–922.

[25] J.K. Patel, M.M. Patel, Stomach specific anti-*Helicobacter pylori* therapy: preparation and evaluation of amoxicillin-loaded chitosan mucoadhesive microspheres, Curr. Drug Deliv. 4 (2007) 41–50.

[26] A. Armuzzi, F. Cremonini, F. Bartolozzi, F. Canducci, M. Candelli, V. Ojetti, G. Cammarota, M. Anti, A. De Lorenzo, P. Pola, G. Gasbarrini, A. Gasbarrini, The effect of oral administration of *Lactobacillus GG* on antibiotic-associated gastrointestinal side-effects during *Helicobacter pylori* eradication therapy, Aliment. Pharmacol. Ther. 15 (2001) 163–169.

[27] M. Obonyo, L. Zhang, S. Thamphiwatana, D. Pornpattananangkul, V. Fu, L. Zhang, Antibacterial activities of liposomal linolenic acids against antibiotic-resistant *Helicobacter pylori*, Mol. Pharm. 9 (2012) 2677–2685.

[28] P. Jain, S. Jain, K.N. Prasad, S.K. Jain, S.P. Vyas, Polyelectrolyte coated multilayered liposomes (nanocapsules) for the treatment of *Helicobacter pylori* infection, Mol. Pharm. 6 (2009) 563–603.

[29] J.-M. Liou, C.-C. Chen, M.-J. Chen, C.-C. Chen, C.-Y. Chang, Y.-J. Fang, J.Y. Lee, S.-J. Hsu, J.-C. Luo, W.-H. Chang, Y.-C. Hsu, C.-H. Tseng, P.-H. Tseng, H.-P. Wang, U.-C. Yang, C.-T. Shun, J.-T. Lin, Y.-C. Lee, M.-S. Wu, Sequential versus triple therapy for the first-line treatment of *Helicobacter pylori*: a multicentre, open-label, randomised trial, Lancet 381 (2013) 205–213.

[30] A. Patel, N. Shah, J.B. Prajapati, Clinical appliance of probiotics in the treatment of *Helicobacter pylori* infection — a brief review, J. Microbiol. Immunol. Infect. (2013) 1–9.

[31] J. Vítor, F.F. Vale, Alternative therapies for *Helicobacter pylori*: probiotics and phytomedicine, FEMS Immunol. Med. Microbiol. 63 (2011) 153–164.

[32] P.L. Bardonnet, V. Faivre, W.J. Pugh, J.C. Piffaretti, F. Falson, Gastroretentive dosage forms: overview and special case of *Helicobacter pylori*, J. Control. Release 111 (2006) 1–18.

[33] C.H. Prasanthi, N.L. Prasanthi, S.S. Manikiran, N.R. Rao, Focus on current trends in the treatment of *Helicobacter pylori* infection: an update, Int. J. Pharm. Sci. Rev. Res. 9 (2011) 42–51.

[34] K. Blecher, A. Nasir, A. Friedman, The growing role of nanotechnology in combating infectious disease, Virulence 2 (2011) 395–401.

[35] S. Arora, S. Gupta, R.K. Narang, R.D. Budhiraja, Amoxicillin loaded chitosan-alginate polyelectrolyte complex nanoparticles as mucopenetrating delivery system for *H. pylori*, Sci. Pharm. 79 (2011) 673–694.

[36] M.J. Hajipour, K.M. Fromm, A.A. Ashkarran, D.J. Aberasturi, I.R. Larramendi, T. Rojo, V. Serpooshan, W.J. Parak, M. Mahmoudi, Antibacterial properties of nanoparticles, Trends Biotechnol. 30 (2012) 499–511.

[37] A. Jung, Y. Kwon, "Nanoantibiotics": a new paradigm for treating infectious diseases using nanomaterials in the antibiotics resistant era, J. Control. Release 156 (2011) 128–145.

[38] R.Y. Pelgrift, A.J. Friedman, Nanotechnology as a therapeutic tool to combat microbial resistance, Adv. Drug Deliv. Rev. 65 (2013) 1803–1815.

[39] S. Hassani, Y. Pellequer, A. Lamprecht, Selective adhesion of nanoparticles to inflamed tissue in gastric ulcers, Pharm. Res. 26 (2009) 1149–1154.

[40] D.A. Norris, N. Puri, P.J. Sinko, The effect of physical barriers and properties on the oral absorption of particulates, Adv. Drug Deliv. Rev. 34 (1998) 135–154.

[41] D. Luo, J. Guo, F. Wang, J. Sun, G. Li, X. Cheng, M. Chang, X. Yan, Preparation and evaluation of anti-*Helicobacter pylori* efficacy of chitosan nanoparticles *in vitro* and *in vivo*, J. Biomater. Sci. 20 (2009) 1587–1596.

[42] É.L. Silva, J.F. Carvalho, T.R.F. Pontes, E.E. Oliveira, B.L. Francelino, A.C. Medeiros, E.S.T. Egito, J.H. Araujo, A.S. Carriço, Development of a magnetic system for the treatment of *Helicobacter pylori* infections, J. Magn. Magn. Mater. 321 (2009) 1566–1570.

[43] R. Sambathkumar, N. Venkateswaramurthy, M. Vijayabaskaran, P. Perumal, Formulation of clarithromycin loaded mucoadhesive microspheres by emulsification-internal gelation technique for anti-*Helicobacter pylori* therapy, Int. J. Pharm. Pharm. Sci. 3 (Suppl. 2) (2011) 171–177.

[44] M. Fernandes, I.C. Goncalves, S. Nardecchia, I.F. Amaral, M.A. Barbosa, M.C. Martins, Modulation of stability and mucoadhesive properties of chitosan microspheres for therapeutic gastric application, Int. J. Pharm. 454 (2013) 116–124.

[45] A.A. Salyers, D.W. Dixie, Bacterial Pathogenesis: A Molecular Approach, 2nd ed. ASM Press, Washington DC, 2002.

[46] A. Allen, G. Flemström, Gastroduodenal mucus bicarbonate barrier: protection against acid and pepsin, Am. J. Physiol. Cell Physiol. 288 (2005) C1–C19.

[47] D.Y. Singh, N.K. Prasad, Double liposomes mediated dual drug targeting for treatment of *Helicobacter pylori* infections, Pharmazie 66 (2011) 268–273.

[48] Z. Drulis-Kawa, A. Dorotkiewicz-Jach, Liposomes as delivery systems for antibiotics, Int. J. Pharm. 387 (2010) 187–198.

[49] P.L. Bardonnet, V. Faivre, P. Boullanger, M. Ollivon, F. Falson, Glycosylated liposomes against *Helicobacter pylori*: behavior in acidic conditions, Biochem. Biophys. Res. Commun. 383 (2009) 48–53.

[50] P. Sutton, Y.T. Chionh, Why can't we make an effective vaccine against *Helicobacter pylori*? Expert Rev. Vaccines 12 (2013) 433–441.

[51] W. Zhao, W. Wu, X. Xu, Oral vaccination with liposome-encapsulated recombinant fusion peptide of urease B epitope and cholera toxin B subunit affords prophylactic and therapeutic effects against *H. pylori* infection in BALB/c mice, Vaccine 25 (2007) 7664–7673.

[52] S.F. Moss, L. Moise, D. Soo, W. Kim, S. Zhang, J. Lee, A.B.. Rogers, W. Martin, A.S. Groot, HelicoVax: epitope-based therapeutic *Helicobacter pylori* vaccination in a mouse model, Vaccine 29 (2011) 2085–2091.

[53] J.W. Lim, H. Kim, K.H. Kim, NF-κB, inducible nitric oxide synthase and apoptosis by *Helicobacter pylori* infection, Free Radic. Biol. Med. 31 (2001) 355–366.

[54] A.K. Jain, A. Agarwal, H. Agrawal, G.P. Agrawal, Double liposome based dual-drug delivery system as vectors for effective management of peptic ulcer, J. Liposome Res. 22 (2012) 205–214.

[55] G. Fontana, M. Licciardi, S. Mansueto, D. Schillaci, G. Giammona, Amoxicillin-loaded polyethylcyanoacrylate nanoparticles: influence of PEG coating on the particle size, drug release rate and phagocytic uptake, Biomaterials 22 (2001) 2857–2865.

[56] L.M. Ensign, R. Cone, J. Hanes, Oral drug delivery with polymeric nanoparticles: the gastrointestinal mucus barriers, Adv. Drug Deliv. Rev. 64 (2012) 557–570.

[57] Y. Akiyama, N. Nagahara, T. Kashihara, S. Hirai, H. Toguchi, *In vitro* and *in vivo* evaluation of mucoadhesive microspheres prepared for the gastrointestinal tract using polyglycerol esters of fatty acids and a poly(acrylic acid) derivative, Pharm. Res. 12 (1995) 397–405.

[58] M. Cuña, M.J. Alonso, D. Torres, Preparation and *in vivo* evaluation of mucoadhesive microparticles containing amoxycillin-resin complexes for drug delivery to the gastric mucosa, Eur. J. Pharm. Biopharm. 51 (2001) 199–205.

[59] S. Harsha, Dual drug delivery system for targeting *H. pylori* in the stomach: preparation and *in vitro* characterization of amoxicillin-loaded Carbopol(R) nanospheres, Int. J. Nanomedicine 7 (2012) 4787–4796.

[60] A.O. Elzoghby, W.M. Samy, N.A. Elgindy, Protein-based nanocarriers as promising drug and gene delivery systems, J. Control. Release 161 (2012) 38–49.

[61] S. Ramteke, N.K. Jain, Clarithromycin- and omeprazole-containing gliadin nanoparticles for the treatment of *Helicobacter pylori*, J. Drug Target. 16 (2008) 65–72.

[62] R.B. Umamaheshwari, N.K. Jain, Receptor mediated targeting of lectin conjugated gliadin nanoparticles in the treatment of *Helicobacter pylori*, J. Drug Target. 11 (2003) 415–424.

[63] R.B. Umamaheshwari, S. Ramteke, N.K. Jain, Anti-*Helicobacter pylori* effect of mucoadhesive nanoparticles bearing amoxicillin in experimental gerbils model, AAPS PharmSciTech. 5 (2004) 1–9.

[64] S. Ramteke, R.B. Umamaheshwari, N.K. Jain, Clarithromycin based oral sustained release nanoparticulate drug delivery system, Indian J. Pharm. Sci. 68 (2006) 479–484.

[65] S. Ramteke, N. Ganesh, S. Bhattacharya, N.K. Jain, Triple therapy-based targeted nanoparticles for the treatment of *Helicobacter pylori*, J. Drug Target. 16 (2008) 694–705.

[66] J. Wang, Y. Tauchi, Y. Deguchi, K. Morimoto, Y. Tabata, Y. Ikada, Positively charged gelatin microspheres as gastric mucoadhesive drug delivery system for eradication of *H. pylori*, Drug Deliv. 7 (2000) 237–243.

[67] S. Harsha, Pharmaceutical suspension containing both immediate/sustained-release amoxicillin-loaded gelatin nanoparticles: preparation and *in vitro* characterization, Drug Des. Dev. Ther. 7 (2013) 1027–1033.

[68] I.C. Goncalves, A. Magalhaes, M. Fernandes, I.V. Rodrigues, C.A. Reis, M.C. Martins, Bacterial-binding chitosan microspheres for gastric infection treatment and prevention, Acta Biomater. 9 (2013) 9370–9378.

[69] R. Hejazi, M. Amiji, Stomach-specific anti-*H. pylori* therapy. I: preparation and characterization of tetracyline-loaded chitosan microspheres, Int. J. Pharm. 235 (2002) 87–94.

[70] F. Nogueira, I.C. Goncalves, M.C. Martins, Effect of gastric environment on *Helicobacter pylori* adhesion to a mucoadhesive polymer, Acta Biomater. 9 (2013) 5208–5215.

[71] Y.H. Lin, S.C. Tsai, CH. Lai, C.H. Lee, Z.S. He, G.C. Tseng, Genipin-cross-linked fucose-chitosan/heparin nanoparticles for the eradication of *Helicobacter pylori*, Biomaterials 34 (2013) 4466–4479.

[72] J.-H. Lee, D.-U. Lee, C.-S. Jeong, *Gardenia jasminoides* Ellis ethanol extract and its constituents reduce the risks of gastritis and reverse gastric lesions in rats, Food Chem. Toxicol. 47 (2009) 1127–1131.

[73] S. Shah, R. Qaqish, V. Patel, M. Amiji, Evaluation of the factors influencing stomach-specific delivery of antibacterial agents for *Helicobacter pylori* infection, J. Pharm. Pharmacol. 51 (1999) 667–672.

[74] A. Portero, C. Remunan-Lopez, M.T. Criado, M.J. Alonso, Reacetylated chitosan microspheres for controlled delivery of anti-microbial agents to the gastric mucosa, J. Microencapsul. 19 (2002) 797–809.

[75] C. Remuñán-López, A. Portero, M. Lemos, J.L. Vila-Jato, M.J. Nuñez, P. Riveiro, J.M. López, M. Piso, M.J. Alonso, Chitosan microspheres for the specific delivery of amoxycillin to the gastric cavity, STP Pharm. Sci. 10 (2000) 69–76.

[76] J.A. Raval, J.K. Patel, M.M. Patel, Formulation and *in vitro* characterization of spray dried microspheres of amoxicillin, Acta Pharma. 60 (2010) 455–465.

[77] J. Patel, P. Patil, Preparation and characterization of amoxicillin mucoadhesive microparticles using solution-enhanced dispersion by supercritical CO_2, J. Microencapsul. 29 (2012) 398–408.

[78] R. Hejazi, M. Amiji, Stomach-specific anti-*H. pylori* therapy. II. Gastric residence studies of tetracycline-loaded chitosan microspheres in gerbils, Pharm. Dev. Technol. 8 (2003) 253–262.

[79] R. Hejazi, M. Amiji, Stomach-specific anti-*H. pylori* therapy Part III: effect of chitosan microspheres crosslinking on the gastric residence and local tetracycline concentrations in fasted gerbils, Int. J. Pharm. 272 (2004) 99–108.

[80] M.M. Amiji, Tetracycline-containing chitosan microspheres for local treatment of *Helicobacter pylori* infection, Cellulose 14 (2006) 3–14.

[81] K.Y. Lee, D.J. Mooney, Alginate: properties and biomedical applications, Prog. Polym. Sci. 37 (2012) 106–126.

[82] M. Leonard, M.R. Boisseson, P. Hubert, F. Dalencon, E. Dellacherie, Hydrophobically modified alginate hydrogels as protein carriers with specific controlled release properties, J. Control. Release 98 (2004) 395–405.

[83] Y. Miyazaki, K. Ogihara, S. Yakou, T. Nagai, K. Takayama, *In vitro* and *in vivo* evaluation of mucoadhesive microspheres consisting of dextran derivatives and cellulose acetate butyrate, Int. J. Pharm. 258 (2003) 21–29.

[84] Y.-H. Lin, C.-H. Chang, Y.-S. Wu, Y.-M. Hsu, S.-F. Chiou, Y.-J. Chen, Development of pH-responsive chitosan/heparin nanoparticles for stomach-specific anti-*Helicobacter pylori* therapy, Biomaterials 30 (2009) 3332–3342.

[85] N. Nagahara, Y. Akiyama, M. Nakao, M. Tada, M. Kitano, Y. Ogawa, Mucoadhesive microspheres containing amoxicillin for clearance of *Helicobacter pylori*, Antimicrob. Agents Chemother. 42 (1998) 2492–2494.

[86] R.B. Umamaheshwari, S. Jain, N.K. Jain, A new approach in gastroretentive drug delivery system using cholestyramine, Drug Deliv. 10 (2003) 151–160.

[87] M.-K. Chun, H. Sah, H.-K. Choi, Preparation of mucoadhesive microspheres containing antimicrobial agents for eradication of *H. pylori*, Int. J. Pharm. 297 (2005) 172–179.

[88] Z. Liu, W. Lu, L. Qian, X. Zhang, P. Zeng, J. Pan, *In vitro* and *in vivo* studies on mucoadhesive microspheres of amoxicillin, J. Control. Release 102 (2005) 135–144.

[89] P.S. Rajinikanth, L.N. Karunagaran, J. Balasubramaniam, B. Mishra, Formulation and evaluation of clarithromycin microspheres for eradication of *Helicobacter pylori*, Chem. Pharm. Bull. 56 (2008) 1658–1664.

[90] J.K. Patel, J.R. Chavda, Formulation and evaluation of stomach-specific amoxicillin-loaded carbopol-934P mucoadhesive microspheres for anti-*Helicobacter pylori* therapy, J. Microencapsul. 26 (2009) 365–376.

[91] S.K. Jain, M.S. Jangdey, Lectin conjugated gastroretentive multiparticulate delivery system of clarithromycin for the effective treatment of *Helicobacter pylori*, Mol. Pharm. 6 (2008) 295–304.

[92] S.K. Jain, M. Gupta, A.K. Sahoo, A.N. Pandey, A.K. Jain, Lectin conjugated gastroretentive microspheres of amoxicillin for effective treatment of *Helicobacter pylori*, Curr. Sci. 106 (2014) 267–276.

[93] Y.S. Thorat, V.S. Modi, S.C. Dhavale, Use of carbomers to design mucoadhesive microspheres for an anti-*H. pylori* drug, clarithromycin, Int. J. Pharm. Technol. Res. 1 (2009) 1421–1428.

[94] S. Ramteke, N. Ganesh, S. Bhattacharya, N.K. Jain, Amoxicillin, clarithromycin, and omeprazole based targeted nanoparticles for the treatment of *H. pylori*, J. Drug Target. 17 (2009) 225–234.

[95] C.-H. Chang, Y.-H. Lin, C.-L. Yeh, Y.-C. Chen, S.-F. Chiou, Y.-M. Hsu, Y.-S. Chen, C.-C. Wang, Nanoparticles incorporated in pH-sensitive hydrogels as amoxicillin delivery for eradication of *H. pylori*, Biomacromolecules 11 (2010) 133–142.

[96] J.A. Ko, H.J. Lim, H.J. Park, Effect of microencapsulated precipitants of *Lactobacillus casei* ATCC 393 on *Helicobacter pylori* eradication, Process Biochem. 46 (2011) 631–635.

[97] M. Moogooee, H. Ramezanzadeh, S. Jasoori, Y. Omidi, S. Davaran, Synthesis and *in vitro* studies of cross-linked hydrogel nanoparticles containing amoxicillin, J. Pharm. Sci. 100 (2010) 1057–1066.

[98] N. Venkateswaramurthy, R. Sambathkumar, M. Vijayabaskaran, P. Perumal, Clarithromycin mucoadhesive microspheres for anti-*Helicobacter pylori* therapy: formulation and *in vitro* evaluation, Int. J. Curr. Pharm. Res. 2 (2010) 24–27.

[99] N. Venkateswaramurthy, R. Sambathkumar, P. Perumal, *In vivo* evaluation of amoxicillin trihydrate and clarithromycin-loaded mucoadhesive microspheres for *H. pylori* eradication, Trop. J. Pharm. Res. 12 (2013) 143–147.

[100] N. Venkateswaramurthy, R. Sambathkumar, M. Vijayabaskaran, P. Perumal, Formulation and *in vitro* evaluation of furazolidone mucoadhesive microspheres, Int. J. Pharm. Pharm. Sci. 2 (2010) 104–106.

[101] N. Venkateswaramurthy, P. Perumal, R. Sambathkumar, Design and evaluation of controlled release mucoadhesive microspheres of amoxicillin for anti *Helicobacter pylori* therapy, Asian J. Pharm. 5 (2011) 238–245.

[102] N. Venkateswaramurthy, R. Sambathkumar, Formulation and evaluation of stomach specific amoxicillin loaded mucoadhesive microspheres, Iran. J. Pharm. Sci. 6 (2010) 227–233.

[103] N. Venkateswaramurthy, R. Sambathkumar, P. Perumal, Controlled release mucoadhesive microspheres of clarithromycin for the treatment of *Helicobacter pylori* infection, Pharm. Lett. 4 (2012) 993–1004.

[104] Y. Liu, J. Zhang, Y. Gao, J. Zhu, Preparation and evaluation of glyceryl monooleate-coated hollow-bioadhesive microspheres for gastroretentive drug delivery, Int. J. Pharm. 413 (2011) 103–109.

[105] R. Pal, A.P.S. Bhadoria, S. Ramteke, Preparation and characterization of sodium alginate-carbopol-924P based mucoadhesive microbeads, Pharm. Lett. 3 (2011) 1–11.

[106] Y.-H. Lin, S.-F. Chiou, C.-H. Lai, S.-C Tsai, C.-W. Chou, S.-F. Peng, Z.-S. He, Formulation and evaluation of water-in-oil amoxicillin-loaded nanoemulsions using for *Helicobacter pylori* eradication, Process Biochem. 47 (2012) 1469–1478.

[107] S.C. Angadi, L.S. Manjeshwar, T.M. Aminabhavi, Novel composite blend microbeads of sodium alginate coated with chitosan for controlled release of amoxicillin, Int. J. Biol. Macromol. 51 (2012) 45–55.

[108] G.K. Tripathi, Formulation and evaluation pH stimuli sensitive multiparticulate delivery system of clarithromycin for the treatment of *Helicobacter pylori*, Int. J. Pharm. Technol. Res. 5 (2013) 07–16.

[109] S. Hao, Y. Wang, B. Wang, Q. Zou, H. Zeng, X. Chen, X. Liu, J. Liu, S. Yu, A novel gastroretentive porous microparticle for anti-*Helicobacter pylori* therapy: preparation, *in vitro* and *in vivo* evaluation, Int. J. Pharm. 463 (2014) 10–21.

[110] C.-H. Chang, W.-Y. Huang, C.-H. Lai, Y.-M. Hsu, Y.-H. Yao, T.-Y. Chen, J.-Y. Wu, S.-F. Peng, Y.-H. Lin, Development of novel nanoparticles shelled with heparin for berberine delivery to treat *Helicobacter pylori*, Acta Biomater. 7 (2011) 593–603.

[111] X. Zhu, D. Zhou, S. Guan, P. Zhang, Z. Zhang, Y. Huang, Preparation and characterization of novel multi-core chitosan microspheres for stomach-specific delivery of hydrophilic antibiotics, J. Mater. Sci. Mater. Med. 23 (2012) 983–990.

[112] P. Pan-In, A. Tachapruetinun, N. Chaichanawongsaroj, W. Banlunara, S. Suksamran, S. Wanichwech-Arungruang, Combating *Helicobacter pylori* infections with mucoadhesive nanoparticles loaded with *Garcinia mangostana* extract, Nanomedicine 9 (3) (2013) 457–468.

[113] M. Ali, K. Dhar, M. Jain, V. Pandit, Mucoadhesive microparticulate drug delivery system of curcumin against *Helicobacter pylori* infection: design, development and optimization, J. Adv. Pharm. Technol. Res. 5 (2014) 48.

[114] R.P. Raffin, D.S. Jornada, M.I. Ré, A.R. Pohlmann, S.S. Guterres, Sodium pantoprazole-loaded enteric microparticles prepared by spray drying: effect of the scale of production and process validation, Int. J. Pharm. 324 (2006) 10–18.

[115] S.-Y. Kim, H.-J. Doh, M.-H. Jang, Y.-J. Ha, S.-l. Chung, H.-J. Park, Oral immunization with *Helicobacter pylori*-loaded poly(D, L-lactide-co-glycolide) nanoparticles, Helicobacter 4 (1999) 33–39.

[116] J.-M. Ren, Q.-M. Zou, F.-K. Wang, Q. He, W. Chen, W.-K. Zen, PELA microspheres loaded *H. pylori* lysates and their mucosal immune response, World J. Gastroenterol. 8 (2002) 1098–1102.

[117] L. Figueiredo, C.C.R. Calado, A.J. Almeida, L.M.D. Gonçalves, Protein and DNA nanoparticulate multiantigenic vaccines against *H. pylori*: *in vivo* evaluation, 2nd Portuguese Meeting in Bioengineering (ENBENG), Coimbra, 2012.

[118] S. Thamphiwatana, V. Fu, J. Zhu, D. Lu, W. Gao, L. Zhang, Nanoparticle-stabilized liposomes for pH-responsive gastric drug delivery, Langmuir 29 (2013) 12228–12233.

[119] A.K. Jain, S.K. Jain, Development and characterization of nanolipobeads-based dual drug delivery system for *H. pylori* targeting, J. Drug Target. 21 (2013) 593–603.

[120] S. Chakraborti, S. Bhattacharya, R. Chowdhury, P. Chakrabarti, The molecular basis of inactivation of metronidazole-resistant *Helicobacter pylori* using polyethyleneimine functionalized zinc oxide nanoparticles, PLoS ONE 8 (2013).

[121] M.G. Russo, E.G. Vega Hissi, A.C. Rizzi, C.D. Brondino, Á.G. Salinas Ibañez, A.E. Vega, H.J. Silva, R. Mercader, G.E. Narda, Synthesis, physicochemical characterization, DFT calculation and biological activities of Fe(III) and Co(II)–omeprazole complexes. Potential application in the *Helicobacter pylori* eradication, J. Mol. Struct. 1061 (2014) 5–13.

[122] M. Amin, F. Anwar, M.R. Janjua, M.A. Iqbal, U. Rashid, Green synthesis of silver nanoparticles through reduction with *Solanum xanthocarpum* L. berry extract: characterization, antimicrobial and urease inhibitory activities against *Helicobacter pylori*, Int. J. Mol. Sci. 13 (2012) 9923–9941.

[123] Y. Luo, C. Wang, Y. Qiao, M. Hossain, L. Ma, M. Su, *In vitro* cytotoxicity of surface modified bismuth nanoparticles, J. Mater. Sci. Mater. Med. 23 (2012) 2563–2573.

[124] R. Chen, M.H. So, J. Yang, F. Deng, C.M. Che, H. Sun, Fabrication of bismuth subcarbonate nanotube arrays from bismuth citrate, Chem. Commun. (2006) 2265–2267.

[125] R. Chen, G. Cheng, M.H. So, J. Wu, Z. Lu, C.-M. Che, H. Sun, Bismuth subcarbonate nanoparticles fabricated by water-in-oil microemulsion-assisted hydrothermal process exhibit anti-*Helicobacter pylori* properties, Mater. Res. Bull. 45 (2010) 654–658.

[126] P. Nazari, R. Dowlatabadi-Bazaz, M.R. Mofid, M.R. Pourmand, N.E. Daryani, M.A. Faramarzi, Z. Sepehrizadeh, A.R. Shahverdi, The antimicrobial effects and metabolomic footprinting of carboxyl-capped bismuth nanoparticles against *Helicobacter pylori*, Appl. Biochem. Biotechnol. 172 (2014) 570–579.

[127] J.M. Irache, I. Esparza, C. Gamazo, M. Agueros, S. Espuelas, Nanomedicine: novel approaches in human and veterinary therapeutics, Vet. Parasitol. 180 (2011) 47–71.

[128] Y. Inoue, S. Yoshimura, Y. Tozuka, K. Moribe, T. Kumamoto, T. Ishikawa, K. Yamamoto, Application of ascorbic acid 2-glucoside as a solubilizing agent for clarithromycin: solubilization and nanoparticle formation, Int. J. Pharm. 331 (2007) 38–45.

[129] N. Al-Jaber, The relationship between antioxidant and anti-ulcer activities in Saudi honey samples harvested from various regions in different seasons, Food Nutr. Sci. 04 (2013) 131–138.

[130] S. Arora, J.M. Rajwade, K.M. Paknikar, Nanotoxicology and *in vitro* studies: the need of the hour, Toxicol. Appl. Pharmacol. 258 (2012) 151–165.

Chapter 2.4

Oral administration of lipid-based delivery systems to combat infectious diseases

This book chapter was written in consequence of the review paper shown in Chapter 2.3. We found out that lipid nanoparticles have not been applied to treat *H. pylori* infections. Nevertheless, its usefulness to treat other infectious diseases by oral administration was unquestionable. Hence, this chapter aimed to summarize the main characteristics of the gastrointestinal tract that should be considered when designing nanoparticles to be orally administrated. The main purpose was to be able to translate this knowledge to the rational design of the drug delivery system.
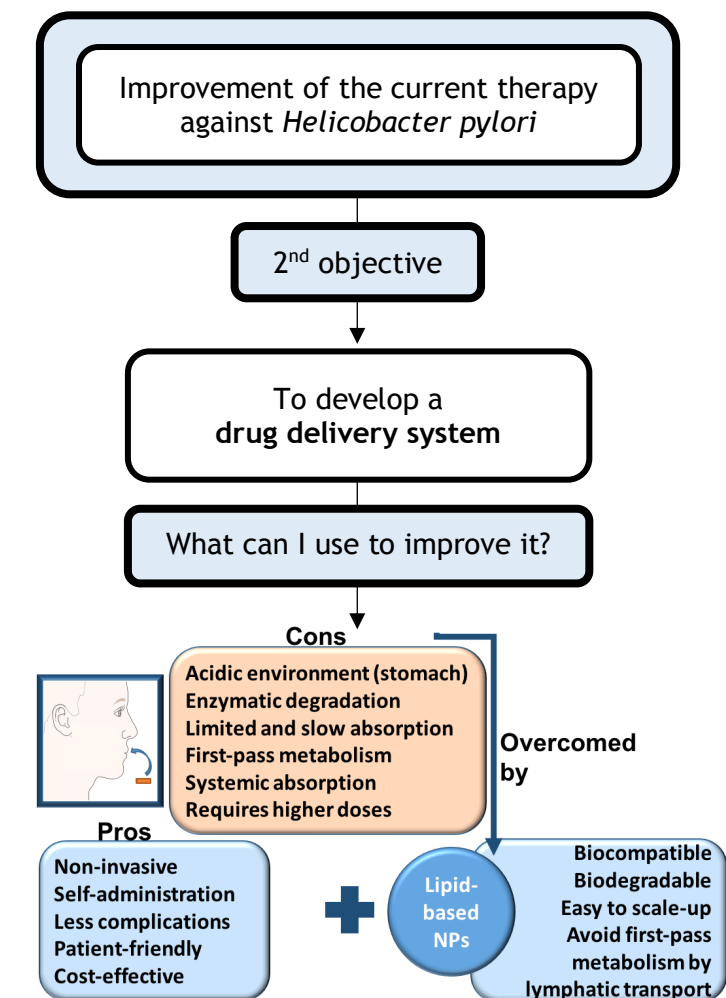
Reproduced with permission of Pan Stanford Publishing (Appendix A).

Chapter 4

Oral Administration of Lipid-Based Delivery Systems to Combat Infectious Diseases

Rita M. Pinto,[a,*] Daniela Lopes,[a,*] Cláudia Nunes,[a] Bruno Sarmento,[b,c] and Salette Reis[a]

[a]*UCIBIO, REQUIMTE, Department of Chemical Sciences, Faculty of Pharmacy, University of Porto, Portugal*
[b]*I3S - Institute of Research and Innovation in Health, University of Porto, Portugal*
[c]*CESPU - Institute for Advanced Research and Training in Health Sciences and Technologies and University Institute of Health Sciences, Gandra, Portugal*
shreis@ff.up.pt

According to the World Health Organization (WHO), infectious diseases are still one of the leading causes of death worldwide, englobing direct and indirect associations (e.g., cancers caused by infectious diseases). Furthermore, the increase of resistance with loss of drug efficacy and the lack of new antimicrobial drugs have become a worldwide challenge to provide adequate treatment against infectious diseases. The drawbacks associated with this

*Rita M. Pinto and Daniela Lopes contributed equally to the chapter.

problem lead daily to high costs to society and to health-care systems. Therefore, microparticles and NPs emerged as a promising drug delivery strategy to improve the current treatment against infectious diseases. Among all, lipid particles have been highlighted for their BA and their ability to incorporate both lipophilic and hydrophilic drugs, protecting them against in vivo degradation. Further, they can be produced on an industrial scale and can be orally administered, which play a key role in the increase of therapeutic compliance. However, different characteristics of the gastrointestinal tract must be taken into account in the design of delivery systems that aim for oral absorption and stability. This section aims to review these characteristics as well as the design of lipid micro- and nanoparticles to be applied in the treatment of infectious diseases.

4.1 Introduction

At the beginning of the twentieth century, infectious diseases were the leading cause of death at a worldwide level [1]. However, with the development of antimicrobial drugs and specially with the production of penicillin in the 1940s, the fight against microbial agents emerged [2]. Consequently, this phenomenon led to a significant decrease in morbidity and mortality resultant from infectious diseases [2]. Nevertheless, in 1999, the World Health Organization (WHO) reported that infectious diseases were the cause of 32% of deaths at a global level, most of the cases being from developing countries [3, 4]. The same organization also reported that infectious diseases were responsible for killing over 14 million people worldwide [5, 6]. Nowadays, the developed world is also being severely affected by infectious diseases, as a consequence of antimicrobial resistance (AMR) [7]. In the United States, AMR is estimated to be responsible for US$20 billion in extra costs to the health-care system and US$35 billion in costs to society per year [7, 8]. Besides, this phenomenon leads to more than 8 million additional days in hospitals [7]. AMR is also a concern in the European Union, since it is estimated that this phenomenon causes 25,000 deaths and costs more than US$1.5 billion per year [9]. These costs include both health-care expenses and loss in productivity [9].

AMR is a natural evolutionary process in microorganisms, since AMR genes existed long before the therapeutic application of antimicrobial drugs [7, 10]. For instance, in bacteria the occurrence of mutations in an infection cycle is highly probable due to the large number of bacteria, the rapid generation time, and the high intrinsic rate of mutation [11]. However, AMR is not exclusive to bacteria, since other microorganisms, such as parasites, viruses, and fungi, can acquire AMR [7]. In the last decades, this phenomenon has been rapidly evolving and spreading due to the wide use of antimicrobial agents in humans and animals [7]. In fact, the ability of antimicrobial drugs to induce genetic mutations in microbial pathogens is already proven [12]. This association is more significant when sublethal concentrations are used [12]. Consequently, there is no assurance that new antimicrobial drugs can respond to the increasing rates of resistance in a timely manner [2, 7, 13]. Thus, AMR is becoming a worldwide threat to efficient treatment of infectious diseases [14].

There are also other drawbacks of the current antimicrobial therapy. Oral administration is usually the primordial route due to its commodity and security [15]. However, it is also associated with poor bioavailability (BA) due to poor aqueous solubility and/or poor permeability of drugs [15]. The acidic pH of the stomach can also reduce the BA of drugs through their degradation [15]. Further, hepatic first-pass metabolism contributes to reducing the concentration of drugs in the systemic circulation, since drug metabolism occurs during this process [15, 16]. Consequently, infection conditions usually require high doses of antimicrobial drugs in order to achieve an adequate concentration in serum, which commonly lead to side effects [17]. However, even applying an aggressive antimicrobial treatment, the complete eradication of the infection can be difficult to achieve due to drugs' degradation or low efficacy [17]. The therapeutic effect of most antimicrobial agents is also compromised by intrinsic factors [18]. These factors include poor cellular penetration, limited intracellular retention, inefficient subcellular distribution, and decreased intracellular activity [18].

Novel and effective strategies are needed to overcome these limitations. One field that has been evolving in the last years is nanotechnology. Nanoparticles (NPs) protect drugs from the acidic conditions of the stomach, improve their half-life, and maintain a sustained drug release at the target site, leading to higher

concentrations of antimicrobial drugs near the microorganism, even with lower doses [19]. Hence, these delivery systems can minimize drugs' side effects and improve their therapeutic efficacy, decreasing the potential development of microbial resistance [19]. NPs are also capable of loading multiple antimicrobial agents within their structures [8]. As a consequence, AMR mechanisms are unlikely to develop, since it requires multiple and simultaneous gene mutations in the microbial DNA [8]. Combining these advantages with the possibility of vectorization to a specific target, NPs have been developed to be applied in several diseases, including infectious diseases. This section aims to summarize several approaches to combat infectious diseases by resorting to lipid-based delivery systems for oral administration. Further, studies to assess pharmacokinetic properties and therapeutic efficacy will also be discussed.

4.2 Oral Administration

Oral administration is the most convenient and safest route for drug administration [15]. This route is cost effective, has fewer complications, and is less intrusive than intravenous administration [15, 20]. Further, the possibility of self-administration and its feature as a patient-friendly route increase the therapeutic compliance [21]. However, the selection of the administration route should be dependent on the purpose and on the target site [22]. For instance, to target muscles or skin, a topical route is more advantageous [22]. On the other hand, to target the liver or the spleen, the intravenous route is preferential, but with a higher risk of local and vascular infection and patient discomfort [15, 20, 22].

Although oral administration is the most common route, it implies contact with an extremely acidic medium, with digestive enzymes, and with biliary salts [23, 24]. These drawbacks are associated with low BA of drugs in vivo, because of their degradation, poor solubility, and low ability to cross biological barriers [21]. One strategy to overcome these limitations is to use NPs to protect the drug from the harsh conditions of the environment and to enhance its permeability [21]. Still, it is necessary to take into account all the conditions and barriers of the GI tract (Fig. 4.1) in

order to surpass its restraints and, if possible, to take advantage of its characteristics to design the NP [21].
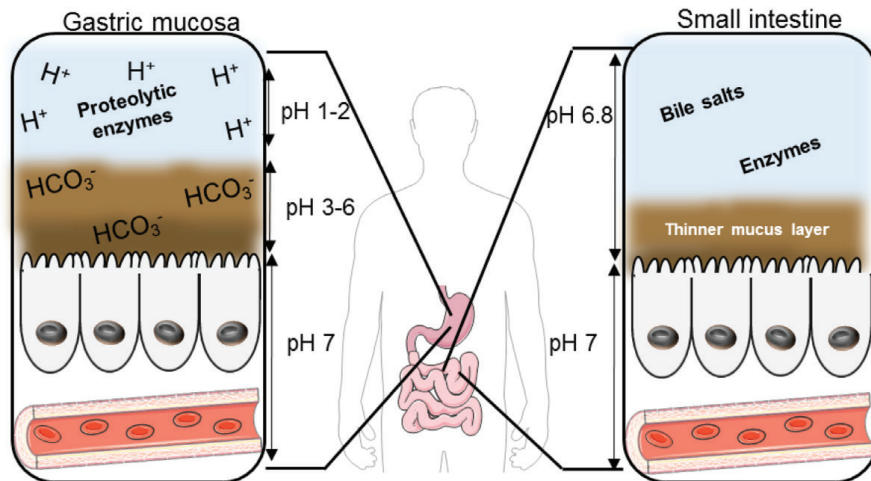
Figure 4.1 Schematic representation of the main differences between the gastric mucosa and the small intestine barrier. The pH of the lumen and the thickness of the mucus layer are the major differences.

The mucus layer is the first barrier for oral administration, and it is composed of water, salts, lipids, phospholipids, and different macromolecules, among which mucins are highlighted [25, 26]. It is divided in two different layers: the outer layer, which is loosely attached and has larger pores, and the inner layer, which is more packed [25]. Although the pore of the mucin fibers is around 100 nm, they are also able to pack, creating larger pores [25]. This barrier works simultaneously as a physical barrier to prevent the penetration of foreign substances and microorganisms and as a permeable gel that allows the diffusion of several molecules, including nutrients [25]. The mucus layer protects epithelial cells, which have restricted permeability [24]. Still, NPs are able to cross epithelial cells by transcellular or paracellular pathways [21].

In general, three different strategies have been used to enhance NP absorption through the mucus layer: (i) mucoadhesiveness, with attraction to a mucosa membrane due to several interactions established (e.g., electrostatic and H-bonds), (ii) mucolytic NPs, which have the disadvantage of favoring infections by disrupting the mucus barrier, and (iii) muco-penetrating NPs, by changing the size or their surface characteristics [19, 21, 27]. NPs are easily entrapped

within the protective outer mucus layer by steric difficulties or mucoadhesion features [24, 28]. As a consequence of high mucoadhesiveness, NP penetration and mobility within the mucosa may be affected [29]. Nevertheless, this entrapment can be very advantageous in gastric or enteric infections, such as by *Helicobacter pylori,* since a local release of the drug can be achieved. The NP-mucus interaction can be a consequence of electrostatic interactions, due to the surface charge, or of hydrophobic interactions [30]. However, it is also important to be aware that given the fast turnover of the gastric mucosa and the natural clearance of the GI tract, mucoadhesion of NPs may be affected, decreasing their permeability [28, 31]. Although the turnover time of the GI mucus is estimated to be higher than in other physiological sites, it is still very fast, especially in the loosely adherent layer [32]. NPs with higher penetration and establishment of interactions with deeper layers of the mucus may be a promising alternative [29, 30]. For that purpose, particles with a hydrophilic and uncharged surface may prevent the establishment of interactions with the mucus [27]. One promising strategy is the use of poly(ethylene glycol) (PEG), which is a hydrophilic compound and has an additional advantage of mucoadhesiveness and stability [24]. However, to treat bacterial infections, this strategy has been avoided since PEG prevents the fusion and the contact with bacterial membranes [33].

Mucin molecules are organized into a porous structure, which should be taken into account when the purpose is local penetration [27]. In general, the drug delivery system should be small enough to be able to overcome the steric obstruction caused by the mucus [27]. Furthermore, smaller particles are promptly distributed throughout the human body due to their ability to cross membrane or mucosa pores and to circulate in small vessels like capillaries [22]. Small size NPs are also highlighted by their therapeutic efficacy [22]. Using muco-penetrating NPs, it is possible to release the drug near the epithelial cells or even improve their intracellular delivery or uptake [24].

One important advantage of the GI tract is its large surface of absorption, which in total reaches around 300–400 m^2 [21]. The thickness varies along the GI tract, with the thinnest firmly adherent layer in the small intestine [21, 23]. Thus, this area is primary in the absorption of NPs [21]. One of the strategies used by

microorganisms to attach to and colonize the mucosa of the GI tract is the alteration of its bioequilibrium [25]. More specifically, they are able to disturb the equilibrium between the turnover rate and the secretion of mucus, which determines its thickness [34]. Learning from microorganisms' abilities, intelligent delivery systems can be designed, for instance, using ligands to epithelial receptors (e.g., bacterial lipopolysaccharide [LPS] or flagellin), which lead to the inhibition of the synthesis of mucus glycoproteins [25]. It is also possible to use lectins, vitamins, sugars, or adhesins to target the GI tract [24].

The GI tract has also several enzymes, such as lipases, that are able to degrade lipids [30]. Furthermore, the pH of the GI tract varies from 1.0 in the stomach lumen to 7.0 in the colon [30]. Even in the stomach, a pH gradient exists, given the low pH of the lumen and the physiologic pH near epithelial cells [35]. On the other hand, in the intestine, the pH is higher (around 6.8) [30]. These characteristics should be taken into consideration when designing particles for oral delivery, due to their instability under harsh conditions. Moreover, the intestinal barrier has a high immunologic ability, leading to a high loss of NPs by the action of the immune cells [30]. Nevertheless, their nanoparticulate state promotes the uptake by M cells of Peyer's patches [36]. Consequently, lipid NPs enable the system to bypass the effect of first-pass metabolism, through lymphatic absorption [36, 37].

It is inevitable to mention that a growing concern is the toxicity of NPs delivered through the oral route. The topical contact between NPs and epithelial cells can lead to a local toxicity, and the specific properties of the NP surface can interact with the GI tract, changing the cellular uptake of the NPs [21]. Usually, in vitro studies are performed; however, they are insufficient for a translation to a toxicity in the human body [24]. Studies of the effect of NPs on genes or on the immune system after oral administration are still lacking [24]. Lipid NPs are classified as biodegradable, since the human body is able to degrade these NPs [38]. However, even biodegradable NPs should be studied, since the products of their degradation can have toxic effects [21, 24]. The cytotoxicity of different lipid NPs was evaluated, and they all showed 90% cell viability, using Caco-2 cells [39]. In vivo studies of orally administered lipid NPs composed of

glycerol monostearate, tristearin, and Pluronic-F68 as a surfactant were also performed in rats, and they did not cause any damage to the intestinal epithelium [40]. Lipids are usually safe, and the use of surfactants and cosurfactants is more worrisome [21, 41]. Nevertheless, lipid NPs are still identified as well tolerated in living systems [41].

4.3 Lipid-Based Delivery Systems

4.3.1 Lipid-Based Nanoparticles

In the last decades, many colloidal drug carriers have been studied to improve drug solubility by oral administration [42]. For the majority of the NPs, a low-cost large-scale production method is currently not available [42]. Nevertheless, lipid-based NPs present the best features of other colloidal systems and have emerged as a strategy to overcome their limitations [42]. These NPs are usually composed of a matrix of physiological or physiologically related lipids characterized by their versatility, biocompatibility, and biodegradability [36, 38, 42]. Lipids are natural materials that can be degraded by natural processes, such as enzymatic activity [38]. Due to these processes, complex lipids are easily and completely degraded in the human body [38]. Therefore, the excipients that compose the matrix of lipid-based NPs are generally recognized as safe (GRAS) for oral and topical administration [41].

Lipid-based NPs exhibit other outstanding advantages, including improved kinetic stability, drug solubility, and controlled drug release [36, 38, 43, 44]. According to the production process, lipid-based NPs can be easily scaled up and their production can avoid the use of organic solvents [36]. Besides, lipid-based NP production is cost effective, which increases the researchers' interest in these nanocarriers [36, 41].

Different types of lipid-based NPs have been engineered, such as liposomes, solid lipid nanoparticles (SLNs), nanostructured lipid carriers (NLCs), lipid-drug conjugate (LDC) NPs, and micelles. In this section, the most commonly studied, which are represented in Fig. 4.2, will be discussed.
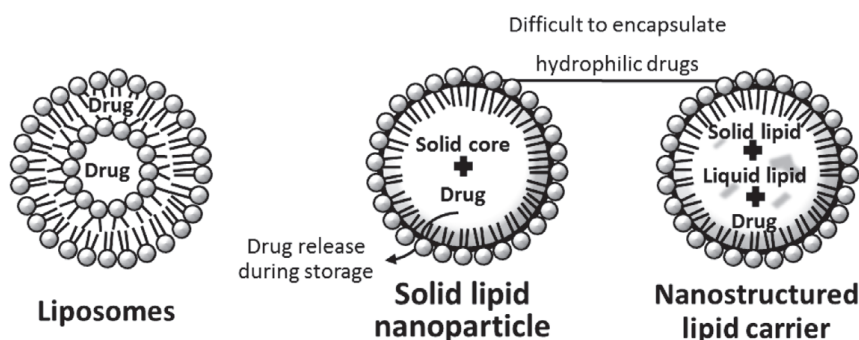
Figure 4.2 The three most common lipid-based NPs: (left) liposomes, (center) solid lipid nanoparticle, and (right) nanostructured lipid carrier.

Liposomes can incorporate both lipophilic and hydrophilic drugs, since they are composed of amphipathic lipids, which self-assemble into spherical vesicles with an aqueous core [45]. Liposomes have been the most studied drug delivery system to deliver antimicrobial drugs [2]. Their major advantages are their low toxicity, their versatility, and the possibility of coencapsulation [45]. Given their similarity to cell membranes, they are able to fuse with microbes [2, 46]. In fact, it has already been shown that the development of AMR is significantly reduced when the contact with the microorganism is by fusion [47].

SLNs were introduced in 1991 as an alternative to colloidal drug carriers, such as liposomes, emulsions, and polymeric microparticles and NPs [48]. SLNs are nanospheres with a mean particle size from 50 to 1000 nm, consisting of a matrix composed of lipids in a solid state at both room and body temperatures [36, 41, 49]. Fatty acids, waxes, monoglycerides, diglycerides, and triglycerides are widely used to construct the rigid core of SLNs [44]. To stabilize the solid matrix, various nontoxic surfactants can be added during SLN preparation, such as poloxamers, polysorbates, and polyvinyl alcohol [44, 50, 51].

To overcome the drawbacks of SLNs, namely the limited drug loading capacity and an early drug release during storage due to a structural reorganization, NLCs were studied [38, 42, 44]. The second generation of lipid-based NPs are composed of a lipid matrix with both solid and liquid lipids [44]. NLC matrices are less ordered and have imperfections due to the presence of the liquid lipid, providing more spaces to incorporate drugs when compared to SLNs

[41, 44]. Consequently, the drug loading capacity is enhanced, while drug release during storage is minimized [42, 44]. Besides, these nanocarriers are less susceptible to gelation during both preparation and storage, having a lower water content when compared to SLNs [38, 44].

4.3.2 Preventing Infectious Diseases by Oral Vaccines

Vaccines have been essential to humans and to the general public health, especially in terms of the global eradication of several infections, such as small pox in 1979 [52]. A more recent discovery was the possibility of using the oral route to administer vaccines against intestinal infections like cholera, rotavirus, and salmonella [53]. The advantages of oral vaccines are unquestionable and include higher compliance, reduction of severe side effects, and the possibility of self-administration, which is important in regions where access to medical care and instrumentation is lacking [53, 54]. Furthermore, regulatory issues related with oral administration are less strict than for injectable vaccines [53]. In fact, sterilization is not required for oral vaccines, facilitating their manufacture [54]. It is also less risky for medical personnel, since the probability of getting a transmittable disease is significantly reduced [53]. Another important advantage is the possibility to induce an immune response at the mucosa, since most of the pathogens (around 90%) infect humans by penetrating mucosal tissues, such as the lung and the GI tract [53, 54]. Although injectable vaccines are more effective in achieving a systemic immune response, they lack in terms of inducing a specific and local mucosa response to work as an immunological barrier to the invasion of pathogens [54]. Nevertheless, the oral route has several drawbacks associated with the high rate of failure in clinical trials, leading to the low number of licensed oral vaccines [53]. One limitation, and probably the most important one, is the instability that results from the features of the GI tract already mentioned, such as the low pH, the poor permeability, and the presence of several enzymes [23, 24]. This is particularly important since the efficacy of peptide or protein antigens is affected by proteolytic degradation [55]. NPs can be potent antigen delivery systems, by protecting and delivering the antigens

only near the immune cells [56]. Moreover, due to the ability of NPs to interact with and activate immune pathways, they can work as an adjuvant and enhance the immune response to the loaded antigen [56]. The use of delivery systems has also been associated with the possibility of single doses being the focus of interest of institutions like WHO, due to the opportunity of having simplified immunization schedules [52]. Besides, the incorporation of different compounds in the same NP, with a controlled release of each one, may also help the simplification of the immunization schedules [57].

Despite controversy, in general, smaller particles in the nanometer range are shown as the most promising ones for the immune stimulation, due to their ability to cross intestinal barriers [52]. However, as mentioned in Section 4.2, Peyer's patches allow a way of penetration through lymphatic absorption [36]. In the GI tract, the ileum has a predominance of these patches, making it a preferential region for the absorption of oral vaccines [53]. This pathway of absorption allows the use of bigger NPs with high efficacy [52]. If this pathway is chosen, it is important to design the NP according to that purpose. For instance, the functionalization with PEG is known to increase the stability of liposomes in vivo [58]. However, Minato et al. showed by administering PEG-modified and unmodified liposomes to mice that, for higher doses, the systemic immunity was higher in unmodified liposomes [58]. This may be a consequence of the protecting effect promoted by PEG, which suppresses the uptake by macrophages and probably the uptake by Peyer's patches [58]. Other properties, such as the sustained release and the physicochemical properties of the surface, are also important for a strong immune response [52]. For instance, surface hydrophobicity is essential for a good interaction between antigen presenting cells and NPs [59]. Cationic surfaces are also recognized as a higher potentiator of the antigen presenting cells, due to electrostatic interactions established with negative membranes [56]. However, they are still associated with higher toxicity in vivo [53]. Another key factor recently suggested by Liu et al. was the location of the antigen within the NP [60]. They used cationic lipid-poly(lactide-co-glycolide) acid (PLGA) hybrid NPs to test different locations of the antigen: (i) adsorbed, (ii) encapsulated, and (iii)

both adsorbed and encapsulated [60]. They reported, through in vivo studies, higher immunologic efficiency when the antigen was both adsorbed and encapsulated, providing simultaneously an initial antigen exposure and a controlled release and a long-term exposure of the antigen encapsulated [60].

Liposomes have been indicated as a potent adjuvant for immunization against several bacteria and viruses [55]. The use of multilamellar liposomes instead of unilamellar may be a better option due to their higher stability against detergents and their higher loading capacity of antigens [58]. Due to their composition, which includes an aqueous core and a hydrophobic bilayer, liposomes can load different types of antigens, including peptides and DNA [61]. For instance, Wang et al. proved that liposomes loading mycobacterium DNA were able to induce antigen-specific mucosal and humoral immune response against tuberculosis after oral administration to mice [62]. Furthermore, since they are usually endocytosed by antigen presenting cells, they are able to promote an effective adjuvant induction of the immune system, even when carrying weaker antigens [53, 61]. The similarity of these lipid nanocarriers to cell membranes allows their use in the encapsulation of toxins that interact with cell membranes in vivo [63]. Thus, this strategy has been used to develop toxoid vaccines [63]. It is also possible to use functionalization to improve the targeting and the uptake by immune cells [53]. Wang et al. used mannosylated liposomes for oral immunization against hepatitis B virus [64]. Due to the presence of mannose, liposomes were internalized by mononuclear cells via mannose receptors [64].

The use of other components, such as fucose and Ulex europaeus agglutinin-1 (UEA-1), has already shown enhanced uptake by M cells [53]. Moreover, the conjugation with specific antibodies also enhances the uptake in the GI tract [53].

Archaeosomes, which are liposomes composed of lipids from archaebacterial membranes, have also been used due to their adjuvant effect and their good tolerance [65]. Given their structure, archaeosomes are very stable, resisting oxidation, enzymes, bile salts, and even temperature and low pH [61]. Further, they are less permeable and their usefulness as oral vaccine carrier has

been proved [61, 65]. Other types of liposomes, such as lipoplex, lipopolyplex, and niosome, have also been used for vaccine formulations [66]. A comprehensive overview of the application of these liposomal structures is described elsewhere [66, 67].

Nanoemulsions have also been used due to their safety and immunogenicity, already proved in a phase I study [61]. These emulsions vary in size, from dozens to hundreds of nanometers, and can exist in an oil-in-water structure or the inverse, a water-in-oil structure [56]. A combination of strategies is also possible. For instance, Liau et al. used liposomes in a double emulsion for oral vaccines [68]. Due to their compartmental structure, with liposomes incorporated inside the water vacuoles of the double emulsion, they were able to achieve a prolonged release of the fluorescein isothiocyanate (FITC)-labeled ovalbumin-encapsulated nanoparticles [68]. Another strategy was designed by Hollmann et al. by creating liposomes coated with S-layer proteins from different bacteria [69]. The coating enhanced the liposomes' stability against bile salts, pH, and thermal shock [69].

Although the study of oral vaccine delivery systems has been exponentially increasing, there is still a long way to go for clinical application in humans [53]. Lipid NPs containing immunostimulatory compounds are still pointed out as one of the most advanced nanocarriers [52].

4.3.3 Treating Infectious Diseases

As previously mentioned, oral delivery is the most cost-effective routes and simultaneously the most comfortable to the patient [15]. However, due to the severe conditions of the GI tract, several lipid-based delivery systems have been widely studied to improve antimicrobial drugs' pharmacokinetics and to treat a wide range of infections. A summary of the advantages and drawbacks of oral administration and the usefulness of lipid-based NPs is presented in Fig. 4.3. Infectious diseases are disorders promoted by the invasion of pathogenic agents, including bacteria, viruses, fungi, and parasites. Herein we will give a few examples of how lipid-based NPs are advantageous for treating infectious diseases.
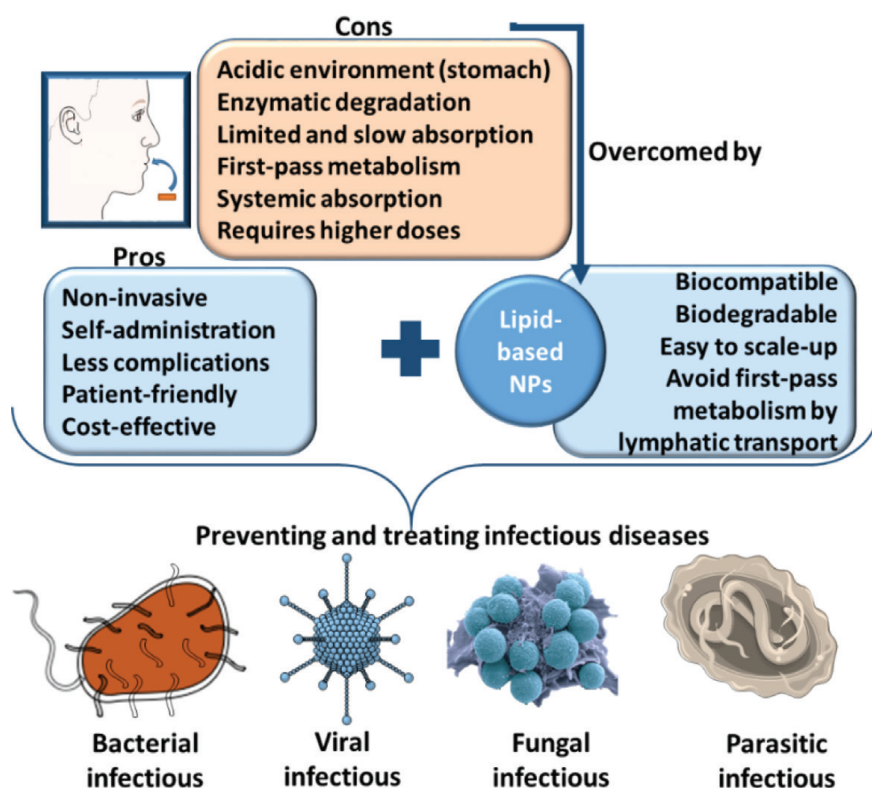
Figure 4.3 Schematic summary of the pros and cons of the oral administration and application of lipid-based NPs to overcome their limitations.

4.3.3.1 Bacterial infections

Given the limitation of the clinical use of antibiotics, namely their low BA [15, 16], researchers expect to find new and more efficient therapeutic approaches against bacterial infections. Lipid NPs and liposomes have been used to increase BA and aqueous solubility of many antibiotics.

Fluoroquinolones are widely used in clinics due to their safety and antibacterial efficacy [70, 71]. Norfloxacin is a synthetic third-generation fluoroquinolone with bactericidal activity against most of the gram-negative pathogens, being also active against some gram-positive bacteria [71, 72]. Nonetheless, this antimicrobial agent is associated with a poor aqueous solubility and low permeability [73]. Therefore, it has a low BA when administered by the oral route [71, 73]. To enhance its oral BA and pharmacological activity, Dong et al.

synthetized SLNs composed of SA as the solid lipid and polyvinyl acetate (PVA) as the emulsifier [73]. Plasma concentrations were higher for SLNs when compared with those of the free drug at all time points [73]. Antibacterial activity studies concluded that the SLNs remained effective against *Staphylococcus aureus* for a longer period of time when compared to that of the free drug [73]. Furthermore, cytotoxicity studies revealed that SLNs were biocompatible and presented low toxicity [73]. In conclusion, SLNs effectively enhanced BA and antibacterial activity of the drug, which can lead to lower doses and, consequently, decreased side effects and toxicity [73].

Besides antibiotics, many investigators are focusing their research on natural compounds with antimicrobial activity against a broad range of bacteria, such as free fatty acids [74]. For instance, linolenic acid has been highlighted due to its huge potential against all strains of *H. pylori*, including the ones resistant to metronidazole, which is one of the antibiotics usually administered in the standard treatment [75]. Therefore, Thamphiwatana et al. developed liposomal formulations to encapsulate linolenic acid in an innovative therapeutic approach [75]. To synthetize the liposomes, linolenic acid, L-α-phosphatidylcholine (EggPC), and cholesterol were mixed in a ratio of 3:6:1 [75]. The authors observed by fluorescence imaging that the liposomes were able to fuse with *H. pylori* [75]. To support this result, in vivo antibacterial studies were performed using C57BL/6 mouse as a model [75]. The animals were infected with the bacteria and further treated with the liposomal formulations, the standard triple therapy and PBS or bare liposome as control [75]. The results from this experiment showed that mice treated with the formulations had a reduced *H. pylori* burden of around 2.5 orders of magnitude compared to the negative controls [75]. On the other hand, triple therapy antibiotics only reduce it by around 1.4 orders of magnitude [75]. Moreover, a significant portion of liposomal formulations were able to accumulate within the mucus layer for at least 24 h, without compromising the gastric mucosal integrity [75]. Toxicological effects were evaluated in uninfected mice and demonstrated that the developed formulation was safe due to no apparent increase in gastric epithelial apoptosis [75]. Taking into account the previous results, it can be concluded that liposomes encapsulating linolenic acid have a huge potential to treat infections caused by *H. pylori* [75].

4.3.3.2 Viral infections

Viral infections are identified as one of the primary causes of death around the world [76]. Among the most worrisome viruses, the ones that are able to cause persistent infections that lead to cancer (e.g., hepatitis B virus and hepatitis C virus) or to immunodeficiency (e.g., HIV) are highlighted [76]. The main limitations of the current therapies are associated with the emergence of new viruses and the resistance mechanisms of the common viruses [77]. Since viruses are able to use the machinery of the host cell, the possibility of finding virus-specific proteins or enzymes that could be inhibited is extremely low [77]. Furthermore, when a virus-specific compound is found, it is usually particular for that virus, hindering the design of a broad-spectrum antivirus [77]. Another main drawback is the lack of antivirals able to combat latent infections [77].

Several NPs have been developed to improve the current antiviral treatment, including nanoemulsions, SLNs, and liposomes [78]. The advantages are well recognized. For instance, SLNs loading lapinavir, a poorly absorbed antiretroviral drug, proved their benefit by improving the drug's oral BA [79, 80]. These results were proven through in vivo studies, analyzing blood and lymph samples of Wistar rats [79, 80]. The higher oral BA was linked to intestinal lymphatic uptake, which avoids both the P-glycoprotein (Pgp) efflux pump and metabolism at the liver by cytochrome P450 [79]. The same benefit was highlighted by Makwana et al., when encapsulating efavirenz in SLNs composed of Gelucire 44/14, Compritol 888 ATO, Lipoid S75, and Poloxamer 188 [81]. In fact, SLNs were able to induce the secretion of chylomicron by enterocytes and, consequently, they increased the uptake through intestinal lymphatics [81]. This pathway of absorption is a key aspect when thinking of coadministration with other drugs that interact by inhibition or acceleration of metabolism at the liver [81].

NLCs have also been investigated as options to load antiviral drugs. For instance, Beloqui et al. loaded saquinavir in NLCs composed of Precirol ATO5, Miglyol 812, Tween 80, and Poloxamer 188 [82]. By changing their proportion, they reported sizes that varied from 165 nm to 1090 nm [82]. In vitro permeability studies showed that the amount of surfactant and the size were critical to the mechanism of transcytosis and to overcome the Pgp efflux

pump [82]. A year later, they evaluated the advantages of coating with dextran-protamine [83]. Using Caco-2 cell monolayers and Caco-2/HT29-MTX cell monolayers as models for enterocytes and mucus, respectively, they showed that dextran coating improved the permeability of the NPs [83]. In the mucus model, the improved effect was observed only when the surface was almost neutrally charged [83].

Liposomes have also been extensively used, and they have already proved their usefulness in lowering drug cytotoxicity as well as in improving the plasma half-life of antiviral drugs [78]. For instance, Zhong et al. synthetized liposomes composed of soya lecithin and cholesterol to incorporate a codrug composed of lamivudine and ursolic acid, which are used against the hepatitis B virus [84]. According to what was observed in the in vitro release, pharmacokinetic studies in rats showed that the time of circulation of the drug was enhanced when administered as a liposomal suspension [84]. Furthermore, the absorption was significantly improved, with a relative BA of 11-fold higher than the codrug suspension [84]. It is also possible to improve the stability of the nanosystem in the GI tract using tetraether lipids [85]. That strategy was applied by Uhl et al. to encapsulate Myrcludex B [85]. This peptide has activity against hepatitis B virus, and it is currently under evaluation in clinical trials [85]. However, its use is limited to subcutaneous application due to its degradation on oral administration [85]. In vivo studies revealed an improvement in the oral uptake of this peptide when incorporated in the liposomes [85].

The advantages of NPs in the treatment of viral infections are recognized, especially concerning the improvement of BA and the possibility to reduce the number of doses [77]. Consequently, the treatment can become a more cost-effective solution [77]. However, there are still ethical and scientific limitations that must be overcome to translate this technology into the clinic [77].

4.3.3.3 Fungal infections

In the last few decades, fungal infections have been an increasing concern, special due to nosocomial infections, which are a crucial cause of morbidity and mortality in hospitalized patients [86, 87]. One of the predominant nosocomial fungal pathogens is the *Candida* spp., among other fungi [87].

Due to the necessity to find new and more promising therapies against opportunistic fungi, a few studies reporting the use of both lipid NPs and liposomes were recently published. For instance, a recent work performed by Aljaeid et al. was focused on the development of SLNs as a drug delivery system to encapsulate miconazole, a broad-spectrum antifungal drug with poor aqueous solubility [88, 89]. The final formulation was composed of Precirol ATO5, Cremophor RH40, lecithin, and dicetylphosphate [90]. It showed an initial in vitro release of 45% of the drug (in the first 2 h), followed by a sustained release [90]. Nonetheless, an in vivo pharmacokinetic study was also performed, using albino male rabbits [90]. This experiment confirmed the results obtained in vitro, revealing a 2.5-fold increase of the drug's BA when compared to the capsule formulation currently existing in the market [90]. Furthermore, antifungal activity against *Candida albicans* was evaluated, showing that miconazole capsules exhibited enhanced antifungal activity compared to that of the powder alone [90]. However, SLNs showed the maximum inhibition zone compared to the previous two formulations [90]. Hence, the authors concluded that SLNs loading miconazole for oral administration enhanced its BA and were more efficient in the treatment of *C. albicans* infections [90].

Due to the relevance of miconizole as an antifungal agent, the encapsulation of this drug was evaluated in a study performed by Mendes and his coworkers [91]. Miconazole was encapsulated in NLCs to target the oral mucosa [91]. The optimal formulation was composed of Gelucire 43/01 as the solid lipid and Miglyol 812 as the lipid liquid, being posteriorly tested against *C. albicans* [91]. According to the results, the NLCs required lower concentrations of the drug to inhibit the total agent growth when compared to the concentrations of the drug needed in the free form [91]. The placebo formulations were also evaluated, and it was observed that the NPs per se have antifungal activity [91]. In a further experiment, the NLCs were incorporated in a hydrogel composed of glycerin and benzalkonium chloride to improve the local delivery to the oral mucosa [91]. The hydrogel showed a similar antimicrobial effect against *C. albicans* using a 17-fold lower drug dose compared to the oral gel available in the market [91]. Therefore, a lower drug

concentration is needed in each administration and the dosage frequency decreases, minimizing undesirable side effects [91].

Besides miconazole, other active substances were also encapsulated in lipid NPs to improve their therapeutic efficiency against fungal infections, such as oral candidiasis. For instance, Garg et al. formulated both SLNs and NLCs to load eugenol, a phenolic compound of clove oil [92]. In this work, SA was used as a solid lipid and caprylic triglyceride as the liquid lipid [92]. The authors verified that the particle size decreased from 332 nm to 87.7 nm when the liquid lipid was added to the formulation [92]. The antifungal activity of the formulations was further evaluated both in vitro and in vivo [92]. In vitro studies revealed that the eugenol-loaded NPs were able to inhibit *C. albicans* cellular growth after 24 h of incubation [92]. On the other hand, SLNs alone were not efficient [92]. To confirm these results, in vivo studies were performed in immunosuppressed rats orally infected with the fungal agent [92]. In in vivo studies, the authors observed that the animals treated with eugenol-loaded SLNs presented significant reduction of the log CFU (colony forming units) value, concluding that SLNs improve the therapeutic efficacy of eugenol against oral candidiasis [92].

Amphotericin B is also a relevant antifungal agent. Consequently, several liposomal-based drug delivery systems have been used to encapsulate the drug. However, oral delivery of liposomes presents some difficulties due to the hostile GI environment. Still, the drug delivery systems must be stable along the digestive tract. With this purpose, Skiba-Lahiani et al. developed oral amphotericin B–loaded liposomal formulations composed by vegetal ceramides [93]. The structural integrity of the vesicles was evaluated in the GI tract environment using an "artificial stomach-duodenum" model [93]. It was observed that the mean size increased after 30 min. of incubation in the digestive medium [93]. Nonetheless, the presence of ceramides in the formulations seems to limit these size variations when compared to formulations without ceramides [93]. Besides, these formulations were able to resist the hostile simulated GI environment composed of bile salts and digestive enzymes for a longer period of time [93]. In conclusion, liposomes with vegetal ceramides in their composition showed enhanced stability in the GI environment, which can be an advantage for oral administration of amphotericin B [93].

4.3.3.4 Parasitic infections

Parasitic infections are easily transmitted through contaminated food and are associated with high morbidity and mortality, especially in developing countries [94]. Despite the efforts, the fight against parasitic diseases is still unsatisfactory. The development of an effective vaccine is hindered by the fact that the majority of parasites do not induce a significant immune response [95]. Hence, the combat against parasitic infections is reduced to antiparasitic drugs [95]. Nevertheless, the drawbacks of the current treatment plans are several, including the toxicity and ineffectiveness of antiparasitic drugs, the costs of the treatment, and the resistance developed by parasites [96]. In general, antiparasitic drugs have low oral BA due to their degradation under the conditions of the GI tract combined with their low permeability [97]. Furthermore, some parasites are intracellular, hampering the exposure to drugs [96].

The possibility of using metallic-oxide-based NPs has been extensively studied due to their inhibitory effect against several infectious diseases [96]. NPs as drug delivery systems are also promising solutions for these types of diseases. The possibility of encapsulating synergic antimicrobials in the same delivery system, the high load capability with protection of the loaded drug, and the selective targeting may reduce the duration of the treatment, decrease toxic effects, and increase their efficacy [95]. For instance, Omwoyo et al. developed SLNs composed of SA to load dihydroartemisinin against malaria [98]. This drug is insoluble and unstable in acidic pH, which leads to a poor BA and a consequent insufficient efficacy [98]. The authors reported that the small size, of around 260 nm, allowed their uptake in the GI tract in a passive manner [98]. The protection of the drug against the severe conditions of the GI tract led to in vitro and in vivo efficacy [98]. When compared to the plain drug, the efficacy increased by 24% [98]. Therefore, this system may allow the reduction of the dose and its frequency [98]. Another artemisinin derivative, viz. arteether, was also encapsulated in SLNs composed of glycerol monostearate and three different surfactants (soya lecithin, Tween 80, and Pluronic F68) in different ratios [99]. Given its hydrophobicity, arteether is usually administered as an oily intramuscular injection [99]. In vivo studies showed a better pharmacokinetic profile after oral administration when the drug was incorporated into SLNs [99]. Thus, the use of this NP may

allow a different and more patient-friendly route of administration [99]. Arteether was also incorporated in NLCs to allow their oral administration [100]. In vivo studies showed an almost complete eradication of the *Plasmodium berghei* from blood samples of mice [100]. Further, a longer survival period was also achieved with these NPs [100]. Interestingly, this drug had already been incorporated in liposomes, with higher BA (relative BA around 98% for the NPs versus 32% for the oral suspension) [101].

Lipid-based NPs can also reduce the cytotoxicity of antiparasitic drugs. As an example, de Souza et al. encapsulated praziquantel, a commonly used drug against schistosomiasis, in SLNs composed of SA and Poloxamer 188 [102]. Besides the higher efficacy of the drug delivery system compared to that of the free drug, the authors also reported a lower toxicity in HepG2 cells, which are human hepatoma cells [102]. Since prazinquantel is associated with hepatotoxicity, these in vitro studies showed that the drug-loaded NP is a promising solution for decreasing praziquantel toxicity in vivo [102]. Moreover, the delivery system has a lower intestinal permeation than the plain drug, indicating that SLNs act as a reservoir, allowing a higher dose in mesenteric veins of the intestine, where the parasites are located [102].

Liposomal formulations targeting macrophages have also been studied to treat intracellular infections, such as leishmaniosis [97]. The use of sugars, viz. mannose and fucose, allows the targeting of the mannose-fucose receptors of macrophages [97]. This strategy has also been used for SLNs, with a high antileishmanial activity [97]. An overview of the advantages of SLNs/NLCs versus liposomes in the treatment of parasitic diseases is well described by Date et al. [95].

4.4 Evaluating Lipid-Based Nanoparticles

4.4.1 Studies to Assess Pharmacokinetic Properties

Oral administration requires that NPs be able to overcome the harsh conditions of the GI tract and to cross its barriers to reach the target. These properties have to be fully studied to evaluate the pharmacokinetic properties of the designed NP (Fig. 4.4).
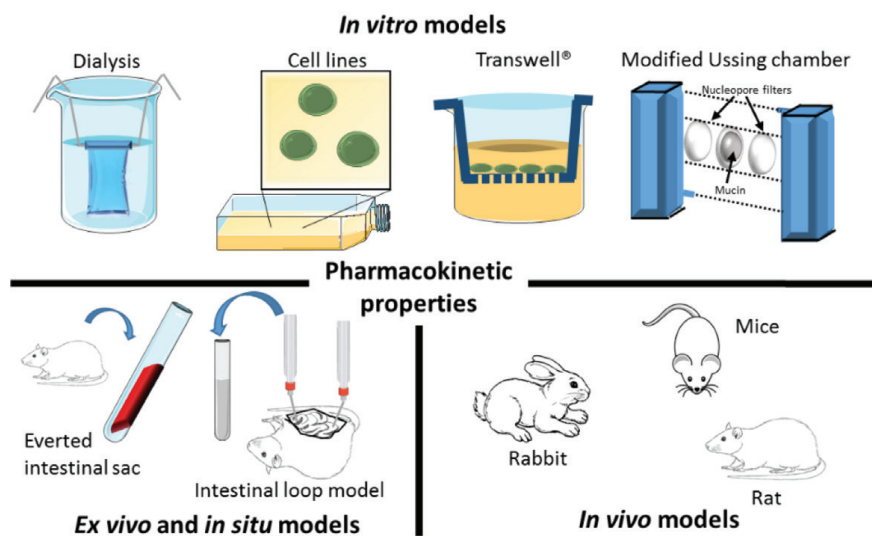
Figure 4.4 Schematic representation of the most common assays performed to evaluate the pharmacokinetic properties of NPs after oral administration. These assays include in vitro, ex vivo, in situ, and in vivo models.

In vitro techniques are the simplest ones to perform and are usually the first step after NP optimization. One of the most common experiments to evaluate the pharmacokinetics of drug delivery systems involves the observation of drug release in vitro. This evaluation is usually performed using the dialysis method, which is widely applied to lipid NPs. In this method, drug-loaded lipid NPs are added to a dialysis bag and dialyzed against a receiver solution [51]. For instance, Xie and coworkers applied this method, where ofloxacin-loaded SLNs were suspended in 0.1 M hydrochloric acid in a dialysis bag and further dialyzed against a higher volume of 0.1 M hydrochloric acid at 37°C under magnetic stirring [51]. At different time points, samples were taken from the receiver solution to determine the amount of drug diffused through the dialysis bag [51]. However, to have a more comprehensive and reliable medium, simulated gastric and intestinal fluids can be used [30]. Nevertheless, these assays are extremely simplistic, since the GI tract has enzymes and ionic strengths that affect the chemical and colloidal stability of the delivery system [30]. The complexity can be increased using cell models, namely Caco-2 cells and cocultures with Caco-2 cells and HT29 cell lines [27]. By combining both cell lines, a more complete model is obtained, with both absorptive and goblet cells [27]. Using

a Transwell setup, the transport of the NPs across the layer of cells can be assessed [30]. To study the possibility of uptake by M cells directly to the mucosal immune system, a coculture of Caco-2 cell lines and lymphocytes can be used [30].

The interaction with the mucus is also a key aspect of the pharmacokinetic, since it is the first barrier of the GI tract. It is also possible to use mucus models to evaluate the interaction established between the delivery system and the mucus. These models can be as simplistic as mucin solutions or as complex as those more similar to in vivo, by resorting to mucus provided by horses, pigs, or humans [103]. A comprehensive overview regarding mucus models is provided elsewhere [103]. Several techniques can be used in this type of studies, from zeta potential, size measurements, and rheological measurements to more complex permeability studies [28]. Besides the most common Transwell device, an Ussing chamber with a donor and an acceptor compartment separated by a vertical layer of mucus is also an alternative to mucus-NP interactions studies [28]. A very recent review was published with a summary of in vitro models of the intestinal barrier and the mechanisms of transport of lipid NPs [104]. More recent and advanced techniques are multiple particle tracking and the gut-on-a-chip setup. The first one uses video microscopy to track NPs, providing useful information regarding their qualitative movement in different environments [28]. The second novelty is a model able to mimic the properties of the intestine and its microbial flora, with fluid flow and mechanical movements [30].

To improve in vitro models and to overcome their limitations, especially regarding the lack of tissue interactions, ex vivo and in situ techniques have been performed [27]. Ex vivo techniques include the isolation of intestinal tissues, which may ultimately damage their properties [27]. On the other hand, in in situ models the connection of the excision with the animal is kept during the experiment and only after a variable period of time the animal is sacrificed [27, 30].

In vitro studies are useful for a preliminary study; however, in vivo models must be used to assess NPs absorption, biodistribution, tissue accumulation, and the ability of the animal to excrete the NPs [24]. The animals used for these experiments can be various, such as rats [73], mice [51], and rabbits [90]. In the work elaborated by Aljaeid and Hosny, albino male rabbits were randomly divided in two groups [90]. One group worked as a control, where the rabbits

were treated with the commercially available formulation in the market [90]. The other group was treated with the optimal solid lipid formulations developed by the authors [90]. At specific time points of the experiment, blood samples were collected and analyzed using high-performance liquid chromatography [90]. Furthermore, lymph samples of animal models can also be evaluated to look for an uptake by the intestinal lymphatic pathway [79].

Despite their unquestionable usefulness, animal models have their limitations that should be taken into account when translating the NP into clinical practice. An interesting and comprehensive overview by Kararli compares the GI tract of humans with the animal models commonly used in the preclinical studies [105]. For instance, the most common in vivo models, viz. rats and mice, have less mucin than humans [106]. On the other hand, models such as rabbits have a different quantity of Peyer's patches and rodents have less acidic stomachs [106].

4.4.2   Studies to Assess Therapeutic Efficacy

In this section, several examples demonstrate that NPs are able to enhance the therapeutic efficacy of antimicrobial agents. In fact, in general, drug-loaded NPs are more effective than the plain drugs [22]. This effect may happen by the improvement of the drug's BA, by improvement in its local concentration through controlled and targeted release, or even by a change in the route of administration to a more patient-friendly one [22]. The assessment of the therapeutic efficacy is then a crucial and key aspect to validate the usefulness of the delivery system. Indeed, it would be pointless to have a higher BA if it would not increase the drug's therapeutic efficacy.

In vitro assays are valuable tools to assess the therapeutic efficacy of antimicrobial NPs. For bacteria, in vitro antimicrobial activity studies are based on the determination of the minimum inhibitory concentration (MIC) and of the minimum bactericidal concentration (MBC) [107]. The MIC can be defined as the lowest concentration of a antimicrobial agent required to inhibit visible growth of an inoculum of the bacterium in a broth dilution test [108]. On other hand, MBC is the minimal concentration of a antimicrobial agent able to kill ≥99.9% of the initial inoculum within 24 h, and it is determined from broth dilution MIC tests by subculturing onto

antibiotic-free agar media [108]. For instance, in the work of Dong et al. serial dilutions of NP suspensions were mixed with *S. aureus* to a final bacterial concentration of 5.5×10^5 CFU/mL [73]. The mixture was posteriorly incubated at 37°C for 12 h and 24 h, with shaking [73]. Usually, the MIC is determined by a visual comparison of the medium turbidity of the cultures and the control tubes [108]. Alternatively, the MIC value can be determined by spectroscopy [110]. MBC is measured by subculturing the broths previously used for MIC measurement onto fresh agar plates at 37°C [73]. Therefore, the microbial colonies are counted when they are observed by the naked eye [73]. Besides the determination of MIC and MBC, studies of NP-pathogen interactions can be performed, such as agglutination assays, epifluorescence studies, TEM technique, and quantification of bacterial adhesion using luminescence [19]. These studies are reported in more detail elsewhere [19].

In the case of fungal infections, the determination of the MIC can also be applied. For instance, Mendes et al. evaluated the antifungal activity of miconazole against *C. albicans* by comparing the MIC of miconazole encapsulated in NLCs to its free form [91]. The same type of assay is also performed with parasites, such as for antimalarial efficacy [98] and against *Schistosoma mansoni* [102].

For viruses, the feasibility of in vitro studies depends on the virus. The recommendation is that in vitro studies be performed if there are currently available cell cultures in which the virus can survive and complete its life cycle [111]. For those viruses where in vitro studies can be performed, these studies can be a good complement before the in vivo studies. As an example, Ron-Doitch et al. infected HaCaT cells with herpes simplex virus 1 (HSV-1) and then evaluated cell viability [112]. In such assays, the EC_{50} (half maximal effective concentration) is used instead of the "inhibitory" concentration once the NPs' effect is determined by their ability to protect an infected cell [112].

Nonetheless, similar to what has been described for pharmacokinetic assays, in vivo efficacy against microbial agents should also be assessed since BA strongly affects NP efficacy. Before the evaluation of the therapeutic efficacy of the delivery system, it is important to establish the infective dose of the pathogen, which is the dose necessary to establish the infection without inducing severe or lethal infections in the animals [113]. On the other hand, the lethal

dose is responsible for deaths in 100% of the cases [113]. To perform this experiment, animals are divided into groups and infected with different concentrations of the pathogen. As an example, Wang et al. tested different concentrations of *Escherichia coli* [113]. The concentration that induces the deaths of all animals was considered the lethal dose [113]. When administering lower concentrations, some mice survived and bacterial counts were determined in several organs: heart, liver, lung, spleen, and kidneys [113]. Below the lethal concentration the bacteria were undetectable in all organs [113]. Therefore, this concentration was considered the infective dose [113]. A posterior mortality protection study was performed by the authors using 70 mice divided into 7 groups [113]. All the animals were injected intraperitoneally with the lethal infection inoculum size of bacteria and further treated with a single dose of norfloxacin-loaded SLNs [113]. Deaths were recorded over a 72 h period [113]. As in bacterial infections, the in vivo therapeutic efficacy of NPs against other pathogenic agents (viz. viruses, fungi, and parasites) can be evaluated by infecting animals with the pathogen of interest. After the infection, the survival rate, the manifestation of symptoms, or the rate of the pathogenic agent can be evaluated.

4.5   Conclusions and Future Perspectives

Among the scientific community, there is no doubt regarding the value of the oral route. Nevertheless, its limitations have also been highlighted, especially concerning the lower efficacy of drugs due to their lower BA after oral administration. Lipid NPs have been extensively studied to overcome several drawbacks of the current treatment of diverse diseases.

Their ability to protect the drug from the harsh conditions of the GI tract is a key advantage of drug delivery systems. This may be particularly interesting for the encapsulation of antimicrobial peptides. This emerging field includes naturally occurring molecules, produced by organisms such as plants and insects [114]. Their activity against several bacteria have been proved [114]. Nevertheless, being peptides, their stability in the GI tract may be compromised, which can be overcome by NPs. However, NPs have to be designed in conformity with the purpose, mainly concerning their stability under acidic conditions and in the presence of degradative

enzymes and their difficulty in crossing the mucus barrier. Several strategies have been made in order to overcome these limitations, such as mucus-penetrating NPs (reviewed in "Developments of Mucus Penetrating Nanoparticles" [27]) and mucoadhesive NPs [106]. However, despite the efforts, there are only a few NPs in the market [22]. One of the drawbacks that hinder the use in the clinic is the translation from the assays performed in the academic field to the administration to humans [22]. For instance, the most common in vivo models have several differences when compared to the anatomy and physiologic of the GI tract in humans [106]. All these factors, combined with different transit times and different commensal colonizations, hamper the translation to the clinic [106]. Furthermore, other limitations rise, such as the difficulty in scaling up and the cost benefit, which are most of the time far from desirable [22]. Another drawback is the lack of toxicity studies [21]. Despite the well-recognized safety of both the oral route and the lipid-based delivery systems, the low cytotoxicity should not be interpreted as nontoxicity in vivo, since other factors, such as genotoxicity and immunogenic toxicity, must be taken into account [24]. These limitations lead to a huge discrepancy between the thousands of papers published reporting NPs against infectious diseases and the only 276 clinical trials till date with such NPs [22]. The future encompasses an interdisciplinary collaboration [22]. To have an ideal NP, it must be effective and nontoxic. Thus, besides the collaboration of health-care researchers, such as physicists and pharmacists, other fields (e.g., biologists, virologists, and toxicologists) must be involved [22, 77].

At the end, and despite the extra cost of NPs in comparison with the current therapies, all the advantages of delivery systems may save financial resources. In fact, the efficacy is highly enhanced when NPs are used, lowering the frequency of dosage and the incidence of side effects. NPs may have an additional interest in cases where two or more drugs are used in the first-line treatment, facilitating the fight against viruses like HIV and bacteria such as *H. pylori* [22].

Acknowledgments

References

1. Cohen, M.L. Changing patterns of infectious disease. *Nature*, 2000, **406**(6797):762–767.

2. Huh, A.J., et al. "Nanoantibiotics": a new paradigm for treating infectious diseases using nanomaterials in the antibiotics resistant era. *J Controlled Release*, 2011, **156**(2):128–145.

3. The world health report 1999: making a difference. 1999, World Health Organization.

4. Fonkwo, P.N. Pricing infectious disease: the economic and health implications of infectious diseases. *EMBO Rep*, 2008, **9**(Suppl 1):S13–S17.

5. Taylor, L.H., et al. Risk factors for human disease emergence. *Philos Trans R Soc Lond B Biol Sci*, 2001, **356**(1411):983–989.

6. The world health report 2000, health systems: improving performance. 2000, World Health Organization.

7. Antimicrobial resistance global report on surveillance: 2014 summary. 2014, World Health Organization.

8. Pelgrift, R.Y., et al. Nanotechnology as a therapeutic tool to combat microbial resistance. *Adv Drug Deliv Rev*, 2013, **65**(13–14):1803–1815.

9. Antibiotic resistance fact sheet. 2015, World Health Organization. [cited 2016; Available from: http://www.who.int/mediacentre/factsheets/antibiotic-resistance/en/.

10. McBain, A.J., et al. Biocide tolerance and the harbingers of doom. *Int Biodeter Biodegrad*, 2001, **47**(2):55–61.

11. Walsh, C. Molecular mechanisms that confer antibacterial drug resistance. *Nature*, 2000, **406**(6797):775–781.

12. Sköld, O. *Antibiotics and Antibiotic Resistance*. John Wiley & Sons, Hoboken, New Jersey, 2011.

13. Hart, C.A. Antibiotic resistance: an increasing problem? *BMJ*, 1998, **316**(7140):1255–1256.

14. Mathers, C., et al. The global burden of disease: 2004 update. 2008, World Health Organization.

15. Harde, H., et al. Solid lipid nanoparticles: an oral bioavailability enhancer vehicle. *Expert Opin Drug Deliv*, 2011, **8**(11):1407–1424.

16. Pond, S.M., et al. First-pass elimination. Basic concepts and clinical consequences. *Clin Pharmacokinet*, 1984, **9**(1):1–25.

17. Beaulac, C., et al. Eradication of mucoid Pseudomonas aeruginosa with fluid liposome-encapsulated tobramycin in an animal model of chronic pulmonary infection. *Antimicrob Agents Chemother*, 1996, **40**(3):665–669.

18. Xie, S., et al. Biodegradable nanoparticles for intracellular delivery of antimicrobial agents. *J Controlled Release*, 2014, **187**:101–117.

19. Lopes, D., et al. Targeting strategies for the treatment of Helicobacter pylori infections, in *Nano Based Drug Delivery*, Naik, J. ed. IAPC Publishing, Croatia, 2015, pp. 339–366.

20. MacGregor, R.R., et al. Oral administration of antibiotics: a rational alternative to the parenteral route. *Clin Infect Dis*, 1997, **24**(3):457–467.

21. Araújo, F., et al. Safety and toxicity concerns of orally delivered nanoparticles as drug carriers. *Expert Opin Drug Metab Toxicol*, 2014, **11**(3):1–13.

22. Zazo, H., et al. Current applications of nanoparticles in infectious diseases. *J Controlled Release*, 2016, **224**:86–102.

23. Bakhru, S.H., et al. Oral delivery of proteins by biodegradable nanoparticles. *Adv Drug Deliv Rev*, 2013, **65**(6):811–821.

24. Ojer, P., et al. Toxicity evaluation of nanocarriers for the oral delivery of macromolecular drugs. *Eur J Pharm Biopharm*, 2015, **97**(Pt A):206–217.

25. Gamazo, C., et al. Mimicking microbial strategies for the design of mucus-permeating nanoparticles for oral immunization. *Eur J Pharm Biopharm*, 2015, **96**:454–463.

26. Boltin, D., et al. Pharmacological and alimentary alteration of the gastric barrier. *Best Pract Res Clin Gastroenterol*, 2014, **28**(6):981–994.

27. Liu, M., et al. Developments of mucus penetrating nanoparticles. *Asian J Pharm Sci*, 2015, **10**(4):275–282.

28. Griessinger, J., et al. Methods to determine the interactions of micro- and nanoparticles with mucus. *Eur J Pharm Biopharm*, 2015, **96**:464–476.

29. Arora, S., et al. Amoxicillin loaded chitosan-alginate polyelectrolyte complex nanoparticles as mucopenetrating delivery system for h. pylori. *Sci Pharm*, 2011, **79**(3):673–694.

30. Gamboa, J.M., et al. In vitro and in vivo models for the study of oral delivery of nanoparticles. *Adv Drug Deliv Rev*, 2013, **65**(6):800–810.

31. Lopes, D., et al. Eradication of Helicobacter pylori: past, present and future. *J Controlled Release*, 2014, **189**:169–86.

32. Boegh, M., et al. Mucus as a barrier to drug delivery - understanding and mimicking the barrier properties. *Basic Clin Pharmacol Toxicol*, 2015, **116**:178–186.

33. Thamphiwatana, S., et al. Nanoparticle-stabilized liposomes for pH-responsive gastric drug delivery. *Langmuir*, 2013, **29**(39):12228–12233.

34. Cone, R.A. Barrier properties of mucus. *Adv Drug Deliv Rev*, 2009, **61**(2):75–85.

35. Allen, A., et al. Gastroduodenal mucus bicarbonate barrier: protection against acid and pepsin. *Am J Physiol Cell Physiol*, 2005, **288**(1):C1–C19.

36. Battaglia, L., et al. Lipid nanoparticles: state of the art, new preparation methods and challenges in drug delivery. *Expert Opin Drug Deliv*, 2012, **9**(5):497–508.

37. Fricker, G., et al. Phospholipids and lipid-based formulations in oral drug delivery. *Pharm Res*, 2010, **27**(8):1469–1486.

38. Pardeike, J., et al. Lipid nanoparticles (SLN, NLC) in cosmetic and pharmaceutical dermal products. *Int J Pharm*, 2009, **366**(1–2):170–184.

39. Silva, A.C., et al. Preparation, characterization and biocompatibility studies on risperidone-loaded solid lipid nanoparticles (SLN): high pressure homogenization versus ultrasound. *Colloids Surf B*, 2011, **86**(1):158–165.

40. Rawat, M.K., et al. In vivo and cytotoxicity evaluation of repaglinide-loaded binary solid lipid nanoparticles after oral administration to rats. *J Pharm Sci*, 2011, **100**(6):2406–2417.

41. Severino, P., et al. Current state-of-art and new trends on lipid nanoparticles (SLN and NLC) for oral drug delivery. *J Drug Deliv*, 2012, **2012**:750891.

42. Das, S., et al. Recent advances in lipid nanoparticle formulations with solid matrix for oral drug delivery. *AAPS PharmSciTech*, 2011, **12**(1):62–76.

43. Anton, N., et al. Design and production of nanoparticles formulated from nano-emulsion templates - a review. *J Controlled Release*, 2008, **128**(3):185–199.

44. Ali Khan, A., et al. Advanced drug delivery to the lymphatic system: lipid-based nanoformulations. *Int J Nanomed*, 2013, **8**:2733–2744.

45. Drulis-Kawa, Z., et al. Liposomes as delivery systems for antibiotics. *Int J Pharm*, 2010, **387**(1–2):187–198.

46. Blecher, K., et al. The growing role of nanotechnology in combating infectious disease. *Virulence*, 2011, **2**(5):395–401.

47. Obonyo, M., et al. Antibacterial activities of liposomal linolenic acids against antibiotic-resistant Helicobacter pylori. *Mol Pharm*, 2012, **9**(9):2677–2685.

48. Muller, R.H., et al. Solid lipid nanoparticles (SLN) for controlled drug delivery - a review of the state of the art. *Eur J Pharm Biopharm*, 2000, **50**(1):161–177.

49. Wilczewska, A.Z., et al. Nanoparticles as drug delivery systems. *Pharmacol Rep*, 2012, **64**(5):1020–1037.

50. Abed, N., et al. Nanocarriers for antibiotics: a promising solution to treat intracellular bacterial infections. *Int J Antimicrob Agents*, 2014, **43**(6):485–496.

51. Xie, S., et al. Preparation and evaluation of ofloxacin-loaded palmitic acid solid lipid nanoparticles. *Int J Nanomed*, 2011, **6**:547–555.

52. Correia-Pinto, J.F., et al. Vaccine delivery carriers: insights and future perspectives. *Int J Pharm*, 2013, **440**(1):27–38.

53. Davitt, C.J., et al. Delivery strategies to enhance oral vaccination against enteric infections. *Adv Drug Deliv Rev*, 2015, **91**:52–69.

54. Marasini, N., et al. Oral delivery of nanoparticle-based vaccines. *Expert Rev Vaccines*, 2014, **13**(11):1361–1376.

55. Almeida, A.J., et al. Solid lipid nanoparticles as a drug delivery system for peptides and proteins. *Adv Drug Deliv Rev*, 2007, **59**(6):478–490.

56. Zhao, L., et al. Nanoparticle vaccines. *Vaccine*, 2014, **32**(3):327–337.

57. das Neves, J., et al. Nanotechnology-based systems for the treatment and prevention of HIV/AIDS. *Adv Drug Deliv Rev*, 2010, **62**(4–5):458–477.

58. Minato, S., et al. Application of polyethyleneglycol (PEG)-modified liposomes for oral vaccine: effect of lipid dose on systemic and mucosal immunity. *J Controlled Release*, 2003, **89**(2):189–197.

59. Yue, H., et al. Polymeric micro/nanoparticles: particle design and potential vaccine delivery applications. *Vaccine*, 2015, **33**(44):5927–5936.

60. Liu, L., et al. Immune responses to vaccines delivered by encapsulation into and/or adsorption onto cationic lipid-PLGA hybrid nanoparticles. *J Controlled Release*, 2016, **225**:230–239.

61. Newsted, D., et al. Advances and challenges in mucosal adjuvant technology. *Vaccine*, 2015, **33**(21):2399–2405.

62. Wang, D., et al. Liposomal oral DNA vaccine (mycobacterium DNA) elicits immune response. *Vaccine*, 2010, **28**(18):3134–3142.

63. Fang, R.H., et al. Engineered nanoparticles mimicking cell membranes for toxin neutralization. *Adv Drug Deliv Rev*, 2015, **90**:69–80.

64. Wang, T., et al. Mannosylated and lipid A-incorporating cationic liposomes constituting microneedle arrays as an effective oral mucosal HBV vaccine applicable in the controlled temperature chain. *Colloids Surf B*, 2015, **126**:520–530.

65. Li, Z., et al. Archaeosomes with encapsulated antigens for oral vaccine delivery. *Vaccine*, 2011, **29**(32):5260–5266.

66. Watson, D.S., et al. Design considerations for liposomal vaccines: influence of formulation parameters on antibody and cell-mediated immune responses to liposome associated antigens. *Vaccine*, 2012, **30**(13):2256–2272.

67. Wang, S., et al. Intranasal and oral vaccination with protein-based antigens: advantages, challenges and formulation strategies. *Protein Cell*, 2015, **6**(7):480–503.

68. Liau, J.J., et al. A lipid based multi-compartmental system: liposomes-in-double emulsion for oral vaccine delivery. *Eur J Pharm Biopharm*, 2015, **97**(Pt A):15–21.

69. Hollmann, A., et al. Characterization of liposomes coated with S-layer proteins from lactobacilli. *Biochim Biophys Acta*, 2007, **1768**(3):393–400.

70. Appelbaum, P.C., et al. The fluoroquinolone antibacterials: past, present and future perspectives. *Int J Antimicrob Agents*, 2000, **16**(1):5–15.

71. Breda, S.A., et al. Solubility behavior and biopharmaceutical classification of novel high-solubility ciprofloxacin and norfloxacin pharmaceutical derivatives. *Int J Pharm*, 2009, **371**(1–2):106–113.

72. Holmes, B., et al. Norfloxacin. A review of its antibacterial activity, pharmacokinetic properties and therapeutic use. *Drugs*, 1985, **30**(6):482–513.

73. Dong, Z., et al. Preparation and in vitro, in vivo evaluations of norfloxacin-loaded solid lipid nanopartices for oral delivery. *Drug Deliv*, 2011, **18**(6):441–450.

74. Desbois, A.P., et al. Antibacterial free fatty acids: activities, mechanisms of action and biotechnological potential. *Appl Microbiol Biotechnol*, 2010, **85**(6):1629–1642.

75. Thamphiwatana, S., et al. In vivo treatment of Helicobacter pylori infection with liposomal linolenic acid reduces colonization and ameliorates inflammation. *Proc NatI Acad Sci USA*, 2014, **111**(49):17600–17605.

76. Galdiero, S., et al. Silver nanoparticles as potential antiviral agents. *Molecules*, 2011, **16**(10):8894–8918.

77. Lembo, D., et al. Nanoparticulate delivery systems for antiviral drugs. *Antivir Chem Chemother*, 2010, **21**(2):53–70.

78. Shao, J., et al. Nanodrug formulations to enhance HIV drug exposure in lymphoid tissues and cells: clinical significance and potential impact on treatment and eradication of HIV/AIDS. *Nanomedicine*, 2016, **11**(5):545–564.

79. Negi, J.S., et al. Development of solid lipid nanoparticles (SLNs) of lopinavir using hot self nano-emulsification (SNE) technique. *Eur J Pharm Sci*, 2013, **48**(1–2):231–239.

80. Aji Alex, M.R., et al. Lopinavir loaded solid lipid nanoparticles (SLN) for intestinal lymphatic targeting. *Eur J Pharm Sci*, 2011, **42**(1–2):11–18.

81. Makwana, V., et al. Solid lipid nanoparticles (SLN) of Efavirenz as lymph targeting drug delivery system: elucidation of mechanism of uptake using chylomicron flow blocking approach. *Int J Pharm*, 2015, **495**(1):439–446.

82. Beloqui, A., et al. Mechanism of transport of saquinavir-loaded nanostructured lipid carriers across the intestinal barrier. *J Controlled Release*, 2013, **166**(2):115–123.

83. Beloqui, A., et al. Dextran-protamine coated nanostructured lipid carriers as mucus-penetrating nanoparticles for lipophilic drugs. *Int J Pharm*, 2014, **468**(1–2):105–111.

84. Zhong, Y., et al. Preparation and evaluation of liposome-encapsulated codrug LMX. *Int J Pharm*, 2012, **438**(1–2):240–248.

85. Uhl, P., et al. A liposomal formulation for the oral application of the investigational hepatitis B drug Myrcludex B. *Eur J Pharm Biopharm*, 2016, **103**:159–166.

86. Jarvis, W.R. Epidemiology of nosocomial fungal infections, with emphasis on Candida species. *Clin Infect Dis*, 1995, **20**(6):1526–1530.

87. Perlroth, J., et al. Nosocomial fungal infections: epidemiology, diagnosis, and treatment. *Med Mycol*, 2007, **45**(4):321–346.

88. Jain, S., et al. Design and development of solid lipid nanoparticles for topical delivery of an anti-fungal agent. *Drug Deliv*, 2010, **17**(6):443–451.

89. Pedersen, M., et al. Formation and antimycotic effect of cyclodextrin inclusion complexes of econazole and miconazole. *Int J Pharm*, 1993, **90**(3):247–254.

90. Aljaeid, B.M., et al. Miconazole-loaded solid lipid nanoparticles: formulation and evaluation of a novel formula with high bioavailability and antifungal activity. *Int J Nanomed*, 2016, **11**:441–447.

91. Mendes, A.I., et al. Miconazole-loaded nanostructured lipid carriers (NLC) for local delivery to the oral mucosa: improving antifungal activity. *Colloids Surf B*, 2013, **111**:755–763.

92. Garg, A., et al. Enhancement in antifungal activity of eugenol in immunosuppressed rats through lipid nanocarriers. *Colloids Surf B*, 2011, **87**(2):280–288.

93. Skiba-Lahiani, M., et al. Development and characterization of oral liposomes of vegetal ceramide based amphotericin B having enhanced dry solubility and solubility. *Mater Sci Eng C Mater Biol Appl*, 2015, **48**:145–149.

94. Torgerson, P.R., et al. World Health Organization estimates of the global and regional disease burden of 11 foodborne parasitic diseases, 2010: a data synthesis. *PLoS Med*, 2015, **12**(12):e1001920.

95. Date, A.A., et al. Parasitic diseases: liposomes and polymeric nanoparticles versus lipid nanoparticles. *Adv Drug Deliv Rev*, 2007, **59**(6):505–521.

96. Yah, C.S., et al. Nanoparticles as potential new generation broad spectrum antimicrobial agents. *Daru*, 2015, **23**:43.

97. Pham, T.T., et al. Strategies for the design of orally bioavailable antileishmanial treatments. *Int J Pharm*, 2013, **454**(1):539–552.

98. Omwoyo, W.N., et al. Development, characterization and antimalarial efficacy of dihydroartemisinin loaded solid lipid nanoparticles. *Nanomedicine*, 2016, **12**(3):801–809.

99. Dwivedi, P., et al. Pharmacokinetics study of arteether loaded solid lipid nanoparticles: an improved oral bioavailability in rats. *Int J Pharm*, 2014, **466**(1–2):321–327.

100. Ali, Z., et al. Development and characterization of arteether-loaded nanostructured lipid carriers for the treatment of malaria. *Artif Cells Nanomed Biotechnol*, 2014, **44**(2):545–549.

101. Bayomi, M.A., et al. In vivo evaluation of arteether liposomes. *Int J Pharm*, 1998, **175**:1–7.

102. de Souza, A.L., et al. In vitro evaluation of permeation, toxicity and effect of praziquantel-loaded solid lipid nanoparticles against Schistosoma mansoni as a strategy to improve efficacy of the schistosomiasis treatment. *Int J Pharm*, 2014, **463**(1):31–37.

103. Groo, A.C., et al. Mucus models to evaluate nanomedicines for diffusion. *Drug Discov Today*, 2014, **19**(8):1097–1108.

104. Beloqui, A., et al. Mechanisms of transport of polymeric and lipidic nanoparticles across the intestinal barrier. *Adv Drug Deliv Rev*, 2016, 106(Pt B):242–255.

105. Kararli, T.T. Comparison of the gastrointestinal anatomy, physiology, and biochemistry of humans and commonly used laboratory animals. *Biopharm Drug Dispos*, 1995, **16**:351–380.

106. Ensign, L.M., et al. Oral drug delivery with polymeric nanoparticles: the gastrointestinal mucus barriers. *Adv Drug Deliv Rev*, 2012, **64**(6):557–570.

107. Andrews, J.M. Determination of minimum inhibitory concentrations. *J Antimicrob Chemother*, 2001, **48**(Suppl 1):5–16.

108. French, G.L. Bactericidal agents in the treatment of MRSA infections-the potential role of daptomycin. *J Antimicrob Chemother*, 2006, **58**(6):1107–1117.

109. Hazzah, H.A., et al. Gelucire-based nanoparticles for curcumin targeting to oral mucosa: preparation, characterization, and antimicrobial activity assessment. *J Pharm Sci*, 2015, **104**(11):3913–3924.

110. Severino, P., et al. Sodium alginate-cross-linked polymyxin B sulphate-loaded solid lipid nanoparticles: antibiotic resistance tests and HaCat and NIH/3T3 cell viability studies. *Colloids Surf B*, 2015, **129**:191–197.

111. Guidance for industry; Antiviral product development - conducting and submiting virology studies to the agency. Department of Health and Human Services (Food and Drug Administration), 2006.

112. Ron-Doitch, S., et al. Reduced cytotoxicity and enhanced bioactivity of cationic antimicrobial peptides liposomes in cell cultures and 3D epidermis model against HSV. *J Controlled Release*, 2016, **229**:163–171.

113. Wang, Y., et al. Preparation and stability study of norfloxacin-loaded solid lipid nanoparticle suspensions. *Colloids Surf B*, 2012, **98**:105–111.

114. Steckbeck, J.D., et al. Antimicrobial peptides: new drugs for bad bugs? *Expert Opin Biol Ther*, 2014, **14**(1):11–14.

Chapter 2.5

Targeting strategies for the treatment of *Helicobacter pylori* infections

This book chapter was written by invitation, following the publication of the review paper shown in Chapter 2.3. In the literature, several studies use passive and active targeting strategies to *H. pylori*. Hence, this chapter was written to summarize the possibilities of targeting the bacteria and the gastric mucosa, as well as the techniques to quantify the efficacy of the targeting. Within the thesis, the main purpose was to choose a targeting agent to functionalize lipid nanoparticles.

Chapter

13
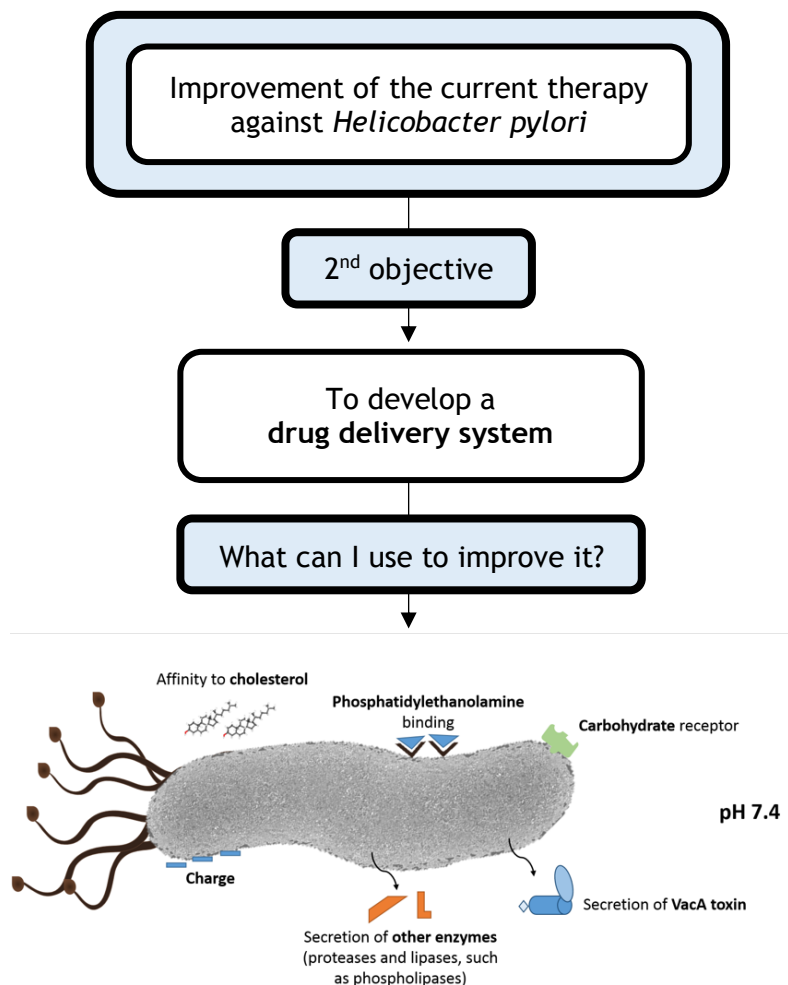
TARGETING STRATEGIES FOR THE TREATMENT OF *HELICOBACTER PYLORI* INFECTIONS

Daniela Lopes[1], Cláudia Nunes[1], M. Cristina L. Martins[2,3], Bruno Sarmento[2,4], and Salette Reis[1]*

[1] UCIBIO/REQUIMTE, Departamento de Ciências Químicas, Faculdade de Farmácia, Universidade do Porto, Porto, Portugal
[2] INEB – Instituto de Engenharia Biomédica, Universidade do Porto, Porto, Portugal
[3] ICBAS – Instituto de Ciências Biomédicas Abel Salazar, Universidade do Porto, Porto, Portugal
[4] IINFACTS – Instituto de Investigação e Formação Avançada em Ciências e Tecnologias da Saúde, Instituto Superior de Ciências da Saúde-Norte, Gandra-PRD, Portugal

*Corresponding author: shreis@ff.up.pt

Contents

13.1. INTRODUCTION

Helicobacter pylori (*H. pylori*) are gram-negative bacteria which are able to colonise the gastric mucosa due to several factors [1,2]. These virulent factors are both promoters of cytotoxicity and enhancers of its survival, even in an austere environment such as the acidic pH of the stomach [1,2]. *H. pylori* are therefore able to penetrate within the mucosa and attach themselves to the surface between the mucous layer and epithelial cells [2,3]. They infect a high percentage of the world's population, with infection rates of approximately 50 % [4]. Once colonised, the majority of the population does not manifest symptoms [4], however, 20 % of the infected population evolves from histological signs of chronic gastritis to gastrointestinal symptoms of gastritis and peptic ulcers [5]. Persistent infections may even evolve into cancer, which led to the classification of the bacterium as a human carcinogen (Group 1) by the International Agency for Research on Cancer (IARC) and the World Health Organization (WHO) [4]. In fact, its relationship to gastric cancer and lymphomas of mucosa-associated lymphoid tissue has been proved [6]. Although there is no clear explanation for it, it has also been related to other extradigestive conditions, such as idiopathic thrombocytopenic purpura, iron deficiency anaemia, ischemic heart disease, stroke, Parkinson's disease and Alzheimer's disease [7].

The severity of *H. pylori* is exacerbated by the difficulty of eradication. There is much controversy regarding the development of an effective vaccine, due to the difficulty of achieving a full protective immune response [8,9]. Clinical trials have generally failed and the investment necessary by pharmaceutical companies is high [8,9]. The current approach against *H. pylori* infection is treatment whenever symptoms justify it and includes a drug to reduce the contact between the ulcer and gastric acid, and two or three antibiotics, such as amoxicillin, clarithromycin and metronidazole, for at least 7 days [10,11]. The treatment has evolved over the years, but it still has several problems. In fact, eradication rates of 80 % were achieved by prolonging the first-line treatment for 14 days (14-day triple therapy) and in some countries rates of only 20–45 % have been reported [10,12]. These rates are still far from those desirable for infectious diseases and those proposed by the WHO [11].

The difficulty of eradicating *H. pylori* is a consequence of a sequence of events. Some drugs, viz. amoxicillin and clarithromycin, are degraded by gastric acid [13], and antibiotics do not remain for a sufficient time in the stomach, resulting in increased difficulty in achieving significant concentrations capable of crossing the mucous layer barrier and reaching the surface where *H. pylori* resides [14,15]. These issues both lead to the necessity of higher doses and, consequently, to the exacerbation of gastrointestinal side effects, such as nausea, vomiting and abdominal pain [16]. In fact, the frequency of side effects

combined with the duration of therapy, which varies between 7 and 14 days, and the discomfort resulting from the multiple doses, causes people to give up on the therapy [16,17]. This lack of therapeutic compliance complicates the success of eradication and ultimately it can have a tremendous effect on the development of antibiotics resistance. Actually, the bacterium has developed resistance to several antibiotics, such as metronidazole, with the percentage of resistance at 40 % and 90 % in developed and developing countries, respectively [18].

Different strategies have been attempted in order to overcome these limitations: other approaches to the treatment plan (*e.g.* bismuth-containing quadruple therapy, sequential and concomitant therapy), use of probiotics and phytomedicine [7,19-21]. A nanotechnology approach has also been applied to the development of effective systems to eradicate *H. pylori* [22]. Diverse nano- and microparticles have been tested, such as liposomes, polymeric, magnetic and metallic particles [22]. These systems have strong and specific advantages for each kind of nanoparticle. One approach common to the systems in general is the possibility of using passive and active targeting in order to improve the therapy [22]. Targeting allows the enhancement of the affinity between the nano- or microsystem and the gastric mucosa or the *H. pylori*. In the special case of *H. pylori* infection, vectorization can thus be used to improve the residence time of antibiotics in the stomach and to increase drug concentration at the action site, minimising the side effects. It is also possible to use specific ligands to the bacterium to decrease its adhesion to the gastric mucosa, improving eradication rates [15]. Herein, we will summarise several approaches to targeting both the gastric mucosa and *H. pylori*.

13.2. HOW CAN TARGETING OVERCOME DRUG RESISTANCE?

One of the most worrying problems in the treatment of *H. pylori* infection is the development of resistance to antimicrobial drugs. Some commonly used drugs, such as metronidazole and clarithromycin, are already resisted by *H. pylori*. Rates of 40 % of resistance to metronidazole have already been reported in developed countries [18]. For clarithromycin, rates of 30 % in America and 92 % in Africa have been reported [23]. Some studies also reported resistance to other drugs, such as amoxicillin, tetracycline and levofloxacin [23]. Multidrug resistance achieved rates of around 9 % in Europe and Asia [23]. Antibiotic resistance is disquieting, especially because persistent infections can lead to gastric cancer and it is difficult to use other antimicrobial drugs, as they are degraded by pH [4,13].

Nanoparticles can be used to improve the pharmacokinetic properties of drugs and to protect them from the hostile environment of the stomach.

Improvement of their half-life and a sustained and local release of the drug result in lower doses and a higher efficacy [24]. With a complement of targeting and stimuli-release systems, nanoparticles can be used to achieve higher concentrations of antimicrobial drugs near the bacterium even at low doses [25]. This can minimise side effects and improve the therapeutic efficacy, killing the bacterium and decreasing the potential of developing resistance. This can be improved due to the prospect of using multiple antimicrobial drugs in therapeutic doses [24]. It is unlikely that the bacterium will develop multiple simultaneous gene mutations to resist different mechanisms in the same nanosystem [25]. Given the possibility of using higher doses of the antimicrobial drug, it is possible to saturate transmembrane pumps [25].

Specific mechanisms of the interaction of nanoparticles with bacteria have also proved their usefulness in overcoming bacterial resistance. For instance, the fusion of liposomes with the bacterial membrane and the direct release of its contents inside the bacterium allow the use of sub-minimal inhibitory concentrations (sub-MIC) of antimicrobial drugs [26]. Given the well-known resistance mechanisms related to the membrane, namely the decrease of its permeability and the activation of efflux systems, fusion between liposomes and bacterial membranes can overcome both these mechanisms [26]. Dendrimers have also proved their efficacy since their positive charges promote their link with negative membranes, increasing permeability [25]. Ultimately, they can even destroy the microbial cell membrane [25]. Other kinds of nanoparticles, such as metallic nanoparticles, are unlikely to induce drug resistance for either multiple mechanisms and efficacy even in lower doses [22].

13.3. TARGETING THE GASTRIC MUCOSA

There is a close relationship between the gastric mucosa and *H. pylori* infection. First, these bacteria are able to penetrate within the mucosa and colonise the surface under the mucus layer [1,2]. Their virulence can also damage the gastric mucosa, causing peptic ulcers and ultimately gastric cancer [1,4]. The pharmacokinetic of antimicrobial drugs involves absorption and diffusion across the mucus to reach the bacterium, hence it is significantly affected by the gastric mucosa [14,15]. It is also the first barrier that nanoparticles have to cross to reach their target, and therefore, it is important to know the physicochemical properties of the gastric mucosa in order to take advantage of those characteristics to optimise the nanosystem.

One important feature of the mucosa is its hydrophobicity, which avoids the diffusion of hydrogen ions [27]. Their composition in phospholipids, as well as in other surface groups, viz. sialic acid, carboxyl and sulphate groups, play an important role in the interaction with nanoparticles. These surface groups on the mucosa are negatively charged and can establish several interactions with

nanoparticles, such as electrostatic attraction, hydrogen bond (H-bond) formation and van-der-Waal forces [28-30]. The mucus layer is also characterised by its composition, highly rich in mucins, which are high-molecular-mass oligomeric glycoproteins [31]. Taking this into account, systems with mucoadhesive properties may have an extended residence time at the target and improve contact with biological membranes [30]. The gastric mucosa also has a pH gradient, which is extremely acidic (1 or 2) in the lumen of the stomach and near neutral at the interface between the mucosa and epithelial cells [32,33]. This pH gradient results from the secretion of HCO_3 molecules and from the restricted diffusion of protons by the mucus layer [32]. The place to release the antimicrobial drug may thus be chosen using different pH-sensitive nanosystems.

A summary of all characteristics which can be used to treat *H. pylori* infections through the targeting of the gastric mucosa is presented in Figure 1.
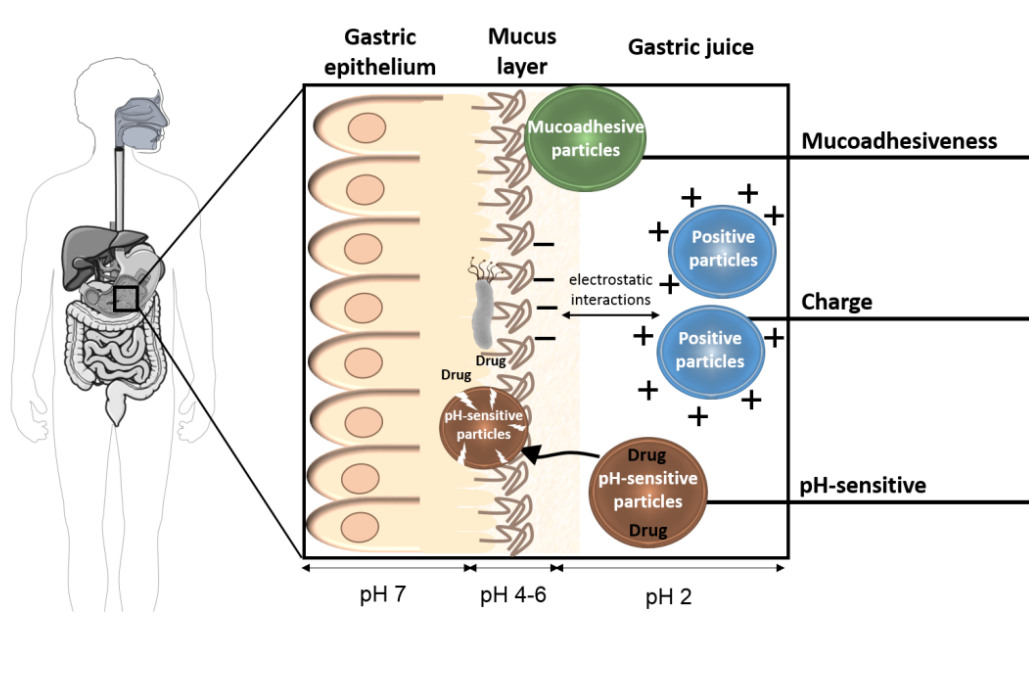
Figure 1. Scheme of the different strategies that can be used to target the gastric mucosa

13.3.1. Mucoadhesiveness

Mucoadhesiveness is a characteristic of some compounds reflected in their attraction to a mucosal membrane, which results in a temporary retention [34]. This can be very advantageous both for the increment of the amount of drugs locally released and for the improvement of direct contact with the biological membrane involved in the absorption of the drug [30].

Consequently, this strategy has been applied to the treatment of several disorders, through the target of different human mucosa, such as to nasal [35], buccal [36], ocular [37] and vaginal [38] mucosa, among others. Diverse polymers can be used, including natural polymers, such as alginate, chitosan, pectin, xanthan gum, hyaluronic acid and gelatin, synthetic polymers, as poly(ethylene glycol), poly(ethylene oxide), poly(acrylic acid), poly(methacrylic acid) and poly(vinyl amine), and semi-synthetic polymers, namely cellulose derivatives [39].

Due to the complexity of adhesion to the mucosa, several theories have emerged to explain this phenomenon. The electronic theory relies on the existence of electron transference in the origin of electrostatic interactions [34]. In the adsorption theory, other interactions are taken into account, such as H-bonds, van-der-Waals forces, hydrophobic interactions and chemisorption process [34]. Some polymers, namely thiolated polymers or thiomers, can establish disulphide bonds with the mucus gel layer [40]. The wetting theory suggests that the ability of mucoadhesive compounds in the liquid state to extend themselves on the mucosa is due to the surface tension of both mucus and polymers [34]. It is also hypothesised that diffusion events are related to mucoadhesion, which depends on the gradient of concentration, molecular weight, size and mobility of molecules [34]. Adhesion is also related to the force required to detach the material from the mucosa (fracture theory) and with the increased contact area of rough and porous materials (mechanical theory) [34].

Although without certainties concerning the mechanisms involved in mucoadhesion, several bioadhesive polymers have been extensively used. In the special case of *H. pylori* infection, affinity to the gastric mucosa is a useful strategy since the enhancement of the retention time in the stomach is important in overcoming the direct transit through the gastrointestinal tract [41]. Polymeric systems with bioadhesive properties have therefore been used to eradicate *H. pylori*. Polymeric particles have additional advantages, such as their mechanical stability and loading capacity [15]. Several polymers are recognised as biocompatible and some such as gelatin, are classified as GRAS (generally regarded as safe) by the Food and Drug Administration (FDA) [22]. Some mucoadhesive polymers, such as poly(acrylic acid) and poly(allylamine hydrochloride) can decrease the adhesion of *H. pylori* to the gastric mucosa [28].

Table 1 summarises different mucoadhesive polymers reported in nanosystems applied to the treatment of *H. pylori* infection. For instance, poly(acrylic acid) or carbopol was used to develop microspheres. In fact, mucoadhesion properties of carbopol had already been demonstrated by *in vitro* and *in vivo* studies [42]. Proteins such as gliadin and gelatin, can also be used, highlighting their additional advantages, which are their nutritional value and the existence of renewable sources [43]. Polymeric carbohydrate molecules, more specifically chitosan, have emerged as a promising drug

delivery system for *H. pylori*. Due to their positive charge and their mucoadhesiveness, chitosan particles can establish strong electrostatic interactions between their protonated glucosamine residues and the abovementioned negatively charged groups of the gastric mucosa [44,45]. Chitosan was therefore used to develop nano- and microparticles loading different antibiotics. In consequence of its broad-spectrum antimicrobial effect, it has also been used in direct action against the bacteria [46,47]. Another approach is the use of chitosan to plug, seal and remove the bacterium from the body [47]. Other polymers with mucoadhesion properties were also used in microparticles composed of mixture of polymers, such as carboxyvinyl polymers, cholestyramine, glycerol monooleate, hydroxypropyl methylcellulose among others.

The problem of extensive mucoadhesiveness is the lower ability to penetrate within the mucosa [29]. Arora *et al.* (2011) thus modified the charge of chitosan and decreased the particle size to less than the mesh size of mucin fibres [29]. Results revealed the permanency of microparticles in the deepest layers of the mucosa for over 6 h [29].

Table 1. Summary of different mucoadhesive polymers used in nano- and microsystems to eradicate *H. pylori* through distinct mechanisms

Polymer		Mechanism of action/Reference
Poly(acrylic acid) or carbopol		Load amoxicillin [48,49]
Proteins	Gliadin	Load acetohydroxamic acid [50]; amoxicillin [51]; clarithromycin [52]; dual therapy [53] and triple therapy [54]
	Gelatin	Load amoxicillin [55,56]
Chitosan		Deliver dual therapy [57,58]; amoxicillin [17,59]; tetracycline [44]; Antibacterial properties of chitosan [46,60,61]
Copolymers		Deliver antibiotics (several systems with different mixture of polymers, summarised in [22]); probiotics [62]; phytomedicine [63-66] and antacids [67].

13.3.2. Charge

As mentioned above, gastric mucosa is negatively charged, and thus positively charged nanoparticles can be used as means of targeting. Bearing in mind that electrostatic interaction may play an important role in the mucoadhesion process, positively charged nanoparticles can be particularly interesting [55]. Wang *et al*. (2000) demonstrated that positively charged gelatin microspheres

have increased mucoadhesiveness to nasal mucosa compared to negatively charged particles [55]. Applying this strategy to load amoxicillin, they were able to demonstrate through the use of rhodamine isothiocyanate (RITC)-labelled microspheres in a rat stomach, a higher interaction between the mucosa and modified gelatin microspheres than with gelatin microspheres [55]. The adhesion increased with the increase of the number of amino groups [55]. As several facts may affect the results, such as the labelling with RITC, the perfusion speed and time and the number of microspheres, further studies are still necessary [55]. Cholestyramine also has positively charged amino groups, being used by Umamaheshwari *et al.* (2003) [68]. The use of a cellulose acetate butyrate polymer to coat these microparticles masked their surface charge and led to a decrease in their mucoadhesiveness [68].

A different approach was developed by Lin *et al.* (2009), using nanoparticles composed of positively charged chitosan and negatively charged heparin [69]. Once the chitosan:heparin ratio was significantly high, the positive charges of chitosan exceeded the negative charges of heparin [69]. Thus, the final charge of the particle was between $+15\,mV$ and $+33\,mV$ [69]. They were able to demonstrate the adhesion and uptake of nanoparticles by gastric cells using fluorescence studies [69]. These particles were able to interact with sites of *H. pylori* infection [69].

There are other systems which can be applied to the concept of positively charged nanoparticles. For instance, cationic liposomes have been widely studied for gene therapy and cancer treatment and their application can be extended to target the gastric mucosa [70]. Liposomes in general are recognised for their safety and biocompatibility, however positive charges have been associated with cytotoxicity [70]. In order to overcome this issue, a novel strategy has been adopted, more specifically the cover with biodegradable anionic polymers, which are non-toxic [70]. This would obviously decrease interaction with the gastric mucosa, however, Jain *et al.* (2009) developed positively charged liposomes composed of egg phosphatidylcholine, cholesterol and stearylamine, and coated with poly(acrylic acid) (negative) and then with poly(allylamine hydrochloride) (positive) [28]. This strategy allowed a coating of liposomes, increasing their stability [28]. Simultaneously, it was possible to take advantage of the positive charge of the outer layer to enhance interaction with the mucosa [28]. Their ability to bind both gastric mucosa and the bacteria, which are negatively charged, was proven through agglutination and adherence studies [28]. Nevertheless, it is necessary to take into account toxicity issues concerning the use of cationic polymers [28]. In fact, in general it has been proved that cytotoxicity is related with the surface charge, as cationic nanoparticles are more toxic than anionic and neutral nanoparticles [71].

13.3.3. pH-sensitive nanoparticles

Given the pH gradient of the gastric mucosa, it is possible to develop nanoparticles able to respond to external stimuli. According to the purpose, nanoparticles, either sensitive to acidic pH or sensitive to neutral pH, have been developed. Taking into account the pH of the gastrointestinal tract and the extremely acidic pH of the lumen of the stomach, a local and controlled delivery to acidic pH can be useful to optimise absorption and minimise premature drug degradation [72]. On the other hand, sensitivity to neutral pH will allow the release of the content near the bacterium. Both strategies will be discussed herein.

Concerning the release at acidic pH, it is well known that drugs can be degraded at extremely acidic pH, as in the pH of the lumen of the stomach. For instance, Ramteke *et al.* (2009) reported that amoxicillin, clarithromycin and omeprazole are degraded in acidic pH within 3 h [73]. This degradation can be avoided by encapsulation in a nanoparticle, which can help to conserve an effective concentration at the site of action for long periods of time [73]. Ramteke *et al.* developed a nanoparticle composed of chitosan and glutamic acid conjugates [73]. Glutamate salt dissolves slowly in acidic pH, which allowed sustained release over 5–6 h [73]. The authors also reported that functionalization with fucose, which is a strategy of active targeting that will be discussed later in this chapter (see 13.4.6. Carbohydrate receptors), decreased the exposure to acidic pH and consequently retarded the release [73]. Another strategy was developed by Liu *et al.* (2011), combining buoyancy and mucoadhesion through the use of microspheres of Eudragit® E PO as the modulator of drugs release and glyceryl monooleate as a bioadhesive polymer [74]. The matrix is a polymer soluble at low pH, and thus the drug release rate is higher at acid pH [74]. There are several other examples with a higher release at extremely acidic pH than at neutral pH, which were applied to the eradication of *H. pylori* [22]. This is normally due to the instability of the nanosystem and not necessarily in consequence of an initial plan for the design of pH-sensitive nanoparticles, however, a controlled and sustained release can be achieved with the majority of the systems [22]. Nevertheless, the development of pH-sensitive nanoparticles is a strategy widely applied to other diseases. For instance, both cancer and inflammatory diseases are characterised by an acidic extra-cellular environment [75,76]. Thus, pH-sensitive nanoparticles can be used to a target delivery of drugs, decreasing drugs release at physiologic pH, consequently, decreasing side effects and improving therapy [76]. Their application can be extended to diagnostic and gene therapy [76]. Herein, we will summarise some possible strategies for different nanoparticles.

Liposomes are one of the most studied nanoparticles for delivering antimicrobial drugs [22] and it is possible to develop pH-sensitive liposomes. One approach widely studied is the use of polymorphic lipids, highlighting

unsaturated phosphatidylethanolamine (PE), such as diacetylenic--phosphatidyl-ethanolamine (DAPE), palmitoyl-oleoyl-phosphatidyl--ethanolamine (POPE) and dioleoyl-phosphatidyl-ethanolamine (DOPE) [76]. These phospholipids are usually combined with stabilisers, such as cholesteryl hemisuccinate (CHEMS), which self-assembles into bilayers at neutral pH [76,77]. It was shown by Hafez and Cullis (2000) that CHEMS itself has pH-sensitive properties [77]. When in contact with acidic pH, CHEMS became protonated and, consequently, the liposome reverts from a bilayer to an inverted hexagonal II phase [78]. It is also possible to use liposomes stabilised by external compounds sensitive to pH changes. For instance, carboxyl modified gold nanoparticles were used to stabilise liposomes of 1,2-di-(9Z--octadecenoyl)-3-trimethylammonium-propane (DOTAP) and egg phosphatidylcholine. At pH values below the pK_a of the carboxylic group (pK_a around 5), modified gold nanoparticles are protonated and detach from the liposome, increasing its fusion ability [79]. Solid lipid nanoparticles are a possible alternative for application in the eradication of the bacterium, being useful to protect drugs against hostile environments and to control the release of antimicrobial agents [22]. Kashanian *et al.* (2011) created solid lipid nanoparticles, composed of polysorbate 80, tripalmitin glyceride and *N*-glutaryl PE [80]. Results revealed higher release at acid pH comparatively with physiological pH [80]. Polymeric nanoparticles are also an attractive alternative, using either hydrogels triggered when exposure to a particular pH range or polymeric nano- or microparticles whose physical properties change in response to an external stimuli [81,82]. Different polymeric classes can be used to respond to differences in pH, more specifically poly(methacrylicacid)s, poly(vinylpyridine)s and poly(vinylimidazole)s [82].

Targeting through the release in response to the neutral pH is possible partly due to the abovementioned secretion of HCO_3-molecules and the restricted diffusion of protons through the mucus layer, and partly due to a specific survival mechanism of *H. pylori* [1,32]. More specifically, one of the enzymes secreted by the bacterium, urease, is able to produce ammonia [1]. This secretion results on one strategy for its survival, since it results in the conservation of periplasmic and cytoplasmic pH near to neutral [1]. It is therefore possible to benefit from the difference between the pH of the gastric mucosa and the pH of the medium nearby *H. pylori*. For instance, Thamphiwatana *et al.* (2013) used small gold nanoparticles modified with chitosan to stabilise liposomes at acidic pH [83]. Modified gold nanoparticles were charged at acidic pH, being attached to liposomes composed of egg phosphatidylcholine and 1,2-dioleoyl-*sn*-glycerol-3-phosphate (sodium salt) [83]. At neutral pH, however, modified gold nanoparticles became deprotonated and, consequently, detached from liposomes [83]. This detachment allows the destabilisation of the phospholipid bilayer and fusion with the bacterial membrane (Figure 2) [83]. The efficacy of this method was proved by the increased fusion and higher release rates at pH 7.4 [83].

Another approach was used by Silva *et al.* (2009), who used a mixture of pH-sensitive polymers, more specifically, methacrylic acid and methyl methacrylate ester copolymer, known as Eudragit®S100 [84]. This polymer is soluble at pH above 7.0 and, consequently, was used to protect magnetite particles from gastric dissolution and to load amoxicillin [84]. In general, poly(methacrylic acid-*co*-ethylacrylate) copolymers, commercially known as Eudragits, are widely used to develop pH-sensitive nanoparticles and include a large class of different polymers [85]. They are usually mixed with other polymers [85].
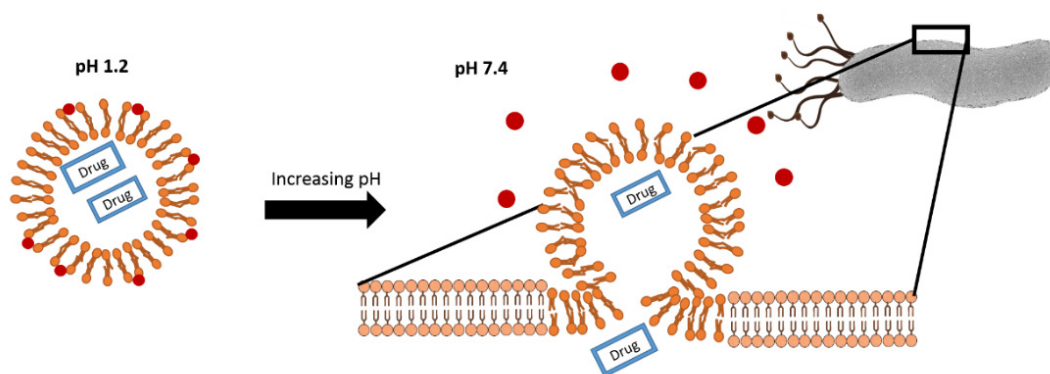
Figure 2. Scheme representative of the action mechanism of pH-sensitive liposomes by the stabilisation with modified gold nanoparticles at acidic pH. When the surrounded medium becomes neutral, modified gold nanoparticles become deprotonated and detach from liposomes. The destabilisation allows the fusion of liposomes with the bacterial membrane (adapted from [83]).

A mixture of chitosan and heparin was used to synthetise pH-sensitive nanoparticles by Lin *et al.* (2009), for application in *H. pylori* eradication [86]. At acid pH (4.5–6.5), which simulates the pH gradient of the gastric mucosa, chitosan is positively charged and heparin is negatively charged [86], and thus, polyelectrolyte complexes are formed by electrostatic interactions [86]. At pH 7.0, however, chitosan is deprotonated, which results in the collapse of the nanoparticle [86]. It is also possible to use pH-sensitive hydrogels to incorporate nanoparticles, as was done by Chang *et al.* (2010) through the incorporation of chitosan/poly-γ-glutamic acid nanoparticles in calcium--alginate-gelatin hydrogel [87]. Results showed pH-sensitive properties of hydrogel, which protected amoxicillin from the acidic pH [87].

13.4. TARGETING *HELICOBACTER PYLORI*

H. pylori are gram-negative bacteria, which have a spiral-shaped or a coccoid form depending on the hostility of the environment [1,2]. They can colonise an aggressive environment like the stomach due to virulent factors, such as their ability to adhere to the target cells through adhesins, and four to six flagella, which enhance their mobility [1,2]. They are also able to produce urease, cytotoxins and phospholipases which support their subsistence and their toxicity [1,2].

These virulent factors are related to the toxicity of the bacteria and have a close relationship to gastric cancer. They can however be used to eradicate *H. pylori*. Through several mechanisms discussed in this section, it is possible to take advantage of these virulent factors to release the content of the nanoparticle near the bacterium, improving drugs concentration and decreasing side effects. Figure 3 summarises the strategies discussed in this subchapter.
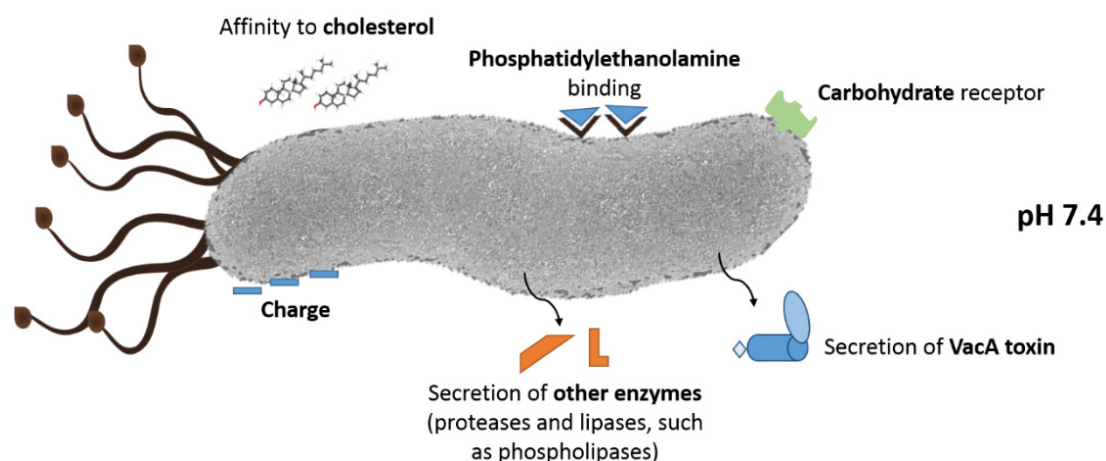
Figure 3. Summary of different virulent factors, which can be used for actively targeting the bacterium

13.4.1. Phosphatidylethanolamine

The ability of *H. pylori* to colonise the surface between the mucus gel layer and epithelial cells is directly related to their affinity to gastric glycerolipids [88]. In 1989, Langwood *et al.* reported the affinity of this bacterium to a lipid demonstrated through solid-phase thin-layer chromatography (TLC) overlay procedure [88]. This lipid was found in higher amounts in human antral mucosa comparatively with fundal mucosa and in adults comparatively to infants [88]. This explained the tendency of colonisation of the antrum and the higher rate of infection in adults [88]. In this work, the glycerolipid recognised by *H. pylori* was isolated from the antrum of human stomach and from human

erythrocytes [89]. A few years later (1992), Langwood *et al.* analysed high performance liquid chromatography (HPLC) fatty acid profiles and the ability of the bacterium to bind different phospholipids through TLC overlay [89]. The main conclusion of their work was that the glycerolipid receptor for *H. pylori* is PE [89]. Due to the well-characterised PE from erythrocytes, they only analysed the erythrocytes receptor [89], however, they speculated that the receptor was the same in the human mucosa, possibly with changes in the fatty acids [89]. The hypothesis of Langwood *et al.* concerning the importance of PE was supported by Dytoc *et al.* (1993), with the study of adhesion of *H. pylori* to different culture cells [90]. Although other mechanisms are involved, there is an evident correlation between the ability of *H. pylori* to adhere to eukaryotic cells with PE [90].

Taking into account the binding of *H. pylori* to PE in the gastric mucosa, PE can be used as an active targeting strategy to treat *H. pylori* infection. PE constitutes one class of lipids, which assemble into nonbilayer structures under physiological conditions [77]. To overcome this limitation, different approaches have been used, such as a mixture of lipids and phospholipids anchored to polymeric beads (Figure 4). For instance, Bardonnet *et al.* (2008) used epikuron 170 (phosphatidylcholine > 72 %, PE > 10 %, phosphatidylinositol < 3 %, lyso-phosphatidylcholine < 4 % and free fatty acids 10 %) and cholesterol to produce liposomes [13]. The formulation was however negatively charged and, given the charge of *H. pylori*, electrostatic repulsion occurred and prevented strong interactions [13]. Double liposomes composed of phosphatidylcholine, cholesterol and PE were also evaluated and both growth inhibition percentage and agglutination assays showed a higher efficiency of the system with PE [91]. Lipobeads composed of an acylated poly(vinyl alcohol) (PVA) core surrounded by a PE bilayer were also used to encapsulate acetohydroxamic acid [15]. Using agglutination assays, it was shown that all *H. pylori* strains recognised PE on the lipobeads as well as commercial PE [15]. Interestingly, lipobeads were able to plug and seal the PE receptor and, consequently, block the adhesion of *H. pylori* to KATO-III cells, which was concluded from radiolabelling assays [15]. This may imply that this specific targeting can optimise the treatment of *H. pylori* infections not only by a specific binding and local deliver of antibiotics near the bacterium, but also by precluding the attachment of the bacterium to the gastric mucosa.
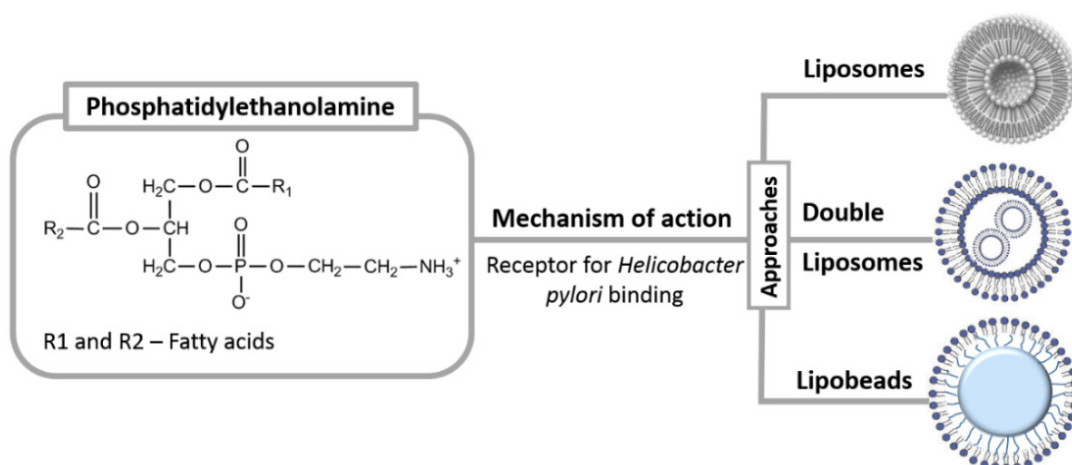
Figure 4. Different approaches to using PE in the active targeting of *H. pylori*. These approaches include liposomes, double liposomes and lipobeads, with a phospholipid bilayer anchored to a polymeric core.

13.4.2. Cholesterol

Cholesterol is a steroid with a planar tetracyclic ring system and an extended carbon chain towards the bilayer centre [92]. It is very common in eukaryotic cells, namely in the gastric mucosa [93], and thus, Ansorg *et al.* (1992) evaluated the affinity of *H. pylori* for cholesterol through several studies, such as gas-liquid chromatography, adsorption procedures and agglutination assays [94]. Results showed a high affinity for cholesterol, and, more interestingly, washings were not sufficient to detach the cholesterol from the bacteria, which can indicate a strong binding or an uptake [94]. This feature of *H. pylori* strains (both reference and wild strains) does not extend to other bacteria, such as *Staphylococcus epidermidis* and *Escherichia coli* [93].

The relation between *H. pylori* and cholesterol is not merely affinity. *H. pylori* follows a cholesterol gradient and is able to extract this lipid from gastric epithelial membranes [95]. In fact, excessive cholesterol enhances phagocytosis of *H. pylori* and, consequently, inflammation [95]. Nevertheless, the glucosylation of cholesterol by the bacteria allows escape from the phagocytosis [95]. Cholesterol in combination with sphingolipids and phospholipids may create a rigid domain, called lipid rafts [96]. It is believed that the bacteria use these lipid rafts both to deliver bacterial virulence factors and to invade inside the host cells [96]. The knowledge of these mechanisms may be explored to develop drugs able to inhibit lipid rafts [96] or drugs to inhibit cholesterol glucosylation [95], in order to difficult the long-term persistent infection.

This affinity was also explored to test the potential of steroid hormones as antimicrobial agents against *H. pylori* due to their similarity with cholesterol

[97]. Hosoda *et al.* (2011) reported that progesterone inhibits the absorption of free cholesterol by the bacteria, suggesting that *H. pylori* may have a steroid-binding protein at the cell surface [97]. This may be very useful in order to develop a new strategy to target the bacteria and several nanoparticles were tested using cholesterol in their composition. For instance, Barbonnet *et al.* (2008) tested liposomes composed of epikuron 170 or 1,2-dipalmitoyl-*sn*-glycero-3-phosphocholine (DPPC) to load antimicrobial agents (ampicillin and metronidazole) [13]. Using epifluorescence microscopy, the authors visualized liposome-bacteria interactions that could be explained by the presence of cholesterol [13]. Obonyon *et al.* (2012) also evaluated liposomes composed of cholesterol, hydrogenated L-α-phosphatidylcholine and linolenic acid [18]. They observed that the interaction between liposomes and the bacteria was by fusion and not by adsorption or aggregation [18]. Fusion with the bacterial membrane is a significant advantage because it was reported that this mechanism outrides efflux pumps and barely induces drug resistance [18,24]. Both in double liposomes and lipobeads mentioned in the section 13.4.1., they also used cholesterol in the composition of the phospholipid bilayer [15,91]. Thus, positive results in agglutination and adherence studies were possibly enhanced by the presence of cholesterol. As well as the possibility of using cholesterol for specific targeting, it can be useful as a membrane stabiliser, particularly in the case of liposomes [92].

13.4.3. Vacuolating cytotoxin A

The ability of the bacteria to produce a factor that induces vacuolization in cultured cells was reported by Leunk *et al.* in 1988 [98]. In 1992, Cover *et al.* purified and characterised the vacuolating cytotoxin A (VacA) [99] and over the years knowledge concerning its mechanism and its influence on the toxicity of the bacterium has evolved. In fact, several mechanisms have been associated with this toxin, such as alteration of endo-lysossomal function, permeabilisation of the membrane and pore formation in the plasma membrane [100]. It has also been related to the formation of reactive oxygen species and gastric cancer [101].

Given its effect on the membrane, it is possible to use the VacA toxin to release antimicrobial agents, since near the bacterium the toxin will destabilise the phospholipid bilayer of liposomes through the formation of channels (Figure 5) [13]. The content of the liposomes would thus be locally released. This effect was proven using different liposomes. Moll *et al.* (1995) demonstrated that VacA toxin induces efflux of potassium from liposomes of asolectin [102]. In 2000, Pagliaccia *et al.* used liposomes of egg L-α-phosphatidylcholine and asolectin in order to prove the self-induced binding of VacA toxin into membranes and its ability to destabilise the membrane, resulting in the release of a fluorescent probe called calcein [103]. It was thus proposed that VacA toxin would bind to the lipid membrane and through a structural change would induce membrane leakage [103]. In fact, it

is known that VacA toxin binds as a monomer to lipid membrane, with a special affinity to lipid rafts, then oligomerises and penetrates [104]. Consequently, a channel is created, and given this evidence, VacA has been classified as a nonconventional pore-forming toxin with multifunctions [104]. The formation of channels was demonstrated using planar lipid bilayers of egg L-α-phosphatidylcholine, dioleoylphosphatidylserine and cholesterol [105]. Using atomic force microscopy, it was possible to see that the channel is a hexamer composed of assembly of monomers of VacA toxin [105].

Another approach is to use heparin nanoparticles, since a subunit of VacA can bind both heparin and heparin sulphate which would likely improve a local release [63].
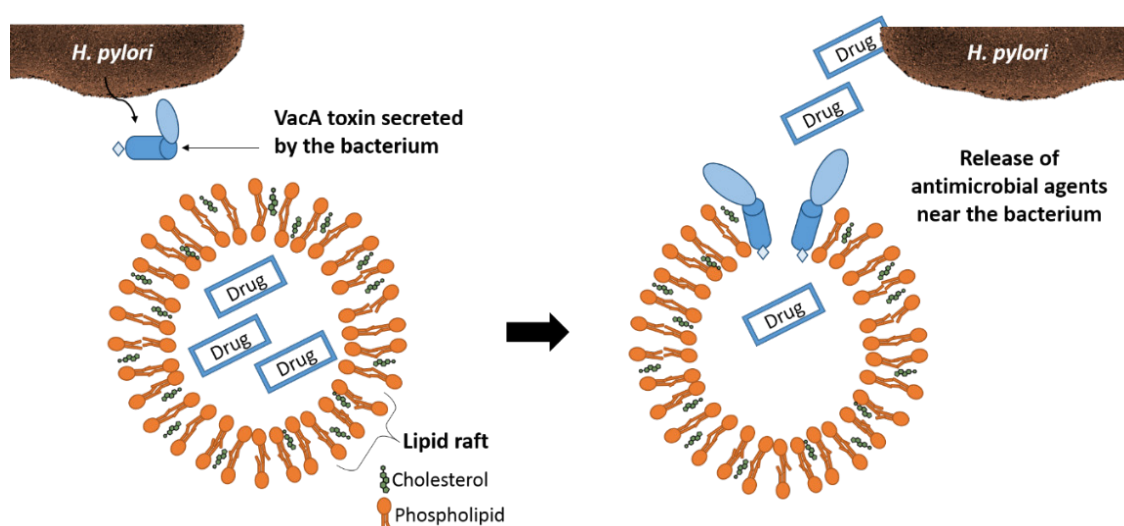
Figure 5. Using the ability of VacA toxin to produce pores in the membrane (based on [104]) to local release of the content of a liposome

13.4.4. Enzymes

Similarly to the possibility of use VacA toxin to destabilise the nanoparticle, *H. pylori* is able to secrete different enzymes. For instance, phospholipases secreted by the bacteria are considered pathogenic factors, being related to increased risk of developing ulcers and gastric cancer [106,107]. The bacterium secretes several phospholipases (A1, A2, C and D) which can modify and degrade the gastric mucus [106]. The presence of sphingomyelinases in the bacterium has also been reported [108]. They are also able to induce the production of phospholipases from leukocytes [109], and therefore, liposomes or other type of nanoparticles with a phospholipid bilayer, such as a core-shell nanoparticle, can be used and destabilised by these enzymes. They are able to cleave phospholipids in specific locations, modifying their components and, as

a result, their structure [106]. Consequently, the content will be released near the bacterium and the inflammation. Other enzymes are also secreted by *H. pylori*, such as lipases and proteases [110], which can be used to destabilise lipid and protein nanoparticles.

13.4.5. Charge

In 1990, Smith *et al.* studied the surface hydrophobicity and surface charge of *H. pylori* in order to understand the mechanisms involved in their adhesion to the gastric mucosa [111]. Different studies were performed, namely hydrophobic interaction chromatography and measurement of contact angles with water, among other things [111]. These complementary methods revealed that *H. pylori* have a hydrophilic and negatively charged surface [111]. The negative charge of *H. pylori* was also reported by Pruul *et al.* in the same year [112]. Positively charged nanoparticles, mentioned in subchapter 13.3.2, may therefore be useful, and can simultaneously target the gastric mucosa and the bacterium. The importance of the charge was reported by Bardonnet *et al.* (2008), since less electronegative liposomes showed the best results due to less electrostatic repulsion between the nanoparticle and *H. pylori* [13]. The charge of the bacterium can be changed as a resistance mechanism. For instance, the majority of gram-negative bacteria are able to mask lipid A negative charges, reducing the affinity of positively charged drugs to the outer membrane [113]. In the special case of *H. pylori*, they are able to modify its majority surface component [lipopolysaccharide (LPS)], through the modification of lipid A [114,115]. The lipid A 1-phosphate group is substituted by a residue of PE in the hydroxyl of the carbon-1 [115]. This results in a reduction of the negative charge [115], which has to be taken into account if the charge only is chosen as a target mechanism.

13.4.6. Carbohydrate receptors

Currently, it is well recognised that *H. pylori* can adhere to the gastric mucosa through specific adhesins. In 1998, Ilver *et al.* identified the adhesin binding fucosylated Lewis b (Leb) histo-blood group antigen (BabA) as a receptor for the adherence of *H. pylori* to the gastric mucosa [116]. A few years later (2002), Mahdavi *et al.* reported sialyl-dimeric-Lewis x glycosphingolipid (SabA) as a receptor for *H. pylori*, relating this fact to chronic inflammation [117]. BabA and SabA adhesins differ from each other in terms of amino acid composition and affinity for specific glycans, as the specific affinity of SabA to sialic acid and BabA to fucose [118,119]. Given the individual glycan profile of human gastric mucosa, *H. pylori* can benefit from having diverse adhesins [118].

Nanotechnology can take advantage of these adhesins on the surface of the bacterium (Figure 6), such as by using lectins, which are a diverse class of carbohydrates with the advantage of being non-immunogenic [120]. They are also bioadhesives, improving their retention time in the stomach [120].

Different lectins, namely *Ulex Europaeus Agglutinin* I (UEA I) and Conconavalin A (Con A) were tested by Umamaheshwari and Jain (2003) [50]. These lectins were covalently bounded to gliadin nanoparticles, which were chosen due to their mucoadhesiveness, and used to encapsulate acetohydroxamic acid [50]. Agglutination assays showed the efficacy of the binding between both lectins and the bacterium, compared with the absence of agglutination with non-conjugated gliadin nanoparticles [50]. The binding was inhibited by fucose and mannose, reflecting the involvement of the receptors [50]. The results were also confirmed using *in situ* adherence assays, where the carbohydrate receptors were completely plugged and sealed by the nanoparticles conjugated with lectins [50]. In the presence of these nanoparticles, the binding between *H. pylori* receptors and gastric mucosa carbohydrates was significantly affected, hindering the adhesion to the gastric mucosa [50]. Applying this strategy, triple drug loaded-nanoparticles were developed by Ramteke *et al.* and the results showed a superior *in vivo* clearance to that of non-conjugated formulations and free drugs [54]. Con A was also conjugated with ethylcellulose microspheres to encapsulate clarithromycin [121] and in conjugation with Eudragit S100 microspheres to encapsulate amoxicillin trihydrate [122].
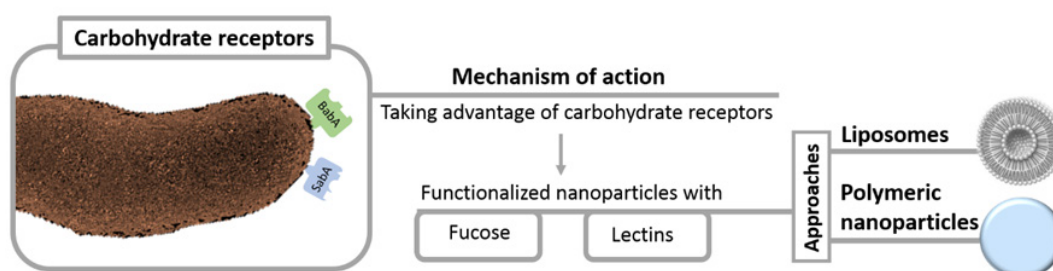
Figure 6. Different approaches to targeting *H. pylori* using the linkage of fucose and lectins to carbohydrate receptors in the bacterium

Bardonnet *et al.* (2008) developed liposomes of DPPC or epikuron in conjugation with a synthetic glycolipid, which was composed of a cholesterol group, four ethylene glycol units and fucose [13]. The same group had already proved that liposomes with fucosyl neoglycolipids on the surface were stable [123]. Epifluorescence studies showed an enhancement of the interaction of liposomes with the bacterium when the fucosylated neoglypid was present [13]. They were able to bind both spiral and coccoid forms [13]. However, this was not possible in all strains, since some *H. pylori* strains do not express babA2 gene and, consequently, do not have the receptor to bind the fucose [13].

Fucose was also used in other kinds of nanoaparticles, such as conjugated with chitosan-glutamate nanoparticles to deliver amoxicillin, clarithromycin and omeprazole [73]. The specific binding was confirmed through agglutination assays [73]. The targeting improved the clearance of the bacteria *in vivo* [73]. Lin *et al.* (2013) developed genipin-cross-linked fucose-chitosan/heparin nanoparticles to encapsulate amoxicillin and demonstrated the targeting through electronic microscopy and fluorescence studies [124].

13.5. STUDIES TO EVALUATE THE EFFICACY OF THE TARGETING

After optimising a nanoparticle for different parameters, such as size, zeta--potential, entrapment efficiency, profile of release at different pH and stability, it is essential to evaluate their efficacy. General studies can be performed, such as *in vitro H. pylori* growth inhibition, and specific assays can be chosen to evaluate their interaction with either the gastric mucosa or the bacterium.

13.5.1. Nanoparticle-gastric mucosa interactions

Mucoadhesiveness is one strategy extensively applied in the case of *H. pylori* infection. There are several possibilities for evaluating this property, including indirect and direct methods [39]. Indirect methods include microgravimetric methods, atomic force microscopy and diffusion/particle tracking methods [39]. Direct methods involve cytoadhesion methods and *ex vivo* and *in vivo* administration and imaging [39]. Herein, we will focus on different assays applied directly to the study of nano- and microparticles to be applied in the eradication of *H. pylori*. For instance, a piece of rat stomach, tied onto plastic, can be used to spread nanoparticles [125], then, disintegrating test apparatus is used to promote regular up and down movements of the system with the tissue and distilled water [125]. After 4 h, the number of microspheres still adhered is counted [125]. A more complex assay was performed by Liu *et al.* (2005), using cut stomachs incubated with microspheres in a chamber at 93 % relative humidity and room temperature [126]. After 20 min, tissues were fixed on a polyethylene support at an angle of 45° and washed with pH 1.3 HCl-physiological saline for 5 min (22 ml min^{-1}) [126]. The remaining microspheres were counted [126]. The results can be expressed in different ways, such as by the percentage of the remaining microspheres [126] or by the percentage of mucoadhesion, which can be calculated using the Equation 1 [127].

$$\% \, Mucoadhesion = \frac{W_0 - W_1}{W_o} \times 100 \tag{1}$$

where w_0 and w_1 are the weight of microspheres applied initially and the weight of microspheres rinsed off, respectively.

Scanning electron microscopy was also used to monitor the *in vitro* wash-off test for mucoadhesive microspheres at different time points [128].

Another approach was applied by Wang *et al.* (2000) using male wistar rats to remove stomach under anesthesia [55]. After washing the content of the stomach, RITC-labeled microspheres suspended in simulated gastric fluid were filled into the stomach [55]. After incubation for 30 min, the stomach was washed and perfused with simulated gastric fluid for 30 min (1.0 ml min^{-1}) [55]. Fluorescence spectrophotometry was then used to determine the percentage of microspheres retained in the stomach after degradation of the microspheres with trypsine [55].

Another *in vivo* approach was used by Liu *et al.* (2005), using thirty rats divided into six groups, of which three were administered with microspheres and three with placebo [126]. They were sacrificed at 2, 4 and 7 h and microspheres remained in the gastrointestinal tract were counted [126]. *In vivo* mucoadhesion was evaluated by Ramteke *et al.* (2008) using nanoparticles containing barium sulphate as a contrast agent [54]. The authors used albino rats which were recorded by X-ray photographs at different times [54].

It is also possible to evaluate the ability of the nanoparticle to block the binding of *H. pylori* to mucosa. For this purpose, Umamaheshwari *et al.* (2004) performed adherence assays using labelled *H. pylori* and KATO-III cells (gastric epithelial cells) [15]. *H. pylori* preincubated with lipobeads were washed and added to the suspension of KATO-III cells [15]. Six washes were used to remove non-adherent bacteria [15]. The number of bacteria adherent was counted using disintegrations *per* minute in a scintillation counter after trypsination to remove adherent bacteria and KATO-III cells from the wells [15]. *In situ* adherence assays can also be used for the same purpose [15]. Fluorescein isothiocyanate-labeled (FITC-labeled) bacteria preincubated with lipobeads for 2 h were washed and then added to tissue sections of samples of oesophagus, stomach, duodenum and colon [15]. *In situ* binding was demonstrated through fluorescence microscopy [15].

13.5.2. Nanoparticle-*H. pylori* interactions

Agglutination assays can be performed by mixing the same amount of bacterial suspension and the nanoparticle formulation [50]. The agglutination reaction can then be scored according to the size of clumps [50]. This assay can also be used to confirm whether a specific ligand is involved, pre-incubating with specific inhibitors of agglutination [50]. The agglutination can be however affected by the self-aggregation of some strains [13]. Bardonnet *et al.* (2008) used epifluorescence studies, with the bacteria stained with DAPI by fluorescent *in situ* hybridization technique and liposomes marked with NBD-PC

[13]. The mixture was observed by epifluorescence microscopy and the superimposition of the two dyes suggested that liposomes were aggregated around *H. pylori* [13].

Another labelling technique was used by Gonçalves *et al.* (2013), using *H. pylori* previously marked with FITC [61]. The interaction with auto-fluorescent chitosan microspheres was demonstrated through confocal laser scanning microscopy (Figure 7) [61].
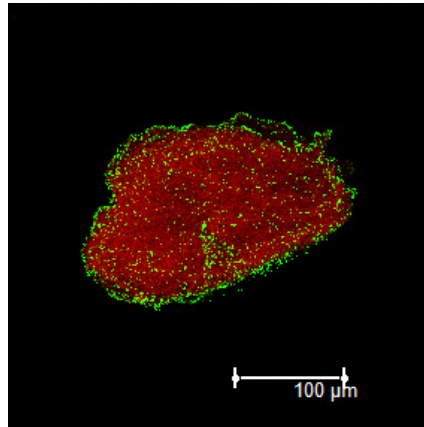
Figure 7. Confocal microscopy image of chitosan microspheres (in red) with adherent FITC-labelled *H. pylori* strain (17875/Leb) (in green) under pH 6.0 (adapted from [61]). The scale-line is representative of the whole system.

Quantification of adhesion of ^{35}S-labeled *H. pylori* can be achieved using a luminescence counter through the determination of the radioactivity of each well of polyethylene terephthalate plates [61]. Knowing the concentration in colony-forming unit (CFU).ml^{-1} of the initial *H. pylori* inoculum ($C_{Hp}^{i} C$), the activity of *H. pylori* adherent in c.p.m. ($A_{Hp}^{mic} A$), the activity of the initial *H. pylori* inoculum in c.p.m.ml^{-1} ($A_{Hp}^{i} A$) and knowing the number of microspheres of each well (N_{mic}), which can be counted using a camera coupled to a stereomicroscope, it is possible to determine the number of adherent bacteria *per* microsphere (Equation 2) [61].

$$\frac{Number\ of\ adherent\ bacteria}{microsp\,here}\,(\text{CFU } per \text{ microsphere}) = \frac{(C_{Hp}^{i} \times A_{Hp}^{mic} \div A_{Hp}^{i})}{N_{mic}} \quad (2)$$

Other techniques of microscopy can be used, such as transmission electron microscopy (TEM) to demonstrate both the distribution of the nanoparticle around the bacteria and their effect on the morphology of the bacteria [124].

13.6. CONCLUSION

Nanotechnology is a growing and promising field, which has been extensively studied in order to overcome limitations of current therapies in several diseases. In the special case of *H. pylori* infection, nanoparticles have been proving their utility in improving the efficacy of antibiotics, by protecting them from the environment and by promoting a controlled, sustained and local delivery of drugs. The local delivery can be achieved by targeting gastric mucosa or the bacterium.

In the development of a targeting nanoparticle is important to initially choose the nanoparticle and the strategy most suitable for the purpose in mind. In this process, it is essential to take into account the balance between various approaches. Extreme mucoadhesiveness may be prejudicial to penetration within the mucosa due to the decrease of mobility and it is affected by the high turnover of the gastric mucosa [29,129]. The pH gradient is also a key point, since the gastric medium is around pH 1.2 whereas the surrounding medium of the bacterium is at neutral pH. This large pH gradient can also affect the charge of the nanoparticles if it includes the pK_a of the nanoparticles components. The charge of the bacterium can be changed by resistance mechanisms, and therefore it is important to take these possible changes into account. Other mechanisms, such as translocation, coordinated response of tissues, enzymes and toxicokinetics, may affect the specificity of the targeting and even be involved in toxicity mechanisms [130].

Above all, the possibility of combining different strategies in order to increase the local release is very attractive, and advantageous to decreasing the development of antibacterial resistance.

ACKNOWLEDGMENTS

REFERENCES

1.   L. Boyanova, I. Mitov, B. Vladimirov, *Helicobacter pylori*, Caister Academic Press, Norfolk, UK, 2011.
2.   H.L.T. Mobley, G.L. Mendz, S.L. Hazell, (Eds.), *Helicobacter pylori*: physiology and genetics, ASM Press, Washington DC, USA, 2001.
3.   H.L.T. Mobley. *Gastroenterology* **113** (1997) S21–S28.
4.   IARC Working Group on the Evaluation of the Carcinogenic Risks to Human, Lyon, France, 2009.
5.   S.S. Kim, V.E. Ruiz, J.D. Carroll, S.F. Moss. *Cancer Lett.* **305** (2011) 228–238.
6.   P.L. Bardonnet, V. Faivre, W.J. Pugh, J.C. Piffaretti, F. Falson. *J. Control. Release* **111** (2006) 1–18.
7.   S.D. Georgopoulos, V. Papastergiou, S. Karatapanis. *Expert Opin. Pharmacother.* **14** (2013) 211–223.
8.   P. Sutton, Y.T. Chionh. *Expert Rev. Vaccines* **12** (2013) 433–441.
9.   A. Müller, J.V. Solnick. *Helicobacter* **16** (2011) 26–32.
10.   A. Zullo, C. Hassan, L. Ridola, V.d. Francesco, D. Vaira. *Eur. J. Intern. Med.* **24** (2012) 16–19.
11.   P. Malfertheiner, F. Megraud, C.A. O'Morain, J. Atherton, A.T. Axon, F. Bazzoli, G.F. Gensini, J.P. Gisbert, D.Y. Graham, T. Rokkas, E.M. El-Omar, E.J. Kuipers. *Gut* **61** (2012) 646–664.
12.   M. Selgrad, P. Malfertheiner. *Curr. Opin. Pharmacol.* **8** (2008) 593–597.
13.   P.-L. Bardonnet, V. Faivre, P. Boullanger, J.-C. Piffaretti, F. Falson. *Eur. J. Pharm. Biopharm.* **69** (2008) 908–922.
14.   L. Yang, J. Eshraghi, R. Fassihi. *J. Control. Release* **57** (1999) 215–222.
15.   R.B. Umamaheshwari, N.K. Jain. *J. Control. Release* **99** (2004) 27–40.
16.   A. Armuzzi, F. Cremonini, F. Bartolozzi, F. Canducci, M. Candelli, V. Ojetti, G. Cammarota, M. Anti, A. De Lorenzo, P. Pola, G. Gasbarrini, A. Gasbarrini. *Aliment. Pharmacol. Ther.* **15** (2001) 163–169.
17.   J.K. Patel, M.M. Patel. *Curr. Drug Deliv.* **4** (2007) 41–50.
18.   M. Obonyo, L. Zhang, S. Thamphiwatana, D. Pornpattananangkul, V. Fu, L. Zhang. *Mol. Pharm.* **9** (2012) 2677–2685.
19.   J.-M. Liou, C.-C. Chen, M.-J. Chen, C.-C. Chen, C.-Y. Chang, Y.-J. Fang, J.Y. Lee, S.-J. Hsu, J.-C. Luo, W.-H. Chang, Y.-C. Hsu, C.-H. Tseng, P.-H. Tseng, H.-P. Wang, U.-C. Yang, C.-T. Shun, J.-T. Lin, Y.-C. Lee, M.-S. Wu. *Lancet* **381** (2013) 205–213.
20.   A. Patel, N. Shah, J.B. Prajapati. *J. Microbiol. Immunol. Infect.* **47** (2013) 1–9.
21.   J. Vítor, F.F. Vale. *FEMS Immunol. Med. Microbiol.* **63** (2011) 153–164.
22.   D. Lopes, C. Nunes, M.C. Martins, B. Sarmento, S. Reis. *J. Control. Release* **189** (2014) 169–186.
23.   W. Wu, Y. Yang, G. Sun. *Gastroenterol. Res. Pract.* **2012** (2012) 1–8.
24.   A.J. Huh, Y.J. Kwon. *J. Control. Release* **156** (2011) 128–145.
25.   R.Y. Pelgrift, A.J. Friedman. *Adv. Drug Deliv. Rev.* **65** (2013) 1803–1815.
26.   Z. Drulis-Kawa, A. Dorotkiewicz-Jach. *Int. J. Pharm.* **387** (2010) 187–198.
27.   W. Bernhard, A.D. Postle, M. Linck, K.-F. Sewing. *Biochim. Biophys. Acta* **1255** (1995) 99–104.
28.   P. Jain, S. Jain, K.N. Prasad, S.K. Jain, S.P. Vyas. *Mol. Pharm.* **6** (2009) 563–603.
29.   S. Arora, S. Gupta, R.K. Narang, R.D. Budhiraja. *Sci. Pharm.* **79** (2011) 673–694.
30.   C.-M. Lehr, H.E. Boddé, J.A. Bouwstra, H.E. Junginger. *Eur. J. Pharm. Sci.* **1** (1993).

31. H. Nordman, J.R. Davies, I. Carlstedt. *Biochem. J.* **331** (1998) 687–694.
32. A. Allen, G. Flemström. *Am. J. Physiol.* **288** (2005) C1–C19.
33. A.A. Salyers, D.W. Dixie, *Bacterial Pathogenesis: A Molecular Approach*, 2nd ed., ASM Press, Washington DC, USA, 2002.
34. V.V. Khutoryanskiy. *Macromol. Biosci.* **11** (2011) 748–764.
35. M.I. Ugwoke, R.U. Agu, N. Verbeke, R. Kinget. *Adv. Drug Deliv. Rev*. **57** (2005) 1640–1665.
36. N. Salamat-Miller, M. Chittchang, T.P. Johnston. *Adv. Drug Deliv. Rev*. **57** (2005) 1666–1691.
37. A. Ludwig. *Adv. Drug Deliv. Rev.* **57** (2005) 1595–1639.
38. C. Valenta. *Adv. Drug Deliv. Rev.* **57** (2005) 1692–1712.
39. A. Sosnik, J. das Neves, B. Sarmento. *Prog. Polym. Sci*. **39** (2014) 2030–2075.
40. A. Bernkop-Schnurch. *Adv. Drug Deliv. Rev.* **57** (2005) 1569–1582.
41. L.M. Ensign, R. Cone, J. Hanes. *Adv. Drug Deliv. Rev*. **64** (2012) 557–570.
42. Y. Akiyama, N. Nagahara, T. Kashihara, S. Hirai, H. Toguchi. *Pharm. Res.* **12** (1995) 397–405.
43. A.O. Elzoghby, W.M. Samy, N.A. Elgindy. *J. Control. Release* **161** (2012) 38–49.
44. R. Hejazi, M. Amiji. *Int. J. Pharm*. **235** (2002) 87–94.
45. I.C. Gonçalves, P.C. Henriques, C.L. Seabra, M.C.L. Martins. *Expert Rev. Anti-Infect. Ther*. (2014) 1–12.
46. D. Luo, J. Guo, F. Wang, J. Sun, G. Li, X. Cheng, M. Chang, X. Yan. *J. Biomater. Sci*. **20** (2009) 1587–1596.
47. F. Nogueira, I.C. Goncalves, M.C. Martins. *Acta Biomater.* **9** (2013) 5208–5215.
48. M. Cuña, M.J. Alonso, D. Torres. *Eur. J. Pharm. Biopharm*. **51** (2001) 199–205.
49. S. Harsha. *Int. J. Nanomed.* 7 (2012) 4787–4796.
50. R.B. Umamaheshwari, N.K. Jain. *J. Drug Target.* **11** (2003) 415–424.
51. R.B. Umamaheshwari, S. Ramteke, N.K. Jain. *AAPS PharmSciTech* **5** (2004) 1–9.
52. S. Ramteke, R.B. Umamaheshwari, N.K. Jain. *Indian J. Pharm. Sci.* **68** (2006) 479–484.
53. S. Ramteke, N.K. Jain. *J. Drug Target.* **16** (2008) 65–72.
54. S. Ramteke, N. Ganesh, S. Bhattacharya, N.K. Jain. *J. Drug Target.* **16** (2008) 694–705.
55. J. Wang, Y. Tauchi, Y. Deguchi, K. Morimoto, Y. Tabata, Y. Ikada. Drug Deliv. **7** (2000) 237–243.
56. S. Harsha. *Drug Des. Dev. Ther.* **7** (2013) 1027–1033.
57. S. Shah, R. Qaqish, V. Patel, M. Amiji. *J. Pharm. Pharmacol*. **51** (1999) 667–672.
58. A. Portero, C. Remunan-Lopez, M.T. Criado, M.J. Alonso. *J. Microencapsulation* **19** (2002) 797–809.
59. J. Patel, P. Patil. *J. Microencapsulation* **29** (2012) 398–408.
60. M. Fernandes, I.C. Goncalves, S. Nardecchia, I.F. Amaral, M.A. Barbosa, M.C. Martins. *Int. J. Pharm.* **454** (2013) 116–124.
61. I.C. Goncalves, A. Magalhaes, M. Fernandes, I.V. Rodrigues, C.A. Reis, M.C. Martins. *Acta Biomater*. **9** (2013) 9370–9378.
62. J.A. Ko, H.J. Lim, H.J. Park. *Process Biochem*. **46** (2011) 631–635.
63. C.-H. Chang, W.-Y. Huang, C.-H. Lai, Y.-M. Hsu, Y.-H. Yao, T.-Y. Chen, J.-Y. Wu, S.-F. Peng, Y.-H. Lin. *Acta Biomater*. **7** (2011) 593–603.
64. X. Zhu, D. Zhou, S. Guan, P. Zhang, Z. Zhang, Y. Huang. *J. Mater. Sci. Mater. Med*. **23** (2012) 983–990.

65. P. Pan-In, A. Tachapruetinun, N. Chaichanawongsaroj, W. Banlunara, S. Suksamrarn, S. Wanichwech-Arungruang. *Nanomedicine* (2013).

66. M. Ali, K. Dhar, M. Jain, V. Pandit. *J. Adv. Pharm. Technol. Res.* 5 (2014) 48–56.

67. R.P. Raffin, D.S. Jornada, M.I. Ré, A.R. Pohlmann, S.S. Guterres. *Int. J. Pharm.* **324** (2006) 10–18.

68. R.B. Umamaheshwari, S. Jain, N.K. Jain. *Drug Deliv.* **10** (2003) 151–160.

69. Y.-H. Lin, C.-H. Chang, Y.-S. Wu, Y.-M. Hsu, S.-F. Chiou, Y.-J. Chen. *Biomaterials* **30** (2009) 3332–3342.

70. G. Shim, M.-G. Kim, J.Y. Park, Y.-K. Oh. *Asian J. Pharm. Sci.* **8** (2013) 72–80.

71. M.Y. Wani, M.A. Hashim, F. Nabi, M.A. Malik. *Adv. Phys. Chem.* **2011** (2011) 1–15.

72. V.R. Patel, M.M. Amiji. *Pharm. Res.* **13** (1996) 588–593.

73. S. Ramteke, N. Ganesh, S. Bhattacharya, N.K. Jain. *J. Drug Target.* **17** (2009) 225–234.

74. Y. Liu, J. Zhang, Y. Gao, J. Zhu. *Int. J. Pharm.* **413** (2011) 103–109.

75. L. Tian, Y.H. Bae. *Colloids Surf. B* **99** (2012) 116–126.

76. X. Liu, G. Huang. *Asian J. Pharm. Sci.* **8** (2013) 319–328.

77. I.M. Hafez, P.R. Cullis. *Biochim. Biophys. Acta* **1463** (2000) 107–114.

78. S. Simões, V. Slepyshkin, N. Düzgünes, M.C.P.d. Lima. *Biochim. Biophys. Acta* **1515** (2001) 23–27.

79. D. Pornpattananangkul, S. Olson, S. Aryal, M. Sartor, C.M. Huang, K. Vecchio, L. Zhang. *ACS nano* **4** (2010) 1935–1942.

80. S. Kashanian, A.H. Azandaryani, K. Derakhshandeh. *Int. J. Nanomed.* **6** (2011) 2393–2401.

81. R.A. Siegel. *J. Control. Release* **190** (2014) 337–351.

82. H. Priya James, R. John, A. Alex, K.R. Anoop. *Acta Pharm. Sin. B* **4** (2014) 120–127.

83. S. Thamphiwatana, V. Fu, J. Zhu, D. Lu, W. Gao, L. Zhang. *Langmuir* **29** (2013) 12228–12233.

84. É.L. Silva, J.F. Carvalho, T.R.F. Pontes, E.E. Oliveira, B.L. Francelino, A.C. Medeiros, E.S.T. do Egito, J.H. Araujo, A.S. Carriço. *J. Magn. Magn. Mater.* **321** (2009) 1566–1570.

85. X.Q. Wang, Q. Zhang. *Eur. J. Pharm. Biopharm.* **82** (2012) 219–229.

86. Y.H. Lin, C.H. Chang, Y.S. Wu, Y.M. Hsu, S.F. Chiou, Y.J. Chen. *Biomaterials* **30** (2009) 3332–3342.

87. C.-H. Chang, Y.-H. Lin, C.-L. Yeh, Y.-C. Chen, S.-F. Chiou, Y.-M. Hsu, Y.-S. Chen, C.-C. Wang. *Biomacromolecules* **11** (2010) 133–142.

88. C.A. Lingwood, A. Pellizari, H. Law, P. Sherman, B. Drumm. *Lancet* (1989) 238–241.

89. C.A. Lingwood, M. Huesca, A. Kuksis. *Infect. Immun.* **60** (1992) 2470–2474.

90. M. Dytoc, B. Gold, M. Louie, M. Huesca, L. Fedorko, S. Crowe, C. Lingwood, J. Brunton, P. Sherman. *Infect. Immun.* **61** (1993) 448–456.

91. D.Y. Singh, N.K. Prasad. *Pharmazie* **66** (2011) 268–273.

92. T.P. McMullen, R.N. McElhaney. *Curr. Opin. Colloid Interface Sci.* **1** (1996) 83–90.

93. C. Trampenau, K.-D. Müller. *Microbes Infect.* **5** (2003) 13–17.

94. R. Ansorg, K.-D. Müller, G. Von Recklinghausen, H.P. Nalik. *Int. J. Med. Microbiol.* **276** (1992) 323–329.

95. C. Wunder, Y. Churin, F. Winau, D. Warnecke, M. Vieth, B. Lindner, U. Zahringer, H.J. Mollenkopf, E. Heinz, T.F. Meyer. *Nat. Med.* **12** (2006) 1030–1038.
96. C.-H. Lai, Y.-M. Hsu, H.-J. Wang, W.-C. Wang. *BioMedicine* **3** (2013) 27–33.
97. K. Hosoda, H. Shimomura, S. Hayashi, K. Yokota, Y. Hirai. *FEMS Microbiol. Lett.* **318** (2011) 68–75.
98. R.D. Leunk, P.T. Johnson, B.C. David, W.G. Kraft, D.R. Morgan. *J. Med. Microbiol.* **26** (1988) 93–99.
99. T.L. Cover, M.J. Blaser. *J. Biol. Chem.* **267** (1992) 10570–10575.
100. E. Papini, M. Zoratti, T.L. Cover. *Toxicon* **39** (2001) 1757–1767.
101. J. Rassow, M. Meinecke. *Microbes Infect.* **14** (2012) 1026–1033.
102. G. Moll, E. Papini, R. Colonna, D. Burroni, J. Telford, R. Rappuoli, C. Montecucco. *Eur. J. Biochem.* **234** (1995) 947–952.
103. C. Pagliaccia, X.-M. Wang, F. Tardy, J.L. Telford, J.-M. Ruysschaert, V. Cabiaux. *Eur. J. Biochem.* **267** (2000) 104–109.
104. P. Boquet, V. Ricci. *Trends Microbiol.* **20** (2012) 165–174.
105. H. Iwamoto, D.M. Czajkowsky, T.L. Cover, G. Szabo, Z. Shao. *FEBS Lett.* **450** (1999) 101–104.
106. P. Lusini, N. Figura, M. Valassina, F. Roviello, C. Vindigni, L. Trabalzini, R. Nuti, C. Lenzi, C. Gonnelli, M. Nardi, P. Martelli, A. Santucci. *Dig Liver Dis.* **37** (2005) 232–239.
107. T. Tannaes, I.K. Bukholm, G. Bukholm. *FEMS Immunol. Med. Microbiol.* **44** (2005) 17–23.
108. Y.-L. Lin, J.-S. Liu, K.-T. Chen, C.-T. Chen, E.-C. Chan. *FEBS Lett.* **423** (1998) 249–253.
109. N. Dorrell, M.C. Martino, R.A. Stabler, S.J. Ward, Z.W. Zhang, A.A. McColm, M.J.G. Farthing, B.W. Wren. *Gastroenterology* **117** (1999) 1098–1104.
110. D.T. Smoot. *Gastroenterology* **113** (1997) S31–S34.
111. J.I. Smith, B. Drumm, A.W. Newmann, Z. Policova, P.M. Sherman. *Infect. Immun.* **58** (1990) 3056–3060.
112. H. Pruul, C.S. Goodwin, P.J. McDonald, G. Lewis, D. Pankhurst. *J. Med. Microbiol.* **32** (1990) 93–100.
113. J.S. Gunn, K.B. Lim, J. Krueger, K. Kim, L. Guo, M. Hackett, S.I. Miller. *Mol. Microbiol.* **27** (1998) 1171–1182.
114. T.W. Cullen, D.K. Giles, L.N. Wolf, C. Ecobichon, I.G. Boneca, M.S. Trent. *PLoS Pathog.* **7** (2011) 1–18.
115. A.X. Tran, J.D. Whittimore, P.B. Wyrick, S.C. McGrath, R.J. Cotter, M.S. Trent. *J. Bacteriol.* **188** (2006) 4531–4541.
116. D. Ilver, A. Arnqvist, J. Ogren, I.-M. Frick, D. Kersulyte, E.T. Incecik, D.E. Berg, A. Covacci, L. Engstrand, T. Bore, Science, **279** (1998) 373–377.
117. J. Mahdavi, B. Sonden, M. Hurtig, F.O. Olfat, L. Forsberg, N. Roche, J. Angstrom, T. Larsson, S. Teneberg, K.A. Karlsson, S. Altraja, T. Wadstrom, D. Kersulyte, D.E. Berg, A. Dubois, C. Petersson, K.E. Magnusson, T. Norberg, F. Lindh, B.B. Lundskog, A. Arnqvist, L. Hammarstrom, T. Boren. *Science* **297** (2002) 573–578.
118. M. Aspholm, A. Kalia, S. Ruhl, S. Schedin, A. Arnqvist, S. Lindén, R. Sjöström, M. Gerhard, C. Semino-Mora, A. Dubois, M. Unemo, D. Danielsson, S. Teneberg, W.K. Lee, D.E. Berg, T. Borén. *Methods. Enzymol.* **417** (2006) 293–339.
119. A. Magalhães, C.A. Reis. *Braz. J. Med. Biol. Res.* **43** (2010) 611–618.
120. A.O. Elzoghby, W.M. Samy, N.A. Elgindy. *J. Control. Release* **161** (2012) 38–49.

121. S.K. Jain, M.S. Jangdey. *Mol. Pharm.* **6** (2008) 295–304.
122. S.K. Jain, M. Gupta, A.K. Sahoo, A.N. Pandey, A.K. Jain. *Curr. Sci.* **106** (2014) 267–276.
123. P.L. Bardonnet, V. Faivre, F. Pirot, P. Boullanger, F. Falson. *Biochem. Biophys. Res. Commun.* **329** (2005) 1186–1192.
124. Y.H. Lin, S.C. Tsai, C.H. Lai, C.H. Lee, Z.S. He, G.C. Tseng. *Biomaterials* **34** (2013) 4466–4479.
125. J.A. Raval, J.K. Patel, M.M. Patel. *Acta Pharm.* **60** (2010) 455–465.
126. Z. Liu, W. Lu, L. Qian, X. Zhang, P. Zeng, J. Pan. *J. Control. Release* **102** (2005) 135–144.
127. A.O. Adebisi, B.R. Conway. *Int. J. Pharm.* **470** (2014) 28–40.
128. J.K. Patel, J.R. Chavda. *J. Microencapsulation* **26** (2009) 365–376.
129. S. Hassani, Y. Pellequer, A. Lamprecht. *Pharm. Res.* **26** (2009) 1149–1154.
130. S. Arora, J.M. Rajwade, K.M. Paknikar. *Toxicol. Appl. Pharmacol.* **258** (2012) 151–165.

Chapter 3

Motivation and objectives

"If you are working on something exciting that you really care about,
you don't have to be pushed. The vision pulls you."

Steve Jobs

There are three assertions that are currently recognized among the *H. pylori* experts:

1) *H. pylori* can cause gastric cancer, which is supported by epidemiology, molecular, animal, and eradication studies in humans [1];

2) *H. pylori* eradication reduces active inflammation in gastric mucosa, improves the mucosal status, heals chronic gastritis, prevents the progression to precancerous lesions, and reduces the incidence of gastric cancer [1];

3) The screening and the treatment of *H. pylori* infections are cost-effective. This is valid not only for communities with higher risk of gastric cancer, but also for developed countries due to the reduction in dyspepsia and peptic ulcers costs [1].

It is crucial to eradicate the bacteria as soon as there are clinical signs. The main problem raises from the limitations of the current therapy, which were mentioned in the previous chapter. Even when the treatment plan is strictly followed, the eradication rates are usually between 70-80% [2, 3]. This is still distant from the desirable for infectious diseases [1]. In fact, the success of any treatment against infectious diseases should be near 100%, specially to avoid repeated treatments and the development of antimicrobial resistance [4]. When the treatment against *H. pylori* fails, the rate of ulcer recurrence can be higher than 55%, which demonstrates the importance of completely eradicate *H. pylori* [5]. In those cases, the risk of gastric cancer development is indeed three-fold increased [5].

Among the new strategies that have been arising, the sequential and the concomitant therapy have been highlighted by several guidelines as alternative treatment plans. Nevertheless, these treatments have several limitations. They imply the administration of three or four drugs, taken two to four times a day, to up 14 days [3]. Therefore, the

probability of having adverse side effects (malaise, nausea, and diarrhoea) is high [3]. This is particularly frequent in the concomitant therapy due to the large number of pills [6]. In fact, these treatment plans are complex and require a committed compliance by the patient [3]. The sequential therapy requires a switch halfway, which hinders even more the therapeutic compliance [6]. Consequently, there is a serious risk of abandonment of the treatment, which can contribute to the development of antimicrobial resistance. Probiotics have also been publicized for being useful against *H. pylori*. There are indeed some studies that suggest probiotics as an alternative treatment [7, 8]. Nevertheless, the benefit of using probiotics are more associated with the reduction of side effects than with the effective death of *H. pylori* [1].

There is no optimal treatment so far, and *H. pylori* has been called an old but ever-challenging bug. Therefore, the main purpose of this thesis was to **improve the current therapy against *H. pylori* infections**. For that, two objectives were followed in this work:

1) To understand some **pharmacokinetic limitations** of the current therapy (viz., a proton-pump inhibitor, omeprazole, and two antibiotics, metronidazole and amoxicillin), by studying their interaction with biomembrane models (liposomes, monolayers, multilayers in capillaries, and modelled membranes);

2) To develop a **drug delivery system** with the ability to resist to the acidic pH and to interact and eradicate *H. pylori*.

These two objectives were pursued by stablishing specific objectives, that can be enumerated as follows:

- Understanding at a molecular level the interaction of the drugs with biological lipid membranes using a biophysical approach with the combination of experimental and computational techniques;

- Evaluation of the effect of each drug on the structure, the molecular packing, the organization, and the conformation of the phospholipids within a biomembrane model;

- Correlation of the studied properties with therapeutic and toxic effects;

- Development of a new and biocompatible drug delivery system using a rational design. The system should be able to resist to the harsh conditions of the gastrointestinal tract, should interact with the gastric mucus layer, and should interact and eradicate *H. pylori* at the site of infection.

References

[1] P. Malfertheiner, F. Megraud, C.A. O'Morain, J.P. Gisbert, E.J. Kuipers, A.T. Axon, F. Bazzoli, A. Gasbarrini, J. Atherton, D.Y. Graham, R. Hunt, P. Moayyedi, T. Rokkas, M. Rugge, M. Selgrad, S. Suerbaum, K. Sugano, E.M. El-Omar, Management of *Helicobacter pylori* infection-the Maastricht V/Florence Consensus Report, Gut 66(1) (2017) 6-30.

[2] A. Zullo, C. Hassan, L. Ridola, V.d. Francesco, D. Vaira, Standard triple and sequential therapies for *Helicobacter pylori* eradication: An update, Eur. J. Intern. Med. 24(1) (2012) 16-19.

[3] *Helicobacter pylori* in developing countries, World Gastroenterology Organisation Global Guidelines, 2010, pp. 1-15.

[4] S.D. Georgopoulos, V. Papastergiou, S. Karatapanis, Current options for the treatment of *Helicobacter pylori*, Expert Opin. Pharmacother. 14(2) (2013) 211-223.

[5] A. Talebi Bezmin Abadi, *Helicobacter pylori* treatment: New perspectives using current experience, J. Glob. Antimicrob. Resist. 8 (2017) 123-130.

[6] S.Y. Kim, D.J. Choi, J.-W. Chung, Antibiotic treatment for *Helicobacter pylori*: is the end coming?, World J Gastrointest. Pharmacol. Ther. 6(4) (2015) 183-198.

[7] A. Patel, N. Shah, J.B. Prajapati, Clinical appliance of probiotics in the treatment of *Helicobacter pylori* infection - A brief review, J. Microbiol. Immunol. Infect. 47(5) (2013) 1-9.

[8] J. Vítor, F.F. Vale, Alternative therapies for *Helicobacter pylori:* probiotics and phytomedicine, FEMS Immunol. Med. Microbiol. 63 (2011) 153-164.

Chapter 4

Methods to evaluate drug-lipid membrane interactions

"'Eureka' moments are very, very rare in my experience. It normally takes several weeks of experiments to tease out the truth, even when you have a really pretty good idea of what is going on."

Tim Hunt

Biological membranes work as barriers *in* vivo. Consequently, they affect the pharmacokinetic properties of drugs, such as their diffusion, transport, distribution, and accumulation [1]. Biophysical studies of drug-lipid membrane interactions were used to understand some limitations of the pharmacokinetic properties of the current therapy. For that purpose, three drugs were evaluated (omeprazole, metronidazole, and amoxicillin) for being classified as first-line drugs against *H. pylori* infections by several guidelines [2, 3]. Mimetic membrane models were used once the fragility, heterogeneity, and complexity of biological cells hinder the study of drug-lipid membrane interactions [1]. There are different membrane model systems in which the lipid organization and composition can be used to mimic biological lipid membranes. In this thesis, **dipalmitoylphosphatidylcholine (DPPC)** was chosen to compose the membrane models. There are several reasons that underlie this choice:

- Biological cells and, in particular, the gastric mucosa and the mucus layer, are composed of phosphatidylcholines [4];

- DPPC tails are composed of sixteen carbons, which resembles the acyl chains length of the main phospholipid of the gastric mucosa (palmitoyl-oleoyl-phosphatidylcholine, POPC, C16:0/C18:1) [4];

- The saturated acyl chains enable the study of different lipid phases. For instance, the surface pressure-area isotherm of DPPC has well-defined lipid phases whereas no defined lipid phases are visualized in Langmuir isotherms of unsaturated phospholipids, such as POPC [5];

127

- DPPC has been used to assess drug-membrane interactions in several studies, including to mimic the gastric mucosa [6]. Therefore, reference values are easily found in the literature, which enables a better validation of the work.

In this thesis, different models and techniques were combined to ensure a more comprehensive picture of the interaction between each drug and biological membranes (Figure 1). Liposomes, monolayers, multilayers, and modelled membranes composed of DPPC were used. In each model, several techniques were performed, and this chapter will describe the theoretical background behind those techniques.
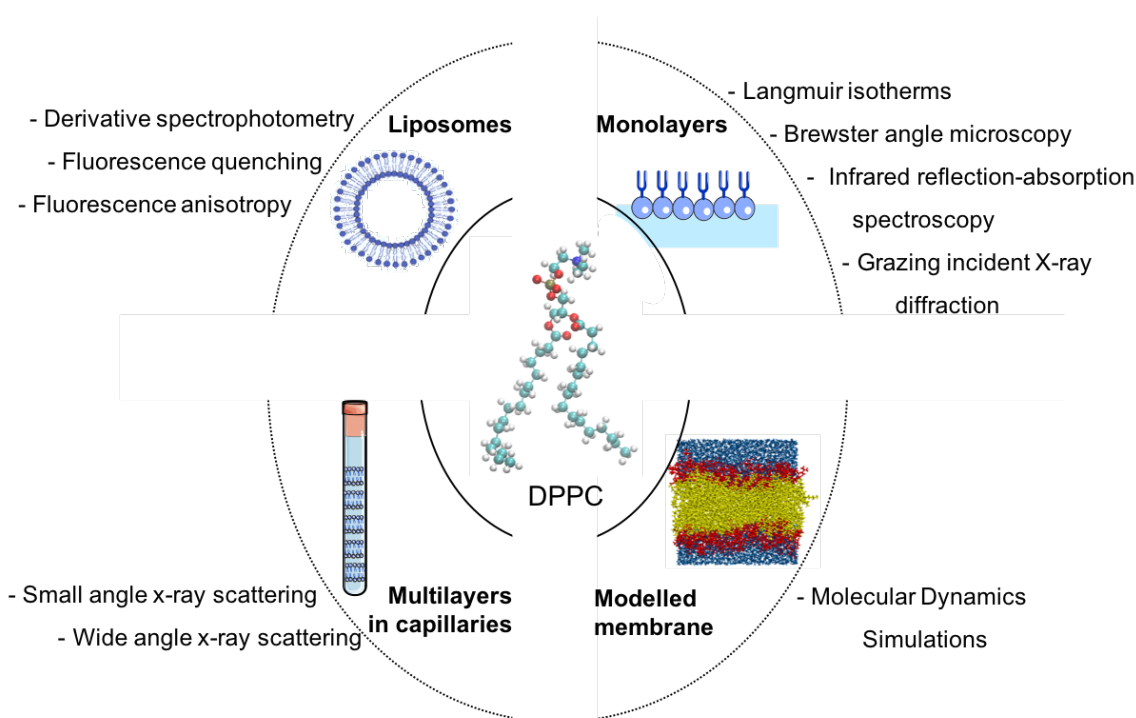
Figure 1. Representation of the several membrane model systems (liposomes, monolayers, multilayers, and modelled membranes) that were formed by DPPC moieties. The techniques that were performed using each model are also mentioned.

1. Liposomes

Amphipathic phospholipids, such as DPPC, can self-assemble into vesicles composed of one or more bilayers. Their anisotropic environment is similar to the one existent in biological cells [1]. Furthermore, the curvature of vesicles composed of zwitterionic vesicles in which the diameter ranged from 60 to 180 nm showed a negligible curvature, as cell membranes [7]. Therefore, unilamellar vesicles (LUVs) are commonly used to study drug-membrane interactions [1, 6, 8]. There are several methods to prepare liposomes. In this work, LUVs of DPPC of 100 nm were prepared by the classic thin-film hydration method

followed by extrusion [9]. Using this model, derivative spectrophotometry, fluorescence quenching and anisotropy studies were performed (Figure 2).
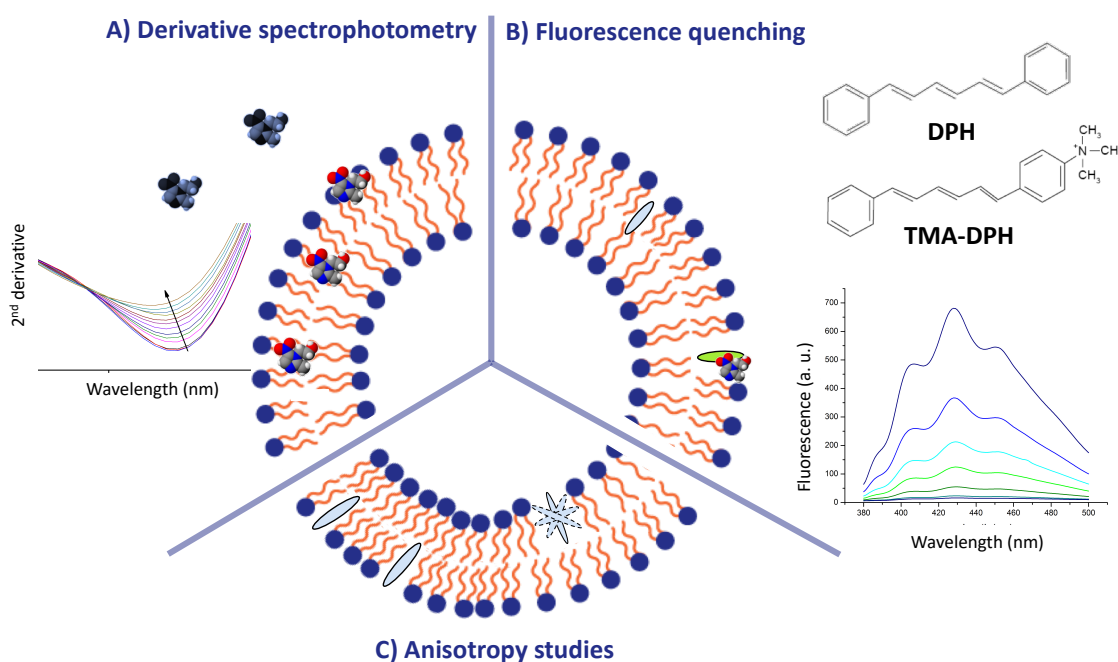
Figure 2. Liposomes were used as mimetic membrane models in which derivative spectrophotometry, fluorescence quenching, and anisotropy studies were performed.

1.1   Derivative spectrophotometry

The pharmaceutical industry usually uses the octanol/water system to determine the partition coefficient [1]. Nevertheless, this system is an isotropic biphasic system, where drug partitioning is governed only by hydrophobic interactions [10]. Due to the amphipathic properties of phospholipids and to the anisotropic environment of biological membranes, the partition of drugs *in vivo* may be also governed by electrostatic interactions, especially hydrogen and ionic bonds for ionized drugs [10]. Therefore, liposomes are better models to study the partition of ionizable molecules. There are different techniques that enable the determination of partition coefficients in liposomes, namely, potentiometry, isothermal titration calorimetry, and fluorescence studies. However, potentiometry requires high concentrations of the analytes; isothermal titration calorimetry is associated with a time-consuming optimization process; and fluorescence spectroscopy is only suitable for fluorescent drugs [11]. Hence, partition coefficients were determined though derivative spectrophotometry.

The basis of derivative spectrophotometry is that the absorption parameters (molar absorptivity and/or the wavelength of maximum absorbance) varies according to the polarity of the environment [12]. Therefore, when the drug partitions into the phospholipid bilayer, either close to the polar heads or more deeply in the membrane, its absorption spectra will change. In fact, there are deviations that can be graphically visualized (Figure 2, A). The use of absorbance derivative enables the elimination of the background signal that results from the light scattered by membrane models. It also improves the resolution of overlapping bands [13]. The partition coefficient is then calculated through a non-linear regression curve, using the following equation [13]:

$$D_t = D_w + \frac{b\, K_p[L]}{1 + K_p[L]} \qquad (1)$$

In this equation, D_t and D_w are the total and the aqueous derivative of the drug absorbance; K_p is the partition coefficient in L.mol^{-1}; and [L] is the concentration of the lipid. b is a constant defined by $b = (\varepsilon_m - \varepsilon_w) \times C_T$, in which ε is the drug molar absorptivity in lipid (m) and in water (w), and C_T is the total molar concentration of the drug.

1.2 Fluorescence quenching studies

The location of a drug within a membrane is extremely useful to understand the type of interactions that may be leading to changes on the biophysical properties of the membrane. Since half of the current commercial drugs have a membrane protein as a target, their location can also provide new insight on their pharmacodynamic properties [1].

In this thesis, we used fluorescent probes with a well-known location within a DPPC membrane, namely, 1,6-diphenyl-1,3,5-hexatriene (DPH) and 1-(4-Trimethylammoniumphenyl)-6-Phenyl-1,3,5-Hexatriene p-Toluenesulfonate (TMA-DPH) (molecular structures are shown in Figure 2, B). DPH is one of the most commonly used and characterized probes. It is mainly located parallel to the acyl chains of phospholipids whereas TMA-DPH has a more superficial location due to the cationic group that anchors to the phosphate group of DPPC [14]. The extent of the quenching depends on the proximity between the quencher and the fluorophore [14]. Therefore, the location can be indirectly estimated by the rate of fluorescence quenching.

The deactivation of fluorescence can be generally described through the Stern-Volmer equation (Equation 2). This equation can be applied when the deactivation is linearly proportional to the increasing concentration of the quencher [14].

$$\frac{I_0}{I} - 1 = K_{SV}[Q]_m \tag{2}$$

where I_0 and I are the steady-state fluorescence intensity of the probe without and with the drug, respectively, and K_{SV} is the constant of Stern-Volmer. Since the quenching depends on the amount of drug that is interacting with the phospholipid bilayer, a membrane effective concentration of the drug was also calculated ($[Q]_m$). This value is calculated using Equation 3, which takes into account the partition coefficient (K_p), the total concentration of the drug ($[Q]_t$), the lipid molar volume (V_φ), and the lipid molar concentration ([L]).

$$[Q]_m = \frac{K_p[Q]_t}{1+(K_p-1)(V_\varphi[L])} \tag{3}$$

Drugs may absorb light at the wavelength of excitation of the fluorophore, which would lead to an apparent quenching phenomenon. To avoid these false positive results, Equation 4 is used to eliminate the inner filter effect [15].

$$I_{corr} = I \frac{A_Q 1-10^{-A_F}}{A_F 1-10^{-A_Q}} \tag{4}$$

I_{corr} stands for the corrected fluorescence intensity, I is the experimental fluorescence intensity. A is the absorbance values at the excitation wavelength of the fluorophore in the absence (A_F) and the presence (A_Q) of the drug.

Fluorescence quenching analysis can benefit from lifetime measurements. Two main methods can be used to determine the lifetime of a probe, namely, time-domain and frequency-domain methods [14]. The influence of a drug on the fluorophore lifetime can give insights about the type of quenching. The static quenching does not affect the lifetime of the unquenched fluorophore once it involves the formation of a complex between the probe and the drug [14]. On the other hand, the dynamic or collisional quenching

encompasses diffusion encounters and, consequently, it changes the lifetime of the probe [14].

There are deviations to the Stern-Volmer equation. In this work, the combined dynamic and static quenching was used to fit positive deviations to the Stern-Volmer equation [14] (Equation 5).

$$\frac{I_0}{I} - 1 = (K_D + K_S)[Q]_m + K_D K_S [Q]_m^2 \tag{5}$$

where K is the constant of the dynamic (D) or the static (S) quenching.

1.3 Anisotropy studies

Fluorescence anisotropy (Figure 2, C) is related with the extent of polarization of the emission light [14]. A sample is usually excited with vertically polarized light, and the intensity of emission (*I*) is measured through a polarizer which is oriented parallel (II) or perpendicular ($\perp$) to the excitation polarizer [14]. Anisotropy can then be calculated using Equation 6 [14].

$$r = \frac{I_\parallel - I_\perp}{I_\parallel + 2I_\perp} \tag{6}$$

Anisotropy is a dimensionless quantity that do not depend on the fluorescence intensity of the sample once the total intensity ($I_\parallel + 2I_\perp$) is used for normalization [14]. Fluorescence anisotropy depends on the fluorophore rotational movement and, consequently, it is a very useful technique to study the packing of phospholipids. In this thesis, temperature- and time-resolved anisotropy were used.

1.3.1 Temperature-dependent steady-state anisotropy

Thermotropic phase transitions of phospholipids are important physicochemical properties, being extensively used to study drug-membrane interactions [16]. Usually, phospholipids pass from crystalline to liquid-crystalline with the increase of temperature [16]. Some phospholipids, such as DPPC, also pass through an intermediate phase, which

is called the ripple phase [17]. These lipid phase transitions play a crucial role *in vivo*, for instance for the regulation of protein function [18].

The rate of rotational diffusion of fluorophores within phospholipids bilayers are dependent on the viscosity of the environment. Hence, the steady-state fluorescence anisotropy (r_s) can be used to evaluate the membrane fluidity. r_s was calculated using Equation 6, in which an instrumental correction factor (G) was considered by multiplying $I_\perp$ by G on both parts of the fraction. The G factor is given by the ratio of the sensitivities of the detection system for vertically and horizontally polarized lights (Equation 7) [14].

$$G = \frac{I_\perp}{I_\parallel} \tag{7}$$

The temperature (T_m) and the cooperativity (B) of the main phase transition can be obtained by changes on the steady-state anisotropy in function of the temperature (Equation 8) [19].

$$r_s = r_{S1} + p_1 T + \frac{r_{S2} - r_{S1} + p_2 T - p_1 T}{1 + 10^{B(1/T - 1/T_m)}} \tag{8}$$

where T is the temperature, p_1 and p_2 are the slopes of the linear fits of the variation of anisotropy before and after the phase transition, and r_{S1} and r_{S2} are the corresponding y-intercepts.

1.3.2 Time-resolved anisotropy

Time-resolved anisotropy is based on the measurement of the values of anisotropy following pulsed excitation [14]. Anisotropy decays over time depend on the flexibility of the fluorophore [14]. Therefore, time-resolved anisotropy can provide direct insights on the dynamics of processes that result on polarization loss [20]. Once the profile of the anisotropy decay depends on the environment, it is also possible to infer domains formation through the existence of more complex "dip-and-rise" decays [20].

The anisotropy decay ($r(t)$) was described as a sum of discrete exponential terms (Equation 9), including the amplitude (β_i) and the rotational correlation time (ϕ_i) of the ith decay component of the anisotropy, and the limiting anisotropy (r_∞).

$$r(t) = \sum_{i=1}^{n} \beta_i \, exp\left(\frac{-t}{\phi_i}\right) + r_\infty \qquad (9)$$

2. Monolayers

Langmuir monolayers have been used to study membrane biophysics at 30 mN.m^{-1} once this is the lateral membrane pressure existent in the outer layer of a cell membrane. Thus, the lipid packing is similar is both situations [21, 22]. Moreover, the physical behaviour of monolayers and bilayers are similar at this pressure [23]. Lipid monolayers are stable bidimensional systems that are formed by lateral compression of amphipathic molecules that had been spread onto an aqueous surface. They can be used to perform different experimental techniques (Figure 3), such as, Langmuir isotherms, Brewster angle microscopy (BAM), infrared reflection-absorption spectroscopy (IRRAS), and grazing incidence X-ray diffraction (GIXD) studies.
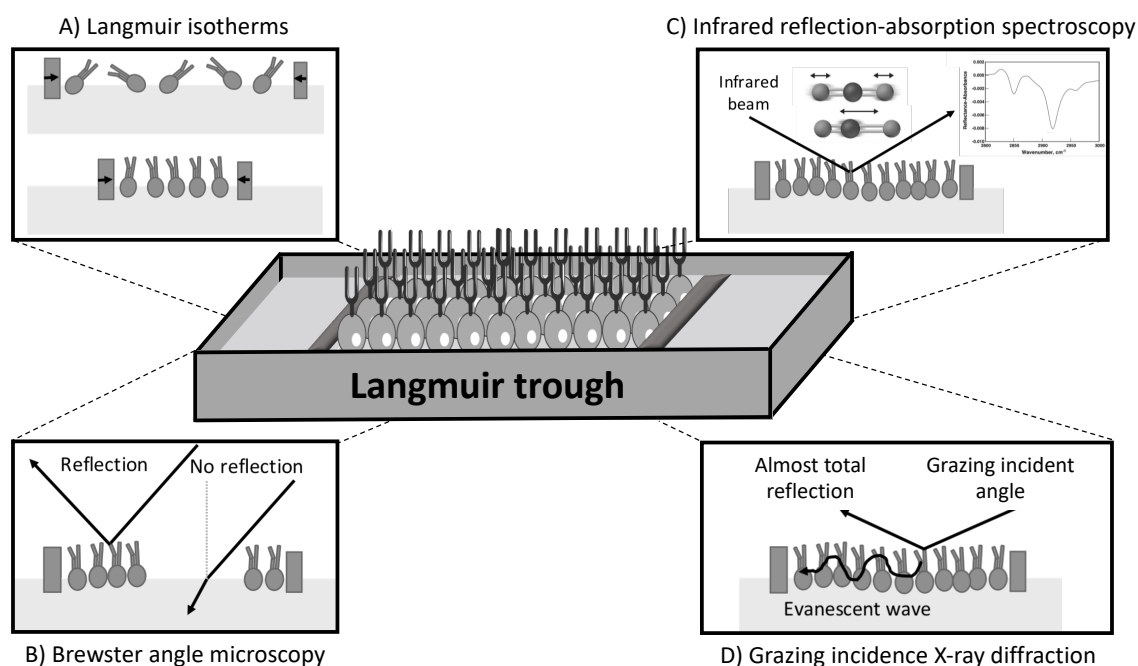
Figure 3. Monolayers were used as mimetic membrane models in which Langmuir isotherms, BAM, IRRAS, and GIXD studies were performed.

2.1 Langmuir isotherms

The monolayer can pass through different order transitions (gaseous, liquid expanded, tilted condensed, and untitled condensed) just by increasing the lateral pressure [22] (Figure

3, A). The surface pressure-molecular area (π/A) isotherms of DPPC monolayers are well characterized [24], and they have been used to study the topical action of drugs on the gastric mucosa [25, 26]. Changes on the outline of the π/A isotherm reflects the effect of a molecule on phospholipids packing.

The minimal area per lipid is used to characterize a lipid monolayer. In this thesis, it was calculated through the intersection of the x axis with a straight line obtained by the linear fitting of the condensed phase [27], in a range of pressures that included the biological lateral pressure. The elastic modulus was also used to characterize the compressibility of the membrane, and it can be calculated through the following equation [28]:

$$C_s^{-1} = -A \left(\frac{d\pi}{dA} \right) \qquad (10)$$

The elastic modulus of biological membranes is an important parameter to assess interactions that occur *in vivo*, such as among lipids or between lipids and proteins [29]. Furthermore, drops in the elastic modulus values reflect a discontinuity in the lateral packing [30]. Hence, it can be useful to unveil the effect of a drug on the formation of domains.

2.2 Brewster angle microscopy

BAM is based on changes in the reflectivity of a polarized laser beam when it interacts with a monolayer [31] (Figure 3, B). Hence, BAM can be used to assess the shape and the texture of phospholipids domains [31]. Once it does not resort to probes to visualize the membrane, BAM enables the visualization of the actual morphological changes during the dynamic process of compression [32]. In BAM images, darker regions correspond to more fluid phases whereas more condensed domains have a high reflective index and appear lighter.

2.3 Infrared reflection-absorption spectroscopy

Langmuir isotherms and BAM images provide information about the packing and the phase domains of monolayers. IRRAS can be used to complete the previous techniques by providing insights on chains conformation and hydrogen and ionic interactions. This technique enables the determination of the frequency of the molecular vibrations of phospholipids that are spread onto an aqueous solution [33]. The polarization modulation IRRAS (PM-IRRAS) considers the differences between the reflectivity of the light in a plane

parallel (s-polarizer) and in a plane perpendicular (p-polarizer) to the surface. By this, it is possible to minimize the signal of interfering molecules as the water and the carbon dioxide, which makes this technique highly sensitive and suitable for monolayer analysis [34]. In this work, four modes of vibration were analysed. Their wavenumbers and the corresponding structural information are provided in Table 1.

Table 1. Infrared vibration modes used for analysis of PM-IRRAS spectra.

Vibration mode	Wavenumber (cm^{-1})	Information
CH_2 symmetric stretch	2849-2854	Conformational order. Lower wavenumbers imply a more ordered membrane
CH_2 asymmetric stretch	2916-2924	
PO_2^- asymmetric stretch	1220-1260	Lower wavenumbers mean more hydrogen bonds/more hydration
C=O (esther)	1710-1740	

2.4 Grazing incidence X-ray diffraction

In GIXD, the incident beam is almost totally reflected and only an evanescent wave is able to travel along the interface [35, 36]. This technique is one of the main techniques that provides information regarding the structural arrangements and the conformation of phospholipids at the air/water interface [35, 36].

In this technique, spectra are obtained by varying the angle between the incident and the diffracted beam projected on the horizontal plane. For each angle, the vertical distribution of the scattered intensity is also collected. Hence, two separate components can be obtained from the scattering wave vector Q. Q_{xy} corresponds to the in-plane component, and it gives information about the periodic structure of the monolayer [37]. The distance among lattice planes is calculated from the first-order peaks of the the in-plane component ($d=2\pi/Q_{xy}$) [35]. The correlation length (ξ), which is a qualitative measurement of the extend of order, is calculated using the full-width at half-maximum (w_{hk}) values of the Bragg peaks ($\xi=2/w_{hk}$) [38]. On the other hand, Q_z is the out-of-plane component, from which it is possible to calculate the tilt angle [37] (Equation 11).

$$Q_z = Q_{xy} \cos(\psi) \tan(t) \tag{11}$$

Where ψ is the azimuth angle, with is equal to zero in the case of a next neighbour tilt.

3. Multilayers in capillaries

Multilayers in capillaries or stacked bilayers are easily prepared through the dispersion of multilamellar vesicles (MLVs) [39]. After the formation of MLVs through the hydration of a lipid film, the samples are aged overnight at 4 °C. After shaken by vortex, the samples are transferred into capillaries and kept at 4 °C until the experiment. This model possess long range periodicity and short range disorder, being useful for small and wide angle X-ray scattering studies (SAXS and WAXS, respectively) [40] (Figure 4).

SAXS

Lamellar phase
1:1/1:2/1:3/1:4/...

Hexagonal phase
1:1/1:√3/1:√4/1:√7/...

Cubic phase
1:1/1:√2/1:√3/1:√4/...

WAXS

Hexagonal phase — d_1

Pseudo-hexagonal phase — d_1, d_2
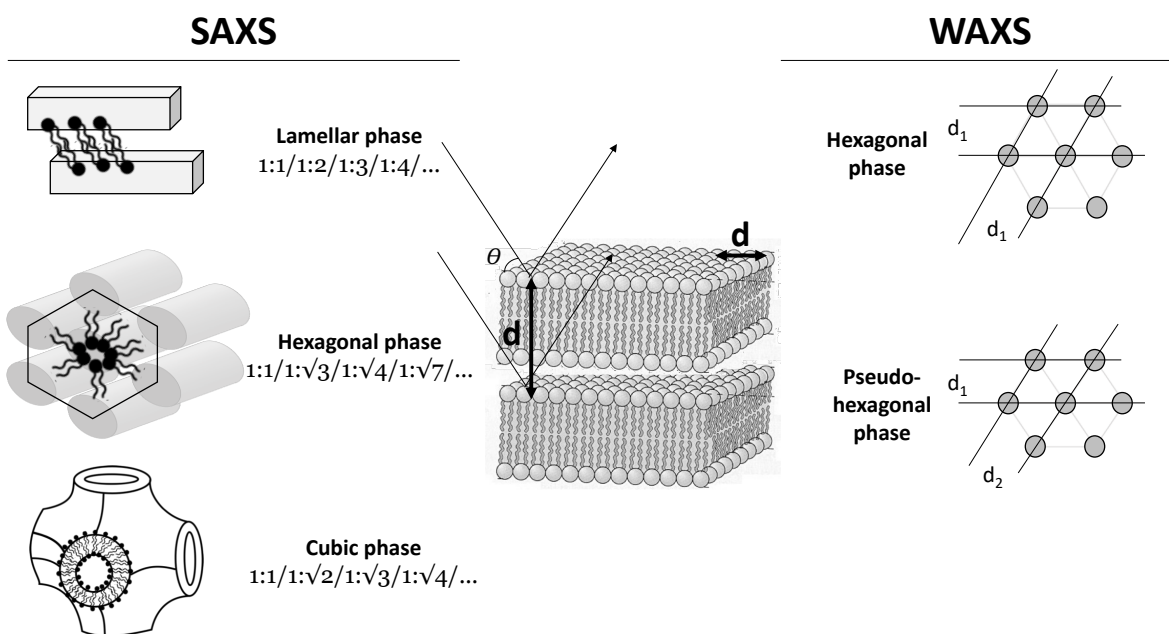
Figure 4. Multilayers in capillaries or stacked bilayers were used to perform SAXS and WAXS experiments. Representation of the different structural information that can be acquired from each experiment.

3.1 Small and Wide angle X-ray scattering

Multilayers in capillaries are organized in plain bilayers, whose interfaces are parallel and periodic. The basis of the X-ray scattering studies is that the incident beam is scattered when it faces these periodic structures, and the intensity of the scattered beam is measured in function of the scattering angle [41]. Based on Bragg's law, the scattered intensity is expressed in terms of the scattering vector (q), which is calculated through the wavelength of the scattered radiation (λ) and the scattering angle relatively to the incoming beam (2θ) [41] (Equation 12). From this, the repeated distances can be calculated (d).

$$q = \frac{4\pi}{\lambda}\sin\theta = \frac{2\pi}{d} \tag{12}$$

SAXS and WAXS provide different information once the long range order of the model appears in the small angle region ($\theta < 5°$C) and the short range order, such as the packing of the acyl chains, appears in the wide angle region ($5°$C $< \theta < 180$ $°$C) [40]. Furthermore, the correlation length (ξ) can also be calculated from the full width at half maximum (fwhm) (Equation 13). This parameter indicates the variability among the different distances, which means that a high correlation length in SAXS indicates that many bilayers have the same bilayer thickness whereas in WAXS it means that many hydrophobic chains have the same packing distance.

$$\xi = \frac{4\pi^2}{fwhm} \tag{13}$$

SAXS and WAXS also provide insights on the different lipid phases within the sample. On SAXS, it is possible to infer the type of structure (lamellar, hexagonal, cubic, etc.) from the ratio between the positions of the diffractions peaks (Figure 4). These non-bilayer phases also have biological relevance, for instance for events such as membrane fusion, exocytosis, and endocytosis [40]. From WAXS, it is possible to infer the spatial organization of the acyl chains packing, such as the hexagonal and the pseudo-hexagonal phase (Figure 4). This relevant information can be provided in gel phases and not in the liquid-crystalline phase once there is high diffusion of WAXS Bragg peaks.

4. Modelled membranes

Pre-assembled membranes are important for efficiently simulate drug-membrane interactions. For small bilayer patches, with only a few lipid moieties, the construction of membranes can be manually performed by each researcher [42]. Nevertheless, there are currently several tools that can be used to arrange lipids into a bilayer configuration, such as CHARMM-GUI, Membuilder, LipidBuilder, and Packmol [42]. Some of these tools can even create phospholipid structures besides planar membranes (e.g. micelles, vesicles, and hexagonal phases) [42]. In this thesis, phospholipid bilayers (Figure 5) were used to mimic the most common state of biological membranes.
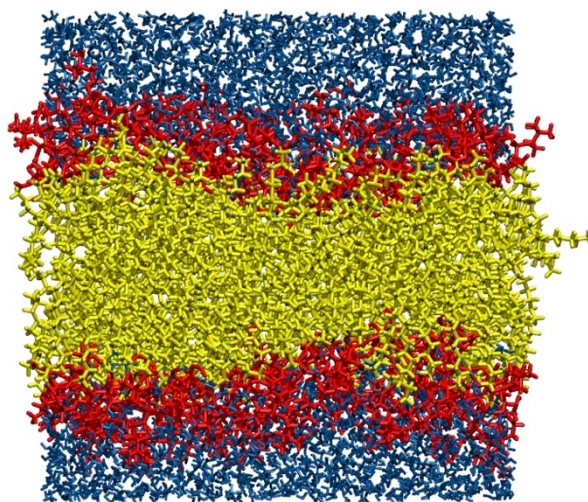
Figure 5. Membrane of DPPC modelled using the CHARMM-GUI builder. Water molecules are shown in blue, and phospholipids are shown in red (polar heads) and yellow (hydrophobic chains).

4.1 Molecular dynamics simulations

Molecular dynamics (MD) simulations for biomolecular systems started when McCammon et al. (1977) simulated the dynamics of folded proteins [43]. Nowadays, MD simulations are worldwide used. The usefulness of MD relies not only on the study of properties that can be measured or observed by experimental techniques, but especially for those where experiments are impossible, dangerous or too expensive [44]. Therefore, MD simulations were carried out in this thesis as a complementary piece to understand drug-membrane interactions with an atomic and time-resolution. The basis of this technique as well as all the parameters that must be optimized for each run are described in Chapter 2.2. A special highlight must be made to umbrella sampling simulations once they enable the determination of the partition coefficient and the free energy profiles of compounds that do not spontaneously visit all regions of the membrane [45].

References

[1] D. Lopes, S. Jakobtorweihen, C. Nunes, B. Sarmento, S. Reis, Shedding light on the puzzle of drug-membrane interactions: Experimental techniques and molecular dynamics simulations, Prog. Lipid Res 65 (2017) 24-44.

[2] P. Malfertheiner, F. Megraud, C.A. O'Morain, J.P. Gisbert, E.J. Kuipers, A.T. Axon, F. Bazzoli, A. Gasbarrini, J. Atherton, D.Y. Graham, R. Hunt, P. Moayyedi, T. Rokkas, M. Rugge, M. Selgrad, S. Suerbaum, K. Sugano, E.M. El-Omar, Management of *Helicobacter pylori* infection-the Maastricht V/Florence Consensus Report, Gut 66(1) (2017) 6-30.

[3] C.A. Fallone, N. Chiba, S.V. van Zanten, L. Fischbach, J.P. Gisbert, R.H. Hunt, N.L. Jones, C. Render, G.I. Leontiadis, P. Moayyedi, J.K. Marshall, The Toronto Consensus for the Treatment of *Helicobacter pylori* Infection in Adults, Gastroenterol. 151(1) (2016) 51-69 e14.

[4] W. Bernhard, A.D. Postle, M. Linck, K.-F. Sewing, Composition of phospholipid classes and phosphatidylcholine molecular species of gastric mucosa and mucus, Biochim. Biophys. Acta 1255 (1995) 99-104.

[5] C. Grauby-Heywang, F. Morote, M. Mathelie-Guinlet, I. Gammoudi, N.R. Faye, T. Cohen-Bouhacina, Influence of oxidized lipids on palmitoyl-oleoyl-phosphatidylcholine organization, contribution of Langmuir monolayers and Langmuir-Blodgett films, Chem. Phys. Lipids 200 (2016) 74-82.

[6] C. Pereira-Leite, C. Nunes, S. Reis, Interaction of nonsteroidal anti-inflammatory drugs with membranes: *in vitro* assessment and relevance for their biological actions, Prog. Lipid Res. 52 (2013) 571-584.

[7] D. Berti, G. Caminati, P. Baglioni, Functional liposomes and supported lipid bilayers: towards the complexity of biological archetypes, Phys. Chem. Chem. Phys. 13(19) (2011) 8769-82.

[8] A.C. Alves, D. Ribeiro, C. Nunes, S. Reis, Biophysics in cancer: The relevance of drug-membrane interaction studies, Biochim. Biophys. Acta 1858(9) (2016) 2231-2244.

[9] Liposomes: Methods and Protocols, 2nd ed., Humana Press2017.

[10] G.P. van Balen, C. Martinet, G. Caron, G. Bouchard, M. Reist, P.A. Carrupt, R. Fruttero, A. Gasco, B. Testa, Liposome/water lipophilicity: methods, information content, and pharmaceutical applications, Med. Res. Rev. 24(3) (2004) 299-324.

[11] D.R.P. Loureiro, J.X. Soares, D. Lopes, T. Macedo, D. Yordanova, S. Jakobtorweihen, C. Nunes, S. Reis, M.M.M. Pinto, C.M.M. Afonso, Accessing lipophilicity of drugs with biomimetic models: A comparative study using liposomes and micelles, Eur. J. Pharm. Sci. 115 (2018) 369-380.

[12] L.M. Magalhaes, C. Nunes, M. Lucio, M.A. Segundo, S. Reis, J.L. Lima, High-throughput microplate assay for the determination of drug partition coefficients, Nat. Protoc. 5(11) (2010) 1823-30.

[13] B.d. Castro, P. Gameiro, J.L.F.C. Lima, C. Matos, S. Reis, A fast and reliable spectroscopic method for the determination of membrane-water partition coefficients of organic compounds, Lipids 36(1) (2001) 89-96.

[14] J.R. Lakowicz, Principles of Fluorescence Spectroscopy, 3rd ed., Springer, Singapure, 2006.

[15] A. Coutinho, M. Prieto, Ribonuclease T1 and alcohol dehydrogenase fluorescence quenching by acrylamide: a laboratory experiment for undergraduate students, J. Chem. Educ. 70(5) (1993) 425-428.

[16] J.K. Seydel, M. Wiese, Drug-membrane interactions: analysis, drug distribution, modeling, Wiley-VCH2002.

[17] M. Rappolt, G. Rapp, Structure of the stable and metastable ripple phase of dipalmitoylphosphatidylcholine, Eur. Biophys. J. 24(381-386) (1996).

[18] A.H.d. Vries, S. Yefimov, A.E. Marck, S.J. Marrink, Molecular structure of the lecithin ripple phase, PNAS 102(15) (2005) 5392-5396.

[19] A. Grancelli, A. Morros, M.E. Cabañas, Ò. Domènech, S. Merino, J.L. Vázquez, M.T. Montero, M. Viñas, J. Hernández-Borrelli, Interaction of 6-Fluoroquinolones with Dipalmitoylphosphatidylcholine Monolayers and Liposomes, Langmuir 18 (2002) 9177-9182.

[20] T.A. Smith, K.P. Ghiggino, A review of the analysis of complex time-resolved fluorescence anisotropy data, Methods Appl. Fluoresc. 3(2) (2015) 022001.

[21] C. Peetla, A. Stine, V. Labhasetwar, Biophysical Interactions with Model Lipid Membranes: Applications in Drug Discovery and Drug Delivery, Mol. Pharm. 6(5) (2009) 1264-1276.

[22] V.M. Kaganer, H. Möhwald, P. Dutta, Structure and phase transitions in Langmuir monolayers, Rev. Mod. Phys 71(3) (1999) 779-819.

[23] A. Blume, A comparative study of the phase transitions of phospholipids bilayers and monolayers, Biochim. Biophys. Acta 557 (1979) 32-44.

[24] C.W. McConlogue, T.K. Vanderlick, A close look at domain formation in DPPC monolayers, Langmuir 13 (1997) 7158-7164.

[25] C. Nunes, G. Brezesinski, D. Lopes, J.L. Lima, S. Reis, M. Lucio, Lipid-drug interaction: biophysical effects of tolmetin on membrane mimetic systems of different dimensionality, J. Phys. Chem. B 115(43) (2011) 12615-23.

[26] C. Nunes, G. Brezesinski, C. Pereira-Leite, J.L. Lima, S. Reis, M. Lucio, NSAIDs interactions with membranes: a biophysical approach, Langmuir 27(17) (2011) 10847-58.

[27] L.K. Buehler, Cell membranes, Garland Science Taylor & Francis Group, New York, 2015.

[28] Z. Wang, X. Li, S. Yang, Studies of dipalmitoylphosphatidylcholine (DPPC) monolayers embedded with endohedral metallofullerene (Dy@C82), Langmuir 25(22) (2009) 12968-73.

[29] N. Fa, L. Lins, P.J. Courtoy, Y. Dufrene, P. Van Der Smissen, R. Brasseur, D. Tyteca, M.P. Mingeot-Leclercq, Decrease of elastic moduli of DOPC bilayers induced by a macrolide antibiotic, azithromycin, Biochim. Biophys. Acta 1768(7) (2007) 1830-8.

[30] J.M. Smaby, V.S. Kulkarni, M. Momsen, R.E. Brown, The interfacial elastic packing interactions of galactosylceramides, sphingomyelins, and phosphatidylcholines, Biophys. J. 70 (1996) 868-877.

[31] D. Vollhardt, V.B. Fainerman, Characterisation of phase transition in adsorbed monolayers at the air/water interface, Advances in colloid and interface science 154(1-2) (2010) 1-19.

[32] P.U. Muller, C.C. Akpo, K.W. Stockelhuber, E. Weber, Novel amphiphiles with preorganized functionalities-formation of Langmuir-films and efficiency in mineral flotation, Advances in colloid and interface science 114-115 (2005) 291-302.

[33] R. Mendelsohn, C.R. Flach, Infrared Reflection–Absorption Spectrometry of Monolayer Films at the Air–Water Interface, John Wiley & Sons Ltd (2002) 1028-1031.

[34] M.A. Ramin, G. Le Bourdon, N. Daugey, B. Bennetau, L. Vellutini, T. Buffeteau, PM-IRRAS investigation of self-assembled monolayers grafted onto SiO_2/Au substrates, Langmuir 27(10) (2011) 6076-84.

[35] C. Stefaniu, G. Brezesinski, Grazing incidence X-ray diffraction studies of condensed double-chain phospholipid monolayers formed at the soft air/water interface, Advances in colloid and interface science 207 (2014) 265-79.

[36] C. Stefaniu, G. Brezesinski, X-ray investigation of monolayers formed at the soft air/water interface, Curr. Opin. Colloid Interface Sci. 19(3) (2014) 216-227.

[37] M. Lúcio, B. Frank, S. Reis, J.L.F.C. Lima, G. Brezesinski, Binding of Nonsteroidal Anti-inflammatory drugs to DPPC: Structure and Thermodynamic Aspects, Langmuir 24 (2008) 4132-4139.

[38] F. Neville, Y. Ishitsuka, C.S. Hodges, O. Konovalov, A.J. Waring, R. Lehrer, K.Y. Lee, D. Gidalevitz, Protegrin interaction with lipid monolayers: Grazing incidence X-ray diffraction and X-ray reflectivity study, Soft matter 4(8) (2008) 1665-1674.

[39] J.F. Nagle, S. Tristram-Nagle, Structure of lipid bilayers, Biochim. Biophys. Acta 1469(3) (2000) 159-195.

[40] A.I.I. Tyler, R.V. Law, J.M. Seddon, Chapter 16: X-Ray diffraction of lipid model membranes, in: D.M. Owen (Ed.), Methods in Membrane Lipids, Methods in Molecular Biology, Springer Science+Business Media, New York, USA, 2015.

[41] C.J. Garvey, T. Lenne, K.L. Koster, B. Kent, G. Bryant, Phospholipid membrane protection by sugar molecules during dehydration-insights into molecular mechanisms using scattering techniques, Int. J. Mol. Sci. 14(4) (2013) 8148-63.

[42] M. Javanainen, H. Martinez-Seara, Efficient preparation and analysis of membrane and membrane protein systems, Biochim. Biophys. Acta 1858(10) (2016) 2468-2482.

[43] J.A. McCammon, B.R. Gelin, M. Karplus, Dynamics of folded proteins, Nature 267(16) (1977) 585-590.

[44] W.F. van Gunsteren, D. Bakowies, R. Baron, I. Chandrasekhar, M. Christen, X. Daura, P. Gee, D.P. Geerke, A. Glattli, P.H. Hunenberger, M.A. Kastenholz, C. Oostenbrink, M. Schenk, D. Trzesniak, N.F. van der Vegt, H.B. Yu, Biomolecular modeling: Goals, problems, perspectives, Angewandte Chemie 45(25) (2006) 4064-92.

[45] J. Kästner, Umbrella sampling, WIREs Comput. Mol. Sci. 1(6) (2011) 932-942.

Chapter 5

Methods to develop and characterize the drug delivery systems

"Ideas do not always come in a flash but by diligent trial-and-error
experiments that take time and thought."

Charles K. Kao

This chapter aims to describe the basic theoretical concepts behind the different techniques (Figure 1) that were used to design and characterize the nanoparticles. A rational design (Box-Behnken design) was initially performed, and the drug delivery system was characterized in terms of its physical features (size, zeta-potential, and morphology) and its efficacy against *H. pylori.*

Box-Behnken design

Characterization

Size

Dynamic Light Scattering

Zeta-potential

Electrophoretic Light Scattering

Morphology

Scanning and Transmission Electron Microscopy

Interaction with the bacteria

Imaging Flow Cytometry by ImageStream$^{X®}$

In vitro Infection Model
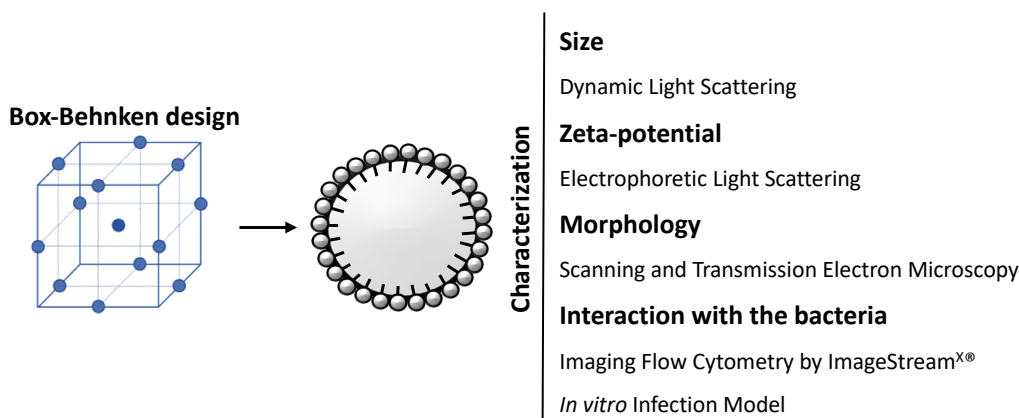
Figure 1. Techniques that were used to design and characterize the drug delivery system.

1. Box-Behnken design

The optimization of the composition of a nanoparticle is an initial crucial step once it affects all the physico-chemical features. In a traditional methodology, the optimization is performed one-variable-at-a-time, keeping constant the other variables [1, 2]. This methodology usually leads to sub-optimal formulations, and it is time and money-consuming [2, 3]. The higher number of experiments also requires a high consumption of reagents and materials [1, 2]. New strategies have been developed to overcome these limitations, such as the response surface methodologies. An initial screening is necessary to define the independent and the dependent variables as well as to delimit the experimental regions [2].

After that, the experimental data set is obtained with fewer experiments. Rational approaches use mathematical and statistic methods to obtain a linear or square polynomial equation that describe the behaviour of the experimental data set [2]. Through that, it is possible to predict the effect of each variable on the final formulation features [4]. By changing several variables simultaneously, these rational techniques also enable the assessment of the interactive effect of several variables at once [5].

Box-Behnken design consists of a mathematical approach where the independent variables are adjusted at three equally distributed levels (-1, 0, +1) [2]. This approach usually requires 15 to 17 runs for 3 or 4 dependent variables, and the results are represented in a multidimensional cube (Figure 1). A central point is used to calculate the error of the experiment by producing three replicas of that composition. At the end, the optimum value for each variable is predicted [2].

2. Dynamic Light Scattering

The behaviour of nanoparticles *in vivo* are correlated with their physico-chemical features, with a special highlight to their size [6]. In fact, particles size affect their cellular uptake, internalization via, permeability and retention effects, circulation time, among other pharmacokinetic features [6]. Particles size is extremely important for gastric diffusion. For instance, it was shown that particles with more than 200 nm have a decreased diffusion through the gastric mucosa [7]. Moreover, the size also affects the mucoadhesion to inflamed tissues of the gastric ulcers [8].

Dynamic light scattering is a commonly used technique to calculate the hydrodynamic size and the size distribution of nanoparticles [9]. This technique uses the Stokes-Einstein theory to predict the size of particles knowing the diffusion coefficient (D), the temperature (T), and the viscosity (η) of the medium [10]. The basis is that larger particles have smaller diffusion constants and, consequently, slower fluctuations of light scattered intensity over time (Figure 2). Considering these Brownian motions, the apparent radius (R) of the hydrated/solvated particle can be calculated through the Stokes-Einstein equation ($D = \kappa_B T / 6\pi\eta R$), where κ_B is the Boltzmann constant [9].
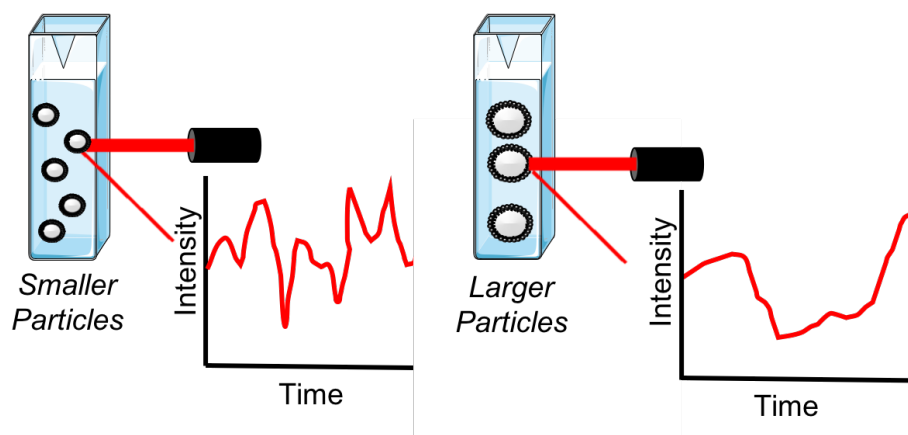
Figure 2. Dynamic light scattering of particles with different sizes: smaller particles show faster fluctuations of light scattering (left) whereas larger particles have slower ones (right).

3. Electrophoretic Light Scattering

The surface charge is important for biodistribution, opsonisation, and toxicity *in vivo* [6]. It is also crucial for the stability of the system once negatively or positively charged particles ($> |30$ mV$|$) are less likely to aggregate due to charged repulsions [6, 11]. In the case of *H. pylori* infections, the surface charge can even be used as a passive targeting agent against either the gastric mucosa or the bacteria [12].

Most liquids, especially the media used for biological assays, are composed of ions, either positive or negative ones. These ions tend to act as counter-ions of particles, being distributed around a charged particle (Stern layer) [13]. Loosely associated ions surround that layer, which leads to an electrical double layer [13]. The charge of the surface is called zeta potential, and it is usually determined by electrophoretic mobility [13]. When an electrical field is applied, the charge of a particle influences its mobility towards an electrode, which can be measured [13].

4. Scanning and Transmission Electron Microscopy

Electron microscopy can enlarge an image 1 million times, which makes it a useful technique to study small biological events, even individual proteins [14]. There are two main categories of electron microscopy: scanning electron microscopy (SEM) and transmission electron microscopy (TEM).

In SEM, a high-energy electron beam interacts with the surface of the sample, which is normally coated with a thin film of gold to improve contrast [14]. As result, different types of electron signals are emitted and process to give an image of the topography at three dimensions [14]. Hence, SEM can be useful to unveil morphological features of isolated

organisms [15]. In this thesis, SEM was used to evaluate the effect of lipid nanoparticles on the *H. pylori* morphology. One of the main difficulties when performing SEM observations is the dehydration of the samples, which can lead to collapse, shrinkage, and distortion of the results [15]. To overcome this problem, several methods have been developed, such as the critical point drying [15]. In TEM, the incident electron beam is transmitted, and the scattered or unscattered electrons that are consequently formed are focused and projected on a screen [13]. This technique has a high spatial resolution, which makes it a useful tool to study morphological and structural properties of nanomaterials [13]. TEM produces two dimensional images [14].

5. **Imaging Flow Cytometry (ImageStream^X®)**

Imaging flow cytometry (IFC) is an emergent technique that gathers together the conventional flow cytometry and the ability to capture multi-spectral images of each event (e.g. cell, bacteria, etc.) [16]. For that, imaging channels are used, which capture label-dependent fluorescence signals [16]. The existence of multiple lasers, detectors and the configuration of filters enable the analysis of the fluorescence through multiple channels [17]. The decomposition into different subimages allows the individual quantification of the signals obtained from overlapping regions [17]. The ability of this technique to couple fluorescent signals to a spatial context enables the study of co-localized events [16]. Therefore, this technique was used to access the affinity of the lipid nanoparticles to target the bacteria.

6. *In vitro* **infection model**

In vivo, *H. pylori* lives within the gastric mucosa, protected by the surrounding mucus layer or more frequently close to epithelial cells [18]. This is one of the limitations of the current therapy and one of the reasons of the incongruity between the efficacy of antibiotics *in vitro* and *in vivo* [19]. Therefore, we designed and developed an *in vitro* infection model (Figure 3) that could recreate in a simplistic way the infection that occurs *in vivo*.

The main purpose of this *in vitro* infection model was to ensure that the developed nanosystem was able to reach and kill *H. pylori* even when the bacteria is protected from an epithelial and a mucus barrier. Thus, the cell-line was selected considering its ability to keep the barrier after *H. pylori* infection. MKN-74 cells were chosen once they keep their cell morphology and cellular adhesion even after 96h after the infection [20]. Furthermore, *H. pylori* does not affect the cell cycle progression of those cells [21]. The chosen bacterial strain was the *H. pylori* J99 or ATCC 700824, which is a human strain firstly isolated from

a patient with duodenal ulcer and duodenitis [22]. It is classified as a type I strain once it produces both CagA and VacA, and it induces the secretion of interleukin-8 by gastric epithelial cells [23]. It also has BabA adhesins [23], and it is positive for other outer membrane proteins, such as SabA and OipA [24, 25]. Therefore, the strain *H. pylori* J99 was chosen for being a human pathogenic strain.
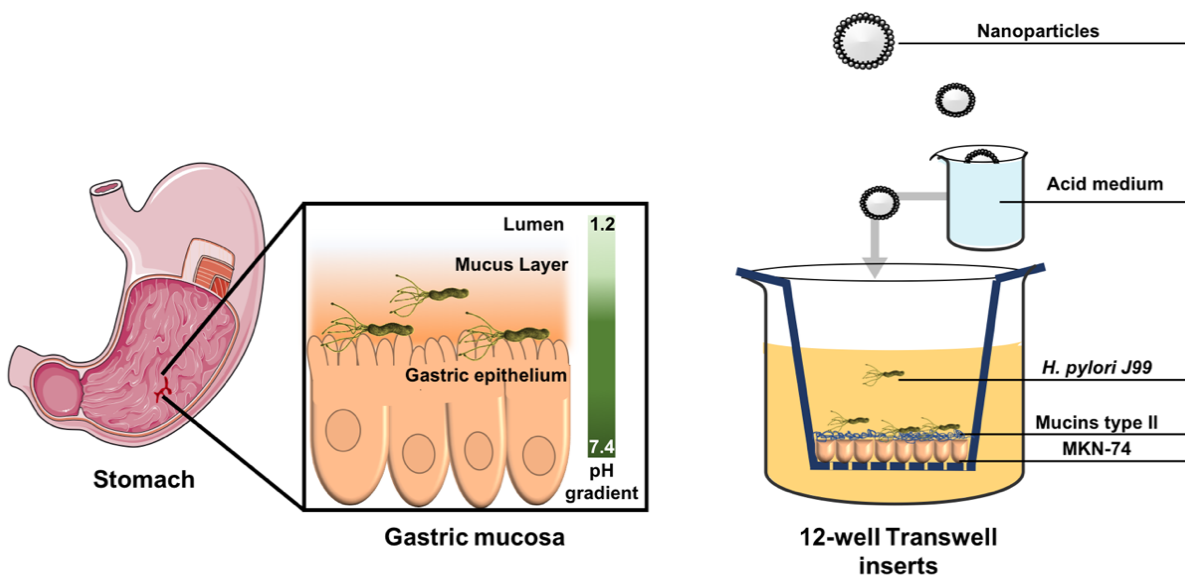
Figure 3. Infection of the gastric mucosa by *H. pylori.* Representation (right) of the developed *in vitro* infection model, where gastric cells (MKN-74), artificial mucins (mucins type II), a human pathogenic strain of *H. pylori* (J99), and an acid medium were used.

Gastric cells were seeded in 12-well transwell inserts and grown for 7 days. The use of transwell devices enable the measurement of the transepithelial electric resistance, which ensures a dense barrier, with functional tight junctions. Porcine mucins type II were added by adapting a reported protocol [26]. The addition of mucins was followed by a soft orbital shaken to enable a homogeneous distribution of the mucins onto the surface of the gastric epithelium. Then, *H. pylori* was incubated with the system for 24 h to guarantee enough time for the bacteria to migrate across mucins, adhered, and infect gastric cells. The contact of the nanoparticles or the drug with the acidic medium of the stomach lumen was mimicked by the previous incubation with acid medium for 1 h. The time of treatment was 24 h.

References

[1] B. Singh, R. Kapil, M. Nandi, N. Ahuja, Developing oral drug delivery systems using formulation by design: vital precepts, retrospect and prospect, Expert. Opin. Drug Deliv. 8(10) (2011) 1341-1360.

[2] M.A. Bezerra, R.E. Santelli, E.P. Oliveira, L.S. Villar, L.A. Escaleira, Response surface methodology (RSM) as a tool for optimization in analytical chemistry, Talanta 76(5) (2008) 965-77.

[3] B. Singh, R. Bhatowa, C.B. Tripathi, R. Kapil, Developing micro-/nanoparticulate drug delivery systems using "design of experiments", Int. J. Pharm. Investig. 1(2) (2011) 75-87.

[4] T. Lundstedt, E. Seifert, L. Abramo, B. Thelin, A. Nystrom, J. Pettersen, R. Bergman, Experimental design and optimization, Chemom. Intell. Lab. Syst. 42 (1998) 3-40.

[5] S.L. Ferreira, R.E. Bruns, H.S. Ferreira, G.D. Matos, J.M. David, G.C. Brandao, E.G. da Silva, L.A. Portugal, P.S. dos Reis, A.S. Souza, W.N. dos Santos, Box-Behnken design: an alternative for the optimization of analytical methods, Anal. Chim. Acta 597(2) (2007) 179-86.

[6] I. Kalashnikova, N. Albekairi, S. Al-Enazy, E. Rytting, Chapter 4: Characterization of drug-loaded nanoparticles, in: J. Naik (Ed.), Nano Based Drug Delivery, IAPC Publishing, Zagreb, Croatia, 2015.

[7] D. Lopes, C. Nunes, M.C. Martins, B. Sarmento, S. Reis, Eradication of *Helicobacter pylori*: past, present and future, J. Control. Release 189 (2014) 169-186.

[8] S. Hassani, Y. Pellequer, A. Lamprecht, Selective adhesion of nanoparticles to inflamed tissue in gastric ulcers, Pharm. Res. 26(5) (2009) 1149-1154.

[9] R. Pecora, Dynamic light scattering measurement of nanometer particles in liquids, J. Nanopart. Res. 2(2) (2000) 123-131.

[10] BS ISO 22412:2008 Particle size analysis - Dynamic light scattering (DLS), (2008).

[11] K.E. Sapsford, K.M. Tyner, B.J. Dair, J.R. Deschamps, I.L. Medintz, Analyzing nanomaterial bioconjugates: a review of current and emerging purification and characterization techniques, Anal. Chem. 83(12) (2011) 4453-88.

[12] D. Lopes, C. Nunes, M.C.L. Martins, B. Sarmento, S. Reis, Chapter 13: Targeting strategies for the treatment of *Helicobacter pylori* infections, in: J. Naik (Ed.), Nano Based Drug Delivery, IAPC Publishing, Zagreb, Croatia, 2015.

[13] P.C. Lin, S. Lin, P.C. Wang, R. Sridhar, Techniques for physicochemical characterization of nanomaterials, Biotechnol. Adv. 32(4) (2014) 711-26.

[14] Chapter 5: Microscopy, in: M. Carter, J. Shieh (Eds.), Guide to research techniques in neurosciences, Elsevier, U.S.A., 2015.

[15] C.G. Golding, L.L. Lamboo, D.R. Beniac, T.F. Booth, The scanning electron microscope in microbiology and diagnosis of infectious disease, Sci. Rep. 6 (2016) 26516.

[16] H. Hennig, P. Rees, T. Blasi, L. Kamentsky, J. Hung, D. Dao, A.E. Carpenter, A. Filby, An open-source solution for advanced imaging flow cytometry data analysis using machine learning, Methods 112 (2017) 201-210.

[17] E.K. Zuba-Surma, M. Kucia, A. Abdel-Latif, J.W.L. Jr., M.Z. Ratajczak, The ImageStream system: a key step to a new era in imaging, Folia Histochem. Cytobiol. 45(4) (2007) 279-290.

[18] S.J. Hessey, J. Spencer, J.I. Wyatt, G. Sobala, B.J. Rathbone, A.T.R. Axon, M.F. Dixon, Bacterial adhesion and disease activity in *Helicobacter* associated chronic gastritis, Gut 31 (1990) 134-138.

[19] F. Mégraud, P. Trimoulet, H. Lamouliatte, L. Boyanova, Bactericidal effect of amoxicillin on *Helicobacter pylori* in an *in vitro* model using epithelial cells, Antimicrob. Agents Chemother. 35(5) (1991) 869-872.

[20] S. Schneider, G. Carra, U. Sahin, B. Hoy, G. Rieder, S. Wessler, Complex cellular responses of Helicobacter pylori-colonized gastric adenocarcinoma cells, Infect. Immun. 79(6) (2011) 2362-71.

[21] P. Sommi, *Helicobacter pylori* Releases a Factor(s) Inhibiting Cell Cycle Progression of Human Gastric Cell Lines by Affecting Cyclin E/cdk2 Kinase Activity and Rb Protein Phosphorylation through Enhanced p27KIP1 Protein Expression, Exp. Cell Res. 281(1) (2002) 128-139.

[22] *Helicobacter pylori*: physiology and genetics, ASM Press, Washington DC, 2001.

[23] P. Doig, B.L. Jonge, R.A. Alm, E.D. Brown, M. Uria-Nickelsen, B. Noonan, S.D. Mills, P. Tummino, G. Carmel, B.C. Guild, D.T. Moir, G.F. Vovis, T.J. Trust, *Helicobacter pylori* physiology predicted from genomic comparison of two strains, Microbiol. Mol. Biol. Rev. 63(3) (1999) 675-707.

[24] J. Mahdavi, B. Sonden, M. Hurtig, F.O. Olfat, L. Forsberg, N. Roche, J. Angstrom, T. Larsson, S. Teneberg, K.A. Karlsson, S. Altraja, T. Wadstrom, D. Kersulyte, D.E. Berg, A. Dubois, C. Petersson, K.E. Magnusson, T. Norberg, F. Lindh, B.B. Lundskog, A. Arnqvist, L. Hammarstrom, T. Boren, *Helicobacter pylori* SabA adhesin in persistent infection and chronic inflammation, Science 297(5581) (2002) 573-8.

[25] S. Odenbreit, K. Swoboda, I. Barwig, S. Ruhl, T. Boren, S. Koletzko, R. Haas, Outer membrane protein expression profile in *Helicobacter pylori* clinical isolates, Infect. Immun. 77(9) (2009) 3782-90.

[26] L. Garcia-Gonzalez, L. Yepez-Mulia, A. Ganem, Effect of beta-cyclodextrin on the internalization of nanoparticles into intestine epithelial cells, Eur. J. Pharm. Sci. 81 (2016) 113-8.

Chapter 6

Progress beyond the state of the art

"It is always wise to look ahead, but difficult to look further than you can see."

Winston Churchill

The manuscripts that this thesis has originated will be presented in the following subchapters:

1- Topical interaction with lipid membranes as a new additional mechanism of action of immediate-release omeprazole

2- Molecular mechanisms behind the new additional mechanism of action of immediate-release omeprazole

3- Metronidazole within phosphatidylcholine lipid membranes: new insights to improve the design of imidazole derivatives (Submitted)

4- Proof of pore formation and biophysical perturbations through a 2D amoxicillin-lipid membrane interaction approach (Biochim. Biophys. Acta 1859 (2017) 803-812)

5- Delivering amoxicillin at the infection site – a rational design through lipid nanoparticles

6- Targeting and killing the ever-challenging ulcer bug: an antibiotic-free strategy

7- Efficacy of amoxicillin-loaded lipid nanoparticles on an *in vitro* infection model of *Helicobacter pylori*

Chapter 6.1

Topical interaction with lipid membranes as a new additional mechanism of action of immediate-release omeprazole

This work was designed around the first objective, which was to understand some pharmacokinetic limitations of the current therapy. Omeprazole is commonly used to treat peptic ulcers caused by *H. pylori*. Nevertheless, we found out a controversy between the use of a local release of the drug at the stomach (immediate-release omeprazole) and a systemic distribution (enteric-coated omeprazole). Once these routes of absorption imply the contact with different pH values, we studied the effect of pH on the topical interaction of omeprazole with lipid membrane models.
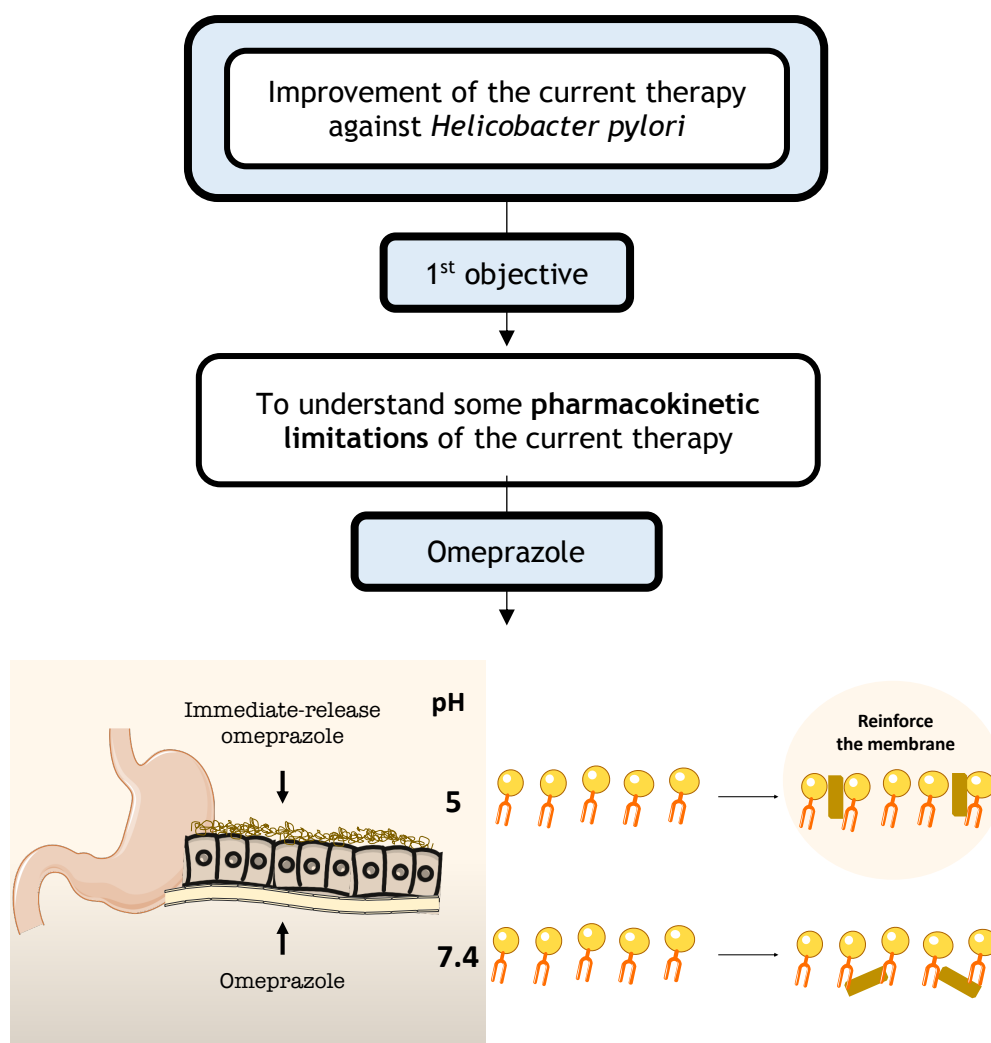
Chapter 6.1

Topical interaction with lipid membranes as a new additional mechanism of immediate-release omeprazole

Daniela Lopes-de-Campos[1], Catarina Pereira-Leite[1], Ana Coutinho[2,3], Joana C. Ricardo[2], Aleksander Fedorov[2], Manuel Prieto[2], Bruno Sarmento[4,5,6], Sven Jakobtorweihen[7], Cláudia Nunes[1], and Salette Reis[1*]

[1]LAQV, REQUIMTE, Departamento de Ciências Químicas, Faculdade de Farmácia, Universidade do Porto, Portugal

[2]CQFM-IN and IBB-Institute for Bioengineering and Biosciences, Instituto Superior Técnico, Universidade de Lisboa, Lisboa, Portugal

[3]Departamento de Química e Bioquímica, Faculdade de Ciências, Universidade de Lisboa, Lisboa, Portugal

[4]INEB - Instituto de Engenharia Biomédica, Universidade do Porto, Porto, Portugal

[5]i3S - Instituto de Investigação e Inovação em Saúde, Universidade do Porto, Porto, Portugal

[6]IINFACTS, Instituto de Investigação e Formação Avançada em Ciências e Tecnologias da Saúde, Instituto Universitário de Ciências da Saúde, Gandra, Portugal

[7]Institute of Thermal Separation Processes, Hamburg University of Technology, Hamburg, Germany

Omeprazole is a proton pump inhibitor usually administered under an enteric-coating. A new already FDA-approved strategy combines omeprazole with sodium bicarbonate to release the drug in the stomach lumen. This strategy showed to be more effective in increasing the intragastric pH and reducing the risk of bleedings. The aim of this study was to assess the effect of the absorption route by evaluating the topical effects of this drug on the phospholipids of the gastric mucosa, at different pH values and lipid phases.

Liposomes of dipalmitoylphosphatidylcholine were used as mimetic models. pH 5.0 mimicked an absorption through the gastric mucosa whereas pH 7.4 was used to mimic a systemic circulation. Distribution coefficients, free energy profiles, and fluorescence studies were combined to evaluate the membrane partitioning of omeprazole and its effect on the structure and dynamics of lipid bilayers.

Results showed that the partition and the preferential location of omeprazole depends on the drug ionization state, becoming more superficial for the charged form, which exists at pH 5.0. Fluorescence studies showed that omeprazole can decrease the cooperativity of the lipid main phase transition and induce the appearance of ordered domains at pH 5.0. Overall, the results showed that the existence of a protonated state at pH 5.0 enables the omeprazole intercalation among phospholipids. Hence, we propose here a new additional mechanism of action, where omeprazole at pH 5 can act like a phospholipid and, consequently, reinforce and protect the gastric mucosa.

Keywords: Immediate-release omeprazole, liposomes, partition coefficient, fluorescence studies, free energy profiles, molecular dynamics simulations.

1. Introduction

Omeprazole (OME) is a proton pump inhibitor (PPI) that is composed of heterocyclic groups, including a pyridine and a benzimidazole group [1]. OME was the first clinically used PPI, and it has been used for more than 25 years [1]. The interaction of OME with the gastric mucosa is crucial for its pharmacodynamic properties. Its main mechanism of action is the inhibition of the proton pumps located in the parietal cells of the gastric mucosa [2]. Furthermore, the inhibition of the gastric mucosa carbonic anhydrase was also indicated as one additional mechanism [3]. The pH is also an important key for its efficacy. OME acts as a "pro-drug" that needs to be activated by the acidic pH to undergo a molecular rearrangement into a sulphonamide intermediate [2]. PPIs are administered under enteric-coated tablets or capsules that protect the drug from the early activation at the stomach lumen [4]. Therefore, PPIs are absorbed at the intestine and distributed into the blood stream [4]. This promotes a delayed release and, consequently, a delayed absorption [5]. A new FDA-approved strategy to overcome this limitation is an immediate-release OME (IR-OME) [5]. This strategy combines OME and sodium bicarbonate to increase the intragastric pH and to protect OME from the acidic degradation [5]. Thus, OME can be locally and faster absorbed at the gastric mucosa [5]. Besides the higher efficacy already proved in increasing the intragastric pH [5-7], IR-OME reduces the risk of upper gastrointestinal bleeding [8].

Considering the interaction of IR-OME with both epithelial cells and the mucus layer, the aim of this study was to assess the topical effects of IR-OME on lipid membranes. Biological membranes, including epithelial cells from the gastric mucosa, and the mucus layer are mostly composed of phosphatidylcholines [9, 10]. Furthermore, membranes are heterogeneous fluid lipid phases, where ordered lipid microdomains are also present [11, 12]. Although unsaturated phospholipids are more common *in vivo*, the use of saturated phospholipids enables the evaluation of the effect of the lipid phase in drug-membrane interactions. Hence, here liposomes of dipalmitoylphosphatidylcholine (DPPC) were used to mimic lipid membranes. The effect of pH was also assessed in this study. IR-OME is able to keep the median 24-h gastric pH around 4.7 (3.2-5.8) [6]. Thus, the studies of OME-DPPC interactions were performed at both pH 5.0 (mimicking the local interaction at the gastric mucosa) and pH 7.4 (physiological pH). These pH values also enable the study of different protonation states of OME (Figure 1), which are important for the interaction with zwitterionic molecules, such as DPPC. Different experimental techniques (derivative spectrophotometry and fluorescence techniques) were used to an *in vitro* assessment of OME-DPPC interactions. Furthermore, molecular dynamics (MD) simulations were used to obtain the free energy profile of both protonation states along the DPPC bilayer.

1

2

pH	1 (%)	2 (%)	Others
5.0	62.8	37.2	0.0
7.4	98.5	0.2	1.3
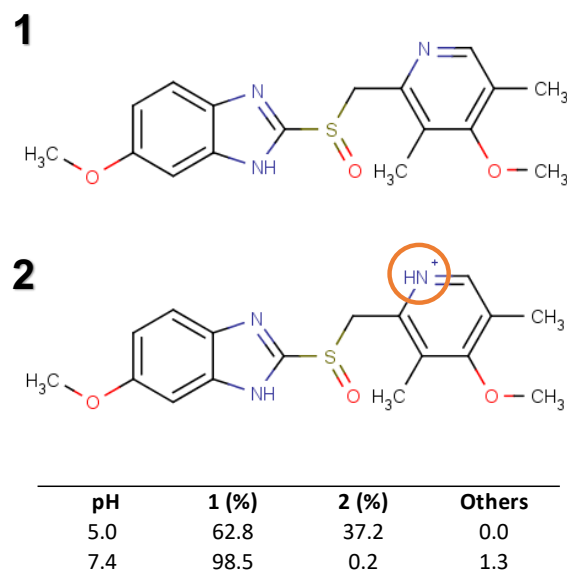
Figure 1. Protonation states of OME and their relative percentage at pH 5.0 and pH 7.4. These values were predicted by the *pK$_a$* plugin of MarvinSketch (ChemAxon®).

2. Materials and methods

2.1 Materials

1,2-Dipalmitoyl-*sn*-glycero-3-phosphocholine was obtained from Avanti® Polar Lipids, Inc (Alabaster, AL, USA). Trimethylammonium-diphenylhexatriene (TMA-DPH) and diphenylhexatriene (DPH) were purchased from Molecular Probes (Invitrogen Corporation, Carlsbad, California, USA). Unless otherwise stated, other reagents, such as OME and Ludox® AM-30 colloidal silica, were obtained from Sigma-Aldrich. All compounds were used without further purification.

All drug solutions and liposome suspensions were prepared using specific buffers (acetate buffer, *I*=0.13 M, for pH 5 and Hepes buffer, *I*=0.1 M, for pH 7.4). All solutions were prepared using double-deionized water (conductivity inferior to 0.1 μS.cm^{-1}).

2.2 Experimental section

2.2.1 Liposomes preparation

Liposomes were prepared using the method of the thin film hydration [13]. DPPC, previously solubilized in a mix of chloroform/methanol in a proportion of 3:2 (v/v), was evaporated under a nitrogen stream in a rotative evaporator. The lipid film was hydrated with the specific buffer. Large unilamellar vesicles (LUVs) were obtained after the

extrusion at 45 °C through polycarbonate filters (100 nm). For the fluorescence studies, both probes (DPH and TMA-DPH) were solubilized in chloroform/methanol (3:2) and then co-dried with the lipid in a final molar ratio of 300:1 (lipid:probe).

2.2.2 Determination of the distribution coefficients of OME

The distribution coefficients of OME at both pH values was assessed by a derivative spectrophotometry method [14]. OME was added to suspensions of increasing concentration of DPPC (from 0 M to 0.001 M) to a final drug concentration of 30 µM. Ethanol (1.25%, v/v) was used to help the solubilisation of OME. The samples were then incubated for 30 min at 45 °C. A Cary 1E UV/Vis Spectrophotometer coupled with a Cary Varian Peltier control was used to obtain the absorption spectra (200-400 nm) at a temperature below (37 °C) and above (45 °C) the main phase transition temperature of DPPC [15]. The distribution coefficients were calculated through a K_p calculator routine using a non-linear least-squares regression method described by Eq. (1) [14].

$$D_t = D_w + \frac{b\,K_p[L]}{1+K_p[L]} \tag{1}$$

where D_T and D_w are the derivative intensity of the absorbance spectra of the total amount of drug and the amount of drug in the aqueous phase; K_p is the partition coefficient; [L] is the molar concentration of the lipid; and b is a constant defined by $b = (\varepsilon_m - \varepsilon_w) \times C_T$, in which ε is the drug molar absorptivity within the lipid (m) or the water (w) phase and C_T is the total molar concentration of drug. The second and the third derivative of the absorbance spectra were calculated to eliminate the light scattering promoted by vesicles and to enhance the resolution of the bands. The obtained K_p was divided by the lipid molar volume of DPPC (0.70 Lmol^{-1} [16]) to obtain dimensionless K_p. The results from the derivative spectrophotometry are shown in Log D (Log D$_{DS}$).

2.2.3 Determination of OME location using fluorescence quenching

The membrane location of OME was estimated using steady-state fluorescence quenching and lifetime measurements. Fluorescent probes (TMA-DPH and DPH) with well-known locations within a DPPC membrane were used [17]. Buffered suspensions of DPPC (500 µM) in the presence of increasing concentrations of OME (0-100 µM) were incubated in the dark for 30 min at 45 °C for both pH values.

Steady-state fluorescence quenching studies were performed in a Biotek Synergy HT microplate reader using filters that encompass the wavelength of excitation and emission of both probes (λ_{exc}=357 nm for DPH and λ_{exc} = 359 nm for TMA-DPH, and λ_{em} = 429 nm for both probes). Fluorescence intensity values were recorded at 37 °C and 45 °C and further corrected by considering the absorbance of the sample at the excitation wavelength (inner filter effect). The methods behind the data analysis are described in the supporting information.

Frequency-domain fluorescence lifetime measurements were performed in a Fluorolog Tau-3 Lifetime system (Horiba) at 37 °C and 45 °C. Modulation frequencies were recorded from 6 to 200 MHz, with an integration time of 10 s. The manual slits were kept at 0.5 mm, and the slits for the excitation and the emission monochromators were 7.0/0.7 mm and 7.0/7.0 (side entrance/side exit), respectively. Ludox® was used as a reference standard with a lifetime of 0.00 ns.

2.2.4 Lipid phase transition through steady-state fluorescence anisotropy measurements

Steady-state fluorescence anisotropy measurements were used to determine the cooperativity and the temperature of the main phase transition of DPPC. For that, DPPC LUVs (500 μM) were incubated with OME (30 μM) for 30 min at 45 °C for both pH values. A Jasco FP-6500 Spectrofluorometer coupled with a Peltier Jasco ADP-303T Temp-controller was used. Excitation and emission slits were kept to 3 nm, and data was recorded from 25 to 55 °C (1 °C data pitch). From the changes in the steady-state anisotropy (r_s) values, the temperature (T_m) and the cooperativity (B) of the main phase transition were calculated (Eq. (A.4) of the supporting information).

2.2.5 Membrane organization through time-resolved fluorescence anisotropy studies

Time-resolved fluorescence anisotropy decays of DPH-labelled LUVs of DPPC (500 μM), with and without OME (30 μM), were obtained using the time-correlated single-photon timing technique. The samples were incubated for 30 min in the dark at 45 °C. A home-built set-up [18, 19] composed of a frequency-doubled laser of Rhodamine 6G (Coherent 701-2), a Jobin-Yvon HR320 monochromator, and a Hamamatsu R-2809U microchannel plate was used. The anisotropy decays were obtained considering the

intensity decays [17]. The parallel and the perpendicular fluorescence decays ($I_{VV}(t)$ and $I_{VH}(t)$, respectively) were alternatively measured using a λ_{exc} of 340 nm and λ_{em} of 429 nm. A time window of 1024 channels, with a time-scale of 58.6 ps/channel, 50,000 counts in the peak channel of the instrument response function (IRF), and 20,000 counts in the sample decay curves were used. A Ludox® dispersion was used to scatter the excitation beam while recording the IRF. A detailed description of the subsequent data analysis is provided in the supporting information.

Steady-state fluorescence anisotropy data was acquired to calculate a G' factor (Eq. A.6) able to minimize the influence of experimental artefacts on the time-resolved fluorescence studies. For that purpose, a SLM Aminco 8100 spectrofluorimeter (SLM Instruments, INC.) coupled to a thermostatic sample holder at 37 °C or 45 °C was used. The λ_{exc} and λ_{em} were set to 345 nm and 429 nm, respectively. Background fluorescence intensities promoted by the light scattering of the LUVs were considered. The four components of the polarized fluorescence emission were measured 10 times for each sample.

2.3 Calculation details
2.3.1 Prediction of the protonation states of OME

The *pK$_a$* plugin of ChemAxon®, MarvinSketch application, version 15.4.13.0, was used to predict the relative percentage of the protonation state of OME at pH 5.0 and pH 7.4.

2.3.2 Calculation of free energy profiles

The main settings of the MD simulations are described here. Further simulation details are provided in the supporting information. The CHARMM36 force field was used to model the interactions of the atoms [20]. However, for OME, some parameters are missing in the CHARMM force filed. Therefore, the general automated atomic model parameterization (GAAMP) was used to calculate the missing parameters [21].

In the MD umbrella sampling simulations, a reaction coordinate has to be defined (see also the supporting information). Here, the reaction coordinate for the free energy profile was the center of mass distance of the OME molecule to the bilayer center. Rather than taking all lipids into account for the definition of the membrane center, we used a so-called cylinder-based definition [22, 23]. In this case, only lipids that are within a cylinder parallel to the bilayer normal and located around the OME center of mass were

considered. The contribution of the lipid atoms to the membrane center are weighted, where the weight was switched from one to zero between the cylinder center and the cylinder radius. A cylinder radius of 2 nm was used. This cylinder-based definition of the membrane center was shown to be advantageous compared to taking all lipids into account [22-24].

To obtain the initial systems, snapshots are taken randomly from an equilibrated MD trajectory that contained the lipid bilayer, water, ions, but none OME molecules. OME molecules are then placed at their desired positions (distance to the membrane center). Since the system is so dense, there are no voids that fit an OME molecule. To avoid removing overlapping molecules, the interactions of the OME molecules with the rest of the system are slowly switched on in alchemical simulations. First the Lennard-Jones interactions were switched on, followed by the electrostatic interactions, where the OME molecules are harmonically restrained to their start positions.

Different methods were proposed to calculate the partition coefficient from the free energy profiles. Here we used the equation that corrects for the water content in the lipid phase [25]. Furthermore, as the experimental partition coefficients were dimensionless (see above), the coefficients from the MD results were calculated such that they are also dimensionless (based on the molar concentrations c [25]). The distribution coefficient for pH 7.4 can be directly taken from the simulation of neutral OME. However, the distribution coefficient for pH 5 was calculated from the MD simulations of the neutral and charged form according to their percentage at this pH (see Figure 1) Log D_{US}(pH 5) = Log (0.63 * K_{US}(neutral OME) + 0.37 * K_{US}(protonated OME)). We note here that the error margins of the partition coefficients are rather high. The OME molecule is quite flexible (large number of possible conformations) and maybe different conformations are sampled for the two OME molecules. However, the results obtained here are sufficient for this study. We will further investigate the OME conformations and their influence in a subsequent publication.

3. Results and Discussion

3.1 OME distribution coefficients

The ability of a drug to penetrate a biological membrane is crucial for its diffusion, transport, and distribution *in vivo* [26]. In the case of PPI, it is even important for its mechanism of action. OME has to be able to cross the plasma and the canalicular membrane to inhibit the proton pump [27]. The Log P value for OME octanol/water partition that is mentioned in the literature is around 2.36 [28]. Nevertheless, this determination has three limitations: i) It is performed in an octanol/water system, and thus

it does not consider the anisotropic environment that exists in biological membranes; ii) it does not consider the effect of pH on the charge state of the molecule and, consequently, on its ability to interact with charged molecules, such as phospholipids; and iii) it does not allow to study the effect of the lipid phase on the drug permeation through biological membranes. Hence, we used derivative spectrophotometry to determine the distribution coefficients (Log D) of OME at both pH values (5.0 and 7.4) and in different lipid phases. At 37 °C, DPPC is in a pre-transition state (ripple phase or $P_{\beta'}$), which is composed of periodic ordered and disordered domains [12]. Above the main phase transition temperature, DPPC is in a liquid-crystalline phase (L_α), which is the most common state of biological membranes [11]. Derivative spectrophotometry enables the determination of the partition in mimetic colloid systems, such as liposomes, without perturbing the equilibrium [26]. The basis and the protocol of this method is well described elsewhere [14]. Briefly, a deviation of the maximum of absorbance of the drug reflects a variation of the polarity of the environment that surrounds the drug (Figure A.1 of the supporting information). Furthermore, the existence of isosbestic points confirms the entire elimination of the scattering promoted by the LUVs [14]. The obtained Log D_{DS} values are shown in Table 1.

Table 1. Log D values obtained using derivative spectroscopy (Log D_{DS}) and umbrella sampling simulations (Log D_{US}) in different lipid phases and pH values.

pH	Lipid phase	Log D_{DS}	Log D_{US}
5.0	$P_{\beta'}$	2.23 ± 0.05	-
	L_α	2.52 ± 0.06	2.1 ± 0.3
7.4	$P_{\beta'}$	2.57 ± 0.07	-
	L_α	2.72 ± 0.02	2.3 ± 0.3

The understanding of OME partitioning within the lipid membrane was deepened by carrying out umbrella sampling simulations. The different protonation states of OME (Figure 1) were independently modelled to evaluate the effect of the charge on the drug partitioning. The simulations were carried out only in the liquid-crystalline phase due to the complexity of modelling the DPPC ripple phase. The results of Log D_{US} are also shown in Table 1. Umbrella sampling simulations allow the calculation of the free energy in regions of the membrane that would be barely visited in an unbiased simulation [29]. This thermodynamic parameter reflects the stability of a specific configuration and,

consequently, the preferential location of OME within the phosphatidylcholine membrane. The free energy profiles of each ionization state of OME are shown in Figure 2.
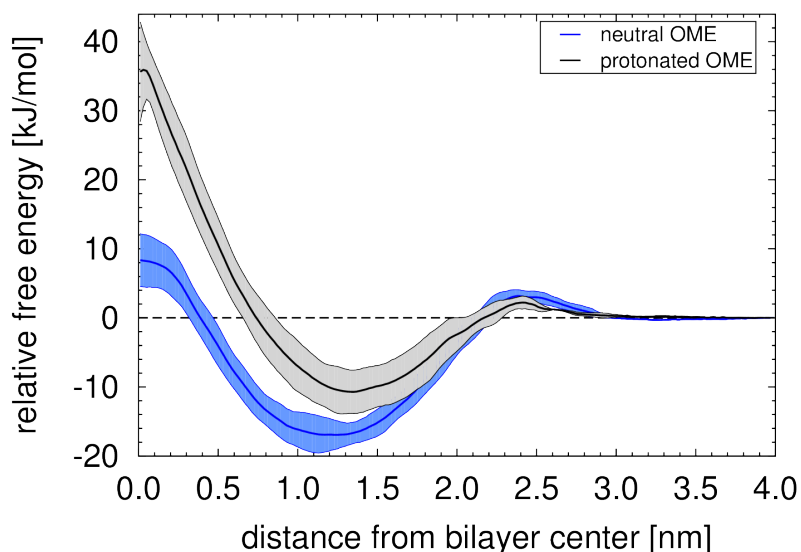
Figure 2. Free energy profiles of OME in its neutral and protonated state, obtained by umbrella sampling simulations at 50 °C. The free energy of the water phase was used as reference by defining it to be zero. All profiles are shown for half of the bilayer, and the colour regions represent the error margins.

At both pH 5.0 and pH 7.4, OME partitioning depends on the lipid phase, with higher affinity for the liquid-crystalline phase (Table 1). This effect was already shown for other drugs [30] due to the higher packing of phospholipids in some regions of the ripple phase, which hinders the penetration of the drug. Within the same lipid phase, the Log D is higher at pH 7.4. This result is probably related to the ionic forms of OME existing at each pH value. Predicted values of pK_a indicate that, at pH 7.4, neutral OME predominates, while the pyridine moiety become partially protonated at pH 5.0 (Figure 1). It is noteworthy that pK_a of acids usually increases in phospholipid bilayers, while pK_a of bases often decreases [31]. No significant alterations in the pK_a of a pyridine moiety were previously reported due to partitioning in phosphatidylcholine bilayers [32]. The same seems to be applied in this case once the Log D values decreased at pH 5.0, suggesting the presence of charged OME with lower affinity for the DPPC bilayer. Indeed, the Umbrella sampling simulations confirmed this, Log D_{us} showed the same trend as Log D_{DS}. OME in its deprotonated state (neutral) exhibited a preference for deeper regions of the membrane, which is shown by the minimum free energy closer to the bilayer center than that observed for charged OME (Figure 2). Furthermore, there is a higher energetic barrier for

163

the penetration of the protonated state of OME towards the center of the membrane in comparison with that observed for neutral OME.

In the case of PPI, a too high lipophilicity would lead to an accumulation near the hydrophobic chains of the membrane, which would hinder the access to its target [27]. On the other hand, a very low Log D would reduce the ability to cross membranes and, consequently, to access the acid space, where OME is activated to interact with the proton-pump [27]. Our results show that both charge forms (protonated and deprotonated) of OME have suitable Log D values to penetrate parietal cells. Nevertheless, its location within the membrane may be different. Further studies were carried out using fluorescence studies to unveil the location of OME within the membrane at both pHs.

3.2 Insights into OME location using fluorescence quenching

The location of OME was experimentally estimated through fluorescence quenching studies. TMA-DPH and DPH were used as probes due to their well-known location within phospholipid bilayers. DPH is mainly located among phospholipids, parallel to the apolar chains of phospholipids [26]. TMA-DPH has a more superficial location due to the trimethylammonium group that anchors to the polar heads of phospholipids [26]. The ability of OME to interact with the probes was evaluated through the decrease of their fluorescence – quenching phenomenon. The quenching of a fluorophore can be driven by a dynamic process due to diffusion encounters or by a static mechanism, with the formation of a complex between the probe and the drug [17]. The type of quenching can be distinguished by measuring the influence of the drug on the lifetime of the probe. A static quenching does not affect the lifetime of a probe once the lifetime of the fluorophore moieties that are unquenched is maintained [17]. The lifetime of the DPH probe as well as the deactivation of its fluorescence in presence of OME at both pH values are provided in the supporting information (Figure A.2 of the supporting information). The type of quenching is strongly affected by pH. At pH 5.0, a positive deviation is observed, and a combined dynamic and static quenching (Eq. (A.3) of the supporting information) was used to fit the upward-curving plot [17]. At pH 7.4, a linear relation between the fluorescence decrease and the drug concentration (Eq. (A.2) of the supporting information) was verified, with the existence of both dynamic and static quenching. The same trend was obtained with the TMA-DPH probe. The values of the quenching constants determined for both pH values and lipid phases are shown in Table 2.

Table 2. Fluorescence quenching constants obtained with TMA-DPH- or DPH-labelled LUVs of DPPC at two different pH values (5.0 and 7.4), each one assessed in two different lipid phases.

pH	Lipid phase	Probe	K_s (M^{-1})	K_D (M^{-1})	K_{sv} (M^{-1})
5.0	$P_{\beta'}$	TMA-DPH	545 ± 100	138 ± 24	684 ± 101
		DPH	591 ± 107	154 ± 38	745 ± 107
	L_α	TMA-DPH	249 ± 34	99 ± 14	348 ± 34
		DPH	242 ± 36	159 ± 35	400 ± 36
7.4	P_β	TMA-DPH	7 ± 1	4.7 ± 0.8	12 ± 1
		DPH	9 ± 2	4 ± 1	13 ± 2
	L_α	TMA-DPH	9 ± 2	5 ± 2	13 ± 2
		DPH	9.7 ± 0.4	5.2 ± 0.4	14.9 ± 0.4

At both pH values and lipid phases, OME can effectively quench both probes (Table 2), which immediately shows that OME can penetrate the membrane. The quenching of both probes occurs in a similar extent in each condition. This indicates that independently of pH and lipid phase, OME can interact with both DPH (deeper in the membrane) and TMA-DPH (more superficial). These results are in agreement with the results obtained by umbrella sampling simulations (Figure 2), as the negative free energy is extended throughout different regions of the membrane.

The quenching is significantly higher at pH 5.0 than at pH 7.4. Nitrogen is a known quencher, specially within an amine or a pyridine group [17]. For most of the quenching reactions, the distance between the quencher and the fluorophore must be short [17]. Hence, molecular contact is crucial [17]. OME has three nitrogen atoms that are included in a benzimidazole and a pyridine group (Figure 1). The difference between the type and the extent of quenching between both pH values may depend on the orientation of OME within the membrane. At pH 5.0, the positive charge of OME can stablish electrostatic interactions with the phosphate group of DPPC, and the benzimidazole group can stablish hydrophobic interactions with the apolar chains of DPPC. Therefore, OME may be intercalated among DPPC molecules, promoting a higher quenching of the probes by locating parallel to TMA-DPH or DPH. At pH 7.4, OME is predominantly neutral, which enables an aleatory distribution within deeper regions of the membrane by establishing hydrophobic interactions with the acyl chains of DPPC. This conclusion is consistent with the free energy profiles (Figure 2), as the minimum free energy of charged OME (preferential location) is closer to the polar heads of DPPC than that of neutral OME. Furthermore, it is also corroborated by the higher efficiency of quenching observed in the

ripple than in the liquid-crystalline phase at pH 5.0. The higher packing of phospholipids in the ripple phase may increase the proximity between OME and the probes, leading to a higher static deactivation due to the insertion of charged OME parallel to DPPC molecules (Table 2). On the other hand, at pH 7.4, the quenching did not depend on the lipid phase. This suggests that neutral OME is probably located in the more disordered region of the DPPC bilayer, that is, the acyl chains region.

3.3 Effect of OME on lipid phase transition through fluorescence anisotropy

The effect of OME on the phase transition temperature of DPPC was assessed through fluorescence anisotropy measurements of both TMA-DPH and DPH. The fluorescence anisotropy depends on the rotational movement of the probe, which is dependent on the packing of the membrane [17]. Figure 3 shows the variation of the DPH fluorescence anisotropy within DPPC LUVs as a function of temperature at pH 5.0 and 7.4. The temperature-dependent fluorescence anisotropy plots for TMA-DPH are provided in the supporting information (Figure A.3 of the supporting information).
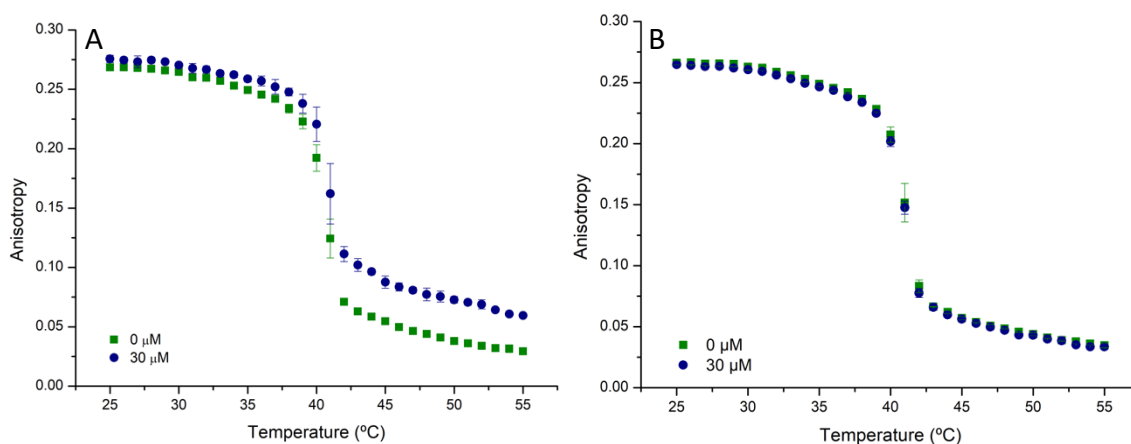
Figure 3. Temperature dependence of the steady-state fluorescence anisotropy of DPH-labelled LUVs of DPPC in presence of different concentrations of OME (0 μM in green and 30 μM in blue), at pH 5.0 (A) and pH 7.4 (B).

The obtained temperature (T_m) and the cooperativity (B) values of the main phase transition are provided in Table 3. At pH 7.4, OME does not affect B or T_m. Nevertheless, at pH 5.0, the cooperativity decreased either with TMA-DPH or DPH. Cooperativity lowering is associated with a drug location within the first nine carbons of the hydrocarbon chains [33, 34]. This result is consistent with the different locations of OME charge states previously discussed (see last section). Indeed, charged OME located parallel to the DPPC acyl chains exist only at pH 5.0, and this charge state may strongly affect the cooperativity unit of the DPPC bilayer. On the other hand, at pH 7.4, neutral OME located deeper within the DPPC acyl chains would have a less impact on the first carbons of the DPPC hydrophobic chains, and the cooperativity of DPPC bilayers would not be affected, as observed herein.

In the liquid-crystalline phase at pH 5.0 (Figure 3 (A)), it is clear that OME increased the fluorescence anisotropy of DPH. According to the Perrin equation [17], this result may be due to the effect of OME on the lifetime and/or the rotation correlation time of the probe. As OME was already shown to be a collisional quencher of DPH, time-resolved polarized fluorescence measurements were performed to study the OME effect on the molecular organization of DPH-labelled LUVs of DPPC, independently of the former effect.

Table 3. Temperature (T_m) and cooperativity (B) of the main phase transition of DPPC LUVs labelled with TMA-DPH or DPH according to OME concentration, at pH 5.0 and 7.4.

pH	[OME] (µM)	TMA-DPH		DPH	
		B	T_m (°C)	B	T_m (°C)
5.0	0	1037 ± 98	40.2 ± 0.1	1108 ± 126	40.2 ± 0.2
	30	705 ± 123	40.5 ± 0.3	923 ± 96	40.6 ± 0.2
7.4	0	1063 ± 93	40.6 ± 0.1	1098 ± 61	40.7 ± 0.1
	30	1110 ± 99	40.5 ± 0.1	951 ± 80	40.8 ± 0.2

3.4 Effect of OME on membrane structure through time-resolved fluorescence anisotropy

Fluorescence anisotropy decays depend on the flexibility and on the rotational movement of the fluorophore inside the membrane [17]. Therefore, time-resolved fluorescence anisotropy studies were used to assess the effect of OME on the structure of the DPPC membrane. The assays were performed using DPH-labelled LUVs, once the effect of OME on steady-state fluorescence anisotropy was similar for both probes, as shown in the preceding sections. The anisotropy decays of DPH (Figure 4) were usually biphasic for both pH values and lipid phases, with an initial anisotropy rapidly decreasing to a residual, almost constant, positive value. The correlation times (ϕ), the residual anisotropies (r_∞), and the order parameters (S) determined from the anisotropy decays are shown in Table 4.
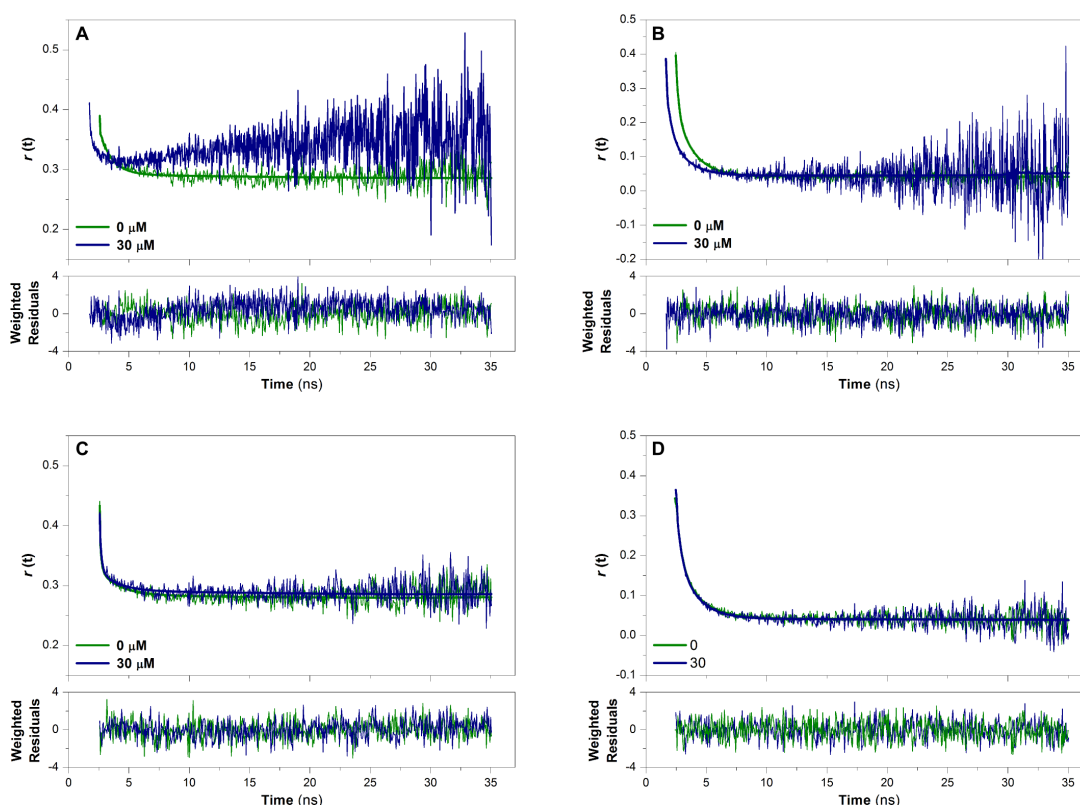
Figure 4. Fluorescence anisotropy decays of DPH-labelled LUVs of DPPC with 0 µM (green) and 30 µM (blue) of OME in four different conditions: pH 5.0 and 37 °C (A); pH 5.0 and 45 °C (B); pH 7.4 and 37 °C (C); and pH 7.4 and 45 °C (D). Solid lines represent the best fits of Eq. A.10 of the supporting information, and the weighted residuals of each fit are also shown.

The initial anisotropy ($r(0)$) of the decays of DPH in all systems were close to the fundamental anisotropy of DPH ($r_0 = 0.40$ in both lipid phases [35]). Distinct values of residual anisotropy were obtained with DPH-labelled LUVs of DPPC at different lipid phases. Higher values of r_∞ and S were obtained at 37 °C, due to the higher degree of membrane organization of the $P_{\beta'}$ phase. No significant alterations of the time-resolved fluorescence anisotropy parameters were observed upon OME addition at pH 7.4 (both lipid phases) and at pH 5.0 at the fluid phase (Table 4). At pH 5.0 and in the ripple phase, the anisotropy decay in the presence of OME was not biphasic (Figure 4 (A)). The called "dip-and-rise" complex behaviour was observed, as previously reported for other compounds [36]. The anisotropy increase after the first decay is probably due to the existence of another fluorescent species with a higher lifetime and a lower rotational correlation time [36, 37]. The second species must have a larger intrinsic value of r_∞, such as when the environment is more ordered [37]. The rotational correlation time and the lifetime of DPH varies depending on the DPPC lipid phase (ϕ=0.80 ns and τ=10.5 ns in gel phase; ϕ=0.89 ns and τ=8 ns in the liquid-crystalline phase [35]). As the ripple phase of DPPC is composed of gel-like and fluid-like domains [12] and the Log D of OME decreased in the ripple phase, it is conceivable that OME have more affinity to fluid-like domains. The insertion of OME in the more disordered regions of the ripple phase may promote a higher packing of the surrounded phospholipids, putatively in the gel-like domains. In the regions where OME is inserted, the lifetime of the probe is significantly decreased (τ=2.9 ns). On the other hand, the long-range packing may increase, and the lifetime of DPH in more ordered regions may become closer to that obtained in the gel phase (τ=10.5 ns [35]). Consequently, the obtained "dip-and-rise" anisotropy decay may be due to the presence of DPH molecules in more ordered (higher r_∞) and more disordered (smaller r_∞) regions, suggesting that OME leads to a higher heterogeneity within the DPPC bilayer at 37 °C, inducing the appearance of more ordered regions. This result is consistent with the previously esplanade. We propose here that the protonated state of omeprazole has amphiphilic properties and, consequently, intercalates among DPPC moieties. Amphiphilic molecules that are oriented parallel to phospholipids can in fact increase the order parameter of the apolar chains of phospholipids [38].

Table 4. Time-resolved fluorescence anisotropy parameters[a] of plain DPH-labelled DPPC and in presence of 30 µM of OME at pH 5.0 or pH 7.4. The values were obtained by fitting Eq. A.10 to the anisotropy decays. The order parameter was calculated using Eq. A.11.

pH	Lipid phase	[OME] (µM)	$\langle\phi\rangle$[b]	β_1	ϕ_1 (ns)	ϕ_2 (ns)	r_∞	r(0)	S
5.0	$P_{\beta'}$	0	1.1	0.06	1.1	-	0.291	0.36	0.86
		30[c]	0.2	0.05	0.2	-	0.321	0.38	0.91
	L_α	0	0.9	0.17	0.2	1.5	0.043	0.40	0.33
		30	1.0	0.10	0.3	1.4	0.046	0.29	0.34
7.4	$P_{\beta'}$	0	0.6	0.07	0.1	1.6	0.284	0.39	0.85
		30	0.5	0.07	0.1	1.5	0.291	0.40	0.86
	L_α	0	1.2	0.11	0.4	1.7	0.042	0.30	0.33
		30	1.1	0.10	0.4	1.6	0.041	0.30	0.33

[a] $\langle\phi\rangle$, mean rotational correlation time, $\pm$ 0.2; β_1, amplitude, $\pm$ 0.02; ϕ, rotational correlation time, $\phi_1 \pm$ 0.1 and $\phi_2 \pm$ 0.3; r_∞, limiting anisotropy, $\pm$ 0.003; r(0), initial anisotropy, $\pm$ 0.02, S, order parameter, $\pm$ 0.01.

[b] $\langle\phi\rangle=(\beta_1 \times \phi_1+\beta_2 \times \phi_2)/(\beta_1+\beta_2)$

[c] Data analysis disregarding "dip-and-rise" feature. $\chi^2 > 1.3$.

Peptic ulcers are associated with injuries in the gastric mucosa. The importance of phospholipids in protecting the gastric mucosa has been extensively proven [39, 40]. In fact, a decrease in the concentration of phospholipids in the mucosa has been associated with ulcerative mechanisms [40]. For instance, *H. pylori*, which is recognized as one of the key factors in the etiology of peptic ulcers, reduces the phospholipid concentration due to their lipolytic activity [41]. It was also proven that *H. pylori* can alter the surface hydrophobicity of the mucosa, which is returned after its eradication [41, 42]. Additionally, the administration of phospholipids demonstrated to be protective against ulcers [43, 44]. Therefore, surface-active molecules, such as charged OME, may have a key role in strengthen and protect the gastric mucosa [40].

4. Conclusions

Our work aimed to unveil the topical effects on phospholipid membranes that could result from a local absorption of OME through the gastric mucosa. Our results showed that the effect of OME on DPPC LUVs depends on pH. A small difference on the pH (5.0 to 7.4) affects the distribution coefficient and the preferential location of OME, as distinct ionization states are present. Charged OME, only present in acidic medium, seems to locate closer to the bilayer surface, as well as to induce the formation of ordered domains. Therefore, we propose here a new additional mechanism of action of OME at acidic pH.

Due to its amphiphilic nature of the protonated state, OME can be intercalated among phospholipids. By acting like a phospholipid, OME can contribute to reinforce the protective phospholipid layers of the gastric mucosa. This can be an additional explanation to the higher efficacy of IR-OME. Further studies on the molecular mechanisms of OME-DPPC interactions are ongoing.

Acknowledgments

References

[1] D.S. Strand, D. Kim, D.A. Peura, 25 Years of Proton Pump Inhibitors: A Comprehensive Review, Gut Liver 11(1) (2017) 27-37.

[2] L. Olbe, E. Carlsson, P. Lindberg, A proton-pump inhibitor expedition: the case histories of omeprazole and esomeprazole, Nat. Rev. Drug Discov. 2(2) (2003) 132-9.

[3] I. Puscas, M. Coltau, M. Baican, G. Domuta, Omeprazole has a dual mechanism of action: it inhibits both H+K+ATPase and gastric mucosa carbonic anhydrase enzyme in humans (*In vitro* and *In vivo* experimens), J. Pharmacol. Exp. Ther. 290 (1999) 530-534.

[4] V.F. Roche, The chemically elegant proton pump inhibitors, Am. J. Pharm. Educ. 70(5) (2006) 1-11.

[5] D. Castell, Review of immediate-release omeprazole for the treatment of gastric acid-related disorders, Expert Opin. Pharmacother. 6(14) (2005) 2501-2510.

[6] D. Castell, R. Bagin, B. Goldlust, J. Major, B. Hepburn, Comparison of the effects of immediate-release omeprazole powder for oral suspension and pantoprazole delayed-release tablets on nocturnal acid breakthrough in patients with symptomatic gastro-oesophageal reflux disease, Aliment. Pharmacol. Ther. 21(12) (2005) 1467-74.

[7] P.O. Katz, F.K. Koch, E.D. Ballard, R.G. Bagin, T.C. Gautille, G.C. Checani, D.L. Hogan, V.S. Pratha, Comparison of the effects of immediate-release omeprazole oral suspension, delayed-release lansoprazole capsules and delayed-release esomeprazole capsules on nocturnal gastric acidity after bedtime dosing in patients with night-time GERD symptoms, Aliment. Pharmacol. Ther. 25(2) (2007) 197-205.

[8] S.A. Conrad, A. Gabrielli, B. Margolis, A. Quartin, J.S. Hata, W.O. Frank, R.G. Bagin, J.A. Rock, B. Hepburn, L. Laine, Randomized, double-blind comparison of immediate-release omeprazole oral suspension

versus intravenous cimetidine for the prevention of upper gastrointestinal bleeding in critically ill patients, Crit. Care Med. 33(4) (2005) 760-765.

[9] V. Bernhard, A.D. Postle, M. Linck, K.-F. Sewing, Composition of phospholipid classes and phoshatidylcholine molecular species of gastric mucosa and mucus, Biochim. Biophys. Acta 1255 (1995) 99-104.

[10] F. Gambinossi, M. Puggeli, G. Gabrielli, Enzymatic hydrolysis reaction of phospholipids in monolayers, Colloids Surf. B, Biointerfaces 23 (2002) 273-281.

[11] P.V. Escriba, Membrane-lipid therapy: a new approach in molecular medicine, Trends Mol. Med. 12(1) (2006) 34-43.

[12] M. Eeman, M. Deleu, From biological membranes to biomimetic model membranes, Biotechnol. Agron. Soc. Environ. 14(4) (2010) 719-736.

[13] C. Nunes, G. Brezesinski, D. Lopes, J.L. Lima, S. Reis, M. Lucio, Lipid-drug interaction: biophysical effects of tolmetin on membrane mimetic systems of different dimensionality, J. Phys. Chem. B 115(43) (2011) 12615-23.

[14] L.M. Magalhaes, C. Nunes, M. Lucio, M.A. Segundo, S. Reis, J.L. Lima, High-throughput microplate assay for the determination of drug partition coefficients, Nat. Protoc. 5(11) (2010) 1823-30.

[15] C. Nunes, G. Brezesinski, C. Pereira-Leite, J.L. Lima, S. Reis, M. Lucio, NSAIDs interactions with membranes: a biophysical approach, Langmuir 27(17) (2011) 10847-58.

[16] R. Koynova, A. Koumanov, B. Tenchov, Metastable rippled gel phase in saturated phosphatidylcholines: calorimetric and densitometric characterization, Biochimica et Biophysica Acta 1285 (1996) 101-108.

[17] J.R. Lakowicz, Principles of Fluorescence Spectroscopy, 3rd ed., Springer, Singapure, 2006.

[18] J.A. Poveda, M. Prieto, J.A. Encinar, J.M. González-Ros, C.R. Mateo, Intrinsic Tyrosin Fluorescence as a Tool To Study the Interaction of the Shaker B "Ball" Peptide with Anionic Membranes, Biochem. 42 (2003) 7124-7132.

[19] A.M. Melo, A. Fedorov, M. Prieto, A. Coutinho, Exploring homo-FRET to quantify the oligomer stoichiometry of membrane-bound proteins involved in a cooperative partition equilibrium, Phys. Chem. Chem. Phys. 16(34) (2014) 18105-17.

[20] J.B. Klauda, R.M. Venable, J.A. Freites, J.W. O'Connor, D.J. Tobias, C. Mondragon-Ramirez, I. Vorobyov, A.D. MacKerell, R.W. Pastor, Update of the CHARMM All-Atom Additive Force Field for Lipids: Validation on Six Lipid Types, J. Phys. Chem. B 114(23) (2010) 7830-7843.

[21] L. Huang, B. Roux, Automated Force Field Parameterization for Non-Polarizable and Polarizable Atomic Models Based on Ab Initio Target Data, J. Chem. Theory Comput. 9(8) (2013).

[22] N. Nitschke, K. Atkovska, J.S. Hub, Accelerating potential of mean force calculations for lipid membrane permeation: System size, reaction coordinate, solute-solute distance, and cutoffs, J. Chem. Phys. 145(12) (2016) 125101.

[23] H.A. Filipe, M.J. Moreno, T. Rog, I. Vattulainen, L.M. Loura, How to tackle the issues in free energy simulations of long amphiphiles interacting with lipid membranes: convergence and local membrane deformations, J. Phys. Chem. B 118(13) (2014) 3572-81.

[24] C. Neale, R. Pomes, Sampling Errors in Free Energy Simulations of Small Molecules in Lipid Bilayers, Biochim. Biophys. Acta, Biomembr. 1858(10) (2016) 2539-48.

[25] S. Jakobtorweihen, A.C. Zuniga, T. Ingram, T. Gerlach, F.J. Keil, I. Smirnova, Predicting Solute Partitioning in Lipid Bilayers: Free Energies and Partition Coefficients from Molecular Dynamics Simulations and COSMOmic, J. Chem. Phys. 141(4) (2014) 045102.

[26] D. Lopes, S. Jakobtorweihen, C. Nunes, B. Sarmento, S. Reis, Shedding light on the puzzle of drug-membrane interactions: Experimental techniques and molecular dynamics simulations, Prog. Lipid Res. 65 (2017) 24-44.

[27] I.M. Modlin, G. Sachs, Pharmacology of acid secretion, Acid Related Diseases: Biology and Treatment, Lippincott Williams & Vilkins, Philadelphia, United States of America, 2004.

[28] F.Z. Dörwald, Pyridines, Pyrimidines, and Related Compounds, Lead Optimization for Medicinal Chemistry: Pharmacokinetic properties of Functional Groups and Organic Compounds, Wiley-VCH, Weinheim, Germany, 2012.

[29] J. Kästner, Umbrella sampling, Wiley Interdiscip. Rev. Comput. Mol. Sci. 1(6) (2011) 932-942.

[30] C. Nunes, D. Lopes, M. Pinheiro, C. Pereira-Leite, S. Reis, *In vitro* assessment of NSAIDs-membrane interactions: significance for pharmacological actions, Pharm. Res. 30(8) (2013) 2097-107.

[31] A. Avdeef, Physicochemical profilling (solubility, permeability and charge state), Curr. Top. Med. Chem. 1 (2001) 277-351.

[32] R.P. Austin, A.M. Davis, C.N. Manners, Partitioning of ionizing molecules between aqueous buffers and phospholipid vesicles., J. Pharm. Sci. 84(10) (1995) 1180-3.

[33] M.K. Jain, N.W. Wu, Effect of Small Molecules on the Dipalmitoyl Lecithin Liposomal Bilayer: III. Phase Transition in Lipid Bilayer, J. Membrane Biol. 34 (1977) 157-201.

[34] Q. Liu, Y. Qu, R.V. Antwerpen, N. Farrel, Mechanism of the Membrane Interaction of Polynuclear Platinum Anticancer Agents. Implications for Cellular Uptake, Biochem. 45 (2006) 4248-4256.

[35] L.F. Aguilar, J.A. Pino, M.A. Soto-Arriaza, F.J. Cuevas, S. Sanchez, C.P. Sotomayor, Differential dynamic and structural behavior of lipid-cholesterol domains in model membranes, PLoS One 7(6) (2012) e40254.

[36] T.A. Smith, K.P. Ghiggino, A review of the analysis of complex time-resolved fluorescence anisotropy data, Methods Appl. Fluoresc. 3(2) (2015) 022001.

[37] P.K. Wolber, B.S. Hudson, Bilayer acyl chain dynamics and lipid-protein interaction: The effect of the M13 Bacteriophase coat protein on the decay of the fluorescence anisotropy of parinaric acid, Biophys. J. 37 (1982) 253-262.

[38] J. Barry, M. Fritz, J.R. Brender, P.E.S. Smith, D.-K. Lee, A. Ramamoorthy, Determining the Effects of Lipophilic Drugs on Membrane Structure by Solid-State NMR Spectroscopy: The Case of the Antioxidant Curcumin, J. Am. Chem. Soc. 131 (2009) 4490-4498.

[39] F. Mauch, G. Bode, H. Ditschuneit, P. Malfertheiner, Demonstration of a phospholipid-rich zone in the human gastric epithelium damaged by *Helicobacter pylori*, Gastroenterol. 105(6) (1993) 1698-1704.

[40] L.M. Lichtenberger, Role of phospholipids in protection of the GI mucosa, Dig. Dis. Sci. 58(4) (2013) 891-3.

[41] S. Ishibashi, R. Iwakiri, R. Shimoda, H. Ootani, S. Kawasaki, J. Tadano, A. Kikkawa, A. Ootani, K. Oda, T. Fujise, T. Yoshida, S. Tsunada, H. Sakata, K. Fujimoto, Normalization of Phospholipids Concentration of the Gastric Mucosa was Observed in Patients with Peptic Ulcer after Eradication of *Helicobacter pylori*, Helicobacter 7(4) (2002) 245-249.

[42] P.M. Goggin, J. Marrero, R.T. Spychal, P.A. Jackson, C.M. Corbishley, T.C. Northfield, Surface hydrophobicity of gastric mucosa in Helicobacter pylori infection: Effect of clearance and eradication, Gastroenterol. 103(5) (1992) 1486-1490.

[43] S. Demirbilek, I. Gürses, N. Sezgin, A. Karaman, N. Gürbüz, Protective Effect of Polyunsaturated Phosphatidylcholine Pretreatment on Stress Ulcer Formation in Rats, J. Pediatr. Surg. 39(1) (2004).

[44] F.I. Tovey, Role of dietary phospholipids and phytosterols in protection against peptic ulceration as shown by experiments on rats, World J. Gastroenterol. 21(5) (2015) 1377-84.

Chapter 6.1

Supporting information

1. Data analysis of fluorescence quenching studies

The Stern-Volmer equation (Eq. A.1) was used when the deactivation of fluorescence was linear in presence of increasing concentrations of drug [1]:

$$\frac{I_0}{I} - 1 = K_{SV}[Q]_m \tag{A.1}$$

where I_0 and I are the steady-state fluorescence intensity of the probe without and with the drug, respectively, and K_{SV} is the constant of Stern-Volmer. $[Q]_m$ is the membrane effective concentration of drug, which has in consideration the partition coefficient (K_p), the total concentration of the drug ($[Q]_T$), the lipid molar volume (V_φ), and the lipid molar concentration ($[L]$), according to the following equation [1]:

$$[Q]_m = \frac{K_p[Q]_t}{1+(K_p-1)(V_\varphi[L])} \tag{A.2}$$

The combined dynamic and static quenching was used to fit positive deviations to the Stern-Volmer equation (Eq. A.3) [1].

$$\frac{I_0}{I} - 1 = (K_D + K_S)[Q]_m + K_D K_S[Q]_m^2 \tag{A.3}$$

where K is the constant of the dynamic (D) or the static (S) quenching.

2. Lipid phase transition through fluorescence anisotropy

In the fluorescence anisotropy measurements, the temperature (T_m) and the cooperativity (*B*) of the main phase transition were calculated using the following equation [2]:

$$r_S = r_{S1} + p_1 T + \frac{r_{S2} - r_{S1} + p_2 T - p_1 T}{1 + 10^{B(1/T - 1/T_m)}} \tag{A.4}$$

where *T* is the temperature, p_1 and p_2 are the slopes of the linear fits of the variation of anisotropy before and after the phase transition, and r_{S1} and r_{S2} are the corresponding y-intercepts.

3. Data analysis of the time-resolved anisotropy decays

The data was analyzed using the TRFA Data Processing Package (version 1.4) of the Scientific Software Technologies Center (Belarusian State University, Belarus). The analysis was performed in two steps: 1st) calculation of the fluorescence intensity decay parameters and 2nd) calculation of the anisotropy decay parameters. In the first step, the experimental fluorescence intensity decay (I_m(t)) was calculated using the following equation:

$$I_m(t) = I_{vv}(t) + 2G' I_{vH}(t) \tag{A.5}$$

where I_{VV}(t) and I_{VH}(t) are the parallel and the perpendicular fluorescence decays, respectively. *G'* is a factor that considers the fluorophore photobleaching and the fluctuations in the laser and, consequently, it was used to eliminate artificial artefacts during the data analysis. The *G'* factor was calculated using equation A.6, which considers the steady-state fluorescence anisotropy ($\langle r_S \rangle$). In our measurements, the *G'* factor varied between 0.96 and 1.00.

$$G' = \left(\frac{1 - \langle r_S \rangle}{1 + 2\langle r_S \rangle} \right) \left(\frac{\int I_{VV}(t) dt}{\int I_{VH}(t) dt} \right) \tag{A.6}$$

The fluorescence decay parameters were obtained by the iterative convolution of the fluorescence decay, i_m(t), which is empirically described as a sum of discrete exponentials

(Eq. A.7), with the instrument response function (IRF) and fitting to the experimental data $I_m(t)$ through a nonlinear least-squares regression method.

$$i_m(t) = \sum_{i=1}^{n} \alpha_i exp\left(\frac{-t}{\tau_i}\right) \tag{A.7}$$

α_i is the amplitude, and τ_i is the lifetime of the fluorescence decay component. The lifetime was then fixed for the subsequent analysis.

In the second step, the anisotropy decay parameters were obtained by simultaneous iterative convolution of $i_{VV}(t)$ and $i_{VH}(t)$, which are described by equations A.8 and A.9, respectively.

$$i_{VV}(t) = \frac{i_m(t)}{3}[1 + 2r(t)] \tag{A.8}$$

$$i_{VH}(t) = \frac{i_m(t)}{3}[1 - r(t)] \tag{A.9}$$

The anisotropy decay ($r(t)$) was described as a sum of discrete exponential terms (Eq. A.10), including the amplitude (β_i) and the rotational correlation time (ϕ_i) of the ith decay component of the anisotropy, and the limiting anisotropy (r_∞).

$$r(t) = \sum_{i=1}^{n} \beta_i \, exp\left(\frac{-t}{\phi_i}\right) + r_\infty \tag{A.10}$$

The order parameter (S) of the bilayer was calculated using Eq. A.11:

$$\frac{r_\infty}{r_0} = S^2 \tag{A.11}$$

in which r_0 is the fundamental anisotropy of the probe (0.39 for DPH [1]).

The steady-state fluorescence anisotropy ($\langle r_S \rangle$) used to calculate the G' factor in Eq. A.6 was calculated through the following equation:

$$\langle r_S \rangle = \frac{I_{VV} - GI_{VH}}{I_{VV} + 2GI_{VH}} \tag{A.12}$$

where I_{VV} and I_{VH} are the vertical and the horizontal components of the polarized fluorescence emission. In this case, the *G* factor is an instrumental correction factor ($G=I_{VH}/I_{VH}$) for the transmissivity bias introduced by the detection system.

4. Calculation of free energy profiles

All MD simulations were carried out with GROMACS version 2016.1 [3]. The CHARMM36 force field was used to model the lipids [4] and the ions [5], and the CHARMM TIP3P force field was used for modelling water. As for OME some parameters are missing in the CHARMM general force field [6], the general automated atomic model parameterization (GAAMP) was used to calculate the missing parameters [7]. In the simulations, bonds to hydrogen atoms were constrained. All simulations contained 128 DPPC lipid molecules, 7024 water molecules, 13 chloride ions, and 13 sodium ions. To keep the system neutral, the number of sodium ions was reduced for simulations that contained protonated OME. The Lennard-Jones interactions were cutoff at 1.2 nm, and a force switch was use from 1.0 nm on. The electrostatic interactions were cutoff at 1.2 nm, and the Particle-Mesh Ewald summation [8, 9] was used to take electrostatic interactions behind the cutoff into account. A Verlet list with a radius of 1.2 nm and an update of every tenth step was employed. The time step size was 2 fs. The temperature was kept constant at 323.15 K with the Nosé-Hoover thermostat [10] and a coupling constant of 1 ps. The pressure was kept constant at 1 bar with a semi-isotropic coupling to the Parrinello-Rahman barostat [11, 12] with a coupling constant of 5 ps and the compressibility of water.

To obtain the free energy profiles, MD umbrella sampling (US) simulations were carried out [13]. In this type of simulations, the regions of the membrane are sampled in independent simulations (windows). OME was harmonically restrained (here a force constant of 1000 kJ mol^{-1} nm^{-2} was used) at a different position in each simulation. For an efficient sampling, each simulation contained two OME molecules where the equilibrium positions were separated by 4 nm in the direction parallel to the bilayer normal. The spacing between the windows was 0.1 nm and 40 windows were simulated for each profile. Each umbrella window was simulated for 100 ns where the first 10 ns were considered as equilibration time and, consequently, were not included in the analysis. The weighted histogram analysis method [14] was used as implemented in the g_wham program [15] of the GROMACS package to obtain the free energy profile from the US simulations.

5. OME distribution coefficients
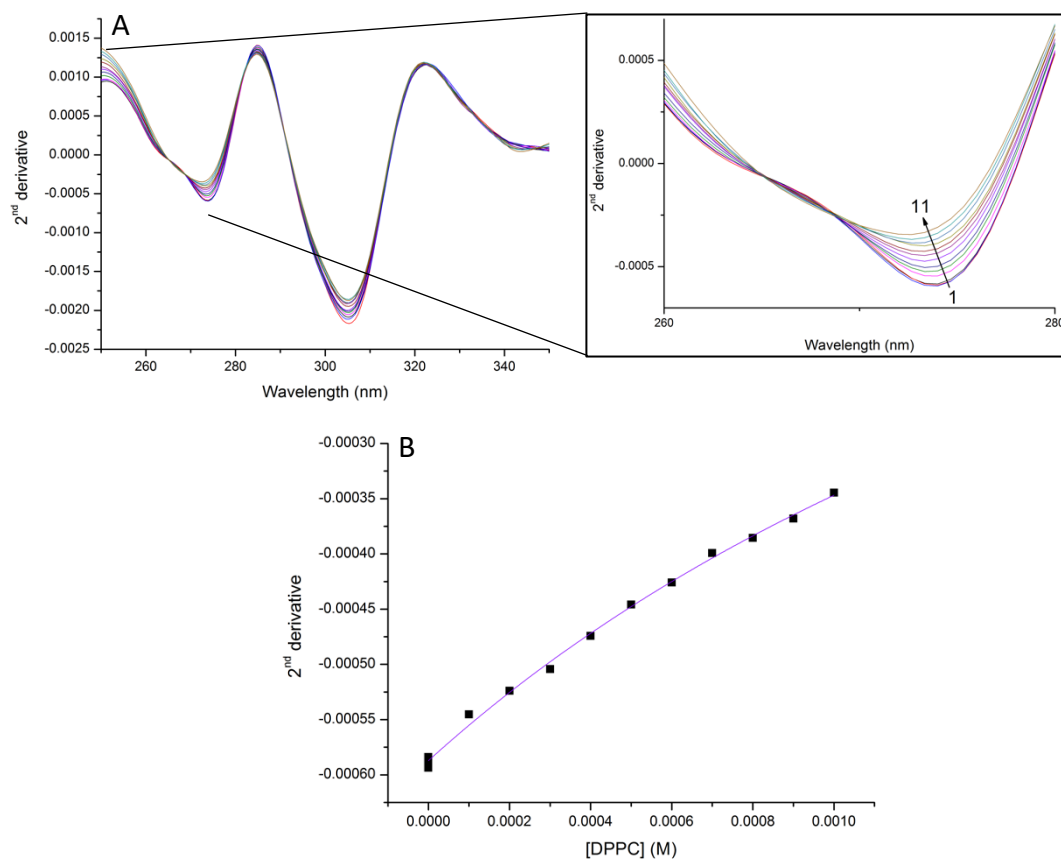
Figure A.1. Second derivative spectra (A) of OME (30 µM) at pH 7.4, incubated with LUVs of DPPC in the liquid-crystalline phase. The deviation of the spectra is visible by increasing the concentration of the lipid phase from 0 M (spectrum 1) to 0.001 M (spectrum 11). The K_p values in L.mol^{-1} are obtained by fitting the values of the derivative with Eq. (1) (B).

6. Insights into OME location using fluorescence quenching
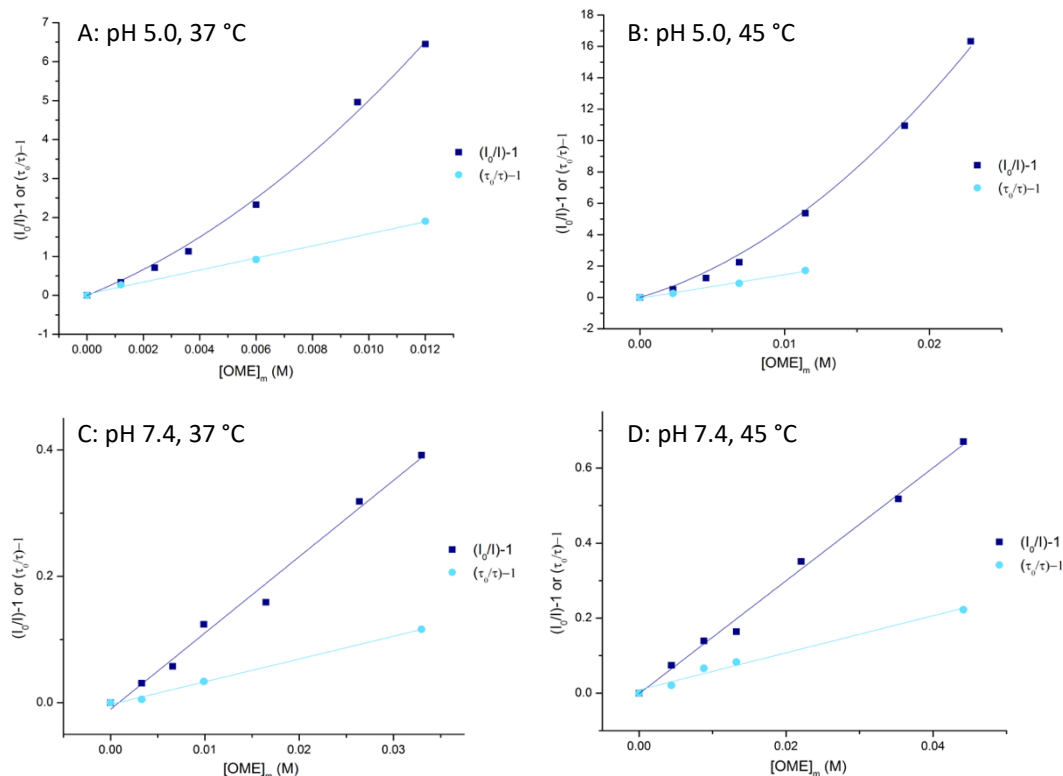
Figure A.2. Stern-Volmer plots of the probe DPH in unilamellar vesicles of DPPC by increasing the concentration of OME at pH 5.0 (A and B) and pH 7.4 (C and D). Both ripple phase (A and C) and liquid-crystalline phase (B and E) are shown. Dark blue represent Stern-Volmer plots obtained by steady-state fluorescence measurements (I_0/I) and light blue represent those from lifetime fluorescence measurements (τ_0/τ).

7. Lipid phase transition through fluorescence anisotropy
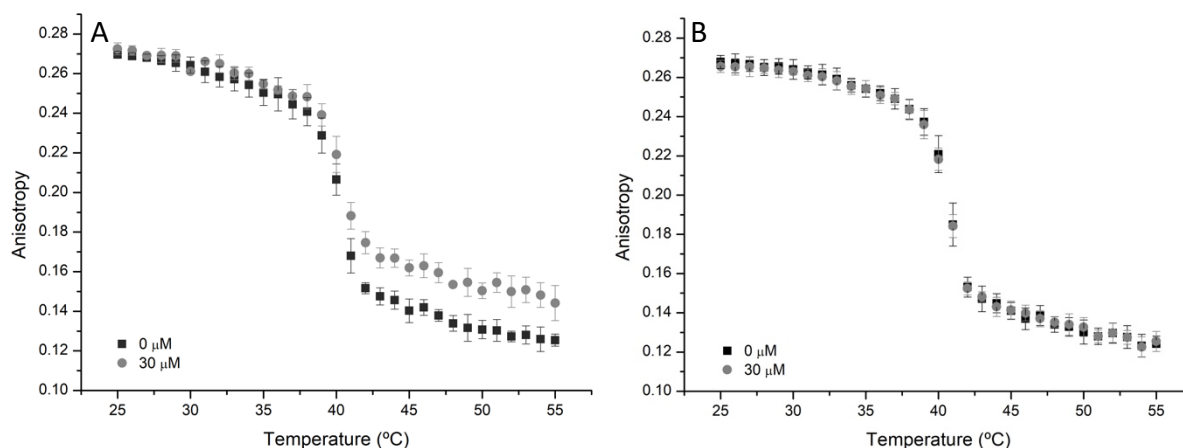
Figure A.3. Temperature dependence of the steady-state anisotropy of TMA-DPH-labelled unilamellar vesicles of DPPC in presence of different concentrations of OME (0 µM in black and 30 µM in light grey), at pH 5.0 (A) and pH 7.4 (B).

References

[1] J.R. Lakowicz, Principles of Fluorescence Spectroscopy, 3rd ed., Springer, Singapure, 2006.

[2] A. Grancelli, A. Morros, M.E. Cabañas, Ò. Domènech, S. Merino, J.L. Vázquez, M.T. Montero, M. Viñas, J. Hernández-Borrelli, Interaction of 6-Fluoroquinolones with Dipalmitoylphosphatidylcholine Monolayers and Liposomes, Langmuir 18 (2002) 9177-9182.

[3] M.J. Abraham, T. Murtola, R. Schulz, S. Páll, J.C. Smith, B. Hess, E. Lindahl, GROMACS: High performance molecular simulations through multi-level parallelism from laptops to supercomputers, SoftwareX 1-2 (2015) 19-25.

[4] J.B. Klauda, R.M. Venable, J.A. Freites, J.W. O'Connor, D.J. Tobias, C. Mondragon-Ramirez, I. Vorobyov, A.D. MacKerell, R.W. Pastor, Update of the CHARMM All-Atom Additive Force Field for Lipids: Validation on Six Lipid Types, J. Phys. Chem. B 114(23) (2010) 7830-7843.

[5] R.M. Venable, Y. Luo, K. Gawrisch, B. Roux, R.W. Pastor, Simulations of Anionic Lipid Membranes: Development of Interaction-Specific Ion Parameters and Validation using NMR Data, J. Phys. Chem. B 117(35) (2013) 10183-92.

[6] K. Vanommeslaeghe, E. Hatcher, C. Acharya, S. Kundu, S. Zhong, J. Shim, E. Darian, O. Guvench, P. Lopes, I. Vorobyov, A.D. Mackerell, Jr., CHARMM General Force Field: A Force Field for Drug-Like Molecules Compatible With the CHARMM All-atom Additive Biological Force Fields, J. Comput. Chem. 31(4) (2010) 671-90.

[7] L. Huang, B. Roux, Automated Force Field Parameterization for Non-Polarizable and Polarizable Atomic Models Based on Ab Initio Target Data, J. Chem. Theory Comput. 9(8) (2013).

[8] T. Darden, D. York, L. Pedersen, Particle mesh Ewald: An N·log(N) method for Ewald sums in large systems, J. Chem. Phys. 98(12) (1993) 10089.

[9] U. Essmann, L. Perera, M.L. Berkowitz, T. Darden, H. Lee, L.G. Pedersen, A smooth particle mesh Ewald method, J. Chem. Phys. 103(19) (1995) 8577-8593.

[10] G.J. Martyna, M.E. Tuckerman, D.J. Tobias, M.L. Klein, Explicit Reversible Integrators for Extended Systems Dynamics, Mol. Phys. 87(5) (1996) 1117-1157.

[11] M. Parrinello, Polymorphic Transitions in Single Crystals: A New Molecular Dynamics Method, J. Appl. Phys. 52(12) (1981) 7182.

[12] S. Nosé, M.L. Klein, Constant Pressure Molecular Dynamics for Molecular Systems, Mol. Phys. 50(5) (2006) 1055-1076.

[13] G.M. Torrie, J.P. Valleau, Nonphysical Sampling Distributions in Monte Carlo Free-Energy Estimation: Umbrella Sampling, J. Comput. Phys. 23 (1977) 187-199.

[14] S. Kumar, D. Bouzida, R.H. Swendsen, P.A. Kollman, J.M. Rosenberg, The Weighted Histogram Analysis Method for Free-Energy Calculations on Biomolecules. I. The Method, J. Comput. Chem. 13(8) (1992) 1011-1021.

[15] J.S. Hub, B.L.d. Groot, D.v.d. Spoel, g_wham - A Free Weighted Histogram Analysis Implementation Including Robust Error and Autocorrelation Estimates, J. Chem. Theory Comput. 6(12) (2010) 3713-3720.

Chapter 6.2

Molecular mechanisms behind the new additional mechanism of action of immediate-release omeprazole

The previous work (Chapter 6.1) led us to a whole new additional mechanism of action of omeprazole when absorbed through the gastric mucosa. Nevertheless, the molecular mechanisms of the reinforcement of the membrane were not completely understood. Hence, this work was designed to use biophysical techniques that enable the study at a molecular level.
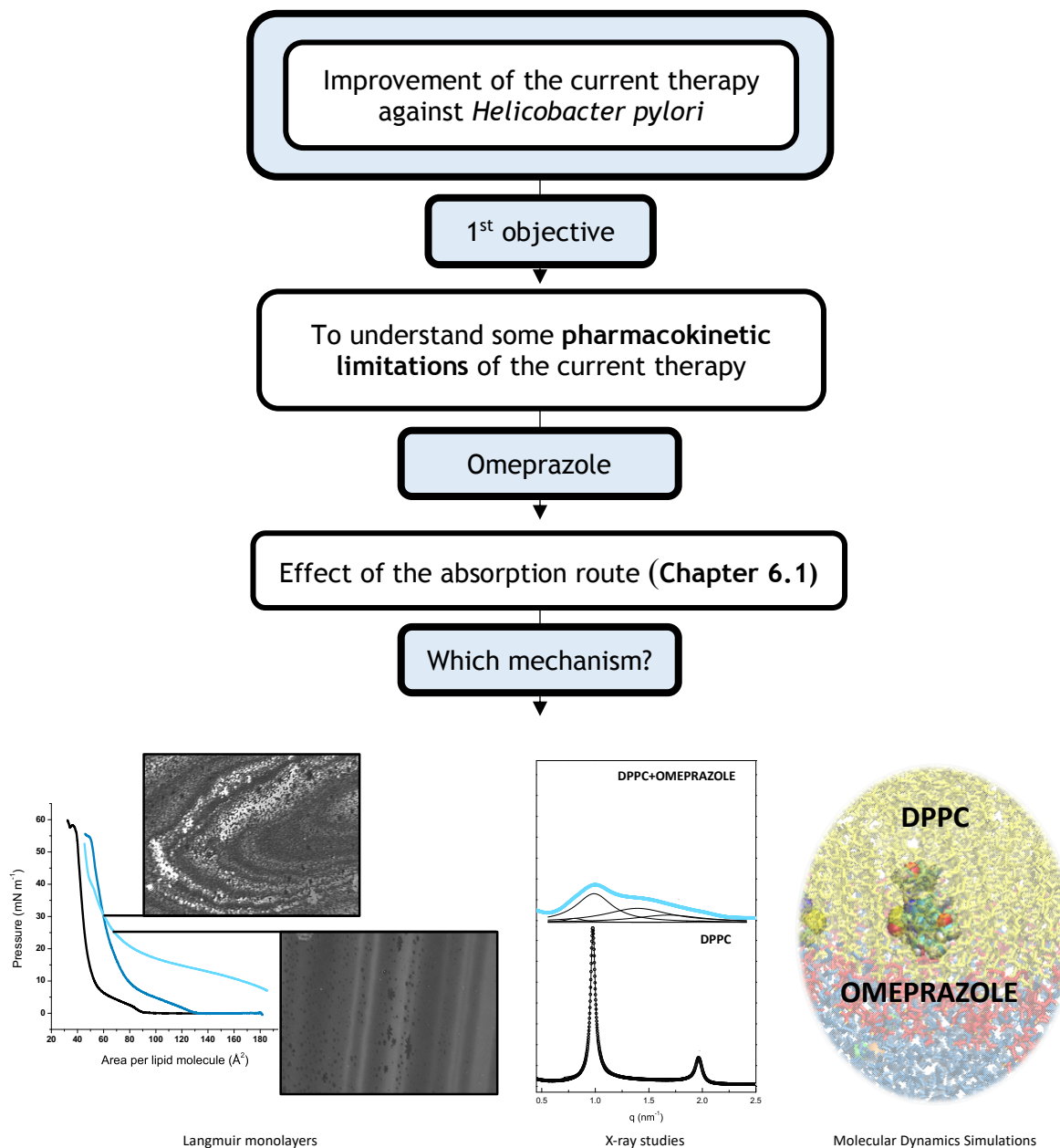
Langmuir monolayers   X-ray studies   Molecular Dynamics Simulations

Chapter 6.2

Molecular mechanisms behind the new additional mechanism of action of immediate-release omeprazole

Daniela Lopes-de-Campos[1], Cláudia Nunes[1*], Philippe Fontaine[2], Bruno Sarmento[3,4,5], Sven Jakobtorweihen[6*], and Salette Reis[1*]

[1]LAQV, REQUIMTE, Departamento de Ciências Químicas, Faculdade de Farmácia, Universidade do Porto, Portugal

[2]Synchrotron SOLEIL, L'Orme des Merisiers, Saint Aubin, BP48, 91192 Gif-sur-Yvette, France

[3]INEB - Instituto de Engenharia Biomédica, Universidade do Porto, Rua Alfredo Allen 208, 4200-393 Porto, Portugal

[4]i3S - Instituto de Investigação e Inovação em Saúde, Universidade do Porto, Rua Alfredo Allen 208, 4200-393 Porto, Portugal

[5]IINFACTS, Instituto de Investigação e Formação Avançada em Ciências e Tecnologias da Saúde, Instituto Universitário de Ciências da Saúde, Gandra, Portugal

[6]Institute of Thermal Separation Processes, Hamburg University of Technology, Germany

Immediate-release omeprazole is a strategy that enables the absorption of omeprazole (OME) through the gastric mucosa. This strategy showed a high efficiency in increasing the intragastric pH and reducing the bleeding. Furthermore, several *in vivo* studies showed a cytoprotective mechanism of the gastric mucosa promoted by orally administered omeprazole that was not related to the inhibition of the proton-pump. Previously we showed that omeprazole increased the order of dipalmitoylphosphatidylcholine (DPPC) membranes at pH 5. Motivated by this finding, the mechanisms behind the interaction of OME with DPPC membranes at pH 5 is unveiled in this study. Therefore, several experimental and computational techniques were combined. Langmuir monolayers coupled with Brewster angle microscopy, grazing incident X-ray diffraction, and Infrared reflection-absorption spectroscopy measurements, and 3-D models for X-ray scattering studies, including small and wide-angle, and molecular dynamics simulations were applied.

The results showed that omeprazole intercalates among DPPC molecules and promotes the formation of domains with highly condensed and untilted phospholipids. Electrostatic and hydrophobic interactions between the drug and the DPPC enables an intercalation that rearranges the conformational state of DPPC. Ultimately, these results show that the local release of OME enables its action as a phospholipid-like drug that can improve the protection of the gastric mucosa. Thus, a new mechanism of action of immediate-release omeprazole is proposed, which can be used if a local absorption is preferred over a systemic distribution.

Keywords: immediate-release omeprazole, X-ray studies, monolayers, molecular dynamics simulations.

1. Introduction

Immediate-release omeprazole (IR-OME) is a new FDA-approved strategy to induce an earlier effect on the inhibition of the proton-pump [1]. This effect results from a rapid absorption of the "naked" drug when comparing to the conventional delayed release of OME from enteric-coated capsules [1, 2]. Once IR-OME contains sodium bicarbonate, OME is protected from the acidic degradation [1, 2]. Previous studies have shown a high efficacy of IR-OME in increasing the intragastric pH and reducing the risk of upper gastrointestinal bleeding [3-6]. Furthermore, a cytoprotective mechanism of orally administered OME that is not involved with the inhibition of the proton-pump was already reported in rats [7-9].

The release of OME at the stomach lumen leads to a local absorption and, consequently, to biophysical interactions with the gastric mucosa. In our previous study, we assessed the effect of the pH on the topic interaction of OME with dipalmitoylphosphatidylcholine (DPPC) membranes (**Chapter 6.1**). DPPC was used due to the existence of phosphatidylcholines in both the mucus layer and the gastric epithelial cells [10, 11]. Furthermore, DPPC enables the study in different lipid phases for being a saturated phospholipid. The results of our previous study showed that OME was able to decrease the cooperativity and to increase the main phase transition temperature and the order parameter of DPPC at pH 5 (**Chapter 6.1**). On the other hand, when OME reaches the gastric mucosa from the blood stream (pH 7.4), the biophysical parameters of DPPC remained unaltered (**Chapter 6.1**). Therefore, we hypothesized that the protonated state of OME that exists at pH 5 may be intercalated among phospholipids due to its amphiphilic properties. This intercalation may organize the DPPC membrane and, consequently, may reinforce the gastric mucosa. Nevertheless, the molecular mechanisms behind this effect were still unknown. Therefore, in this work we used different experimental techniques (Langmuir isotherms, Brewster Angle Microscopy, Infrared reflection-absorption spectroscopy measurements, and X-ray diffraction studies, including small-angle, wide-angle, and grazing incident X-ray diffraction) to further study the mechanism at a molecular level. IR-OME keep the median 24-h gastric pH around 4.7, varying from 3.2 to 5.8 [3]. Therefore, all the experimental studies were performed at pH 5. Furthermore, molecular dynamics (MD) simulations were used to obtain an atomistic picture of the mechanism of each protonation state, that is the neutral (OME^0) and the protonated (OME^+) state (Figure 1).

OME⁰ (63 %) **OME⁺ (37 %)**
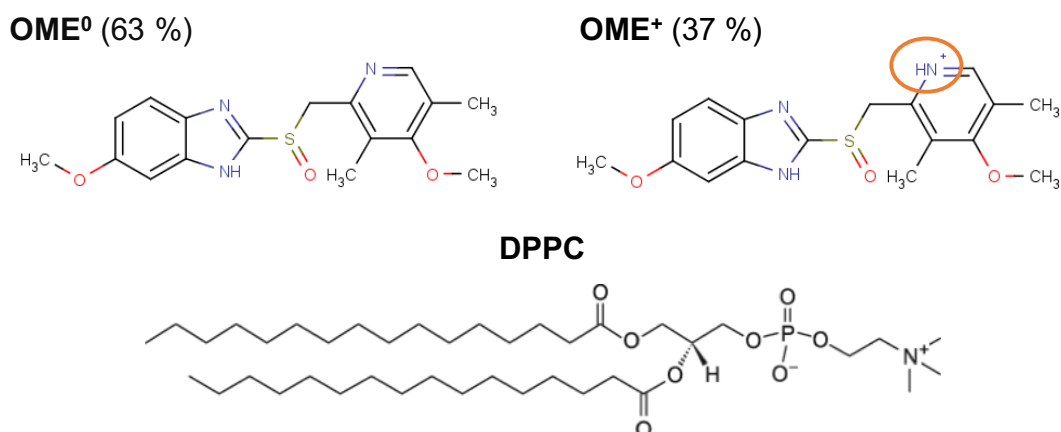
DPPC

Figure 1. Neutral (OME⁰) and charged (OME⁺) state of OME with their relative percentage, and molecular structure of DPPC at pH 5 (computational prediction by the pK_a plugin of ChemAxon®).

2. Materials and methods

2.1 Experimental methods

2.1.1 Materials

OME was purchased from Sigma-Aldrich, and 1,2-dipalmitoyl-*sn*-glycero-3-phosphocholine was obtained from Avanti® Polar Lipids, Inc. All drug solutions were prepared at pH 5, using acetate buffer (I=0.13M) and double-deionized water (conductivity inferior to 0.1 $\mu S.cm^{-1}$).

2.1.2 Langmuir isotherms

A buffered solution of 5 μM or 30 μM of OME at pH 5 was prepared using 1.25 % of ethanol to help the solubilisation process. A DPPC solution in chloroform (1 $mg.ml^{-1}$) was spread onto 420 mL of a buffered subphase. Acetate buffer was used as control. After spreading the lipid, the monolayer was equilibrated until full stabilization of the pressure or for at least 10 min to enable the evaporation of chloroform. Surface pressure-area isotherms were obtained using two symmetric barriers in a KSV NIMA Langmuir trough. The rate of compression was 5 Å/molecule/min. A Wilhelmy microbalance with a filter paper plate (accuracy > 0.1 $mN.m^{-1}$) was used to measure the surface tension. All assays were performed at 20 $\pm$ 1 °C.

The elastic modulus (C_s^{-1}) was calculated using the following equation [12]:

$$C_s^{-1} = -A\left(\frac{d\pi}{dA}\right) \tag{1}$$

2.1.3 Brewster Angle Microscopy

Microscopic images of the lipid domains were obtained using a KSV NIMA Brewster Angle Microscope (BAM) with a lateral resolution of 2 μm. The microscope is coupled with a Langmuir trough. Hence, it is possible to obtain a real-time visualization of the compression of a phospholipid monolayer. DPPC monolayers were prepared as described in the 2.1.2 section, using an OME concentration of 30 μM. All assays were performed at 20 ± 1 °C.

2.1.4 Infrared reflection-absorption spectroscopy measurements

Infrared measurements were performed using a KSV NIMA Polarization Modulation Infrared Reflection Absorption Spectrophotometer. This technique enables the elimination of the background signal that is promoted by environmental molecules, such as water and CO_2 [13]. The angle of incidence was set to 80 ° to the surface normal, and the height was optimized in each assay to get an interferogram higher than 6.5. OME concentration was set to 37.5 μM to keep the same lipid:drug ratio used in the previous sections in a trough of 45 ml. The background was subtracted by measuring the subphase before the spreading of DPPC. 10 scans per second were obtained for each spectrum during 300 s. The spectra resolution was 8 cm^{-1}. All measurements were done at 20 ± 1 °C.

2.1.5 Small-angle and wide-angle X-ray diffraction studies

OME was added to a DPPC solution in chloroform/methanol (3:2 v/v) in a molar ratio of 0.06 (drug:lipid). Lipid films were formed by drying the sample at 50 °C, under a stream of N_2. All samples were left under reduced pressure overnight to ensure the evaporation of the organic solvents. The samples were then transferred into X-ray transparent glass capillaries with 1 mm diameter (Hilgenberg GmbH, Germany), which were sealed and stored for 1 weak at 4 °C. The non-crystalline diffraction (NCD) beamline of ALBA synchrotron (Cerdanyola del Vallès, Barcelona, Spain) was used to perform the

measurements. SAXS and WAXS detectors were calibrated using silver behenate and chromium trioxide, respectively. At each temperature (20 and 37 °C), SAXS and WAXS diffraction patterns were acquired with 5 s and 1 s of exposure, respectively.

Lorentzian fittings of the diffraction patterns were used to obtain the q-values and the full-width at half-maximum (w). Both long- and short-range distances (d) were calculated considering the q-values of the peak maximum (d=2π/q), and the correlation length (ξ) was calculated considering the w (ξ=4π^2/w).

2.1.6 Grazing incident X-ray diffraction studies

Grazing incident X-ray diffraction studies (GIXD) were used to assess changes in the structural arrangements of DPPC in presence of OME. For that, monolayers of DPPC were prepared similarly to what was described in the section 2.1.2, using 30 μM of OME. The volume of the trough was 400 mL, and it was enclosed in a sealed chamber to keep the temperature at 20 $\pm$ 1 °C. Helium was flushed into the chamber to reduce gas scattering and to avoid the damage of the monolayer by the beam. The monolayer was compressed to reach a surface pressure of 30 mN.m^{-1}. The measurements were performed on the SIRIUS beamline at the SOLEIL synchrotron, using an incident X-ray beam of 10.5 keV (λ = 0.118 nm) and a beam size of 0.1 x 2 mm^2 (V x H). The details and the optics of the facility are described elsewhere [14]. The incident angle was set to 1.70 mrad, which is below the critical angle of the air-water interface (2.04 mrad at 10.5 keV). The evanescent wave that travelled along the interface allowed the study of a layer of 5 nm beneath the interface. The wave vector resolution is 0.03 nm^{-1}. A 1D gas detector fixed on the 2-axis detector arm of the beamline's diffractometer was used, which enable the measurement of the scattered intensity with very low noise. To collimate the scattered beam, the Soller slit system is used in front of the detector.

The mathematical analysis is described elsewhere [15]. Briefly, the scattering intensity can be divided in an in-plane component (Q_{xy}) and an out-of-plane component (Q_z) [16, 17]. The distance among lattice planes was calculated using the first component (d=2π/Q_{xy}) [17]. The correlation length (ξ) was calculated by considering the full-width at half-maximum (w) of the Bragg peaks (ξ=2/w) [18]. Lattice parameters (a and b) were calculated using Eq. (2) and (3), respectively.

$$a = \frac{4\pi}{\sqrt{2Q_{xy\,1\bar{1}}^2 + 2Q_{xy\,11}^2 - Q_{xy\,02}^2}} \tag{2}$$

$$b = \frac{4\pi}{Q_{xy\,02}^{2}} \tag{3}$$

The tilt angle (t) was calculated considering the out-of-plane component and the azimuth angle (ψ) (Eq. (4)).

$$Q_z = Q_{xy} \cos(\psi) \tan(t) \tag{4}$$

2.2 Computational methods

2.2.1 Prediction of the protonation state of OME

The protonation state of OME was predicted by the pK_a plugin of ChemAxon®, MarvinSketch application, version 15.4.13.0.

2.2.2 Molecular dynamics simulations

All MD simulations were carried out with GROMACS version 2016.1 [19]. The CHARMM36 force field was used as interaction model for the lipids [20] and ions [21] and the CHARMM TIP3P model for water. The CHARMM general force field [22] contains parameters for drug molecules. Unfortunately, for OME some parameters are missing. Therefore, we used the general automated atomic model parameterization [23] to calculate charges and bonded parameters for neutral and charged OME. The simulation details were the same as in our earlier publication (**Chapter 6.1**). In total four constant pressure (1 bar), constant temperature (20 °C) MD simulations were analysed. All simulations contained 128 DPPC lipids, a water to lipid ratio of ca. 55, 13 chlorine ions and 13 sodium ions. If OME^+ molecules were present the number of sodium ions was reduced to keep the system neutral. The four systems differ in the amount of OME: (i) no OME molecules, (ii) eight OME^0 molecules, (iii) eight OME^+ molecules, and (iv) five OME^0 plus three OME^+ molecules. All simulations were carried out for 250 ns, where the first 100 ns ((ii) and (iv)) or the first 150 ns ((i) and (iii)) were not analysed. These equilibration times were determined mainly according to the equilibration of the area per lipid. The initial systems were based on equilibrated membrane systems and the corresponding numbers of OME molecules were placed into the water phase, then the interactions with the rest of the system were slowly switched on with short alchemical simulations. Thereafter, the systems containing OME molecules were run for 1 μs at a temperature of

50 °C to let the OME molecules distribute across the membrane. The system without OME molecules were run for 250 ns at 50 °C. The end snapshots of these systems were used as start for the simulations at 20 °C.

3. Results

3.1 Langmuir isotherms

Langmuir monolayers are good models to study membrane biophysics due to the similarity between the lipid packing of a monolayer at a lateral pressure of 30 mN.m^{-1} with the outer layer of a cell membrane [24, 25]. The physical behaviours of monolayers and bilayers are in fact similar at this pressure [26]. Furthermore, lipid monolayers are stable bidimensional systems that can pass through different order transitions (gaseous, liquid expanded, tilted condensed, and untilted condensed) just by increasing the lateral pressure [25]. If a compound affects the packing of phospholipids, the outline of the surface pressure-molecular area (π/A) isotherm will change. The effect of omeprazole (OME) at pH 5 is shown in Figure 2 (A). The isotherm of plain DPPC is in agreement with the one reported by our research group [15]. OME can expand the monolayer of DPPC to higher areas per lipid. The minimal area per lipid was calculated through the intersection of the x axis with a straight line obtained by fitting the condensed phase in a range of pressures that included 30 mN.m^{-1} [15]. The area per lipid increased from 50.1 $\pm$ 0.7 Å^2 to 99 $\pm$ 4 Å^2 in presence of 30 μM of OME. The expansion of the area per lipid is in fact visualized through all the different lipid phases, starting in the correspondent gaseous phase of DPPC alone, for the highest concentration of OME. The transition from liquid-expanded to liquid condensed in a DPPC isotherms is reflected in a plateau where both phases coexist [25]. For plain DPPC, that transition occurred from approximately 3 to 6.5 mN.m^{-1}, which is in agreement with the literature [27]. In presence of 5 μM of OME, the transition seems to be expanded to a larger interval of pressure (1.5 to 8 mN.m^{-1}). This is coherent with our previous results, which showed that OME decreased the cooperativity of phase transition in a DPPC vesicle (**Chapter 6.1**). The formation of domains with different packings was indeed suggested in our previous work (**Chapter 6.1**). The C_s^{-1} enables to monitor two-dimension phase transitions [28]. Figure 2 shows the effect of OME on the C_s^{-1}, with the existence of an additional peak. A drop in C_s^{-1} values reflect a discontinuity in the lateral packing and, therefore, a phase transition [28]. Thus, these results are coherent with the hypothesis of domains formation.
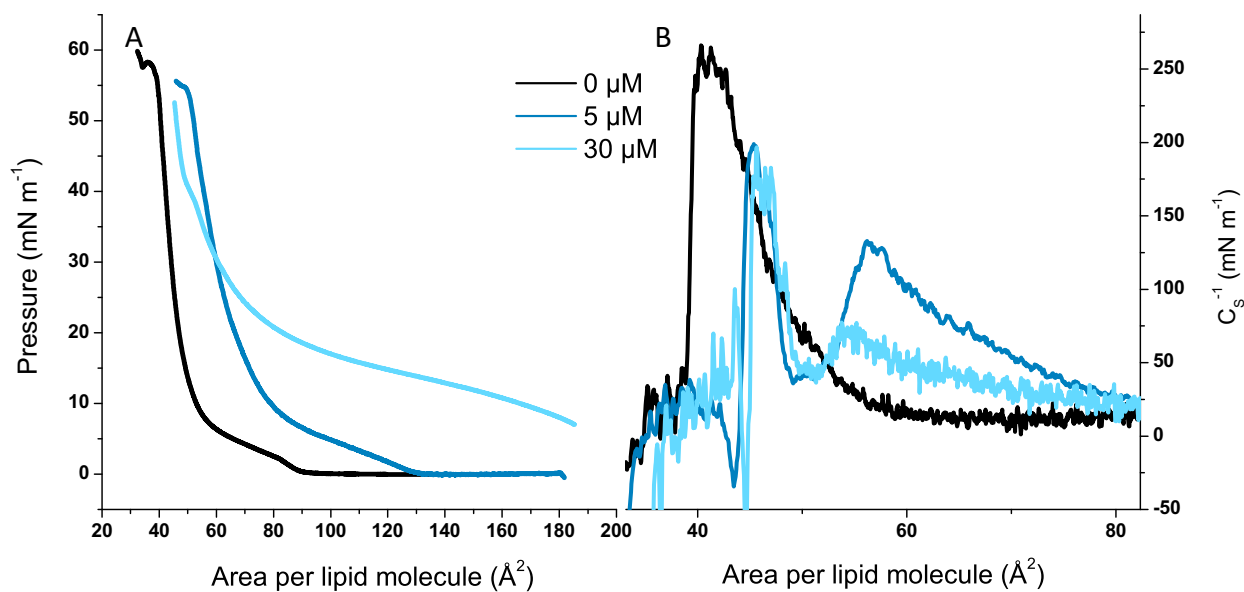
Figure 2. Surface pressure-area (π/A) isotherms (A) of DPPC spread onto increasing concentrations of OME (0 (black), 5 (dark blue), and 30 μM (light blue)). Respective C_s^{-1} of the isotherms (B).

3.2 Brewster Angle Microscopy

The results obtained from the Langmuir isotherms point towards the possibility of the coexistence of phases with different lipid packings in presence of OME. Therefore, Brewster angle microscopy was used once it enables the study of the shape and the texture of phospholipid domains [29]. This technique is based on the ability of a condensed domain to reflect more the incident laser beam [29]. The results are shown in Figure 3. The DPPC alone presented spherical domains, which had been already reported by our research group [15]. The effect of OME is evident. At 20 mN.m^{-1}, DPPC is not organized in spherical domains. Instead, OME promotes a different organization of the lipid phase, with linear packed regions. At higher pressures, those regions become highly condensed, which is visualized by their high refractive index. The existence of more disordered domains (darker regions) within the highly packed regions is noteworthy. In our previous work (**Chapter 6.1**), we suggested that OME was able to intercalate DPPC molecules and, consequently, to promote the packing of the surrounded phospholipids. These results are in good agreement, showing small fluid regions surrounded by condensed domains. Both the expansion of the monolayer (Figure 2, A) and the formation of domains (Figure 2, B, and Figure 3) can be a consequence of a fluidizing effect that commonly result from electrostatic interactions with the polar heads of phospholipids [30] or due to the saturation/intercalation within the membrane that result from hydrophobic

interactions [31]. PM-IRRAS was then used to have more insight of which type of interactions are occurring.
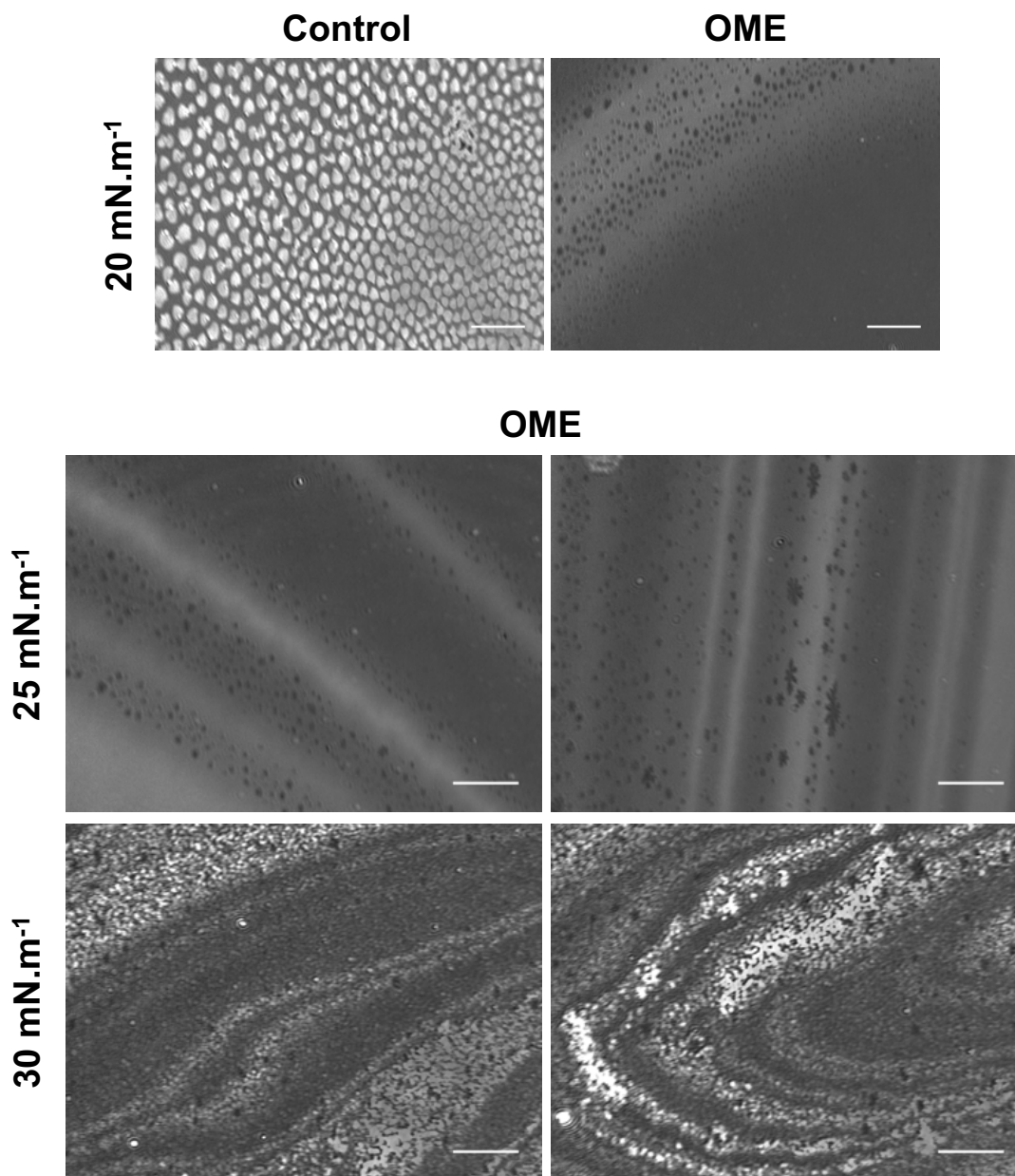
Figure 3. Brewster angle microscopic images of Langmuir monolayers of DPPC at pH 5 and at different surface pressures (20 mN.m^{-1} (top), 25 mN.m^{-1} (middle), and 30 mN.m^{-1} (bottom)). At 20 mN.m^{-1}, the control shows plain DPPC. All the other images correspond to DPPC monolayers spread onto 30 μM of OME. The scale is visualized by a straight white line of 100 μm.

3.3 Infrared reflection-absorption spectroscopy measurements

PM-IRRAS was used to unveil the effect of OME on the frequency of the molecular vibrations of phospholipids [32]. DPPC (Figure 1) has different constituent groups. Their vibration modes depend on the packing and on the hydration of the monolayer. Groups that belong to the polar head of DPPC (e. g. phosphate (PO_2^-) and carbonyl (C=O)) are located closer to the membrane surface. The establishment of new bonds, such as H-bonds, and the increase of the hydration of those groups changes their vibrational modes to lower wavenumbers [32]. Methylene groups (CH_2) belong to the hydrocarbon chains of phospholipids. Consequently, changes of their vibrational wavenumbers reflect changes in the conformational order of the monolayer [32]. Figure 4 shows the results of the PM-IRRAS measurements (detailed wavenumbers in Table A.1 of the supporting information).
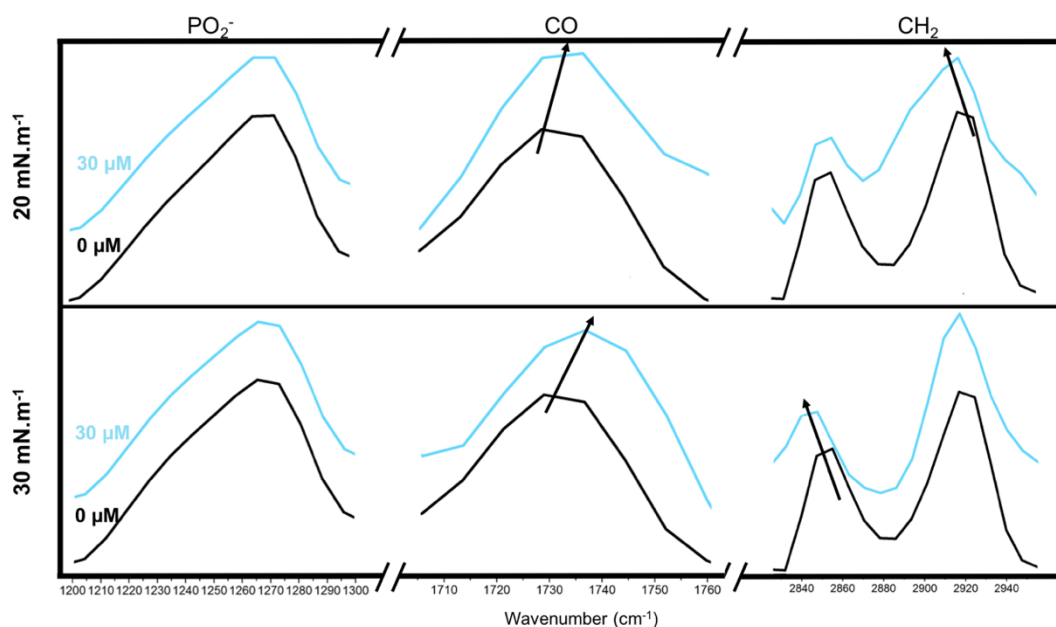
Figure 4. PM-IRRAS spectra of DPPC in presence of OME (0 (black) and 30 μM (light blue)) at different pressures (20 and 30 mN.m^{-1}). The frequency of the molecular vibration of the main groups of DPPC are shown, namely, the phosphate (left), the carbonyl (middle), and the methylene (right) groups.

The results show that OME increases the wavenumber of vibration of the carbonyl group from 1730 to 1737 cm^{-1}, which indicates a lower hydration of the group. Simultaneously, OME causes a blue shift of vibration of the methylene asymmetric stretch. The variation from 2920 to 2014 cm^{-1} at 20 mN.m^{-1} and to 2018 cm^{-1} at 30 mN.m^{-1} reflect a higher packing of the hydrophobic chains of DPPC. These results are coherent with the hypothesis of OME causing the packing of the surrounded phospholipids. Its effect on the organization of DPPC molecules were further studies using X-ray diffraction studies.

3.4 Small-angle and wide-angle X-ray diffraction studies

X-ray diffraction studies have successfully been applied to study disordered materials, such as biomimetic membranes, once they provide dynamic and structural insights [33]. Both SAXS and WAXS were used, and results are shown in Figure 5 and Table 1. The essays were performed at 20 °C and 37 °C since our previous results (**Chapter 6.1**) showed that the organizing effect was not significant in the liquid-crystalline phase.
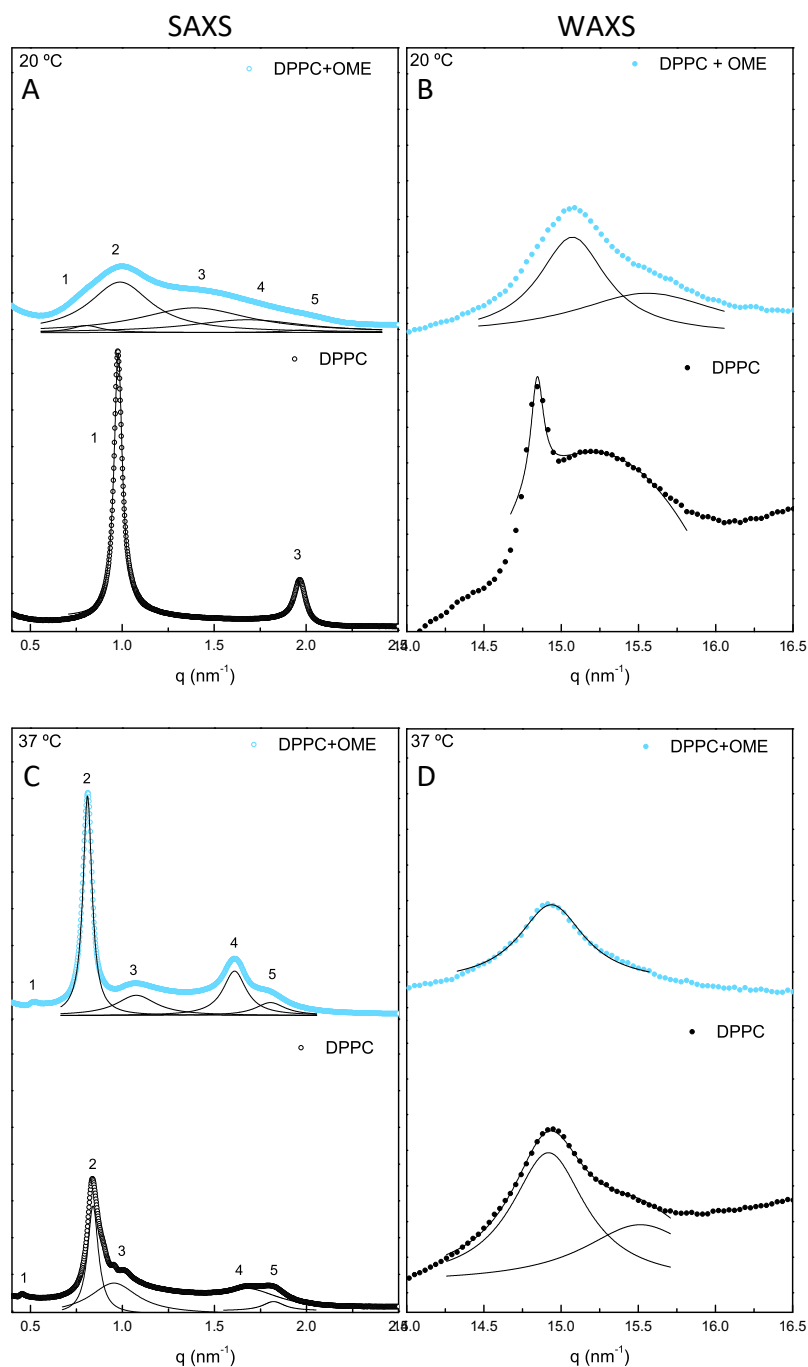
Figure 5. SAXS (left) and WAXS (right) patterns of DPPC in absence (DPPC) and in presence of OME (DPPC+OME) in a molar ratio of 0.06, at 20 °C (top) and at 37 °C (bottom).

At 20 °C, DPPC is in the gel phase ($L_{\beta'}$), which is characterized by a lamellar phase (Figure 5, A). The long-range distance (SAXS)) is 64.3 Å, which is coherent with the described in the literature [34]. Nevertheless, in presence of OME, DPPC is organized in two lipid phases (Figure 5, A). The lamellar phase that exists in plain DPPC seems to stay almost unaltered, with similar long-range distances. Although with similar long-range distances, the existence of broad peaks indicates a less cooperative process. This is visualized by the significantly lower correlation length, which can indicate the existence of different phases within the membrane. This lamellar phase is important to preserve a cell structure and compartmentalization [35]. OME promotes the formation of a second phase in a hexagonal structure (diffraction spacing in the order $1:1/1:\sqrt{3}/1:2$). The critical micellar concentration of OME is described to be 3×10^{-6} M [36]. Therefore, considering the packing of the DPPC molecules in the gel phase, OME may prefer to be organized in inverted micellar structures inside the bilayer. WAXS patterns (Figure 5, B) show two Bragg peaks that result from a pseudo-hexagonal lattice of DPPC chains. OME decreases both the distances among phospholipids and the correlation length. These results indicate the existence of a more packed/ordered membrane.

At 37 °C, DPPC is organized in a stable ripple phase (Figure 5, C). The SAXS pattern is coherent with the reported in the literature [37]. One of the phases has larger long-range distances than at 20 °C. At this temperature, DPPC is in a ripple phase, which is characterized by an undulation of the membrane due to the co-existence of domains in the gel and in the liquid-crystalline phase [38]. d_2 is in fact similar to the distance reported for the liquid-crystalline phase of DPPC (74.6 Å [34]). In presence of OME, DPPC remains in the stable ripple phase. The existence of higher correlation lengths for some distances show that there are some phases with a higher packing. WAXS patterns (Figure 5, D) show a transition from a pseudo-hexagonal to a hexagonal packing of the hydrophobic chains in presence of OME. The higher packing of DPPC molecules is visualized through the smaller distance and the higher correlation length.

OME can promote the formation of phases with higher long-range distances at both temperatures. This reflects an increase of the bilayer thickness, which can result from a larger solvation region and/or from the bending of the membrane. Additionally, it can result from an intercalation among lipid chains that leads to higher order parameters and lower tilt angles of the hydrophobic chains [39]. Considering the previous results, all hypothesis must be considered. OME can increase the order and the packing of phospholipids (**Chapter 6.1**). PM-IRRAS results showed a lower hydration of the carbonyl group. This dehydration can result from the expulsion of the water molecules due to membrane packing, which can increase the solvation region. The bending of the membrane was also

visualized by BAM and by the formation of a hexagonal phase at 20 °C. The distance obtained for DPPC+OME (77.9 Å) at 20 °C is in fact similar to the second order peak of plain DPPC at 37 °C (74.7 Å), which can indicate the existence of undulated regions. At both temperatures, the packing of DPPC was visualized. Grazing incident X-ray diffraction was then used to evaluate the effect of OME on the tilt of DPPC.

Table 1. Long-range and short-range distances (d) determined from SAXS and WAXS patterns, respectively, in absence (DPPC) and in presence (+OME) of the drug. The corresponding correlation lengths (ξ), for the first order peaks, are also shown. The essays were performed at pH 5.0 and at 20 °C and 37 °C.

		1st order peaks				2nd and 3rd order peaks		
		d_1 (Å)	ξ_1 (Å^{-1})	d_2 (Å)	ξ_2 (Å^{-1})	d_3 (Å)	d_4 (Å)	d_5 (Å)
			T (°C)					
SAXS	DPPC	64.26 ± 0.02	7604 ± 90	-		31.98 ± 0.02	-	-
	+OME	77.9 ± 0.3	2005 ± 95	63.5 ± 0.2	962 ± 16	45.0 ± 0.4	37.5 ± 0.5	31.6 ± 0.2
	DPPC	137.4 ± 0.3	14144 ± 1500	74.66 ± 0.03	5525 ± 167	62.6 ± 0.6	37.69 ± 0.08	34.50 ± 0.05
	+OME	119.5 ± 0.2	6764 ± 78	77.54 ± 0.01	6711 ± 337	58.4 ± 0.3	39.05 ± 0.03	34.83 ± 0.05
WAXS	DPPC	4.2333 ± 0.002	2687 ± 453	4.101 ± 0.008	343 ± 381			
	+OME	4.169 ± 0.003	738 ± 58	4.04 ± 0.02	345 ± 33			
	DPPC	4.212 ± 0.002	674 ± 35	4.050 ± 0.007	440 ± 80			
	+OME	4.206 ± 0.002	758 ± 42	-				

(Note: T = 20 for the first DPPC/+OME pair in each block, T = 37 for the second pair.)

3.5 Grazing incident X-ray diffraction studies

In GIXD measurements, almost all the incident beam is reflected and only an evanescent wave travels along the interface [16, 17]. Therefore, it is a very useful technique to study structural arrangements, tilt variations and conformational changes of phospholipids within a monolayer [16, 17]. At pH 5, DPPC has two Bragg peaks (Figure 6), which reflects a rectangular lattice structure with tilted chains. The results of this control were already reported by our research group [15], and they are in agreement with previous results [40]. For this type of structure, the first order peaks indexations are set to $1\bar{1}$ (out-of-plane) and 02 (in-plane). The results are shown in Table 2.
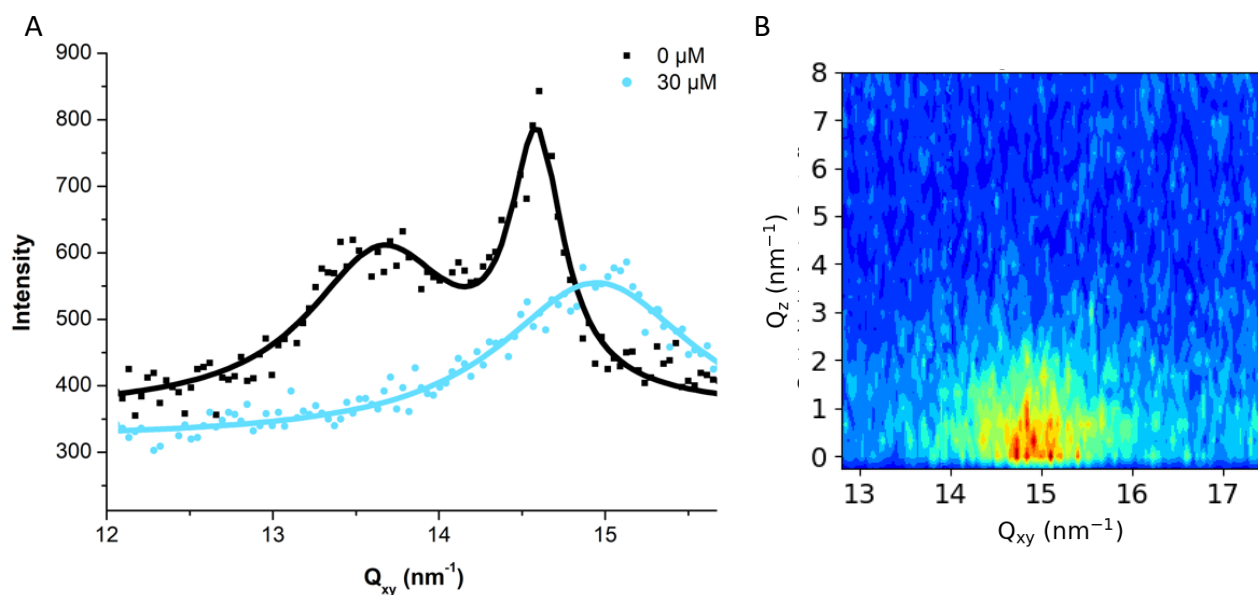
Figure 6. Q_z Integrated scattered intensity vs. Q_{xy} (A), obtained at pH 5 and at 30 mN.m^{-1} in presence of different concentrations of OME (0 (black) and 30 µM (light blue)). The Q_{xy}-Q_z intensity map (B) corresponds to DPPC spread onto a buffered OME solution.

When DPPC was spread onto an OME subphase, one Bragg peak at higher Q_{xy} value was measured. This reflects a hexagonal organization, with a very low correlation length (3 nm) in comparison to plain DPPC in the 02 direction (29 nm). Lower correlation lengths indicate a more laterally disorganized membrane. The absence of an out-of-plane peak (Figure 6, B) indicates that the acyl chains are no longer tilted. Hence, the lateral disorganization may be due to the existence of more condensed and untilted domains. In fact, the distance between the phospholipids of those domains was smaller than the ones observed for plain DPPC (Table 2). Furthermore, the area per unit cell of plain DPPC is 0.48 nm^2 whereas in presence of OME it is 0.24 nm^2. Hence, these results show that the macroscopic area per lipid molecule significantly decreased, which is coherent with the existence of highly packed domains as visualized by BAM. Considering the higher long-range distance that was measured by the SAXS experiments, the existence of untilted phospholipids was hypothesized. These GIXD results show not only that OME causes the packing of untilted DPPC molecules, but also the existence of different domains. Furthermore, DPPC acquires a hexagonal organization, which is coherent with the results from WAXS. To have more insight of what is happening at a molecular level, MD simulations were carried out.

Table 2. Peaks positions (Q), distance (d), correlation length (ξ), deduced lattice parameters (a, b), and tilt angle (t) in absence and in presence of 30 μM of OME, at pH 5 and at 30 mN.m⁻¹.

	$Q_{1\bar{1}}$ (nm⁻¹) ±0.04	$d_{1\bar{1}}$ (Å) ±0.03	Q_{02} (nm⁻¹) ±0.03	d_{02} (Å) ±0.03	ξ_{11} (nm)	ξ_{02} (nm)	a (nm)	b (nm)	tilt (deg.)
DPPC (Chapter 6.4)	13.31	4.72	14.57	4.31	2.8	28.6	0.56	0.86	23
			Q_{10} (nm⁻¹) ±0.03	d_{10} (Å) ±0.03		ξ_{10} (nm)	a (nm)	b (nm)	tilt (deg.)
DPPC+OME			14.92	4.21		3.0	0.49	0.49	-

3.6 MD Simulations

MD simulations is a powerful tool to obtain insights beyond the experimental techniques. The main advantage of this complement is the possibility of studying OME-DPPC interactions on the atomistic-scale [41]. The effect of concentration is important to this type of studies once any perturbation of the lipid membrane would be difficult to obtain using only one drug molecule to 128 lipid molecules [42]. The OME concentration is important as the drug to lipid ratio will influence the extent of the membrane perturbation. Therefore, 8 molecules of OME were used in the MD simulations that contained 128 lipids to maintain the ratio of 30 μM of OME to 500 μM of DPPC that was used to study the effect on the order through the fluorescence studies (**Chapter 6.1**). At pH 5, OME is in different protonation states (Figure 1). To understand the effect of each one independently, both the protonated (OME⁺) and the neutral (OME⁰) state were modelled. Moreover, the effect at pH 5 was simulated considering the percentage of each state. The results of the order parameter of DPPC are shown in Figure 7.

OME causes an increase on the order parameter of DPPC throughout the membrane, with exception of the first carbons. In general, both protonation states promoted a higher order of the membrane. The order parameter reflects the spatial restriction of the motion of the C-H bond [43]. Therefore, these simulations are in line with the results obtained from the X-ray diffraction studies that showed the existence of domains with higher packing. The effect of OME⁺ is significantly more pronounced. This was already expected once amphiphilic molecules that can be inserted within the membrane, parallel to phospholipids, can increase the order of the methylene groups of DPPC [44]. This effect was already visualized through PM-IRRAS experiments, where the wavenumber of vibration of the methylene groups decreased.
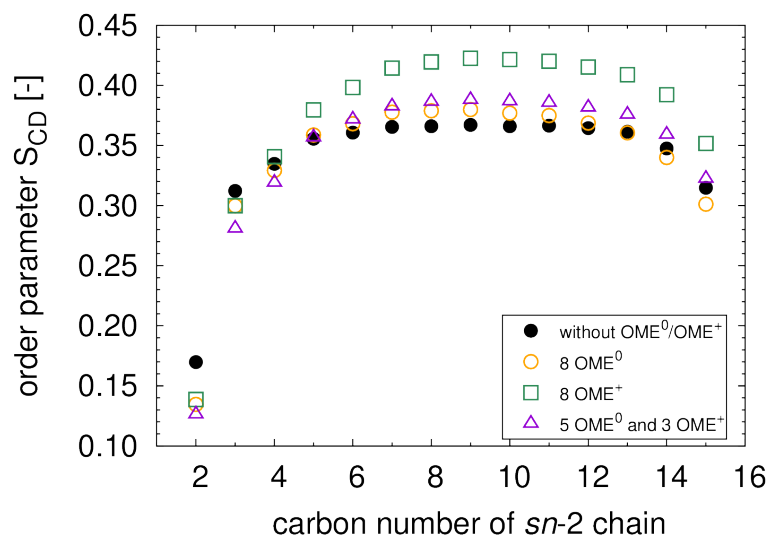
Figure 7. Deuterium order parameter (S_{CD}) profiles of the CH_2 groups along the *sn*-2 tail of DPPC membranes without (black) and with 8 molecules of OME in different protonated states, namely, neutral (OME^0 in orange), positively charged (OME^+ in green), and a mix of neutral and positively charged OME (purple) at 20 °C. The error bars are smaller than the symbol size.

Radial distribution functions (RDF) were calculated to study in detail the types of interactions that can occur between OME^+ and DPPC. The results are shown in Figure 8. The charged pyridine of OME^+ can from electrostatic interactions with the phosphate group of DPPC (Figure 8, A), as it can be seen through the RDF peak at small distances. On the other hand, the benzimidazole group, represented by C3-C5 and C8, can stablish hydrophobic interactions with methylene groups C2-C6 of the apolar chains of DPPC (Figure 8, B). These interactions are dependent on the position of OME within the membrane. Density profiles (Figure A.1 of the supporting information) show that the benzimidazole group is preferably located within 0.5-2.0 nm to the bilayer center, with a maximum close to C8 of DPPC. On the other hand, the density maximum of the pyridine group overlaps with the density of the phosphate group. The most disorder effect happens for the carbons 7 to 13 of DPPC (Figure 7). Nevertheless, the probability of interaction between OME and the carbons 10 to 16 from DPPC is very low (Figure 8). Therefore, the organizing effect seems to be a consequence of changes on the conformation of DPPC molecules and not a direct consequence of the hydrophobic interactions that may occur.
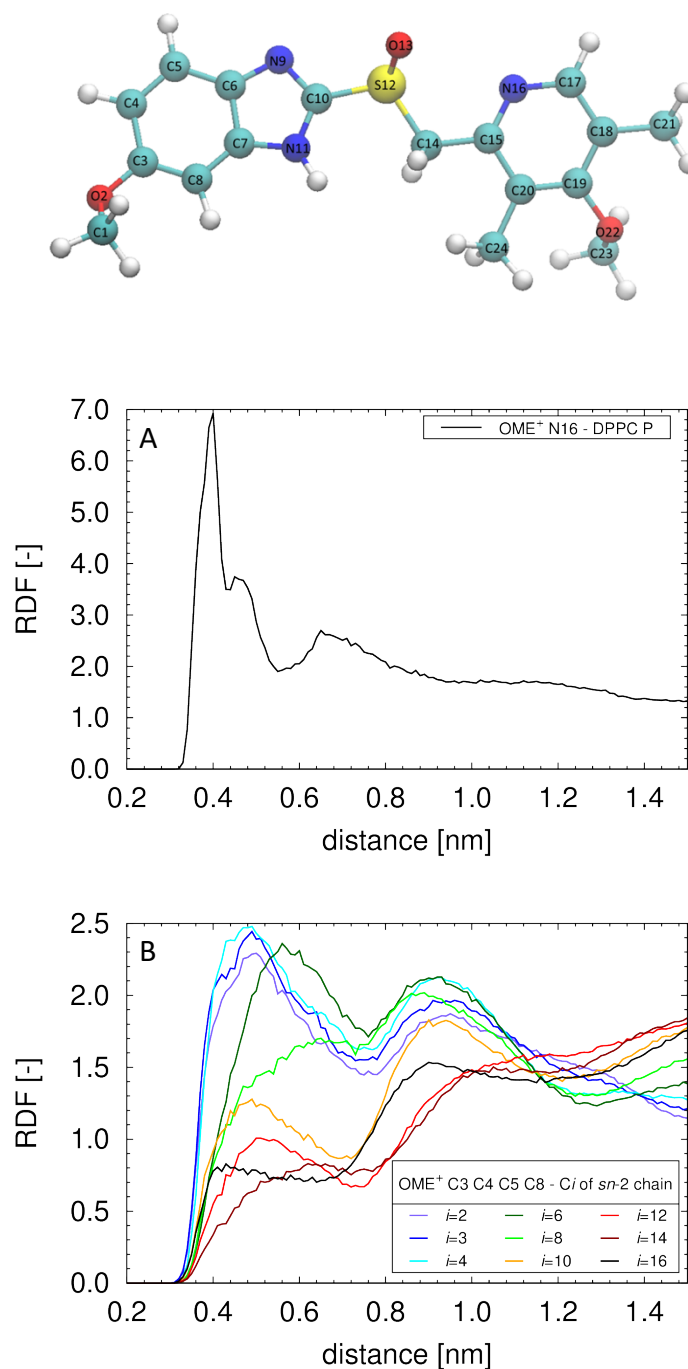
Figure 8. Radial distribution functions between selected OME atoms and atoms of the DPPC membrane. A) pyridine group (N16) of OME – phosphate group of DPPC. B) benzimidazole group (C3, C4, C5, and C8) of OME – hydrophobic chains of DPPC.

Combining all the results and considering the snapshots obtained through the unbiased simulation (Figure 9), we conclude that the effect of OME at pH 5 is due to the existence of 37% of positively charged molecules. OME$^+$ is oriented in parallel to the phospholipids whereas the neutral state is aleatory oriented within the membrane (Figure 9). The intercalation of OME$^+$ molecules is due to the electrostatic interactions stablished

between the pyridine group and the phosphate group of DPPC and the hydrophobic interactions between the benzimidazole group and the first methylene groups of DPPC (Figure 8). At 37 °C, the DPPC membrane is in the ripple phase, which mimics the co-existence of fluid and ordered microdomains in biological cells [45]. OME can increase the packing of DPPC molecules in some regions, keeping however the ripple phase structure.

The ability of OME to be cytoprotective of the gastric mucosa had already been noticed in rats [7-9]. The protective effect of OME was found neither to be dependent on its mechanism as a proton-pump inhibitor nor on the biosynthesis of prostaglandins [8]. Moreover, the protection against experimentally induced gastric lesions was not verified when OME was given intravenously [7]. We propose here that the additional mechanism of action of OME is the intercalation among phospholipid molecules. Due their positive charge, it can contribute to the repulsion of protons that are involved in the development or in the aggravation of injuries. Furthermore, OME promotes a rearrangement of the surrounded DPPC molecules, increasing its packing and changing its conformation from pseudo-hexagonal to hexagonal. The effect of increasing the packing of phospholipids was already pointed out as one explanation for the increase of the hydrophobicity of the gastric mucosa [46]. Therefore, a topical interaction can in fact explain the cytoprotective action of OME.
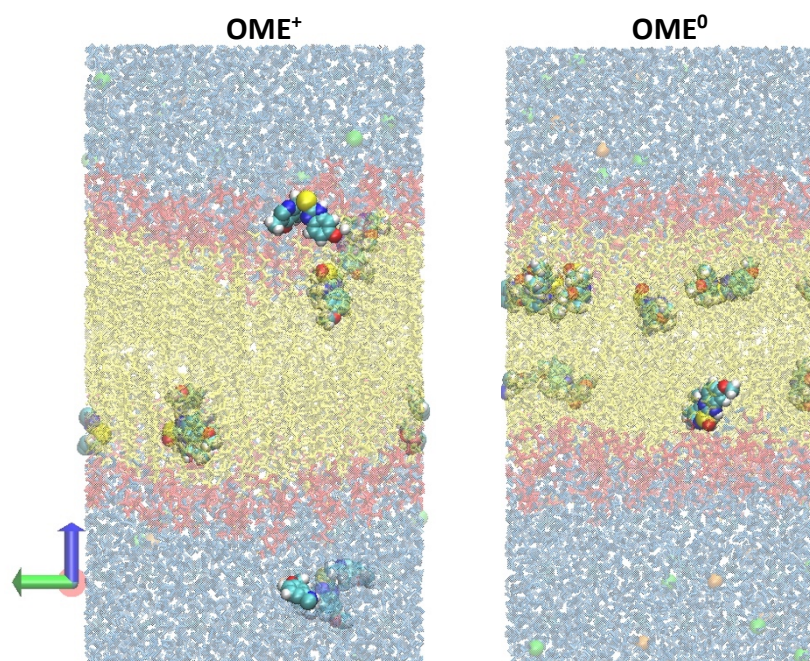
Figure 9. Snapshot of a DPPC membrane at 20 °C simulated for 250 ns with 8 molecules of the positively charged state of OME (OME$^+$) or with 8 neutral OME (OME^0).

4. Conclusions

Our results show that, at lower pH values, OME has an additional mechanism of action through the intercalation among DPPC molecules, that rearrange themselves into more packed domains. This pH was chosen to mimic the local absorption through the gastric mucosa when IR-OME is used. Ultimately, IR-OME can be used for membrane-lipid therapy. This type of treatment is based on the regulation of the membrane lipid structure to reverse a pathological state [1]. By binding to membrane lipids, this type of drugs can regulate the organization of lipids [1]. In the case of gastric ulcers, membrane injuries are promoted by a decrease in the mechanisms of defence of the gastric mucosa against the aggressions of the medium (pH and pepsin). It was already reported that the administration of phospholipids can help in the healing of ulcers [47, 48]. IR-OME allows OME to be a phospholipid-like drug that can improve the ability of the mucus layer to protect the gastric mucosa from the harsh conditions of the stomach lumen. Thus, we propose a new mechanism of action that occurs when a local absorption is preferred over a systemic distribution.

References

[1] E. Altal, Blondeau, Kathleen, A. Pauwels, R. Farré, J. Tack, Evolving pharmacological approaches in gastroesophageal reflex disease, Expert Opin. Emerg. Drugs 17(3) (2012) 347-359.

[2] V.F. Roche, The chemically elegant proton pump inhibitors, Am. J. Pharm. Educ. 70(5) (2006) 1-11.

[3] D. Castell, R. Bagin, B. Goldlust, J. Major, B. Hepburn, Comparison of the effects of immediate-release omeprazole powder for oral suspension and pantoprazole delayed-release tablets on nocturnal acid breakthrough in patients with symptomatic gastro-oesophageal reflux disease, Aliment. Pharmacol. Ther. 21(12) (2005) 1467-74.

[4] P.O. Katz, F.K. Koch, E.D. Ballard, R.G. Bagin, T.C. Gautille, G.C. Checani, D.L. Hogan, V.S. Pratha, Comparison of the effects of immediate-release omeprazole oral suspension, delayed-release lansoprazole capsules and delayed-release esomeprazole capsules on nocturnal gastric acidity after bedtime dosing in patients with night-time GERD symptoms, Aliment. Pharmacol. Ther. 25(2) (2007) 197-205.

[5] D. Castell, Review of immediate-release omeprazole for the treatment of gastric acid-related disorders, Expert Opin. Pharmacother. 6(14) (2005) 2501-2510.

[6] S.A. Conrad, A. Gabrielli, B. Margolis, A. Quartin, J.S. Hata, W.O. Frank, R.G. Bagin, J.A. Rock, B. Hepburn, L. Laine, Randomized, double-blind comparison of immediate-release omeprazole oral suspension versus intravenous cimetidine for the prevention of upper gastrointestinal bleeding in critically ill patients, Crit. Care Med. 33(4) (2005) 760-765.

[7] H. Mattsson, K. Andersson, H. Larsson, Omeprazole provides protection against experimentally induced gastric mucosal lesions, Eur. J. Pharmacol. 91 (1983) 111-114.

[8] S.J. Konturek, T. Brzozowski, T. Radecki, Protective action of omeprazole, a benzimidazole derivative, on gastric mucosal damage by aspirin and ethanol in rats, Digestion 27 (1983) 159-164.

[9] M.J. Manna, S.Y.N. Matloub, Cytoprotective actions of omeprazole in indomethacin - induced gastric mucosal injury in rats, J. Fac. Med. Baghdad 52(1) (2010) 80-83.

[10] V. Bernhard, A.D. Postle, M. Linck, K.-F. Sewing, Composition of phospholipid classes and phoshatidylcholine molecular species of gastric mucosa and mucus, Biochim. Biophys. Acta 1255 (1995) 99-104.

[11] F. Gambinossi, M. Puggeli, G. Gabrielli, Enzymatic hydrolysis reaction of phospholipids in monolayers, Colloids Surf. B, Biointerfaces 23 (2002) 273-281.

[12] Z. Wang, X. Li, S. Yang, Studies of dipalmitoylphosphatidylcholine (DPPC) monolayers embedded with endohedral metallofullerene (Dy@C82), Langmuir 25(22) (2009) 12968-73.

[13] Nanomaterials and Nanoarchitectures: a complex review of the current hot topics and their applications, Springer, Dordrecht, 2013.

[14] P. Fontaine, G. Ciatto, N. Aubert, M. Goldmann, Soft Interfaces and Resonant Investigation on Undulator Source: A Surface X-ray Scattering Beamline to Study Organic Molecular Films at the SOLEIL Synchrotron, Sci. Adv. Mater. 6(11) (2014) 2312-2316.

[15] D. Lopes, C. Nunes, P. Fontaine, B. Sarmento, S. Reis, Proof of pore formation and biophysical perturbations through a 2D amoxicillin-lipid membrane interaction approach, Biochim. Biophys. Acta 1859(5) (2017) 803-812.

[16] C. Stefaniu, G. Brezesinski, X-ray investigation of monolayers formed at the soft air/water interface, Curr. Opin. Colloid Interface Sci. 19(3) (2014) 216-227.

[17] C. Stefaniu, G. Brezesinski, Grazing incidence X-ray diffraction studies of condensed double-chain phospholipid monolayers formed at the soft air/water interface, Adv. Colloid Interface Sci. 207 (2014) 265-79.

[18] F. Neville, Y. Ishitsuka, C.S. Hodges, O. Konovalov, A.J. Waring, R. Lehrer, K.Y. Lee, D. Gidalevitz, Protegrin interaction with lipid monolayers: Grazing incidence X-ray diffraction and X-ray reflectivity study, Soft Matter 4(8) (2008) 1665-1674.

[19] M.J. Abraham, T. Murtola, R. Schulz, S. Páll, J.C. Smith, B. Hess, E. Lindahl, GROMACS: High performance molecular simulations through multi-level parallelism from laptops to supercomputers, SoftwareX 1-2 (2015) 19-25.

[20] J.B. Klauda, R.M. Venable, J.A. Freites, J.W. O'Connor, D.J. Tobias, C. Mondragon-Ramirez, I. Vorobyov, A.D. MacKerell, R.W. Pastor, Update of the CHARMM All-Atom Additive Force Field for Lipids: Validation on Six Lipid Types, J. Phys. Chem. B 114(23) (2010) 7830-7843.

[21] R.M. Venable, Y. Luo, K. Gawrisch, B. Roux, R.W. Pastor, Simulations of Anionic Lipid Membranes: Development of Interaction-Specific Ion Parameters and Validation using NMR Data, J. Phys. Chem. B 117(35) (2013) 10183-92.

[22] K. Vanommeslaeghe, E. Hatcher, C. Acharya, S. Kundu, S. Zhong, J. Shim, E. Darian, O. Guvench, P. Lopes, I. Vorobyov, A.D. Mackerell, Jr., CHARMM General Force Field: A Force Field for Drug-Like Molecules Compatible With the CHARMM All-atom Additive Biological Force Fields, J. Comput. Chem. 31(4) (2010) 671-90.
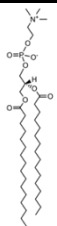
[23] L. Huang, B. Roux, Automated Force Field Parameterization for Non-Polarizable and Polarizable Atomic Models Based on Ab Initio Target Data, J. Chem. Theory Comput. 9(8) (2013).

[24] C. Peetla, A. Stine, V. Labhasetwar, Biophysical Interactions with Model Lipid Membranes: Applications in Drug Discovery and Drug Delivery, Mol. Pharm. 6(5) (2009) 1264-1276.

[25] V.M. Kaganer, H. Möhwald, P. Dutta, Structure and phase transitions in Langmuir monolayers, Rev. Mod. Phys. 71(3) (1999) 779-819.

[26] A. Blume, A comparative study of the phase transitions of phospholipids bilayers and monolayers, Biochim. Biophys. Acta 557 (1979) 32-44.

[27] M. Pinheiro, M. Arede, J.J. Giner-Casares, C. Nunes, J.M. Caio, C. Moiteiro, M. Lucio, L. Camacho, S. Reis, Effects of a novel antimycobacterial compound on the biophysical properties of a pulmonary surfactant model membrane, Int. J. Pharm. 450(1-2) (2013) 268-77.

[28] J.M. Smaby, V.S. Kulkarni, M. Momsen, R.E. Brown, The interfacial elastic packing interactions of galactosylceramides, sphingomyelins, and phosphatidylcholines, Biophys. J. 70 (1996) 868-877.

[29] D. Vollhardt, V.B. Fainerman, Characterisation of phase transition in adsorbed monolayers at the air/water interface, Adv. Colloid Interface Sci. 154(1-2) (2010) 1-19.

[30] T.M. Nobre, F.J. Pavinatto, L. Caseli, A. Barros-Timmons, P. Dynarowicz-Łątka, O.N. Oliveira, Interactions of bioactive molecules & nanomaterials with Langmuir monolayers as cell membrane models, Thin Solid Films 593 (2015) 158-188.

[31] K. Bialkowska, M. Bobrowska-Hägerstrand, H. Häger-strand, Expansion of phosphatidylcholine and phosphatidylserine/phosphatidylcholine monolayers by differently charged amphiphiles, Zeitschrift für Naturforschung C: A Journal of Biosciences 56(9-10) (2001) 826–830.

[32] R. Mendelsohn, C.R. Flach, Infrared reflection-absorption spectrometry of monolayer films at the air-water interface, John Wiley & Sons Ltd. (2002).

[33] G. Pabst, N. Kucerka, M.P. Nieh, M.C. Rheinstadter, J. Katsaras, Applications of neutron and X-ray scattering to the study of biologically relevant model membranes, Chem. Phys. Lipids 163(6) (2010) 460-79.

[34] C. Nunes, G. Brezesinski, J.L. Lima, S. Reis, M. Lucio, Synchrotron SAXS and WAXS study of the interactions of NSAIDs with lipid membranes, J. Phys. Chem. B 115(24) (2011) 8024-32.

[35] J. Jouhet, Importance of the hexagonal lipid phase in biological membrane organization, Front. Plant Sci. 4 (2013) 494.

[36] A.N. Nagappa, P.V. Pandi, P.K. Mishra, R.K. Girish, I. Shanmukh, Transport through liquid membranes containing omeprazole and lansoprazole, Indian J. Biochem. Biophys. 39 (2002) 406-409.

[37] M. Rappolt, G. Rapp, Structure of the stable and metastable ripple phase of dipalmitoylphosphatidylcholine, Eur. Biophys. J. 24 (1996) 381-386.

[38] J. Katsaras, S. Tristram-Nagle, Y. Liu, R.L. Headrick, E. Fontes, Clarification of the ripple phase of lecithin blayers using fully hydrated, aligned samples, Phys. Rev. E 61(5) (2000) 5668-5677.

[39] J.W. Patrick, R.C. Gamez, D.H. Russell, The Influence of Lipid Bilayer Physicochemical Properties on Gramicidin A Conformer Preferences, Biophys. J. 110(8) (2016) 1826-1835.

[40] F. Neville, M. Cahuzac, O. Konovalov, Y. Ishitsuka, K.Y. Lee, I. Kuzmenko, G.M. Kale, D. Gidalevitz, Lipid headgroup discrimination by antimicrobial peptide LL-37: insight into mechanism of action, Biophys. J. 90(4) (2006) 1275-87.

[41] D. Lopes, S. Jakobtorweihen, C. Nunes, B. Sarmento, S. Reis, Shedding light on the puzzle of drug-membrane interactions: Experimental techniques and molecular dynamics simulations, Prog. Lipid Res. 65 (2017) 24-44.

[42] M.B. Boggara, R. Krishnamoorti, Partitioning of nonsteroidal antiinflammatory drugs in lipid membranes: a molecular dynamics simulation study, Biophys. J. 98(4) (2010) 586-95.

[43] Handbook of Modern Biophysics: Biomedical Applications of Biophysics, Humana Press2010.

[44] J. Barry, M. Fritz, J.R. Brender, P.E.S. Smith, D.-K. Lee, A. Ramamoorthy, Determining the Effects of Lipophilic Drugs on Membrane Structure by Solid-State NMR Spectroscopy: The Case of the Antioxidant Curcumin, J. Am. Chem. Soc. 131 (2009) 4490-4498.

[45] M. Eeman, M. Deleu, From biological Membranes to Biomimetic Model Membranes, Biotechnol. Agron. Soc. Environ. 14(4) (2010) 719-726.

[46] P.M. Goggin, J. Marrero, R.T. Spychal, P.A. Jackson, C.M. Corbishley, T.C. Northfield, Surface hydrophobicity of gastric mucosa in Helicobacter pylori infection: Effect of clearance and eradication, Gastroenterol. 103(5) (1992) 1486-1490.

[47] S. Demirbilek, I. Gürses, N. Sezgin, A. Karaman, N. Gürbüz, Protective Effect of Polyunsaturated Phosphatidylcholine Pretreatment on Stress Ulcer Formation in Rats, J. Pediatr. Surg. 39(1) (2004).

[48] F.I. Tovey, Role of dietary phospholipids and phytosterols in protection against peptic ulceration as shown by experiments on rats, World J. Gastroenterol. 21(5) (2015) 1377-84.

Chapter 6.2

Supporting information

Table A.1. Wavenumber of molecular vibrations of a DPPC monolayer in absence or in presence of AMX, at three different pHs (pH 1.2, pH 5 and pH 7.4) and pressures (10 and 20 mN.m^{-1}).

	Pressure	*20 mN.m^{-1}*		*30 mN.m^{-1}*	
		Buffer	**Omeprazole**	**Buffer**	**Omeprazole**
	υ_{as} (PO$_2^-$) (cm^{-1})	1263 ± 1	1263 ± 1	1263 ± 1	1262 ± 1
	υ (CO) (cm^{-1})	1730 ± 1	1737 ± 3	1730 ± 1	1736 ± 3
	υ_s (CH$_2$) (cm^{-1})	2850 ± 1	2852 ± 4	2847 ± 1	2848 ± 5
DPPC	υ_{as} (CH$_2$) (cm^{-1})	2920 ± 1	2914 ± 2	2920 ± 3	2918 ± 3
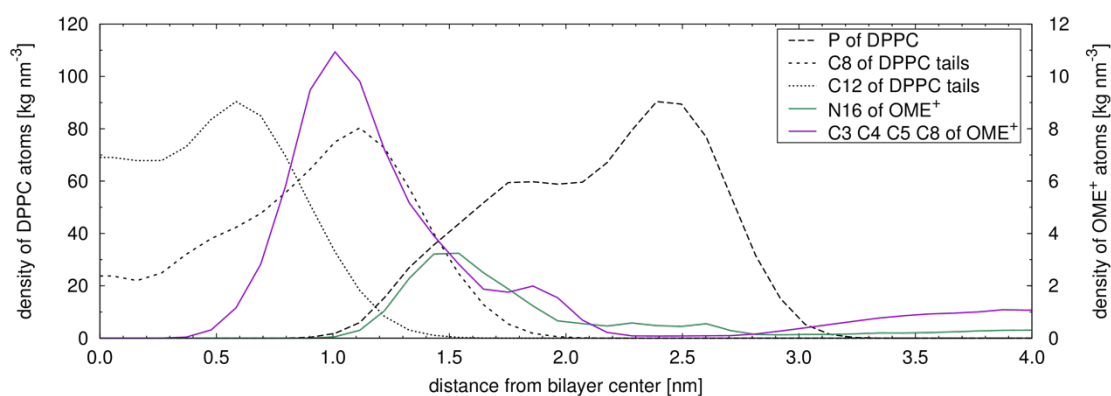
Figure A.1 Density profiles of DPPC (left axis) and positively charged state of omeprazole (right axis) atoms. From DPPC, the phosphor and the carbons 8 and 12 are shown. From omeprazole, the density of the positively charged nitrogen of omeprazole and the carbons 3, 4, 5, and 8 are shown.

Chapter 6.3

Metronidazole within phosphatidylcholine lipid membranes: new insights to improve the design of imidazole derivatives

Metronidazole belongs to the group of imidazole derivatives, which have been studied due to their antimicrobial, antiparasitic, and even anticancer properties. They possess the same pharmacophore and different substituents. Those lateral chains are usually designed according to structure-activity or structure-toxicity relationships. Hence, the aim of this study was to have new insights of the effect of metronidazole functional groups on the interaction with phosphatidylcholine membranes.
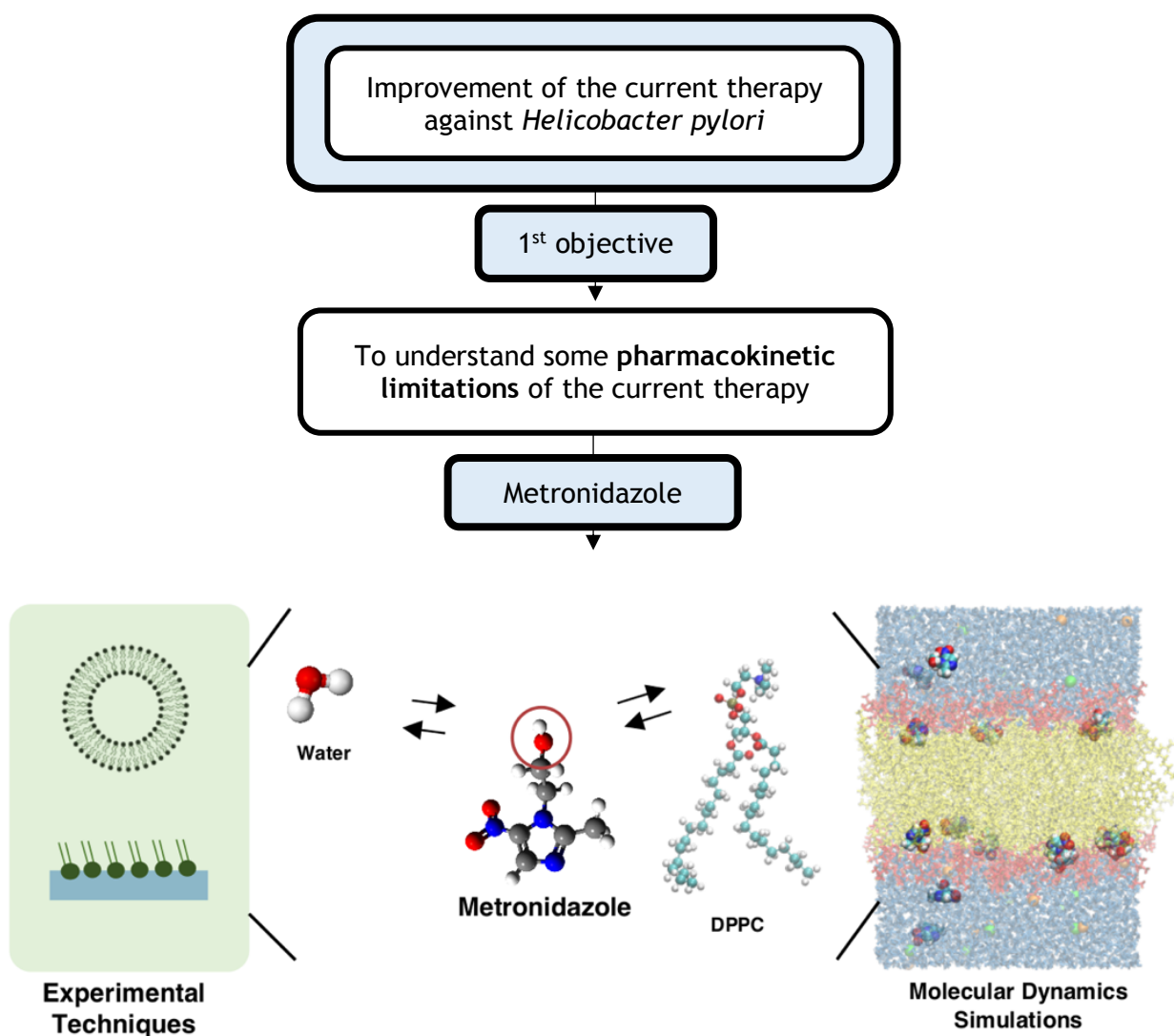
Chapter 6.3

Metronidazole within phosphatidylcholine lipid membranes: new insights to improve the design of imidazole derivatives

Daniela Lopes-de-Campos[1], Cláudia Nunes[1], Bruno Sarmento[2,3,4], Sven Jakobtorweihen[5], Salette Reis[1]

[1]LAQV, REQUIMTE, Departamento de Ciências Químicas, Faculdade de Farmácia, Universidade do Porto, Portugal

[2]INEB - Instituto de Engenharia Biomédica, Universidade do Porto, Rua Alfredo Allen 208, 4200-393 Porto, Portugal

[3]i3S - Instituto de Investigação e Inovação em Saúde, Universidade do Porto, Rua Alfredo Allen 208, 4200-393 Porto, Portugal

[4]IINFACTS, Instituto de Investigação e Formação Avançada em Ciências e Tecnologias da Saúde, Instituto Superior de Ciências da Saúde, Gandra, Portugal

[5]Institute of Thermal Separation Processes, Hamburg University of Technology, Germany

Metronidazole is a imidazole derivative with antibacterial and antiprotozoal activity. Despite its therapeutic efficacy, several studies have been developing new imidazole derivatives with lower toxicity. Considering that drug-membrane interactions are key factors for drugs pharmacokinetic and pharmacodynamic properties, the aim of this work is to provide new insights into the structure-toxicity relationships of metronidazole within phosphatidylcholine membranes. For that purpose, lipid membrane models (liposomes and monolayers) composed of dipalmitoylphosphatidylcholine were used. Experimental techniques (determination of partition coefficients and Langmuir isotherm measurements) were combined with molecular dynamics simulations. Different pHs and lipid phases were evaluated to enable a better extrapolation for in vivo conditions. The partition of metronidazole depends on the pH and on the biphasic system (octanol/water or DPPC/water system). At pH 1.2, metronidazole is hydrophilic. At pH 7.4, metronidazole disturbs the order and the packing of phospholipids. For this toxic effect, the hydroxyl group of the side chain of metronidazole is a key by interacting with the water embedded in the membrane and with the phosphate group and the apolar chains of phospholipids.

Keywords: metronidazole, imidazole derivatives, structure-toxicity relationship, monolayers, liposomes, molecular dynamics simulations, drug design.

1. Introduction

Metronidazole is a imidazole derivative [1] with antibacterial and antiprotozoal activity. It is widely used to treat anaerobic infections, such as gastric, gynecologic, respiratory, and urinary tract infections [2]. It is also considered a first-line drug against *Helicobacter pylori,* which colonizes the gastric mucosa [3, 4]. One of the main advantages of metronidazole is its pharmacokinetic profile, with a broad distribution throughout the human body, including the central nervous system and abscess cavities [2]. However, what is an advantage in a bioavailability perspective can also be

disadvantageous in terms of side effects. In fact, the toxicity of metronidazole has been expressed through gastric (nausea, vomiting and abdominal pain), central nervous system, respiratory, and pancreatic side effects, among others [1, 5, 6]. *In vivo*, drug-membrane interactions are strongly related to the pharmacokinetic properties and the bioavailability of drugs [7, 8]. These interactions depend on the molecular structure of the drug and may ultimately be related with drugs efficacy and side effects [8]. Lipid membrane models have been used for the *in vitro* assessment of these interactions [8]. The influence of some variables, such as the pH of the medium, the temperature, and the ionic strength, can be easily evaluated using these models. On the other hand, the adjustment of these variables is difficult to perform in cell membranes due to their heterogeneity and their dependence on a homeostatic environment [9]. Thus, lipid membrane models can be used to extrapolate and predict the interaction of drugs with biological lipid membranes. This can ultimately provide new insights for a rational drug design [7]. In this study, lipid membrane models composed of dipalmitoylphosphatidylcholines (DPPC) were selected to mimic lipid membranes of biological cells. Phosphatidylcholines are the most common polar head of phospholipids in biological membranes, including the gastric mucosa and the mucus layer [10, 11]. Despite the prevalence of unsatured phospholipids, DPPC (saturated) was selected once its surface pressure-area isotherm has well-defined lipid phases [12]. Thus, it is possible to evaluate the effect of the drug in different lipid phases.

In this context, the purpose of this study was to unveil the structure-toxicity relationship of metronidazole within biological membranes using lipid membrane models. When metronidazole is administered by the oral route, it crosses different pHs that affect its protonation state. For instance, the gastric mucosa has a pH gradient that varies from acidic pH in the stomach lumen to neutral pH near the epithelial cells [13]. In this work, the partition of metronidazole was assessed at two different pHs (pH 1.2 and pH 7.4) for being close to the extremes of the pH range found *in vivo*. Moreover, these pHs enable the study of different protonation states (Figure 1) of both the lipid (the pK_a of the phosphate group is 3.8) and the drug molecule (pK_a is approximately 2.5) [14, 15]. The acid-base properties of metronidazole may play a significant role in its pharmacokinetic and pharmacodynamics properties. This is particularly important for interactions with charged membranes, such as a DPPC membrane. Due to its pK_a, 80% of DPPC is positively charged at pH 1.2, and almost 100% of DPPC is in its zwitterionic state at pH 7.4 (data ChemAxon®, MarvinSketch application, version 15.4.13.0). In addition to pH, the lipid phase of the model system is also important for drug-membrane interactions. Although the physiological state of biological membranes is the liquid-crystalline phase (L_α), more

ordered lipid domains also exist [16]. Nowadays, it is well recognized that membranes are not a homogeneous fluid lipid phase [17]. Membranes have lipid microdomains in which fluid and ordered phases coexist [17]. In the case of phosphatidylcholine membranes, there is a pre-transition state (ripple phase or $P_{\beta'}$) composed of periodic ordered and disordered lipid domains [17]. Therefore, 310 K and 323 K were used to study the interaction of metronidazole with DPPC in a $P_{\beta'}$ and in a L_α phase, respectively.
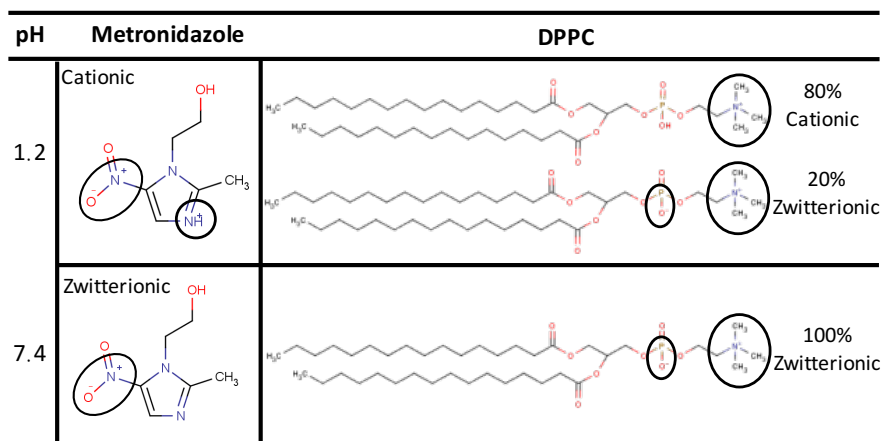
Figure. 1. Different protonation states of metronidazole and DPPC and their relative percentage, when applied, at different pHs. These results were obtained from a computational prediction made by the pK_a plugin of ChemAxon®, MarvinSketch application, version 15.4.13.0.

Experimentally, two lipid-membrane models were used: i) liposomes, to assess the partition of metronidazole by derivative spectrophotometry, and ii) monolayers, to evaluate the effect of the drug on the packing of phospholipids through isotherm measurements. These techniques were complemented with molecular dynamics (MD) simulations to have additional information at an atomistic scale. New insights regarding drugs location, their orientation, their effect on the neighbouring atoms, and the interactions established within a lipid membrane were obtained through these simulations. Therefore, a deeper understanding of the structure-toxicity relationship of metronidazole was obtained by combining different lipid membrane models and computational simulations [8].

2. Materials and methods

2.1 Materials

Metronidazole and *1*-octanol were obtained from Sigma-Aldrich. 1,2-dipalmitoyl-*sn*-glycero-3-phosphocholine was brought from Avanti® Polar Lipids. All reagents were used without further purification. All drug solutions and lipid membrane models were prepared

using buffers: simulated gastric fluid for pH 1.2 and Hepes (I=0.1M) for pH 7.4. The simulated gastric fluid was prepared according to the European Pharmacopoeia 8.0, with 2 g.L^{-1} of NaCl and 7 mL.L^{-1} of concentrated HCl. The final ionic strength (I) was around 0.12 M. All the solutions were prepared using double-deionized water (conductivity inferior to 0.1 µS.cm^{-1}).

2.2 Experimental work

2.2.1 Determination of the partition coefficient using the shake flask method

The shake flask method was adapted from the OECD guideline [18]. The two solvents (*n*-octanol and the buffer) were mutually saturated by heavily shaking the bottles for 6 hours, and then left them rest overnight. Considering the preliminary estimation of the partition coefficient and the solubility of metronidazole in each solvent, the volume ratios of the solvents were stablished (Table 1).

Table 1. Volumes of octanol ($V_{octanol}$), volumes of buffer (V_{buffer}), and volume ratios used in the determination of the Log $D_{octanol/water}$.

pH	$V_{octanol}$ (mL)	V_{buffer} (mL)	$V_{n-octanol}/V_{buffer}$
1.2	7	3	2.33
	8.24	1.76	4.67
7.4	1.76	8.24	0.22
	4.62	5.38	0.86

The vessels with the mixture of solvents were vortexed and shaken by rotating the tube throughout 180° about its transverse axis. The phases were then separated by centrifugation, during 20 minutes at 9 G (Allegra® X-15R Centrifuge from Beckman Coulter). Metronidazole was quantified in each phase by UV-Vis spectrophotometry. Duplicate vessels of each ratio were evaluated, with a total of four independently measured vessel at each pH. The assay was performed at room temperature.

2.2.2 Preparation of liposomes

Liposomes were prepared using the thin film hydration method [19]. Briefly, a DPPC solution in chloroform/methanol (3:2 (v/v)) was evaporated under a nitrogen stream in a rotative evaporator. After the evaporation, the lipid film was hydrated and vortexed with

the specific buffer, leading to the formation of multilamellar vesicles (MLVs). Unilamellar liposomes (LUVs) of 100 nm were obtained after the extrusion through polycarbonated filters at a temperature above the main phase transition temperature of the lipid.

2.2.3 Determination of partition coefficients using derivative spectrophotometry

The determination of the partition coefficients was based on a derivative spectrophotometry method [20]. Buffered solutions of metronidazole (60 µM) were added to suspensions of increasing concentration of DPPC (from 0 to 1000 µM). The absorption spectra (200 – 400 nm) of the samples were recorded in a Biotek Synergy HT microplate reader, applying the protocol developed by our research group [20]. A more sensitive equipment (Cary 1E UV/Vis Spectrophotometer coupled with a Cary Varian Peltier control) was also used to confirm the results. The averages and the standard deviations presented in the results section correspond to the assays performed in both equipments. All assays were carried out at a temperature below (310.15 K) and above (318.15 K) the main transition temperature of DPPC [21].

The partition coefficients were obtained using the K_p calculator routine [20]. The second and the third derivative of the absorbance spectra were determined to eliminate the light scattering promoted by the LUVs. The K_p calculator determines the K_p in M^{-1} through a non-linear least-squares regression. The Log D_{DS} is obtained from the dimensionless K_p, which is calculated by dividing the K_p in M^{-1} by the lipid molar volume.

2.2.4 Langmuir isotherms

Langmuir isotherm (π/A) measurements were performed according to a previously described method [22]. A DPPC solution in chloroform (1 mM) was spread onto 420 mL of a buffer solution (Hepes buffer, pH 7.4, I=0.1 M) or a buffered solution of metronidazole (60 µM). After 10 minutes for equilibration, the monolayer was compressed at a rate of 5 $Å^2$/molecule/min, and the surface tension was measured using an Wilhelmy microbalance with a filter paper plate with an accuracy superior to 0.1 $mN.m^{-1}$. All assays were performed in a KSV NIMA Langmuir trough with two symmetric compressor barriers at 298.15 K.

2.3 Calculation details

2.3.1 Prediction of the protonation state of metronidazole and DPPC

The protonation state of both the drug and DPPC at pH 1.2 and pH 7.4 were predicted by the pK_a plugin of ChemAxon®, MarvinSketch application, version 15.4.13.0.

2.3.2 Membrane simulations

The protonation state of DPPC was chosen considering the pK_a of the phosphate group (3.8) [15]. At pH 7.4, membranes are composed of zwitterionic DPPC, with an overall neutral charge. At pH 1.2, the phosphate group is mainly in its neutral state. Hence, the membrane is composed of 80% positively charged DPPC and 20% zwitterionic DPPC. Therefore, membranes were designed accordingly. 104 charged DPPC molecules plus 24 zwitterionic DPPC molecules were used to mimic the membrane at pH 1.2, whereas 128 zwitterionic DPPC molecules were used at pH 7.4. The initial lipid membrane at pH 7.4 was obtained using the CHARMM-GUI membrane builder [23]. After equilibrating this membrane, the membrane at pH 1.2 was obtained by adding hydrogens to the phosphate group of randomly chosen lipids, with the constrain that the proportion of the charged and neutral form of DPPC is the same in both leaflets. For the charged DPPC, chloride ions were used as counterions. Water molecules were added in a water/lipid ratio of approximately 55 to guarantee a full hydration of the membrane. More specifically, 7024 and 6922 water molecules were added to the membrane at pH 7.4 and at pH 1.2, respectively. Both membranes were equilibrated during 100 ns at three different temperatures: 298.15 K (room temperature), 310.15 K (physiological temperature) and 323.15 (temperature above the main transition temperature of DPPC [21]). 13 Na and Cl ions were added in replacement of 26 water molecules (ionic strength of approximately 0.1 M) to the systems at 310.15 K and at 323.15 K. Both membranes were simulated for 100 ns and used as starting structures for the following simulations.

All simulations were carried out using the GROMACS 4.5.7 package [24, 25]. Fixed number of particles (*N*), pressure (*P*), and temperature (*T*) were used (NPT ensemble). The pressure was kept constant at 1 bar using the Parrinello-Rahman barostat [26, 27] with a semiisotropic coupling, a compressibility of 4.5×10^5 bar^{-1}, and a coupling constant of 5 ps. The Nosé-Hoover thermostat was used to maintain a constant temperature [28]. A leap-frog algorithm was used to integrate Newton's equation of motion with a time step of 2 fs. Periodic boundary conditions were used, and a Lennard-Jones cutoff radius of 1.2 nm was employed, with a smooth switch to zero starting at 0.8 nm. For the electrostatic interactions, a cutoff radius of 1 nm was used, and the long-range part was taken into

account with the Particle-Mesh Ewald (PME) summation [29, 30]. A neighbour list was used and updated every 10th step. These parameters were used in all simulations.

2.3.3 Computation of free energy profiles

Umbrella sampling simulations were carried out to obtain the free energy profiles of metronidazole within the membrane [31-33]. Equilibrated membrane systems from the simulations described in the previous section were used as starting points. First, one molecule of metronidazole was inserted into the water phase of each system. This molecule was then pulled to the center of the bilayer with a force constant of 1000 kJ.mol^{-1}.nm^{-2} and a pulling rate of 0.0001 nm ps^{-1}. Lipids, water, and ions were restrained with a constant force of 500 kJ.mol^{-1}.nm^{-2} to avoid their movement along with the pulled solute molecules. A second molecule is used in each US simulation to enhance sampling [34]. Therefore, another metronidazole molecule was placed into the water phase. Both solutes were then pulled in the same direction with a constant force of 1000 kJ.mol^{-1}.nm^{-2} and pulling rates of 0.0001 nm.ps^{-1}. The direction was chosen such that the first metronidazole was pulled in the opposite direction of the first pull. From the last pulling simulation, the starting configurations for all windows along the *z*-axis were obtained. Therefore, the two solutes are at a distance that they do not influence each other. The free energy profiles shown in this work are averages of the individual profiles of two metronidazole molecules. A summary of the systems and the number of windows used in each umbrella sampling are shown in Table 2. Two different protonation states of metronidazole were investigated, namely, a positively charge at pH 1.2 and a zwitterionic with an overall neutral charge at pH 7.4.

Table 2. Summary of the systems used in the umbrella sampling simulation.

pH	Drug $^{overall\ charge}$	N°. of lipid molecules$^{overall\ charge}$	Ions	T (K)	N°. of windows
1.2	Metronidazole^{+}	104 DPPC^{+} 24 DPPC^{0}	117 Cl^{-} 11 Na^{+}	310.15	38
	Metronidazole^{+}	104 DPPC^{+} 24 DPPC^{0}	117 Cl^{-} 11 Na^{+}	323.15	37
7.4	Metronidazole^{0}	128 DPPC^{0}	13 Cl^{-} 13 Na^{+}	310.15	41
	Metronidazole^{0}	128 DPPC^{0}	13 Cl^{-} 13 Na^{+}	323.15	39

Each umbrella window was simulated with the solute harmonically restrained in the *z*-direction with a force constant of 3000 kJ.mol^{-1}.nm^{-2} for 80 ns. However, it could freely move in the *x-y* plane. The spacing between the windows was 0.1 nm. The first ns was discarded due to equilibration processes. The weighted histogram analysis method (WHAM) [35, 36] was used to obtain the free energy profile of the solute, with the energy in the bulk water set to zero as reference. The WHAM implementation of the g_wham program was used [37]. The convergence of the free energy profiles of each solute should be checked carefully [38, 39]. Figure A.1 of the supporting information shows the convergence of the partitions coefficients over the simulation time for all simulated systems.

2.3.4 Unbiased simulation

Two unbiased MD simulations over 1 μs were carried out at 323.15 K, using the membrane composed of 128 molecules of zwitterionic DPPC and 13 molecules of NaCl. One of these simulations included two zwitterionic metronidazole molecules and the other one 16 zwitterionic metronidazole molecules. As the free energy barriers were not too high for these conditions, the simulations were used to determine another two free energy profiles and the corresponding Log D values. 16 molecules of metronidazole were selected to model the lipid:drug ratio used for the intermediary concentration of DPPC in the derivative spectrophotometry method (500 μM of DPPC to 60 μM of metronidazole, which is its plasmatic concentration [14, 40]). The concentration of 500 μM of DPPC is also commonly used in experiments that evaluate drugs effect on biophysical properties of lipid membrane models [21, 41]. 6977 and 6692 molecules of water were used in the system with 2 and with 16 molecules of metronidazole, respectively. If not otherwise mentioned, the simulation with 16 metronidazole molecules was analysed for the last 900 ns. However, only the first ns was not analysed when free energy profiles were calculated from the unbiased simulations to have a better water phase sampling.

2.3.5 Force field

The CHARMM36 all-atom force field was used to model the lipids [42, 43]. However, the cationic form of DPPC is not included in the official CHARMM version. Nevertheless, since the introduction of cardiolipin models, all parameters are available to model the cationic form of DPPC [23]. The calculated area per lipid was compared to our experimental data to validate the parameters of the charged DPPC (see Table A.1 of the supporting information). An optimized CHARMM36 force field was used for the salt ions

[44]. Water molecules were modelled with the CHARMM TIP3P force field. For drug molecules, the CHARMM general force field (CGenFF) exists [45]. However, we checked with the CHARMM ParamChem tool [46, 47] for metronidazole parameters and found that some parameters are missing, and a reliable assignment by analogy was not possible. Therefore, we used the general automated atomic model parameterization (GAAMP) [48] to calculate charges and bonded parameters for zwitterionic and cationic metronidazole molecules, whereby the CGenFF was used as the initial model. GAAMP is an automatic parametrization tool, relying on QM data capable of calculating parameters compatible with the CHARMM force field.

3. Results and Discussion

3.1 Determination of the distribution coefficient of metronidazole

The partition coefficient reflects the ability of a drug to penetrate from a polar (e.g., physiologic medium) to a more apolar environment (e.g., lipid membranes). Hence, its determination can be very useful to modify or design new drugs and even to optimize already commercialized drugs. The distribution coefficient (Log D) reveals the lipophilicity of ionizable compounds, and it is extremely important for drugs with ionizable groups [41]. This is the case of metronidazole once it has a nitrogen side chain with a zwitterionic charge and a deprotonable nitrogen atom in the imidazole ring with a pK_a of 2.5 [14]. In this work, the distribution coefficient was determined by three different techniques: i) MD simulations of metronidazole within a DPPC membrane (Log D_{MD}); ii) the shake flask method using an octanol/water system (Log $D_{o/w}$); and iii) a derivative spectroscopic technique using liposomes of DPPC as membrane models (Log D_{DS}).

MD simulations were used to understand the partition of metronidazole with atomistic and picosecond resolution. The pH was simulated by modelling different protonation states (Figure 1), and the lipid phase was obtained by simulating the membrane at 310 or at 323 K. Considering that both the charge state and the lipid phase change among the different systems, the validation of the modelled membrane is an important step before further studies. The validation was achieved through the comparison of the area per lipid at both pHs and the order parameter at pH 7.4 with the experimental values (Table A.1 and Figure A.2 of the supporting information, respectively). Both parameters were in good agreement with the experimental results. Thus, the interaction models used in the MD simulations are suitable for this study.

Free energy profiles can be obtained from MD simulations. This thermodynamic parameter reflects the stability of a specific configuration. Hence, it can also be used to

calculate other properties, such as the pK_a and the partition coefficient. The umbrella sampling method was used to obtain the free energy also in regions that were barely visited in an equilibrium (unbiased) simulation [31]. In this method, the system is divided into small layers (windows) along the direction of the bilayer normal. Then, a biased simulation for each window is carried out, with the drug molecule harmonically restraint in the *z*-direction. Results (Figure 2) show that the minimum of the free energy changes depending on the lipid phase of the membrane and on the protonation state of both the drug and the lipid. At pH 1.2 (Figure 2, left column), the free energy in the membrane is always higher than the free energy in the water. This profile indicates that the state where the drug is within the membrane is not thermodynamically favourable. Thus, the drug has a hydrophilic character at this pH. On the opposite, at pH 7.4 (Figure 2, right column), there is a negative free energy in the membrane (higher affinity to the membrane). At both temperatures, the minimum of the free energy is at *z*=1-1.5 nm, which shows that the drug's preferential location is between the center of the bilayer and the headgroups of the phospholipids. At both pHs, two energetic barriers can be visualized: i) near the polar heads, which constitutes a barrier to the penetration of the drug, and ii) in the center of the bilayer, indicating a low affinity for that region. Two unbiased simulations were also carried out to obtain the free energy profile at pH 7.4 and 323 K (Figure 2, D). The profiles obtained by both methods (umbrella sampling and unbiased simulation) are similar, as depicted by the overlapping of the free energy profiles. Differences are mainly visualized near the center of the bilayer and at *z*=2-2.5 nm, with a higher barrier predicted by umbrella sampling. This difference is probably due to insufficient sampling in this region in the unbiased simulations. However, the very good agreement of both profiles validates the methods. The umbrella sampling simulation represents infinite dilution (two separated metronidazole molecules, see also calculation details section), whereas the unbiased simulations present a lipid/metronidazole ratio of 64 and 8, respectively. Therefore, the similarity of the free energy profiles shows that the partition is concentration independent in this concentration range.

There are different equations to determine the partition coefficient from the free energy profile (see reference [49] for a detailed discussion). Commonly, the system is divided into two parts, where one represents the membrane phase and the other represents the bulk water phase. Klamt *et al.* (2008) suggested an equation with a water correction [50]. In this equation, it is assumed that part of the free energy in each region of the membrane is attributed to the water content of that region [49, 50]. This equation has the advantage that the size of the membrane phase does not have to be defined. Furthermore, it is more suitable for hydrophilic compounds [50]. We compared our

simulations using both types of equations (with and without a water correction). For lipophilic solutes, the difference between the partition coefficients in log scale was less than 0.3 (see also reference [49]). Nevertheless, for hydrophilic compounds it was larger than 2. As this study comprises hydrophilic compounds, the equation with the water correction was used to calculate the partition coefficients from the MD data. To be consistent with the experimental results (see below) all partition coefficients are dimensionless (i.e., L_{water}/L_{lipid} also named $K^{(c,c)}$ in reference [49]). Log D_{MD} values obtained by umbrella sampling and by unbiased simulations are shown in Table 3.
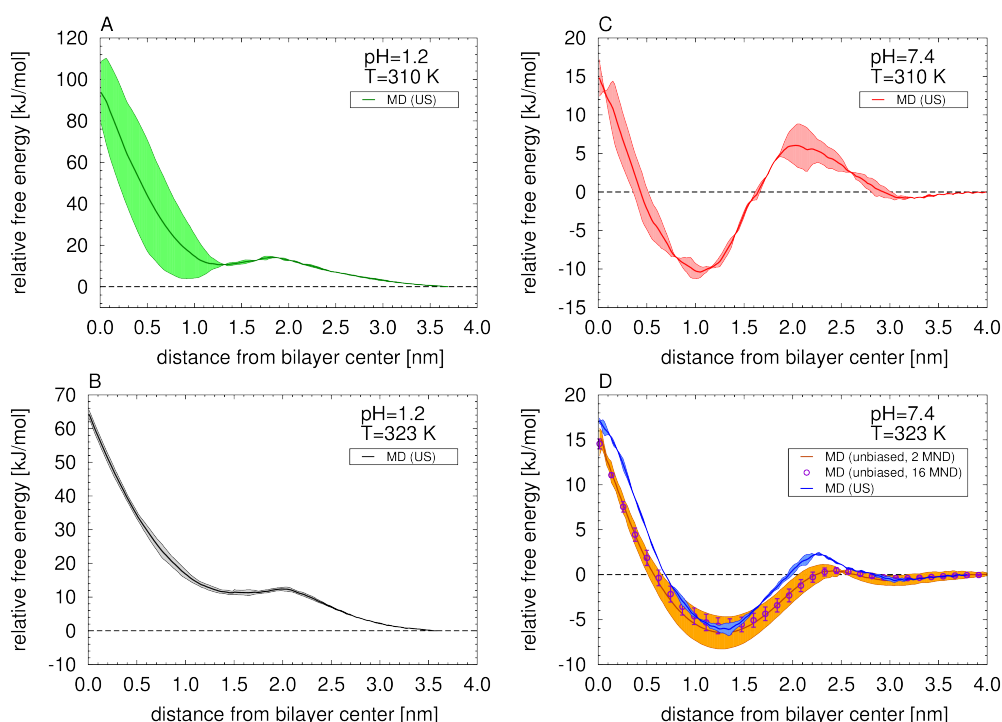
Figure 2. Free energy profiles obtained at four different conditions: A) pH 1.2, 310 K, B) pH 1.2, 323 K, C) pH 7.4, 310 K, and D) pH 7.4, 323 K. These conditions enabled the study of different lipid phases and different protonation states of both the drug and DPPC. The free energy profiles were obtained from MD simulations (umbrella sampling (A-D) and two unbiased simulations (D)). The free energy of the water phase was defined as reference by setting it to zero, and all profiles are shown for one half of the bilayer. The coloured areas show the error margins. For better visualization, the results of the unbiased MD simulation with 16 metronidazole (MND) molecules are shown with error bars to represent their error margin.

The partition coefficient of metronidazole was also assessed using experimental techniques. The most commonly used technique is the "shake flask method", which measures the octanol/water partition. For ionizable compounds, the Organisation for Economic Co-operation and Development (OECD) guideline suggests to use an appropriate buffer (with a pH of at least one unit below or above the pK_a) instead of water

[18]. Since the pK$_a$ of metronidazole is 2.5 [14] both pHs 1.2 and 7.4 cover the stated by the guideline. Log D$_{o/w}$ values are shown in Table 3. Recently, new alternatives have been emerged. For instance, a liposome/water system can be used to determine more accurately a partition coefficient that is governed by electrostatic and hydrogen bonds [51, 52]. This type of interactions is not considered in an octanol/water partition once it is limited by completely separated apolar and polar media [51, 52]. Among all the possible techniques that can be used to determine the partition in a liposome/water system, UV-Vis derivative spectrophotometry was used for allowing the determination of partition coefficients without a physical separation and, consequently, without disturbing the equilibrium [53]. In this method, the deviation of the maximum of absorbance is determined. This deviation indicates that the environment that surrounds the drug is changing, as it happens when a drug moves from an aqueous to a lipid phase [20]. The derivative is used instead of the absorbance once it enables a better resolution of the overlapping bands and an elimination of the spectral interference of liposomes [20]. The partition coefficient is calculated from a non-linear regression using the following equation [54]:

$$D_t = D_w + \frac{b\, K_p[L]}{1 + K_p[L]} \tag{1}$$

where D_t and D_w are the total and the aqueous derivative of the absorbance of the drug; K_p is the partition coefficient; and [L] is the concentration of the lipid. b is a constant defined by $b = (\varepsilon_m - \varepsilon_w) \times C_T$, in which ε_m and ε_w represent the drug molar absorptivity in each phase (lipid – m and water – w), and C_T is the total molar concentration of the drug. The K$_p$ is determined in L.mol^{-1}, and it can be divided by the lipid molar volume (0.70 L.mol^{-1} for DPPC [55]) to obtain a dimensionless K$_p$. However, derivative spectrophotometry cannot be applied for hydrophilic compounds [20]. Thus, at pH 1.2, it was not possible to determine the partition coefficient through this technique. Figure 3 (A) shows the second derivate of the absorbance spectra of metronidazole in a liposome/buffer suspension at pH 7.4. A deviation of the maximum of the derivative is shown, and the partition coefficient was calculated applying Eq. (1) (Figure 3, B).
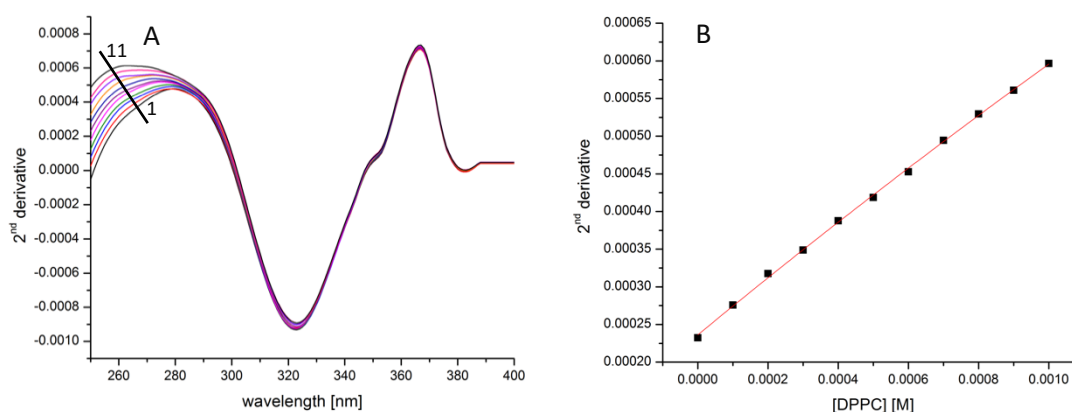
Figure 3. Second-derivative spectra (A) of metronidazole (60 µM) at pH 7.4, incubated with large unilamellar vesicles (LUVs) of DPPC in the liquid-crystalline phase. The black straight line shows the deviation of the spectra from a DPPC concentration of 0 M (spectrum 1) to 0.001 M (spectrum 11). The derivative values of that deviation were used to fit Eq. (1) to obtain a non-linear regression (B).

The Log D values obtained through the different techniques are shown in Table 3. At pH 1.2, both Log $D_{o/w}$ and Log D_{MD} are negative, which reflects the hydrophilic character of metronidazole. The Log D_{MD} is lower than the Log $D_{o/w}$. In fact, at this pH, both metronidazole and DPPC are positively charged, with the possible existence of repulsion forces. This repulsion does not exist in an octanol/water system. Thus, at pH 1.2, the partition of metronidazole is less probable in a membrane/water model than in an octanol/water system.

Table 3. Log D values obtained through different approaches: MD simulations (Log D_{MD}) and experimental techniques. For the Log D_{MD} calculations, the US simulations and the unbiased simulations with 2 or 16 molecules of metronidazole (MND) were used. In the experimental work, the derivative spectrophotometry (Log D_{DS}) and the shake flask method using the octanol/water system (Log $D_{o/w}$) are presented.

pH	Lipid membrane phase	MD simulations (Log D_{MD})			Experimental work	
		US simulation	Unbiased simulation		Log D_{DS}	Log $D_{O/W}$
			2 MND	16 MND		
1.2	$P_{\beta'}$	-3.2 ± 0.7	N/A*	N/A*	N/A*	-1.49 ± 0.06
	L_α	-3.6 ± 0.6				
7.4	$P_{\beta'}$	1.07 ± 0.07			1.0 ± 0.2	-0.22 ± 0.09
	L_α	0.48 ± 0.04	0.7 ± 0.3	0.7 ± 0.4	1.1 ± 0.2	

N/A: not available due to the limitation of the technique.

The partition of metronidazole is higher at pH 7.4 than at pH 1.2. This is in coherency with the trend of non-charged drugs to easily cross membranes by passive diffusion. Thus, when the intragastric pH is higher (e.g., when an antacid is administered), the ability of metronidazole to cross cell membranes is improved [14]. For one of the main applications of metronidazole, which is *Helicobacter pylori* infections [3], a higher absorption at the stomach would be preferential. This bacterium is usually located in the interface between epithelial cells and the gastric mucosa [4]. Therefore, a higher diffusion through the gastric mucus would enhance the local concentration and the efficacy of metronidazole and would decrease the prevalence of side effects.

The Log $D_{o/w}$ of metronidazole at pH 7.4 is -0.22, which is coherent with the literature [14]. Although higher than at pH 1.2, it still reflects a hydrophilic character. Nevertheless, both Log D_{MD} and Log D_{DS} are positive and in good agreement. This was expected once the use of membrane models enables a more accurate determination of the Log D, especially when the partition is governed by electrostatic and hydrogen bonds [51, 52]. In fact, at pH 7.4, metronidazole can form electrostatic and hydrogen bonds with the polar heads of DPPC. Table 3 also shows that the Log D_{DS} and the Log D_{MD} are more similar at 310 K than at 323 K. However, all three MD results for 323 K and pH 7.4 have overlapping error bars, showing again the good agreement for the different metronidazole concentrations used in these simulations.

The effect of the lipid phase is negligible when comparing the experimental values. However, it seems to be an important variable for the MD simulations, with better agreement to the experiment in the $P_{\beta'}$ (310 K) than in the L_{α} phase (323 K).

These results show that the membrane/water partition of metronidazole at pH 7.4 is higher than reflected by the octanol/water literature values due to the limitations of the octanol/water system. Moreover, there is a correlation of the experimental and the simulated values, which corroborates the classification of MD simulations as a powerful tool for drug design. Below, the effect of metronidazole in the biophysical properties of the membrane was evaluated by experimental techniques and complemented with MD simulations for a comprehensive understanding of metronidazole-membrane interactions.

3.2 Langmuir isotherms to assess the packing of DPPC monolayers

Langmuir isotherms have been used for decades, and they are a very useful tool to study air-water interfaces [56]. By lateral compression, a monolayer can pass from a gas to a liquid expanded phase [57]. By continuing the compression, a plateau of a first-order transition may appear, reflecting the coexistence of the liquid expanded and the liquid condensed phases [57]. Then, an abrupt increase of the pressure is observed in the liquid

condensed phase, until the collapse is reached [57]. Surface pressure-area (π-A) isotherms of DPPC spread onto buffer or onto a buffered solution of metronidazole are shown in Figure 4. Metronidazole affects the transition from the liquid expanded to the liquid condensed phase. Furthermore, at the same pressure, the area per lipid is higher in the presence of metronidazole, which suggests that this drug promotes a lower packing of DPPC.
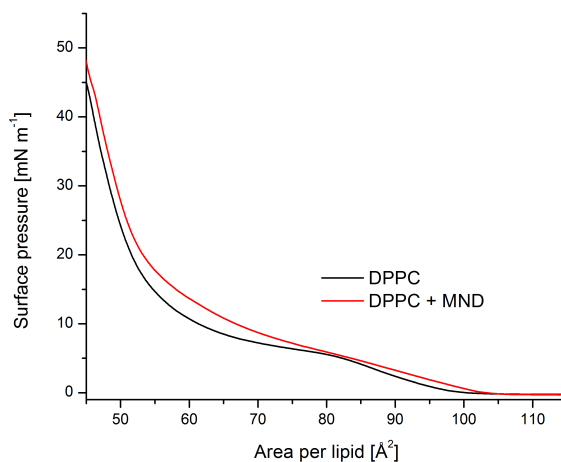
Figure 4. Surface pressure-area (π-A) isotherms of DPPC spread onto a buffer subphase (black) or onto a buffered subphase of metronidazole (MND) in a concentration of 60 μM (red) at pH 7.4.

The area per lipid is an important feature of phospholipid bilayers. It can be calculated from the isotherms profile through the intersection of a straight line of the isotherm on the condensed phase with the *x*-axis [58]. The area per lipid of DPPC spread onto a buffer solution was 57.3 ± 0.4 Å^2, whereas in presence of metronidazole it increased to 58.4 ± 0.4 Å^2. This difference is in agreement with the changes in the isotherm profile, and it reflects the tendency of metronidazole to decrease the packing of DPPC. The elastic modulus (C_s^{-1}) can also be calculated from the isotherm profile, according to the following equation:

$$C_s^{-1} = -A \left(\frac{d\pi}{dA} \right)$$ (2)

This parameter reveals the elastic properties and the compressibility of the membrane [59]. The elastic modulus of DPPC spread onto a buffer subphase is 217 ± 7 mN.m^{-1}, which is coherent with the literature [12]. After the addition of metronidazole, the elastic modulus decreases to 195 ± 6 mN.m^{-1}. A lower elastic modulus points towards a more compressible and more fluid membrane, which is in agreement with the higher area per lipid. This biophysical perturbation, manifested as a fluidizing effect, was already

identified as one of the toxic mechanisms of several drugs [60, 61]. Therefore, in the following section MD simulations were used to get a deeper understanding of the relation between the molecular structure of metronidazole and its fluidizing effect.

3.3 MD simulations to assess metronidazole-membrane interactions

3.3.1 Effect on the order parameter

The order parameter (S_{CD}) is usually calculated using the angle (θ) formed between the C-H bond and the normal to the lipid bilayer:

$$S_{CD} = \left\langle \frac{3}{2}(cos^2\theta) - \frac{1}{2} \right\rangle \tag{3}$$

Indirectly, it can reveal the packing and the alignment of the phospholipids chains. An unbiased simulation with 16 molecules of metronidazole was carried out for allowing the study of a concentration similar to the plasmatic concentration (60 μM) [14, 40]. Furthermore, the L_α phase (323 K) and the physiological pH (pH 7.4) were selected for allowing a better extrapolation to *in vivo* interactions. A snapshot of the system and the order parameter obtained after a 1 µs unbiased simulation are represented in Figure 5. In the snapshot (Figure 5, left), most of the metronidazole molecules is located near the first carbons of the hydrophobic tails of DPPC, which was already predicted by the free energy profile.
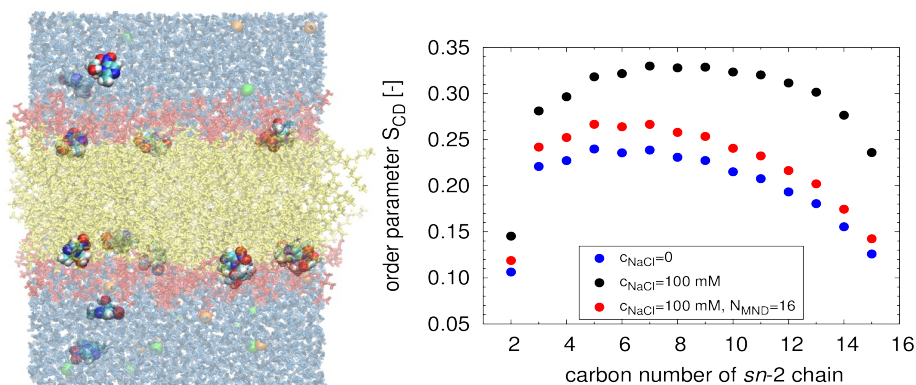
Figure 5. Snapshot of the simulated system (left) with 16 molecules of zwitterionic metronidazole at 323 K within a DPPC membrane. DPPC head groups are shown in red and hydrophobic tails in yellow, water is shown in blue. Chlorine and sodium are shown as green and orange spheres. The atoms of metronidazole are shown as spheres (carbon in cyan, hydrogen in white, oxygen in red, and nitrogen in blue). Deuterium order parameter (S_{CD}) profiles of the CH_2 groups along the *sn*-2 tail (right) of DPPC membrane without (blue) and with 13 molecules of NaCl (black), and in presence of 16 molecules of metronidazole (red).

Figure 5 (right) shows a significant increase in the order parameters of DPPC in the presence of NaCl. The presence of ions also affected the area per lipid and the thickness of the membrane (data not shown). These effects were already reported by other authors [62, 63], and they were explained by the strong binding of sodium ions to the polar heads of the lipids. However, when 16 molecules of metronidazole were added to the system, the order parameters decreased. This disorder effect corroborates the results from the surface pressure-area (π-A) isotherms, where metronidazole promoted a lower packing and a higher area per lipid.

3.3.2 The location and orientation of metronidazole within the membrane model

A deeper analysis of the unbiased simulation was carried out to understand the key factors for the disorder effect. Figure 6 (left) shows the order parameter of the *sn*-2 tail of DPPC over time. This simulation was started from an equilibrated system without metronidazole by initially placing all metronidazole molecules into the water phase. The order parameter decreased in the first 100 ns, and then it was almost stable over the last 900 ns of the simulation. In the first 100 ns, metronidazole was able to penetrate the membrane, as evidenced by the changes in the mass density of metronidazole (Figure 6, right). The mass density of metronidazole decreased over the first 100 ns in the water phase ($z > 3.0$ nm) and increased in the membrane. Therefore, the change of the order parameters is a direct consequence of DPPC-metronidazole interaction. Furthermore, after equilibration, the maximum of the mass density is at a distance of 1.2 nm from the bilayer center. This value is in agreement to the preferential location predicted by the free energy profile (minimum at z=1.3 nm).
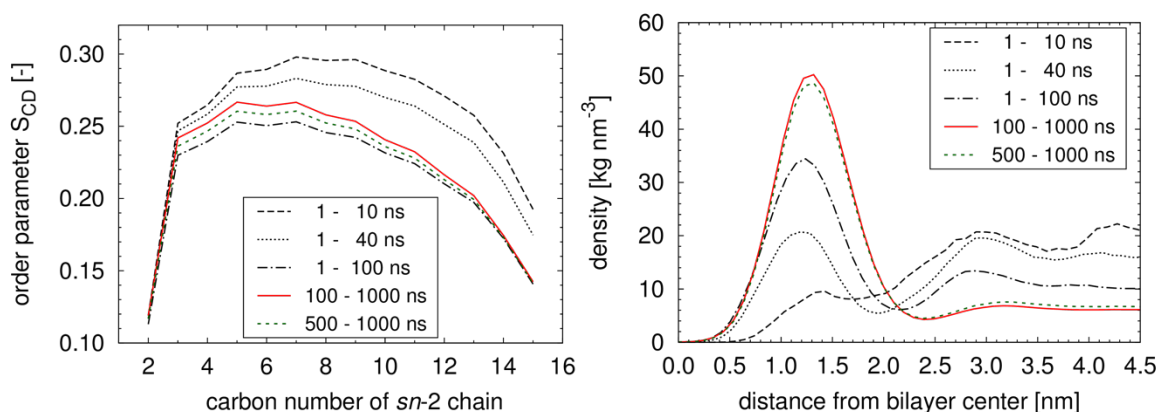
Figure 6. Deuterium order parameter (S_{CD}) profiles of the CH$_2$ groups along the *sn*-2 tail (left) averaged over different time intervals of an unbiased simulation of a DPPC membrane with 13 molecules of NaCl and 16 molecules of zwitterionic metronidazole, at 323 K. Mass density profile (right) of the 16 zwitterionic metronidazole molecules along the membrane normal.

Individual windows from the umbrella sampling were also analysed to disclose the effect of the location of metronidazole within the membrane on the order parameter of the nearest phospholipids (Figure 7). As in the umbrella sampling simulations metronidazole is located in a defined region of the membrane, it is possible to elucidate which effect metronidazole has on the nearest lipids (metronidazole-lipid distance < 0.9 nm). The range of 0.7 to 2.1 nm from the bilayer center corresponds to the distances where the free energy was negative and, consequently, where the state of metronidazole within the membrane is thermodynamically favourable (see Figure 2, D). The position of metronidazole has a noteworthy impact on the order parameter. The highest effect is observed when metronidazole is at 0.7-1.1 nm from the bilayer center. Overall, the effect is quite pronounced from 0.7 to 1.5 nm, which coincides with the position of the hydrophobic tails (see also Figure A.3 of the supporting information). The effect is less noticeable near the polar heads (from 1.7-2.1 nm).
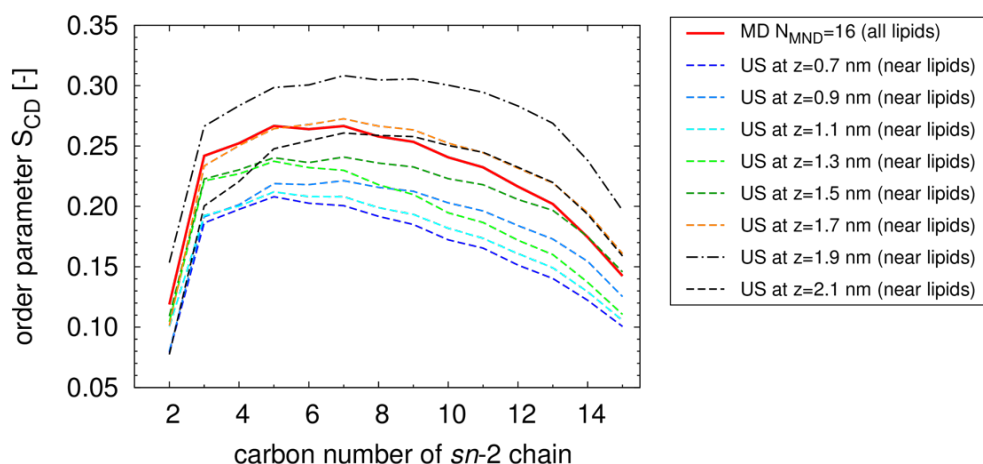
Figure 7. Deuterium order parameter (S_{CD}) profiles along the *sn*-2 tail of the nearest DPPC phospholipids, found in a radius of 0.9 nm around a metronidazole molecule. Umbrella sampling windows (pH 7.4, 323 K), with metronidazole at different *z* positions (here the position of the harmonic restrain is given), were used. The red profile corresponds to the average order of all DPPC phospholipids, after 1 μs of the unbiased simulation.

The orientation of a drug within a membrane can affect its partition, its effect on the biophysical properties of the membrane, and, ultimately, its interaction with specific sites of membrane proteins. The orientation of a drug within a membrane can be assessed by defining a vector to be compared with the normal of the bilayer. For metronidazole, this vector was defined by two carbons on opposite sides of the imidazole ring (Figure 8, left). These atoms were selected for being more rigid than the substituents of the ring. The angle of orientation is parallel to the normal of the bilayer for 0° and 180°. The angle is set to zero when the carbon to which the nitro group is bound is pointing to the bilayer center.

On the other hand, the angle is 90º when it is perpendicular to the normal to the bilayer. The results of the orientation are shown in Figure 8 (right). The maximum of the angle distribution is around 90º in the water phase. This is not a consequence of the preferential orientation of metronidazole in the water phase. Instead, it is based on geometrical reasons. In a homogeneous phase, all orientations have the same probability. However, when using an axis to obtain a relative orientation, an angle of 0º is only obtained for one vector [49]. On the opposite, an angle of 90º is the most probable due to the highest number of possible arrangements. In the region near the polar headgroups ($z \cong 2.0$ nm), the preferential orientation of metronidazole is approximately 30°. One possible explanation is the magnitude of the partial charges on the nitrogen named N3 and the carbon named C2 of the imidazole ring (please see Figure A.4 of the supporting information). The magnitudes of these charges are larger than the charges on the nitro group, which is located on the opposite side of the imidazole ring. Therefore, the C2/N3 side of the imidazole ring can be oriented towards the charges of the zwitterionic polar heads of DPPC. Different orientations are adopted by metronidazole during its penetration into the membrane, with a higher angle near the center of the bilayer. This is because here both sides of the bilayer influence metronidazole, and it will rotate near the center while crossing the membrane.
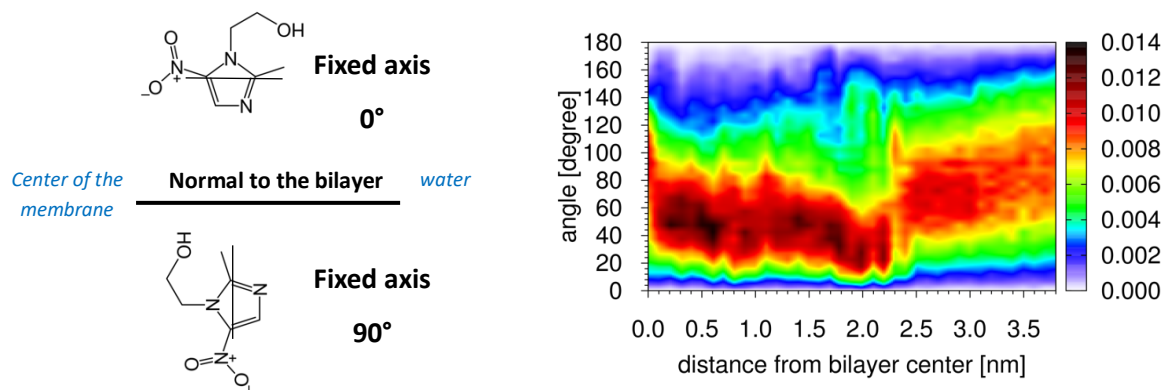
Figure 8. Orientation of metronidazole in function of its position within the membrane. The angle is defined by a fixed axis that crosses two carbon atoms of the imidazole ring (illustrated on the left) and by the bilayer normal. Colour maps indicate angle distribution, coloured from white (lower probability) to black (higher probability).

3.3.3 Interaction of metronidazole with water, DPPC, and ions

Radial distribution functions (RDFs) were calculated to have a deeper understanding of the type of interactions between metronidazole and other molecules of the system. RDFs reflect the probability of finding an atom in the proximity of a reference atom. Since

the RDF is normalized with the ideal gas density, RDF values below one are considered insignificant. In general, four main interactions may occur when metronidazole penetrates the membrane: i) metronidazole – water embedded in the membrane; ii) metronidazole – polar heads of DPPC; iii) metronidazole – hydrophobic chains of DPPC; and iv) metronidazole – ions embedded in the membrane. The last one was not significant since the RDFs were below 1 (data not shown). Hence, it will not be discussed in this paper. The other interactions will be discussed in detail. All main possible interactions were evaluated, and the RDFs of the most significant ones are presented in Figure 9.
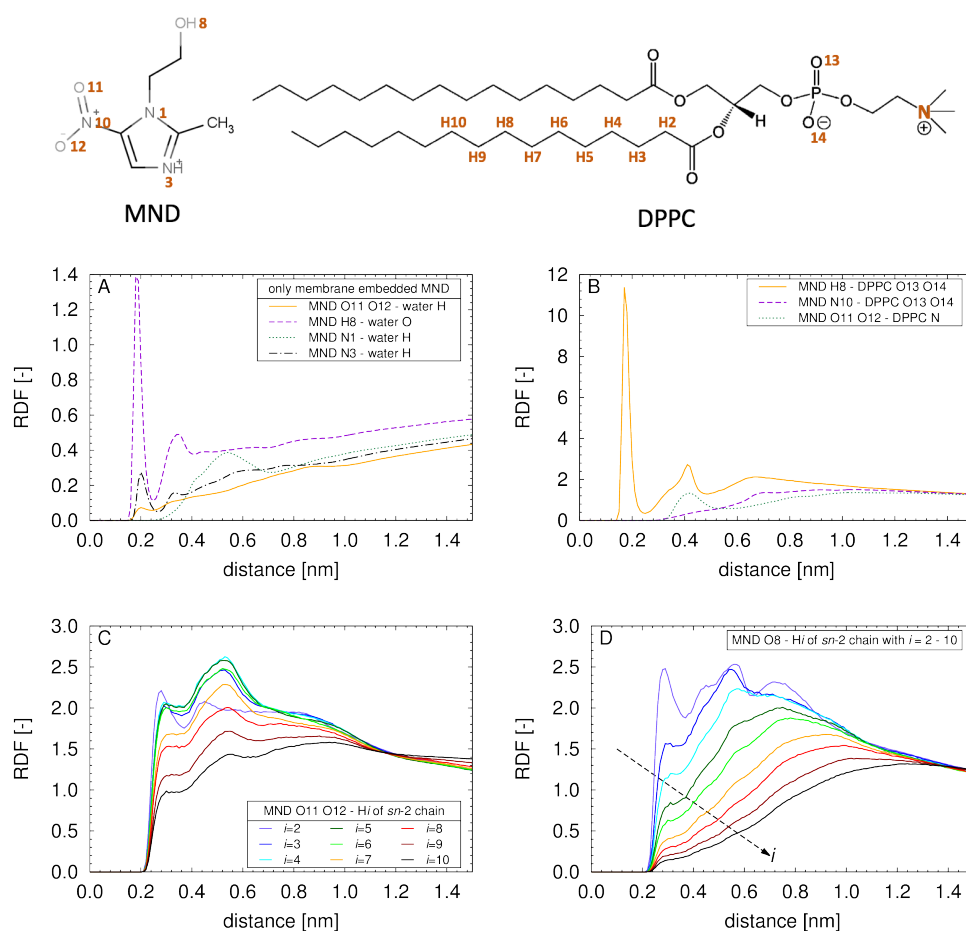
Figure 9. RDFs of the main interactions of metronidazole (MND) within a membrane. A) Metronidazole-water distances, where only metronidazole molecules that are located within the membrane, more specifically, between the center of masses of the phosphor atoms of the two leaflets, were considered. Note that for metronidazole groups in B-D all metronidazole molecules are taken into account. The reference atoms of metronidazole were the oxygen atoms (O11 and O12), the hydrogen of the hydroxyl group (H8), and the nitrogen atoms of the imidazole ring (N1 and N3). B) Distances between metronidazole and polar heads of DPPC. The reference atoms of metronidazole were H8, the nitrogen of the side chain (N10), and the oxygen atoms (O11 and O12). The atoms of the polar heads evaluated were the negative oxygen atoms of the phosphate group (O13 and O14) and the nitrogen group of the choline (N). C and D) Distances between metronidazole and hydrophobic chains of DPPC. The reference atoms of metronidazole were the oxygen atoms: O11 and O12 in C, and O8 in D. Both RDFs (C and D) are relative to the hydrogen atoms bounded to the carbons 2 to 10 of the *sn*-2 chain.

The interaction between metronidazole embedded in the membrane and water plays an important role in a possible perturbation of the hydrophobicity of the membrane [64]. The RDFs of this possible interaction are shown in Figure 9 (A). In general, the possibility of the majority of the interactions is not significant, with RDFs below one. Nevertheless, the interaction between the hydroxyl group of metronidazole and the oxygen of the water molecules within the membrane is noteworthy. Although the height of the first maximum is decreased when compared to the RDF for the water phase (see Figure A.5 of the supporting information), it still reflects a moderate interaction (maximum height of approximately 1.4 at 0.2 nm). This shows proximity and a possible interaction between metronidazole embedded in the membrane and water. Even deeply buried metronidazole shows this type of contact (see Figure A.5 of the supporting information). A deeper penetration of water molecules may destabilize the biophysical properties of the membrane [64]. In long exposures, it can promote the formation of pores [64]. Thus, this type of interactions may be related with drugs toxicity.

Due to its chemical structure (Figure 9, top), the phosphatidylcholine group of DPPC is only a hydrogen bond acceptor. Electrostatic interactions may also play a key role in the interaction with charged molecules, such as metronidazole. Thus, the RDFs of the three possible metronidazole-phosphatidylcholine interactions were determined (Figure 9, B). More specifically, i) between the hydrogen of the hydroxyl group of metronidazole (H8) and the two negative oxygen atoms of the phosphate group of DPPC (O13 and O14); ii) between the positively charged nitrogen of the side chain of metronidazole (N10) and the oxygen atoms (O13 and O14) of DPPC; and iii) between the negative oxygen atoms of metronidazole (O11 and O12) and the charged nitrogen of the amino group of DPPC (N). The last interaction may occur in a moderate extent (RDF > 1 at 0.4 nm). Nevertheless, the main interaction is the first one mentioned (MND H8 – DPPC O13 O14), with a significant RDF of almost 12. We checked for hydrogen bonds using the GROMACS tool g_hbond with the standard criteria (donor-acceptor distance smaller than 0.35 nm and hydrogen-donor-acceptor angle smaller than 30°). On average, 11 $\pm$ 8 % of the 16 metronidazole molecules are forming a hydrogen bond with the phosphate group of DPPC. As two acceptors of DPPC (O13 and O14) are available, we also checked for three-centred hydrogen bonds. It turned out that this type is not relevant, with an occurrence below 0.07 %.

Figure 9 (C) shows the RDFs of the oxygen atoms (O11 and O12) of metronidazole in relation to the hydrogen atoms (H2-H10) bounded to the carbons of the *sn-2* chain of DPPC. The carbons present at the end of the hydrophobic chain (C11-C16) were excluded since their positions coincide with a high free energy. Therefore, the existence of

interactions with these methylene groups is improbable. In addition, Figure 9 (D) shows the RDFs of the oxygen of the hydroxyl group of metronidazole (O8) in relation to the same hydrogen atoms mentioned for the Figure 9 (C) (H2-H10). Both RDFs show that the possibility of interactions is higher with the hydrogens of the first carbons, with narrow peaks at small distances. In the case of interactions with the oxygen atoms (O11 and O12) of metronidazole, the RDFs with the hydrogens of the first eight carbons of the DPPC tail are higher than two at the maximum, which is located at 0.5 nm. The carbons C4 to C8 are located in the region where the local disorder was higher (0.7 – 1.5 nm). Thus, these interactions (MND O11 and O12 – hydrogens of the *sn*-2 chain of DPPC) may play an important role in the disorder effect. On the other hand, the effect on the order parameter is not so pronounced in more superficial hydrogens (H2-H3) even with a higher probability of interaction with metronidazole. For the interaction between the oxygen of the hydroxyl group of metronidazole (O8) and the hydrogens of the *sn*-2 chain of DPPC (Figure 9, D), the shift of the peak of the RDFs to higher distances for deeper hydrogens is graphically visible. This interaction is less probable than the previously mentioned interaction (MND O11 O12 – Hydrogens of the *sn*-2 chain of DPPC, Figure 9, C). Nevertheless, it still happens in a moderate extent.

In summary, the hydroxyl group of the side chain of metronidazole forms interactions with the water embedded in the membrane, with the phosphate group of the DPPC polar heads, and with the hydrogens of the *sn-2* chain of DPPC. Thus, this group may have a key role in the disturbance of the biophysical properties of the DPPC membrane. It is worth mentioning that the oxygen atoms (O11 and O12) of metronidazole are also establishing interactions with the hydrogens of the apolar chains.

4. Conclusions

As metronidazole can be administered by the oral route, the interaction with biological membranes at different pHs is a key issue for its absorption. At acidic pH, the hydrophilic character of metronidazole may imply a lower absorption at the stomach and a subsequent higher absorption at the intestine, leading to a systemic distribution. At pH 7.4, metronidazole has a higher affinity to the membrane. Nevertheless, the penetration of metronidazole is associated with a disturbance of the order and the packing of the phospholipids. This biophysical perturbation was already referred as one of the toxic mechanisms of several drugs [60, 61]. MD simulations showed that the hydroxyl group of metronidazole is important for the interactions with water molecules embedded in the membrane. Thus, the partitioning of metronidazole promotes the penetration of water

molecules, which can be associated with a decrease of the hydrophobicity of the membrane and a destabilization of its biophysical properties [64]. The hydroxyl group of metronidazole also forms interactions with the phosphate group of the DPPC polar heads. In addition, the oxygen atoms bounded to the nitrogen of the side chain of metronidazole are important for the partitioning of metronidazole, by forming interactions with the hydrogens of the hydrophobic chains.

The nitroimidazole ring of metronidazole is essential for its mechanism of action [40]. Our results show that substituents of the side chain of metronidazole are important for its interaction with phosphatidylcholine lipid membranes and, consequently, for the disturbance of the membrane. Several studies have been trying to develop new imidazole derivatives (e.g., [65-67]). Ultimately, the structure-toxicity relationship of metronidazole within phosphatidylcholine membranes can provide new insights for the modification and design of new imidazole derivatives with lower toxicity.

Acknowledgments

References

[1] Meyler's Side Effects of Drugs: The international Encyclopedia of Adverse Drug Reactions and Interactions, 15th ed., Elsevier, 2006.

[2] J.E. Bennett, R. Dolin, M.J. Blaser, Principles and Practise of Infectious Diseases, Eighth ed., Elsevier, Philadelphia, 2015.

[3] P. Malfertheiner, F. Megraud, C.A. O'Morain, J. Atherton, A.T. Axon, F. Bazzoli, G.F. Gensini, J.P. Gisbert, D.Y. Graham, T. Rokkas, E.M. El-Omar, E.J. Kuipers, Management of *Helicobacter pylori* infection: the Maastricht IV/ Florence Consensus Report, Gut, 61 (2012) 646-664.

[4] D. Lopes, C. Nunes, M.C. Martins, B. Sarmento, S. Reis, Eradication of *Helicobacter pylori*: Past, Present and Future, J. Control. Release, 189 (2014) 169-186.

[5] A. Kuriyama, J.L. Jackson, A. Doi, T. Kamiya, Metronidazole-Induced Central Nervous System Toxicity: A Systematic Review, Clin. Neuropharmacol., 34 (2011) 241-247.

[6] A. Bendesky, D. Menéndez, P. Ostrosky-Wegman, Is Metronidazole Carcinogenic?, Mutat. Res., 511 (2002) 133-144.

[7] C. Peetla, A. Stine, V. Labhasetwar, Biophysics Interactions with Model Lipid Membranes: Applications in Drug Discovery and Drug Delivery, Molecular Pharmaceutics, 6 (2009) 1264-1276.

[8] D. Lopes, S. Jakobtorweihen, C. Nunes, B. Sarmento, S. Reis, Shedding Light on the Puzzle of Drug-Membrane Interactions: Experimental Techniques and Molecular Dynamics Simulations, Prog. Lipid Res., 65 (2017) 24-44.

[9] M. Lúcio, C. Nunes, J. Lima, S. Reis, A biophysical Aproach to the Study of the Therapeutic and Toxic Effects of Non-steroidal Anti-inflammatory Drugs, in: A. Jurado (Ed.) A toxicological/pharmacological Approach to Chemico-Biological Interactions at a Membrane level, Transworld Research Network, 2012.

[10] W. Bernhard, A.D. Postle, M. Linck, K.-F. Sewing, Composition of Phospholipid Classes and Phosphatidylcholine Molecular Species of Gastric Mucosa and Mucus., Biochim. Biophys. Acta, 1255 (1995) 99-104.

[11] F. Gambinossi, M. Puggelli, G. Gabrielli, Enzymatic Hydrolisis Reaction of Phospholipids in Monolayers, Colloids Surf. B Biointerfaces, 23 (2002) 273-281.

[12] D. Lopes, C. Nunes, P. Fontaine, B. Sarmento, S. Reis, Proof of Pore Formation and Biophysical Perturbations through a 2D Amoxicillin-Lipid Membrane Interaction Approach, Biochim. Biophys. Acta, Biomembr., 1859 (2017) 803-812.

[13] A. Allen, G. Flemstrom, Gastroduodenal Mucus Bicarbonate Barrier: Protection Against Acid and Pepsin, Am. J. Physiol. Cell Physiol., 288 (2005) C1-19.

[14] A.F. Goddard, M.J. Jessa, D.A. Barrett, P.N. Shaw, J.-P. Idstrom, C. Cederberg, R.C. Spiller, Effect of Omeprazole on the Distribution of Metronidazole, Amoxicillin, and Clarithromycin in Human Gastric Juice, Gastroenterology, 111 (1996) 358-367.

[15] H. Nakahara, S. Lee, Y. Shoyama, O. Shibata, The Role of Palmitic Acid in Pulmonary Surfactant Systems by Langmuir Monolayer Study: Lipid–Peptide Interactions, Soft Matter, 7 (2011) 11351.

[16] P.V. Escriba, Membrane-lipid Therapy: a New Approach in Molecular Medicine, Trends Mol. Med., 12 (2006) 34-43.

[17] M. Eeman, M. Deleu, From biological Membranes to Biomimetic Model Membranes, Biotechnol. Agron. Soc. Environ., 14 (2010) 719-726.

[18] Partition Coefficient (n-octanol/water): Shake Flask Method, in, Organisation for Economic Co-operation and Development (OECD), 1995.

[19] C. Pereira-Leite, C. Nunes, J.L. Lima, S. Reis, M. Lucio, Interaction of Celecoxib with Membranes: the Role of Membrane Biophysics on its Therapeutic and Toxic Effects, J. Phys. Chem. B, 116 (2012) 13608-13617.

[20] L.M. Magalhaes, C. Nunes, M. Lucio, M.A. Segundo, S. Reis, J.L. Lima, High-throughput Microplate Assay for the Determination of Drug Partition Coefficients, Nat. Protoc., 5 (2010) 1823-1830.

[21] C. Nunes, G. Brezesinski, C. Pereira-Leite, J.L. Lima, S. Reis, M. Lucio, NSAIDs Interactions with Membranes: a Biophysical Approach, Langmuir, 27 (2011) 10847-10858.

[22] M. Pinheiro, M. Arede, J.J. Giner-Casares, C. Nunes, J.M. Caio, C. Moiteiro, M. Lucio, L. Camacho, S. Reis, Effects of a Novel Antimycobacterial Compound on the Biophysical Properties of a Pulmonary Surfactant Model Membrane, Int. J. Pharm., 450 (2013) 268-277.

[23] E.L. Wu, X. Cheng, S. Jo, H. Rui, K.C. Song, E.M. Davila-Contreras, Y. Qi, J. Lee, V. Monje-Galvan, R.M. Venable, J.B. Klauda, W. Im, CHARMM-GUI Membrane Builder Toward Realistic Biological Membrane Simulations, J. Comput. Chem., 35 (2014) 1997-2004.

[24] B. Hess, C. Kutzner, D. van der Spoel, E. Lindahl, GROMACS 4: Algorithms for Highly Efficient, Load-Balanced, and Scalable Molecular Simulation, J. Chem. Theory Comput., 4 (2008) 435-447.

[25] S. Pronk, S. Pall, R. Schulz, P. Larsson, P. Bjelkmar, R. Apostolov, M.R. Shirts, J.C. Smith, P.M. Kasson, D. van der Spoel, B. Hess, E. Lindahl, GROMACS 4.5: a High-Throughput and Highly Parallel Open Source Molecular Simulation Toolkit, Bioinformatics, 29 (2013) 845-854.

[26] M. Parrinello, Polymorphic Transitions in Single Crystals: A New Molecular Dynamics Method, J. Appl. Phys., 52 (1981) 7182.

[27] S. Nosé, M.L. Klein, Constant Pressure Molecular Dynamics for Molecular Systems, Mol. Phys., 50 (2006) 1055-1076.

[28] G.J. Martyna, M.E. Tuckerman, D.J. Tobias, M.L. Klein, Explicit Reversible Integrators for Extended Systems Dynamics, Mol. Phys., 87 (1996) 1117-1157.

[29] T. Darden, D. York, L. Pedersen, Particle mesh Ewald: An N·log(N) method for Ewald sums in large systems, J. Chem. Phys., 98 (1993) 10089.

[30] U. Essmann, L. Perera, M.L. Berkowitz, T. Darden, H. Lee, L.G. Pedersen, A smooth Particle Mesh Ewald Method, J. Chem. Phys., 103 (1995) 8577.

[31] J. Kästner, Umbrella Sampling, Wiley Interdiscip. Rev.: Comput. Mol. Sci., 1 (2011) 932-942.

[32] G.M. Torrie, J.P. Valleau, Monte Carlo Free Energy Estimates Using Non-Boltzmann Sampling: Application to the sub-Critical Lennard-Jones Fluid, Chem. Phys. Lett., 28 (1974) 578-581.

[33] G.M. Torrie, J.P. Valleau, Nonphysical Sampling Distributions in Monte Carlo Free-Energy Estimation: Umbrella Sampling, J. Comput. Phys,., 23 (1977) 187-199.

[34] J.L. MacCallum, W.F. Bennett, D.P. Tieleman, Distribution of Amino Acids in a Lipid Bilayer from Computer Simulations, Biophys. J., 94 (2008) 3393-3404.

[35] S. Kumar, D. Bouzida, R.H. Swendsen, P.A. Kollman, J.M. Rosenberg, The Weighted Histogram Analysis Method for Free-Energy Calculations on Biomolecules. I. The Method, J. Comput. Chem., 13 (1992) 1011-1021.

[36] M. Souaille, B. Roux, Extension to the Weighted Histogram Analysis Method: Combining Umbrella Sampling with Free Energy Calculations, Comput. Phys. Commun., 135 (2001) 40-57.

[37] J.S. Hub, B.L.d. Groot, D.v.d. Spoel, g_wham - A Free Weighted Histogram Analysis Implementation Including Robust Error and Autocorrelation Estimates, J. Chem. Theory Comput., 6 (2010) 3713-3720.

[38] C. Neale, W.F. Bennett, D.P. Tieleman, R. Pomes, Statistical Convergence of Equilibrium Properties in Simulations of Molecular Solutes Embedded in Lipid Bilayers, J. Chem. Theory Comput., 7 (2011) 4175-4188.

[39] M. Paloncyova, K. Berka, M. Otyepka, Convergence of Free Energy Profile of Coumarin in Lipid Bilayer, J. Chem. Theory Comput., 8 (2012) 1200-1211.

[40] R.J. Anderson, P.W. Groundwater, A. Todd, A.J. Worsley, Antibacterial Agents: Chemistry, Mode of Action, Mechanisms of Resistance and Clinical Applications, Wiley, Chichester, 2012.

[41] M. Pinheiro, M. Arede, C. Nunes, J.M. Caio, C. Moiteiro, M. Lucio, S. Reis, Differential Interactions of Rifabutin with Human and Bacterial Membranes: Implication for its Therapeutic and Toxic Effects, J. Med. Chem., 56 (2013) 417-426.

[42] A.D. MacKerell, D. Bashford, M. Bellott, R.L. Dunbrack, J.D. Evanseck, M.J. Field, S. Fischer, J. Gao, H. Guo, S. Ha, D. Joseph-McCarthy, L. Kuchnir, K. Kuczera, F.T.K. Lau, C. Mattos, S. Michnick, T. Ngo, D.T. Nguyen, B. Prodhom, W.E. Reiher, B. Roux, M. Schlenkrich, J.C. Smith, R. Stote, J. Straub, M. Watanabe, J. Wiórkiewicz-Kuczera, D. Yin, M. Karplus, All-Atom Empirical Potential for Molecular Modeling and Dynamics Studies of Proteins, J. Phys. Chem. B, 102 (1998) 3586-3616.

[43] J.B. Klauda, R.M. Venable, J.A. Freites, J.W. O'Connor, D.J. Tobias, C. Mondragon-Ramirez, I. Vorobyov, A.D. MacKerell, R.W. Pastor, Update of the CHARMM All-Atom Additive Force Field for Lipids: Validation on Six Lipid Types, J. Phys. Chem. B, 114 (2010) 7830-7843.

[44] R.M. Venable, Y. Luo, K. Gawrisch, B. Roux, R.W. Pastor, Simulations of Anionic Lipid Membranes: Development of Interaction-Specific Ion Parameters and Validation using NMR Data, J. Phys. Chem. B, 117 (2013) 10183-10192.

[45] K. Vanommeslaeghe, E. Hatcher, C. Acharya, S. Kundu, S. Zhong, J. Shim, E. Darian, O. Guvench, P. Lopes, I. Vorobyov, A.D. Mackerell, Jr., CHARMM General Force Field: A Force Field for Drug-Like Molecules Compatible With the CHARMM All-atom Additive Biological Force Fields, J. Comput. Chem., 31 (2010) 671-690.

[46] K. Vanommeslaeghe, A.D. MacKerell, Jr., Automation of the CHARMM General Force Field (CGenFF) I: bond perception and atom typing, J. Chem. Inf. Model., 52 (2012) 3144-3154.

[47] K. Vanommeslaeghe, E.P. Raman, A.D. MacKerell, Jr., Automation of the CHARMM General Force Field (CGenFF) II: assignment of bonded parameters and partial atomic charges, J. Chem. Inf. Model., 52 (2012) 3155-3168.

[48] L. Huang, B. Roux, Automated Force Field Parameterization for Non-Polarizable and Polarizable Atomic Models Based on Ab Initio Target Data, J. Chem. Theory Comput., 9 (2013).

[49] S. Jakobtorweihen, A.C. Zuniga, T. Ingram, T. Gerlach, F.J. Keil, I. Smirnova, Predicting Solute Partitioning in Lipid Bilayers: Free Energies and Partition Coefficients from Molecular Dynamics Simulations and COSMOmic, J. Chem. Phys., 141 (2014) 045102.

[50] A. Klamt, U. Huniar, S. Spycher, J. Keldenich, COSMOmic: A Mechanistic Approach to the Calculation of Membrane-Water Partition Coefficients and Internal Distributions within Membranes and Micelles, J. Phys. Chem. B, 112 (2008) 12148-12157.

[51] K. Bittermann, S. Spycher, K.U. Goss, Comparison of Different Models Predicting the Phospholipid-Membrane Water Partition Coefficients of Charged Compounds, Chemosphere, 144 (2016) 382-391.

[52] G.P. van Balen, C. Martinet, G. Caron, G. Bouchard, M. Reist, P.A. Carrupt, R. Fruttero, A. Gasco, B. Testa, Liposome/water lipophilicity: methods, information content, and pharmaceutical applications, Med. Res. Rev., 24 (2004) 299-324.

[53] N.C. Santos, M. Prieto, M.A.R.B. Castanho, Quantifying Molecular Partition into Model Systems of biomembranes: an Emphasis on Optical Spectroscopic Methods, Biochim. Biophys. Acta, 1612 (2003) 123-135.

[54] B.d. Castro, P. Gameiro, J.L.F.C. Lima, C. Matos, S. Reis, A Fast and Reliable Spectroscopic Method for the Determination of Membrane-Water Partition Coefficients of Organic Compounds, Lipids, 36 (2001) 89-96.

[55] R. Koynova, A. Koumanov, B. Tenchov, Metastable Ripple Gel Phase in Saturated Phosphatidylcholine: Calorimetric and Densitometric Characterization, Biochim. Biophys. Acta, 1285 (1996) 101-108.

[56] R. Mendelsohn, G. Mao, C.R. Flach, Infrared Reflection-Absorption Spectroscopy: Principles and Applications to Lipid-Protein Interaction in Langmuir Films, Biochim. Biophys. Acta, Biomembr., 1798 (2010) 788-800.

[57] V.M. Kaganer, H. Möhwald, P. Dutta, Structure and Phase Transitions in Langmuir Monolayers, Rev. Mod. Phys., 71 (1999) 779-819.

[58] L. Buehler, Cell Membranes, Garland Science Taylor & Francis Group, 2015.

[59] Z. Wang, X. Li, S. Yang, Studies of Dipalmitoylphosphatidylcholine (DPPC) Monolayers Embedded with endohedral metallofullerene (Dy@C82), Langmuir, 25 (2009) 12968-12973.

[60] C. Pereira-Leite, C. Nunes, S. Reis, Interaction of Nonsteroidal Anti-inflammatory Drugs with Membranes: *In Vitro* Assessment and Relevance for their Biological Actions, Prog. Lipid Res., 52 (2013) 571-584.

236

[61] A.C. Alves, D. Ribeiro, C. Nunes, S. Reis, Biophysics in Cancer: The Relevance of Drug-Membrane Interaction studies, Biochim. Biophys. Acta, Biomembr., 1858 (2016) 2231-2244.

[62] H. Khandelia, S. Witzke, O.G. Mouritsen, Interaction of Salicylate and a Terpenoid Plant Extract with Model Membranes: Reconciling Experiments and Simulations, Biophys. J., 99 (2010) 3887-3894.

[63] R.A. Bockmann, A.H. Hac, Thomas Grubmuller, Helmut Effect of Sodium Chloride on a Lipid Bilayer, Biophys. J., 85 (2003) 1647-1655.

[64] M. Markiewicz, M. Pasenkiewicz-Gierula, Comparative Model Studies of Gastric Toxicity of Nonsteroidal Anti-inflammatory Drugs, Langmuir, 27 (2011) 6950-6961.

[65] K. Bowden, J. Izadi, Multifunctional Derivatives of Metronidazole, Il farmaco, 53 (1998) 58-61.

[66] A.J. Atia, Synthesis and Antibacterial Activities of new Metronidazole and Imidazole Derivatives, Molecules, 14 (2009) 2431-2446.

[67] D.Y. Alawadi, H.A. Saadeh, H. Kaur, K. Goyal, R. Sehgal, T. Ben Hadda, N.A. ElSawy, M.S. Mubarak, Metronidazole Derivatives as a New Class of Antiparasitic Agents: Synthesis, Prediction of Biological Activity, and Molecular Properties, Med. Chem. Res., 24 (2014) 1196-1209.

Chapter 6.3

Supporting information
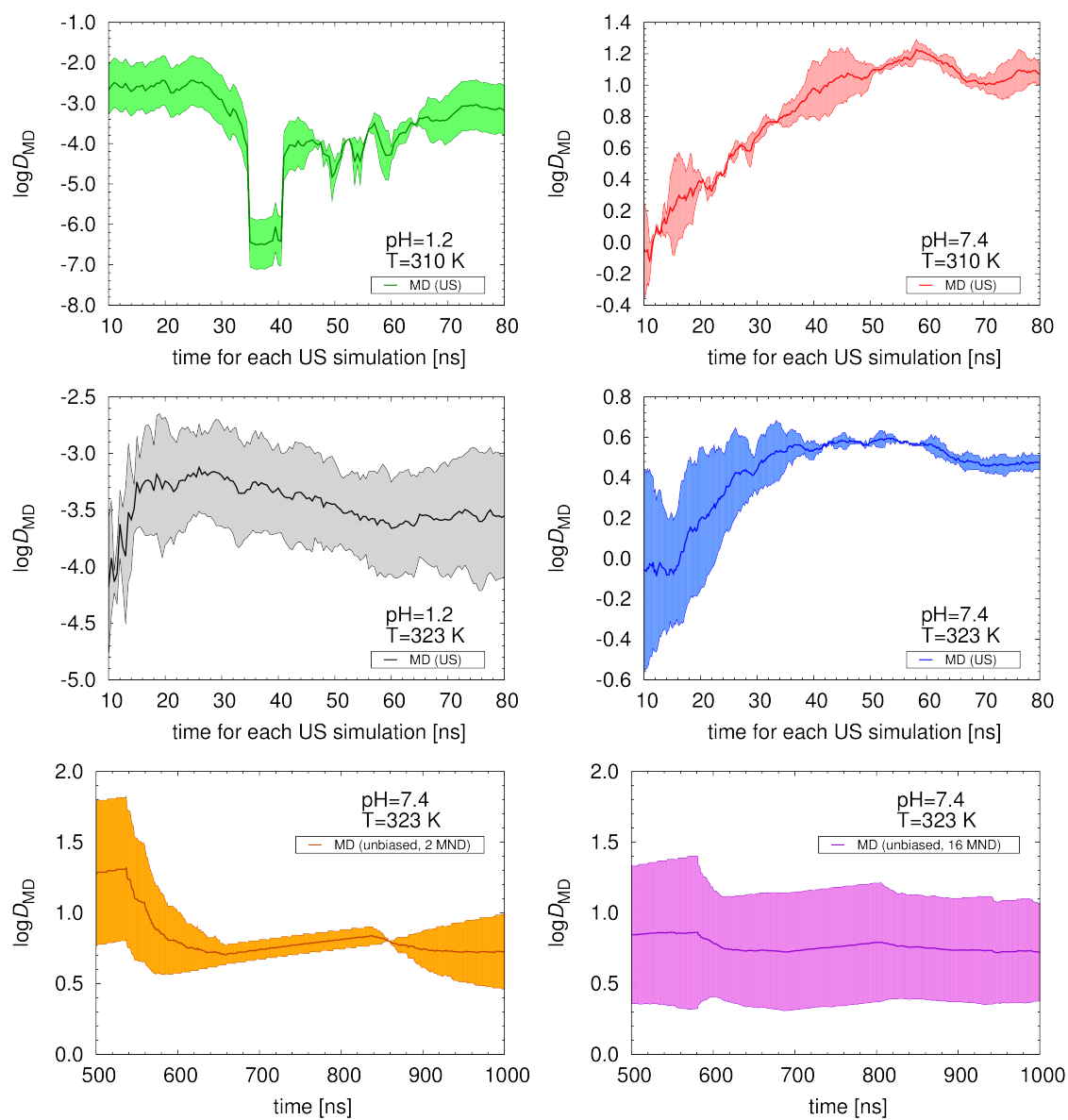
Figure A.1. Partition coefficients over the simulation time for all modelled systems: pH 1.2, 310 K (A); pH 1.2, 323 K (B); pH 7.4, 310 K (C); pH 7.4, 323 K (D and E). A-D were taken from umbrella sampling simulations, and E was obtained from an unbiased simulation. The average of two independent metronidazole molecules were considered, and the colored areas show the error margin of the results.

Validation of the modelled membrane

The area per lipid is the average area occupied by one lipid, and it is one of the most important characterization features. In fact, it changes depending on the bilayer structure, on their charge, and on the saturation of the hydrophobic tails [1], Both the modelled and the experimental areas per lipid are shown in Table S1. At pH 1.2, the area per lipid obtained by MD simulations is 0.046 nm^2 higher than the experimental value. This difference is lower than the range of experimental areas found in different sources, as presented for pH 7.4. Note for pH 1.2 only one experimental value is available [2]. At physiological pH, the areas per lipid obtained by MD simulations are in the range of the experimental values.

Table A.1. Modelled (MD) and experimental (exp.) areas per lipid (A_L), at two different pHs (pH 1.2 and pH 7.4) and two different lipid phases, namely gel (298 K) and liquid-crystalline phase (323 K).

T [K]	pH	A_L MD [nm^2]	A_L exp. [nm^2]
298	1.2	0.551	0.505 [2]
298	7.4	0.529	0.486 – 0.523 [3]
323	7.4	0.601	0.57 – 0.712 [3]

Another important feature is the packing of the membrane, which depends on the temperature. The main transition temperature of DPPC is around 313 K [4]. Thus, a pre-transition phase characterized by a ripple and a liquid-crystalline phase should be modelled at 310 K and 323 K, respectively [5]. The simulated order parameters of the membrane in the liquid-crystalline phase at pH 7.4 are in good agreement with the order determined experimentally (Fig. S1).
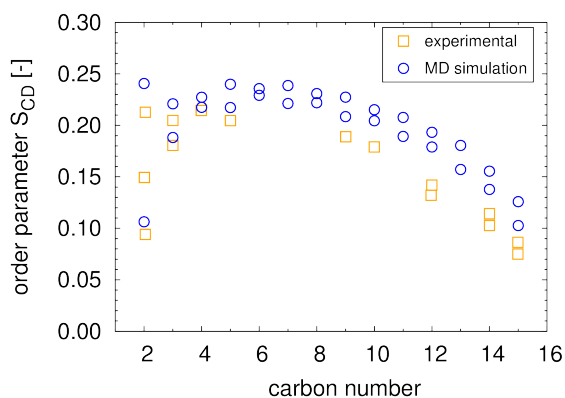
Figure A.2. Modeled (MD) and experimental [6] order parameter profiles of the CH$_2$ groups along the hydrophobic tails, for pH 7.4 and *T*=323 K.

Mass density profiles along the membrane normal
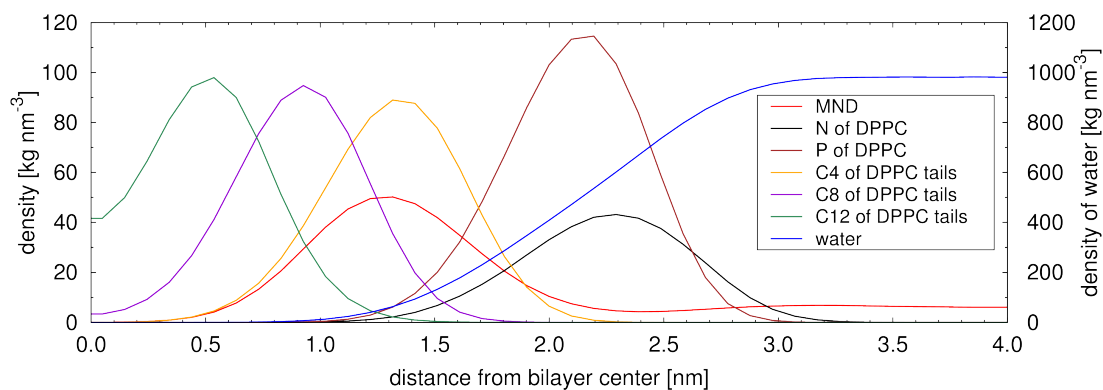
Figure A.3. Mass density profiles along the membrane normal shown for one leaflet of the bilayer. Calculated from the MD simulation with 16 metronidazole (MND) molecules (T=323 K, pH 7.4). Distribution of metronidazole, water and some selected atom groups of DPPC are shown.

Partial charges of metronidazole
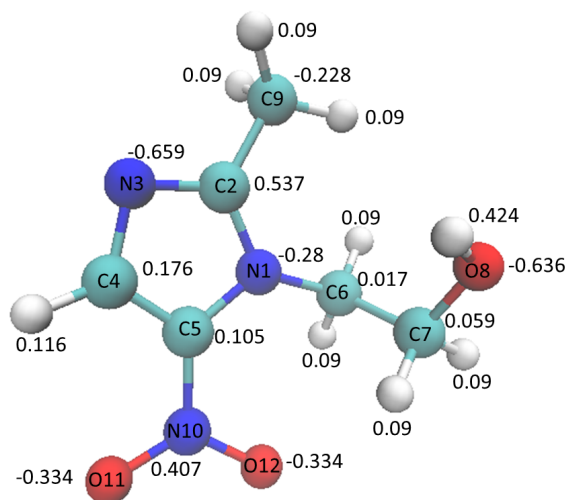
Figure A.4. Partial charges, calculated with GAAMP [7], of zwitterionic metronidazole as used in the MD simulations. The atoms are colored according to their atom type (carbon in cyan, hydrogen in white, oxygen in red, and nitrogen in blue), and names are assigned to all non-hydrogen atoms.

RDFs of metronidazole-water interactions
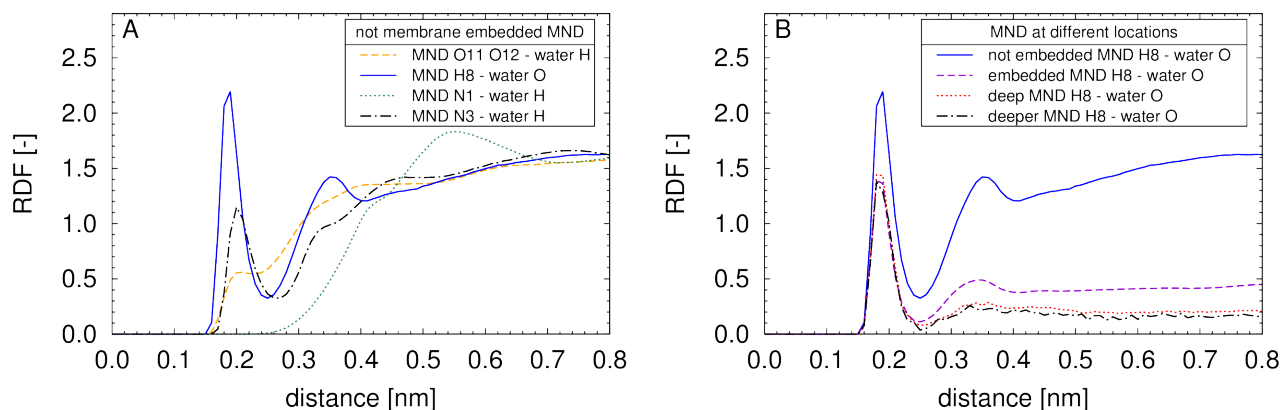
Figure A.5. RDFs of metronidazole (MND): (A) MND - water distances, where only MND molecules that are located outside the membrane (outside the boundaries formed by the center of masses of phosphor atoms of the two leaflets) were considered. Hence, only the MND molecules that are not considered for Figure 9 A are considered here. The reference atoms of metronidazole were the oxygen atoms (O11 and O12), the hydrogen of the hydroxyl group (H8), and the nitrogen atoms of the imidazole ring (N1 and N3) (see also Figure 9). (B) MND (at different positions) – water distances, when: i) only MND molecules that are outside the membrane are considered (solid blue, which is the same line as shown in A); ii) only MND molecules embedded in the membrane are taken into account (dashed purple, which is the same line as in Figure 9 A); iii) only MND molecules that are deeper in the membrane are considered (dotted red, when MND molecules are between the center of masses of the C12 atoms of the hydrophobic tails of the two leaflets; and dashed dotted black, when MND molecules are located even deeper inside the membrane, namely, between the center of masses of the C14 atoms of the hydrophobic tails of the two leaflets).

References

[1] T. Hianik, Structure and Physical properties of Biomembranes and Model Membranes, Acta Physica Slovaca, 56 (2006) 687-805.

[2] D. Lopes, C. Nunes, P. Fontaine, B. Sarmento, S. Reis, Proof of Pore Formation and Biophysical Perturbations through a 2D Amoxicillin-Lipid Membrane Interaction Approach, Biochim. Biophys. Acta, Biomembr., 1859 (2017) 803-812.

[3] J.F. Nagle, S. Tristam-Nagle, Structure of Lipid Bilayers, Biochim. Biophys. Acta, 1469 (2000) 159-195.

[4] C. Nunes, G. Brezesinski, C. Pereira-Leite, J.L. Lima, S. Reis, M. Lucio, NSAIDs Interactions with Membranes: a Biophysical Approach, Langmuir, 27 (2011) 10847-10858.

[5] J. Katsaras, S. Tristram-Nagle, Y. Liu, R.L. Headrick, E. Fontes, Clarification of the Ripple Phase of Lecithin Bilayers using Fully Hydrated, Aligned Samples, Phys. Rev. E, 61 (2000) 5668-5677.

[6] J.B. Klauda, R.M. Venable, J.A. Freites, J.W. O'Connor, D.J. Tobias, C. Mondragon-Ramirez, I. Vorobyov, A.D. MacKerell, R.W. Pastor, Update of the CHARMM All-Atom Additive Force Field for Lipids: Validation on Six Lipid Types, J. Phys. Chem. B, 114 (2010) 7830-7843.

[7] L. Huang, B. Roux, Automated Force Field Parameterization for Non-Polarizable and Polarizable Atomic Models Based on Ab Initio Target Data, J. Chem. Theory Comput., 9 (2013).

Chapter 6.4

Proof of pore formation and biophysical perturbations through a 2D amoxicillin-lipid membrane interaction approach

This work was designed within the first objective. The association between the gastrointestinal and renal toxicity of amoxicillin with lower pH values had been reported. Since the pH affects the protonation state of both amoxicillin and the polar heads of some phospholipids, this work was design to assess the effect of pH on drug-lipid membrane interactions.
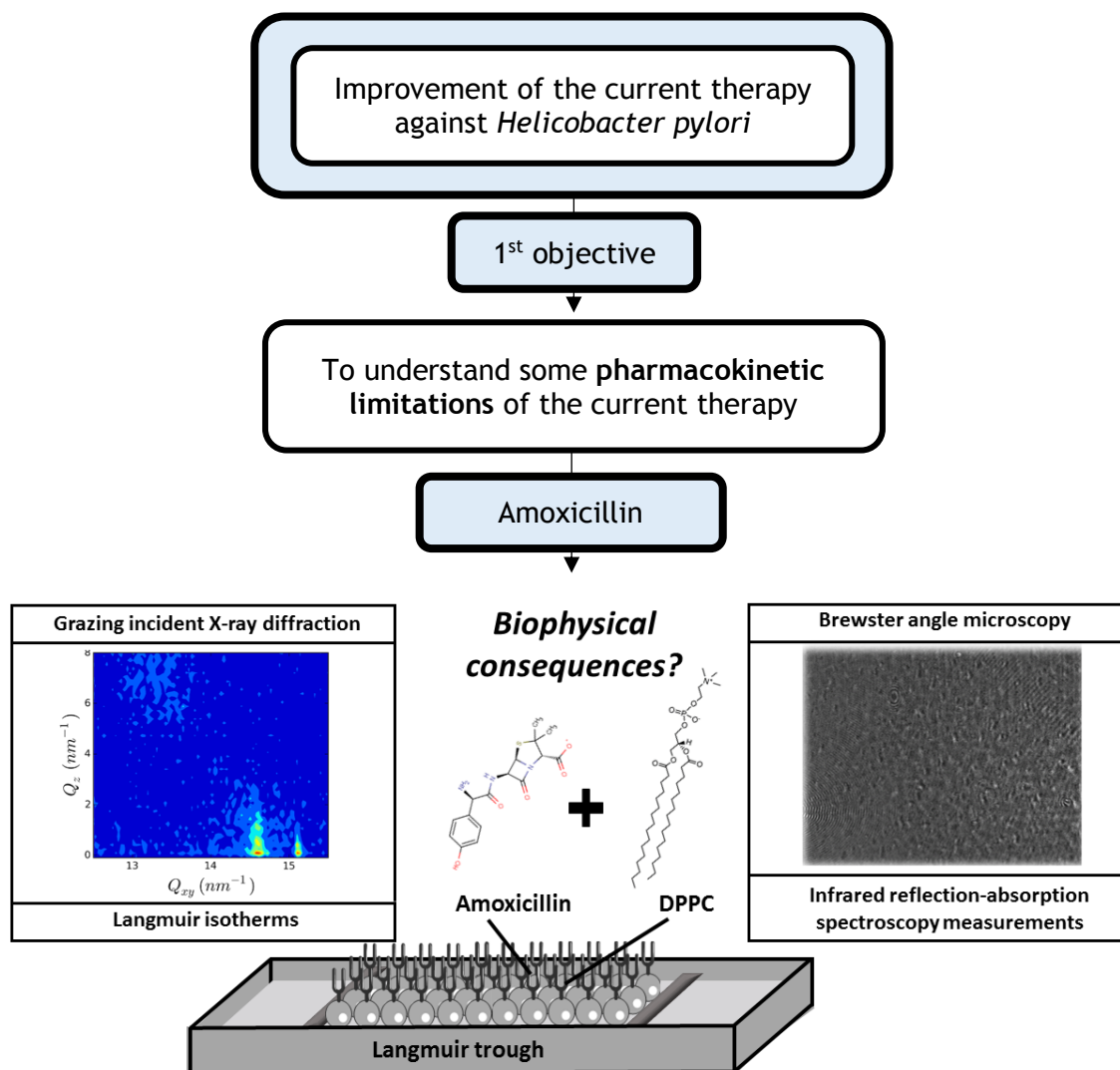
Proof of pore formation and biophysical perturbations through a 2D amoxicillin-lipid membrane interaction approach

CrossMark

Daniela Lopes [a], Cláudia Nunes [a], Philippe Fontaine [b], Bruno Sarmento [c,d], Salette Reis [a,*]

[a] UCIBIO, REQUIMTE, Departamento de Ciências Químicas, Faculdade de Farmácia, Universidade do Porto, Portugal
[b] Synchrotron SOLEIL, L'Orme des Merisiers, Saint Aubin, BP48, 91192, Gif-sur-Yvette, France
[c] I3S, Instituto de Investigação e Inovação em Saúde and INEB – Instituto de Engenharia Biomédica, Portugal
[d] CESPU, Instituto de Investigação e Formação Avançada em Ciências e Tecnologias da Saúde, Portugal

ARTICLE INFO

ABSTRACT

Amoxicillin is a worldwide used antibiotic, and it is classified as a first-line drug against *Helicobacter pylori* gastric infections. However, the current treatment of these infections has several limitations, such as the side effects and the low therapeutic compliance. Amoxicillin has been associated with gastrointestinal and renal side effects, with higher toxicity when the pH is lower. By considering this association and the well-known pH gradient of the gastric mucosa, this work aims to evaluate the influence of pH on the toxicity of amoxicillin. For that purpose, 1,2-dipalmitoyl-*sn*-glycero-3-phosphocholine (DPPC) monolayers were used since phosphatidylcholines are the most common phospholipid headgroup of biological membranes. To have insight of the effects of amoxicillin, different techniques were employed, namely, isotherm measurements, infrared reflection-absorption spectroscopy, grazing incident X-ray diffraction and Brewster angle microscopy. The monolayers of DPPC spread onto different buffer solutions (pH 1.2, pH 5 and pH 7.4) showed different structural and packing properties. The interaction with amoxicillin also depended on the pH. At pH 7.4, the highest effect was visualized at lower pressures, with partial restoration of the biophysical properties of the monolayer at 30 mN.m^{-1}. A higher perturbation is shown at acidic pH, in which pores were visualized by Brewster angle microscopy. These perturbations may ultimately be related with amoxicillin toxicity.

© 2017 Elsevier B.V. All rights reserved.

1. Introduction

Amoxicillin (AMX) is a semi-synthetic antibiotic that belongs to the penicillin group due to its molecular structure composed of a β-lactam ring and a thiazolidine ring. Its mechanism of action relies on the inhibition of bacterial enzymes that are involved in the synthesis of the bacterial cell wall [1]. Consequently, it can promote the lysis and the death of several bacteria [1]. AMX is used worldwide and it is reported as the most often prescribed antibiotic in 22 of the 30 European Union countries [2]. Moreover, in the United States, it has been in the top 3 of the antibiotics prescribed to people aged 65 or over [3]. In a worldwide perspective, broad-spectrum penicillins have been the most used class of antibiotics [3].

AMX is considered a first-line drug against different bacterial infections, such as against *Helicobacter pylori (H. pylori)* [4]. These bacteria

were classified as a human carcinogenic (group I) by the World Health Organization [5]. However, there are still several efforts to be made to overcome the limitations of the current treatment plan [6]. As a consequence of the location of *H. pylori in vivo*, antibiotics have to cross the mucus layer to reach the bacterium on the epithelium layer [6]. Nevertheless, this is hindered by the low diffusion rate of antibiotics and their low residence time in the stomach [6]. Another limitation is the presence of gastrointestinal side effects, such as abdominal pain, nausea and vomiting, that lead to lower therapeutic compliance [1,6]. Furthermore, AMX and other β-lactam antibiotics have also been associated with renal toxicity [1,7]. Its relation with urine pH was already reported, with higher toxicity when the pH is lower [7]. By considering this association and knowing the well-recognized pH gradient of the gastric mucosa [8], our hypothesis is that the pH may affect AMX toxicity. Therefore, it is important to evaluate the perturbation of the biophysical properties of membranes after their interaction with the drug at different pHs.

The present study encompasses the evaluation of the biophysical consequences on the phospholipids present on the mucus layer after their interaction with AMX. For that purpose, monolayers at the air/liquid interface were used as a simplified membrane model, to avoid the interference of trans-bilayer events and to maintain the properties of

245

biomembranes [9]. Both the phospholipid composition and the pH were selected according to the aim of the study. Phosphatidylcholines are the main headgroup of the phospholipids in the gastric mucosa and in the mucus layer [10]. Moreover, unsaturated phospholipids are more common than the saturated ones [10]. Nevertheless, the purpose of the study encompasses the study of the effect of AMX in different lipid phases. Therefore, dipalmitoylphosphatidylcholine (DPPC) was selected due to its surface pressure-area (π-A) isotherm, with well-defined lipid phases. In the π-A isotherms of unsaturated phospholipids, such as palmitoyloleoylphosphatidylcholines, defined lipid phases are not visualized [11]. Thus, the effect of AMX on the different lipid phases would be impossible to evaluate. DPPC has also been used to study the gastric toxicity of nonsteroidal anti-inflammatory drugs [12], which facilitates the access to data for comparison.

The mucus layer has a protective mechanism, which is its ability to resist to proton diffusion [8]. This creates a pH gradient from acid in the stomach lumen to neutral near the epithelial cells [8]. Consequently, the pH can vary from 1 to 2, especially when the mucus layer is injured (e.g., in *H. pylori* infections), to almost physiological pH (pH 7.4) near epithelial cells [13]. The neutral pH is also maintained by the secretion of the urease by *H. pylori* [14]. In this study, three different pHs will be evaluated, namely, pH 1.2, pH 5 and pH 7.4, to cover the extremes of the pH gradient. The gastrointestinal pH gradient that AMX crosses *in vivo* affects its protonation state since AMX has two ionisable groups (viz. an amino and a carboxyl group). Thus, there are different species of AMX *in vivo*, depending on the pH (Fig. 1). Despite the role of the acid-base characteristics of AMX in its interaction with charged membranes, such as a DPPC membrane, these properties have barely been studied. In fact, DPPC also changes its protonation state depending on the pH, with 80% positively charged at pH 1.2 and almost 100% in a zwitterionic state at both pH 5 and pH 7.4 (data ChemAxon®, MarvinSketch application, version 15.4.13.0).

Using the same membrane model, different techniques were performed: (i) isotherm measurements, (ii) polarization modulation infrared reflection-absorption spectroscopy (PM-IRRAS), (iii) grazing incident X-ray diffraction (GIXD) and (iv) Brewster angle microscopy (BAM). All techniques combined provide an overview of the molecular consequences that result upon the interaction of AMX with the monolayer. In particular, information related to the different organizational states of the membrane, the establishment of hydrogen or ionic bonds, the effect on the formation of condensed phase domains, and the lattice structure and the tilt angle of the hydrophobic chains are provided [15,

16]. The effect of AMX was evaluated at different lateral pressures (10 mN.m^{-1}, 20 mN.m^{-1} and 30 mN.m^{-1}) to analyse its effect on different organizational phases. Moreover, 30 mN.m^{-1} is the lateral pressure of biological membranes, which ensures a more reliable extrapolation to *in vivo* interactions [17,18]. This pressure affects the density of the lipid packing and, consequently, it affects biological activities, such as the regulation of membrane proteins [19]. For mimetic model systems, this lateral pressure ensures the similarity of the lipid packing of a monolayer to the outer layer of a cell membrane [18]. Moreover, it was already proven that the physical behaviours of monolayers and bilayers are similar at this pressure, with the same area changes [20]. Therefore, the present study can provide new insight with respect to the interaction of AMX in different protonation states with the membrane, which ultimately can give new information about its mechanisms of toxicity.

2. Experimental methods

2.1. Materials

AMX trihydrated was obtained from Sigma-Aldrich and 1,2-dipalmitoyl-*sn*-glycero-3-phosphocholine (DPPC) was obtained from Avanti® Polar Lipids, Inc. All compounds were used without further purification.

All drug solutions were buffered to obtain the different pHs. Simulated Gastric Fluid (SGF, pH 1.2) was prepared according to the European Pharmacopoeia 8.0, with 2 g.L^{-1} of NaCl and 7 mL.L^{-1} of concentrated HCl. The final ionic strength (I) was around 0.12 M. The pH 5 and the pH 7.4 were obtained using the acetate Buffer ($I = 0.13$ M) and the Hepes Buffer ($I = 0.1$ M), respectively. All solutions were prepared using double-deionized water (conductivity inferior to 0.1 μS.cm^{-1}).

2.2. Langmuir isotherms

DPPC, solubilized in chloroform (1 mg.ml^{-1}), was spread onto a buffer subphase (SGF – pH 1.2, Acetate – pH 5.0 or Hepes – pH 7.4) in a trough of 420 mL, with or without AMX in a concentration of 64 μM. After spreading the lipid, the monolayer was equilibrated for 10 min to evaporate the chloroform. Surface pressure-area isotherms were then obtained through the compression made by two symmetric barriers in a KSV NIMA Langmuir trough. The monolayers were compressed at a rate of 5 Å^2/molecule/min and the surface tension was measured

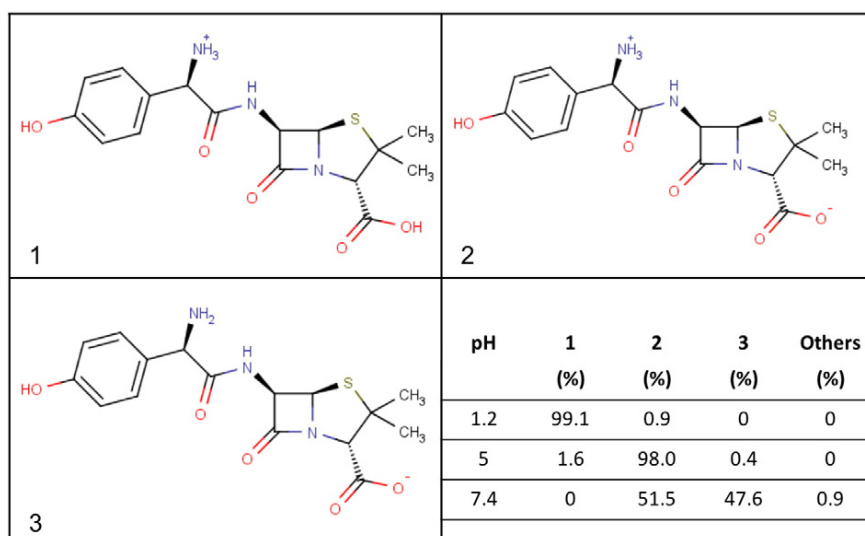| pH	1 (%)	2 (%)	3 (%)	Others (%)
1.2	99.1	0.9	0	0
5	1.6	98.0	0.4	0
7.4	0	51.5	47.6	0.9

Fig. 1. Structures of AMX in different protonation states and their relative percentage at different pHs. These results were obtained from a computational prediction made by the pK$_a$ plugin of ChemAxon®, MarvinSketch application, version 15.4.13.0.

using a Wilhelmy microbalance, with a filter paper plate with an accuracy superior to 0.1 mN.m^{-1}. Between different assays, the trough was cleaned with ethanol and double-deionized water, such a way that by compressing a water subphase a surface pressure of zero mN.m^{-1} was obtained. All assays were performed at 21 ± 1 °C.

2.3. Infrared reflection-absorption spectroscopy measurements

A KSV NIMA Polarization Modulation Infrared Reflection Absorption Spectrometer (PM-IRRAS) was used for infrared analysis. The modulation of the polarization enables the elimination of the interference of the environmental signal, such as from water and CO_2, which makes it highly sensitive and suitable for monolayer analysis [21,22]. The angle of incidence with respect to the surface normal was 80° and the height was optimized in each assay to get an interferogram higher than 6.5. By considering the limitation of the maximum of compression that is possible in a trough of 45 mL, a higher amount of lipid was used to reach an initial pressure of approximately 5 mN.m^{-1}. Therefore, a more concentrated drug solution (75 μM) was used to maintain the lipid:drug ratio used for other assays. The subphase was measured before spreading the lipid, and the correspondent spectrum was subtracted in the following measurements. The spectrum was recorded for 300 s, with a rate of 10 scans per second, and with a spectra resolution of 8 cm^{-1}. All measurements were performed at 21 ± 1 °C.

2.4. Grazing incident X-ray diffraction

The X-ray scattering measurements were performed on the SIRIUS beamline at the SOLEIL synchrotron. The details and the optics of the facility are described elsewhere [23]. The energy of the incident X-ray was 10.5 keV (λ = 0.118 nm) and the beam size was 0.1 × 2 mm^2 ($V \times$ H) at the sample position. The subphase surface was illuminated at an incident angle of 1.70 mrad, below the critical angle of the air–water interface (2.04 mrad at 10.5 keV). Thus, the incident wave was almost totally reflected, while the refracted wave became evanescent. Consequently, a layer of about 5 nm beneath the interface was explored. The scattered intensity was collected with very low noise, using a 1D gas detector fixed on the 2-axis detector arm of the beamline's diffractometer, which has 2048 channels at 150 mm. The Soller slit system is positioned in front of the detector to collimate the scattered beam. The resulting wave vector resolution is 0.03 nm^{-1}.

The spectra were obtained by varying the angle, 2θ, between the incident and the diffracted beam projected on the horizontal plane, and by recording for each angle the vertical distribution of the scattered intensity. Two separate components can be considered in the scattering wave vector Q: Q_{xy} or in-plane component and Q_z or out-of-plane component [24,25]. The resulting spectrum consists of a Q_{xy}-Q_z intensity map that can be vertically integrated along Q_z. Through a Lorentzian fitting of the Q_z-integrated spectrum, the peaks position, width and intensity, that give information concerning the periodic structure of the monolayer, can be determined [26]. The Q_z is used to calculate the tilt angle of the chains [26]. The distance among the lattice planes is calculated from the first-order peaks of the Q_{xy} component, according to the following equation [24]:

$$d = \frac{2\pi}{Q_{xy.}}$$

The correlation length (ξ), which is a qualitative measurement of the extend of order, is calculated for each direction of the crystal lattice, using the full-width at half-maximum (w_{hk}) values of the Bragg peak [27]:

$$\xi_{hk} = \frac{2}{w_{hk}}$$

A Langmuir trough was enclosed in a temperature controlled environment, with a sealed chamber, and flushed with helium during the data collection, to reduce the gas scattering and to avoid beam damage to the monolayer. For a more detailed description of the technique, please see the following reviews [16,28]. A drug solution of 60 μM and a lipid concentration of 1 mM were used in a trough of 400 mL, to maintain the lipid:drug ratio that was used for other assays. All measurements were performed at 20 ± 1 °C.

2.5. Brewster Angle microscopy

A KSV NIMA Brewster Angle Microscope (BAM) with a lateral resolution of 2 μm was used to obtain microscopic images of the lipid domains. The system is coupled to a Langmuir trough, which enables a real-time visualization at different pressures. Conditions similar to those used in the measurements of the pressure-area isotherms were used, viz. a drug solution of 64 μM in a trough of 420 mL and a lipid concentration of 1 mg.ml^{-1}. The images were submitted to a following treatment to achieve a better contrast by scaling the brightness of each image and removing the background. All images were recorded at 21 ± 1 °C.

3. Results

3.1. Langmuir isotherms

The area per lipid molecule is one of the main characteristics of lipid layers since it is the average area occupied by one lipid. It depends on the phospholipids structure, on the charge of their polar heads and on the saturation of their hydrophobic tails [29]. By increasing the lateral pressure applied to the monolayer, the area per lipid molecule changes, with the existence of different order transitions (gaseous, liquid expanded, tilted condensed and untitled condensed) [28]. The minimal area per lipid molecule can be calculated through the intersection of the x axis with a straight line obtained by the linear fitting of the isotherm on the condensed phase [17]. In this work, the fitting was made in a range of pressures that included the biological lateral pressure (30 mN.m^{-1}). Furthermore, the following equation can be used to calculate the elastic modulus (C_s^{-1}), which reflects the elastic properties and the compressibility of the monolayer [30]:

$$C_s^{-1} = -A\left(\frac{d\pi}{dA}\right)$$

The elastic modulus of biological membranes is associated with important interactions in vivo, such as the interactions among lipids and between lipids and proteins [31]. To analyse the effect of AMX in the above-mentioned properties, surface pressure-area (π-A) isotherms were measured and the correspondent elastic moduli were calculated (Fig. 2).

The isotherm of DPPC at pH 1.2 does not have a so well-defined plateau as the ones observed at both pH 5 and pH 7.4. This plateau is characteristic of a mix of the condensed and the liquid expanded phases. Thereby, at pH 1.2, the transition to the liquid condensed phase happened at a higher area per lipid molecule, which indicates a more packed lipid film. Furthermore, the area per lipid molecule decreases, whereas the elastic modulus increases (Table 1). A higher value of the elastic modulus points toward a less compressible membrane and, consequently, a less fluid membrane. Therefore, the lipid film formed at pH 1.2 has a lower area per lipid molecule, a lower compressibility and a higher packing. According to what was expected, the isotherms of DPPC at pH 5.0 and at pH 7.4 are similar since DPPC is almost 100% in its zwitterionic state at both pHs. However, both the areas per lipid molecule and the elastic moduli of DPPC are different (Table 1). These results are in agreement with the results already reported by our research group in 2011 [32].

247
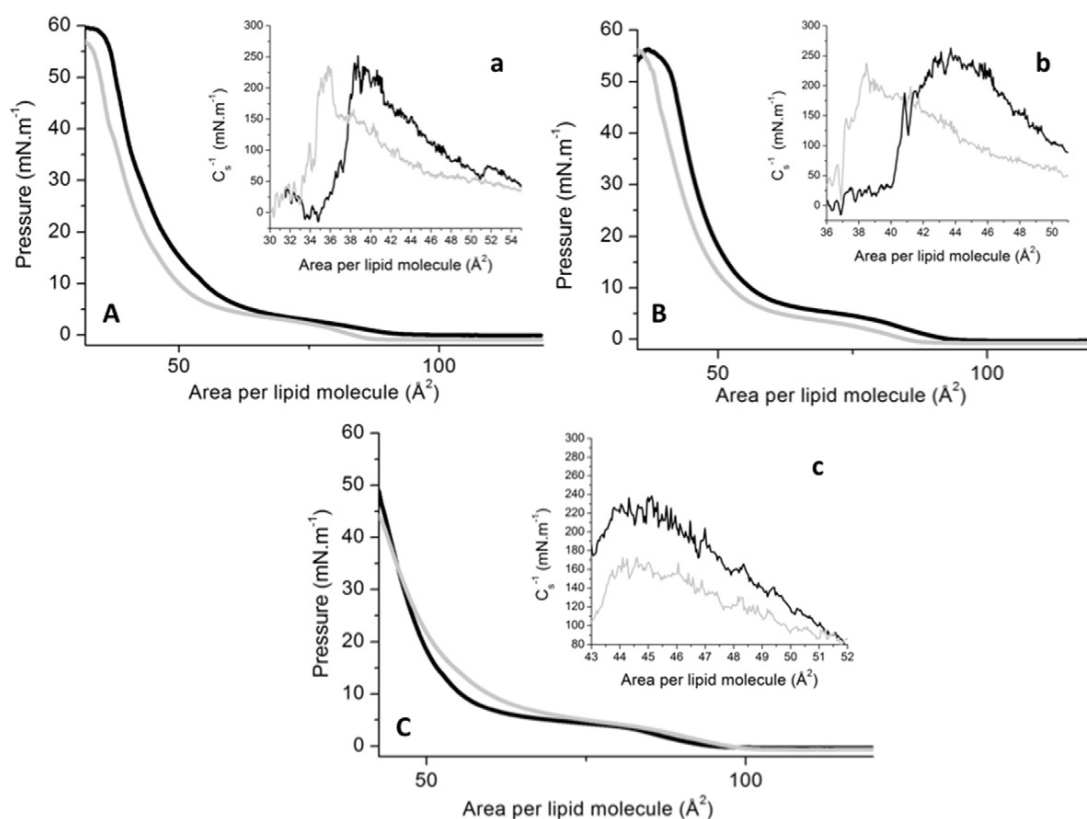
Fig. 2. Surface pressure-area (π-A) isotherms of DPPC on a buffer subphase (black) or on an AMX subphase (grey) at three different pHs: pH 1.2 (A), pH 5 (B) and pH 7.4 (C). Insets a, b and c represent the respective elastic modulus (C_s^{-1}) of the isotherms A, B and C.

At pH 7.4, AMX seems to be squeezed-out from the monolayer in the lipid condensed phase, which is visualized by the overlapping of the isotherms at lower areas per lipid molecule. At pH 1.2 and pH 5, this effect does not happen. An opposite trend is indeed visualized depending on the pH, namely, a higher packing at both pH 1.2 and pH 5, and a lower packing at pH 7.4. This is coherent with the tendency observed in the effect of AMX on the areas per lipid molecule and on the elastic moduli (Table 1). At acidic pH (pH 1.2 and pH 5), AMX decreases the area per lipid molecule and increases the elastic modulus. Furthermore, the entire graphic of the elastic modulus is shifted to lower areas per lipid molecule (Fig. 2, a and b). Hence, AMX promotes the packing and the organization of the DPPC monolayer at those pHs. However, at pH 7.4, AMX increases the area per lipid molecule and decreases the elastic modulus. This is in agreement with the effect observed in the Langmuir isotherms and with the decrease of the maximum value of the elastic modulus, which can be graphically visualized (Fig. 2, c).

3.2. Infrared reflection-absorption spectroscopy measurements

The infrared reflection-absorption spectroscopic technique enables the determination of the frequency of the molecular vibrations of phospholipids that are spread onto an aqueous solution [33]. This is possible due to the transmission-reflection of the infrared radiation that is detected in an angle equal to the incident angle [15]. The PM-IRRAS technique considers the differences between the reflectivity of the light in a plane parallel (s-polarizer) and in a plane perpendicular (p-polarizer) to the surface. Therefore, this technique enables the evaluation of the molecular perturbations by analysing the differences in the wavenumbers of vibration.

Both the phosphate (PO_2^{2-}) and the carbonyl (C = O) groups are localized near the polar heads of phospholipids. Changes on their vibrational wavenumber are related to the establishment of bonds, such as H-bonds [15]. In more detail, changes to lower wavenumbers mean new H-bonds, which can also indicate a more local hydration. On the other hand, the hydrophobic chains of DPPC are composed of methylene groups (CH_2) and, consequently, alterations in the conformational order of the monolayer are reflected in the deviation of the methylene band [15]. Fig. 3 shows the PM-IRRAS spectra of DPPC, with and without AMX, at 30 mN.m^{-1}. The results obtained at 10 and 20 mN.m^{-1} are shown in the Table S1 of the supplementary information.

Comparing DPPC at different pHs, the wavenumber of vibration of the carbonyl group decreased at pH 1.2, which indicates the establishment of new bonds. This blue shift may be associated with the formation of dipole-dipole interactions, which will be further detailed in the discussion section. The wavenumber of the phosphate group is, however, maintained. On the other hand, the effect of AMX is more evident than the effect of the pH. At pH 1.2 and at 30 mN.m^{-1}, AMX induces the deviation of the carbonyl vibrational band to higher wavenumbers (Fig. 3, middle column, bottom line), which reflects a lower hydration. Furthermore, the methylene vibrational band was shifted to lower wavenumbers (Fig. 3, right column, bottom line), which indicates a higher packing. This effect of AMX is also visualized at pH 5 (Fig. 3, right column, middle line), which shows the higher organization promoted by the drug. At pH 7.4, the tendency was the opposite (Fig. 3,

Table 1
Area per lipid molecule and the maximum value of the elastic modulus of a DPPC monolayer, in absence and in presence of AMX, at three different pHs (pH 1.2, pH 5 and pH 7.4).

pH	Area per lipid molecule (Å^2)		Elastic modulus (mN.m^{-1})	
	Buffer	AMX	Buffer	AMX
1.2	50.5 ± 0.4	48.7 ± 0.7	234 ± 6	242 ± 6
5	53.3 ± 0.3	50.7 ± 0.5	223 ± 1	234 ± 2
7.4	55.5 ± 0.2	57.6 ± 0.6	212 ± 4	186 ± 3
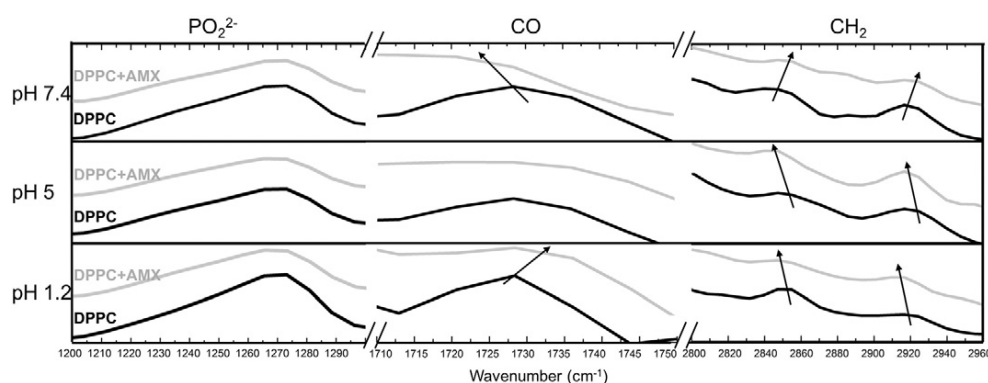
Fig. 3. PM-IRRAS spectra of DPPC on a buffer subphase (black) or on an AMX subphase (grey) at three different pHs: pH 1.2 (bottom), pH 5 (middle) and pH 7.4 (top). The frequency of the molecular vibrations of the phosphate (left), the carbonyl (middle), and the methylene (right) groups are shown.

right column, top line), with the lower packing revealed by the deviation of the methylene vibrational band to higher wavenumbers. Simultaneously, the hydration of the carbonyl group increases (lower wavenumbers) in the presence of AMX. This effect is more perceptible at 10 mN.m^{-1} (Table S1 of the supplementary information), with deviations also visible in the vibrational wavenumber of the phosphate group.

3.3. Grazing incident X-ray diffraction

Grazing incident X-ray diffraction (GIXD) is a technique in which almost all of the incident beam is reflected and only an evanescent wave is able to travel along the interface [24,25]. The use of the grazing incident angle enables the elimination of the scattering promoted by the subtract and enhances the resolution by improving the ratio between the signal and the bulk scattering [34]. This raises this technique to one of the main techniques to study the structural arrangements and the conformation of phospholipids in the air/water interface [24,25].

The position of the peaks and the correspondent distances, the lattice parameters, the tilt angles and the correlation lengths for all the GIXD experiments are gathered in Table 2. In a 2D powder diffraction, the first order peak indexations are 1$\bar{1}$ and 02 for a rectangular lattice.

The structural arrangement of DPPC changes depending on the pH of the buffer. At pH 5, DPPC is in a rectangular lattice structure (two Bragg peaks), with tilted chains. These results are in agreement to what was already observed when spreading DPPC onto other buffers [35,36]. At pH 1.2 and at pH 7.4, three Bragg peaks were measured. Two of the three peaks are in-plane, which indicates that they could not be attributed to a single structure. We interpret this phenomenon as a coexistence of two types of domains, one with DPPC molecules organized as visualized at pH 5 and the other with more condensed and untitled DPPC molecules. Despite the presence of domains in the hexagonal lattice, we selected the rectangular unit cell for simplicity and considering the presence of domains in the usual rectangular lattice.

The results of DPPC at pH 1.2 are shown in Fig. 4. The main effect of AMX is the reduction of the tilt value, as visualized through the leftmost peak. At pH 7.4 (Table 2), the effect of AMX is similar but significantly more pronounced at 10 mN.m^{-1}, with the reduction of the tilt angle to approximately 0°.

At pH 5, the effect of AMX is more perceptible (Fig. 5). Given the presence of two Bragg peaks in the absence of AMX, the structure is in a rectangular lattice (a, b, $\gamma = 90°$) with one molecule per unit cell. Traditionally [24], the out-of-plane and the in-plane peaks are indexed to peak 1$\bar{1}$ and 02, respectively. Lattice parameters are calculated according to the following equations:

$$a = \frac{4\pi}{\sqrt{2Q_{xy\,1\bar{1}}^2 + 2Q_{xy\,11}^2 - Q_{xy\,02}^2}}$$

Table 2
Peaks positions, distance (d), correlation length (ξ), deduced lattice parameters (a, b), unit cell area (A), and tilt angle (t) in absence and in presence of AMX, at three different pHs (1.2, 5 and 7.4) and pressures (10, 20 and 30 mN.m^{-1}).

pH	π (mN.m^{-1})	Subphase	$Q_{z1\bar{1}}$ (nm^{-1}) ±0.03	$Q_{1\bar{1}}$ (nm^{-1}) ±0.03	$d_{1\bar{1}}$ (Å) ±0.03	Q_{02} (nm^{-1}) ±0.03	d_{02} (Å) ±0.03	a (nm)	ξ$_{11}$ (nm)	b (nm)	ξ$_{02}$ (nm)	A (nm^2)	tilt (deg.)
1.2	10	Buffer	14.00	7.10	4.48	14.69	4.27	0.530	3.3	0.850	40.0	0.450	28.2
		AMX	14.20	6.40	4.42	14.57	4.31	0.471	2.5	0.862	50.0	0.406	25.0
	20	Buffer	14.22	5.80	4.42	14.64	4.29	0.515	4.0	0.858	28.6	0.442	22.2
		AMX	13.85	5.70	4.53	14.64	4.29	0.534	2.5	0.858	21.0	0.459	22.1
	30	Buffer	14.06	5.06	4.46	14.70	4.27	0.524	3.3	0.855	22.2	0.448	19.6
		AMX	14.16	5.25	4.43	14.68	4.28	0.519	3.3	0.856	22.2	0.444	20.4
5	10	Buffer	13.05	7.10	4.81	14.54	4.32	0.580	3.0	0.864	16.7	0.501	28.6
		AMX	13.07	7.27	4.81	14.55	4.31	0.579	3.3	0.864	22.2	0.500	29.1
	20	Buffer	13.35	6.88	4.71	14.58	4.31	0.562	2.0	0.662	13.3	0.484	27.3
		AMX	13.48	6.46	4.66	14.59	4.31	0.554	2.5	0.861	10.5	0.477	25.6
	30	Buffer	13.31	5.82	4.72	14.57	4.31	0.564	2.8	0.862	28.6	0.486	23.0
		AMX	13.40	6.10	4.68	14.57	4.31	0.564	2.8	0.862	25.0	0.482	23.8
7.4	10	Buffer	13.31	6.83	4.72	14.57	4.31	0.564	47.0	0.862	40.0	0.486	27.2
		AMX	14.50	~0	4.33	14.50	4.33	0.500	2.2	0.867	28.6	0.437	~0
	20	Buffer	13.43	6.90	4.67	14.62	4.30	0.558	2.2	0.860	20.0	0.479	27.2
		AMX	13.49	6.80	4.66	14.61	4.30	0.554	2.0	0.861	14.3	0.477	26.8
	30	Buffer	13.81	6.00	4.55	14.64	4.29	0.537	2.2	0.858	10.0	0.460	23.4
		AMX	13.68	6.10	4.59	14.63	4.29	0.544	2.2	0.859	6.7	0.467	24.2

Fig. 4. Q_z Integrated scattered intensity vs. Q_{xy}, obtained at pH 1.2 and at 10 mN.m^{-1}, and associated Q_{xy}-Q_z intensity maps, without (left) and with (right) AMX in the subphase.

$$b = \frac{4\pi}{Q^2_{xy\ 02}}$$

At pH 5, the lattice parameters are a = 0.56 nm and b = 0.86 nm, with a correspondent area per unit cell of 0.48 nm^2, which correspond to the macroscopic area per lipid molecule.

From the Q_{xy}-Q_z intensity map, it is possible to visualize that the $1\bar{1}$ degenerate peak is out-of-plane and the peak 02 is in-plane. This indicates that the tilt of the hydrophobic chains is toward the Next Neighbour (NN-tilt). In this case, the tilt value (t) is calculated according to the following equation:

$$Q_z = Q_{xy}\ \cos(\psi^*)\ \tan(t)$$

where ψ is the azimuth angle, which is equal to zero in the case of a NN-tilt. As shown in the Table 2, the NN tilt is not very sensitive to the surface pressure, as already mentioned in the literature [28].

When AMX is added to the subphase at pH 5 (Fig. 5), a third peak appears at Q_{xy} = 15.1 nm^{-1}. Two of the three peaks are in-plane, as visualized from the Q_{xy}-Q_z plot. Consequently, and similar to what happens to DPPC at pH 1.2 and pH 7.4, these peaks could not be attributed to a single structure. Thus, we interpret this phenomenon as a coexistence of un-affected DPPC domains (correspondent to the out-of-plane peak 11 and the first in-plane peak 02) and domains in which the chains are untitled. These latter domains may correspond to a structure organized on a hexagonal lattice correspondent to the 15.1 nm^{-1} peak,

which demonstrates a close packing of the hydrocarbon chains. In this case, the three diffraction peaks 11, $1\bar{1}$, and 02 are degenerated and all located at 15.1 nm^{-1}, which leads to different lattice parameters (a = 0.48 nm and b = 0.83 nm, A = 0.40 nm^2). This corresponds indeed to close packed chains. This is coherent with the decrease in the area per lipid molecule from 53.3 Å^2 (DPPC) to 50.7 Å^2 (in presence of AMX). Since this third peak is in-plane, the chains are upright with no tilt. This diffraction peak is resolution limited, which means that these type of domains have a higher correlation length than DPPC structures on pure water or at pH 5.

The main conclusion of the GIXD study in that AMX promotes the packing of DPPC, which results in two type of domains, one kind with the classical organization of DPPC (tilted chains) and another kind with close-packed upright chains.

3.4. Brewster Angle microscopy

The application of the Brewster Angle Microscopy (BAM) to study monolayers is based on the changes in the reflectivity of the polarized laser beam when it interacts with a condensed monolayer [16]. Thus, the shape of the phospholipid domains and their texture can be visualized [16]. The results are shown in Fig. 6. Comparing the monolayers of DPPC spread onto different buffers, differences in the size and in the shape of the condensed phase domains can be visualized. In particular, the lipid domains are almost spherical at pH 1.2, whereas at pH 7.4 they have a cloverleaf shape, which was already reported in the
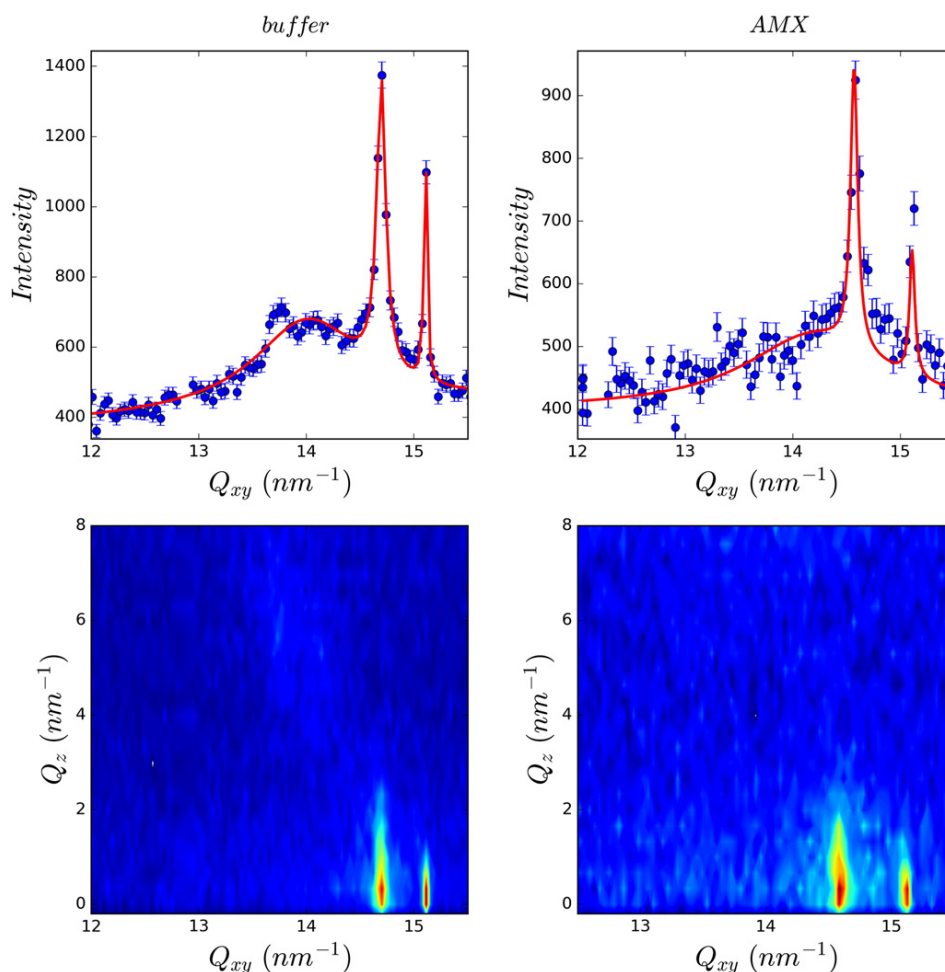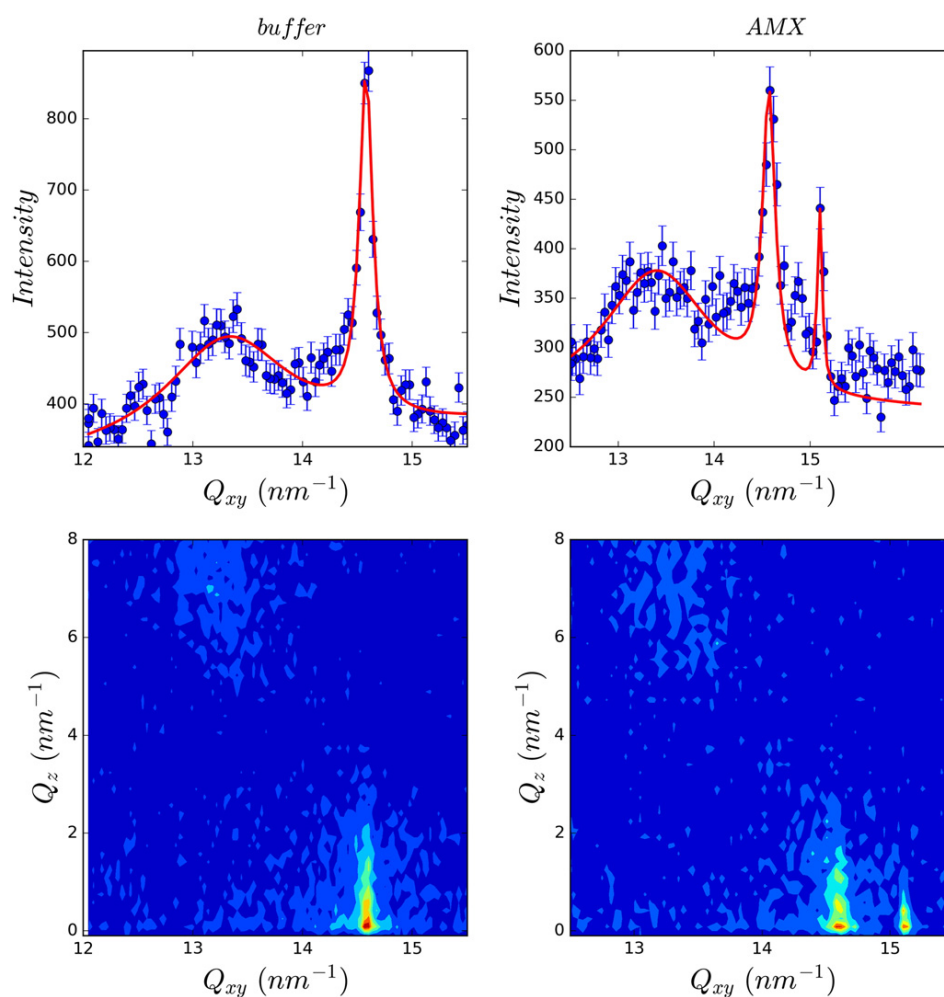
Fig. 5. Q_z Integrated scattered intensity vs. Q_{xy}, obtained at pH 5.0 and at 30 mN.m^{-1} (top), and associated Q_{xy}-Q_z intensity maps, without (left) and with (right) AMX in the subphase.

literature [37,38]. Although DPPC is in the same protonation state at both pH 5 and pH 7.4, the shape of the domains is not similar. The effect of AMX also depends on the pH. At pH 1.2, the shape of the domains does not change with an AMX subphase. However, the same structure is visualized at different pressures, namely, at 10 mN.m^{-1} (buffer subphase) and at 5 mN.m^{-1} (AMX subphase). At higher pressures (Fig. S1 of the supplementary information), AMX promotes the formation of pores in the lipid film. At pH 5 and at lower pressures, the effect of AMX is negligible. At 15 mN.m^{-1}, there is a more compact lipid film in the presence of AMX than in the plain DPPC. Nevertheless, the lipid film has some imperfections, namely, a rough texture and the presence of pores, similar to what was observed at pH 1.2. This effect is also maintained at higher pressures (30 mN.m^{-1}), with a continuous lipid film in the plain DPPC monolayer and pores in the presence of AMX. At pH 7.4, the effect of the drug was only observed at lower pressures, with different domains shapes.

4. Discussion

The interaction between AMX and a DPPC monolayer depends on the protonation state of both AMX and DPPC, which changes depending on the pH. In a general overview, several differences were found when comparing DPPC at different pHs, namely, with respect to the Langmuir isotherms, the areas per lipid molecule and the elastic modulus. In particular, the transitions between different packing states were affected in the DPPC monolayer at pH 1.2, and the area per lipid molecule

decreased from 53.3 Å^2 (pH 5) and 55.5 Å^2 (pH 7.4) to 50.5 Å^2 (pH 1.2), which reflects a higher packing. Accordingly, the elastic modulus was higher at pH 1.2 (234 mN.m^{-1}) than at both pH 5 (223 mN.m^{-1}) and pH 7.4 (212 mN.m^{-1}). These results reflect a lower compressibility at pH 1.2 due to a higher organization. At acidic pH, 80% of DPPC is positively charged, which induces a repulsion of the polar heads. However, a previous study showed that the decrease of pH induced a transition from the liquid-crystalline to the gel phase [39]. Furthermore, the authors reported that the main temperature of phase transition was higher at lower pHs [39]. The protonation at acidic pHs of the phosphate group decreases its interaction with water and, consequently, there is a lower water content in the membrane [39]. Hence, the area per lipid molecule decreases [39], which is coherent with the above-mentioned shifts in the area per lipid molecule and in the elastic modulus. Nevertheless, DPPC has two C = O groups, which have permanent electric dipoles [39]. Due to the proximity of the adjacent phospholipids, dipole-dipole interactions are possible and may overcome the repulsive effect of the positive charges [39]. These dipole-dipole interactions can cause deviations in the PM-IRRAS, more specifically to lower wavenumbers [40]. This was visualized in the PM-IRRAS results. Furthermore, the results obtained from the GIXD experiments showed a higher tilt angle at higher pH, which is in accordance with an increased packing at pH 1.2. Remarkably, although DPPC is in the same protonation state at both pH 5 and pH 7.4, there are some noteworthy differences in the area per lipid molecule, in the elastic modulus, in the number of Bragg peaks and in the shape of the domains. These results

DPPC

DPPC + AMX

$\pi = 10$ mN/m   pH 1.2 $\pi = 5$ mN/m

pH 5.0 $\pi = 10$ mN/m

pH 5.0 $\pi = 15$ mN/m

pH 5.0 $\pi = 30$ mN/m

pH 7.4 $\pi = 10$ mN/m
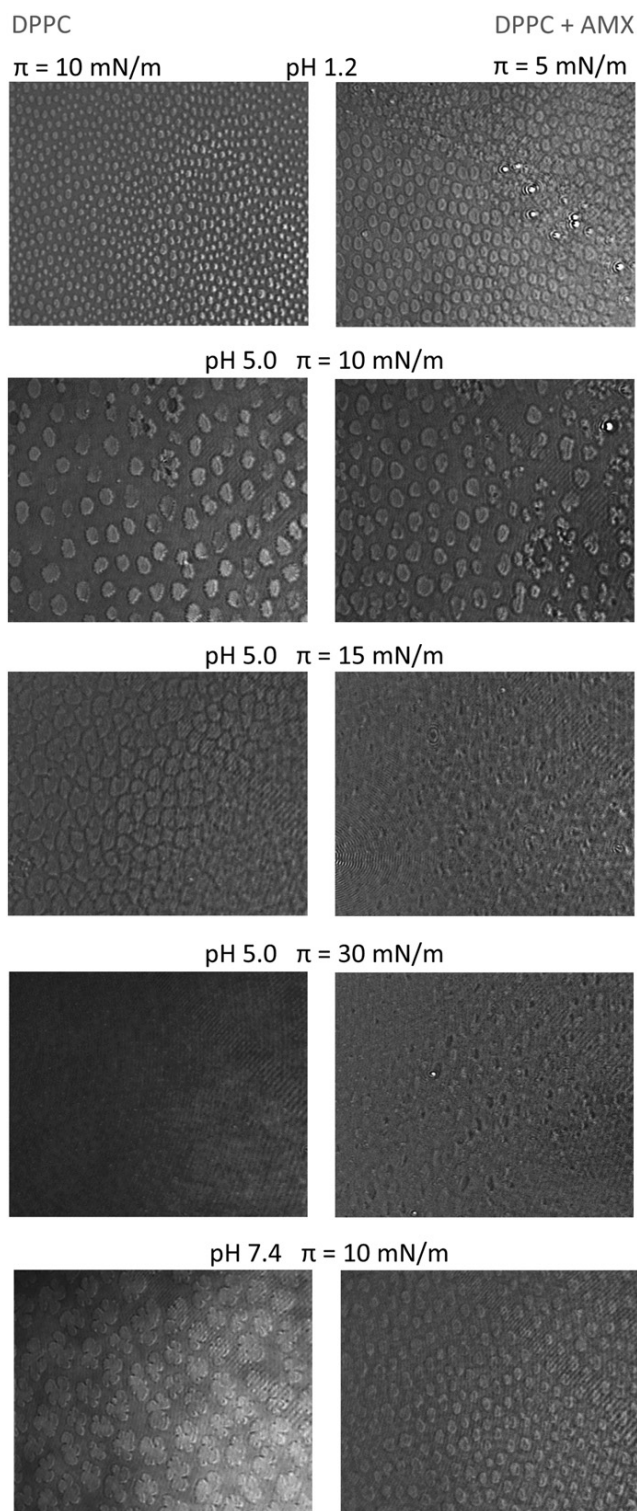
Fig. 6. Brewster angle microscopic images of Langmuir monolayers of DPPC at pH 1.2 at 5 and 10 mN.m^{-1} (top), at pH 5 at 10 mN.m^{-1}, 15 mN.m^{-1} and 30 mN.m^{-1} (middle) and pH 7.4 at 10 mN.m^{-1} (bottom). The left and the right column correspond to a buffer and a buffered solution of AMX as subphase, respectively.

indicate that the buffer may affect the structural conformation of the monolayer. In accordance, other differences were already reported by our research group using other membrane models of DPPC in these buffers. For instance, the cooperativeness and the temperature of

phase transition in liposomes of DPPC changed depending on the buffer [32].

The effect of the pH on the interactions between AMX and the DPPC monolayers was also studied. At pH 1.2, the presence of AMX leads to a highly packed monolayer, as confirmed by the Langmuir isotherm and the lower area per lipid molecule (from 50.5 Å^2 to 48.7 Å^2). The higher elastic modulus (from 234 mN.m^{-1} to 242 mN.m^{-1}) also reflects a less compressible membrane. Furthermore, the shift of the carbonyl band to higher wavenumbers and the deviation of the methylene band to lower wavenumbers reflect the lower hydration and the more organized conformational state. The GIXD results showed a higher effect at lower pressures, with alteration of the tilt angle of the hydrophobic chains. These results were also confirmed by the BAM results, with the same domains visible at different pressures. This means that a similar packing was reached at lower pressures when AMX was present. From the BAM images, the formation of pores was also visualized in presence of an AMX subphase (Fig. S1 of the supplementary information).

At pH 5, 98% of AMX is zwitterionic and 2% is positively charged, whereas DPPC is almost totally zwitterionic. The distance between the two charged groups of AMX is higher than the distance between the charged groups of DPPC, which hampers a double electrostatic interaction. Additionally, the overall effect of AMX is similar to what was observed at pH 1.2. The Langmuir isotherm, the changes in the area per lipid molecule (from 53.3 Å^2 to 50.7 Å^2) and in the elastic modulus (from 223 mN.m^{-1} to 234 mN.m^{-1}) are coherent with a higher packing of the phospholipids in presence of AMX. This effect is also reflected in the PM-IRRAS results and in the BAM results, in which at 15 mN.m^{-1} a lipid film is visualized in presence of AMX, whereas separated domains are visible in plain DPPC. The presence of pores is also visualized even though the protonation states of both DPPC and AMX are different from the ones verified at pH 1.2. The changes in the structural arrangement of DPPC are reflected in the additional Bragg peak in the presence of AMX. We hypothesize that the presence of AMX may induce the formation of two types of domains. The existence of Bragg peaks similar to the ones measured in a plain DPPC monolayer reflects the presence of unperturbed domains. However, the additional in-plane Bragg peak ($Q_{xy} = 15.1$ nm^{-1}) reflects a possible existence of other domains, in which AMX perturbed the structural arrangement of DPPC and promoted a higher packing. This hypothesis is coherent with the higher organization visualized in the other experimental techniques. Furthermore, looking to the BAM results and, in particular, to the effect of AMX at 30 mN.m^{-1}, three different structures are visualized: i) one similar to the lipid film visualized in the plain DPPC, ii) more brightly and white domains characteristic of domains with higher packing and iii) more dark structures (pores).

AMX has been associated with gastrointestinal and renal side effects [1,6]. Due to the pH gradient of the gastric mucosa and the decrease of the urine pH by different phenomena, such as dehydration [7], AMX may be positively charged *in vivo*. A homeostatic environment and the integrity of membranes are essential to preserve biological functions [41]. Furthermore, a special attention must be given to the layer of surfactant-like phospholipids, which are presented on the interface between the mucus layer and the stomach lumen [32]. Its role is related with the homeostasis and the protection of the gastric mucosa from aggressions like the acidic pH of the stomach [32]. Additionally, in renal tissues, defects in basement membranes were already associated with kidney disorders [42]. Therefore, the perturbation of the biophysical properties of the membrane and the formation of pores at acidic pH may indicate disturbance of biological membranes, which ultimately can be related with AMX toxicity. Two main explanations for the formation of pores by drugs are reported in the literature, in addition to the well-known mechanism of antimicrobial peptides [43]. One explanation is a stable association between the drug and the phospholipid that rearranges itself to form pores in channel-shape [44]. Given the results obtained in the PM-IRRAS experiments, a strong interaction between AMX and DPPC is improbable. Another explanation is the

aggregation of drug molecules, heterogeneously distributed in the lipid film, that induces the formation of pores by the higher local concentration associated with the self-aggregation [45]. One of the degradation products of AMX at acidic pH is the penicilloic acid, which results from the opening of the β-lactam ring [46]. This degradation pathway leads to a free carboxyl group that can interact with the amino group of another molecule [46,47]. Therefore, at acidic conditions, the formation of pores may be explained by the local concentration of dimers of AMX.

At pH 7.4 and at 10 mN.m^{-1}, AMX decreases the organization of the monolayer, which is visualized in the Langmuir isotherm, in the higher area per lipid molecule (from 55.5 Å^2 to 57.6 Å^2), in the lower elastic modulus (from 212 mN.m^{-1} to 186 mN.m^{-1}) and in the changes of the tilt angle showed by the GIXD measurements. Additionally, the results of the PM-IRRAS experiments showed that AMX increases the hydration of the carbonyl group (shift to lower wavenumbers) and decreases the packing of DPPC (shift of the methylene band to higher wavenumbers). This effect is even more perceptible at 10 mN.m^{-1} (Table S1 of the supplementary information), with a higher hydration also shown by the deviation of the phosphate band to lower wavenumbers. At this pH, approximately 50% of the AMX is in the zwitterionic state and 50% has the carboxyl group negatively charged. By considering the GIXD results and the overall effect of AMX, we suggest that at 10 mN.m^{-1} electrostatic interactions are established between the negative charge of AMX and the positive charge of the choline of DPPC. Thus, the rest of the molecule may be intercalated among phospholipid chains, which prevents the tilt of DPPC phospholipids and changes its structural arrangement. According to the Langmuir isotherm, AMX also enhances the fluidity of the lipid film. At lower pressures, the interaction may be established due to the reduced packing. However, at higher pressures, AMX seems to be squeezed out from the lipid film, which is visualized in the Langmuir isotherm. The results from the BAM technique are also coherent, since at 10 mN.m^{-1} AMX changes domains shape, having however no visual effect at higher pressures.

5. Conclusion

From the results obtained, it is possible to conclude that the pH affects the structural conformation of plain DPPC and its packing, in particular at pH 1.2. Although in the same protonation state, differences in the DPPC monolayer at pH 5 and at pH 7.4 were also visualized, probably due to the interference of salts. With respect to the effect of AMX, a similar effect was visualized at both pH 1.2 and pH 5. It is noteworthy that AMX is able to induce the formation of pores in the lipid film of DPPC at both pH 1.2 and pH 5, possibly due to dimerization of AMX under acidic conditions. The disturbance of biological barriers and, ultimately, the formation of pores may be related with *in vivo* toxicity. In contrast, at pH 7.4 the interaction between AMX and DPPC is more perceptible at 10 mN.m^{-1}, with expulsion of the drug at higher pressures.

To conclude, changes in the pH affect the protonation state of both AMX and DPPC and, consequently, their interaction. Ultimately, this may affect the toxic effects of AMX observed *in vivo*.

Transparency Document

The Transparency document associated with this article can be found, in online version.

Acknowledgements

Appendix A. Supplementary data

Supplementary data to this article can be found online at http://dx.doi.org/10.1016/j.bbamem.2017.01.031.
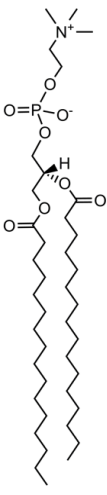
References

[1] Meyler's Side Effects of drugs: The international encyclopedia of adverse drug reactions and interactions, 15th ed. Elsevier B.V., 2006
[2] K. Weist, A. Muller, D. Monnet, O. Heuer, Surveillance of antimicrobial consumption in Europe 2012, European centre for disease prevention and control (ECDC), Stockholm, 2014.
[3] H. Gelband, M. Miller-Petrie, S. Pant, S. Gandra, J. Levinson, D. Barter, A. White, R. Laxminarayan, The state of the world's antibiotics 2015, The Center for Disease Dynamics, Economics & Policy (CDDEP), Washington, D.C., 2015
[4] P. Malfertheiner, F. Megraud, C.A. O'Morain, J. Atherton, A.T. Axon, F. Bazzoli, G.F. Gensini, J.P. Gisbert, D.Y. Graham, T. Rokkas, E.M. El-Omar, E.J. Kuipers, Management of *Helicobacter pylori* infection - the Maastricht IV/ Florence Consensus Report, Gut 61 (2012) 646–664.
[5] A review of human carcinogens, Part B: biological agents, IARC Working Group on the Evaluation of the Carcinogenic Risks to Humans, Lyon, France, 2009.
[6] D. Lopes, C. Nunes, M.C. Martins, B. Sarmento, S. Reis, Eradication of *Helicobacter pylori*: Past, present and future, J. Control. Release 189 (2014) 169–186.
[7] G. Fritz, Amoxicillin-induced acute renal failure, Nephrol. Dial. Transplant. 18 (2003) 1660–1662.
[8] A. Allen, G. Flemström, Gastroduodenal mucus bicarbonate barrier: protection against acid and pepsin, Am. J. Physiol. Cell Physiol. 288 (2005) C1–C19.
[9] C. Nunes, G. Brezesinski, D. Lopes, J.L. Lima, S. Reis, M. Lucio, Lipid-drug interaction: biophysical effects of tolmetin on membrane mimetic systems of different dimensionality, J. Phys. Chem. B 115 (2011) 12615–12623.
[10] W. Bernhard, A.D. Postle, M. Linck, K.-F. Sewing, Composition of phospholipid classes and phosphatidylcholine molecular species of gastric mucosa and mucus, Biochim. Biophys. Acta 1255 (1995) 99–104.
[11] C. Grauby-Heywang, F. Morote, M. Mathelie-Guinlet, I. Gammoudi, N.R. Faye, T. Cohen-Bouhacina, Influence of oxidized lipids on palmitoyl-oleoyl-phosphatidylcholine organization, contribution of Langmuir monolayers and Langmuir-Blodgett films, Chem. Phys. Lipids 200 (2016) 74–82.
[12] C. Pereira-Leite, C. Nunes, S. Reis, Interaction of nonsteroidal anti-inflammatory drugs with membranes: *In vitro* assessment and relevance for their biological actions, Prog. Lipid Res. 52 (2013) 571–584.
[13] D.Y. Singh, N.K. Prasad, Double liposomes mediated dual drug targeting for treatment of *Helicobacter pylori* infections, Pharmazie 66 (2010) 368–373.
[14] *Helicobacter pylori*: Physiology and Genetics, ASM Press, Washington, D.C., 2001
[15] R. Mendelsohn, G. Mao, C.R. Flach, Infrared reflection-absorption spectroscopy: principles and applications to lipid-protein interaction in Langmuir films, Biochim. Biophys. Acta 1798 (2010) 788–800.
[16] D. Vollhardt, V.B. Fainerman, Characterisation of phase transition in adsorbed monolayers at the air/water interface, Adv. Colloid Interf. Sci. 154 (2010) 1–19.
[17] L.K. Buehler, Cell membranes, Garland Science Taylor & Francis Group, New York, 2015.
[18] C. Peetla, A. Stine, V. Labhasetwar, Biophysical interactions with Model Lipid Membranes: Applications in Drug Discovery and Drug Delivery, Mol. Pharm. 6 (2009) 1264–1276.
[19] P.A. Janmey, P.K. Kinnunen, Biophysical properties of lipids and dynamic membranes, Trends Cell Biol. 16 (2006) 538–546.
[20] A. Blume, A comparative study of the phase transitions of phospholipid bilayers and monolayers, Biochim. Biophys. Acta 557 (1979) 32–44.
[21] Nanomaterials and Nanoarchitectures: a complex review of the current hot topics and their applications, Springer, Dordrecht, 2013.
[22] M.A. Ramin, G. Le Bourdon, N. Daugey, B. Bennetau, L. Vellutini, T. Buffeteau, PM-IRRAS investigation of self-assembled monolayers grafted onto SiO$_2$/Au substrates, Langmuir 27 (2011) 6076–6084.
[23] P. Fontaine, G. Ciatto, N. Aubert, M. Goldmann, Soft Interfaces and Resonant Investigation on Undulator Source: A Surface X-ray Scattering Beamline to Study Organic Molecular Films at the SOLEIL Synchrotron, Sci. Adv. Mater. 6 (2014) 2312–2316.
[24] C. Stefaniu, G. Brezesinski, Grazing incidence X-ray diffraction studies of condensed double-chain phospholipid monolayers formed at the soft air/water interface, Adv. Colloid Interf. Sci. 207 (2014) 265–279.
[25] C. Stefaniu, G. Brezesinski, X-ray investigation of monolayers formed at the soft air/water interface, Curr. Opin. Colloid Interface Sci. 19 (2014) 216–227.

[26] M. Lúcio, B. Frank, S. Reis, J.L.F.C. Lima, G. Brezesinski, Binding of Nonsteroidal Anti-inflammatory drugs to DPPC: Structure and Thermodynamic Aspects, Langmuir 24 (2008) 4132–4139.

[27] F. Neville, Y. Ishitsuka, C.S. Hodges, O. Konovalov, A.J. Waring, R. Lehrer, K.Y. Lee, D. Gidalevitz, Protegrin interaction with lipid monolayers: Grazing incidence X-ray diffraction and X-ray reflectivity study, Soft Matter 4 (2008) 1665–1674.

[28] V.M. Kaganer, H. Möhwald, P. Dutta, Structure and phase transitions in Langmuir monolayers, Rev. Mod. Phys. 71 (1999) 779–819.

[29] T. Hianik, Structure and physical properties of biomembranes and model membranes, Acta Phys. Slovaca 56 (2006) 687–805.

[30] Z. Wang, X. Li, S. Yang, Studies of dipalmitoylphosphatidylcholine (DPPC) monolayers embedded with endohedral metallofullerene (Dy@C82), Langmuir 25 (2009) 12968–12973.

[31] N. Fa, L. Lins, P.J. Courtoy, Y. Dufrene, P. Van Der Smissen, R. Brasseur, D. Tyteca, M.P. Mingeot-Leclercq, Decrease of elastic moduli of DOPC bilayers induced by a macrolide antibiotic, azithromycin, Biochim. Biophys. Acta 1768 (2007) 1830–1838.

[32] C. Nunes, G. Brezesinski, C. Pereira-Leite, J.L. Lima, S. Reis, M. Lucio, NSAIDs interactions with membranes: a biophysical approach, Langmuir 27 (2011) 10847–10858.

[33] R. Mendelsohn, C.R. Flach, Infrared Reflection–Absorption Spectrometry of Monolayer Films at the Air–Water Interface, John Wiley & Sons Ltd, 2002 1028–1031.

[34] P. Fontaine, M. Goldmann, M. Bordessoule, A. Jucha, Fast and adjustable-resolution grazing-incidence x-ray liquid surface diffraction, Rev. Sci. Instrum. 75 (2004) 3097–3106.

[35] F. Neville, M. Cahuzac, O. Konovalov, Y. Ishitsuka, K.Y. Lee, I. Kuzmenko, G.M. Kale, D. Gidalevitz, Lipid headgroup discrimination by antimicrobial peptide LL-37: insight into mechanism of action, Biophys. J. 90 (2006) 1275–1287.

[36] C.E. Miller, D.D. Busath, B. Strongin, J. Majewski, Integration of ganglioside GT1b receptor into DPPE and DPPC phospholipid monolayers: an X-ray reflectivity and grazing-incidence diffraction study, Biophys. J. 95 (2008) 3278–3286.

[37] S. Perkovic, H.M. McConnel, Cloverleaf Monolayer Domains, J. Phys. Chem. B 101 (1997) 381–388.

[38] C.W. McConlogue, T.K. Vanderlick, A Close Look at Domain Formation in DPPC Monolayers, Langmuir 13 (1997) 7158–7164.

[39] S. Furuike, V.G. Levadny, S.J. Li, M. Yamazaki, Low pH Induces an Interdigitated Gel to Bilayer Gel Phase Transition in Dihexadecylphosphatidylcholine Membrane, Biophys. J. 77 (1999) 2015–2023.

[40] K. Anic, A.V. Bukhtiyarov, H. Li, C. Rameshan, G. Rupprechter, CO Adsorption on Reconstructed Ir(100) Surfaces from UHV to mbar Pressure: A LEED, TPD, and PM-IRAS Study, J. Phys. Chem. C 120 (2016) 10838–10848.

[41] A.M. Seddon, D. Casey, R.V. Law, A. Gee, R.H. Templer, O. Ces, Drug interactions with lipid membranes, Chem. Soc. Rev. 38 (2009) 2509–2519.

[42] J.H. Miner, Renal basement membrane components, Kidney Int. 56 (1999) 2016–2024.

[43] H. Sato, J.B. Feix, Peptide-membrane interactions and mechanisms of membrane destruction by amphipathic alpha-helical antimicrobial peptides, Biochim. Biophys. Acta 1758 (2006) 1245–1256.

[44] M. Ashrafuzzaman, C.Y. Tseng, M. Duszyk, J.A. Tuszynski, Chemotherapy drugs form ion pores in membranes due to physical interactions with lipids, Chem. Biol. Drug Des. 80 (2012) 992–1002.

[45] S. Schreier, S.V.P. Malheiros, E.d. Paula, Surface active drugs: self-association and interaction with membranes and surfactantes. Physicochemical and biological aspects, Biochim. Biophys. Acta 1508 (2000) 210–234.

[46] E. Nagele, R. Moritz, Structure elucidation of degradation products of the antibiotic amoxicillin with ion trap MS(n) and accurate mass determination by ESI TOF, J. Am. Soc. Mass Spectrom. 16 (2005) 1670–1676.

[47] C.-Y. Lu, C.-H. Feng, Identification of dimer impurities in ampicillin and amoxicillin by capillary LC and tandem mass spectrometry, J. Sep. Sci. 30 (2007) 329–332.

Chapter 6.4

Supporting information

Table S1. Wavenumber of molecular vibrations of a DPPC monolayer in absence or in presence of AMX, at three different pHs (pH 1.2, pH 5 and pH 7.4) and pressures (10 and 20 mN.m⁻¹).

Pressure	*10 mN.m⁻¹*		*20 mN.m⁻¹*	
Subphase pH 1.2	**Buffer**	**AMX**	**Buffer**	**AMX**
υ_{as} (PO₂⁻) (cm⁻¹)	1264 ± 1	1265 ± 1	1265 ± 1	1264 ± 1
υ (CO) (cm⁻¹)	1729 ± 1	1730 ± 1	1729 ± 1	1727 ± 1
υ_s (CH₂) (cm⁻¹)	2854 ± 1	2854 ± 1	2853 ± 2	2853 ± 1
υ_{as} (CH₂) (cm⁻¹)	2920 ± 3	2917 ± 1	2919 ± 1	2917 ± 1
Subphase pH 5	**Buffer**	**AMX**	**Buffer**	**AMX**
υ_{as} (PO₂⁻) (cm⁻¹)	1265 ± 1	1271 ± 1	1265 ± 2	1263 ± 1
υ (CO) (cm⁻¹)	1732 ± 2	1730 ± 1	1733 ± 1	1729 ± 2
υ_s (CH₂) (cm⁻¹)	2850 ± 1	2857 ± 1	2851 ± 2	2852 ± 1
υ_{as} (CH₂) (cm⁻¹)	2921 ± 2	2920 ± 1	2919 ± 1	2920 ± 1
Subphase pH 7.4	**Buffer**	**AMX**	**Buffer**	**AMX**
υ_{as} (PO₂⁻) (cm⁻¹)	1266 ± 1	1262 ± 1	1266 ± 1	1266 ± 2
υ (CO) (cm⁻¹)	1735 ± 1	1722 ± 1	1734 ± 1	1729 ± 1
υ_s (CH₂) (cm⁻¹)	2855 ± 2	2863 ± 1	2853 ± 2	2853 ± 1
υ_{as} (CH₂) (cm⁻¹)	2919 ± 3	2919 ± 2	2915 ± 1	2920 ± 2

DPPC

Figure S1. Brewster angle microscopic images of Langmuir monolayers of DPPC spread onto an amoxicillin subphase at pH 1.2 and 30 mN.m⁻¹ of surface pressure.

Chapter 6.5

Delivering amoxicillin at the infection site – a rational design through lipid nanoparticles

From what we have learnt from the bibliographic review, we chose lipid nanoparticles once 1) they were barely used to treat *H. pylori* infections; 2) they are promising delivery systems for commercial purposes; 3) they showed potentiality to treat infectious diseases by oral administration. We combined antimicrobial compounds and a targeting agent within the particle, and we used a Box-Behnken design to select the physical properties that would enable a higher retention at the site of infection. This work is the full design, development, and characterization of the produced nanoparticles.
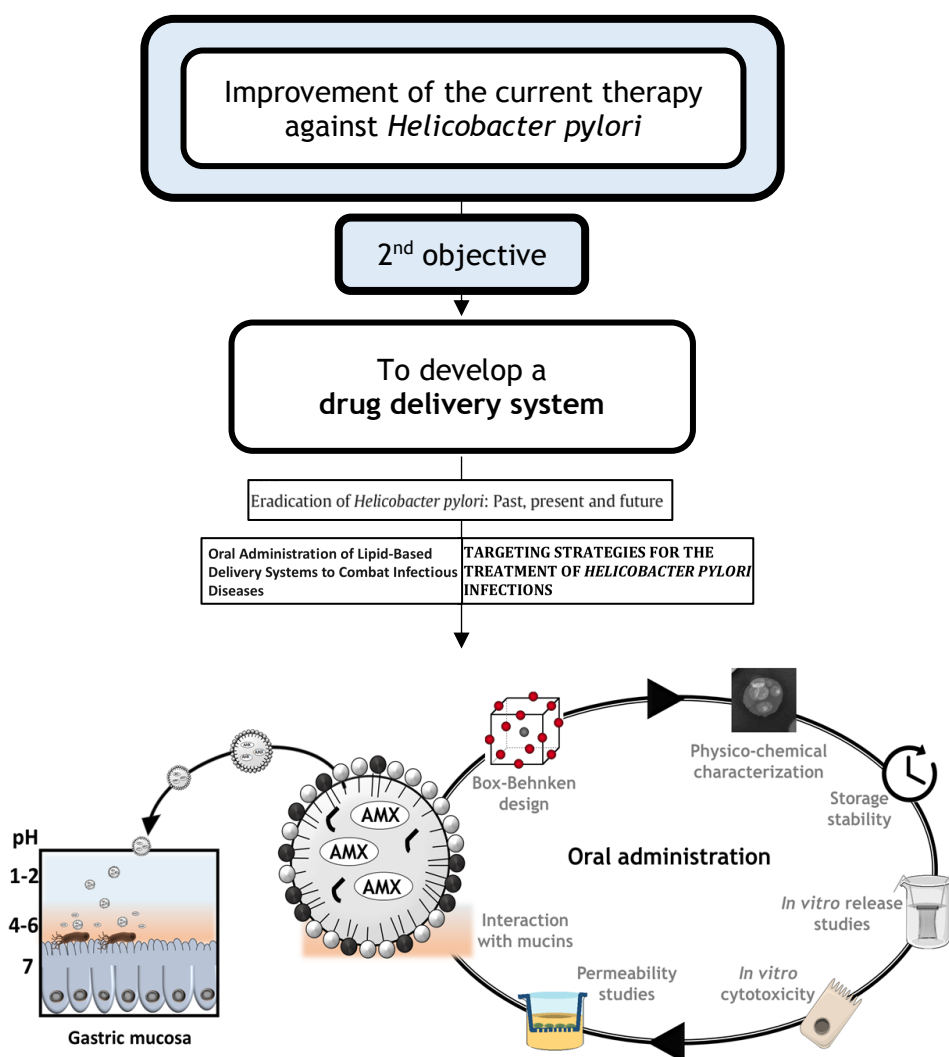
Chapter 6.5

Delivering amoxicillin at the infection site – a rational design through lipid nanoparticles

Daniela Lopes-de-Campos[1,#], Rita M. Pinto[1,#], Sofia A. Costa Lima[1], Tiago Santos[2,3], Bruno Sarmento[2,3,4], Cláudia Nunes[1] and Salette Reis[1*]

[1]LAQV, REQUIMTE, Departamento de Ciências Químicas, Faculdade de Farmácia, Universidade do Porto, Portugal

[2]INEB - Instituto de Engenharia Biomédica, Universidade do Porto, Rua Alfredo Allen 208, 4200-393 Porto, Portugal

[3]i3S - Instituto de Investigação e Inovação em Saúde, Universidade do Porto, Rua Alfredo Allen 208, 4200-393 Porto, Portugal

[4]IINFACTS, Instituto de Investigação e Formação Avançada em Ciências e Tecnologias da Saúde, Instituto Universitário de Ciências da Saúde, Gandra, Portugal

[#]These authors contributed equally to this work

Hypothesis: Amoxicillin is a commonly used antibiotic, though degraded by the acidic pH of the stomach. This is an important limitation for the treatment of *Helicobacter pylori* infections. The encapsulation of amoxicillin in lipid nanoparticles can increase the retention time at the site of infection (gastric mucosa) while protecting the drug from the harsh conditions of the stomach lumen.

Experiments: The nanoparticles were produced by the double emulsion technique and optimized by a three-level Box-Behnken design. Tween 80 and linolenic acid were used as potential therapeutic adjuvants and dioleoylphosphatidylethanolamine (DOPE) as a targeting agent to *Helicobacter pylori*. Nanoparticles were characterized regarding their physico-chemical features, their storage stability, and their usability for oral administration (assessment of *in vitro* release, *in vitro* cell viability, permeability, and interaction with mucins).

Findings: The nanoparticles were stable for at least 6 months at 4°C. *In vitro* release studies revealed a high resistance to harsh conditions (acidic pH, bile salts, lecithin, and temperature). The nanoparticles have a low cytotoxicity effect in both fibroblasts and gastric cell lines, and they have potential to be retained at the gastric mucosa. Overall, the designed formulations present suitable physico-chemical features for being henceforward used by oral administration to treat *Helicobacter pylori* infections.

Keywords: amoxicillin, linolenic acid, lipid nanoparticles, Box-Behnken design, permeability, mucins.

1. Introduction

Amoxicillin (AMX) is a commonly used β-lactam antibiotic that acts by inhibiting the synthesis of bacterial cell walls [1]. AMX is recommended by international guidelines to be a first-line drug against *Helicobacter pylori (H. pylori)* infections [2]. These bacteria have been associated with chronic gastritis, peptic ulcers, and cancer [3, 4]. Nevertheless, its eradication rates are distant from the desirable for infectious diseases [2]. The main

limitations are caused by the pharmacokinetic properties of antibiotics. For instance, AMX is degraded under the acidic pH of the stomach lumen mainly due to the hydrolysis of its β-lactam ring [5-7]. The degradation of AMX leads to a need of higher doses and, consequently, to more side effects [8]. Our research group have already shown that at acidic pHs AMX can promote pore formation in a monolayer of phosphatidylcholines [9]. The low residence time of AMX in the stomach is also a drawback once *H. pylori* is located in the gastric mucosa [3, 10]. Therefore, the treatment of *H. pylori* infections is not feasible in monotherapy [8]. Instead, two or three antibiotics (e.g. amoxicillin, clarithromycin, and metronidazole) are needed, which increases the incidence of side effects and decreases the therapeutic compliance [8].

Several micro- and nanoparticles have been suggested as promising strategies to improve the pharmacokinetic properties of antibiotics [8, 11]. AMX has being the focus of several studies due to its efficacy. For example, AMX is still effective against *H. pylori*, with generally low resistance rates (1-3%), contrary to clarithromycin (16-24%) and metronidazole (20-40%) [12]. AMX has been encapsulated in several delivery systems [8], such as polymeric nanoparticles (e.g. [13-15]), gastroretentive tablets (e.g. [16, 17]), and liposomes (e.g. [18]). However, lipid nanoparticles (LNPs) have not yet been used to encapsulate AMX. LNPs are generally cost-effective and easily scaled-up, which enhance their interest for commercial purposes [19, 20]. They are also biocompatible and biodegradable [19, 20]. *H. pylori* secrete lipolytic enzymes, including carboxylesterases [21, 22]. These enzymes may degrade the lipid matrix, which promotes a local release of the antibiotic. Additionally, Seabra *et al.* (2017) showed the efficacy of LNPs against *H. pylori* [23]. There is also the possibility of functionalizing LNPs to target bacteria and to release the drug near the site of infection [11, 24]. There are in fact some targeting options for both *H. pylori* and the gastric mucosa [25], that have been used in this work.

The purpose of this study was to design and optimize LNPs to load AMX and target *H. pylori* and to overcome the need of multiple antibiotics by using the antibacterial properties of the LNPs components. Tween 80 was chosen as surfactant due to its ability to detach *H. pylori* outer membrane [26]. Consequently, it has a synergistic effect with some antibiotics [26]. Two additional compounds (viz. linolenic acid and dioleoylphosphatidylethanolamine (DOPE)) were also added. Four LNPs formulations, which are distinguished by the presence or the absence of the two additional compounds (Figure 1), were studied and characterized. Linolenic acid is an unsaturated fatty acid. These fatty acids are known for their antibacterial properties, their generally low cost, and their abundance in the nature [27, 28]. Linolenic acid is one of the most potent ones against *H. pylori,* perturbing the integrity of the bacterial membrane [27, 29]. Its effect in both coccoid and spiral forms of resistant *H.*

pylori was already proven [30]. On the other hand, DOPE enables an active targeting to *H. pylori* due to the existence of receptors to phosphatidylethanolamine in these bacteria [31]. It is in fact with these receptors that these bacteria attach themselves to the antrum of human stomach [31]. Thus, DOPE may block the bacterial adhesion to the gastric mucosa, hindering its colonization [25].
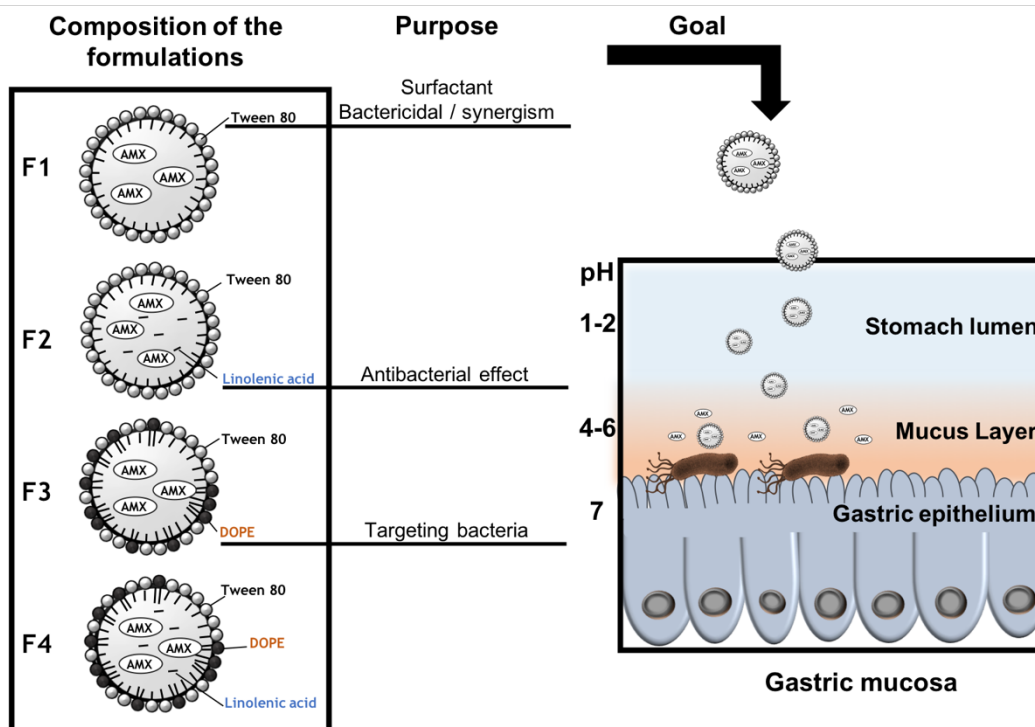
Figure 1. AMX-loaded LNPs, which were designed to release AMX near *H. pylori*. The double-emulsion LNPs are composed of cetyl palmitate, Tween 80, linolenic acid, and DOPE.

The present work encompasses the full design, development, and characterization of AMX-loaded LNPs for oral administration. By protecting AMX from the acidic pH and combining additional antibacterial strategies, an effective formulation for oral delivery is expected. A Box-Behnken factorial design (BBD) was used to improve the optimization process once it avoids the analysis of one variable at a time, and it evaluates simultaneous interactions among different variables [32]. Ultimately, it minimizes the costs associated with the optimization process with respect to both time and financial costs [33]. A comprehensive physical characterization (morphology, particle size, polydispersity (PDI), zeta potential, and loading capacity (LC)) was performed. Moreover, the storage stability, the *in vitro* release at different pHs, the cytotoxicity in two cell lines, the permeability through gastric cell monolayers, and nanoparticle-mucin interactions were also assessed.

2. Materials and methods

2.1 Materials

The lipids Gelucire® 43/01, Gelucire® 44/14, Cetyl palmitate, Compritol® 888 ATO and Precirol® ATO5 were a kind gift from Gattefossé (Gattefossé, France). Softisan® 100, Dynasan® 116, Imwitor® 900 K, and Imwitor® 491 were gently offered by Sasol (Johannesburg, South Africa). 1,2-di-(9Z-octadecenoyl)-*sn*-glycero-3-phosphoethanolamine (DOPE) was purchased from Avanti® Polar Lipids (Alabaster, AL, USA). Acetonitrile 99%, chloroform, and acetic glacial acid were obtained from VWR International LLC (Radnor, PA, USA). SIF® Powder was obtained from Biorelevant (Whitechapel, London, United Kingdom). Hydrochloric acid was purchased from Fisher Scientific International Inc. (Pittsburgh, PA, USA). Dulbecco's Modified Eagle's Medium (DMEM), Roswell Park Memorial Institute (RPMI) medium, trypsin-EDTA (1x), Penicillin-Streptomycin (Pen Strep), Dulbecco's Phosphate Buffered Saline 10x pH 7.4 (PBS), Fetal Bovine Serum (FBS), and Hanks' Balanced Salt Solution (HBSS) with $CaCl_2$ and $MgCl_2$ were purchased from Gibco® (Invitrogen Corporation, Paisley, UK). L929 cells (ATCC® CCL-1TM) were acquired from ATCC® (Manassas, VA, USA). MKN-74 cell line was acquired from the BioBank of Instituto de Investigação e Inovação em Saúde (i3S). Amoxicillin trihydrate, linolenic acid, Tween 80, coumarin-6, and mucins type II were obtained from Sigma-Aldrich® (St. Louis, MO, USA). All components were used without further purification.

2.2 Methods

2.2.1 Preparation of the AMX-loaded LNPs

Two different methods of synthesis were evaluated, namely, i) modified free organic-solvent emulsification/sonication method and ii) double emulsion method. In the first method, the solid lipid (cetyl palmitate) and the surfactant Tween 80 were melted in a hot bath at a temperature above their melting point (from 60°C to 80°C). AMX was solubilized in Milli-Q water using an ultrasounds bath. The lipid phase was then dispersed in 6 mL of the pre-heated AMX solution at the same temperature. The emulsion was promoted by sonication for 5 min at 70% amplitude and cooled in ice for 30 sec. In the double emulsion method, the solid lipid and, when applied, the linolenic acid, were dissolved in chloroform (2 mL). AMX was dissolved in a small volume of NaOH (1 M), and Milli-Q water was added until a final volume of 0.5 mL. This solution was then added to the lipid phase. The emulsion was promoted by sonication for 30 sec at 70% amplitude. When applicable, DOPE (20 mg) was added after dissolution in a small volume of chloroform. A solution of Tween 80 (4 mL,

different concentrations) was added to the emulsion, which was then sonicated for 2 min at 70% amplitude. A solution of Tween 80 in a lower concentration (4 mL, 12.5 mg.mL^{-1}) was then added and the resulting LNPs suspensions were placed in a stirring plate at room temperature for 3 h to evaporate the chloroform. In both methods, the LNPs were protected from light during the entire process of synthesis and storage. Unloaded LNPs were prepared by replacing the drug solution with Milli-Q water. For the permeability studies, coumarin-6 was previously dissolved in a small volume of chloroform, and then it was added to the solid lipid dissolved in the same solvent. The final concentration of coumarin-6 was 0.3 % of the total mass of LNPs.

2.2.2 Experimental design

The BBD was used to optimize and evaluate the effect of different variables on the characteristics of AMX-loaded LNPs [32]. In this study, a 15-run, 3-factor, 3-level BBD was used, in which the solid lipid mass (X_1), the concentration of Tween 80 (X_2), and the AMX mass (X_3) were defined as the independent variables. The concentration of Tween 80 in the second addition was kept constant (12.5 mg.mL^{-1}) and only the mass used in the first addition varied. These variables were studied at three different levels (low (-1), medium (0) and high (1)) (Table A.1 of the supporting information), which were stablished from preliminary experiments. The dependent variables were the size (Y_1), the PDI (Y_2), and the LC (Y_3), and the correspondent constraints are also summarized in Table A.1. The experimental runs were generated and further evaluated using STATISTICA Software (v12, StatSoft Inc; Tulsa, OK, USA). The response values that were predicted for the dependent variables were compared with the experimental ones.

2.2.3 Association efficiency and loading capacity

The association efficiency (AE) was calculated by knowing the amount of AMX encapsulated in the LNPs. The formulations were diluted (1:50) in Milli-Q water and transferred into an Amicon® Ultra-4 Centrifugal Filter Device, ultracel - 50k (50000 NMWL) (MERK Milipore, Ltd; Cork, Ireland). After centrifugation at 524 g until complete separation of the LNPs from the supernatant AMX, the filter unit was centrifuged in an inverted position at 4713 g during 5 min. The pellet of the AMX-loaded LNPs was then dissolved in 2 mL of acetonitrile and centrifuged at 5251 g until full deposition of the lipid. The entrapped AMX, solubilized in acetonitrile, was quantified using UV-Vis spectroscopy (V-660, Jasco Corporation, Software: Spectra Manager V.2, Jasco Corporation; Easton, MD, USA) at 273 nm. The AE was calculated as follows (Eq. 1):

$$AE(\%) = \frac{\text{Entrapped AMX amount}}{\text{Total AMX amount}} \times 100 \qquad (1)$$

The AE was used to calculate the LC, which was defined by the ratio of the percentage of the drug incorporated into the LNPs and the total amount of lipid in the LNPs (Eq. 2):

$$LC(\%) = \frac{\text{Association efficiency} \times \text{Total AMX amount}}{\text{Total lipid amount}} \times 100 \qquad (2)$$

2.2.4 Physical characterization of LNPs

Both the size and the PDI were determined in a Particle Size Analyser by Dynamic Light Scattering (Brookhaven Instruments Corporation; Software: Particle Sizing v.5 Brookhaven Instruments; Holtsville, NY, USA). The results correspond to the mean hydrodynamic diameter (size) and the mean PDI. In the determination of the zeta potential, a Zeta Potential Analyser (ZetaPALS, Brookhaven Instruments Corporation; Software: PALS Zeta Potential Analyser v.5 Brookhaven Instruments; Holtsville, NY, USA) was used. The system was operating at a fixed light incidence angle of 90°, at 25°C. The LNPs suspensions were diluted (1:100) in Milli-Q water prior to measurements.

Transmission electron microscopy (TEM) was used to assess the morphology of LNPs. LNPs suspensions were diluted (1:4) in Milli-Q water. LNPs suspension (10 µL) were then placed on a copper-mesh grid. After 1 to 2 min, the excess was removed, and 0.75% (w/v) uranyl acetate solution (10 µL) was used for 30 sec at room temperature to obtain a negative staining. The samples were observed in a JEM-1400 Transmission Electron Microscope (JEOL Ltd., Tokyo, Japan), with an acceleration voltage of 80 kV.

2.2.5 Assessment of the storage stability

The LNPs in liquid suspension were stored at 4°C for 6 months. The physico-chemical stability was evaluated by measuring the particles size, the PDI, the zeta potential, and the LC over time. All these properties were assessed according to the procedures mentioned in the previous sections. All formulations were protected from light.

2.2.6 *In vitro* **AMX release study**

In vitro release was assessed using the dialysis diffusion technique under sink conditions. A cellulose dialysis bag (Float-A-Lyzer®G2 Dialysis Device, 3.5 – 5 kD MWCO, SpectrumLabs; Rancho Dominguez, CA, USA) was filled with LNPs suspensions (1.5 mL) and placed into a preheated (37°C), light protected, and stirred dissolution media (75 mL). The release was assessed in three different pHs to mimic the pH gradient of the gastric mucosa, namely, extremely acidic pH in the stomach lumen, the intermediate pH in the mucus layer, and the pH near to neutral in the epithelial cells (Figure 1) [34]. Thus, this study intended to simulate the release of AMX during the absorption of AMX-loaded LNPs through the gastric mucosa after oral administration. For that purpose, three conditions were defined: i) 3h in fasted state simulated gastric fluid (FaSSGF: NaCl/HCl solution, pH 1.6 with SIF®Powder, with bile salts and lecithin); ii) 1h in acetate buffer solution (pH 5, I=0.13 M), and iii) 22h in Hepes buffer solution (pH 7.4, I=0.1 M using NaCl). Several aliquots were collected to a UV-Vis microplate (Corning® 96-well UV Microplates, Corning Inc.; Corning, NY, USA) at specific time points and replaced with the same volume of fresh medium. The release rate was quantified by UV-Vis spectroscopy at 277 nm using a microplate reader (BioTek Instruments Inc., Synergy HT, Software: Gen5 v1.08.4, BioTek Instruments Inc.; Winooski, VT, USA). Mathematical models were fitted to the experimental data, namely, zero order, first order, Higuchi and Hixon-Crowell to assess the main mechanisms that lead to the release of AMX [7]. Regression coefficients (r^2) were used to evaluate the best fitting model.

2.2.7 *In vitro* **cell viability studies**

Cell viability studies were performed using two different cell lines. Mammalian mouse fibroblast cell lines, L929, are recommended by the ISO international standard 10993-5 as a standard cell line for biocompatibility assessment [35]. MKN-74, a gastric cancer cell line, was used to evaluate any potential gastric cytotoxicity. These cell lines were previously cultured at 37°C, in a 5% CO_2 atmosphere. L929 cells were cultured in DMEM supplied with 10% FBS and 1% Pen Strep, whereas MKN-74 cells were cultured in RPMI culture medium equally supplied with 10% FBS and 1% Pen Strep. A MTT assay was performed to assess cell viability. Briefly, after 80 to 90 % of confluence, cells were detached from the culture flask by physical detachment using a cell scraper (L929 cell line) or by chemical detachment using 0.25% (w/v) trypsin-EDTA (MKN-74 cell line). The collected cells were seeded in 96-well tissue culture test microplates at a density of 10^5 cells/well. After adhesion, they were incubated with the LNPs suspensions in different solid lipid concentrations (0.5, 1.0, 2.0,

4.0, and 8.0 mg.mL^{-1}) for 24h (L929 cell line) or for 4h (MKN-74 cell line). The medium was then replaced by the MTT solution (100 μL, 0.5 mg.mL^{-1} in fresh medium), and incubated for 2h (L929 cells) or 3h (MKN-74 cells). Formazan crystals were dissolved in DMSO (100 μL) and its absorbance was measured at 590 and 630 nm using a microplate reader (BioTek Instruments Inc., Synergy HT, Software: Gen5 v1.08.4, BioTek Instruments Inc.; Winooski, VT, USA). The latter was used for background subtraction.

2.2.8 Permeability studies

Considering that *H. pylori* is located in the interface between the gastric epithelium and the mucus layer of the gastric mucosa [3, 10], it is important to assess the ability of the AMX-loaded LNPs to be retained by the gastric cells. For that purpose, MKN-74 cells (passage number from 5-12) were cultured in the same conditions as in the cell viability studies. The cells were seeded on Transwell inserts (polyethylene terephthalate membranes with a pore size of 8 μm, Corning Incorporated; Corning, NY, USA) in a cell density of 1x10^5 cells per well (growth area of 0.3 cm^2). After 5 days, the formation of cell monolayers was evaluated using an epithelial VOM2 Voltohmmeter (World Precision Instruments) to measure the transepithelial electric resistance (TEER). The TEER was also measured at the end of the experiment to assess the integrity of the monolayer.

For the permeability studies, 600 and 400 μL of Hank's salt (HBSS) were used at the basolateral and the apical side, respectively. The study was performed using cell monolayers without and with the addition of porcine mucins type II to mimic the mucus layer. In the cases where mucins were added, the protocol was adapted from [36]. Briefly, 50 μL of mucins at 1% *w/v* were added to MKN-74 cells in the apical compartment and incubated for 30 min at 37°C and at 100 r.p.m. in an orbital shaker. The same volume of HBSS was added to the other cells and incubated in the same conditions. Afterwards, 350 μL of AMX-loaded LNPs labelled with coumarin-6 were added to a final concentration of 2 mg.mL^{-1} of solid lipid. After 3h of incubation, the amount of labelled LNPs in each compartment was determined (λ_{exc} = 420 nm and λ_{em} = 504 nm). Transwell inserts without cells were used as positive controls, and transwell inserts only with mucins were used to evaluate the ability AMX-loaded LNPs to be retained by mucins.

The % of permeability was calculated as follows (Eq. 3):

$$\%_{permeability} = \left[\left(\frac{F_{basolateral}}{F_{apical+basolateral}} \right) \middle/ \left(\frac{F_{basolateral\ without\ cells}}{F_{apical+basolateral\ without\ cells}} \right) \right] \times 100 \qquad (3)$$

where F stands for the fluorescence at the maximum of emission (504 nm). The apparent permeability coefficient (P_{app}) was calculated according to the following equation (Eq. 4):

$$P_{app}(cm.s^{-1}) = \frac{m(LNPs)_{normalized}}{A \times [LNPs]_0 \times t} \qquad (4)$$

where $m(LNPs)_{normalized}$ stands for the amount of AMX-loaded LNPs (mg) that permeated the monolayer, normalized by considering the positive control. A is the diffusion area (cm^2), $[LNPs]_0$ is the initial concentration of AMX-loaded LNPs (mg.mL^{-1}), and t is the time in sec.

2.2.9 Nanoparticle-mucin interaction studies

AMX-loaded LNPs were diluted to a final concentration of 2 mg.mL^{-1} in a solution of HBSS or HBSS with mucins in a concentration of 1% *w/v* and then incubated for 3h at 37°C. The size, the PDI, and the zeta potential were assessed according to the methodology described in the section 2.2.4.

2.2.10 Statistical analysis

Statistical analysis was performed using GraphPad Prism Software (v6.01 for Windows; GraphPad Software Inc, San Diego, CA, USA). All assays were performed at least three independent times, and the data is expressed as mean ± SD. The data was analysed using two-way analysis of variance (ANOVA). A *p*-value under 0.05 was considered statistically significant.

3. Results and discussion

An initial lipid screening was performed using 9 different solid lipids (Gelucire® 43/01, Cetyl palmitate, Compritol® 888 ATO, Precirol® ATO 5, Softisan® 100, Gelucire® 44/14, Dynasan® 116, Imwitor® 900 k, and Imwitor® 491) to prepare LNPs by the modified free organic-solvent emulsification/sonication method. The affinity of AMX to each lipid was evaluated through both the AE and the LC. Furthermore, physical characterization (size, PDI, and zeta potential) was also performed. Cetyl palmitate was selected due to the highest LC, the lower size, and the zeta potential of the LNPs. Furthermore, two different methods of synthesis were evaluated, namely, modified free organic-solvent emulsification/sonication and double emulsion synthesis. Once more, physical characterization, AE and LC were the key parameters used to evaluate the method of synthesis. AMX-loaded LNPs produced by the double emulsion technique gave the most promising results.

3.1 Experimental design

After the initial screening, preliminary batches of LNPs were used to evaluate the key variables that affected the physical properties and the LC of AMX-loaded LNPs. The key variables, considered as independent variables for the BBD, were the amount of solid lipid, the concentration of Tween 80, and the amount of AMX. Since F4 (see Figure 1) is the most complex formulation, it was selected to be optimized by the experimental design. The mass of both DOPE (20 mg) and linolenic acid (5 mg) was kept constant.

Fifteen formulations suggested by the software were produced and fully characterized. Three out of the fifteen formulations corresponded to a central point, which is used to estimate the experimental error. The size, PDI, and LC were selected as dependent variables. The R^2 values obtained from the correlation between the experimentally measured values and the predicted values were used to evaluate the best fitting model. The quadratic model (Eq. A.1) was selected due to the higher R^2 values (Figure A.1 of the supporting information). A detailed description of the BBD results is provided in the supporting information. An ideal formulation (F4) was suggested by the STATISTICA v12 software (detailed composition in Table 1) by considering the effects of each factor in each dependent variable and the constraints applied for each one. The particle size is an important parameter for gastric diffusion. It is known that particles with more than 200 nm have a decreased diffusion through the gastric mucosa [8]. Furthermore, nanoparticles with smaller sizes (50 and 200 nm) showed higher mucoadhesion than particles of 750 nm to the inflamed tissue of gastric ulcers [37]. On the other hand, the reduction of the size of

nanoparticles promotes early drug release in the gastrointestinal tract [37, 38]. Thus, Table A.1 shows the constraints applied for the size of the LNPs, with low desirability for sizes above 250 nm. For the other dependent variables, the ideal was a minimum PDI and a higher LC.

The produced LNPs had 197 nm, a PDI of 0.137, and a LC of 7.5, which is not statically different from the predicted values (average size of 184 nm, average PDI of 0.103, and an average LC of 7.5). These results validate the experimental design and show the robustness of the model.

3.2 Physical-chemical characterization

After the optimization of the F4 formulation, other three formulations (F1, F2, F3) were produced (Table 1). The difference among the four formulations was their composition (Figure 1) relatively to the presence or absence of linolenic acid and DOPE. The main goal of studying these formulations is to provide insights on the influence of these compounds in the physical properties of the LNPs. Given the usefulness of linolenic acid as an antibacterial adjuvant [30] and DOPE as an active targeting [31], the full characterization of these systems will support future studies of LNPs-*H. pylori* interactions. The respective unloaded LNPs (P1, P2, P3, and P4) were also studied to evaluate the influence of AMX on the physical properties of the LNPs. The composition of each formulation and the respective physico-chemical characterization are presented in Table 1.

All AMX-loaded LNPs and the correspondent unloaded LNPs were white, milky, and with low viscosity. Furthermore, LNPs aggregation or AMX deposits were not visible in any formulation. The encapsulation of AMX does not significantly affect any of the studied physical properties (*p*>0.05 when comparing the formulation with the respective unloaded LNP). The concentration of Tween 80 may stabilize the aqueous vacuoles, and AMX may be entrapped in those vacuoles and not in the lipid matrix of the LNPs. Thus, the interaction with the lipid phase is minimal, and similar physical properties of the unloaded LNPs and the AMX-loaded LNPs are expected. Moreover, both the PDI and the zeta potential are also similar among all formulations (*p*>0.05). Lower values of particle size distribution (PDI < 0.15) and negative zeta potential values (< - 35 mV) indicate that all formulations are stable, with low tendency to aggregate [39, 40]. These results are coherent with the visible aspect of the formulation.

Table 1. Composition and physical characterization (size, PDI, zeta potential, and LC) of the four AMX-loaded LNPs and the corresponding unloaded LNPs.

Formulation	P1	F1	P2	F2	P3	F3	P4	F4
[mg]								
Cetyl palmitate	178.5	178.5	178.5	178.5	178.5	178.5	178.5	178.5
Tween 80	130	130	125	125	110	110	105	105
Linolenic acid	-	-	5	5	-	-	5	5
DOPE	-	-	-	-	20	20	20	20
AMX	-	19.9	-	19.9	-	19.9	-	19.9
Size [nm]	291 ± 5	284 ± 11	243 ± 17	240 ± 16	237 ± 12	236 ± 18	178 ± 9	197 ± 2
PDI (± 0.02)	0.14	0.14	0.12	0.12	0.12	0.14	0.11	0.12
ζ [mV]	-48 ± 1	-40 ± 1	-39 ± 5	-46 ± 4	-42 ± 4	-37 ± 4	-42 ± 2	-43 ± 3
LC [%]	-	6.3 ± 0.1	-	6.8 ± 0.4	-	5.7 ± 0.6	-	7.5 ± 0.2

The amount of Tween 80, linolenic acid, and DOPE affect the size of the LNPs, which are smaller when linolenic acid and/or DOPE are used to replace part of the Tween 80. The difference between the average size among all formulations are statistically different, with the exception of the comparison between F2 and F3. Given the chemical structural of linolenic acid, it is probably entrapped in the lipid matrix. Therefore, it may be stablishing hydrophobic interactions that can increase the packing of the lipid molecules. Consequently, it can decrease the size of the LNPs. On the other hand, DOPE may have a stabilizing effect, similar to Tween 80, which reduces even more the interfacial tension between the phases with different lipophilicities [41]. These results show that, at least partially, DOPE is at the surface of the LNPs. Hence, it can interact with *H. pylori*, fulfilling its purpose of targeting.

The LC also depends on the presence of Tween 80, linolenic acid, and DOPE. The LC of both F2 and F4 formulations are statistically higher than the LC of the other formulations, which indicates that linolenic acid increases the encapsulation of AMX. This is in agreement with the hypothesis of a higher packing of the lipid matrix caused by the linolenic acid, which can promote the formation of larger aqueous vacuoles. Thus, a higher number of AMX molecules can be entrapped. The molecular structure and the effect of both compounds (linolenic acid and DOPE) on the physical properties of the LNPs indicate that these components are within the particles. Furthermore, the low PDI values decrease the hypothesis of micelles formation.

The morphology of the formulations was also evaluated using TEM (Figure 2). The results revealed that both unloaded and AMX-loaded LNPs have a similar spherical shape with no visible aggregation. This is coherent with the results already determined by dynamic light scattering. TEM images show aqueous vacuoles, which is expected considering the

method of the production of the LNPs. In fact, nanoparticles produced by this technique can contain from few to many small compartments, depending on their size [42].
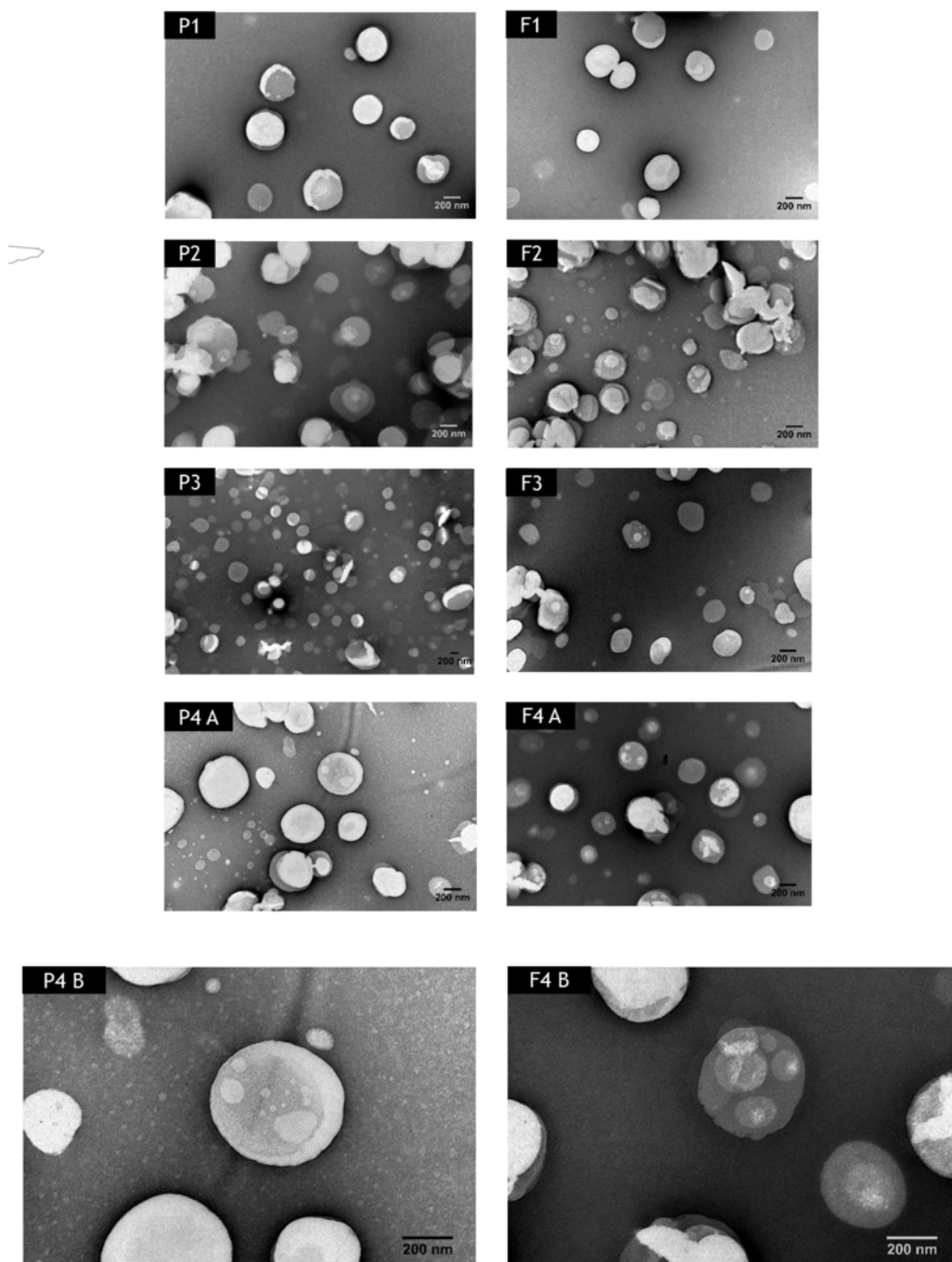
Figure 2. TEM images of the AMX-loaded LNPs and the correspondent unloaded LNPs. P1, F1, P2, F2, F3, P4A, F4A are in a magnification of 50,000 X. P3 is in a magnification of 25,000 X. P4B and F4B are in a magnification of 100,000 X.

3.3 Storage stability

LNPs suspensions were kept for 6 months at 4°C, protected from the light. The particles size, the PDI, the zeta potential, and the LC were evaluated at weeks 0, 1 and 2 and then every month until the end of the study. Given the amount of data, only the results of three months (0, 3, and 6 months) are shown for each property (Figure 3). The detailed results of both unloaded and AMX-loaded LNPs at other time points are presented in the supporting material (Figure A.3 to A.6).
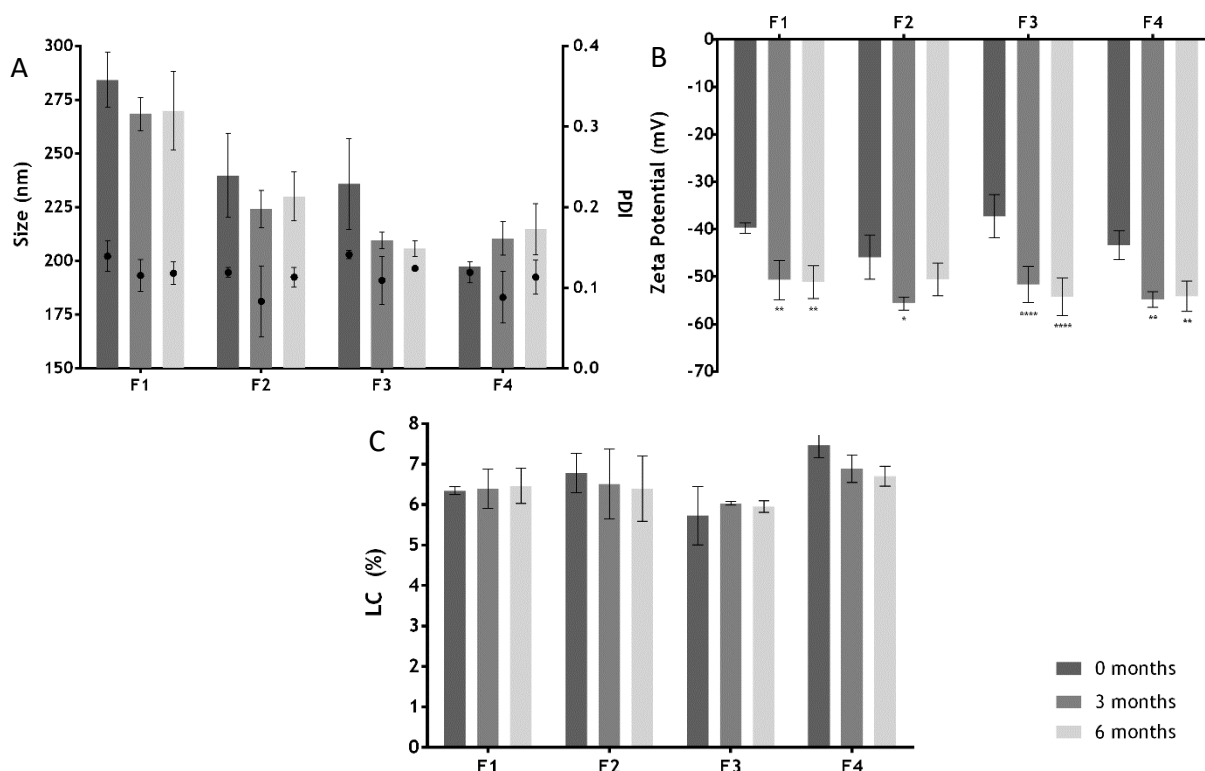
Figure 3. Particles size and PDI (A), zeta potential (B), and LC (C) of the LNPs suspensions, over time (0 months (dark grey), 3 months (intermediate grey) and 6 months (light grey)). In the graphic A, bars represent the size (left Y axis) and dots represent the PDI (right Y axis). Values represent the mean ± SD of three independently produced formulations. *$p < 0.05$, **$p < 0.01$, ***$p < 0.005$, ****$p < 0.0001$ relatively to 0 months.

All AMX-loaded LNPs were stable over at least 6 months with respect to both size and PDI (Figure 3A). No statistically significant variations were verified, excepting for P4 (see Figure A.3 of the supporting information). All the formulations showed a homogenous size distribution (PDI<0.15) with a mean diameter lower than 300 nm. Furthermore, despite the variances over time in the zeta potential value (Figure 3B), their highly negative values (always < -35 mV) reflect the high stability of the LNPs due to lower probability of aggregation [39, 40]. These physical characteristics affect several pharmacokinetic and

pharmacodynamic properties, such as *in vivo* distribution and toxicity [40]. Therefore, their stability is crucial for a drug delivery system [40].

The stability of the LC over time reflects the ability of a nanoparticle to avoid drug release during storage. High rates of drug release during storage implies that a higher number of nanoparticles must be administered to achieve the same therapeutic effect. Consequently, the costs increase due to the need of higher quantities of matrix materials [40]. The LC of all AMX-loaded LNPs (Figure 3C) did not significantly changed (*p*>0.05) during the storage for at least 6 months, which shows a high stability.

3.4 *In vitro* AMX release study

In vitro release studies are usually the simplest method to obtain new insights with respect to the pharmacokinetics of the drug delivery system. The dialysis method was used in different pHs to get closer to the media existent in an absorption through the gastric mucosa, namely, i) gastric medium (pH 1.6) for 3h, ii) mucus layer medium with an intermediate pH (pH 5.0) for 1h, and iii) epithelial cells and systemic circulation environment (pH 7.4) until full release. Furthermore, the mimetic gastric medium also contains bile salts and lecithin (FASSGF) to improve the extrapolation. The results obtained from the *in vitro* release studies of all AMX-loaded LNPs are shown in Figure 4.

The profiles of AMX release are similar for all formulations, which reveal that the presence of linolenic acid and DOPE do not affect the diffusion process of AMX through the LNPs. Moreover, they all followed a Higuchi model release. The release from double emulsions can usually occur by two different ways, namely, disintegration of the thin film that stabilizes the aqueous vacuoles or diffusion/permeation processes [43]. Since Higuchi model is based on the laws of diffusion these results show that AMX is released from the LNPs by diffusion. An initial burst release of approximately 15% occurs within the first hour, which in principle corresponds to the non-encapsulated AMX. This result indicates that the LC may be even higher (around 9.5%) than the measured during LNPs characterization (5.7 to 7.7 %). After the initial burst release, all formulations remained stable under the harsh conditions of the gastric medium (pH 1.6) with low rate of AMX release in the first 3h of study. More precisely, less than 25% was released, which shows that the acidic pH of the gastric medium, the presence of bile salts and lecithin, and the temperature (37°C) do not compromise the integrity of the LNPs. Then a controlled and sustained release was achieved at both pH 5.0 and pH 7.4, with 100% released only after 26h.
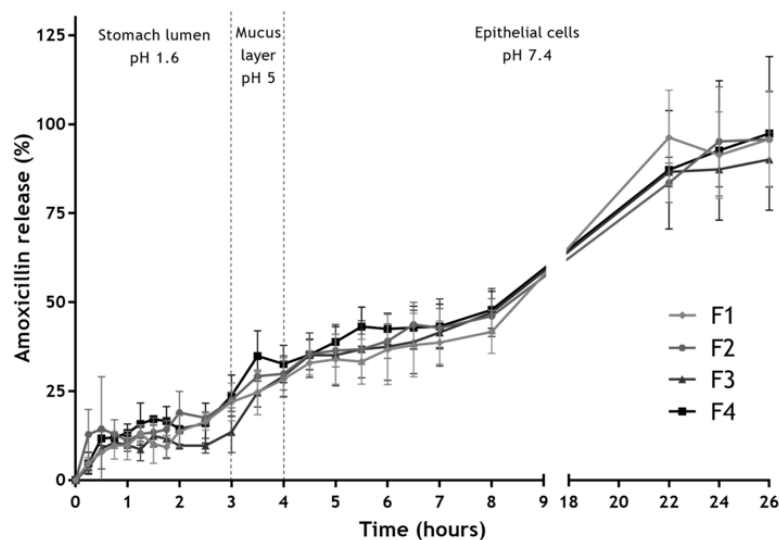
Figure 4. *In vitro* AMX release profiles from the LNPs in three simulated conditions, namely, i) pH 1.6, ii) pH 5.0, and iii) pH 7.4. Vertical lines represent media changes. Values represent the mean ± SD of three independently produced formulations.

3.5 *In vitro* cell viability studies

In vitro cell viability studies are usually the first step to assess the toxicity of drug delivery systems. In this study, two different cell lines were used, namely, fibroblasts (L929) and gastric cells (MKN-74). The first cell line (L929) is recommended by the ISO international standard 10993-5 [35], and the second one (MKN-74) belongs to the first barrier found *in vivo* when the drug delivery system is administrated by the oral route. Considering the location of *H. pylori*, the retention of the LNPs and, consequently, the time of contact near MKN-74 cells would be ideally high. The viability of both cell lines was assessed after incubation with LNPs at different solid lipid concentrations or with plain AMX. It is noteworthy that 0.5 mg.mL^{-1} of solid lipid contain a drug concentration of 0.056 mg.mL^{-1}, which is higher than the AMX plasmatic concentration (0.0146 mg.mL^{-1}) and the AMX concentration in the gastric juice (0.00013 mg.mL^{-1}) [44]. Figure 5 shows the results of the cell viability studies.

The ISO international standard 10993-5 considers that a cytotoxic effect exists when the cell viability is reduced to lower than 70% of the blank [35]. The L929 viability (Figure 5A) was always higher than 70 %, except for 8 mg.mL^{-1} of solid lipid in both P1 and F1 formulations. In the case of MKN-74 (Figure 5B), the percentage of cell viability increased for all formulations with 8 mg.mL^{-1} of solid lipid, with exception of F3 and F4 formulations. There was also a significant increase of the percentage of cell viability when 4 mg.mL^{-1} of the F1 formulation were used. The increased MTT signal can reflect an increase of the

proliferation rate or of the mitochondrial activity [45]. Hence, the formulations with 8 mg.mL^{-1} of solid lipid can interfere either with the normal growth or with the metabolism of MKN-74. This effect is not verified for both F3 and F4 formulations. We believe that there is a balance of effects for F3/F4 formulations. The increase of the MTT signal promoted by Tween 80 is balanced by the reduction of the signal promoted by AMX (reduction to 50% of cell viability). This balance does not happen for F1/F2 formulations due to the higher concentration of Tween 80. This theory is also corroborated by the increase of MTT signal on P3 and P4.
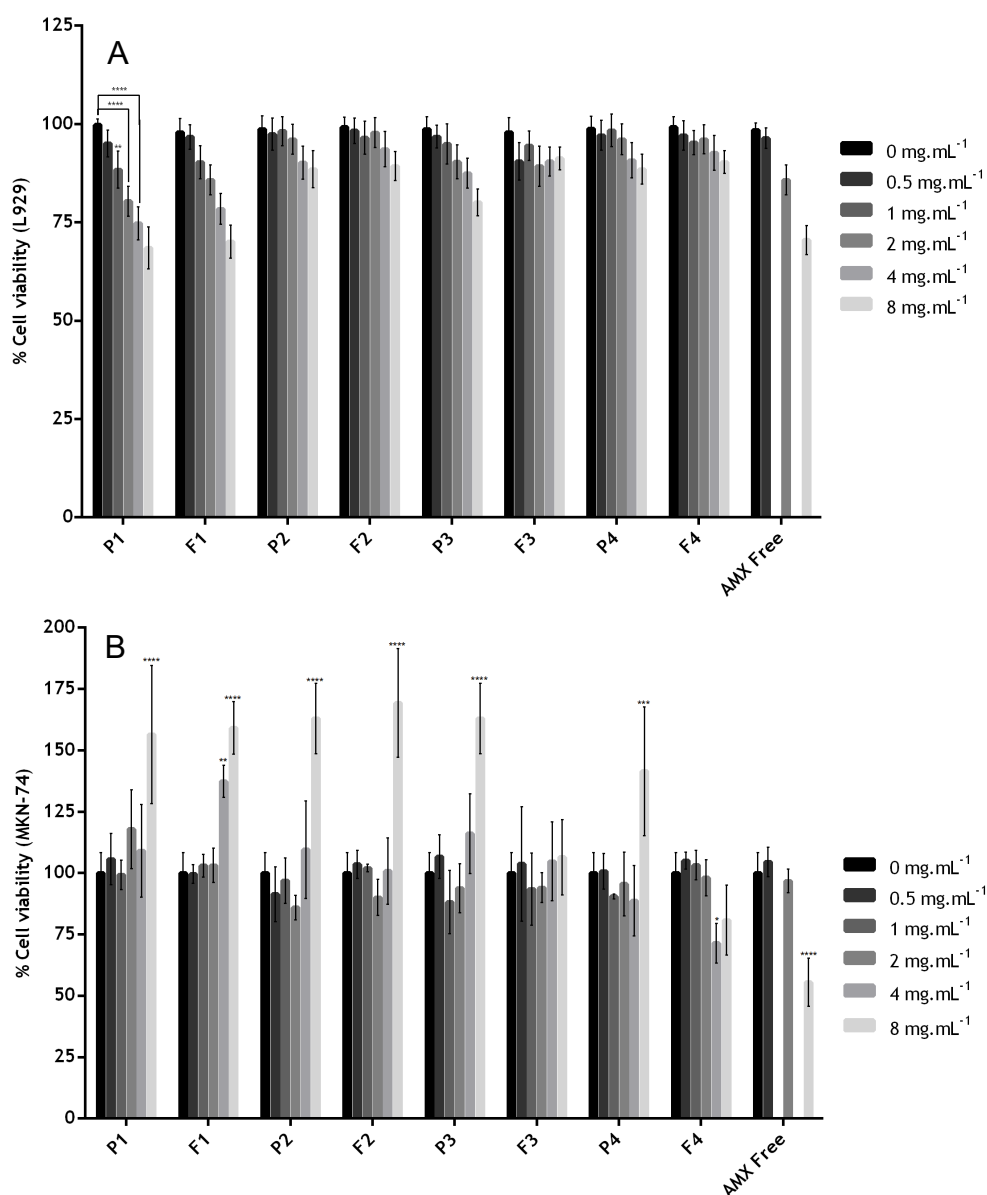
Figure 5. L929 (A) and MKN-74 (B) cell viability of the different formulations in different solid lipid concentrations, from 0 (black) to 8 (light grey) mg.mL^{-1} of solid lipid. For free AMX, the same amount of AMX existent in those concentrations of LNPs was used, with exception of 1 and 4 mg.mL^{-1}. Values represent mean ± SD of three independently produced formulations.*p < 0.05, **p < 0.01, ***p < 0.005, ****p < 0.0001 relatively to 0 mg.mL^{-1}.

The results for both cell lines suggest that the developed AMX-loaded LNPs and the corresponding unloaded LNPs do not interfere with the cell viability until 4 mg.mL^{-1} of solid lipid, with the exception of F1. These doses are significantly higher than the plasmatic concentration of AMX. Therefore, these LNPs have potential to be a safe AMX delivery system for oral administration.

3.6 Permeability assays

For the permeability studies, MKN-74 monolayers were used as a human transwell gastric cell model. Before the addition of the LNPs, the TEER values were above 400 Ω.cm^2. A monolayer with tight junctions similar to those that exist in a gastric epithelium present a TEER value superior to the reference value ranging from 150-200 Ω.cm^2. Therefore, the gastric epithelial barrier was successfully produced. The TEER values were also measured after the incubation with the LNPs. The maintenance of the TEER values (data not shown) suggests that the tight junctions between MKN-74 cells were still functional and the barrier intact.

The permeability of the LNPs were assessed in four distinct systems: i) without cells and without mucins, which worked as a positive control; ii) without cells and with mucins to assess the ability of the LNPs to pass through the network of mucins, which are the major component of the mucus layer; iii) with cells and without mucins to evaluate the permeability of LNPs across gastric epithelial cells; and iv) with cells and with mucins to approximate the model to the *in vivo* gastric mucosa. The results obtained for the percentage of permeability and the apparent permeability coefficient are presented in Table 2. Only AMX-loaded LNPs were evaluated once their physico-chemical properties are similar to the respective unloaded LNPs.

The AMX-loaded LNPs were not able to cross the gastric epithelial cells, even without mucins. Considering that *H. pylori* is mainly attached to the surface of gastric epithelial cells [47], this retention may be a huge advantage to increase the efficacy of the system. This is particularly important in the case of AMX. It was already reported that the effect of AMX is not concentration-dependent as other antibiotics [48]. Instead, it has a time-dependent behaviour [48]. Consequently, a higher retention time near *H. pylori* will increase the efficacy of AMX. In all formulations, roughly 30 % of the AMX-loaded LNPs were able to cross the gel-forming mucins. There are no significant differences among the different AMX-loaded LNPs formulations despite the variation of their sizes. This may lead to the conclusion that the retention of the LNPs is driven by a chemical interaction instead of a physical obstruction. Therefore, nanoparticle-mucin interaction studies were performed.

Table 2. Percentage of permeability and apparent permeability (P_{app}) of the different AMX-loaded LNPs after 3h of incubation in different setups: without cells/with mucins; with cells/without mucins; and with cells/with mucins.

	$\%_{permeability}$			$P_{app} \times 10^{-5}$ (cm.s^{-1})		
	Without cells	With cells		Without cells	With cells	
Mucins	X	-	X	X	-	X
F1	30 ± 1	<LOD	<LOD	3.35 ± 0.06	<LOD	<LOD
F2	31 ± 5	<LOD	<LOD	3.4 ± 0.5	<LOD	<LOD
F3	31 ± 5	<LOD	<LOD	3.5 ± 0.6	<LOD	<LOD
F4	31 ± 4	<LOD	<LOD	3.4 ± 0.4	<LOD	<LOD

* <LOD – below the limit of detection

3.7 Nanoparticle-mucin interactions studies

In a simplistic way, mucoadhesiveness can be defined as the ability of some compounds to be attracted to a mucosa membrane [49]. In this work, nanoparticle-mucin interaction studies were performed by evaluating changes in the physical properties of the AMX-loaded LNPs after incubation with mucins. The results are presented in Figure 6.
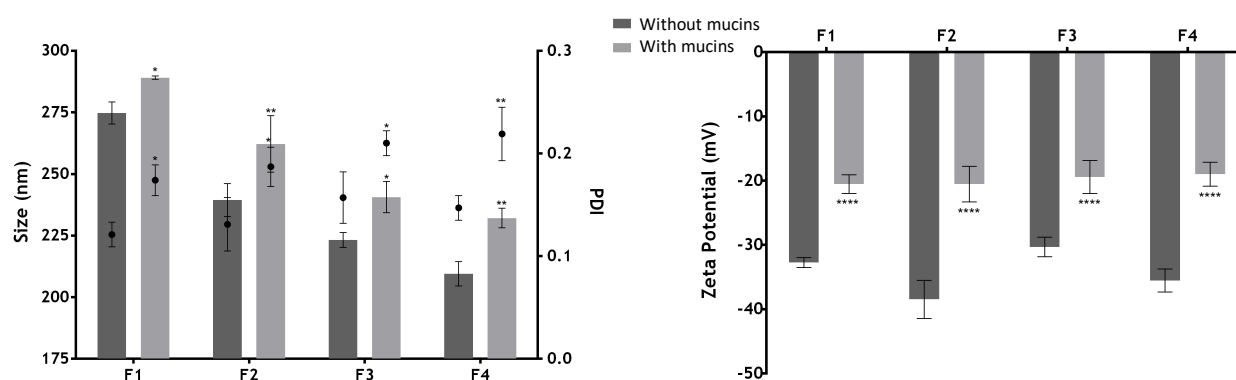
Figure 6. Particles size and PDI (A) and zeta potential (B) of the AMX-loaded LNPs suspensions before (dark grey) and after (light grey) the incubation with mucins. In the graphic A, bars represent the size (left Y axis) and dots represent the PDI (right Y axis). Values represent the mean ± SD of three independently produced formulations. *$p < 0.05$, **$p < 0.01$, ***$p < 0.005$, ****$p < 0.0001$ relatively to the LNPs without mucins.

Mucins have surface groups that are negatively charged, such as sialic and sulfonic groups [50]. Considering the negative charge of the developed LNPs, an electrostatic repulsion would be expected. Interestingly, the incubation with mucins significantly

increased the size, the PDI, and the zeta potential of all formulations, which indicates that the AMX-loaded LNPs can interact with mucins. There are other studies that also show the interaction between negatively charged compounds and mucins [50-52]. There are indeed different theories to explain the complexity of the adhesion to the mucus layer, such as electrostatic interactions, hydrogen bonds, van-der-Waals forces, hydrophobic interactions, among others [49]. Considering the molecular structure of the surface components of the LNPs, Tween 80 and DOPE (Figure A.7 and A.8 of the supporting information, respectively), hydrogen bonds can be stablished between the LNPs and mucins. For instance, carboxylic groups can interact with sugar residues of the monosaccharide side chains [51]. Moreover, mucins also have positively charged groups, namely, the charged amino-acids of mucins non-glycosylated domains [52]. These groups can stablish electrostatic interactions with the negatively charged groups of the surface of the LNPs, if the repulsion is masked. This camouflage effect can happen specially in the presence of salts [50, 52], such as the ones present in the HBSS medium ($CaCl_2$ and $MgCl_2$).

Besides the *H. pylori* that is attached to epithelial cells, there are bacteria that are randomly distributed in the mucus layer [47]. Mucoadhesiveness can in fact be one way of targeting the gastric mucosa, improving the time of contact between the drug and *H. pylori* and, consequently, the efficacy against these bacterial infections [49].

4. Conclusions

In the present work, AMX-loaded LNPs were produced by the double emulsion technique and optimized by a 3-factor, 3-level BBD. As expected by the experimental design, the LNPs have a particle size suitable for diffusion through the mucus layer (around 200 nm) [8, 37]. Furthermore, these LNPs have physico-chemical features suitable for the purpose, namely, a low PDI, a high LC and a long storage stability. *In vitro* release studies revealed that the AMX-loaded LNPs were stable even under harsh conditions (pH 1.6, bile salts, lecithin, and physiological temperature). Since one of the limitations of AMX is its degradation under acidic pH [6], the resistance of the nanoparticle to harsh conditions can overcome that limitation. By taking advantage of the lipolytic enzymes secreted by *H. pylori* [21, 22] and by using an active targeting (DOPE), a local release near the site of infection can be expected. Furthermore, the AMX-loaded LNPs can be retained near the bacteria by the low permeability through gastric epithelial cells and their ability to interact with mucins. Since the effect of AMX is time-dependent [48], a higher retention time near *H. pylori* will increase the efficacy of AMX. Moreover, the development of resistance against these LNPs would be improbable once multiple mutations would be required to fight against different antibacterial compounds (AMX, Tween 80 and linolenic acid) [24]. These results, combined

with the low cytotoxic effect in both fibroblasts and gastric cells, reveal that the produced LNPs may have potential to be administered by oral route against *H. pylori* infections. Studies to evaluate the pharmacodynamic properties of these AMX-loaded LNPs are ongoing.

References

[1] Meyler's Side Effects of drugs: The international encyclopedia of adverse drug reactions and interactions, 15th ed., Elsevier2006.

[2] P. Malfertheiner, F. Megraud, C.A. O'Morain, J. Atherton, A.T. Axon, F. Bazzoli, G.F. Gensini, J.P. Gisbert, D.Y. Graham, T. Rokkas, E.M. El-Omar, E.J. Kuipers, G. European Helicobacter Study, Management of *Helicobacter pylori* infection--the Maastricht IV/ Florence Consensus Report, Gut 61(5) (2012) 646-64.

[3] L. Boyanova, I. Mitov, B. Vladimirov, *Helicobacter pylori*, Caister Academic Press Norfolk, 2011.

[4] S. Mishra, Is *Helicobacter pylori* good or bad?, Eur. J. Clin. Microbiol. Infect. Dis. 32 (2013) 301-304.

[5] A. Tsuji, E. Nakashima, S. Hamano, T. Yamana, Physicochemical properties of amphoteric B-lactam antibiotics I: stability, solubility, and dissolution behavior of amino penicillins as a function of pH, J. Pharm. Sci. 67(8) (1978).

[6] E. Nagele, R. Moritz, Structure elucidation of degradation products of the antibiotic amoxicillin with ion trap MS(n) and accurate mass determination by ESI TOF, J. Am. Soc. Mass Spectrom. 16(10) (2005) 1670-6.

[7] M. Barzegar-Jalali, K. Adibkia, H. Valizadeh, M.R.S. Shadbad, A. Nokhodchi, Y. Omidi, G. Mohammadi, S.H.N. Nezhadi, M. Hasan, Kinetic Analysis of Drug Release From Nanoparticles, J. Pharm. Pharm. Sci. 11(1) (2008) 167-177.

[8] D. Lopes, C. Nunes, M.C. Martins, B. Sarmento, S. Reis, Eradication of *Helicobacter pylori*: Past, present and future, J. Control. Release 189 (2014) 169-86.

[9] D. Lopes, C. Nunes, P. Fontaine, B. Sarmento, S. Reis, Proof of pore formation and biophysical perturbations through a 2D amoxicillin-lipid membrane interaction approach, Biochim. Biophys. Acta 1859(5) (2017) 803-812.

[10] *Helicobacter pylori*: physiology and genetics, ASM Press, Washington DC, 2001.

[11] A.J. Huh, Y.J. Kwon, "Nanoantibiotics": a new paradigm for treating infectious diseases using nanomaterials in the antibiotics resistant era, J Control Release 156(2) (2011) 128-45.

[12] C.A. Fallone, N. Chiba, S.V. van Zanten, L. Fischbach, J.P. Gisbert, R.H. Hunt, N.L. Jones, C. Render, G.I. Leontiadis, P. Moayyedi, J.K. Marshall, The Toronto Consensus for the Treatment of *Helicobacter pylori* Infection in Adults, Gastroenterol. 151(1) (2016) 51-69.e14.

[13] J. Cai, H. Huang, W. Song, H. Hu, J. Chen, L. Zhang, P. Li, R. Wu, C. Wu, Preparation and evaluation of lipid polymer nanoparticles for eradicating H. pylori biofilm and impairing antibacterial resistance in vitro, Int. J. Pharm. 495(2) (2015) 728-37.

[14] Z.W. Jing, Y.Y. Jia, N. Wan, M. Luo, M.L. Huan, T.B. Kang, S.Y. Zhou, B.L. Zhang, Design and evaluation of novel pH-sensitive ureido-conjugated chitosan/TPP nanoparticles targeted to *Helicobacter pylori*, Biomaterials 84 (2016) 276-85.

[15] M. Arif, Q.J. Dong, M.A. Raja, S. Zeenat, Z. Chi, C.G. Liu, Development of novel pH-sensitive thiolated chitosan/PMLA nanoparticles for amoxicillin delivery to treat *Helicobacter pylori*, Mater. Sci. Eng. C Mater. Biol. Appl. 83 (2018) 17-24.

[16] R. Awasthi, G.T. Kulkarni, Development and characterization of amoxicillin loaded floating microballoons for the treatment of *Helicobacter pylori* induced gastric ulcer, Asian J. Pharm. 8(3) (2013) 174-180.

[17] S.K. Dey, P.K. De, A. De, S. Ojha, R. De, A.K. Mukhopadhyay, A. Samanta, Floating mucoadhesive alginate beads of amoxicillin trihydrate: A facile approach for *H. pylori* eradication, Int. J. Biol. Macromol. 89 (2016) 622-31.

[18] D.Y. Singh, N.K. Prasad, Double liposomes mediated dual drug targeting for treatment of *Helicobacter pylori* infections, Pharmazie 66 (2011) 368-373.

[19] L. Battaglia, M. Gallarate, Lipid nanoparticles: state of the art, new preparation methods and challenges in drug delivery, Expert. Opin. Drug Deliv. 9(5) (2012) 497-508.

[20] P. Severino, T. Andreani, A.S. Macedo, J.F. Fangueiro, M.H. Santana, A.M. Silva, E.B. Souto, Current State-of-Art and New Trends on Lipid Nanoparticles (SLN and NLC) for Oral Drug Delivery, J. Drug Deliv. 2012 (2012) 750891.

[21] C. Ruiz, S. Falcocchio, F.I. Pastor, L. Saso, P. Diaz, *Helicobacter pylori* EstV: identification, cloning, and characterization of the first lipase isolated from an epsilon-proteobacterium, Appl. Environ. Microbiol. 73(8) (2007) 2423-31.

[22] G.L. Mendz, T.N. Lim, S.L. Hazell, Fluorinated probes to measure carboxylesterase activities using 19F NMR spectroscopy: application to erythrocytes and Helicobacter pylori, Arch. Biochem. Biophys. 305(2) (1993) 252-260.

[23] C.L. Seabra, C. Nunes, M. Gomez-Lazaro, M. Correia, J.C. Machado, I.C. Goncalves, C.A. Reis, S. Reis, M.C.L. Martins, Docosahexaenoic acid loaded lipid nanoparticles with bactericidal activity against *Helicobacter pylori*, Int. J. Pharm. 519(1-2) (2017) 128-137.

[24] R.Y. Pelgrift, A.J. Friedman, Nanotechnology as a therapeutic tool to combat microbial resistance, Adv. Drug Delivery Rev. 65(13–14) (2013) 1803-1815.

[25] D. Lopes, C. Nunes, M.C.L. Martins, B. Sarmento, S. Reis, Targeting strategies for the treatment of *Helicobacter pylori* infections, in: J. Naik (Ed.), Nano Based Drug Delivery, IAPC Publishing, Zagreb, Croatia, 2015, pp. 339-366.

[26] N. Figura, R. Marcolongo, G. Cavallo, A. Santucci, G. Collodel, A. Spreafico, E. Moretti, Polysorbate 80 and *Helicobacter pylori*: a microbiological and ultrastructural study, BMC Microbiol. 12(217) (2012) 1-10.

[27] C.Q. Sun, C.J. O'Connor, A.M. Roberton, Antibacterial actions of fatty acids and monoglycerides againstHelicobacter pylori, FEMS Immunol. Med. Microbiol. 36(1-2) (2003) 9-17.

[28] J.A. Jackman, B.K. Yoon, D. Li, N.J. Cho, Nanotechnology Formulations for Antibacterial Free Fatty Acids and Monoglycerides, Molecules 21(3) (2016) 305.

[29] S.W. Jung, S. Thamphiwatana, L. Zhang, M. Obonyo, Mechanism of antibacterial activity of liposomal linolenic acid against *Helicobacter pylori*, PLoS One 10(3) (2015) e0116519.

[30] M. Obonyo, L. Zhang, S. Thamphiwatana, D. Pornpattananangkul, V. Fu, L. Zhang, Antibacterial activities of liposomal linolenic acids against antibiotic-resistant *Helicobacter pylori*, Mol. Pharmaceutics 9(9) (2012) 2677-85.

[31] C.A. Lingwood, M. Huesca, A. Kuksis, The Glycerolipid Receptor for *Helicobacter pylori* (and Exoenzyme S) is Phosphatidylethanolamine, Infect. Immun. 60(6) (1992) 2470-2474.

[32] B. Singh, R. Bhatowa, C.B. Tripathi, R. Kapil, Developing micro-/nanoparticulate drug delivery systems using "design of experiments", Int. J. Pharm. Invest. 1(2) (2011) 75-87.

[33] B. Singh, R. Bhatowa, C.B. Tripathi, R. Kapil, Developing micro-/nanoparticulate drug delivery systems using "design of experiments", Int. J. Pharm. Investig. 1(2) (2011) 75-87.

[34] A. Allen, G. Flemstrom, Gastroduodenal mucus bicarbonate barrier: protection against acid and pepsin, Am. J. Physiol. 288(1) (2005) C1-C19.

[35] International Standard ISO 10993-5, Biological evaluation of medical devices–Part 5: tests for in vitro cytotoxicity, Geneva, Switzerland, 2009.

[36] L. Garcia-Gonzalez, L. Yepez-Mulia, A. Ganem, Effect of beta-cyclodextrin on the internalization of nanoparticles into intestine epithelial cells, Eur J Pharm Sci 81 (2016) 113-8.

[37] S. Hassani, Y. Pellequer, A. Lamprecht, Selective adhesion of nanoparticles to inflamed tissue in gastric ulcers, Pharm. Res. 26(5) (2009) 1149-54.

[38] M. Polakovic, T. Görner, R. Gref, E. Dellacherie, Lidocaine loaded biodegradable nanospheres II. Modelling of drug release, J. Control. Release 60 (1999) 169-177.

[39] S. Honary, F. Zahir, Effect of zeta potential on the properties of nano-drug delivery systems-a review (Part 1), Trop. J. Pharm. Res. 12(2) (2013) 255-264.

[40] R. Singh, J.W. Lillard, Jr., Nanoparticle-based targeted drug delivery, Exp. Mol. Pathol. 86(3) (2009) 215-23.

[41] J. das Neves, B. Sarmento, Precise engineering of dapivirine-loaded nanoparticles for the development of anti-HIV vaginal microbicides, Acta Biomater. 18 (2015) 77-87.

[42] M. Iqbal, N. Zafar, H. Fessi, A. Elaissari, Double emulsion solvent evaporation techniques used for drug encapsulation, Int. J. Pharm. 496(2) (2015) 173-90.

[43] K. Pays, J. Giermanska-Kahn, B. Pouligny, J. Bibette, F. Leal-Calderon, Double emulsions: how does release occur?, J. Control. Release 79 (2002) 193-205.

[44] A.F. Goddard, M. Jessa, J., D.A. Barrett, P.N. Shaw, J.-P. Idström, C. Cederberg, R.C. Spiller, Effect of Omeprazole on the Distribution of Metronidazole, Amoxicillin, and Clarithromycin in Human Gastric Juice, Gastroenterology 111 (1996) 358-367.

[45] X.Y. Zhang, T.K. Ng, M.E. Brelen, D. Wu, J.X. Wang, K.P. Chan, J.S. Yung, D. Cao, Y. Wang, S. Zhang, S.O. Chan, C.P. Pang, Continuous exposure to non-lethal doses of sodium iodate induces retinal pigment epithelial cell dysfunction, Sci. Rep. 6 (2016) 37279.

[46] I. Fernandes, V. de Freitas, C. Reis, N. Mateus, A new approach on the gastric absorption of anthocyanins, Food Funct. 3(5) (2012) 508-16.

[47] S.J. Hessey, J. Spencer, J.I. Wyatt, G. Sobala, B.J. Rathbone, A.T.R. Axon, M.F. Dixon, Bacterial adhesion and disease activity in *Helicobacter* associated chronic gastritis, Gut 31 (1990) 134-138.

[48] J.C. Yang, C.W. Lu, C.J. Lin, Treatment of *Helicobacter pylori* infection: current status and future concepts, World J. Gastroenterol. 20(18) (2014) 5283-93.

[49] D. Lopes, C. Nunes, M.C.L. Martins, B. Sarmento, S. Reis, Targeting strategies for the treatment of *Helicobacter pylori* infections, in: J. Naik (Ed.), Nano Based Drug Delivery, IAPC Publishing, Zagreb, Croatia, 2015.

[50] Z. Feldötö, T. Pettersson, A. Dédinaite, Mucin-Electrolyte Interactions at the Solid-Liquid Interface Probed by QCM-D, Langmuir 24 (2008) 3348-3357.

[51] P.C. Griffiths, P. Occhipinti, C. Morris, R.K. Heenan, S.M. King, M. Gumbleton, PSGE-NMR and SANS Studies of the Interaction of Model Polymer Therapeutics with Mucin, Biomacromolecules 11 (2010) 120-125.

[52] I. Bravo-Osuna, M. Noiray, E. Briand, A.M. Woodward, P. Argueso, I.T. Molina Martinez, R. Herrero-Vanrell, G. Ponchel, Interfacial interaction between transmembrane ocular mucins and adhesive polymers and dendrimers analyzed by surface plasmon resonance, Pharm. Res. 29(8) (2012) 2329-40.

Chapter 6.5

Supporting information

Supporting material to the experimental design

Different models can be used (linear, two-factor interaction, and quadratic models), and the most suitable model was selected depending on the correlation between the expected and the observed values. Each model is reflected in an equation, such as the following equation that considers non-linear relationships (non-linear quadratic model) [1].

$$Y = A_0 + A_1X_1 + A_2X_2 + A_3X_3 + A_4X_1X_2 + A_5X_2X_3 + A_6X_1X_3 + A_7X_1^2 + A_8X_2^2 + A_9X_3^2 \qquad (1)$$

in which Y is the measured response; A_0 is an intercept; A_1 to A_3 are the linear coefficients; A_4 to A_6 are the interaction coefficients; A_7 to A_9 are the squared coefficients; and X_1, X_2, X_3 are the coded levels of independent variables [1, 2]. The terms X_1X_2, X_2X_3 and X_1X_3 represent the linear interaction terms, while X_i^2 represents the quadratic term [1]. The predicted R^2 was analysed to evaluate the fitness of the model.
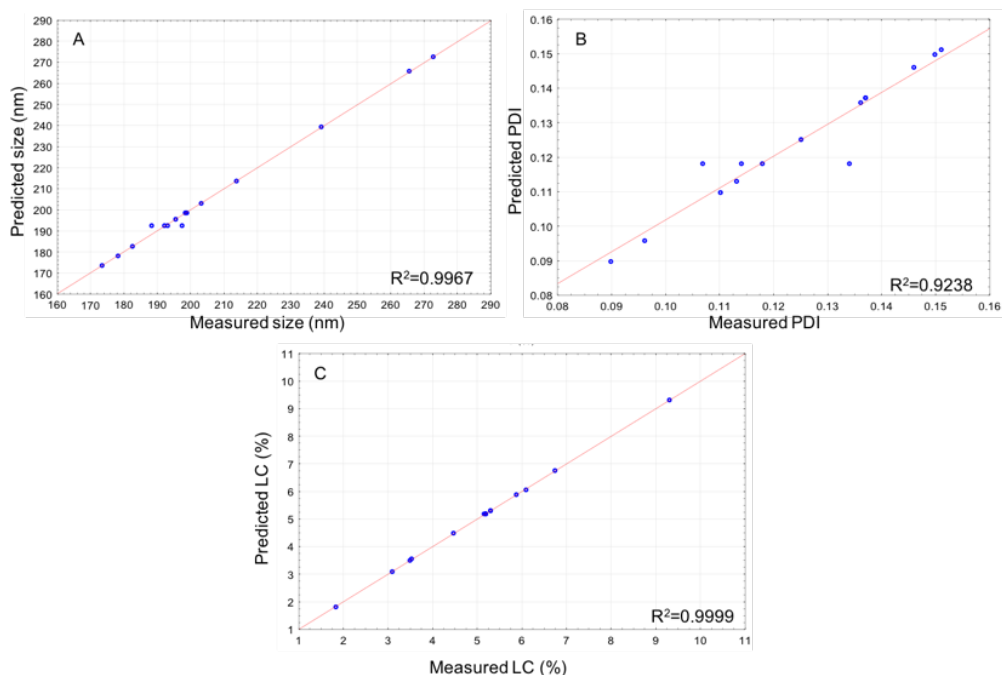
Figure A.1. Correlation between the measured and the predicted values of size (A), PDI (B), and LC (C) and correspondent R^2 values when fitting with the quadratic model.

Table A.1. Independent variables (solid lipid, Tween 80, and AMX mass) and their correspondent levels. Dependent variables (size, PDI, and loading capacity (LC)) and the constraints stablished for the Box-Behnken design.

	Levels		
	-1	0	1
Independent variables			
X_1 = Cetyl Palmitate mass (mg)	150	200	250
X_2 = Tween 80 mass (mg)	15+50	35+50	55+50
X_3 = AMX mass (mg)	10	20	30
Dependent variables	**Desirability**		
	High	**Medium**	**Low**
Y_1 = Size	70	150	250
Y_2 = PDI	0	0.1	0.2
Y_3 = LC	20	4	0

The interaction coefficients and the corresponding *p*-values for each dependent variable are shown in Table A.2. A synergic effect is represented by a positive sign before the interaction coefficient, which means that the response increases with the increase of the independent variable. By opposite, a negative sign represents an antagonistic effect. In general, both the size and the LC of the AMX-loaded LNPs depend on the variance of the factors, in terms of both linear and quadratic effects. On the other hand, the PDI is not affected by the independent variables ($p > 0.05$).

Table A.2. Regression analysis for the particle size (Y_1), the PDI (Y_2), and the LC (Y_3), with the correspondent interaction coefficients for the independent variables (solid lipid amount (Lip), the concentration of Tween 80, and the amount of AMX).

	Particle Size		PDI		LC	
	Coefficient	*p*-value	Coefficient	*p*-value	Coefficient	*p*-value
Int	209.4667	0.000040	0.125750	0.001033	5.01750	0.000001
Lip (L)	8.0667	0.041649	0.015917	0.092883	-0.27000	0.000444
Lip (Q)	-5.1083	0.049967	0.000896	0.828826	0.17979	0.000488
Tween 80 (L)	6.4167	0.063558	-0.004417	0.486725	1.33750	0.000018
Tween 80 (Q)	-9.1083	0.016558	-0.000854	0.836570	-0.49146	0.000065
AMX (L)	16.7167	0.010182	0.010583	0.179917	1.22250	0.000022
AMX (Q)	1.6167	0.306269	-0.005604	0.264096	0.42354	0.000088
Lip (L) * Tween 80 (L)	12.8000	0.030308	-0.004750	0.567698	-1.10500	0.000048
Lip (L) * Tween 80 (Q)	-12.9500	0.015155	-0.014000	0.105725	0.50250	0.000115
Lip (Q) * Tween 80 (L)	-23.2250	0.004786	-0.004000	0.504179	-0.70875	0.000058
Lip (L) * AMX (L)	-11.2500	0.038722	-0.004250	0.605787	-0.46000	0.000276
Lip (Q) * AMX (L)	-3.7250	0.147141	-0.008500	0.228335	-0.08625	0.003898
Tween 80 (L) * AMX (L)	-21.5500	0.011014	0.004250	0.605787	-0.72250	0.000112

Response surface analysis in two dimensions (Figure A.2) were calculated from the quadratic polynomial function (Eq. A.1). These plots enable a better visualization of the response when different factors are varying.

The particle size of the 15 LNPs formulations was found to be in a range of 173-273 nm. The mean was 209 nm, as depicted in the *Int* value in Table A.2. Almost all factors significantly affect the size of the AMX-loaded LNPs. The exceptions are three (Tween 80 (L), AMX (Q), and Lip (Q) * AMX (L)). Tween 80 does not linearly affect the size of the particles. Nevertheless, the quadratic type of interaction has a negative effect (*p*-value < 0.05). For high amounts of Tween 80, the interfacial tension between phases with different lipophilicities is reduced, which stabilizes smaller particles [3]. The amount of lipid has a positive linear effect, with higher diameters for higher amounts of lipid. Since more lipid molecules are available, the molecular density of the lipid phase in the LNPs will increase. AMX also has a linear positive effect on the size of the AMX-loaded LNPs. This effect shows that, depending on the solid lipid mass and on the T80 concentration, the aqueous vacuoles may not be completely stabilized and AMX may coexist in both lipid and aqueous phase. Simultaneous increase of the lipid mass and the surfactant concentration led to bigger AMX-loaded LNPs, which is visualized by the positive value of the regression coefficient

(12.8000) and the dark red on Fig. A.2 (top line, left plot). On the opposite, when both the lipid and the AMX mass increase, the LNPs are smaller (negative effect). A similar effect happens with the simultaneous increase of the AMX mass and the Tween 80 concentration.

The PDI varied from 0.09 to 0.15 (mean of 0.126), with no significant effect of all independent variables. The small range of PDI and the lower PDI values show that the selected double-emulsion method promotes the synthesis of a monodisperse suspension.

The LC was found to be in a range of 1.5-9.5 %, with a mean value of 5%. The *p*-values for the LC analysis are all lower than 0.05 (Table A.2), which reveals that all the linear and quadratic interactions have a statistically significant effect on the LC. The lowest *p*-value (0.000018) is obtained for the linear positive effect of Tween 80 (coefficient = 1.33750). This can be explained by the higher stabilization promoted by Tween 80 of the aqueous vacuoles in which AMX is loaded. AMX also linearly increases the LC since there is a higher amount of drug available for entrapment. On the opposite, higher amounts of lipid decrease the LC since the LC is inversely proportional to the lipid amount (Eq. (2)). The increase of both the lipid mass and the Tween 80 concentration led to a negative effect on the LC, with a regression coefficient of -1.10500 (Table A.2) and a light green in Figure A.2 (bottom line, left graphic). The increase of both AMX mass and surfactant concentration promoted a small negative effect (coefficient = -0.72250). This effect is visualized in Figure A.2 (bottom line, right plot) since the highest LC values are obtained for simultaneous higher values of AMX mass and lower values of Tween 80 concentration or for higher values of Tween 80 concentration and intermediate values of AMX mass. A similar effect happens with the increase of the mass of both the lipid and the AMX. The small negative effect of increasing both the lipid and AMX mass (coefficient = -0.46000) is graphically showed by the intermediate red (upper right corner) in the Figure A.2, bottom line, middle plot.

Figure A.2. Response surface plots in two dimensions for each dependent variable: size (top line), PDI (middle line), and LC (bottom line). The colours represent the response degree, from green (lowest response level) to dark red (highest response level).
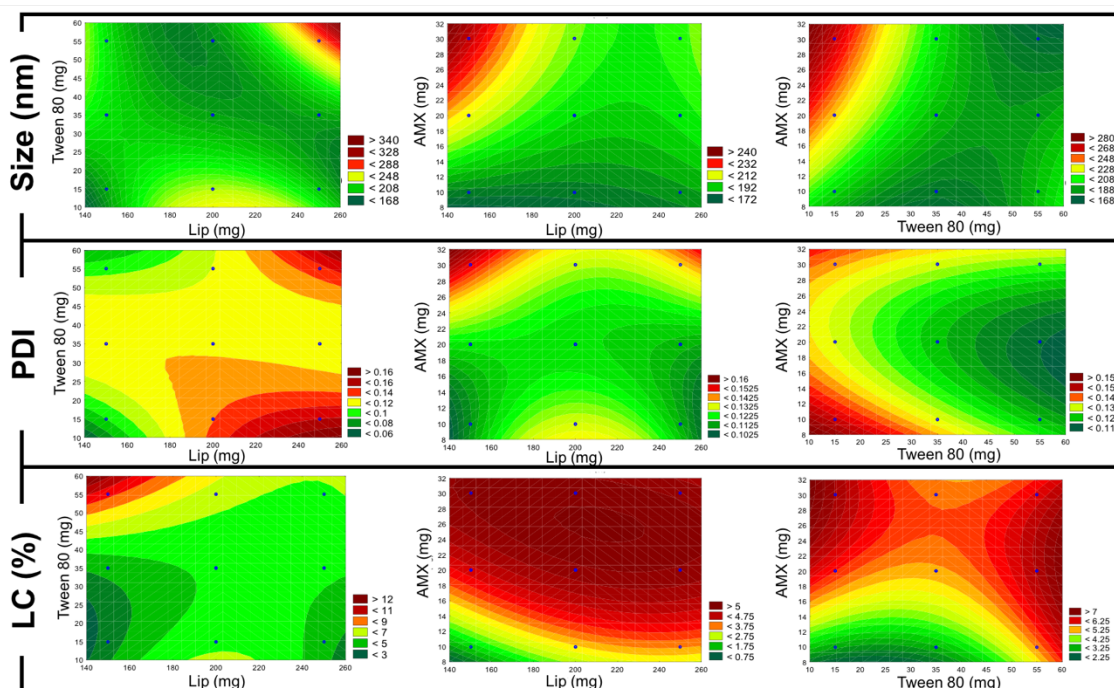
Supporting material to the stabilities studies
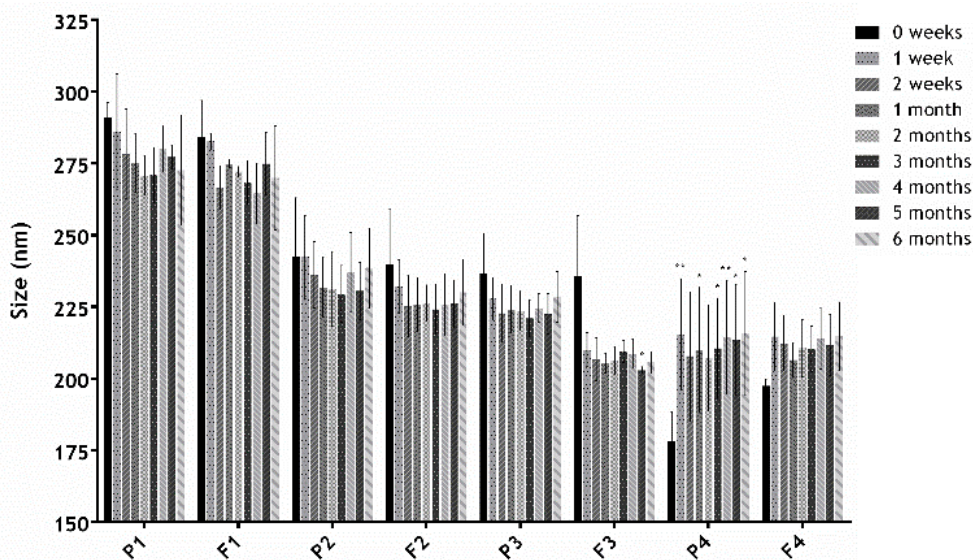
Figure A.3. Size of the lipid nanoparticles suspensions (F1 to F4) and respective unloaded nanoparticles (P1 to P4) over time. Values represent the mean ± SD of three independently synthetized formulations. *p < 0.05, **p < 0.01, ***p < 0.005, ****p < 0.0001 relatively to 0 months.
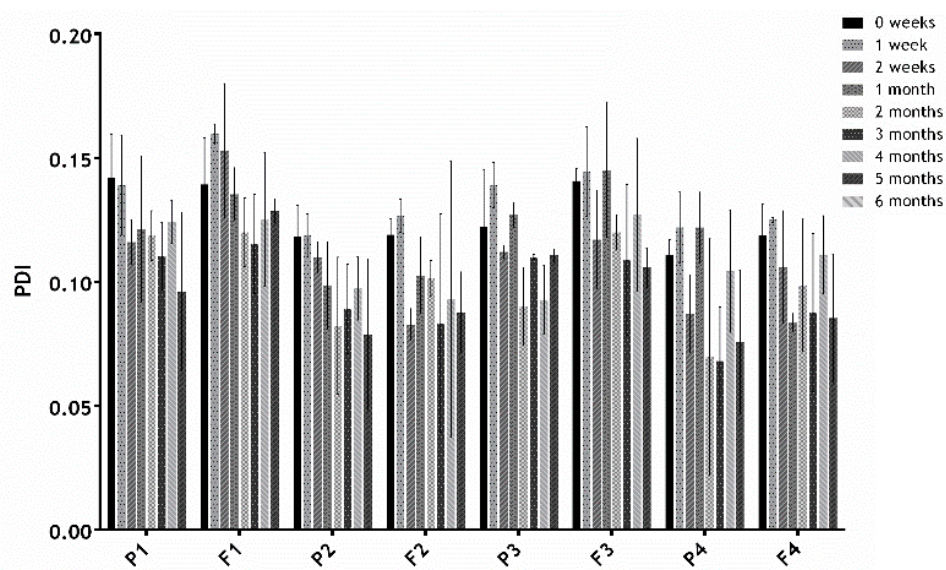
Figure A.4. Polydispersion (PDI) of the lipid nanoparticles suspensions (F1 to F4) and respective unloaded nanoparticles (P1 to P4) over time. Values represent the mean ± SD of three independently synthetized formulations. *p < 0.05, **p < 0.01, ***p < 0.005, ****p < 0.0001 relatively to 0 months.
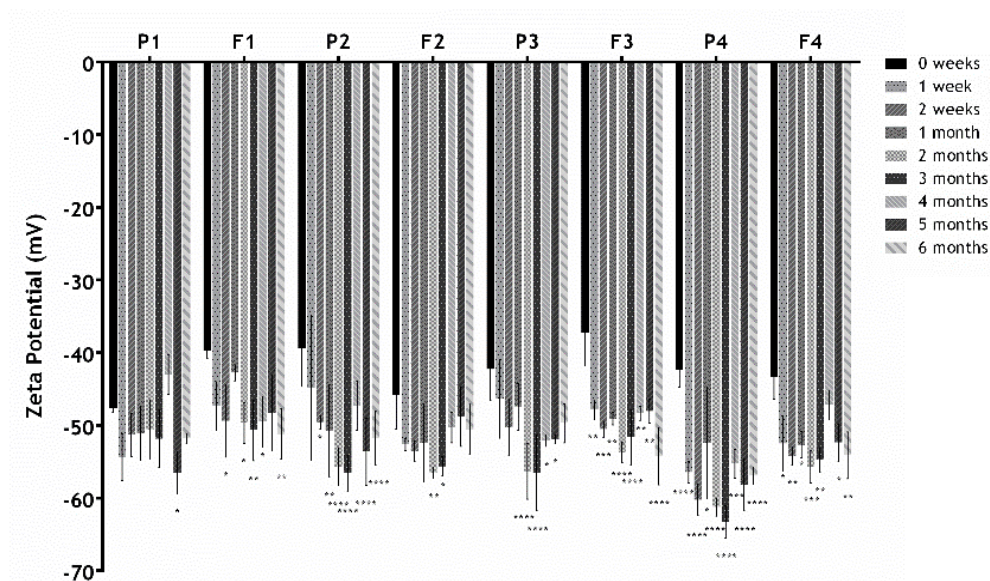
Figure A.5. Zeta potential of the lipid nanoparticles suspensions (F1 to F4) and respective unloaded nanoparticles (P1 to P4) over time. Values represent the mean ± SD of three independently synthetized formulations. *p < 0.05, **p < 0.01, ***p < 0.005, ****p < 0.0001 relatively to 0 months.

Figure A.6. Loading capacity (LC) of the lipid nanoparticles suspensions (F1 to F4) over time. Values represent the mean ± SD of three independently synthetized formulations. *$p < 0.05$, **$p < 0.01$, ***$p < 0.005$, ****$p < 0.0001$ relatively to 0 months.
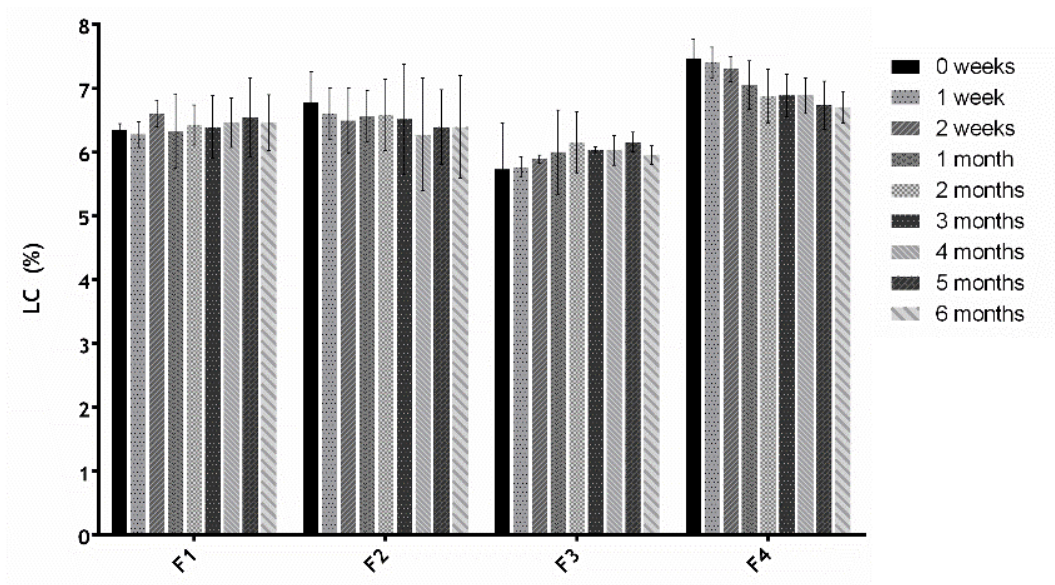
Supporting material to the mucoadhesion studies
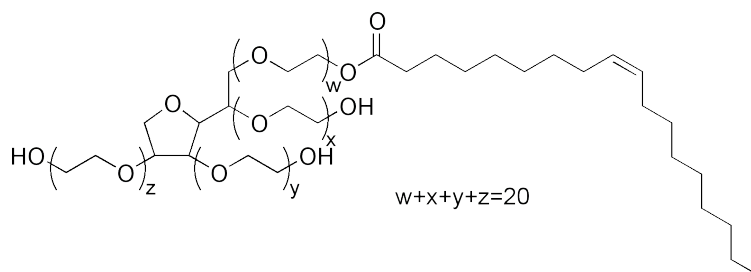
Figure A.7. Molecular structure of Tween 80.
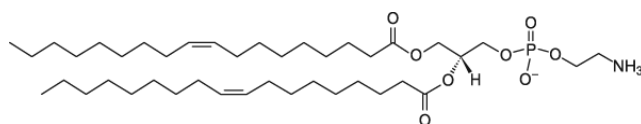
Figure A.8. Molecular structure of dioleoylphosphatidylethanolamine (DOPE).

References

[1] T. Lundstedt, E. Seifert, L. Abramo, B. Thelin, A. Nyström, J. Pettersen, R. Bergman, Experimental design and optimization, Chemom. Intell. Lab. Syst. 42 (1998) 3-40.

[2] J. Hao, X. Fang, Y. Zhou, J. Wang, F. Guo, F. Li, X. Peng, Development and optimization of solid lipid nanoparticle formulation for ophthalmic delivery of chloramphenicol using a Box-Behnken design, Int. J. Nanomed. 6 (2011) 683-92.

[3] J. das Neves, B. Sarmento, Precise engineering of dapivirine-loaded nanoparticles for the development of anti-HIV vaginal microbicides, Acta Biomater. 18 (2015) 77-87.

Chapter 6.6

Targeting and killing the ever-challenging ulcer bug: an antibiotic-free strategy

The previous work (Chapter 6.5) encompassed the rational design behind the development of lipid nanoparticles with potential to be retained at the site of infection. This work was designed to evaluate the antimicrobial efficacy of that system as well as its ability to target the bacteria and inhibit the adhesion to gastric cells.
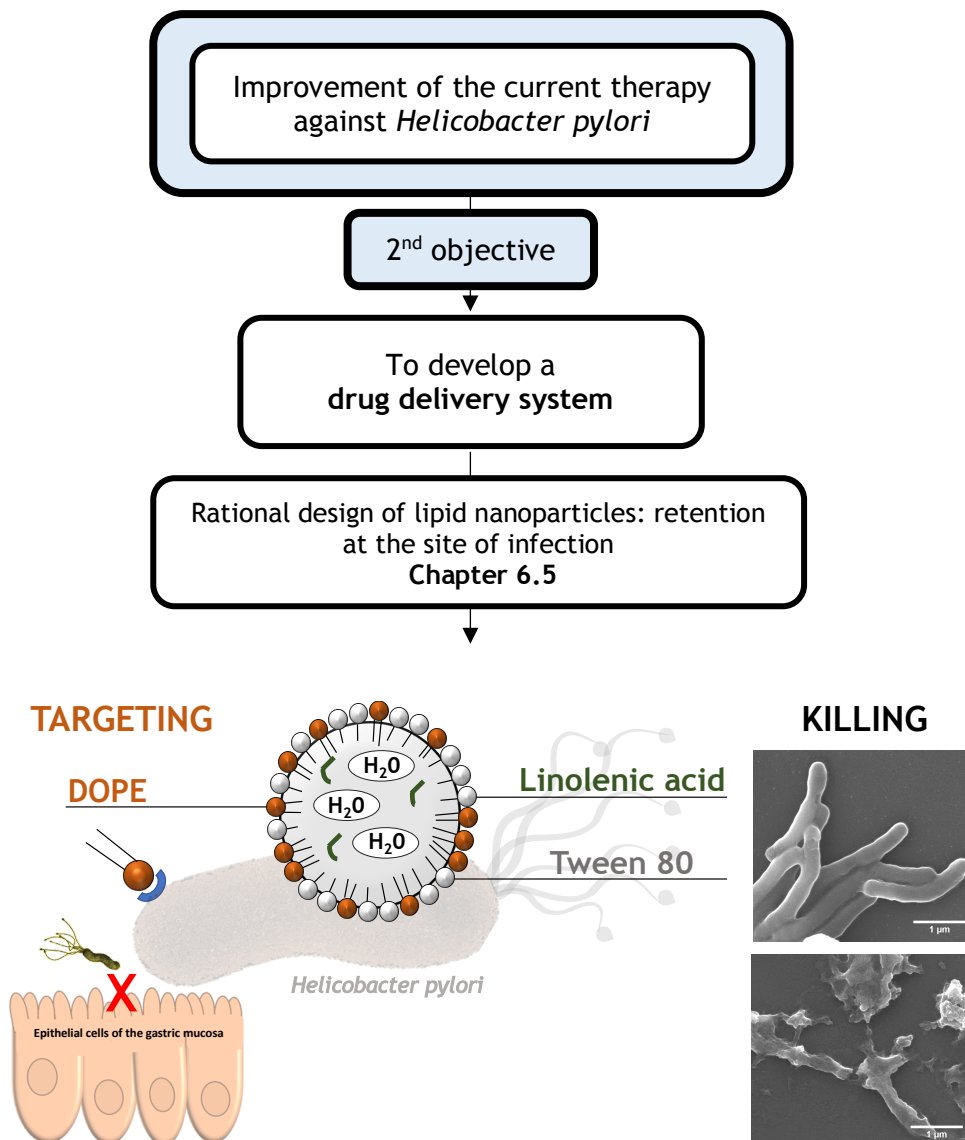
Chapter 6.6

Targeting and killing the ever-challenging ulcer bug: an antibiotic-free strategy

Daniela Lopes-de-Campos[1], Catarina Leal Seabra[2,3], Rita M. Pinto[1], Bruno Sarmento[2,3,4], Cláudia Nunes[1], M. Cristina L. Martins[2,3,5], and Salette Reis[1*]

[1] LAQV, REQUIMTE, Departamento de Ciências Químicas, Faculdade de Farmácia, Universidade do Porto, Portugal

[2] i3S - Instituto de Investigação e Inovação em Saúde, Universidade do Porto, Rua Alfredo Allen 208, 4200-393 Porto, Portugal

[3] INEB - Instituto de Engenharia Biomédica, Universidade do Porto, Rua Alfredo Allen 208, 4200-393 Porto, Portugal

[4] IINFACTS, Instituto de Investigação e Formação Avançada em Ciências e Tecnologias da Saúde, Instituto Universitário de Ciências da Saúde, Gandra, Portugal

[5] ICBAS- Instituto Ciências Biomédicas Abel Salazar, Universidade do Porto, Portugal

Treating *Helicobacter pylori (H. pylori)* infections has been a challenge. These ulcer bugs, as the name implies, are associated with gastric ulceration and gastric cancer. The limitations of the current therapies include antimicrobial resistance and the bacterial location *in vivo*. The aim of this work was to develop lipid nanoparticles (LNPs) that were able to target and inhibit the adhesion of *H. pylori* to the gastric mucosa and to kill the bacteria.

Dioleoylphosphatidylethanolamine (DOPE) was used as surfactant to target *H. pylori*, and Tween® 80 and linolenic acid as antimicrobial agents. Antimicrobial activity was assessed through time-kill kinetic, morphological changes, and membrane permeability of LNPs against bacteria. Imaging flow cytometry (ImageStream[X]®) was used to evaluate the LNPs-bacteria binding rate. A bacteria-gastric cells adhesion model was used to evaluate the ability of the LNPs to inhibit the adhesion of *H. pylori* to MKN-74 cells.

Bactericidal effect of LNPs was observed with Tween®80 and linolenic acid due to the disruption of the bacterial membrane and a leakage of cytoplasmic content. Bioimaging results showed that DOPE enabled a 100% LNPs-bacterial binding after 15 min of incubation. Furthermore, the fully optimized LNPs decreased the percentage of bacteria adhered to gastric cells to 33 %. Considering the emergence of antimicrobial resistance and the importance of adhesion to gastric cells for the pathogenicity of *H. pylori*, these LNPs constitute a powerful strategy to target, seal, and kill *H. pylori*.

Keywords: *Helicobacter pylori*, lipid nanoparticles, Tween 80, Linolenic acid, DOPE, targeting

1. Introduction

Helicobacter pylori (*H. pylori*) were called "ulcer bugs" by Barry Marshall when he discovered the association between these bacteria and gastric ulceration [1, 2]. Since then, the pathogenicity of *H. pylori* has been studied, and the World Health Organization classified these bacteria as a human gastric carcinogenic (Group I) [3]. The eradication of this "ulcer bug" is crucial in several conditions, such as peptic ulcers, mucosa-associated lymphoid tissue lymphoma, atrophic gastritis, post-gastric cancer resection, and in the cases where the patient has relatives with gastric cancer [4]. The first-line treatment is supported by several consensuses worldwide (e.g., [5-9]) and includes at least two antibiotics, such as amoxicillin, clarithromycin, or metronidazole, and a proton-pump inhibitor that should be administered for 7-14 days, twice a day [10].

The eradication rates of *H. pylori* are usually between 70-80%, which is still distant from the 100% that is required for infectious diseases [6, 10]. Several factors are behind the limitations of the current therapy, including antimicrobial resistance, the protective mechanism of the mucus layer, the intracellular location of some bacteria, the low residence time of antibiotics in the stomach, among others [11, 12]. Considering these limitations, several nanoparticles have been developed due to their potential against *H. pylori* infections [13]. Nevertheless, the potentiality of lipid nanoparticles (LNPs) to treat *H. pylori* infections has barely been studied. Seabra *et al*. showed the effect of docosahexaenoic acid-loaded LNPs against these bacteria [14], and the tolerance of the unloaded LNPs to the gut microbiota [15]. LNPs are in fact a great strategy for pharmaceutical applications once they are cost-effective, easily scaled-up, biocompatible, and biodegradable [16, 17]. In a previous work, we designed, developed, and characterized LNPs that were non-cytotoxic and were able to be retained at the gastric mucosa due to their low permeability through gastric cells and the interaction with mucins (**Chapter 6.5**). Their composition (Figure 1) was carefully chosen to have LNPs with potential to target and kill the bacteria.

Dioleoylphosphatidylethanolamine (DOPE) was used as surfactant due to its properties of targeting *H. pylori*. These bacteria have receptors to phosphatidylethanolamine, which are used to attach themselves to the antrum of the human stomach [18]. Therefore, the use of this compound enables the targeting of *H pylori*, and also hampers their adhesion to gastric cells [12]. Tween®80, a well-known surfactant, commonly used by the pharmaceutical industry as an excipient and as a solubilizing agent, was also used. This surfactant enhances the permeability of bacterial cell membranes and avoids biofilm formation in several bacteria, such as *Pseudomonas aeruginosa* [19]. Tween® 80 also inhibits the adhesion of *H. pylori* to host cells [20]. Furthermore, Tween®80 is in fact able to detach the outer membrane of *H. pylori*, having a synergic effect with

several antibiotics [21]. Linolenic acid was also added to enhance the antibacterial activity of these LNPs. In general, fatty acids are recognized for their antibacterial properties, their low cost, and their abundance in nature [22, 23]. Linolenic acid is one of the most potent ones against *H. pylori*, changing the integrity of the bacterial membrane, even when the bacteria are under a coccoid and resistant shape [22, 24].

The aim of this work was to assess if the designed LNPs are able to target, to inhibit the adhesion to the gastric mucosa, and to kill the bacteria. Accordingly, this work aimed to evaluate: the effect of each antibacterial compound (Tween® 80 and linolenic acid) on the growth and on the morphology of the bacteria. The targeting and the sealing effect were evaluated through flow cytometry and an adhesion model using MKN-74 cells.
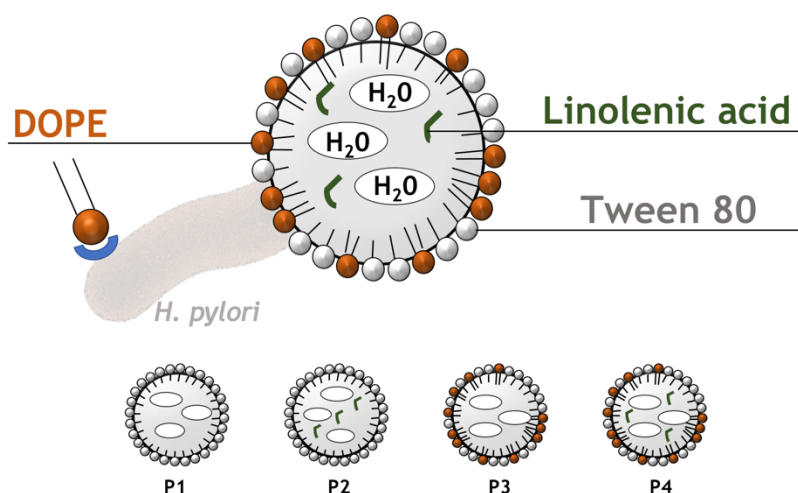
Figure 1. Composition of the LNPs. DOPE was used as a surfactant and a targeting agent, Tween®80 due to its surfactant and antibacterial properties, and linolenic acid as an additional therapeutic agent. P1 to P4 are variants of the LNPs. Only P2 and P4 have linolenic acid, and DOPE was only added to P3 and P4.

2. Materials and Methods

2.1 Materials

Cetyl palmitate was a gift from Gattefossé (Gattefossé, France). 1,2-Dioleoyl-*sn*-glycero-3-phosphoethanolamine (DOPE) was acquired from Avanti® Polar Lipids (Alabaster, AL, USA). Chloroform was obtained from VWR International LLC (Radnor, PA, USA). Roswell Park Memorial Institute (RPMI) medium, trypsin-EDTA (1x), Dulbecco's Phosphate Buffered Saline 10x pH 7.4 (PBS), Penicillin-Streptomycin (Pen-Strep), and Fetal Bovine Serum (FBS) were purchased from Gibco® (Invitrogen Corporation, Paisley,

UK). MKN-74 cell line was provided by the BioBank of Instituto de Investigação e Inovação em Saúde (i3S). Linolenic acid, Tween®80, coumarin-6, Polymixin B, Vancomycin, Amphotericin B, Trimethroprim,Triton™ X-100 and Brucella Broth were obtained from Sigma-Aldrich® (St. Louis, MO, USA). Blood agar base medium was purchased from Liofilchem (Italy) and the defibrinated horse blood from Probiológica (Portugal). Glutaraldehyde (25%) and sodium cacodylate buffer were acquired from Merck (Germany). The BacTiter-Glo™ Microbial Cell Viability assay kit was purchased from Promega Inc (USA).

2.2 Methods

2.2.1 Preparation of the LNPs

The LNPs were prepared by the double emulsion technique, according to the described in a previous paper (**Chapter 6.5**). Briefly, 178.5 mg of cetyl palmitate were dissolved in 2 mL of chloroform, without or with 5 mg of linolenic acid. 0.5 mL of an aqueous solution, previously basified with NaOH (1 M), were dispersed within the lipid solution by sonication for 30 sec at 70% amplitude. When applicable, 20 mg of DOPE solubilized in a small volume of chloroform were added to the emulsion. Afterward, 4 mL of Tween®80 (20, 18.75, 15, or 13.75 mg.mL^{-1} for the P1, P2, P3, or P4 LNPs, respectively) were added to form a double emulsion by sonication (2 min, 70% amplitude). Finally, 4 mL of Tween®80 (12.5 mg.mL^{-1}) were added to all LNPs, and the final suspensions were placed in a stirring plate at room temperature for 3 h to evaporate the organic solvent. For the analysis by imaging flow cytometry, coumarin-6 was dissolved in a small volume of chloroform and added to the solid lipid solution at the beginning of the synthesis. The final concentration of coumarin-6 was 3.15 μg.mL^{-1}.

2.2.2. *H. pylori* culture conditions

H. pylori J99 was provided by the Department of Medical Biochemistry and Biophysics, Umeã University, Sweden. After defrosting, *H. pylori* were firstly cultured in spots in *H. pylori* medium plates, in microaerophilic conditions at 37 °C. After 48 h, bacteria were spread in *H. pylori* medium plate and incubated under microaerophilic conditions, at 37 °C for 48 h. The *H. pylori* medium plates were composed of blood agar base 2 supplemented with 10% defibrinated horse blood and 0.2% of an antibiotic mixture (0.155 g.L^{-1} of Polymixin B, 6.25 g.L^{-1} of Vancomycin, 1.25 g.L^{-1} of Amphotericin B, and 3.125 g.L^{-1} of Trimethroprim). Then, bacteria were cultured for 18-20 h, at 37ºC under 150 rpm in Brucella Broth medium

supplemented with 10% FBS to a final optical density (OD) of 0.1 (λ = 600 nm; Thermo Scientific Spectronic GENESYS 20 Visible Spectrophometer, USA).

2.2.2. Effect on the *H. pylori* growth

H. pylori J99 (ca. 10^7 bacteria.mL^{-1} , OD 0.03) were incubated with different concentrations of LNPs for 24h, at 37 °C, 150 rpm, under microaerophilic conditions. For comparison between the different formulations, LNPs diluted to a final solid lipid concentration of 2 mg.mL^{-1} were used. The concentrations used to assess the individual contribution of Tween® 80 and linolenic acid corresponded to the amount existent in the P4 formulation, namely, 1.2 mg.mL^{-1} (Tween®80) and 56 μg.mL^{-1} (Linolenic acid). Different concentrations of the P4 formulation were also used, namely, 0.5, 1, and 2 mg.mL^{-1} of solid lipid. At different time points (0, 3, 6, 9, 12, 24 h), 200 μL of each suspension was collected, diluted in PBS (pH 7.4) and plated in medium plates. The number of colony forming units (CFU) were counted after 5 days of incubation at 37 °C, in microaerophilic conditions.

2.2.3. Effect on the *H. pylori* morphology

For the scanning electron microscopic analysis, *H. pylori* suspensions similar to those mentioned in the section 2.2.2 were prepared. LNPs were used in a solid lipid concentration of 2 mg.mL^{-1}, and Tween®80 and linolenic acid were used in a concentration similar to the one existent in the P4 formulation (1.2 mg.mL^{-1} and 56 μg.mL^{-1}, respectively). After 3 and 12 h of incubation, 1 mL of each bacteria suspension were washed using PBS (pH 7.4) and centrifuged for 5 min, at 3000 *g*. The bacterial pellet was then fixed with 2.5 % v/v glutaraldehyde in 0.14 M of sodium cacodylate buffer for 30 min at room temperature. 100 µL of the fixed bacterial suspension were placed on a sterilized glass coverslip (Ø13 mm) and then kept for 2 h for adherence. Afterward, the samples were dehydrated with increasing ethanol/water gradient (50% to 99% (v/v)) and then dried using a critical point drying (CPD 7501, Poloran). The sample was then coated with a gold/palladium film over 30 s. The images were acquired using a JEOL JSM-6310F at CEMUP (Centro de Materiais da Universidade do Porto), at 60000x of magnification.

2.2.4. **Effect on the integrity of the plasmatic membrane of** *H. pylori*

The membrane permeability was assessed by quantification of the release of ATP from the bacteria using a BacTilter-Glo™ Microbial Cell Viability Assay kit, adapting the protocol from [24]. Briefly, after 3 h of incubation with the LNPs (in solid lipid concentration of 2 mg.mL^{-1}), the *H. pylori* suspension was centrifuged at 12,000 *g* for 5 min. 100 μL of the supernatant were then mixed in a 96-well white plate with 100 μL of BacTilter-Glo™ reagent. A Synergy™ H Multimode microplate reader, BioTek Instruments (USA), was used to measure the luminescence of the mixture after shaken for 2 min. The results were normalized considering the effect of Triton™ X-100 (positive control) and the medium (negative control) (Eq. (1)).

$$\% \, ATP \, released = \frac{Luminescence_{sample} - Luminescence_{negative \, control}}{Luminescence_{positive \, control} - Luminescence_{negative \, control}} \times 100 \qquad (1)$$

2.2.5. **Efficacy of the targeting to** *H. pylori*

To assess the ability of the LNPs to bind to *H. pylori,* P2 and P4 were labeled with coumarin-6 during their production and then incubated with *H. pylori* J99 under the previously described conditions (section 2.2.2). The LNPs were used in the same solid lipid concentration as in the previous experiments (2 mg.mL^{-1}). After 15 min of incubation with *H. pylori* J99, the bacteria were centrifuged (774 *g* for 10 min) and then fixed with 4% w/v of paraformaldehyde in PBS for 30 min. *H. pylori* DNA was labeled with propidium iodide (0.2 mg.mL^{-1}) for 30 min, at room temperature, and protected from light. Unstained negative control was also prepared. Before analysis, each sample was filtered using a 70 μm mesh filter. The analysis was made by imaging flow cytometer (ImageStream^X®, Amnis, EDM Millipore, Darmstadt, Germany), using a 488 nm laser, a 40x magnification objective of 0.75 N.A (image pixel 0.5 μm^2), and one CDD camera. The INSPIRETM software v4.0 (Amnis, EDM Millipore, Darmstadt, Germany) was used to acquire brightfield images (Channel 1, 420-480 nm), coumarin-6 fluorescence (Channel 2, 480-560 nm), and propidium iodide fluorescence (Channel 4, 560-595 nm). The upper limit was set to 5 μm^2 for Channel 1 and the lower limit was 1 μm^2 for Channel 4. IDEAS® software (Amnis, EDM Millipore, Darmstadt, Germany, version 6.2.64.0) was used for data analysis, by quantifying the percentage of bacteria that were labeled with coumarin-loaded LNPs. Control was used to define the contribution of the samples without coumarin to false positives (positive signal in Channel 2).

2.2.6 Effect of the LNPs on the *H. pylori* adhesion to MKN-74 cells

MKN-74 cells were cultured using RPMI medium supplemented with 10% FBS, at 37 °C in a 5% CO_2 atmosphere (passage 56-60). Supplementation with 1% Pen-Strep was used during the cell culture and removed during the seeding. Trypsin was used to chemically detach MKN-74, which were then seeded in a concentration of 2 x 10^5 cells.mL^{-1} in 24-well tissue culture microplates. After adhesion and confluence (48 h), the medium was replaced by 500 μL of the LNPs (final concentration 2 mg.mL^{-1} of solid lipid) followed by 500 μL of the *H. pylori* J99 suspension (final concentration 10^7 bacteria.mL^{-1}). Both the LNPs and the bacteria were previously diluted in RPMI supplemented with FBS. The microplate was then incubated for 2 h at 37°C. Afterward, the non-adhered and the adhered bacteria were quantified. Non-adherent bacteria were diluted in PBS (pH 7.4) directly from the supernatant and then plated in *H. pylori* medium plates. Adherent bacteria was collected by trypsinization (150 μL for 15 min at 37 °C) and mechanical disruption of the cells through scraping, diluted in PBS (pH 7.4) and plated in *H. pylori* medium plates. After 5 days at 37 °C, number of CFU were counted. *H. pylori* incubated with medium was used as control. Percentages of adherence were calculated through the following equation:

$$\%_{adherence} = \left[\frac{adherent_{bacteria} / (non-adherent_{bacteria}+adherent_{bacteria})}{adherent_{control} / (non-adherent_{control}+adherent_{control})} \right] \times 100 \quad (2)$$

2.2.7 Statistical analysis

Statistical analysis was performed using the GraphPad Prism Software (v5.02 for Windows; GraphPad Softare Inc. San Diego, CA, USA). Data are expressed as mean ± SD from three independent assays. The data were analyzed using one-way analysis of variance (ANOVA). A *p*-value under 0.05 was considered statistically significant.

3. Results and discussion

3.1 Effect of Tween®80 and linolenic acid on *H. pylori* growth

The antimicrobial activity of Tween®80 and linolenic acid present on the LNPs was evaluated over 24h of exposure to *H. pylori* J99. This strain was chosen once it was firstly isolated from a human patient with duodenal ulcer and duodenitis [25]. J99 strain is also considered highly pathogenic due to the secretion of cytotoxins, such as cytotoxin-associated gene A product (CagA) and the vacuolating cytotoxin (VacA) [26]. The kinetic growth of the control (untreated bacteria) is coherent with the literature, with a latency phase, followed by an exponential and a stationary growth [27].

All LNPs have a bactericidal effect, which is dependent on their composition (Figure 2A) and concentration (Figure 2B). The most effective LNPs was P2, with a 3-log-unit of reduction before 6 h of incubation. P1 and P4 had a similar bactericidal profile, with a 3-log reduction after 6 h. P3 was the one with the slowest effect. Considering that Tween®80 detaches the outer membrane of *H. pylori* [21] and that DOPE was included for targeting purposes, it was expected that the LNPs with higher amounts of Tween®80 would have a faster bactericidal effect. Nevertheless, P1 has more Tween®80 than P4, and even so, they have the same bactericidal effect. These results show that the lower amount of Tween®80 in P4 is compensated by the presence of linolenic acid, even in a low concentration. This is corroborated with the slower bactericidal effect of P3, which has a lower amount of Tween®80 and does not have linolenic acid. The effect of linolenic acid is also visualized through the difference between the effect of P1 and P2. Considering these results, we further studied the effect of Tween®80 and linolenic acid in the same amount as they were used in the P4 formulation (Figure 2, B). Linolenic acid had a bacteriostatic effect, with a final reduction of 1-log after 24 h in the growth of *H. pylori*. Nevertheless, when incorporated into the LNPs, linolenic acid activity was faster. This result suggests that LNPs are able to protect fatty acids from oxidation and degradation [14], as with other fatty acids such as docosahexaenoic acid [14]. Another explanation is the increase of the uptake rate of fatty acids when loaded into LNPs [14, 28]. Tween®80 had a bactericidal effect, and the effect of the P4 formulation seems to combine the effects of both linolenic acid and Tween®80. Scanning electron microscopy studies were conducted afterward to evaluate the morphological changes on bacteria.
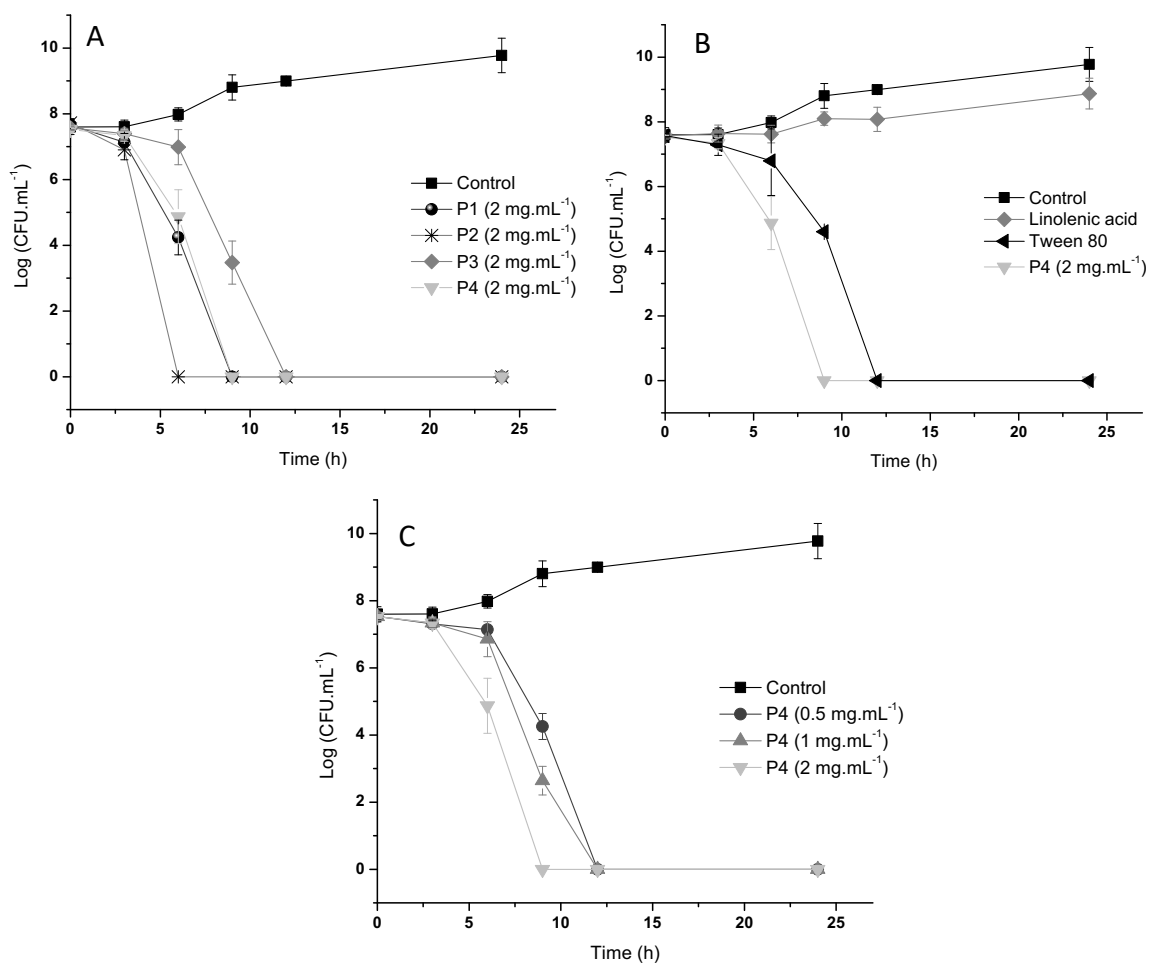
Figure 2. Antimicrobial activity of LNPs against *H. pylori* J99 over 24 h in presence of different LNPs compositions (A) in the same solid lipid concentration (2 mg.mL^{-1}). The contribution of each component was also assessed (B). The concentration used corresponded to the amount existent in the P4 formulation, namely, 56 μg.mL^{-1} and 1.2 mg.mL^{-1} of linolenic acid and Tween®80, respectively. The effect of the concentration of the P4 formulation is also shown (C). Data are expressed as mean ± standard deviation (n=3).

3.2 Effect of Tween®80 and linolenic acid on *H. pylori* morphology

The effect of the LNPs, Tween®80, and linolenic acid on the morphology of *H. pylori* was assessed by scanning electron microscopy. A spiral rod shape was visualized in untreated *H. pylori* J99 (control) after 3 and 12h (Figure 3), as described in the literature [25]. Linolenic acid (Figure 3) induced the formation of coccus after 3 h of incubation, though in a small number. At 12 h, *H. pylori* morphology was similar to the control. This result was predictable once linolenic acid was only bacteriostatic to *H. pylori* J99 in a concentration of 56 μg.mL^{-1} (Figure 2, B). However, linolenic acid changed the aggregation pattern of *H.*

pylori. It was already reported that the majority of linolenic acid is incorporated within the membrane of *H. pylori* [29]. Therefore, linolenic acid may change the surface of *H. pylori,* promoting their aggregation. A similar aggregation effect was shown by Seabra *et al.* with free docosahexaenoic acid [14]. Plain Tween®80 (Figure 3) does not have a significant effect within the first 3 h of incubation. Nevertheless, after 12 h, Tween®80 changed the integrity of the bacterial membrane. This effect is visualized in the rough and irregular surface that is not visualized in the control (Figure 3). These results are in a good agreement to what was reported for Tween®80, with alterations of the bacterial shape and swelling of the bacteria [21].
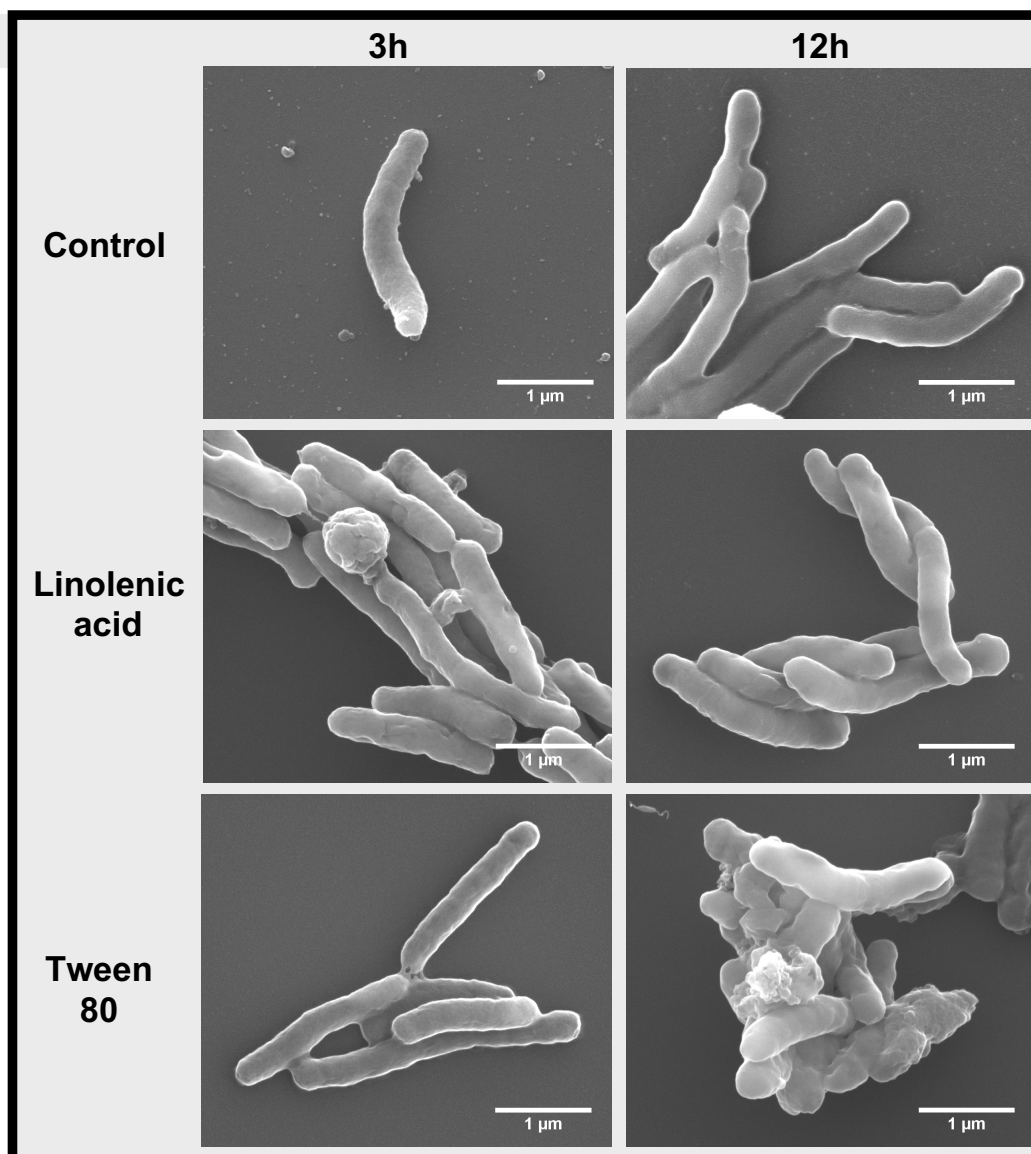
Figure 3. Scanning electron microscopic images of *H. pylori* J99 (control) in presence of linolenic acid (56 μg.mL^{-1}) and of Tween®80 (1.2 mg.mL^{-1}) during 3 or 12 h.
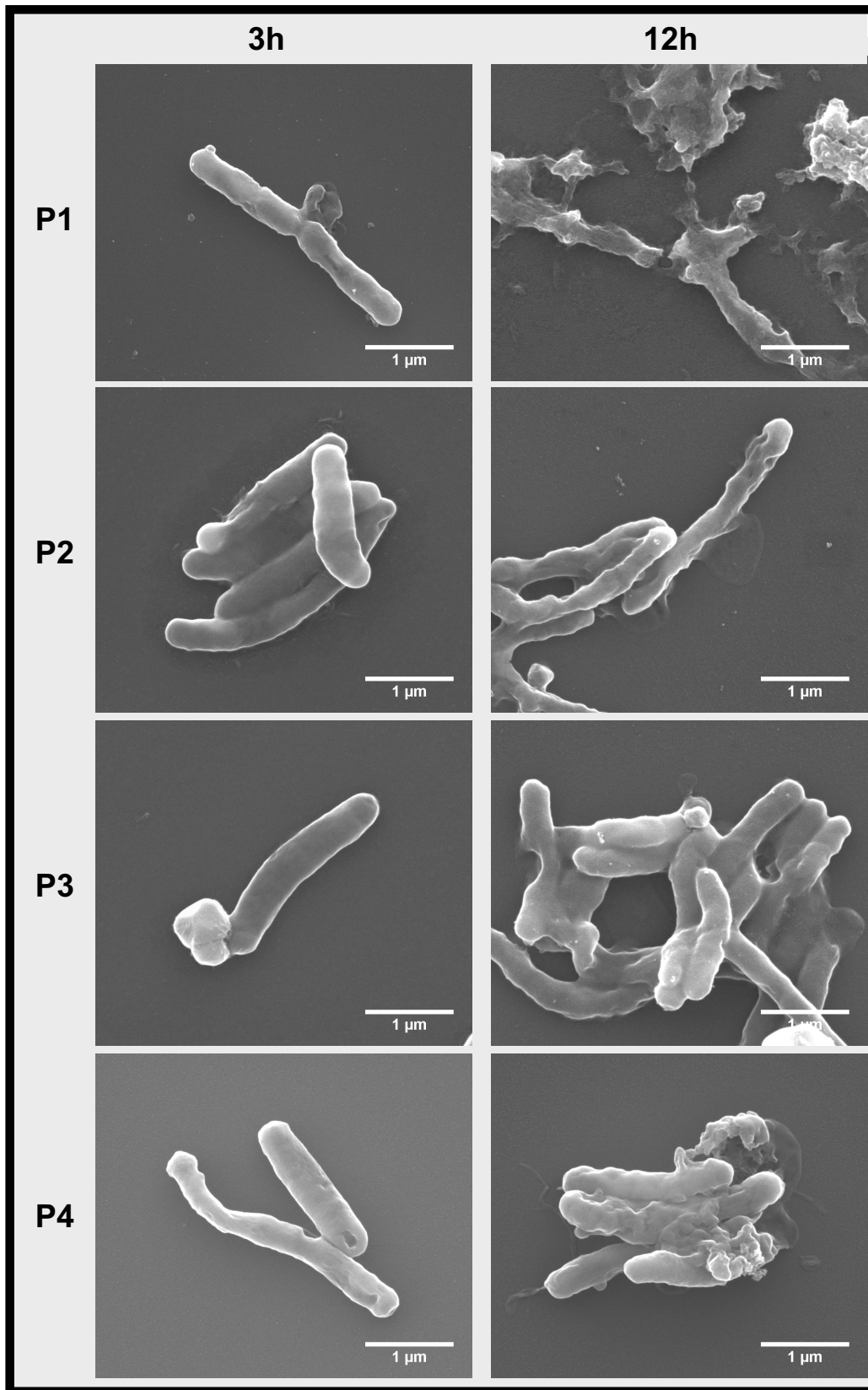
Figure 4. Scanning electron microscopic images of *H. pylori* in presence of P1, P2, P3, and P4 formulations, diluted to a final solid lipid concentration of 2 mg.mL^{-1}, after incubation for 3 or 12 h.

The effect of the LNPs was also assessed through scanning electron microscopy (Figure 4). After 3h of incubation, the effect of both P1 and P2 is visualized with the disruption of the bacterial membrane. Both LNPs have a higher concentration of Tween®80, which may be promoting this effect due to its ability to detach the outer membrane of *H. pylori* [21]. Irregularities of the bacterial membrane are also visualized with the P4 LNPs. However, after 12 h, *H. pylori* have lost their viability in the presence of any of the formulations. Considering the effect of the LNPs in the integrity of the bacterial membrane, we studied the release of adenosine triphosphate (ATP) from the bacteria.

3.3 Effect of the LNPs on the integrity of the plasmatic membrane

The release of ATP is associated with the disruption of the cytoplasmic membrane once its dissolution collapses the proton gradient [30]. This leads to the release of solutes into the medium, such as ATP, which can be quantitatively measured [30]. The results of ATP release normalized by the action of the Triton X-100 are shown in Figure 5. All formulations promoted almost 100 % of ATP release through the plasmatic membrane. The exception is P3, which promoted a release of 87%. Nevertheless, there are no statistically significant differences among the different LNPs. Hence, all LNPs have a permeabilization effect similar to the action of Triton X-100. Due to the detergent properties of Tween®80 [21], it is able to detach the outer membrane of *H. pylori,* which enhances the probability of changing the inner membrane. This may lead to a leakage of the cytoplasmic content, as well as, an increase of ATP release. The lower average of ATP release for the P3 formulation may be associated to the lower amount of Tween®80 present in the formulation. This effect is however counter balanced by the action of linolenic acid (P4 effect) due to ability of linolenic acid to be incorporated into the bacterial membrane and increase its permeability [29]. Fatty acids can also induce the disruption and fragmentation of the bacterial membrane [29].

Interestingly, after 3 h of incubation, there are no significant changes in the viability of the bacteria (Figure 2). Combining this information with the scanning electron microscopic images, these results show that the main mechanism of action of these LNPs may be the disruption of the bacterial membrane, which may be the initial mechanism for a cascade of events that lead to the killing of *H. pylori*.
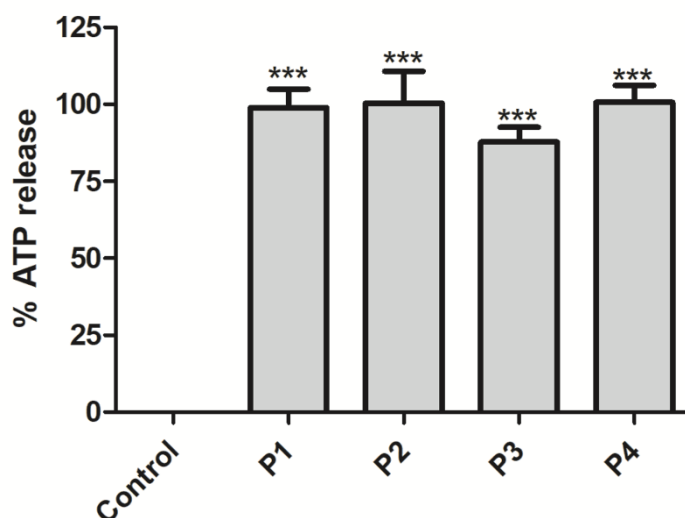
Figure 5. Percentage of ATP release through changes in the permeability of the plasmatic membrane of *H. pylori*. *** $p < 0.005$ means significant differences on the ATP release by bacteria exposure to formulations and control.

3.4 Efficacy of the targeting to *H. pylori*

DOPE was incorporated within the LNPs due to the existence of receptors to phosphatidylethanolamine on the membrane of *H. pylori* [18]. The ability of LNPs to bind to *H. pylori* was then assessed by imaging flow cytometry. The binding of P4 was evaluated for being the most complex formulation. The respective LNPs without DOPE (P2) were also analyzed. Imaging flow cytometry (Figure 6) showed that *H. pylori* are in the rod shape even when incubated with the LNPs. After 15 min of exposure of *H. pylori* with LNPs labelled with coumarin-6, bacteria exhibited a green fluorescence, suggesting a high affinity of LNPs to bind to *H. pylori* membrane. The effect of DOPE is significant once almost 100% of the bacteria are interacting with the P4 LNPs, as it can be seen by the fluorescence intensity of P4 under the positive region. On the contrary, only 75% of the P2 LNPs are bound to *H. pylori*. In fact, a significant percentage of bacteria are not labelled by LNPs (unlabelled-*H pylori* region). It is however noteworthy that the binding of LNPs to the bacteria was fast even for the LNPs without DOPE. The ability of LNPs to interact with *H. pylori* was also shown for other LNPs after 1.5 h [15]. An additional advantage of DOPE is the ability to inhibit the adhesion of the bacteria to gastric cells [12]. Hence, we used a bacteria-gastric cells adhesion model to confirm if this effect is kept under LNPs formulations.
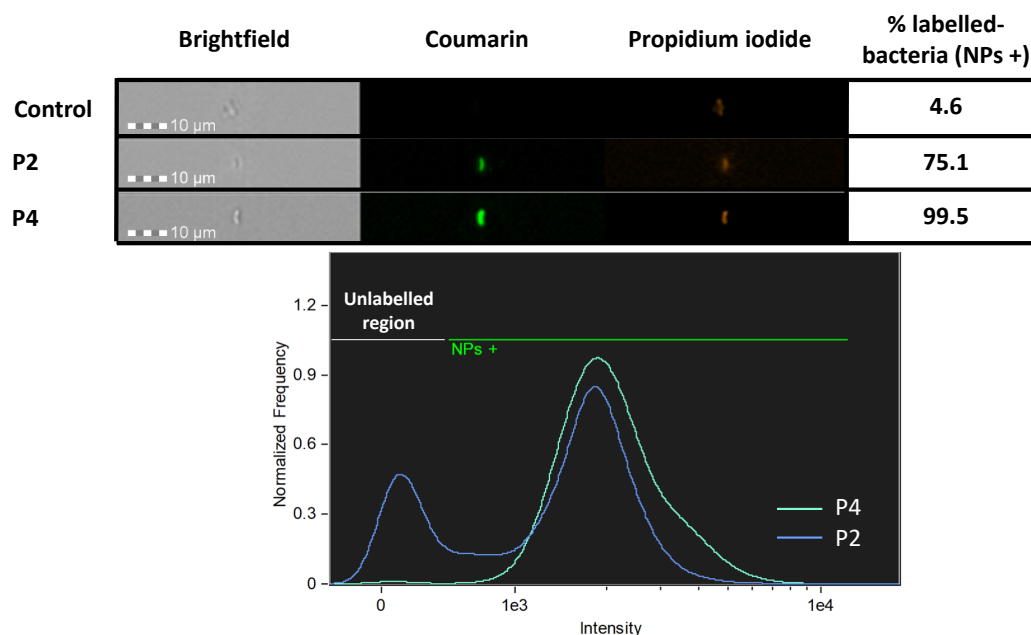
Figure 6. Images acquired by imaging flow cytometry (ImageStream^X®) with the representation of the brightfield (Channel 1), the green fluorescence (Channel 2), and the propidium iodide (Channel 4), and the correspondent percentage of labelled-bacteria. The fluorescence intensity of P2 and P4 is also shown, with the indication of the positive region. The control corresponds to *H. pylori* in medium.

3.5 Effect of the LNPs on the *H. pylori* adhesion to MKN-74 cells

An adhesion model was used to unveil the effect of the LNPs on the adhesion of *H. pylori* J99 to MKN-74. For that purpose, the LNPs were simultaneously incubated with the bacteria. Previous studies showed that the attachment of *H. pylori* to tissue culture cells had taken 1 h to occur [31]. To ensure a good percentage of adhesion without entering within the time frame of *H. pylori* death in presence of LNPs (Figure 2), the incubation was performed for 2 h. The percentage of bacteria that were adhered after this time was calculated using Eq. (2), and the results are shown in Figure 7.

The LNPs that did not contain DOPE (P1 and P2) decreased the percentage of adherence to approximately 70%. The results from imaging flow cytometry showed that *H. pylori* interact with LNPs within short periods of time. Hence, the bacterial membrane may not be free to bind to epithelial cells. In fact, *H. pylori* use interactive surface molecules, such as adhesins, to adhere to human gastric epithelial cells [32]. Furthermore, the inhibitory effect can be due to Tween®80 presence once it inhibits the adhesion of *H. pylori* to host cells [20]. Nevertheless, with DOPE, the LNPs decrease the percentage of adhered bacteria to 53% (P3) and 33% (P4). Therefore, DOPE may plug *H. pylori* and inhibit one of the receptors that these bacteria use to attach themselves to the gastric epithelium, as also

shown by Umamaheshwari *et al.* [12]. Interestingly, while there are no differences between P1 and P2, P3 and P4 are statistically different. P1/P2 and P3/P4 both varied in the inclusion of linolenic acid. Thus, linolenic acid must be at the interface of the LNPs in the P4 formulations whereas it must be internalized in the P2 formulations. The variation of the location of linolenic acid may be a consequence of the lower amount of Tween®80 or the incorporation of DOPE in the P4 formulation. The bacterial cell membrane was considered the prime target of fatty acids as linolenic acid [24]. Thus, the interaction of linolenic acid with the bacterial membrane may also hinder the adhesion of epithelial cells.
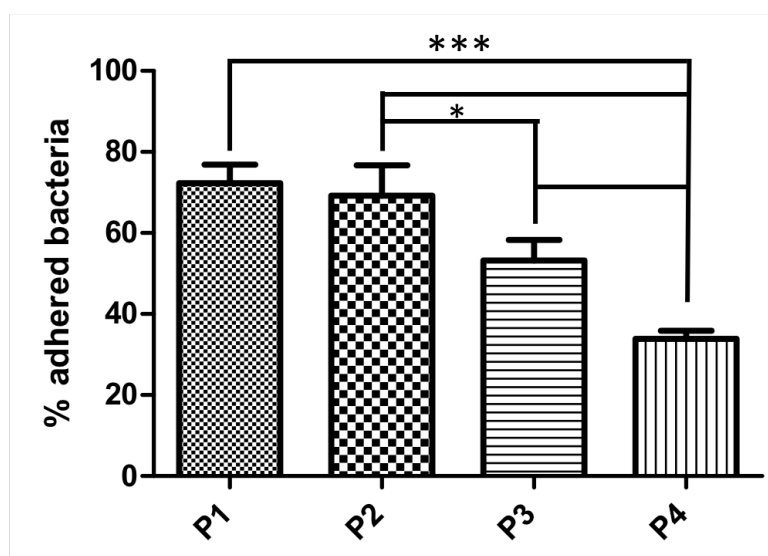
Figure 7. Percentage of *H. pylori* J99 that is adhered to MKN-74 cells after incubation with P1, P2, P3, and P4 for 2 h. The results are normalized by the number of bacteria that were adhered to the control, what was set to 100%. *$p < 0.05$, **$p < 0.01$, ***$p < 0.005$.

4. Conclusions

On this work, the efficacy of the developed LNPs was shown by their ability to adhere to the bacterial membrane, to change its permeability, and to kill the bacteria. Thus, these LNPs may be a good alternative in a world with emergent antimicrobial resistance. Additionally, these LNPs may also be a good basilar structure to load any compound with antimicrobial activity once double emulsion particles can encapsulate both hydrophilic and lipophilic molecules [33]. Furthermore, these LNPs inhibit the adhesion to gastric cells. Adhesion is important for the pathogenicity of *H. pylori.* Differences in the ability of adhesion may decrease the degree of inflammation mediated by the bacteria [34]. This happens because the adhesion to the host cell surface is important to inject bacterial virulence factors [35]. It is also important for the development of chronic infections and to the internalization

by the gastric cells [32, 35]. The efficacy of antimicrobial treatments decreases when the bacteria is internalized, which leads to a need of higher antibiotic doses [35]. Hence, these LNPs and especially the most complex one (P4) can be henceforward used in the treatment of *H. pylori.*

References

[1] M. Kidd, I.M. Modlin, A century of *Helicobacter pylori*, Digestion 59 (1998) 1-15.

[2] World gastroenterology organisation global guideline: *Helicobacter pylori* in developing countries, J. Dig. Dis. 12(5) (2011) 319-26.

[3] A review of human carcinogens. Part B: Biological agents, IARC Working Group on the Evaluation of the Carcinogenic Risks to Human, Lyon, France, 2009.

[4] P. Malfertheiner, F. Mégraud, C. O'Morain, Guidelines for the management of *Helicobacter pylori* infections, Business Briefing: Eur. Gastroenterol. Rev. (2005) 59-62.

[5] R.M. Zagari, M. Romano, V. Ojetti, R. Stockbrugger, S. Gullini, B. Annibale, F. Farinati, E. Ierardi, G. Maconi, M. Rugge, C. Calabrese, F. Di Mario, F. Luzza, S. Pretolani, A. Savio, G. Gasbarrini, M. Caselli, Guidelines for the management of *Helicobacter pylori* infection in Italy: The III Working Group Consensus Report 2015, Dig. Liver Dis. 47(11) (2015) 903-12.

[6] P. Malfertheiner, F. Megraud, C.A. O'Morain, J.P. Gisbert, E.J. Kuipers, A.T. Axon, F. Bazzoli, A. Gasbarrini, J. Atherton, D.Y. Graham, R. Hunt, P. Moayyedi, T. Rokkas, M. Rugge, M. Selgrad, S. Suerbaum, K. Sugano, E.M. El-Omar, Management of *Helicobacter pylori* infection-the Maastricht V/Florence Consensus Report, Gut 66(1) (2017) 6-30.

[7] W.D. Chey, G.I. Leontiadis, C.W. Howden, S.F. Moss, ACG Clinical Guideline: treatment of *Helicobacter pylori* infection, Am. J. Gastroenterol. 112(2) (2017) 212-239.

[8] C.A. Fallone, N. Chiba, S.V. van Zanten, L. Fischbach, J.P. Gisbert, R.H. Hunt, N.L. Jones, C. Render, G.I. Leontiadis, P. Moayyedi, J.K. Marshall, The Toronto Consensus for the Treatment of *Helicobacter pylori* Infection in Adults, Gastroenterol. 151(1) (2016) 51-69 e14.

[9] J.P. Gisbert, J. Molina-Infante, J. Amador, F. Bermejo, L. Bujanda, X. Calvet, M. Castro-Fernández, A. Cuadrado-Lavín, J.I. Elizalde, E. Gene, F. Gomollón, Á. Lanas, C. Martín de Argila, F. Mearin, M. Montoro, Á. Pérez-Aisa, E. Pérez-Trallero, A.G. McNicholl, IV Spanish Consensus Conference on *Helicobacter pylori* infection treatment, Gastroenterología y Hepatología (English Edition) 39(10) (2016) 697-721.

[10] A. Zullo, C. Hassan, L. Ridola, V.d. Francesco, D. Vaira, Standard triple and sequential therapies for *Helicobacter pylori* eradication: An update, Eur. J. Intern. Med. 24(1) (2012) 16-19.

[11] S.D. Georgopoulos, V. Papastergiou, S. Karatapanis, Current options for the treatment of *Helicobacter pylori*, Expert Opin. Pharmacother. 14(2) (2013) 211-223.

[12] R.B. Umamaheshwari, N.K. Jain, Receptor-mediated targeting of lipobeads bearing acetohydroxamic acid for eradication of *Helicobacter pylori*, J. Control. Release 99(1) (2004) 27-40.

[13] D. Lopes, C. Nunes, M.C.L. Martins, B. Sarmento, S. Reis, Eradication of *Helicobacter pylori*: Past, present and future, J Control Release 189 (2014) 169-86.

[14] C.L. Seabra, C. Nunes, M. Gomez-Lazaro, M. Correia, J.C. Machado, I.C. Goncalves, C.A. Reis, S. Reis, M.C.L. Martins, Docosahexaenoic acid loaded lipid nanoparticles with bactericidal activity against *Helicobacter pylori*, Int. J. Pharm. 519(1-2) (2017) 128-137.

[15] C. Leal Seabra, C. Nunes, M. Bras, M. Gomez-Lazaro, C.A. Reis, I.C. Goncalves, S. Reis, M.C.L. Martins, Lipid nanoparticles to counteract gastric infection without affecting gut microbiota, Eur. J. Pharm. Biopharm. (2018).

[16] L. Battaglia, M. Gallarate, Lipid nanoparticles: state of the art, new preparation methods and challenges in drug delivery, Expert. Opin. Drug Deliv. 9(5) (2012) 497-508.

[17] P. Severino, T. Andreani, A.S. Macedo, J.F. Fangueiro, M.H. Santana, A.M. Silva, E.B. Souto, Current State-of-Art and New Trends on Lipid Nanoparticles (SLN and NLC) for Oral Drug Delivery, J. Drug Deliv. 2012 (2012) 750891.

[18] C.A. Lingwood, M. Huesca, A. Kuksis, The glycerolipid receptor for *Helicobacter pylori* (and exoenzyme S) is phosphatidylethanolamine, Infect. Immun. 60(6) (1992) 2470-2474.

[19] C.M. Toutain-Kidd, S.C. Kadivar, C.T. Bramante, S.A. Bobin, M.E. Zegans, Polysorbate 80 inhibition of Pseudomonas aeruginosa biofilm formation and its cleavage by the secreted lipase LipA, Antimicrob. Agents Chemother. 53(1) (2009) 136-45.

[20] M. Huesca, B. Gold, P. Sherman, P. Lewin, C. Lingwood, Therapeutics used to alleviate peptic ulcers inhibit *H. pylori* receptor binding in vitro, Zbl. Bakt. 280(1-2) (1993) 244-252.

[21] N. Figura, R. Marcolongo, G. Cavallo, A. Santucci, G. Collodel, A. Spreafico, E. Moretti, Polysorbate 80 and *Helicobacter pylori*: a microbiological and ultrastructural study, BMC Microb. 12(217) (2012) 1-10.

[22] C.Q. Sun, C.J. O'Connor, A.M. Roberton, Antibacterial actions of fatty acids and monoglycerides against *Helicobacter pylori*, FEMS Immunol. Med. Microbiol. 36(1-2) (2003) 9-17.

[23] J.A. Jackman, B.K. Yoon, D. Li, N.J. Cho, Nanotechnology Formulations for Antibacterial Free Fatty Acids and Monoglycerides, Molecules 21(3) (2016) 305.

[24] S.W. Jung, S. Thamphiwatana, L. Zhang, M. Obonyo, Mechanism of antibacterial activity of liposomal linolenic acid against *Helicobacter pylori*, PLoS One 10(3) (2015) e0116519.

[25] *Helicobacter pylori*: physiology and genetics, ASM Press, Washington DC, 2001.

[26] P. Doig, B.L. Jonge, R.A. Alm, E.D. Brown, M. Uria-Nickelsen, B. Noonan, S.D. Mills, P. Tummino, G. Carmel, B.C. Guild, D.T. Moir, G.F. Vovis, T.J. Trust, *Helicobacter pylori* physiology predicted from genomic comparison of two strains, Microbiol. Mol. Biol. Rev. 63(3) (1999) 675-707.

[27] P. Parreira, A. Magalhaes, I.C. Goncalves, J. Gomes, R. Vidal, C.A. Reis, D.E. Leckband, M.C. Martins, Effect of surface chemistry on bacterial adhesion, viability, and morphology, J. Biomed. Mater. Res. A 99(3) (2011) 344-53.

[28] M. Obonyo, L. Zhang, S. Thamphiwatana, D. Pornpattananangkul, V. Fu, L. Zhang, Antibacterial activities of liposomal linolenic acids against antibiotic-resistant *Helicobacter pylori*, Mol. Pharm. 9 (2012) 2677-85.

[29] S.W. Jung, S.W. Lee, The antibacterial effect of fatty acids on *Helicobacter pylori* infection, Korean J. Intern. Med. 31(1) (2016) 30-5.

[30] J.B. Parsons, J. Yao, M.W. Frank, P. Jackson, C.O. Rock, Membrane disruption by antimicrobial fatty acids releases low-molecular-weight proteins from Staphylococcus aureus, J. Bacteriol. 194(19) (2012) 5294-304.

[31] J.L. Simala-Grant, D. Zopt, D.E. Taylor, Antibiotic susceptibility of attached and free-floating *Helicobacter pylori*, J. Antimicrob. Chemother. 47 (2001) 555-563.

[32] Z.-W. Zhang, N. Dorrel, B.W. Wren, M.J.G. Farthing, *Helicobacter pylori* adherence to gastric epithelial cells: a role for non-adhesin virulence genes, J. Med. Microbiol. 51 (2002) 495-502.

[33] M. Iqbal, N. Zafar, H. Fessi, A. Elaissari, Double emulsion solvent evaporation techniques used for drug encapsulation, Int. J. Pharm. 496(2) (2015) 173-90.

[34] J.G. Kusters, A.H. van Vliet, E.J. Kuipers, Pathogenesis of *Helicobacter pylori* infection, Clin. Microbiol. Rev. 19(3) (2006) 449-90.

[35] Y. Huang, Q.L. Wang, D.D. Cheng, W.T. Xu, N.H. Lu, Adhesion and Invasion of Gastric Mucosa Epithelial Cells by *Helicobacter pylori*, Front. Cell. Infect. Microbiol. 6 (2016) 159.

Chapter 6.7

Efficacy of amoxicillin-loaded lipid nanoparticles on an *in vitro* infection model of *Helicobacter pylori*

Biophysical studies showed that amoxicillin has toxic effects on lipid membranes at acidic pH (**Chapter 6.4**). Hence, its encapsulation and release at the site of infection not only increase its efficacy but also decrease the prevalence of side effects. Additionally, from the previous two works (**Chapter 6.5** and **6.6**) we obtained lipid nanoparticles that are retained at the site of infection and that target, seal, and kill *H. pylori*. Therefore, this work was designed to use the promising nanoparticles to load amoxicillin. We also developed an *in vitro* model infection to mimic the conditions of *H. pylori in vivo*.
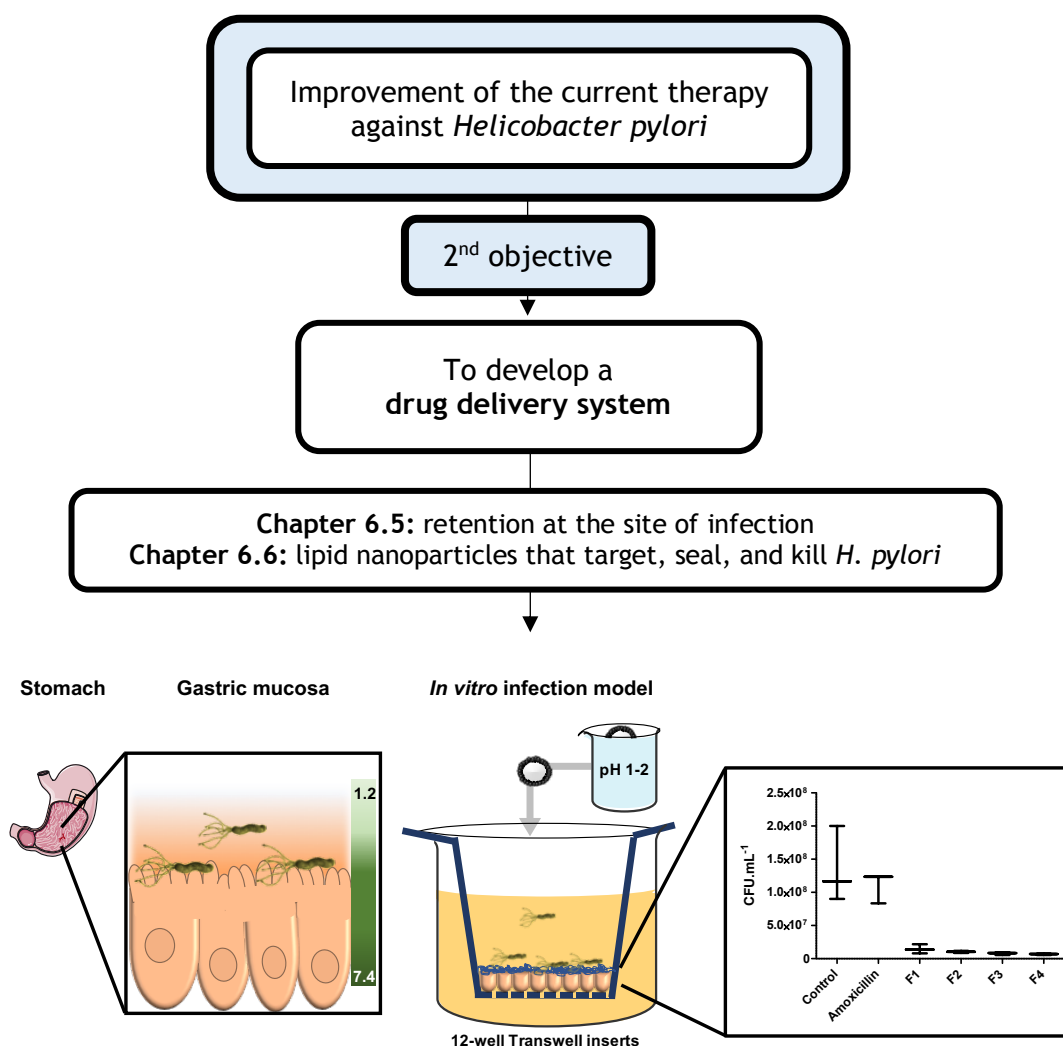
Chapter 6.7

Efficacy of amoxicillin-loaded lipid nanoparticles on an *in vitro* infection model of *Helicobacter pylori*

Daniela Lopes-de-Campos[1], Catarina Leal Seabra[2,3], Rita M. Pinto[1], Bruno Sarmento[2,3,4], Cláudia Nunes[1], M. Cristina L. Martins[2,3,5], and Salette Reis[1*]

[1] LAQV, REQUIMTE, Departamento de Ciências Químicas, Faculdade de Farmácia, Universidade do Porto, Portugal

[2] i3S - Instituto de Investigação e Inovação em Saúde, Universidade do Porto, Rua Alfredo Allen 208, 4200-393 Porto, Portugal

[3] INEB - Instituto de Engenharia Biomédica, Universidade do Porto, Rua Alfredo Allen 208, 4200-393 Porto, Portugal

[4] IINFACTS, Instituto de Investigação e Formação Avançada em Ciências e Tecnologias da Saúde, Instituto Universitário de Ciências da Saúde, Gandra, Portugal

[5] ICBAS- Instituto Ciências Biomédicas Abel Salazar, Universidade do Porto, Portugal

Amoxicillin (AMX) is a first-line drug against Helicobacter pylori (H. pylori) infections. Nevertheless, it faces some pharmacokinetic limitations in vivo. It is degraded under the acidic pH of the stomach, but simultaneously the uptake through the gastric mucosa is decreased when the gastric juice pH is high.

In this work, we assessed the effect of AMX-loaded lipid nanoparticles (LNPs) with different features, on the growth and morphology of H. pylori. We developed an in vitro infection model to mimic the physical and chemical barriers that hinder the treatment in vivo (gastric cells, mucins, and acidic pH) and that take into account the colonization on the interface between the gastric epithelium and the mucus layer. The results showed that the most effective LNPs were composed of Tween®80, linolenic acid, dioleoylphosphatidylethanolamine, and AMX. Although plain AMX was not effective in the in vitro infection model, possibly due to its degradation by the acidic pH, AMX-loaded LNPs significantly decreased the number of bacteria that were adhered or infecting MKN-74 cells. Overall, the in vitro infection model revealed the high potential of the AMX-loaded LNPs to overcome the limitations of the current therapy.

Keywords: *Helicobacter pylori*, lipid nanoparticles, Tween 80, Linolenic acid, DOPE, amoxicillin, *in vitro* infection model

1. Introduction

Helicobacter pylori (*H. pylori*) are bacteria that infect and colonize the antrum of the stomach [1]. At the beginning, the scientific community was sceptical regarding the ability of bacteria to survive to the harsh conditions of the stomach [1]. Nevertheless, their association to peptic ulcers was proven by Barry Marshall, and now they are classified as human carcinogenic (Group 1) by the World Health Organization [2]. *H. pylori* can induce the development of several gastric issues (e.g. chronic gastritis, peptic ulcers, gastric mucosa-associated lymphoma tissue, and adenocarcinomas) and extra-gastric diseases

(e.g. idiopathic thrombocytopenic purpura, iron deficiency anemia, ischemic heart disease, stroke, and Parkinson's and Alzheimer's diseases) [2]. The treatment of *H. pylori* infections is indeed crucial.

"Eradication of the ubiquitous "ulcer bug" is the first step in freeing patients with chronic dyspepsia and/or ulcer disease from an expensive lifetime of chronic medication use." Prof. Barry Marshall [3]. However, there are several factors that limit the current therapy. Some of them are associated with the characteristics of the bacteria, namely, antimicrobial resistances and the number of multiple strains at the site of infection [4]. Other limitations are related to some physiological features of the patient, such as age and enzymatic polymorphisms, as well as their compliance with the treatment [4]. Additionally, in vivo, H. pylori are located near gastric cells and within the mucus layer. Therefore, the protective mechanism of the mucus layer and the intracellular location of some bacteria also hamper the diffusion and the action of antibiotics [4]. Moreover, some antibiotics are degraded by the acidic pH and present a low residence time in the stomach, which lead to a systemic distribution and a lower efficiency [5, 6].

Amoxicillin (AMX) is a first-line drug against *H. pylori* infections [7]. However, it degrades under the acidic pH of the stomach [8-10]. This leads to higher doses and to more side effects, including topical effects on phosphatidylcholine membranes [11]. Nevertheless, the acidic pH is important for its local absorption through the gastric mucosa [12]. To overcome this incongruity and the lower retention of AMX at the site of infection, our research group developed AMX-loaded lipid nanoparticles (LNPs). They were able to retain AMX near the site of infection due to their low permeability through gastric cells and their ability to interact with mucins (**Chapter 6.5**). Moreover, the ability of the unloaded-LNPs to target *H. pylori,* to inhibit their attachment to gastric cells, and to kill the bacteria was also proven (**Chapter 6.6**). This work aimed to evaluate the therapeutic potential of AMX-loaded LNPs (Figure 1) in overcoming the limitations of the current treatment plan. For that purpose, an *in vitro H. pylori* infection model was designed. In fact, there is an incongruity between the efficacy of the antibiotics *in vitro* and *in vivo* once the free-access to the planktonic bacteria is not observed *in vivo* [13]. Therefore, we developed an *in vitro* infection model that can recreate in a simplistic way the infection that occurs *in vivo*.
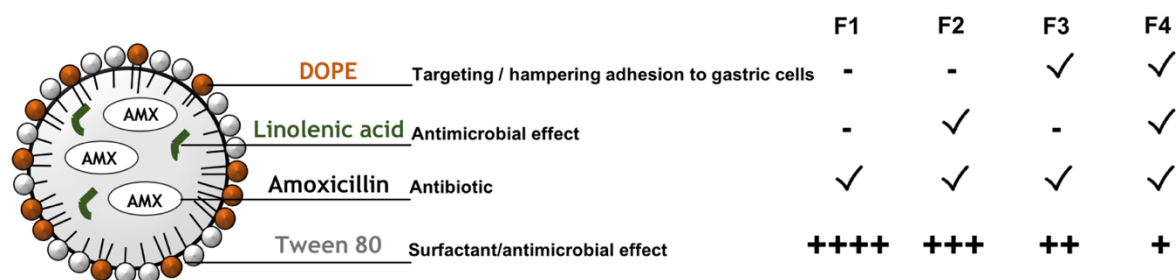
Figure 1. Composition of the different AMX-loaded LNPs. Dioleoylphosphatidylethanolamine (DOPE) is used for targeting, and it is only present in F3 and F4 formulations. Linolenic acid has antimicrobial effects, and it was only added to F2 and F4 formulations. The amount of Tween®80 was decreased for the formulations with a higher complexity.

2. Materials and methods

2.1 Materials

The compounds that composed the LNPs were purchased from Gattefossé, France (cetyl palmitate), Avanti® Polar Lipids, USA (dioleoylphosphatidylethanolamine - DOPE), Sigma-Aldrich ®, USA (Tween 80, linolenic acid, and AMX), and VWR International LLC, USA (chloroform). From Sigma-Aldrich®, it was also obtained Polymixin B, Vancomycin, Amphotericin B, Trimethroprim, Triton™ X-100, and Brucella Broth medium. Roswell Park Memorial Institute (RPMI) medium, trypsin-EDTA (1x), Dulbecco's Phosphate Buffered Saline 10x pH 7.4 (PBS), Penicillin-Streptomycin (Pen-Strep), and Fetal Bovine Serum (FBS) were purchased from Gibco® (Invitrogen Corporation, Paisley, UK). Blood agar base 2 medium was acquired from Liofilchem, Italy. The defibrinated horse blood used for *H. pylori* medium plates was purchased from Probiológica, Portugal. The BioBank of Instituto de Investigação e Inovação em Saúde (i3S) kindly provided the MKN-74 cell line. Glutaraldehyde (25%) and sodium cacodylate buffer were obtained from Merck, Germany, and the BacTiter-Glo™ Microbial Cell Viability assay kit was purchased from Promega Inc, USA.

2.2 Methods

2.2.1 Preparation of the LNPs

The synthesis of the LNPs by the double emulsion technique is well-detailed in previous works (**Chapter 6.7** and **6.6**). Briefly, 178.5 mg of cetyl palmitate, without (F1 and F3) or with (F2 and F4) 5 mg of linolenic acid, were dissolved in chloroform. AMX was

dissolved in a basified aqueous solution (0.5 mL) and then dispersed into the organic solution by sonication, for 30 sec at 70% amplitude. For the F3 and the F4 LNPs, DOPE (20 mg) dissolved in chloroform was added to the emulsion. 4 mL of Tween®80 (20, 18.75, 15, or 13.75 mg.ml^{-1} for F1, F2, F3, or F4, respectively) were added, and the emulsion was sonicated for 2 min at 70% amplitude (tip diameter of 1/4" (6 mm)). Tween®80 (4 mL of 12.5 mg.ml^{-1}) was added again to all formulations. Afterward, the organic solvent was evaporated under stirring for 3 h. During the synthesis, the LNPs were protected from light.

2.2.2 *H. pylori* growth conditions

H. pylori J99 was provided by the Department of Medical Biochemistry and Biophysics, Umeã University, Sweden. It was initially cultured in spots (48 h), followed by spread (48 h), in *H. pylori* medium plates composed of blood agar base 2 with 10% defibrinated horse blood and an antibiotic cocktail with polymixin B (0.155 g.L^{-1}), vancomycin (6.25 g.L^{-1}), amphotericin B (1.25 g.L^{-1}), and trimethroprim (3.125 g.L^{-1}). The medium plates were kept at 37 °C under microaerophilic conditions. For the pre-inoculum suspension, the bacteria were ressuspended in Brucella Broth medium with 10% FBS. The final optical density (OD) was set to 0.1 at 600 nm (Thermo Scientific Spectronic GENESYS 20 Visible Spectrophometer, USA), and the bacteria grew at 37 °C and under microaerophilic conditions, in an orbital shaker of 150 rpm.

2.2.3. Effect of the AMX-loaded LNPs on the kinetic growth of *H. pylori*

H. pylori J99 concentration was adjusted to 10^7 bacteria.mL^{-1} (OD = 0.03, λ = 600 nm) without and with AMX-loaded LNPs at 37 °C, 150 rpm, under microaerophilic conditions. The effect of LNPs was assessed in terms of composition, using the same LNPs concentration, viz. 2 mg.mL^{-1} of solid lipid, and concentration using 0.5, 1, and 2 mg.mL^{-1} of solid lipid of the most complex formulation (F4). In each time point (0, 3, 6, 9, 12, and 24 h), 200 µL of the bacterial suspension were collected, diluted in PBS 1x (pH 7.4) and then plated in *H. pylori* medium plates. After 5 days of incubation at 37 °C, the number of colonies forming units (CFU) were counted.

2.2.4 Effect of the AMX-loaded LNPs on the *H. pylori* morphology

The morphology of *H. pylori* J99 was visualized by scanning electron microscopic analysis. For that purpose, the conditions of incubation with the AMX-loaded LNPs were

the same as those described in the 2.2.3 section, using diluted LNPs (2 mg.ml^{-1} of solid lipid). To assess the effect of AMX, the correspondent amount of drug was used, namely, 0.223 mg.ml^{-1}. In each time point (3 and 12 h), 1 mL of the bacterial suspension was washed in PBS 1x (pH 7.4). The pellet obtained after centrifugation for 5 min at 3,000 *g* was fixed with 2.5 % v/v glutaraldehyde in 0.14 M of sodium cacodylate buffer for 30 min at room temperature. The bacterial suspension (100 µL) adhered on sterilized glass coverslip (Ø13 mm) for 2 h. The samples were then dehydrated with increasing aqueous ethanol solutions (50-90 % (v/v)), dried using a critical point drying (CPD 7501, Poloran), and coated with a gold/palladium film over 30 s. A scanning electron microscopy (JEOL JSM-6310F) from CEMUP (Centro de Materiais da Universidade do Porto) was used to acquire the images at 30,000x and 60,000x of magnification.

2.2.5 Effect of the AMX-loaded LNPs on the integrity of the bacterial membrane

A BacTilter-Glo^{TM} Microbial Cell Viability Assay kit was used to quantify the release of ATP from the bacteria (the protocol is described elsewhere [14]). *H. pylori* J99 were incubated with LNPs diluted to a final solid lipid concentration of 2 mg.mL^{-1}, under the same microaerophilic and temperature conditions as described on the section 2.2.3. After 3 h, bacteria suspension was centrifuged for 5 min at 12,000 *g* and supernatant collected. 100 µL of the supernatant were mixed with 100 µL of the BacTilter-Glo^{TM} reagent in a white 96-well microplate. The luminescence was read in a Synergy^{TM} H Multimode microplate reader, BioTek Instruments (USA) after shaken for 2 min. The results were normalized considering a significant alteration of the bacterial membrane as the positive control (Triton^{TM} X-100) and the normal integrity of the bacterial membrane as the negative control (medium) (Eq. (1)).

$$\% \: ATP \: released = \frac{Luminescence_{sample} - Luminescence_{negative \: control}}{Luminescence_{positive \: control} - Luminescence_{negative \: control}} \times 100 \quad (1)$$

2.2.6 *In vitro* infection model
2.2.6.1 Cell culture conditions

MKN-74 cells (passage number from 56-60) were cultured in RPMI medium supplemented with 10% FBS and 1% Pen-Strep, at 37 °C in an atmosphere with 5% CO_2.

MKN-74 cells were then seeded in 12-well transwell inserts (0.4 μm pore size, Millicell® Hanging Cell Culture Inserts from Millipore, USA) without any antibiotic supplementation. The cells were seeded at a density of 10^5 cells.cm^{-2} and grown for 7 days to obtain a dense barrier, with functional tight junctions. The formation of cell monolayers was evaluated through the transepithelial electric resistance (TEER) using an epithelial VOM2 Voltohmmeter (World Precision Instruments, USA). 1500 and 500 μL of medium were used at the basolateral and the apical side, respectively. The medium was changed every 2/3 days.

2.2.6.2 *H. pylori* infection model

After 7 days, the apical medium was removed, and porcine mucins type II were added by adapting a reported protocol [15]. Briefly, 100 μL of mucins at 1% w/v were added to MKN-74 cells and further incubated at 37 °C for 30 min. In the first 5 min, the tissue culture plate was placed in an orbital shaker (50 rpm) to achieve a homogeneous distribution of the mucins onto the surface of the gastric epithelium. Afterward, 400 μL of a bacterial suspension (1.5 x 10^8 bacteria.mL^{-1}) were added and incubated at 37 °C, under 5% of CO_2, for 24 h to enable migration through mucins, adhesion, and infection of gastric cells. 100 μL of the apical side were then replaced by 100 μL of AMX-loaded LNPs diluted to obtain a final solid lipid concentration of 2 mg.mL^{-1}. The same protocol was followed for the addition of AMX to obtain a final concentration equivalent to the amount of drug existent in the LNPs dilution. Both AMX-loaded LNPs and AMX were previously diluted in acidic medium (pH 1-2) for 1 h, unprotected from light. After 24 h of treatment (48 h post-infection), the number of bacteria that was adhered or infecting gastric cells was obtained by trypsinization (150 μL for 15 min at 37 °C, 50 rpm) and mechanical disruption of the cells through scraping. Then, the adherent and infecting bacteria were diluted in PBS 1x (pH 7.4) and plated in *H. pylori* medium plates. After 5 days at 37 °C, the number of CFU was counted.

2.2.7 Statistical analysis

The GraphPad Prism Software (v5.02 for Windows; GraphPad Software Inc. San Diego, CA, USA) was used to analyze the data by the one-way analysis of variance (ANOVA). The mean ± SD of three independent assays are shown, and a p-value below 0.05 was considered statistically significant.

3. Results and Discussion

## 3.1 Effect of the AMX-loaded LNPs on *H. pylori* growth

The efficacy of the AMX-loaded LNPs was assessed through the growth kinetic of *H. pylori* J99, a human pathogenic strain, which has virulence factors that include the production of the cytotoxin-associated gene A product (CagA), the vacuolating cytotoxin (VacA), the sialic-acid-binding adhesins (SabA) and the blood group antigen-binding adhesins (BabA) [16, 17]. These factors are associated with a higher risk of development of peptic ulcers and gastric cancer [18, 19]. The effect of the AMX-loaded LNPs is shown in Figure 2. The comparison with the unloaded-LNPs is also shown, considering the results already reported in a previous study (**Chapter 6.6**). The effect of the AMX-loaded F1 and F3 was faster than with the corresponding unloaded LNPs (P1 and P3) (Figure 2, A). However, in the formulations with linolenic acid (F2 and F4), the kinetic growth of *H. pylori* was similar to those obtained with the respective unloaded LNPs (**Chapter 6.6**). Thus, the incorporation of AMX does not accelerate the death of the bacteria when linolenic acid is present. Nevertheless, the incorporation of AMX can still be an advantage in those systems, once the treatment of *H. pylori* infections is not feasible in monotherapy [2]. Additionally, the development of antimicrobial resistance is also less probable when the bacteria is attacked through different compounds/mechanisms once multiple mutations would be required [20]. Furthermore, when lower concentrations are used (Figure 2, B), F4 has a faster efficiency rate than the corresponding unloaded LNPs (P4). In fact, the effect of the concentration of P4 is more notorious than of F4. This can be a consequence of two phenomena. The existence of an initial plateau that is not concentration or formulation-dependent (0-3 h) can be due to the resistance of the LNPs under the conditions of the medium. By this, the loading is kept inside of the LNPs, delaying the antibacterial effect. After that initial period, the LNPs may start a disintegration process that leads to a fast bactericidal effect. For instance, for F4 and P4 (2 mg.mL^{-1}), there is a 3-log of reduction (bactericidal effect) at 6 h (3h after the initial plateau). Another explanation for the inexistence of a concentration-effect for the AMX-loaded LNPs is that AMX has a time-dependent effect [21]. Therefore, the retention of the LNPs at the site of infection through the low permeability across MKN-74 cells and the interaction with mucins may have a key role (**Chapter 6.5**).
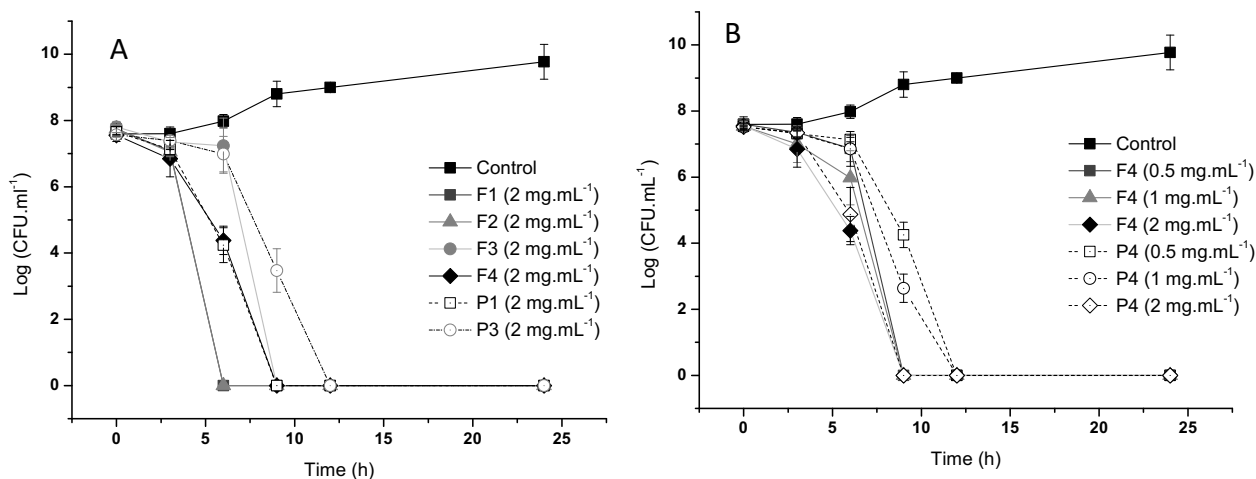
Figure 2. Growth kinetic curves of *H. pylori* J99 over 24 h in presence of different AMX-loaded LNPs compositions (A) in the same solid lipid concentration (2 mg.mL^{-1}). The effect of the solid lipid concentration of the LNPs is also shown (B). The comparison with the effect reported for the unloaded LNPs (P1, P3, and P4) in **Chapter 6.6** is also provided. Data are expressed as mean ± standard deviation (n=3).

3.2 Effect of the AMX-loaded LNPs on *H. pylori* morphology

Scanning electron microscopy can be very useful to unveil morphological changes of isolated organisms [22]. Hence, it was used to assess if the developed LNPs were able to change *H. pylori* morphological features. The results are shown in Figure 3. The control has the typical morphological structure of *H. pylori*, namely, a rod-shaped bacteria (bacilli), with 0.5 x 5 μm in length (Figure 1, A) [1, 23]. The viability of the control is also noticed through the ability of division at 12 h, when the bacteria are in their exponential growth (Figure 2). F1 and F2 formulations promoted a disruption of the bacterial membrane after 3 h of incubation, which led to the release of the cytoplasmic content. F3 did not change *H. pylori* morphology whereas F4 promoted small visual disruptions. The higher effect of F1 and F2 LNPs after 3 h of incubation is not surprising considering the effect of those LNPs on the kinetic growth of *H. pylori* and the ability of Tween®80 to detach the outer membrane of *H. pylori* [24]. However, at 12 h, significant changes on the integrity of the bacterial membrane were visualized to all LNPs. A highlight of the effect of the F1 formulation is shown, where it is possible to visualize that *H. pylori* integrity is totally perturbed. Although in its rod-shape, the bacteria seem to be destroyed and degraded by the AMX-loaded LNPs.
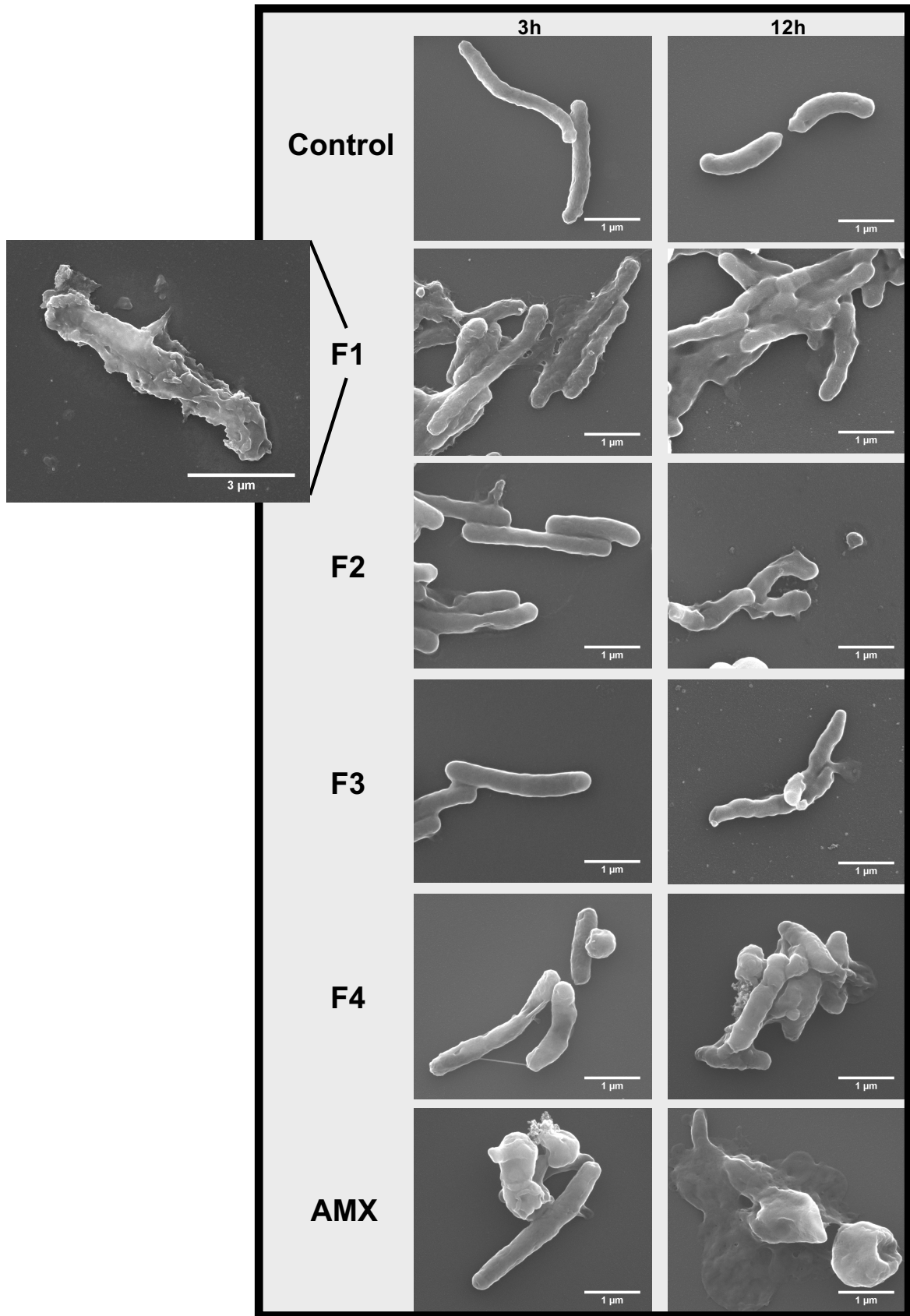
Figure 3. Scanning electron microscopic images of untreated *H. pylori* (control, top line), and treated *H. pylori* with AMX-loaded LNPs (F1 – F4, at a solid lipid concentration of 2 mg.mL^{-1}), and of AMX in the same concentration as it is in the formulations (0.223 mg.mL^{-1}), during 3 or 12 h of incubation.

The effect of plain AMX was also analysed. AMX is a β-lactam antibiotic, whose mechanism of action relies on the inhibition of enzymes that are crucial for the synthesis of the bacterial cell wall [25]. This mechanism can in fact be seen through scanning electron microscopy, with the complete disruption of the bacteria at 12 h. Therefore, both the drug (AMX) and the components of the LNPs (Tween®80 and linolenic acid) seem to contribute to the mechanism of action of the AMX-loaded LNPs. It is noteworthy that the existence of *H. pylori* under its coccoid shape was seen with plain AMX incubation, but only sporadically seen with AMX-loaded LNPs incubation. Some authors suggest that the coccoid form is a passive manifestation of cell death, with the existence of degenerate remains of dead *H. pylori* [26]. However, other authors associated this type of structure with the direct or indirect ability of reinfection [27]. The ability of AMX and antibiotics in general to induce stress conditions that lead to coccoid formation as a mechanism of protection of bacteria was already reported [28]. Nevertheless, the addition of linolenic acid can overcome this effect once it was reported that it can perturb the integrity of the bacterial membrane, even when the bacteria are under a coccoid and resistant shape [14, 29].

3.3 The effect of the AMX-loaded LNPs on the integrity of the bacterial membrane

Scanning electron microscopic images showed the disruption of the cytoplasmic membrane. This effect is followed by the release of solutes, such as ATP, due to the collapse of the proton gradient [30]. Hence, the release of ATP may be quantitatively measured and, indirectly, the permeabilization of the membrane can be inferred [30]. The results show that all AMX-loaded LNPs promote a permeabilization of the bacterial membrane, with an action similar to the effect of Triton X-100 (Figure 4). The ability of linolenic acid and Tween®80 to perturb the bacterial membrane was already shown for the plain compounds [24, 31] and for when they are incorporated in nanoparticles ([14] and **Chapter 6.6**). In fact, the lower effect of the F3 LNPs was also shown for the unloaded-LNPs (**Chapter 6.6**), and it is a consequence of the lower amount of Tween®80. This lower effect is counter balanced by linolenic acid (F4) but not by AMX (comparing to P3 from **Chapter 6.6**). Once the effect of AMX is time-dependent and not concentration-dependent [21], the time of the assay may not be enough for AMX to act. In fact, the effect of AMX does not result from a topical interaction with *H. pylori*. Instead, its mechanism of action depends on the inhibition of enzymes involved in the synthesis of the bacterial cell wall [25]. Therefore, it depends on the multiplication of *H. pylori*. To ensure a more time-dependent pattern within a more realistic model, we developed an *in vitro* infection model.
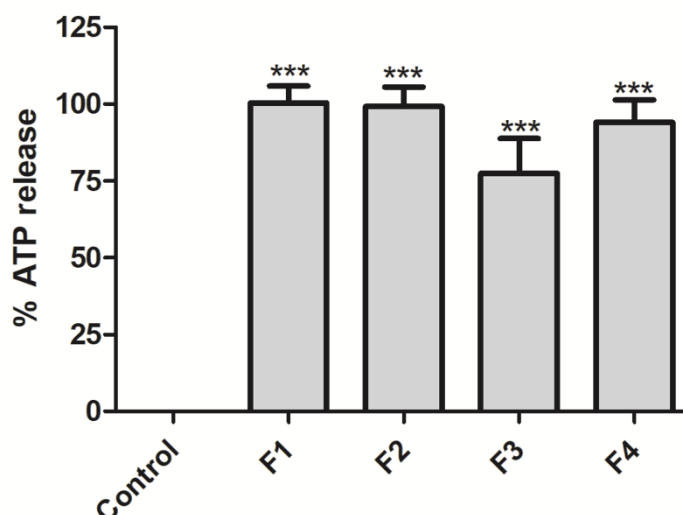
Figure 4. Permeability of bacterial membrane measured by ATP release after 2h of incubactiin. *** $p < 0.005$ significant differences on the ATP release by bacteria exposure to AMX-loaded LNPs formulations and control.

3.4 Efficacy of AMX-loaded LNPs using an *in vitro* infection model

The majority of the efficacy studies against *H. pylori* are performed with planktonic bacteria. These assays are important for a first evaluation; however, they lack in the mimetization of what may occur *in vivo*. *In vivo*, *H. pylori* are protected by the surrounded mucus and by epithelial cells [32] (Figure 5). Hence, the access of drugs to *H. pylori* is limited, and this is one of the reasons for the low biodistribution of antibiotics at infection site and the efficacy of the antibiotics *in vitro* and *in vivo* [13]. Therefore, we designed a model where all the key features that can affect the efficacy of a treatment are represented. First, we used transwell devices to be able to measure the transepithelial electric resistance and, consequently, ensure the formation of an epithelial barrier with functional tight junctions. MKN-74 cell lines were chosen once they keep their cell morphology and cellular adhesion even after 96h after the infection [33]. Consequently, the physical barrier composed of MKN-74 cells would be intact after *H. pylori* infection. Before the addition of mucins, TEER was around 150 $\Omega.cm^2$, which is within the range of the reference to a gastric epithelium (150-200 $\Omega.cm^2$). Mucins were added and homogeneously distributed onto the surface of epithelial cells. *H. pylori* J99 was chosen once it is a human strain with a high pathogenicity. The acid medium is another important feature of *in vivo* administration. We simulated the contact with the pH of the stomach lumen by incubating the LNPs and the AMX for 1 h in acid medium. The time of treatment was 24 h.
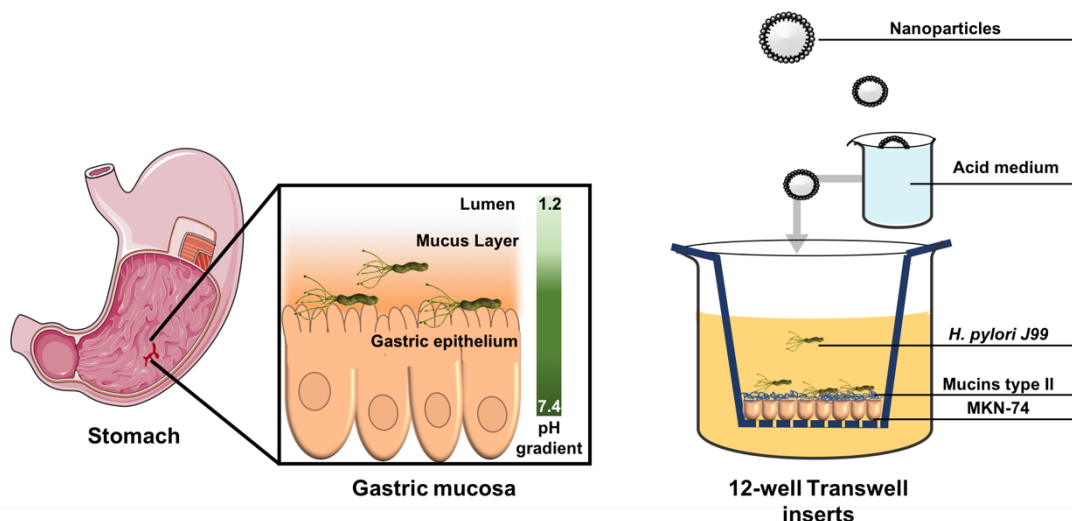
Figure 5. *In vitro* infection model. MKN-74 cell lines were seeded in Transwell devices and then mucins were distributed onto the surface of the formed barrier. The infection by *H. pylori* occurred for 24 h before the administration of the treatment (AMX-loaded LNPs or AMX) for another 24 h. Both treatments were previously incubated for 1 h at acidic pH to mimic the oral administration.

The results are shown in Figure 6. The infection was successfully achieved, as it can be seen by the number of bacteria that were adhered or internalized by MKN-74 cells. A control of *H. pylori* infection without 100 μL of the acidic medium was also performed. 48 h post-infection, there was an average of 1.7 x 10^8 CFU.mL^{-1}, which is within the range of the results of the bacteria with acid (control of Figure 6). Although AMX decreased the average of the number of bacteria, still it was not statistically significant. These results show that AMX is in fact degraded by the acidic pH, which is in agreement to [8-10]. Furthermore, the effect of the AMX-loaded LNPs is statistically significant. Thus, even when *H. pylori* is protected by physical barriers (gastric epithelium and mucins) and by a "chemical barrier" (the acidic pH), the developed AMX-loaded LNPs are effective. Interestingly and although without statistical significance, the average of viable bacteria after the treatment decreased with the increase of the complexity of the LNPs composition. In fact, F4 is the most effective system within an *in vitro* model, probably due to the loading of linolenic acid and DOPE. The first contributed to an additional antimicrobial effect, and the second decreased the ability of the bacteria to adhere and infect cells, increasing its susceptibility to the treatment.
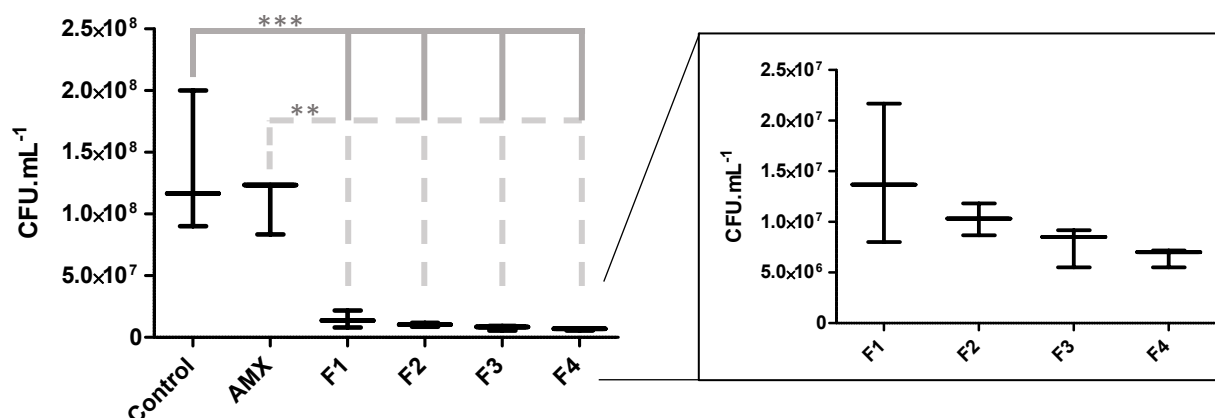
Figure 6. *In vitro* efficacy evaluated by number of CFU of *H. pylori* that were adhered or infecting gastric cells within an *in vitro* infection model, after 24 h of a single-dose treatment using AMX or AMX-loaded LNPs in the same AMX concentration (0.223 mg.mL^{-1}). ** $p < 0.01$ and *** $p < 0.005$.

4. Conclusions

In this work, we have studied the effect of AMX-loaded LNPs against *H. pylori* inclusively by the design and development of an *in* vitro infection model, with all the key features that can affect the efficacy of a treatment. The overall results showed that all components of the LNPs had key roles. Linolenic acid and Tween®80 were important for an initial disruption of the bacterial membrane, DOPE enable the targeting of *H. pylori,* and AMX promoted a faster killing effect of the bacteria. The developed AMX-loaded LNPs had a huge effect within an *in vitro* infection model when compared to plain AMX. Considering that AMX-loaded LNPs can be retained at the site of infection (**Chapter 6.5**), these LNPs are a powerful strategy to overcome the limitations of the current therapy.

References

[1] *Helicobacter pylori*: physiology and genetics, ASM Press, Washington DC, 2001.

[2] D. Lopes, C. Nunes, M.C.L. Martins, B. Sarmento, S. Reis, Eradication of *Helicobacter pylori*: Past, present and future, J. Control. Release 189 (2014) 169-86.

[3] World gastroenterology organisation global guideline: Helicobacter pylori in developing countries, J. Dig. Dis. 12(5) (2011) 319-26.

[4] S.D. Georgopoulos, V. Papastergiou, S. Karatapanis, Current options for the treatment of *Helicobacter pylori*, Expert Opin. Pharmacother. 14(2) (2013) 211-223.

[5] R.B. Umamaheshwari, N.K. Jain, Receptor-mediated targeting of lipobeads bearing acetohydroxamic acid for eradication of *Helicobacter pylori*, J. Control. Release 99(1) (2004) 27-40.

[6] P.-L. Bardonnet, V. Faivre, P. Boullanger, J.-C. Piffaretti, F. Falson, Pre-formulation of liposomes against *Helicobacter pylori:* characterization and interaction with the bacteria, Eur. J. Pharm. Biopharm. 69 (2008) 908-22.

[7] P. Malfertheiner, F. Megraud, C.A. O'Morain, J. Atherton, A.T. Axon, F. Bazzoli, G.F. Gensini, J.P. Gisbert, D.Y. Graham, T. Rokkas, E.M. El-Omar, E.J. Kuipers, G. European Helicobacter Study, Management of *Helicobacter pylori* infection-the Maastricht IV/ Florence Consensus Report, Gut 61(5) (2012) 646-664.

[8] A. Tsuji, E. Nakashima, S. Hamano, T. Yamana, Physicochemical properties of amphoteric B-lactam antibiotics I: stability, solubility, and dissolution behavior of amino penicillins as a function of pH, J. Pharm. Sci. 67(8) (1978).

[9] E. Nagele, R. Moritz, Structure elucidation of degradation products of the antibiotic amoxicillin with ion trap MS(n) and accurate mass determination by ESI TOF, J. Am. Soc. Mass Spectrom. 16(10) (2005) 1670-1676.

[10] M. Barzegar-Jalali, K. Adibkia, H. Valizadeh, M.R.S. Shadbad, A. Nokhodchi, Y. Omidi, G. Mohammadi, S.H.N. Nezhadi, M. Hasan, Kinetic analysis of drug release from nanoparticles, J. Pharm. Sci. 11(1) (2008) 167-177.

[11] D. Lopes, C. Nunes, P. Fontaine, B. Sarmento, S. Reis, Proof of pore formation and biophysical perturbations through a 2D amoxicillin-lipid membrane interaction approach, Biochim. Biophys. Acta 1859(5) (2017) 803-812.

[12] G. Cardaci, J.R. Lambert, R.G. King, N. Onishi, P. Midolo, Reduced amoxicillin uptake into human gastric mucosa when gastric juice pH is High, Antimicrob. Agents Chemother. 39(9) (1995) 2084-2087.

[13] F. Mégraud, P. Trimoulet, H. Lamouliatte, L. Boyanova, Bactericidal effect of amoxicillin on *Helicobacter pylori* in an *in vitro* model using epithelial cells, Antimicrob. Agents Chemother. 35(5) (1991) 869-872.

[14] S.W. Jung, S. Thamphiwatana, L. Zhang, M. Obonyo, Mechanism of antibacterial activity of liposomal linolenic acid against *Helicobacter pylori*, PLoS One 10(3) (2015) e0116519.

[15] L. Garcia-Gonzalez, L. Yepez-Mulia, A. Ganem, Effect of beta-cyclodextrin on the internalization of nanoparticles into intestine epithelial cells, Eur. J. Pharm. Sci. 81 (2016) 113-8.

[16] P. Doig, B.L. Jonge, R.A. Alm, E.D. Brown, M. Uria-Nickelsen, B. Noonan, S.D. Mills, P. Tummino, G. Carmel, B.C. Guild, D.T. Moir, G.F. Vovis, T.J. Trust, *Helicobacter pylori* physiology predicted from genomic comparison of two strains, Microbiol. Mol. Biol. Rev. 63(3) (1999) 675-707.

[17] J. Mahdavi, B. Sonden, M. Hurtig, F.O. Olfat, L. Forsberg, N. Roche, J. Angstrom, T. Larsson, S. Teneberg, K.A. Karlsson, S. Altraja, T. Wadstrom, D. Kersulyte, D.E. Berg, A. Dubois, C. Petersson, K.E. Magnusson, T. Norberg, F. Lindh, B.B. Lundskog, A. Arnqvist, L. Hammarstrom, T. Boren, *Helicobacter pylori* SabA adhesin in persistent infection and chronic inflammation, Science 297(5581) (2002) 573-8.

[18] Y. Yamaoka, Mechanisms of disease: *Helicobacter pylori* virulence factors, Nat. Rev. Gastroenterol. Hepatol. 7(11) (2010) 629-41.

[19] J.C. Atherton, The pathogenesis of *Helicobacter pylori*-induced gastro-duodenal diseases, Annu. Rev. Pathol. Mech. 1 (2006) 63-96.

[20] R.Y. Pelgrift, A.J. Friedman, Nanotechnology as a therapeutic tool to combat microbial resistance, Adv. Drug Delivery Rev. 65(13–14) (2013) 1803-1815.

[21] J.C. Yang, C.W. Lu, C.J. Lin, Treatment of *Helicobacter pylori* infection: current status and future concepts, World J. Gastroenterol. 20(18) (2014) 5283-93.

[22] C.G. Golding, L.L. Lamboo, D.R. Beniac, T.F. Booth, The scanning electron microscope in microbiology and diagnosis of infectious disease, Sci. Rep. 6 (2016) 26516.

[23] L. Boyanova, I. Mitov, B. Vladimirov, *Helicobacter pylori*, Caister Academic Press, Norfolk, 2011.

[24] N. Figura, R. Marcolongo, G. Cavallo, A. Santucci, G. Collodel, A. Spreafico, E. Moretti, Polysorbate 80 and *Helicobacter pylori*: a microbiological and ultrastructural study, BMC Microb. 12(217) (2012) 1-10.

[25] Meyler's side effects of drugs: the international encyclopedia of adverse drug reactions and interactions, 15th ed., Elsevier2006.

[26] J.G. Kusters, M.M. Gerrits, J.A.G.V. Strijp, C.M.J.E. Vandenbroucke-Graus, Coccoid forms of *Helicobacter pylori* are the morphologic manifestation of cell death, Infect. Immun. 65(9) (1997) 3672-3679.

[27] M. Sarem, R. Corti, Role of *Helicobacter pylori* coccoid forms in infection and recrudescence, Gastroenterología y Hepatología (English Edition) 39(1) (2016) 28-35.

[28] V. Berry, K. Jennings, G. Woodnutt, Bactericidal and morphological effects of amoxicillin on *Helicobacter pylori*, Antimicrob. Agents Chemother. 39(8) (1995) 1859-1861.

[29] C.Q. Sun, C.J. O'Connor, A.M. Roberton, Antibacterial actions of fatty acids and monoglycerides againstHelicobacter pylori, FEMS Immunol. Med. Microbiol. 36(1-2) (2003) 9-17.

[30] J.B. Parsons, J. Yao, M.W. Frank, P. Jackson, C.O. Rock, Membrane disruption by antimicrobial fatty acids releases low-molecular-weight proteins from Staphylococcus aureus, J. Bacteriol. 194(19) (2012) 5294-304.

[31] S.W. Jung, S.W. Lee, The antibacterial effect of fatty acids on *Helicobacter pylori* infection, Korean J. Intern. Med. 31(1) (2016) 30-5.

[32] S.J. Hessey, J. Spencer, J.I. Wyatt, G. Sobala, B.J. Rathbone, A.T.R. Axon, M.F. Dixon, Bacterial adhesion and disease activity in *Helicobacter* associated chronic gastritis, Gut 31 (1990) 134-138.

[33] S. Schneider, G. Carra, U. Sahin, B. Hoy, G. Rieder, S. Wessler, Complex cellular responses of *Helicobacter pylori*-colonized gastric adenocarcinoma cells, Infect. Immun. 79(6) (2011) 2362-71.

Chapter 7

Concluding remarks and future perspectives

"When you think you reach the end, just breath… It is just the
beginning to higher ways."

Daniela Lopes-de-Campos

The major aim of this thesis was to improve the current therapy against *H. pylori.* Considering the severity of *H. pylori* infections and the persistent colonization by these bacteria, different strategies were followed to ensure a significant contribution to this field. One strategy was to use fundamental research to study the pharmacokinetic limitations of three first-line drugs against these bacterial infections. The other strategy was to innovate by creating a new treatment to eradicate *H. pylori*. Figure 1 shows an overview of this thesis, from the objectives towards the main findings.

Within the first objective/strategy, we contributed to the state of the scientific and technical knowledge about the usefulness of drug-membrane interactions studies to predict pharmacokinetic and pharmacodynamic properties (**Chapter 2.2**). Following this path, three first-line drugs were further evaluated:

1) **Omeprazole**: One of the major problems that we found on the literature was the controversy between the use of enteric-coated capsules or immediate-release omeprazole. Our studies showed that the pH, which is directly related to the route of absorption, significantly affects the interaction of omeprazole with biological membranes (**Chapter 6.1**). The protonated/charged state of omeprazole that exists at lower pH values (e.g. pH 5) enabled a reinforcement of the lipid membrane. The mechanism behind this effect was also studied (**Chapter 6.2**). The results revealed that at pH 5, omeprazole can stablish electrostatic and hydrophobic interactions with the polar heads and the acyl chains of DPPC, respectively. This intercalation promotes a higher packing of the surrounded DPPC moieties, leading to more condensed and untilted domains. Hence, the protonated state of omeprazole acts as a phospholipid. Phospholipids are important to protect the gastric mucosa, and a decrease of their concentration is associated with ulcerative mechanisms [1, 2]. Therefore, the administration of

surface active molecules is a way to protect and reinforce the gastric mucosa [2-4].

Implications on the clinics: Omeprazole is used to treat peptic ulcers. We have shown that when omeprazole is locally absorbed, it acts as a phospholipid-like drug, which reinforces the gastric mucosa. Therefore, when immediate-release omeprazole, an already FDA approved drug, is preferred over an enteric-coated omeprazole an additional mechanism of action occurs.

2) **Metronidazole**: Nitroimidazole derivatives have been extensively explored once they have a broad therapeutic activity, including antimicrobial, antiparasitic, and anticancer [5]. The chemistry behind nitroimidazole derivatives has been a subject of study for long years [5]. Metronidazole is one of the most important ones and, therefore, we studied its interaction with phosphatidylcholine lipid membranes. We found that the penetration of metronidazole into DPPC membrane models decreased the order and the packing of phospholipids (fluidizing effect) (**Chapter 6.3**). This effect was already pointed as one toxic mechanism of several drugs [6, 7]. Furthermore, there were water molecules in deeper regions of the membrane when metronidazole was present. This reflects a decrease of the hydrophobicity of the membrane and a destabilization of its biophysical properties. We were able to unveil the functional group that was perturbing the DPPC bilayer using molecular dynamics simulations. Our results showed that the hydroxyl group of the side chain of metronidazole interacts with water molecules and with the phosphate group of DPPC polar heads. On the other hand, the oxygen atoms bounded to the nitrogen of metronidazole's side chain are important for the partitioning of the drug.

Implications on the clinics: Several studies have been trying to develop new imidazole derivatives [5, 8-10]. We were able to contribute to the structure-toxicity relationship of metronidazole, by knowing which substituent is useful for metronidazole's partition and which causes toxic effects. These results can help in the design of new imidazole derivatives, which can be applied to treat *H. pylori* and other microbial diseases.
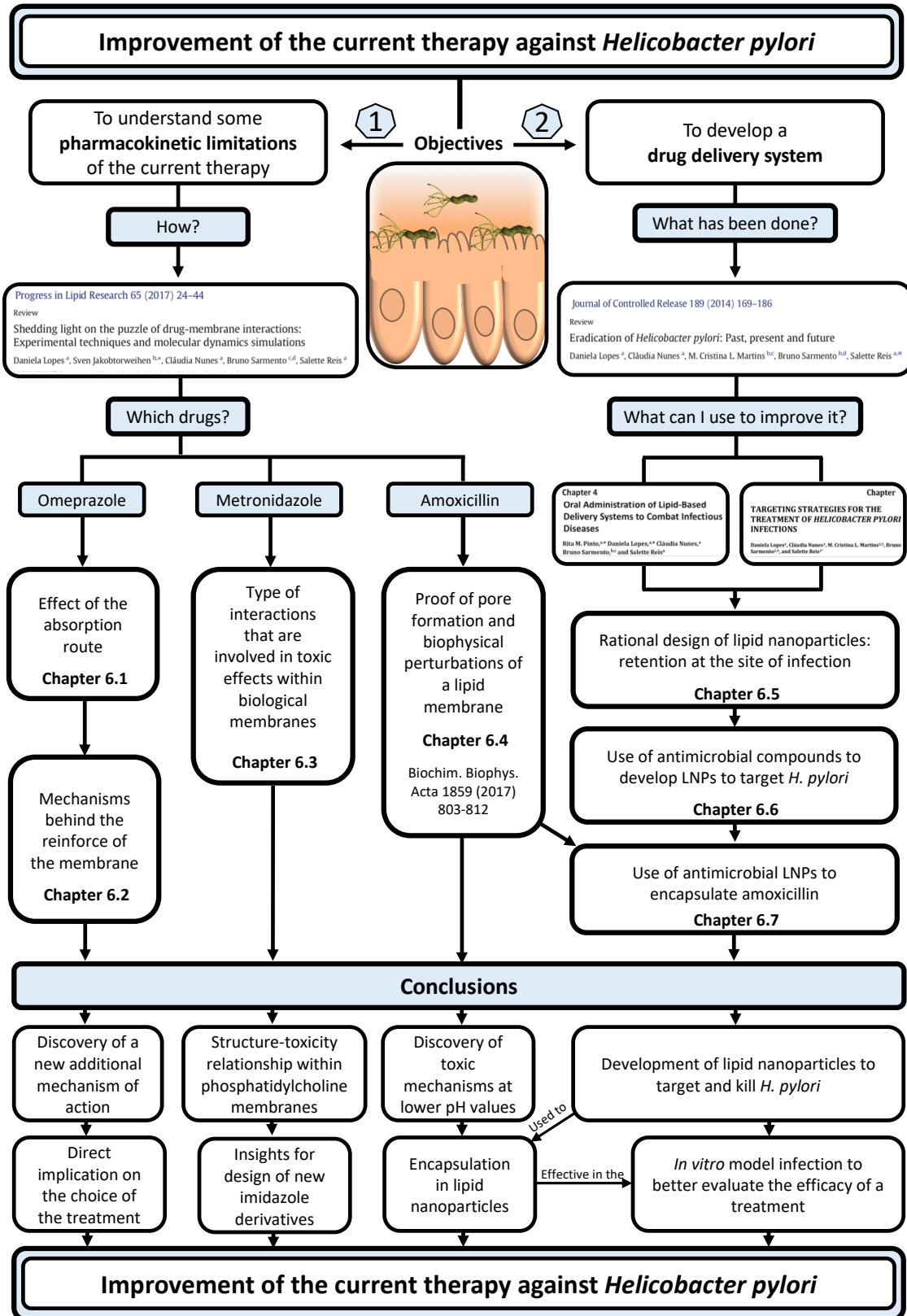
Figure 1. General overview of the objectives and the main findings that result from this thesis.

3) **Amoxicillin**: This drug has been associated with gastrointestinal and renal toxicity, especially when the pH is lower [11, 12]. Hence, we studied the effect of pH on the interaction of amoxicillin with DPPC membranes (**Chapter 6.4**). Our results showed that at lower pH values (pH 1.2 and pH 5) amoxicillin does perturb the biophysical properties of DPPC membranes. Amoxicillin is degraded under acidic pH, which leads to the opening of the β-lactam ring [13]. This leads to a free carboxyl group that is able to interact with the amino group of another molecule, forming dimers of amoxicillin [13, 14]. These dimers may be causing the heterogeneously distribution of amoxicillin within DPPC monolayers, promoting the formation of pores. However, at physiological pH (pH 7.4), amoxicillin did not perturb the DPPC membrane model.

Implications on the clinics: Despite the literature that reports the acidic degradation of amoxicillin, this drug is still administered under non-enteric coated formulations. This leads to a lower efficacy of the drug and, even more worrying, to toxic effects on lipid membranes, as shown by this work. The use of gastro-resistant capsules would however hamper the local effect at the gastric mucosa. Hence, we decided to create a drug delivery system that would be able to protect amoxicillin from the acidic pH of the stomach, releasing the drug near the site of infection.

The results obtained from the drug-membrane interactions led us to a second main objective, which was to develop a drug delivery system. Firstly, we contributed to the state-of-the-art about the use of nanotechnology to treat *H. pylori* infections (**Chapter 2.2**). To know how we could improve what has been done, two book chapters were also written: one about the application of lipid nanoparticles to treat infectious diseases (**Chapter 2.3**) and another one with the targeting strategies to both the bacteria and the gastric mucosa (**Chapter 2.4**). We found out that lipid nanoparticles were extensively explored to treat several bacterial diseases; however, there was only one work [15] with their application to kill *H. pylori*. Therefore, a rational design of lipid nanoparticles was made (**Chapter 6.5**). The rationality was present from the choice of the components (Tween 80 and linolenic acid with antibacterial properties and DOPE for targeting strategies) to the optimization through a quality by design approach. The physico-chemical features (dependent variables of the Box-Behnken design) were chosen to increase the retention time at the site of infection. This was corroborated by the interaction with mucins and the lower permeability through gastric cells. The lipid nanoparticles were able to kill *H. pylori* through the detachment of the bacterial membrane and the release of cytoplasmic content, as shown by scanning electron microscopy and through the percentage of ATP release (**Chapter 6.6**).

Furthermore, the presence of DOPE enabled an adhesion of the lipid nanoparticles to the bacteria within the first 15 min. DOPE also inhibited the adhesion of *H. pylori* to gastric cells. This is particularly important once a lower adhesion decreases the degree of inflammation mediated by these bacteria [16]. *H. pylori* uses the adhesion to inject bacterial virulence factors and to be internalized, hampering the activity of antimicrobial compounds [17, 18]. Thus, we developed a lipid nanoparticle that can be used against *H. pylori* due to their antimicrobial and anti-infection activity. Furthermore, these lipid nanoparticles are promising carriers for antibiotics once they can have a synergic effect with antibiotics. On one hand, most of the antibiotics have to cross the bacterial membrane to reach their target. Consequently, these lipid nanoparticles can enable a higher uptake by increasing the permeability of the bacterial membrane. On the other hand, the developed nanoparticles inhibit the internalization of *H. pylori* by gastric cells, which increases the exposure of the bacteria to the antibiotic. Knowing these advantages and the limitations of amoxicillin, we used these lipid nanoparticles to encapsulate amoxicillin (**Chapter 6.7**). We came across a major difficulty to assess the real efficacy of the lipid nanoparticle. We wanted to have a proof of concept of the drug delivery system. Nevertheless, the main limitations of amoxicillin *in vivo* are the acidic pH and its inability to reach the target site. A significant effect in planktonic bacteria could not reflect its ability to kill bacteria that are protected by the gastric mucosa. In fact, this is one of the incongruities between the efficacy of antibiotics *in vitro* and *in vivo* [19]. Hence, we developed a simplistic model where all the major factors that hamper the therapeutic efficacy *in vivo* could be mimicked. The system was composed of transwell inserts, a gastric cell barrier with functional tight junctions, mucins, and *H. pylori* J99. The acidic pH was also mimicked through a previous incubation of the drug or of the lipid nanoparticles within acidic medium. This *in vitro* infection model can be henceforward used by other researchers to evaluate the efficacy of antimicrobial compounds. Contrary to the observed with plain amoxicillin, amoxicillin-loaded lipid nanoparticles were effective in the *in vitro* infection model. Thus, even when in contact with acidic pH, the developed nanoparticles were able to kill the bacteria that were protected by the gastric cells barrier and by mucins. Therefore, we found a strategy to improve the efficacy of amoxicillin.

Limitations

One of the limitations of the biophysical studies on mimetic models is the oversimplification of biological membranes. In fact, membranes are composed of lipids, proteins, and sugars. Nevertheless, the basic structural unit of biological membranes is the lipid bilayer [20]. Hence, these studies of drug-mimetic models interactions should be seen as an evaluation of the interaction with the skeleton of biological membranes. The use of

more complex systems would hinder the assessment of the molecular mechanisms behind the drug-membrane interaction. In this thesis, DPPC was chosen for all the reasons already mentioned in Chapter 4. Even using a simple model, the drug-membrane interactions studies that were performed (**Chapter 6.1 to 6.4**) provided information regarding therapeutic and toxic mechanisms that involved lipid membranes. Another limitation of biophysical techniques is that their sensitivity usually requires concentrations higher than the plasmatic concentration. However, plasmatic concentrations do not reflect the real distribution of the drug within tissues. For instance, lipophilic drugs may be accumulated in tissues and higher local concentrations are achieved. In the case of interactions with the gastric mucosa, which is the main case of this thesis, the local concentration is significantly higher than the plasmatic concentration. For instance, the maximum concentration of metronidazole in plasma is 9.35 mg.L^{-1} whereas in the gastric juice is 33.58 mg.L^{-1} [21]. The use of probes in the fluorescence techniques and the difficulty to have an accurate force-field in the molecular dynamics simulations can give false results. To avoid this, a special care was taken by using small amounts of probes, according to the indicated by the literature, and by validating computational simulations through the comparison of coefficient partitions. Moreover, different techniques and different models were combined to guarantee that all results pointed towards the same insight.

Considering the development of the drug delivery system, the main limitation is the lack of *in vivo* studies. Despite their unquestionable usefulness, there is no perfect *in vivo* model for *H. pylori* infection. The *in vivo* models that can be easily colonized by *Helicobacter pylori* strains and that have a gastric physiology similar to humans are big animals, such as primates, pigs, and dogs [22]. Nevertheless, they are costly and with low practicality [22]. Small animals are more convenient; however, the manifestation of the bacterial infection is poorly correlated with the human disease [22]. Furthermore, there are only a limited number of *H. pylori* strains that can infect small models, such as mouse models [22]. For instance, *H. pylori* strain SS1, which is the most commonly used in mouse, is a standard mouse-adapted strain [23]. Additionally, the type of model strongly affects the evaluation of the pharmacokinetic properties associated with the oral administration. For instance, rats and mice, which are the most easily and less costly models, have less mucins than humans [24]. Rodents in general have less acidic stomachs [24]. The presence of mucins and the acidic environment are important limitations of the current therapy. Thus, the translation of the pharmacokinetic properties obtained using these models to the human should be carefully done. Therefore, the validation of the lipid nanoparticles as a proof of concept was performed in an *in vitro* infection model in which the *H. pylori* strain could be one of the most pathogenic human strains and where the *in vivo* barriers could be represented.

Future perspectives

Lipid membrane mimetic models revealed to be good platforms to study therapeutic and toxic effects of first-line drugs against *H. pylori* infections. The complexity of the lipid membrane model can be increased through the insertion of proteins or through more complex lipid compositions. The insertion of proteins would be particularly interesting in the case of omeprazole once its main mechanism of action is the inhibition of the proton pump, which is inserted in lipid membranes. Its effect on the packing of phospholipids may also affect the functionality of this protein. In the case of metronidazole and amoxicillin, their interaction with lipid membrane models that mimic the bacterial membrane would also be interesting due to their intracellular targets.

The *in vitro* infection model was a technique that we developed when we faced the need to assess our lipid nanoparticles in a more complex system. Hence, it is a promising platform to be used for other researchers. The optimization of the model can be pursued, with the addition of co-culture of cells or even of co-culture of *H. pylori* strains. Each person is in fact colonized by different strains in simultaneous [25]. Hence, the increase of the complexity of the model could resemble even more an infected gastric mucosa.

After developing the LNPs, their validation was achieved in the *in vitro* infection model as a proof of concept. Therefore, the next step is to perform *in vivo* studies. Considering the above-mentioned limitations, the Mongolian gerbil will be used once they show the same progression of the human disease (chronic gastritis – peptic ulcers – metaplasia- cancer) [22].

References

[1] F. Mauch, G. Bode, H. Ditschuneit, P. Malfertheiner, Demonstration of a phospholipid-rich zone in the human gastric epithelium damaged by Helicobacter pylori, Gastroenterol. 105(6) (1993) 1698-1704.

[2] L.M. Lichtenberger, Role of phospholipids in protection of the GI mucosa, Dig. Dis. Sci. 58(4) (2013) 891-3.

[3] F.I. Tovey, Role of dietary phospholipids and phytosterols in protection against peptic ulceration as shown by experiments on rats, World J. Gastroenterol. 21(5) (2015) 1377-84.

[4] S. Demirbilek, I. Gürses, N. Sezgin, A. Karaman, N. Gürbüz, Protective Effect of Polyunsaturated Phosphatidylcholine Pretreatment on Stress Ulcer Formation in Rats, J. Pediatr. Surg. 39(1) (2004).

[5] D.Y. Alawadi, H.A. Saadeh, H. Kaur, K. Goyal, R. Sehgal, T. Ben Hadda, N.A. ElSawy, M.S. Mubarak, Metronidazole derivatives as a new class of antiparasitic agents: synthesis, prediction of biological activity, and molecular properties, Med. Chem. Res. 24(3) (2014) 1196-1209.

[6] A.C. Alves, D. Ribeiro, C. Nunes, S. Reis, Biophysics in Cancer: The Relevance of Drug-Membrane Interaction studies, Biochim. Biophys. Acta, Biomembr. 1858(9) (2016) 2231-44.

[7] C. Pereira-Leite, C. Nunes, S. Reis, Interaction of Nonsteroidal Anti-inflammatory Drugs with Membranes: *In Vitro* Assessment and Relevance for their Biological Actions, Prog. Lipid Res. 52 (2013) 571-584.

[8] K. Bowden, J. Izadi, Multifunctional Derivatives of Metronidazole, Il farmaco 53 (1998) 58-61.

[9] W.J. Mao, P.C. Lv, L. Shi, H.Q. Li, H.L. Zhu, Synthesis, molecular docking and biological evaluation of metronidazole derivatives as potent Helicobacter pylori urease inhibitors, Bioorg. Med. Chem. 17(21) (2009) 7531-6.

[10] A.J. Atia, Synthesis and Antibacterial Activities of new Metronidazole and Imidazole Derivatives, Molecules 14(7) (2009) 2431-46.

[11] Meyler's Side Effects of drugs: The international encyclopedia of adverse drug reactions and interactions, 15th ed., Elsevier B.V.2006.

[12] G. Fritz, Amoxicillin-induced acute renal failure, Nephrol. Dial. Transplant. 18(8) (2003) 1660-1662.

[13] E. Nagele, R. Moritz, Structure elucidation of degradation products of the antibiotic amoxicillin with ion trap MS(n) and accurate mass determination by ESI TOF, Journal of the American Society for Mass Spectrometry 16(10) (2005) 1670-6.

[14] C.-Y. Lu, C.-H. Feng, Identification of dimer impurities in ampicillin and amoxicillin by capillary LC and tandem mass spectrometry, J. Sep. Sci. 30(3) (2007) 329-332.

[15] C.L. Seabra, C. Nunes, M. Gomez-Lazaro, M. Correia, J.C. Machado, I.C. Goncalves, C.A. Reis, S. Reis, M.C.L. Martins, Docosahexaenoic acid loaded lipid nanoparticles with bactericidal activity against *Helicobacter pylori*, Int. J. Pharm. 519(1-2) (2017) 128-137.

[16] J.G. Kusters, A.H. van Vliet, E.J. Kuipers, Pathogenesis of Helicobacter pylori infection, Clin. Microbiol. Rev. 19(3) (2006) 449-90.

[17] Z.-W. Zhang, N. Dorrel, B.W. Wren, M.J.G. Farthing, *Helicobacter pylori* adherence to gastric epithelial cells: a role for non-adhesin virulence genes, J. Med. Microbiol. 51 (2002) 495-502.

[18] Y. Huang, Q.L. Wang, D.D. Cheng, W.T. Xu, N.H. Lu, Adhesion and Invasion of Gastric Mucosa Epithelial Cells by Helicobacter pylori, Front. Cell. Infect. Microbiol. 6 (2016) 159.

[19] F. Mégraud, P. Trimoulet, H. Lamouliatte, L. Boyanova, Bactericidal effect of amoxicillin on *Helicobacter pylori* in an *in vitro* model using epithelial cells, Antimicrob. Agents Chemother. 35(5) (1991) 869-872.

[20] C. Peetla, A. Stine, V. Labhasetwar, Biophysical interactions with model lipid membranes: applications in drug discovery and drug delivery, Mol. Pharm. 6(5) (2009) 1264-1276.

[21] A.F. Goddard, M.J. Jessa, D.A. Barrett, N.P. Shaw, J.-P. Idström, C. Cederberg, R.C. Spiller, Effect of omeprazole on the distribution of metronidazole, amoxicillin, and clarithromycin in human gastric juice, Gastroenterol. 111 (1996) 358-167.

[22] J.Y. Lee, Animal models of *H. pylori* infection, in: N. Kim (Ed.), *Helicobacter pylori*, Springer Science + Business Media, Singapore, 2016.

[23] A. Lee, J. O'Rourke, M.C.d. Ungria, B. Robertson, G. Daskalopoulos, M.F. Dixon, A standardized mouse model of *Helicobacter pylori* infection: introducing the Sydney strain, Gastroenterol. 112(1386-1397) (1997).

[24] L.M. Ensign, R. Cone, J. Hanes, Oral drug delivery with polymeric nanoparticles: the gastrointestinal mucus barriers, Adv. Drug Deliv. Rev. 64(6) (2012) 557-70.

[25] D.A. Israel, N. Salama, U. Krishna, U.M. Rieger, J.C. Atherton, S. Falkow, *Helicobacter pylori* genetic diversity within the gastric nich of a single human host, PNAS 98(25) (2001) 14625-14630.

APPENDIX

PAN STANFORD PUBLISHING
www.panstanford.com

31st January 2018

To Whom It May Concern

AUTHORISATION LETTER

Pan Stanford Publishing Pte Ltd authorizes Daniela Lopes, the author of Chapter 4: "*Oral administration of lipid-based delivery systems to combat infectious diseases*" in the book: "*Nanoparticles in Life Sciences and Biomedicine*" (ISBN: 978-981-4745-98-7), to reproduce/republish this chapter in her doctoral thesis.

The specifications of the Doctoral Thesis are:

Title: Improvement of the current therapy against Helicobacter pylori: biophysical studies of drug-membrane interaction and development of a dual-drug delivery system
Doctoral Programme: Molecular and Cellular Biotechnology Applied to Health Sciences
Host Institution: Abel Salazar Biomedical Sciences Institute and Faculty of Pharmacy, University of Porto
Doctoral Candidate: Daniela Priscila Rodrigues Lopes de Campos
Affiliation: LAQV, REQUIMTE, Department of Chemical Sciences, Faculty of Pharmacy, University of Porto, Portugal
Supervisor: Prof. Dr. Maria de La Salette de Freitas Fernandes Hipólito Reis Dias Rodrigues
Co-supervisor: Dr. Cláudia Daniela Oliveira de Lacerda Nunes
Co-supervisor: Prof. Dr. Bruno Filipe Carmelino Cardoso Sarmento"

Sincerely,

Jenny Rompas
Director and Publisher
Pan Stanford Publishing Pte. Ltd.

Tel: +65 6829 2268
Fax: +65 6866 3636
Email: jenny@panstanford.com
Web: www.panstanford.com

Improvement of the current therapy against
Helicobacter pylori: biophysical studies of drug-
membrane interaction and development of a dual-
drug delivery system

Daniela Lopes de Campos

INSTITUTO DE CIÊNCIAS BIOMÉDICAS ABEL SALAZAR
FACULDADE DE FARMÁCIA

SEDE ADMINISTRATIVA